Theoretical Investigations of the Acetylene Analogues of Group 14 Elements E_2X_2 (E=Si-Pb, X=F-I)

(Theoretische Untersuchungen der Acetylen Analoga der Gruppe-14-Elemente)

Dissertation

zur Erlangung des
Doktorgrades der Naturwissenschaften
(Dr. rer. nat.)

dem Fachbereich Chemie
der Philipps-Universität Marburg
vorgelegt von

Takayasu Shimizu
（清水 孝保）
aus Kyoto/Japan

Marburg/Lahn 2010

Vom Fachbereich Chemie der
Philipps-Universität Marburg als Dissertation am 20. Juli. 2010
angenommen.

Erstgutachter: Prof. Dr. Gernot Frenking
Zweitgutachter: Prof. Dr. Wolf-Christian Pilgrim

Tag der mündlichen Prüfung war der 8. Sep. 2010.

The Road

Don't fear what happens if you keep going on this road.

With fear, there will be no road.

If you give one step, the step becomes a road.

The step is a road.

Go on without fear, then you will find out.

Tetsuo Kiyosawa

A Japanese Philosophier

此の道を行けば どうなるのかと 危ぶむなかれ

危ぶめば 道はなし

ふみ出せば その一足が 道となる

その一足が 道である

わからなくても 歩いて行け

行けば わかるよ

『道』 清沢 哲夫

Preface

Die vorliegende Arbeit wurde am Fachbereich Chemie der Philipps-Universität Marburg/Lahn unter der Leitung von Herrn Prof. Dr. G. Frenking in der Zeit von April 2006 bis Juni 2010 angefertigt.

Herrn Prof. Dr. G. Frenking danke ich sehr herzlich für die interessante Themenstellung, die geduldige Betreuung, anregende Diskussionen und wertvolle, ideenreiche Ratschläge sowie für hervorragende Arbeitsbedingungen. Meinen Kollegen des AK Prof. Dr. G. Frenking möchte ich für das sehr gute Arbeitsklima und stete Hilfsbereitschaft danken. Ferner Prof. Stefanie Dehnen für die Anfertigung des Zweitgutachtens. Besonderer Dank gebührt Dr. Andreas Krapp, Dr. Ralf Tonnor und Dr. Robin Haunschild, dessen Hilfe am Anfang meines Leben in Marburg und am Verkehrsunfall, Thomas Reuter für eine Vielzahl technischer Hilfen. Calora Rösser, Nicole Holzmann, Moritz von Hopfgarten, Susanne Klein und meine Frende in Marburg, besonders Stephenie Rudd dafür zu danken, sich Mühe gegeben zu haben, die Arbeit zu lesen und zu korrigieren. In besonderer Erinnerung wird mir die Zusammenarbeit mit Dr. Israel Fernández Lopez bleiben, die weit über kollegiales Miteinander hinausging, dabei dennoch viele wegweisende und fruchtbare, fachliche Diskussionen beinhaltete - und unzählige Tischtenisspiel. Mein Dank gilt allen Mitarbeitern der Hochschulrechenzentren der Philipps-Universität Marburg, der Technischen Universität Darmstadt und der Universität Frankfurt.

Besonderer Dank gilt meinen Eltern dafür, dass sie mein Studium finanziell ermöglichten, einen akademischen Grad zu erwerben, und dass sie mir eine Erlaubnis in Marburg zu studieren gegeben hat.

Contents

The most beautiful experience we can have is mysterious.
It is the fundamental emotion
that stands at the cradle of true art and true science.
Albert Einstein

1. Introduction

The chemical research of heavy-atom group 14 analogues of acetylene E_2H_2 and their substituted derivatives E_2R_2 (E = Si-Pb) has fascinated researchers for a long time due to their unusual structures [1, 2, 3]. In the last 25 years, theoretical and experimental researches of E_2R_2 have been done. The starting signal for positive results came from theoretical studies although the experimental attempts of the isolation of the molecules possessing a triple E-E bond with E = Si-Pb were not successful until 2000. In 1982, Moskowitz *et al.* [4] revealed that the linear structure of Si_2H_2 molecules is not a global minimum, which means that Si_2H_2 has a different character from acetylene. In 1983, Lischka and Köhler [5], and some weeks later Binkley *et al.* [6] reported that the singlet potential energy surface of Si_2H_2 is quite different from that of C_2H_2. These reports presented that the doubly bridged structure **A** is found as a global minimum, whereas the acetylene-like linear species HSi≡SiH **G** was found not to be an energy minimum structure but to be a second-order saddle point.

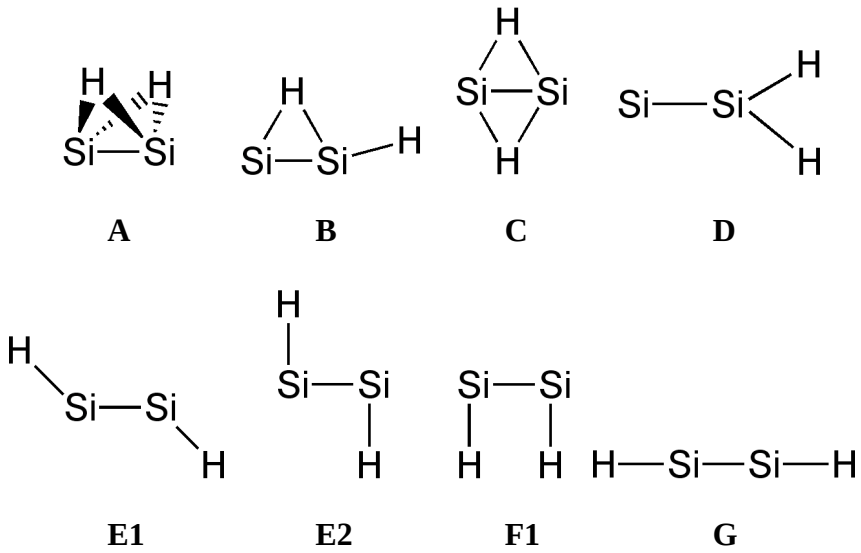

Scheme 1.1 Investigated Si_2H_2 isomers in the previous reports [4, 5]

Scheme 1.1 shows some isomers that were investigated in the previous reports.

These species are denoted as follows: non-planar doubly bridged structure (**A**), singly bridged planar structure (**B**), planar doubly bridged structure (**C**), vinylidene structure (**D**), trans-bent structure (**E**), cis-bent structure (**F**) and linear structure (**G**).

Former studies reported that the global minimum of Si_2H_2 was predicted to be the doubly hydrogen-bridged butterfly structure **A** [5, 6]. The geometry optimization of **G** without linearity symmetry constraint yields the trans-bent structure with the larger angle **E1** as a higher lying local minimum than the butterfly structure **A**. The vinylidene isomer **D** was calculated to be another local minimum on the singlet potential energy surface, where the vinylidene isomer **D** is lower in energy than the trans-bent isomer **E1**. The previous calculations also showed that triplet structures of Si_2H_2 are higher in energy than the singlet forms [5, 6, 7]. Subsequent theoretical studies of Si_2H_2 isomers with higher levels of theory [8-25] confirmed that the doubly bridged structure **A** is the global minimum of Si_2H_2 as predicted by Lischka and Köhler [5], and Binkley [6]. After their works the singly bridged isomer **B** was found as another low-lying energy minimum by Koseki *et al.* [12] and it is proved by the following works with more accurate methods [14, 16, 21, 22, 23, 24, 26].

Some years after the first report of Si_2H_2, theoretical studies of Ge_2H_2 [16, 21, 26, 27, 28, 29], Sn_2H_2 [21] and Pb_2H_2 [21, 31, 32] were reported. These studies showed that the doubly bridged structures **A** are the global minima for these molecules and the order of the stability of the isomers is similar to that of Si_2H_2.

The theoretical researches predicted the stable isomer of E_2H_2, but these isomers were not detected for a long time because of their high reactivity. The spectroscopic investigation in low temperature matrixes by Bogey *et al.* [33, 34] confirmed the theoretical predictions about the unusual structures **A** of Si_2H_2 [5, 6]. The spectroscopic studies also indicate the presence of the structure **B** in low temperature matrixes on Si_2H_2 [35, 36, 37, 38]. Andrews and co-workers have identified the hydrogen-bridged structures **A** for Ge_2H_2, Sn_2H_2 and Pb_2H_2 in low-temperature matrixes [39, 40, 41].

Although Si_2H_2 prefers to have the doubly bridged structure, the theoretical studies of the derivatives of Si_2H_2 show a different trend to Si_2H_2. Thies *et. al.* [42, 43, 44] presented that Si_2Me_2 prefers the vinylidene structure **D**, whereas the doubly

bridged one **A** is the energetically higher lying isomer for Si_2H_2.

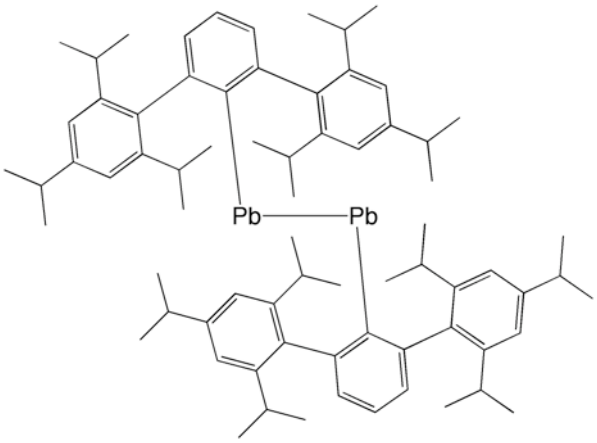

(a)

Figure 1.1. Experimentally isolated Pb_2R_2 isomer (a) by Power *et al.* [45], (R=C_6H_3-2,6-$Trip_2$)PbPb(C_6H_3-2,6-$Trip_2$)

Although the theoretical investigations dominated the study of E_2R_2 molecules for a long time, Power *et al.* made a breakthrough in the experimental research in 2000 [45]. They synthesized the substituted lead compound R*PbPbR* with quite bulky terphenyl substituents R* (R* = C_6H_3-2,6-$Trip_2$; Trip= C_6H_2-2,4,6-$^iPr_3$; Pr = propyl) and they identified the structure by X-ray structure analysis (Figure 1.1). The synthesized isomer does not have the butterfly structure **A** in the previous reports [21, 31, 32], but the trans-bent structure as shown in Figure 1.1, which is a higher-lying local minimum for Pb_2H_2. A peculiar aspect of the molecular structure is the rather long Pb-Pb distance of 3.188 Å and the acute C-Pb-Pb bond angle of 94.3° [45]. In this report, the authors suggested not only that the compound R*PbPbR* has a Pb-Pb single bond due to that the Pb-Pb bond length is longer than the typical single bond, although the Pb-Pb distance is shorter than the interatomic distance in metallic lead, but also that *s* and *p* orbitals of Pb are little hybridized in these isomers and each PbR* fragment carries a σ electron lone-pair and an unpaired electron due to the C-Pb-Pb angle.

A following theoretical study by Frenking *et al.* [26] showed that the structure of R*PbPbR* is quite similar to the trans-bent structure of **E2** for Pb_2H_2 and the structural similarity indicates that Power's compound R*PbPbR* is a derivative of the

trans-bent isomer **E2** of Pb_2H_2 (Scheme 1.1). The orbital analyses of the two types of trans-bent structures **E1** and **E2** of Pb_2H_2 revealed that the HOMO and the LUMO of the two species are exchanged. The **E1** structure has an occupied Pb-Pb π orbital as the HOMO, which is unoccupied in the **E2** structure, whereas the HOMO of **E2** is a σ type Pb-Pb bonding orbital and the orbital is unoccupied in **E1**. After the theoretical study by Frenking *et al.* [32], Power *et al.* [46] reported the theoretical results about MO analyses of MePbPbMe. The report revealed that the orbital figures of the trans isomer **E2** for Pb_2H_2 are common for Pb_2Me_2 and the electronic structure of the trans isomers for Pb_2R_2 molecules depends on the Pb atom.

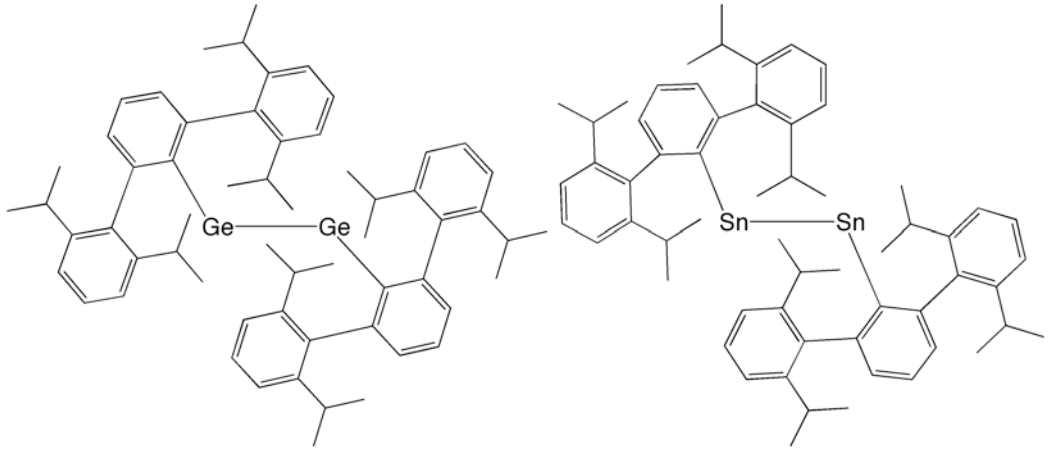

(b) (c)

Figure 1.2. The experimentally conformed ArGeGeAr isomer (b) (C_6H_3-2,6-$Dipp_2$)GeGe(C_6H_3-2,6-$Dipp_2$) [47] and ArSnSnAr isomer (c) (C_6H_3-2,6-$Dipp_2$)SnSn (C_6H_3-2,6-$Dipp_2$) [48]

Shortly after the first report on the synthesis of R*PbPbR* by Power *et al.*, they also succeeded in the isolation and the X-ray structure analysis of R'SnSnR' [47] and R'GeGeR' [48] where R' is a slightly modified terphenyl substituent (R' = C_6H_3-2,6-$Dipp_2$; Dipp = C_6H_3-2,6-$^iPr_2$) (Figure 1.2). Apart form the lead compound R*Pb≡PbR*, the geometries of the germanium and tin analogues of alkynes have rather short E-E distances (2.668 Å and 2.285 Å, respectively) and they have C-E-E angles between 125.2° and 128.7° [47, 48]. The investigation of the geometries indicates that R'SnSnR' and R'GeGeR' are probably derivatives of the structure type **E1** but not **E2** (Scheme 1.1).

A related diaryl compound of ArSiSiAr could not be detected so far, although the isomer is proposed as an intermediate in the C-C formation reaction by reducing terphenyltrifluorosilanes [49]. Other than the diaryl compounds, the synthesis of the molecule $(R_2MeSi)SiSi(SiMeR_2)$ with the bulky alkyl group R = $^{t}Bu_3Si$ has been reported by Wiberg *et al.* [50, 51] (Figure 1.4(d)). The compound was not isolated and not characterized by X-ray structure analysis, but the structure is determined by ^{29}Si-NMR spectra. The spectroscopic results indicate the shorter Si-Si bond length (2.072 Å) than normal double or single Si-Si bonds. The assignment of the observed ^{29}Si-NMR signal to a silicon compound indicates that the isomer synthesized by Wiberg *et al.* [50, 51] has the **E1** structure. The spectroscopic result was supported by quantum chemical calculations of Nagase and coworkers, who calculated not only the theoretical NMR spectra of the model isomer $(H_3Si)SiSi(SiH_3)$ [52], but also the spectra of the spectroscopically detected isomer by Wiberg *et al.* with higher levels of theory [53].

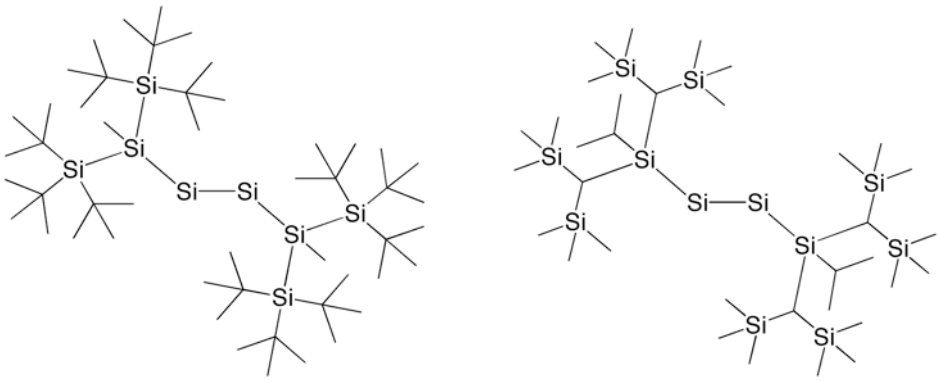

(d) (e)

Figure 1.3. The detected RSiSiR isomer (d) by NMR by Wiberg *et al.* [50, 51] $((^{t}Bu_3Si)_2MeSi)SiSi(SiMe(Si^{t}Bu_3)_2)$, and the isolated RSiSiR isomer (e) $(((Me_3Si)_2CH)_2{}^{i}PrSi)SiSi(Si^{i}Pr(CH(Me_3Si)_2))$ by Sekiguchi *et al.* [54]

A definite proof for the synthesis of a disilyne was recently given in 2004 by Sekiguchi *et al.* [54], who reported on the X-ray structure analysis of $(R_2{}^{i}PrSi)SiSi(Si^{i}PrR_2)$ where R = $CH(Me_3Si)_2$ (Figure 1.4(e)). Some years later they reported both results for the solid-state ^{29}Si-NMR spectra and the calculation [55]. Their studies showed that the theoretical results agree with the results of spectroscopy. Both investigations indicate that $(R_2{}^{i}PrSi)SiSi(Si^{i}PrR_2)$ has the trans-bent structure **E1**,

which is similar to ArGeGeAr and ArSnSnAr compounds.

The first report of the trans-bent structures was published by Nagese *et al.* and they reported the R'SiSiR' with bulky functional group R' and they revealed the stable trans-bent structure is the most stable isomer for R'SiSiR' [56]. After that, many researchers made important theoretical contributions to the understanding of stable group 14 compounds REER where R is a very bulky substituent, both experimentally and theoretically. [57-72] They optimized not only the model compounds HEEH but also the structures that were experimentally found by Power [31, 32] and Wiberg, [33, 34] and they analyzed the influence of the substituent on the stability of the molecules. Nagese and coworkers discussed mainly the bonding situation of the trans-bent structures REER which are derived from **E1** or **E2** (Scheme 1.1) with the geometries [21, 52, 53, 56, 60, 61, 66, 70] and the spectroscopic results [53]. The most important discussion in their papers is the question why R'EER' molecules prefer to have trans-bent distorted geometries and not a linear structure. Another interesting topic was the question whether molecules with the structures **E1** have an E-E triple bond or not. In their papers, they concluded that the bent structures of RSiSiR, RGeGeR and RSnSnR have a triple bond and the Pb-Pb bond of the trans-bent isomer of RPbPbR' is a single bond, although the R'PbPbR' takes a multiple bond structure in solution. However, clear explanations of the unusual structures **A**-**G** of the parent compounds E_2H_2 are not given. The bent structures **E1** and **E2** are the most similar to the linear structure **G**, but they are the highest lying forms of E_2H_2 shown in Scheme 1.1, as reported before [5, 6].

The E_2H_2 molecules and the derivatives of E_2H_2 have been already studied until now. Although the derivatives with the electron donating functional group are investigated [73, 74], the researches about the E_2X_2 isomer containing electron-withdrawing groups are still few. Recently, Li *et al.* reported the isomers of Si_2F_2 and Ge_2F_2 [75, 76]. It was surprising that for Si_2F_2 the vinylidene structure **D** on the triplet state potential energy surface is a global minimum, not the doubly bridged structure **A** [75], although the global minimum of Ge_2F_2 is the doubly bridged structure **A** [76], which is similar to Ge_2H_2 molecules. However, the functions of F atom and the character of E-E bond are not clear.

As shown before, the E-E interaction plays an important role in the E_2R_2 isomers. To understand the E-E bonding, some theoretical investigations were carried out. The preference of molecules RE≡ER where E is Si, Ge, Sn and Pb, has been explained by Popelier *et al.* [77], Pignedoli *et al.* [78], Chesnut [79] and Firme *et al.* [80] in terms of topological analyses of the electron density, and by Shaik *et al.* [62], who employed VB structures. Another method is the MO model employed by Nagase *et al.* [21, 52, 53, 56, 66, 70, 71], Sekiguchi *et al.* [54, 55. 66, 68, 72] and Power *et al.* [46, 57, 58, 59]. The MO model was originally introduced earlier by Trinquier and Malrieu [81, 82] and by Carter and Goddard [83] to explain the E-E bonding structure of X_2E-EX_2. In their works they divided the molecules into the two EX_2 fragments and they discussed their orbital interaction. Trinquier and Malrieu [81, 82] explained the distorted structure of X_2E-EX_2 as donor-acceptor interactions with the two EX_2 fragments in their singlet state, whereas Carter and Goddard [83] used the two triplet CX_2 fragment to describe the X_2C=CX_2 double bond. The MO model could give a good explanation for the double E=E double bond [84, 85, 86]

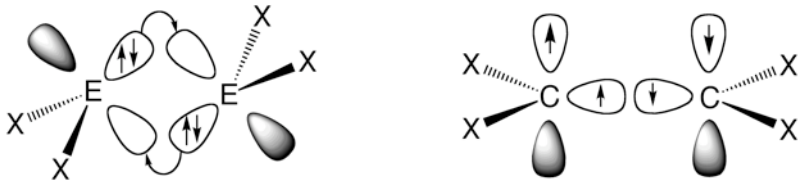

(i) (ii)

Figure 1.4. Two types of orbital interaction models for X_2EEX_2. The donor-acceptor interaction between two EX_2 fragments in their singlet states (i) by Trinquier and Malrieu [81, 82] and the electron-sharing model (ii) in their triplet states by Carter and Goddard [83].

Lein *et al.* [87] reported the results of Energy Decomposition Analyses (EDA) for Si_2H_2, Ge_2H_2, Sn_2H_2 and Pb_2H_2, and they discussed there the reason why the most stable structures of Si_2H_2-Pb_2H_2 are the doubly bridged form **A** followed by the singly bridged **B**. The EDA calculations suggested that an EH donor-acceptor bond is weaker than an E-E σ bond but the donor-acceptor bond is stronger than a π bond and the strength of the E-E σ bond shows the trend **B** > **E1** > **G**. Due to that, the doubly bridged structure is the global minimum and the singly bridged structure is the

following one. Before the report, they employed the EDA to analyze systematically the nature of the interactions in donor-acceptor bonds [88-132] and in electron-sharing bonds [112, 116, 127, 133-141]. They revealed that EDA is a successful and sensible method to understand the character of the bonding.

In this work, the theoretical investigations of E_2X_2 molecules with electron-withdrawing groups (E=Si, Ge, Sn and Pb, X=H, F, Cl, Br and I) have been done (Scheme 1.2). The orbital analyses of E_2X_2 molecules and EX fragments present that the unusual forms of E_2X_2 molecules can be explained in terms of molecular orbital arguments of the interactions between two EX molecules. The bonding analyses of the E-E bonds of these isomers exhibit that the qualitative bonding model is supported and complemented by a quantitative energy decomposition analysis of the binding interactions between the fragments.

The aims of this work are the following four points: The first question is how is the order of stability for each isomer of E_2X_2 molecules. The second question is why E_2X_2 molecules dislike having the linear structure. The third one is the reason why the bridged structures for E_2X_2 except Si_2F_2 are global minima. The last one is the reason why the Si_2F_2 prefers the vinylidene structure **D**, not the linear structure and doubly bridged structure **A**.

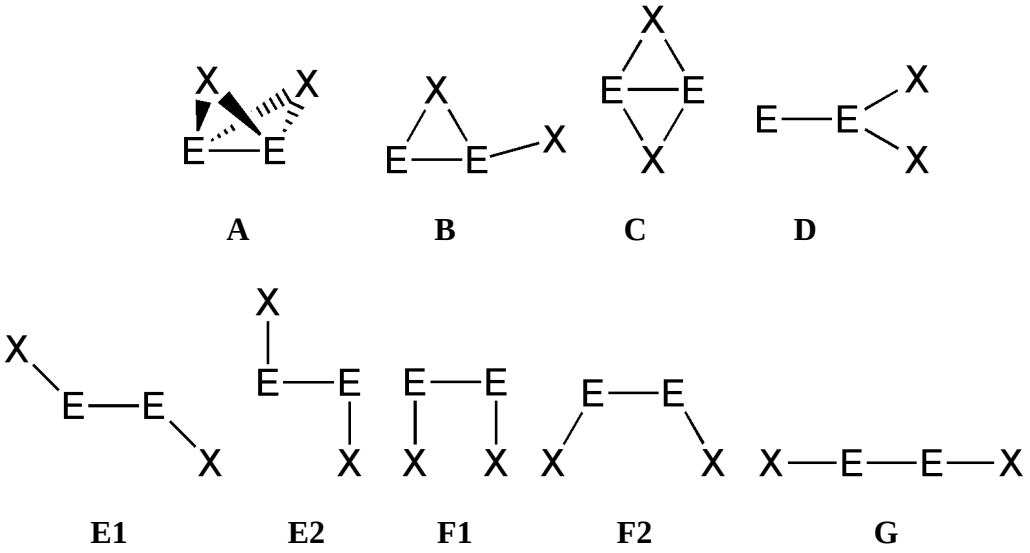

Scheme 1.2 Investigated E_2X_2 isomers in this work.

The underlying physical laws necessary for the mathematical theory of
a large part of physics and the whole of chemistry
are thus completely known,
and the difficulty is only that the exact application of these laws
leads to equations much too complicated to be soluble.
It therefore becomes desirable that approximate practical methods of
applying quantum mechanics should be developed,
which can lead to an explanation of the main features of
complex atomic systems without too much computation.

Paul Dirac

2. Theory

In the last year of the 19th century, Max Planck stated the Planck's laws and he solved the problem of blackbody radiation [142], which violates the laws of classical electrodynamics. This was the dawn of the history of quantum mechanics. In 1905 Einstein gave the explanation for the photoelectron effect using quantum theory [143]. Some decades later de Broglie [144] proposed the idea of matter wave, which is the generalization of the explanation of the photoelectron effect. After that, quantum mechanics were developed by Niels Bohr, Werner Heisenberg, Erwin Schrödinger, Paul Dirac, etc. Quantum mechanics were applied to understand the nature of chemistry and this new region is called quantum chemistry. The developments of the methods and their applications in the region of quantum chemistry are still going on. This chapter gives the overview of the quantum chemical methods which are applied in this study. The details and the discussions of the theoretical methods are given in the original papers and in some textbooks [145-150].

2.1. Schrödinger Equation

Molecular structures, chemical reactivity and the properties of molecules can be understood using chemical and physical theories. The theory of quantum chemistry is based on the Schrödinger equation, which is expressed by a differential equation. This equation was presented by Schrödinger in 1926 [151]. In the non-relativistic case the time-dependent Schrödinger equation is written as follows.

$$-\frac{\hbar}{i}\frac{\partial \Psi(\tau,t)}{\partial t} = \hat{H}(\tau)\Psi(\tau,t) \qquad \text{eq. 1}$$

Here, $\Psi(\tau, t)$ is the wave function of the electronic system dependent on the coordinates τ and time t. The Hamiltonian operator $\hat{H}$ is the analogue of kinetic and potential energy in classical mechanics. When the physical problem is time-independent, the Hamiltonian can be expressed in a time-independent form. The wave function can be divided into a time-independent part and a time-dependent part where the time independent wave function is written as follows.

$$\Psi(\tau,t) = \psi(\tau)\Theta(t) = \psi(\tau)\exp\left(\frac{E}{ih}t\right) \qquad \text{eq. 2}$$

The time-dependent part $\Theta(t)$ is the periodic phase factor. The time-independent Schrödinger equation is expressed by eq. 3.

$$\hat{H}\psi = E\psi \qquad \text{eq. 3}$$

Here, the Hamiltonian operator $\hat{H}$ in the system is presented by eq. 4-1.

$$\hat{H} = -\frac{1}{2}\sum_i \nabla_i^2 - \sum_A \frac{1}{2M_A} - \sum_A \sum_i \frac{Z_A}{r_{iA}} + \sum_A \sum_{B>A} \frac{Z_A Z_B}{r_{AB}} + \sum_j \sum_{i>j} \frac{1}{r_{ij}} \qquad \text{eq. 4-1}$$

which can be written as eq. 4-2.

$$\hat{H} = \hat{T}_e + \hat{T}_N + \hat{V}_{eN} + \hat{V}_{NN} + \hat{V}_{ee} \qquad \text{eq. 4-2}$$

T_e is the kinetic energy of an electron and T_N denotes that of the nucleus. V_{eN}, V_{ee} and V_{NN} denote the potential energy of electron-nucleus interaction, electron-electron interaction and nucleus-nucleus interaction, respectively.

The solution of this differential equation yields the eigenvalues and eigenfunctions. The eigenvalues give the energy of the system while the eigenfuctions describe the stationary state of the system. The square of the wave function is interpreted as the probability of the existence of a particle at the point of τ_1, τ_2, etc. The Schrödinger equation cannot be solved analytically for more than three-body systems. Due to this problem, approximations must be made for larger systems.

One of the most important approximations is the Born-Oppenheimer approximation [152], which states that the movement of nuclei is much slower

compared to the movement of electrons. Therefore the effect of the nuclear movement can be neglected and the nuclear movement can be approximated by the positions of the electrons. Under the Born-Oppenheimer approximation, the kinetic energy of the nuclei is neglected and the electrostatic repulsion between the nuclei is constant. The non-relativistic Schrödinger equation for a molecule under the Born-Oppenheimer approximation is expressed as follows.

$$\hat{H}_e\psi_e = (\hat{T}_e + \hat{V}_{eN} + \hat{V}_{ee})\psi_e = E_e\psi_e \qquad \text{eq. 5}$$

Here, $\hat{H}_e$ is the electronic Hamiltonian operator and E_e is the electronic energy of the system. In this Schrödinger equation, the wave function depends only on the coordination of the atoms. When E_e is calculated for various coordinates of atoms, the potential energy surface of the molecule is obtained, and the molecule moves on the potential energy surface under the Born-Oppenheimer approximation. In most cases the Born-Oppenheimer approximation is a good approximation. The approximation, however, leads to errors and it is not effective when two or more different electronic states in the same geometry are energetically close.

In the solution of the Schrödinger equation the variational principle is employed [153, 154]. This principle states that the energies of trial wave functions $\tilde{\psi}$ are higher or equal to the exact energy.

$$\langle\tilde{\psi}|\hat{H}|\tilde{\psi}\rangle \geq \langle\psi|\hat{H}|\psi\rangle = E_0 \qquad \text{eq. 6}$$

The trial wave function is the practical method to solve the differential function by the variational principle. The eq. 6 is only equal when the exact wavefunction is given.

The connection of the quality δ of the wavefucntion ψ and energy is expressed in eq. 7

$$\delta = 1 - \left|\langle\tilde{\psi}|\psi\rangle\right|^2 \leq \frac{\langle\tilde{\psi}|\hat{H}|\tilde{\psi}\rangle - E_0}{E_1 - E_0} \qquad \text{eq. 7}$$

The equation indicates that the error δ of the wavefunction ψ is small when the difference between the energies of the ground state and the first excited state is larger.

2.2. Hartree-Fock Method

The Pauli-principle states that two electrons with the same quantum numbers cannot exist [155]. The principle directly comes from the antisymmetric character of fermions. The electron is a fermion and the wave function must have antisymmetric character. It means that the sign of the wave function must change on the exchange of the coordinates of two electrons. The n-electron wave function is expressed by the anti-symmetric product of n 1-electron wave functions with spin-orbital orbital [156, 157]. The antisymmetric wave function can be expressed as a Slater-determinant.

$$\Phi = \frac{1}{\sqrt{n!}}\begin{vmatrix} \chi_1(1) & \chi_2(1) & \cdots & \chi_n(1) \\ \chi_1(2) & \chi_2(2) & \cdots & \chi_n(2) \\ \vdots & \vdots & \ddots & \vdots \\ \chi_1(n) & \chi_2(n) & \cdots & \chi_n(n) \end{vmatrix} \qquad \text{eq. 8}$$

The coefficient 1/√n! is the normalization factor of the wave function.

The expectation value for the energy of a Slater-determinant is described in eq. 9.

$$E[\Phi] = \langle \Phi | \hat{H} | \Phi \rangle = E[\{\chi_i\}] \qquad \text{eq. 9-1}$$

$$E[\Phi] = \sum_{i=1}^{N} \langle \chi_i | \hat{h} | \chi_i \rangle + \frac{1}{2}\sum_{i=1}^{N}\sum_{j=1}^{N}\left(\langle \chi_i \chi_j | r_{12}^{-1} | \chi_i \chi_j \rangle - \langle \chi_i \chi_j | r_{12}^{-1} | \chi_j \chi_i \rangle \right) \qquad \text{eq. 9-2}$$

$$\hat{h} = -\frac{1}{2}\nabla_i^2 - \sum_A \frac{Z_A}{r_{iA}}$$

Here, the spin-orbitals are orthogonal. The energy is minimized according to the variation theory. With canonical orbitals, the Hartree-Fock equation is written as follows [158, 159, 160].

$$\hat{f}\chi_a = \varepsilon_a \chi_a \qquad \text{eq. 10}$$

The Hartree-Fock equation is an electron eigenvalue equation, where $\hat{f}$ is the Fock-operator and the eigenvalue ε_a can be interpreted as the orbital energy. The Fock operator $\hat{f}$ is an effective one-electron operator and the operator $\hat{f}$ has the form

of eq. 11.

$$\hat{f} = -\frac{1}{2}\nabla_i^2 - \sum_A \frac{Z_A}{r_{iA}} + v^{HF}(i) \qquad \text{eq. 11}$$

The term v^{HF} means the average potential experienced by the i th electron because of the presence of the other electrons.

As the Fock-operator depends on its eigenfunction due to the potential v^{HF}, the equation is a pseudo-eigenequation and it must be solved iteratively. The procedure is called Self-Consistent Field method (SCF procedure).

When the one-electron function χ_i is expanded as a linear combination of atomic basis functions, the function is as expressed in eq. 12 and the expansion is called Linear Combination of Atomic Orbitals (LCAO).

$$\chi_i = \sum_{\mu}^{K} C_{\mu i}\phi_\mu \quad i=1, 2, \ldots K \qquad \text{eq. 12}$$

It is difficult to solve an integro-differential equation in a matrix eigenvalue equation and it is solved with standard procedures of linear algebra. The Roothan-Hall equation is the matrix equation and it is expressed in eq. 13.

$$\mathbf{FC = SC\varepsilon} \qquad \text{eq. 13}$$

S is the overlap matrix from the basis set ϕ, **F** is the Fock-matrix and **C** is a matrix with the expansion coefficients. **ε** is a diagonal matrix which contains the orbital energy ε. From the solution of the equation, the coefficient matrix is obtained. The Roothan-Hall equation (eq. 13) [161, 162] and the Slater-determinant give the lowest energy for the corresponding system from the coefficient matrix.

2.3. Post Hartree-Fock Methods

In the Hartree-Fock approximation, the movement of electrons with parallel spin is correlated according to the Pauli-principle (exchange correlation). The movement of electrons with anti-parallel spin, however, is not taken into account. Due to the additional repulsion between electrons with anti-parallel spin, the Hartree-Fock energy is always higher than the exact energy. The neglected energy was named correlation energy by Löwdin and the correlation energy is defined by eq. 14 [163].

$$E_{corr.} = E_{exact} - E_{HF} \qquad \text{eq. 14}$$

2.3.1 Configuration Interaction

Most of the quantum chemical procedures to estimate the correlation energy are based on the Hartree-Fock approximation. All of them use the Hartree-Fock wave function and also the Slater-determinant of the occupied orbitals from the SCF calculation as a reference. The Configuration Interaction (CI) method uses a linear combination of excited state Slater-determinants as an ansatz for the CI-wave function.

$$\Psi_{CI} = a_0\Phi_{HF} + \sum_S a_S\Phi_S + \sum_D a_D\Phi_D + \sum_T a_T\Phi_T + \cdots \qquad \text{eq. 15.}$$

Here, Φ_s are the different singly excited Slater-determinants, and Φ_d are the doubly excited Slater-determinants, etc. The coefficients, a_0, a_s, a_d and a_t are expansion coefficients. The CI coefficients are determined by the diagonalisation of the CI matrix (eq. 16).

$$H_{ij} = \left\langle \Phi_i \middle| \hat{H} \middle| \Phi_j \right\rangle \qquad \text{eq. 16}$$

The ground state energy is produced with the lowest CI eigenvalue in the eigenvalue equation. When the CI function includes all excitations, the CI function is called Full-CI and the energy corresponds to the exact energy of the electron systems. In practice, it can hardly be achieved to consider all excited states.

2.3.2 Perturbation Theory

Another method to calculate the correlation energy is perturbation theory [164]. In perturbation theory, the Hamiltonian operator $\hat{H}$ is modified by the perturbation operator $\hat{H}'$ (eq. 17)

$$\hat{H}_{exact} = \hat{H}_0 + \lambda\hat{H}' \qquad \text{eq. 17}$$

The perturbation $\hat{H}'$ must be small compared to $\hat{H}$. The Hamiltonian operator $\hat{H}$, the energy *E* and the wave functions are functions with perturbation parameter λ. In Møller-Plesset perturbation theory, the unperturbed operator is composed from the summation of the Fock-operators. The wave function and the energy are expressed in a Taylor-expansion, which depends on λ. From the expansion, the corrections in the different orders for the energy of the reference system are obtained. $E^{(1)}$ is the first-order correction and it yields the Hartree-Fock energy of the ground state. In practice, second-order Møller-Plesset perturbation theory (MP2) is often used for a second-order correction.

$$E^{(2)} = \sum_{s\neq 0} \frac{\left|\langle \Phi_s | \hat{H} | \Phi_0 \rangle\right|^2}{E_0 - E_s} \qquad \text{eq. 18}$$

Φ_0 is the Hartree-Fock wave function and Φ_s is the Slater-determinate for the excited state. MP2 is a very practical method because it contains 90% of the correlation energy with rather small computational cost. However, perturbation theory fails when the ground state and another state are energetically degenerate or near degenerate, because the second-order correlation energy becomes very large. This is a typical situation in transition metals and transition metal complexes and the error mainly stems from the multi-reference character of the wave function.

An empirical estimation to improve the performance of MP2 methods called SCS-MP2 was suggested by Grimme [165]. In this estimation, the contribution of electrons with the same spin and of those with different spin is scaled with parameters p_T and p_S.

$$E_{corr}^{SCS-MP2} = p_S E_S + p_T E_T \qquad \text{eq. 19}$$

In SCS-MP2, the parameter p_s is 6/5 and p_T is 1/3. The parameter p_s is determined by the correlation energies of H_2 and He, which contain only one spin-pair. In the MP2 method, 80% of the correlation energy can be evaluated in H_2 and He. p_T is empirically determined by benchmark tests. In most cases, the SCS-MP2 method performs much better than MP2 with the same computing effort.

2.3.3 Coupled-Cluster Method

The coupled-cluster (CC) method [166-170] uses electron pair interactions and infinite correlations to greatly improve the accuracy. The excitation operator $\hat{T}$ is defined in eq. 20.

$$\hat{T} = \hat{T}_1 + \hat{T}_2 + \cdots + \hat{T}_n = \sum_{i=0}^{\infty} \hat{T}_i \qquad \text{eq. 20}$$

$\hat{T}$ is the sum of different excitation operators. The excitation operator $\hat{T}_i$ produces all i time excited determinant of the Hartree-Fock wave function Φ_0. The $\hat{T}_1$ and $\hat{T}_2$ operators are expressed in eq. 21.

$$\hat{T}_1\Phi_0 = \sum_{i}^{occ}\sum_{a}^{vir} t_i^a \Phi_i^a \qquad \text{eq. 21-1}$$

$$\hat{T}_2\Phi_0 = \sum_{i<j}^{occ}\sum_{a<b}^{vir} t_{ij}^{ab} \Phi_{ij}^{ab} \qquad \text{eq. 21-2}$$

The coupled-cluster wave function is defined by exponential expressions and the wave function is expressed with the Hartree-Fock reference function Φ_0 in eq. 22.

$$\Psi^{Coupled-Cluster} = e^{\hat{T}}\Phi_0 = \sum_{i=0}^{\infty} \frac{\hat{T}_i}{i!}\Phi_0 \qquad \text{eq. 22}$$

The $e^{\hat{T}}$ operator is represented by a Taylor-series. In the truncated coupled-cluster singles doubles (CCSD) method, the $e^{\hat{T}}$ operator is written as eq. 23.

$$e^{T_1+T_2} = 1 + T_1 + (T_2 + \frac{1}{2}T_1^2) + (T_2T_1 + \frac{1}{6}T_1^3) + (\frac{1}{2}T_2^2 + \frac{1}{2}T_2T_1^2 + \frac{1}{24}T_1^4) + \cdots \qquad \text{eq. 23}$$

With the coupled cluster wave function, eq. 22, the Schrödinger equation can be written in eq. 24.

$$\hat{H}e^{\hat{\mathbf{T}}}\Phi_0 = E_{CC}e^{\hat{\mathbf{T}}}\Phi_0 \qquad \text{eq. 24}$$

The Hamilton operator contains only one and two-electron operators. Consequently, the energy E_{CC} is expressed in eq. 25.

$$\begin{aligned} E_{CC} &= \left\langle \Phi_0 \middle| \hat{H}e^{\hat{\mathbf{T}}} \middle| \Phi_0 \right\rangle \\ &= \left\langle \Phi_0 \middle| \hat{H}\left(1 + \hat{T}_1 + \hat{T}_2 + \frac{1}{2}\hat{T}_1^2\right) \middle| \Phi_0 \right\rangle \end{aligned} \qquad \text{eq. 25}$$

As Φ is the Hartree-Fock wave function and Brillouin's theorem [171] states that singly excited determinants do not interact directly with the Hartree-Fock determinant, the coupled cluster energy is represented by eq. 26.

$$E_{CC} = E_0 + \sum_{i<j}^{occ}\sum_{a<b}^{vir}\left(t_{ij}^{ab} + t_i^a t_j^b - t_i^b t_j^a\right)\left(\left\langle \phi_i\phi_j \middle| \phi_a\phi_b \right\rangle - \left\langle \phi_i\phi_j \middle| \phi_b\phi_a \right\rangle\right) \qquad \text{eq. 26}$$

The CCSD(T) method is a very accurate method and it is developed as a standard method to determine the energy of the system with three Slater-determinants [172]. In this method, non-iterative triple contributions are calculated from a MP4 calculation using CCSD amplitudes.

2.3.4 Multi-Configuration Self-Consistent Field

In some molecules, some frontier orbitals are degenerate or near degenerate and there are various possibilities for the electrons to occupy orbitals. If a restricted HF calculation is carried out in this case, the fully occupied orbitals are optimized for a chosen occupation. It is, however, only the best possible single Slater-determinant wave function formed by the chosen MO and it does not contain the other degenerate frontier orbitals. To treat degenerated orbitals equivalently, the wave function must be expressed as a combination of some various configurations and the orbitals must be optimized for this combination.

$$\Psi_{MCSCF} = a_1\Phi_1 + a_2\Phi_2 + \cdots \qquad \text{eq. 27}$$

This method is called Multi-Configuration Self-Consistent-Field (MCSCF) [173, 174]. In MCSCF, the coefficients in front of the determinants and orbitals are optimized by the variational principle.

When all possible configurations of electrons in a defined space of orbitals are considered in the MCSCF, so to say a complete active space is chosen and the calculation is called CASSCF. In MCSCF or CASSCF, a common notation (*n*,*m*)-CASSCF (MCSCF) is used, and the notation means that *n* electrons are allocated in all possible ways in *m* orbitals.

2.3.5. Multi-Reference Configuration Interaction

In Configuration Interaction (CI), the Hartree-Fock wave function is used as the reference and the configurational state functions are generated by exciting electrons from a single determinant. When an MCSCF wave function is chosen as the reference, the CISD involves excitations of one or two electrons of all determinants in MCSCF and it is defined as Multi-Reference Configuration Interaction (MRCI) [174, 175, 176]. In MRCI, both dynamical correlation and non-dynamical correlation are considered. The MCSCF method recovers the non-dynamical correlation, specifically static correlation, while CI recovers the dynamical correlation.

2.4. Density Functional Theory

Ab initio methods are based on the wave function Ψ while the Density Functional Theory (DFT) is based on the electron density ρ. For an n-electron system, the electron density ρ depends on only 3-spacial coordinates, while the wave function based methods depend on 3N coordinates and N spin-coordinates.

2.4.1 Hohenberg-Kohn Theorems

DFT is based on the first Hohenberg-Kohn theorem [177], which states that the electron density determines the Hamiltonian operator $\hat{H}$ and also all characteristics of a system. The ground state energy E_0 is uniquely expressed by a functional of the electron density and the energy can be described as follows.

$$E_0(\rho_0) = T(\rho_0) + E_{ee}(\rho_0) + E_{Ne}(\rho_0) = T(\rho_0) + \int \rho_0(\vec{r}) V_{Ne} d\vec{r} + E_{ee}(\rho_0) \quad \text{eq. 28}$$

Here, T is the kinetic energy, E_{ee} states the electron-electron interaction term and E_{Ne} describes the nucleus-electron interaction. The system-independent parts T(ρ) and E(ρ) are summarized into the Hohenberg-Kohn functional F_{HK}

$$F_{HK}(\rho_0) = T(\rho) + E_{ee}(\rho) \quad \text{eq. 29}$$

This equation contains the functionals of the kinetic energy T(ρ) and the electron-electron interaction E_{ee}. If the Hohenberg-Kohn functional is known, then this ground state energy is the exact solution of the Schrödinger equation for arbitrary atoms and molecules. The functional is, however, unknown and the functionals at the present try to approximate F_{HK} as accurately as possible. The classical Coulomb repulsion J(ρ) is known and this term is often separated from the term E_{ee} and the E_{ee} part is written in eq. 30.

$$E_{ee}(\rho) = \frac{1}{2} \iint \frac{\rho(\vec{r}_1)\rho(\vec{r}_2)}{r_{12}} d\vec{r}_1 d\vec{r}_2 + E_{ncl}(\rho) = J(\rho) + E_{ncl}(\rho) \quad \text{eq. 30}$$

J(ρ) expresses the charge density. E_{ncl} contains non-classical interactions like exchange correlation, coulomb correlation or the correction for self-interaction.

The second Hohenberg-Kohn theorem [177] states that the variational principle is applicable to Density Functional Theory [178]. In this theorem, E(ρ) exhibits the lowest energy only for the electron density of the ground state. It means that the energy of the trial density is always higher than the exact energy of the system (eq. 31).

$$E_0 = E(\rho_0) \leq E(\tilde{\rho}) \qquad \text{eq. 31}$$

The equal sign hold only when the exact Hohenberg-Kohn functional or the exact Hamiltonian operator is known. Practically, DFT energy is not variational against the exact energy, which means that DFT energies can be lower than exact energies.

2.4.2 Kohn-Sham Ansatz

The Hohenberg-Kohn theorem does not tell us how to find the exact ground state density. Here, Kohn and Sham introduced a new concept of reference system, which has no electron-electron interaction but where the density of the reference system is the same as a real system with the electron-electron interaction [179]. The density of the real system is conformed by the potential V_S. The Hamiltonian operator $\hat{H}_s$ of the hypothetical system is written as follows.

$$\hat{H}_S = -\frac{1}{2}\sum_i^N \nabla_i^2 + \sum_i^N V_S(\vec{r}_i) = \sum_i^N \hat{f}_i^{KS} \qquad \text{eq. 32}$$

The operator is expressed by the summation of N one-electron operators f_i^{KS}. The Kohn-Sham equation is expressed as the analogy to the Hartree-Fock equation using the Slater-determinant and the corresponding energy minima.

$$\hat{f}_i^{KS}\phi_i = \left(-\frac{1}{2}\nabla^2 + V_S(\vec{r})\right)\phi_i = \varepsilon_i\phi_i \qquad \text{eq. 33}$$

The eigenfunction of eq. 34 is given by the Kohn-Sham equations and the density of the reference system comes from the Kohn-Sham orbitals. The Kohn-Sham orbitals are quite similar to molecular orbitals, and it has been proven that the Kohn-Sham orbitals can be interpreted as molecular orbitals [180-183].

$$\rho(\vec{r}) = \sum_{i=1}^{N} |\phi_i|^2 \qquad \text{eq. 34}$$

The potential V_s is written in eq. 35.

$$V_S(\vec{r}_1) = \int \frac{\rho(\vec{r}_2)}{r_{12}} d\vec{r}_2 + V_{XC}(\vec{r}_1) - \sum_{A}^{M} \frac{Z_A}{r_{1A}} \qquad \text{eq. 35}$$

The Kohn-Sham equation must be solved iteratively with the SCF-procedure similar to the Hartree-Fock equation because the potential depends on the Kohn-Sham orbitals. The exchange correlation potential V_{xc} is defined as a functional derivative of the exchange correlation energy. If the exact V_{xc} was known, the exact eigenvalue of the Schrödinger equation could be found.

$$V_{XC} = \frac{\delta E_{XC}}{\delta \rho} \qquad \text{eq. 36}$$

2.4.3 Approximation for the Exchange Correlation Functional

An approximation to calculate the exchange correlation potential V_{xc} is the Local Density Approximation (LDA). When the different densities for α-spin and β-spin are considered, it is called Local Spin Density Approximation (LSDA). In this approximation, the homogeneous electron gas model is assumed and the exchange correlation for LSDA is expressed by eq. 37.

$$E_{XC}^{LSDA}(\rho_\alpha, \rho_\beta) = \int \rho(\vec{r}) \varepsilon_{XC}(\rho_\alpha(\vec{r}), \rho_\beta(\vec{r})) d\vec{r} \qquad \text{eq. 37}$$

ε_{xc} is the exchange and correlation energy per electron in the homogeneous gas. ε_{xc} can be divided into the exchange energy part per electron and the correlation part per electron, $\varepsilon_{xc} = \varepsilon_x + \varepsilon_c$. For ε_x, analytical solutions [184, 185] exist and for ε_c, Vosko, Wilk and Nusair [186] proposed analytical approximations from numerical values of exact Monte Carlo calculations [187] for the homogeneous electron gas.

The electron density strongly depends on the coordinates of atoms and molecules. LSDA is a crude approximation and it must be improved to describe systems more precisely. To achieve greater accuracy, gradients of the electron density are used to form the Generalized Gradient Approximation (GGA). In GGA, the exchange

correlation energy is expressed as follows.

$$E_{XC}^{GGA} = \int f(\rho_\alpha, \rho_\beta, \nabla\rho_\alpha, \nabla\rho_\beta)d\vec{r} \qquad \text{eq. 38}$$

Here, $f(\rho_\alpha, \rho_\beta, \nabla\rho_\alpha, \nabla\rho_\beta)$ is a function of the electron density and the gradient of the electron density. E_{xc} is divided into an exchange part and a correlation part.

$$E_{XC}^{GGA} = E_X^{GGA} + E_C^{GGA} \qquad \text{eq. 39}$$

The most widespread gradient corrected exchange functional was developed by Becke and it is called B88 [188]. The B88 functional is expressed with the LDA exchange functional and additional correction term.

$$E_X^{B88} = E_X^{LSDA} - b\sum_\sigma \int \frac{\rho_\sigma^{4/3} s_\sigma^2}{1 + 6bs_\sigma \sinh^{-1} s_\sigma} d\vec{r} \qquad \text{eq. 40}$$

Here b is an empirical parameter and s is the reduced density gradient in the spin r = α or r = β.

$$s_\sigma = \frac{|\nabla\rho_\sigma(\vec{r})|}{\rho_\sigma^{4/3}(\vec{r})} \qquad \text{eq. 41}$$

A common correlation functional called P86 was developed by Perdew. [189, 190]

$$E_c^{P86} = \int n\varepsilon_c(n_\alpha, n_\beta)d\vec{r} + \int \frac{d^{-1}e^{-\Theta}C(n)|\nabla n|^2}{n^{4/3}} \qquad \text{eq. 42}$$

$$\text{here, } C(n) = 0.001667 + \frac{(0.002568 + \alpha r_s + \beta r_s^2)}{(1 + \gamma r_s + \delta r_s + 10^4 \beta r_s^3)}$$

$$n = (4\pi r_s^3/3)^{-1},\ \Theta = 1.745\tilde{f}[C(\infty)/C(n)]|\nabla n|/n^{7/6},$$

$\alpha = 0.0023266$, $\beta = 7.389\times10^{-6}$, $\gamma = 8.723$ and $\delta = 0.472$.

$\tilde{f} = 0.11$ is a cut-off parameter.

2.5. Basis sets

The one-electron function is expressed as a linear combination of basis functions. The basis functions can be written as a Slater-type function [191],

$$\phi = Nr^{n-1}\exp(-\alpha r)Y_l^m(\theta,\varphi) \qquad \text{eq. 43}$$

or a Gaussian type function.

$$\phi = Nx^i y^j z^k \exp(-\beta r^2)Y_l^m(\theta,\varphi) \qquad \text{eq. 44}$$

Here, N is a normalization coefficient and n is the main quantum number, l is the sub quantum number, m is the magnetic quantum number and Y is a spherical function. Gaussian type orbital shows zero inclination of the function near nucleus and Gaussian type orbital represents the poor behavior near nucleus, while the Slater-type orbitals have cusps and the slope is not zero near the nucleus. Slater-type orbital gives more correct results. Another problem of Gaussian type orbital is that the Gaussian type orbital falls off too rapidly from the nucleus, and it cannot describe the region far from the nucleus, that is, the tail of the wave function, which is important for the chemical bond. Although Slater-type orbitals are more correct than Gaussian type orbitals, it takes longer time to integrate the Slater-type functions because of exp(-αr). To improve the quality of Gaussian type orbital, many Gaussian type orbitals are used to form linear combinations for enough accuracy. Many basis functions per atom orbital can be used to increase the flexibility of the basis sets and to improve the quality of Gaussian type orbital. When two basis functions per atom orbital are used, it is called double ζ basis sets (DZ). The atom orbital constructed from three basis functions and four basis functions are called triple ζ basis sets (TZ) and quadruple ζ basis sets (QZ), respectively. When the number of valence orbital are doubled and the doubling of core orbital is not considered, the produced basis sets is called spit-valence basis sets. The tighter function with large exponent can describe σ bond with large components, while the more diffuse functions with small exponent can give a good description for π and δ orbitals. Higher angler momentum functions are denoted as polarization functions and they can describe polarized orbitals. The polarization functions are added to the basis set and QZ4P means four sets of

polarization functions are added to a quadruple ζ basis set (QZ). Dunning and coworkers have proposed correlation consistent (cc) basis sets and they are invented to recover the correlation energy of valence electrons [192-206]. cc-pVQZ basis set, which is a quadruple ζ basis set of cc basis set, means correlation consistent polarized valence quadruple ζ basis sets. The cc basis set can be augmented with diffuse functions and it is indicated by adding aug- to cc basis sets.

In a chemical bond, valence electrons play more important roles in comparison to inner shell electrons. The core electrons can be substituted by a pseudo potential [207]. The pseudo potential is a one-electron operator and it can substitute the interaction between inner shell electrons with valence electrons. The use of pseudo-potentials reduces the number of basis functions in the calculation and it shortens the calculation time. Relativistic effects are considered in some pseudo potentials, which are obtained by a numerical all-electron-Dirac-HF calculation.

2.6. Relativistic effects

One limit of the Schrödinger equation is the neglect of relativistic effects. Einstein's relativistic theory [208] plays a very important role in the development of relativistic quantum mechanics. His relativistic theory caused dramatic changes in the description of physics. In the relativistic theory, time- and space coordinates exhibit are equivalent and thus, they have to be treated in the same way. The time-dependent Schrödinger equation does not satisfy the demand of the relativistic theory.

In relativistic theory, the speed of light, *c*, is constant and the mass of the electron which moves with *c* increases to m_e

$$m_e = m_0\left[\sqrt{1-\frac{v^2}{c^2}}\right]^{-1} \qquad \text{eq. 45}$$

The first work in this area was carried out by Dirac [209] where he constructed a relativistic Hamiltonian operator which satisfies the Lorentz-invariant relation in the eigenvalue equation. The Dirac equation in an electronic potential is expressed as follows,

$$\left[c\boldsymbol{\alpha}\cdot\mathbf{p}+\boldsymbol{\beta}'mc^2+\mathbf{V}\right]\Psi = E\Psi \qquad \text{eq. 46}$$

$$\text{here, } \boldsymbol{\alpha}_{x,y,z} = \begin{pmatrix} 0 & \boldsymbol{\sigma}_{x,y,z} \\ \boldsymbol{\sigma}_{x,y,z} & 0 \end{pmatrix},\ \boldsymbol{\beta}' = \begin{pmatrix} 0 & 0 \\ 0 & 2\boldsymbol{I} \end{pmatrix}$$

$$\boldsymbol{\sigma}_x = \begin{pmatrix} 0 & 1 \\ 1 & 0 \end{pmatrix},\ \boldsymbol{\sigma}_y = \begin{pmatrix} 0 & -i \\ i & 0 \end{pmatrix},\ \boldsymbol{\sigma}_z = \begin{pmatrix} 1 & 0 \\ 0 & -1 \end{pmatrix},\ \boldsymbol{I} = \begin{pmatrix} 1 & 0 \\ 0 & 1 \end{pmatrix}$$

Here, $\mathbf{p}$ is the momentum operator, and $\boldsymbol{\alpha}$ and $\boldsymbol{\beta}$ are 4×4 matrices. The Dirac equation is a four-dimensional equation. The wave function is expressed with a 4-component vector.

$$\Psi = \begin{pmatrix} \Psi_{L\alpha} \\ \Psi_{L\beta} \\ \Psi_{S\alpha} \\ \Psi_{S\beta} \end{pmatrix} \qquad \text{eq. 47}$$

Ψ_L and Ψ_S are large and small components of the wave function, and α and β represent spin states. In case of c$\rightarrow\infty$, the large component is equal to the solution of the Schrödinger equation. The small component in the electronic wave function gives the interaction with the positronic state. The Dirac equation can be factored out in the two equations.

$$c(\sigma \cdot \mathbf{p})\Psi_S + \mathbf{V}\Psi_L = E\Psi_L \qquad \text{eq. 48-1}$$

$$c(\sigma \cdot \mathbf{p})\Psi_L + (-2mc^2 + \mathbf{V})\Psi_S = E\Psi_S \qquad \text{eq. 48-2}$$

The latter equation is solved for Ψ_S and the wave function of for the small component is written in eq. 49.

$$\Psi_S = (E + 2mc^2 - \mathbf{V})^{-1} c(\sigma \cdot \mathbf{p})\Psi_L \qquad \text{eq. 49}$$

The coefficient of eq. 50. can be divided as follows.

$$(E + 2mc^2 - \mathbf{V})^{-1} = (2mc^2 - \mathbf{V})^{-1}\left(1 + \frac{E}{2mc^2 - \mathbf{V}}\right)^{-1} = (2mc^2 - \mathbf{V})^{-1}\mathbf{K}' \qquad \text{eq. 50}$$

$$\mathbf{K}' = \left(1 + \frac{E}{2mc^2 - \mathbf{V}}\right)^{-1}$$

When the zero-order term is kept, the Zero-Order Regular Approximation (ZORA) is obtained [210-217].

$$\left[\frac{c^2\mathbf{p}^2}{2mc^2 - \mathbf{V}} + \frac{2c^2}{(2mc^2 - \mathbf{V})^2} - \frac{Zs \cdot \mathbf{I}}{r^3} + \mathbf{V}\right]\Psi_L = E\Psi_L \qquad \text{eq. 51}$$

2.6. Geometry Optimization, Statistical Mechanics and Thermodynamics

2.6.1 Geometry Optimization

To find a stationary point on the potential energy surface, the Newton-Raphson procedure is frequently used in geometry optimizations. In this procedure, the energy at a point is expanded to second order by Taylor expansion.

$$E(\vec{x}) \approx E(\vec{x}_0) + \vec{g}^t(\vec{x} - \vec{x}_0) + \frac{1}{2}(\vec{x} - \vec{x}_0)^t \mathbf{H}(\vec{x} - \vec{x}_0) \qquad \text{eq. 52}$$

Here, g is the gradient vector and **H** is the Hessian matrix, which results from the coordinates of the nuclei. At the stationary points, the gradient g at x disappears and the geometry difference from the next point, dx, satisfies the following equation,

$$\Delta x = (\vec{x} - \vec{x}_0) = -\mathbf{H}^{-1}\vec{g} \qquad \text{eq. 53}$$

The calculation of the complete Hessian matrix takes long time with large computational costs. Instead an approximated Hessian matrix is used in the pseudo-Newton-Raphson procedure.

2.6.2. Harmonic Frequency

After the stationary point is found by the pseudo-Newton-Raphson procedure, the Hessian matrix must be calculated and diagonalized.

$$H_{ij} = \frac{\partial E(\vec{x})}{\partial x_i \partial x_j} \qquad \text{eq. 54}$$

When this matrix has only positive values, the point is a minimum. When the matrix has n negative eigenvalues, it means that the point is the n-order transition state. The eigenvalues are harmonic frequencies in each vibrational mode. A frequency calculation is needed not only to characterize the stationary point but also to determine thermodynamic information. In the calculation of Gibbs free energy, the frequencies are used to calculate a zero-point thermal correction energy and vibration

partition functions q_{vib}.

$$G = E_{el} + ZPE - RT \cdot \ln(q_{trans} \cdot q_{rot} \cdot q_{vib}) \qquad \text{eq. 55}$$

Here, E_{el} is the electronic energy and q_{trans} and q_{rot} are the translational partition function and the rotational partition function, respectively. The Gibbs activation energy and the reaction rate constant k in a transition state are calculated using Transition State Theory [218].

$$k = \kappa(T)\frac{k_b T}{h}\exp\left(\frac{-\Delta G^{\ddagger}}{RT}\right) \qquad \text{eq. 56}$$

$\kappa(T)$ is the transmission constant which depends on the temperature.

2.7. Energy Decomposition Analysis

The Energy Decomposition Analysis (EDA) makes it possible to divide the bonding energy of a chemical bond into some energy contributions and to obtain a quantitative interpretation of chemical bonds. EDA is based on the wave function theory of Morokuma [219-223], and Ziegler and Rauk [224-227] developed in the frame of DFT.

The bond formation energy (ΔE) of AB from two fragments A and B is divided in two steps. In the first step, the fragments A and B are deformed from their equilibrium geometry to their geometries and electronic state in the final complex AB. The energy requiring in this step is the preparation energy (ΔE_{prep}).

$$\Delta E = -D_e = \Delta E_{prep} + \Delta E_{\text{int}} \qquad \text{eq. 57}$$

In the second step, the electronic interaction energy (ΔE_{int}) between fragment A and fragment B is estimated. The interaction energy ΔE_{int} is divided into three terms.

$$\Delta E_{\text{int}} = \Delta E_{elstat} + \Delta E_{pauli} + \Delta E_{orb} \qquad \text{eq. 58}$$

The first term, ΔE_{elstat}, is the electrostatic energy, which comes from the interaction between fragments A and B with fixed electronic states in the geometry of AB. The ΔE_{elstat} is expressed in eq. 59.

$$\Delta E_{elstat} = \frac{Z_A Z_B}{R_{AB}} + \iint \frac{\rho^A(r_1)\rho^B(r_2)}{r_{12}} dr_1 dr_2 - \int \frac{Z_B}{r} \rho^A(r) dr - \int \frac{Z_A}{r} \rho^B(r) dr \qquad \text{eq. 59}$$

Here, A and B represent fragments A and B with distance R between them. The first term in eq. 59 is the nuclei-nuclei repulsion and the second term is the Coulomb repulsion between electron clouds. The third and fourth terms are the interactions between electrons in fragment A and fragment B, respectively.

The second term in eq. 58, ΔE_{pauli} , is the Pauli repulsion, which is the energy to antisymmerize and reorthogonalize the wave function of complex, $\Psi_{AB} = \hat{A}N\Psi_A\Psi_B$, from Kohn-Sham orbitals of Ψ_A and Ψ_B. The last term in eq. 50, ΔE_{orb}, is the orbital interaction energy, which is produced in the relaxation from the determinant Ψ_{AB}

$=\hat{A}N\Psi_A\Psi_B$ to the final Kohn-Sham determinant Ψ_{AB}^{min}. The orbital interaction energy contains both inter- and intrafragmental relaxation effects. In a symmetrical molecule, ΔE_{orb} can be decomposed to symmetries of the orbital, e.g. σ, π, δ, etc, enabling one to obtain information on specific orbitals.

2.8 Charge Analyses

2.8.1 Hirshfeld charge

The problem in population analysis is the partition of charge based on basis function and the division of the electron density to the special criterion. In Hirshfeld population analysis [228], the electron density of molecules at r is divided into atomic densities. The promolucular density is defined as the sum of atomic densities located at the nuclear geometries of molecules. The actual molecular electron density at r is divided by weighting factors based on the promolecular contributions.

$$\rho_{promolecular}(\mathbf{r}) = \sum_{A}^{M_{atoms}} \rho_A^{atomic\ density}(\mathbf{r}) \qquad \text{eq. 60}$$

$$w_A(\mathbf{r}) = \frac{\rho_A^{atomic\ density}(\mathbf{r})}{\rho_{promolecular}(\mathbf{r})} \qquad \text{eq. 61}$$

$$Q_A = Z_A - \int w_A(\mathbf{r}) \rho_{promolecular}(\mathbf{r}) d(\mathbf{r}) \qquad \text{eq. 62}$$

2.8.2 Natural Bond Orbital Analysis

Molecular orbitals are localized on atoms and bondings by the transformation and the figures of the localized orbitals are very similar to Lewis structure. The localized molecular orbitals are used in the NBO analysis to analyze bonding situation and partial charges [229, 230]. The analysis is divided to three procedures, occupancy-weighted-symmetric-orthogonalization (OWSO), the division of bonding orbitals and non-bonding orbitals and Jacobi rotation [231, 232]. The occupancy-weighted-symmetric-orthogonalization (OWSO) procedure is the main step in the transformation and it leads to Natural Atomic Orbital (NAO). In this step, orbitals are orthogonalized under the boundary condition. The weakly occupied orbitals are orthogonalized to the strongly occupied orbitals. Partial charges are calculated from the natural atomic orbitals and it is called Natural Population Analysis (NPA) [233]. After the division of non-bonding orbitals and bonding orbitals, OWSO is carried out in the region of bonding orbital to form an orthogonalized set of Natural Hybrid Orbitals (NHO) and they form N/2 Natural Bond Orbitals (NBO). N is

the number of electrons. The orbitals are chosen to describe largest part of electron density and build an optimized Lewis structure. The one-electron density matrix based on NBO consists from the block of the occupied orbitals and that of Rydberg and anti-bonding orbitals. From the Jacobi rotation, the density matrix is expressed by the Natural Localized Orbitals (NLO), which corresponds to the complete localized orbitals of electron density in bonding orbitals and lone pair orbitals.

2.9 Atom In Molecules

The Atom In Molecules (AIM) method [234], which is also called Bader analysis, describes the character of the electron density $\rho(r)$ of a molecule. The interpretation of the chemical bond in the AIM Method is developed based on the partition of the electron density with physical point of view. AIM method focuses on the electron density $\rho(r)$, the gradient of density, $\nabla\rho(r)$, and the laplacian of density $\nabla^2\rho(r)$ (curvature of $\rho(r)$), in a conformation on the minimum of potential energy surface. Especially, the zero point of a gradient of a molecule plays an important role, and the zero point of the gradient of the density, $\nabla\rho(r)=0$, is called "critical point". The critical points of $\rho(r)$ are classified by the curvature of $\rho(r)$, and the critical points of a molecule are categorized into following four groups:

$r_c(3, -3)$: atom critical point

$r_c(3, -1)$: bond critical point

$r_c(3,+1)$: ring critical point

$r_c(3,+3)$: cage critical point

At the atom critical point, all curvatures are negative and $\rho(r)$ is a local maximum because the nuclei have the large positive charge and the nuclei act as a local three-dimensional attractor of the electron density. The (3, -1) critical point is called "bond critical point". At the bond critical points, two curvatures in the directions perpendicular to the axis of the bonding are negative, and $\rho(r)$ is a local maximum in these directions. The third curvature in the plane along the bonding is positive and $\rho(r)$ is a minimum at the critical point. The (3, +1) critical point is called "ring critical point". At the (3, +1) point, two curvatures in the direction of the ring are positive and the last curvature in the plane perpendicular to the ring plane is negative. The (3, +3) critical point is called cage critical point and all curvatures are the positive.

The space is divided into subsystems and the subsystems are separated by a surface. The surface between two atoms is denoted as "zero-flux surface", which determines the border between two atoms.

The curvatures of $\rho(r)$ are obtained as the eigenvalues of the diagonalized Hessian Matrix of $\rho(r)$. The positive eigenvalue of the bond critical point defines a pair of eigenvectors, which begins at the critical point and ends the neighbor atom. The trajectories are called “bonding path”. The bond paths make it possible to understand the character of the interaction between atoms based on the topological analyses.

Quantum theory provides us with a striking illustration of the fact that we can fully understand a connection though we can only speak of it in images and parables.

Werner Heisenberg

3. Methods

The geometries of the molecules have been optimized and the relative energies are calculated at the DFT level of theory using the exchange functional of Becke [188] with the correlation functional of Perdew (BP86) [189, 190]. Uncontracted Slater-type orbitals (STOs) were used as basis functions for the SCF calculations [235]. The basis sets have quadruple-ζ quality augmented by four sets of polarization functions, i.e., two *p* and two *d* functions on hydrogen and two *d* and two *f* functions on the other atoms. This level of theory is denoted BP86/QZ4P. An auxiliary set of s, p, d, f, g and h STOs was used to fit the molecular densities and to represent the Coulomb and exchange potentials accurately in each SCF cycle. Scalar relativistic effects have been considered using the zero-order regular approximation (ZORA) [210-217]. The nature of the stationary points on the potential energy surface was characterized by calculating the Hessian matrices. The calculations were carried out with the program package ADF 2007 [236-238].

The relative energies of singlet isomers have been also calculated at the higher levels of theory, MP2 [239, 240], SCS-MP2 [165, 239, 240], MP4 [239, 240], CCSD [239, 240] and CCSD(T) [239, 240], with Dunning's correlation-consistent quadruple zeta basis sets augmented by diffuse functions (aug-cc-pVQZ) [192-206]. The relative energies of triplet isomers have been also calculated at the higher levels of theory, RMP2 [241], UMP2, SCS-UMP2 [165], UMP4 [242, 243], RCCSD [244, 245] and RCCSD(T) levels [244, 245] with the same basis sets as the singlets. The calculation of adiabatic excitation energies have been done with MRCI-SD/CASSCF [246-253] and MRCI-SD(Q)/CASSCF with aug-cc-pVQZ basis set, where (Q) means the Davidson correction [254]. The program package MOLPRO 2006 [255] was used for the MP2, SCS-MP2, MP4, CCSD, CCSD(T) and MRCI-SD calculations. For the calculations of UMP2 and SCS-UMP2 and UMP4, the program package Gaussian 03 [256] was used.

The pictures of all structures are drawn with the program ChemCraft [257].

The pictures of Kohn-Sham orbitals for orbital analyses are drawn with MOLEKEL program package [258].

The electron density ρ is calculated with BP86/aug-cc-pVQZ basis set by Gaussian 03 [256]. The pictures of the electron density ρ and its Laplacian $\nabla^2\rho$ for the bonding analyses are drawn with a modified version of AIMPAC [259].

Energy decomposition analyses are carried out with BP86/QZ4P level of theory by ADF 2007. In the Energy Decomposition Analysis, the isomers of **A**, **B**, **C**, **E1**, **E2**, **F1**, **F2**, **G** and **H** of E_2X_2 molecules are divided into two EX fragments to analyze the E-E bonding situation. The **SiD** and **SiD(T)** isomers in Si_2X_2 are devided into a Si atom and a SiX_2 fragment.

Let us remember, please, that the search
for the constitution of the world is
one of the greatest and noblest problems
presented by nature.

Galileo Galilei

4. Results and Discussions

This chapter is composed of four sub sections to investigate the effect of halogen atoms X in the E_2X_2 molecules: Si_2X_2, Ge_2X_2, Sn_2X_2 and Pb_2X_2. In each section of the elements E, the effects of halogen atoms in their group are discussed.

4.1 Si_2X_2 Molecules (X=H, F, Cl, Br and I)

4.1.1 Geometries and Relative Energies

Figure 4.1.1.1 – Figure 4.1.1.10 show the optimized geometries of several isomers of Si_2X_2 (X=H, F, Cl, Br and I). The isomers in the singlet state **SiA**-**SiH** and the isomers in the triplet state **SiA(T)**-**SiG(T)** and **SiI(T)** are optimized at the BP86/QZ4P level. In addition to this, single point energies for singlets and triplets are calculated with HF, MP2, SCS-MP2, MP4, CCSD, and CCSD(T). For these calculations, the aug-cc-pVQZ basis sets are used. Table 4.1.1.1, Table 4.1.1.2 and Table 4.1.1.3 show the relative energies of stationary points on the singlet potential energy surface calculated with BP86/QZ4P and HF, MP2, SCS-MP2, MP4, CCSD and CCSD(T) with aug-cc-pVQZ basis sets. Table 4.1.1.4 and Table 4.1.1.5 show the relative energies on the triplet potential energy surface calculated with BP86/QZ4P and HF, MP2, SCS-MP2, MP4, RCCSD and RCCSD(T) with aug-cc-pVQZ basis sets. The energies are given relative to the isomer **SiA**, which is the global minimum of Si_2H_2. The results in the tables and figures show that the optimized geometries and the relative energies are in agreement with previous theoretical calculations on DFT [18, 19, 20, 22, 64, 68, 79, 87] and *ab initio* levels [5-25, 34, 62, 87].

4.1.1.1 Singlet Isomers of Si_2X_2

Scheme 4.1.1.1 shows the different Si_2X_2 isomers investigated here. These species are denoted as follows: non-planar doubly bridged structure (**SiA**), singly

bridged planar structure (**SiB**), planar doubly bridged structure (**SiC**), vinylidene structure (**SiD**), trans-bent structure (**SiE**), cis-bent structure (**SiF**), linear structure (**SiG**) and distorted bent structure (**SiH**).

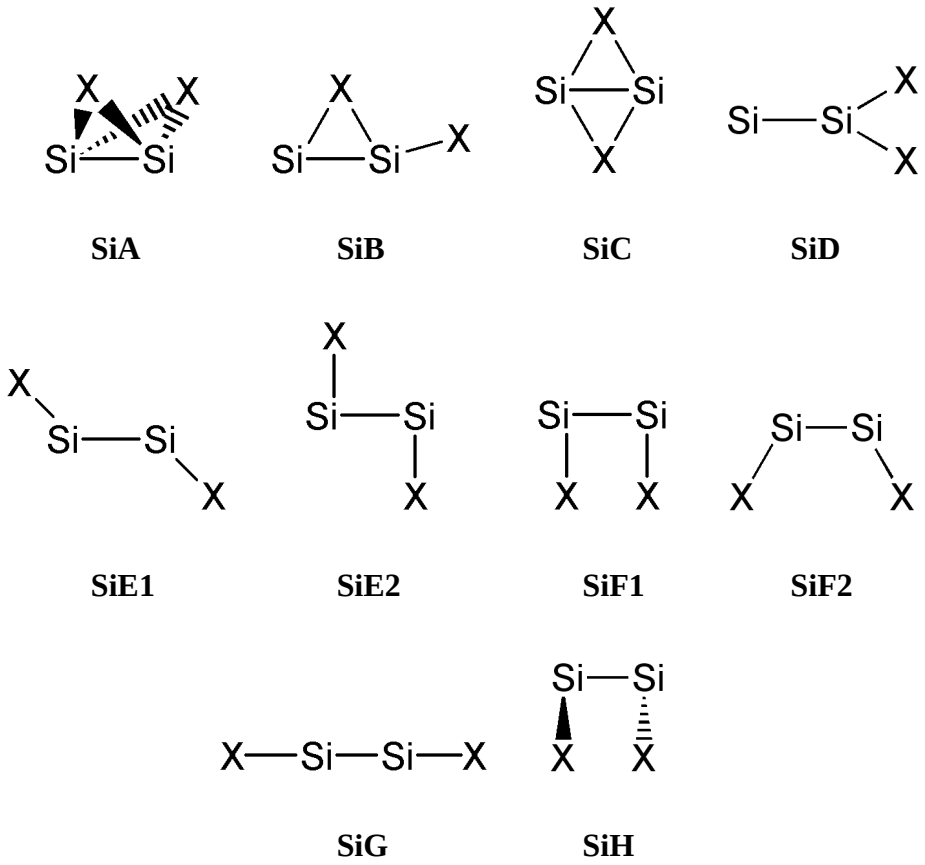

Scheme 4.1.1.1. Investigated singlet isomers of Si_2X_2

The non-planar doubly bridged structures of **SiA** have C_{2v} symmetry (Figure 4.1.1.1) and these isomers are the global minima for Si_2H_2, Si_2Cl_2, Si_2Br_2 and Si_2I_2 molecules, whereas, for Si_2F_2, this structure is only a local minimum. The Si-Si bond lengths correlate well with the mass of the halogen atoms: the Si-Si bond becomes longer as the halogen atom X becomes heavier. The Si-X-Si angle also shows a correlation with the mass of the halogen atoms. Nevertheless, the Si-H-Si angle is the exception because the Si_2H_2 isomer shows a smaller Si-Si distance than the others. Figure 4.1.1.1 shows the Si-X bond length of the SiX fragments and the difference of the Si-X bond lengths suggests that the Si-X bond is more elongated to form the Si-X-Si bridged structure, as the halogen atom X is lighter. The Si-H bond of Si_2H_2 is an outlier because of the different character of the Si-X bond, which is discussed in chapter 4.1.2.1.

The singly bridged planar structures of **SiB** have C_s symmetry (Figure 4.1.1.1) and these isomers are predicted as minima for Si_2X_2 (X=H, Cl, Br and I). Even though, for Si_2F_2, the structure of **SiB** is a transition state. The Si-Si bonds of Si_2Cl_2, Si_2Br_2 and Si_2I_2 are independent of the halogen atoms, and this comes from the differences in the character of the ring structure of **SiB**. Regarding the bond distances of the Si-X bonds in the Si-X-Si ring, it could be said that Si_2H_2, Si_2F_2 and Si_2I_2 have a bridged structure whereas the interactions of the bridging structure for Si_2F_2 and Si_2I_2 are weak.

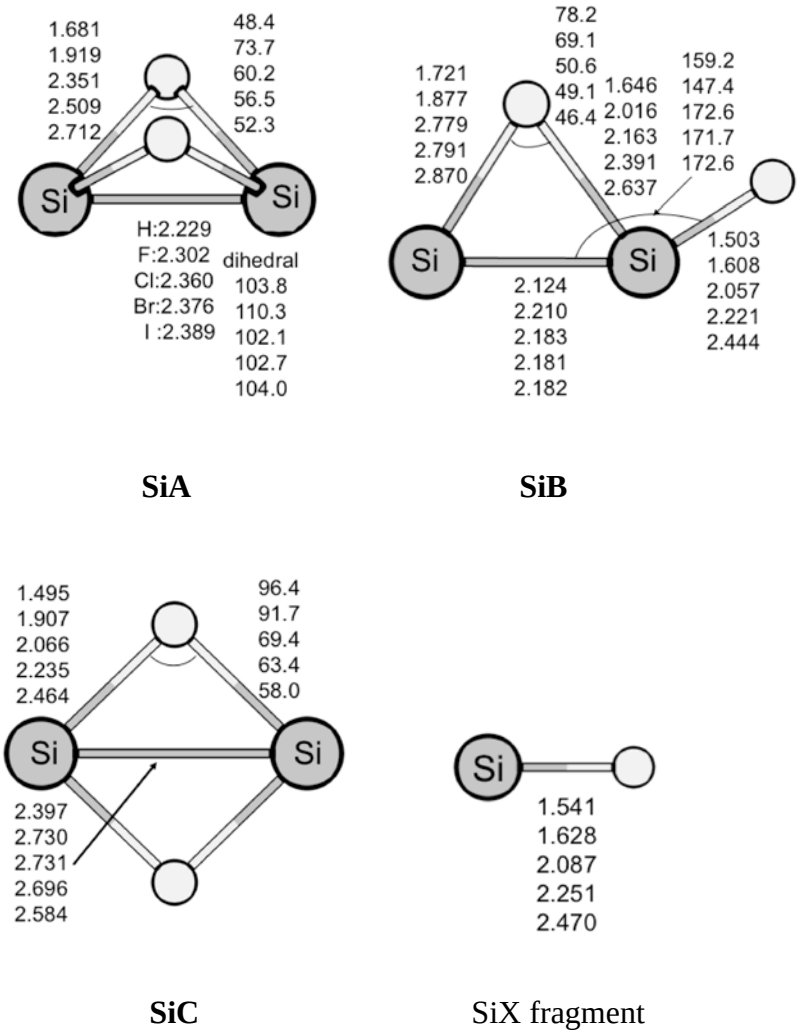

Figure 4.1.1.1. Optimized bridged structures in the singlet state, **SiA**, **SiB** and **SiC**, and the Si-X fragment of the $X^2\Pi$ ground state calculated at BP86/QZ4P level. The bond lengths are given in Å and the angles are given in degree.

The planar doubly bridged structures **SiC** have D_{2h} symmetry (Figure 4.1.1.1) and they are transition states in all cases. The Si-Si bond lengths of **SiC** clearly show

that the two Si atoms of Si_2H_2 interact with each other, while the two Si atoms of Si_2F_2, Si_2Cl_2, Si_2Br_2 and Si_2I_2 interact very weakly. The Si-X interactions here are stronger than those in **SiA** due to the their shorter bond lengths. Therefore, it is found that the main interaction of **SiC** for Si_2F_2, Si_2Cl_2, Si_2Br_2 and Si_2I_2 is the Si-X-Si bridging. The comparison of the Si-X bond lengths in **SiC** with those of the SiX molecules show that the interactions between the Si and X atoms are very strong.

The vinylidene structures **SiD** have C_{2v} symmetry (Figure 4.1.1.2) and they are minima for Si_2X_2 (X=H, F, Cl and Br). For Si_2I_2, this isomer is a transition state. In the vinylidene structures of Si_2X_2 the Si-Si bond length correlates with the mass of the halogen atom and the bond length becomes shorter as the halogen atoms gets heavier.

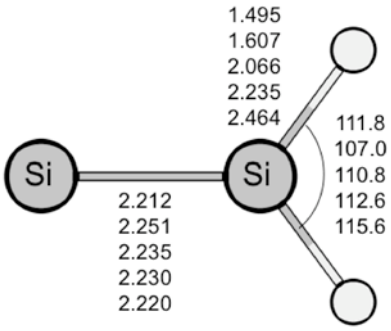

SiD

Figure 4.1.1.2. Optimized vinylidene structures in the singlet state, **SiD**, calculated at BP86/QZ4P level. The bond lengths are given in Å and the angles are given in degree.

The trans-bent structure has two types of isomers, **SiE1** and **SiE2**, both possessing C_{2h} symmetry (Figure 4.1.1.3). The isomers **SiE1** are predicted as minima and the other trans-bent structures **SiE2** are transition states. The isomers, **SiE1** and **SiE2** differ from each other in the Si-Si bond lengths and the Si-Si-X angles. In the **SiE1** isomers, the Si-Si bond lengths correlate with the Si-Si-X angles, and the Si-Si bond becomes shorter as the Si-Si-X angle gets larger. **SiE2** also exhibits the correlation. However, the trend is reversed. The differences of the Si-X bond between **SiE1** and **SiE2** are small (ca. 2-4 %). From these points, the difference between these two isomers stems from the Si-Si bond situation. The Si-Si bond length of **SiE1** of Si_2H_2 is similar to the Si-Si bond length optimized at CCSD(T)/aug-cc-pV5Z levels

(2.108Å), which are reported by Dolgonos [24].

Further, the cis-bent structures also have two types of isomers, **SiF1** and **SiF2**, which both have C_{2v} symmetry (Figure 4.1.1.3). The isomers **SiF1** are transition states. The isomer **SiF2** is a local minimum for Si_2F_2 and the isomers are transition states for Si_2H_2 and Si_2X_2 (X=Cl, Br, I). The isomers, **SiF1** and **SiF2** differ from each other in the Si-Si bond lengths and the Si-Si-X angles, which correspond to the **SiE2** and **SiE1**. **SiF1** and **SiF2** show the clear correlation between Si_2F_2, Si_2Cl_2, Si_2Br_2 and Si_2I_2, where **SiF1** bond become shorter and the Si-Si-Si angle becomes larger as the X atom becomes heavier. In this correlation, Si_2H_2 is an outlier because both the steric effect and the Si-Si bond interactions are important for **SiF1** and **SiF2**. The differences of the Si-X bond between **SiF1** and **SiF2** are small. From these points, these two isomers differ in the Si-Si bond situation and the steric effect of halogen atoms.

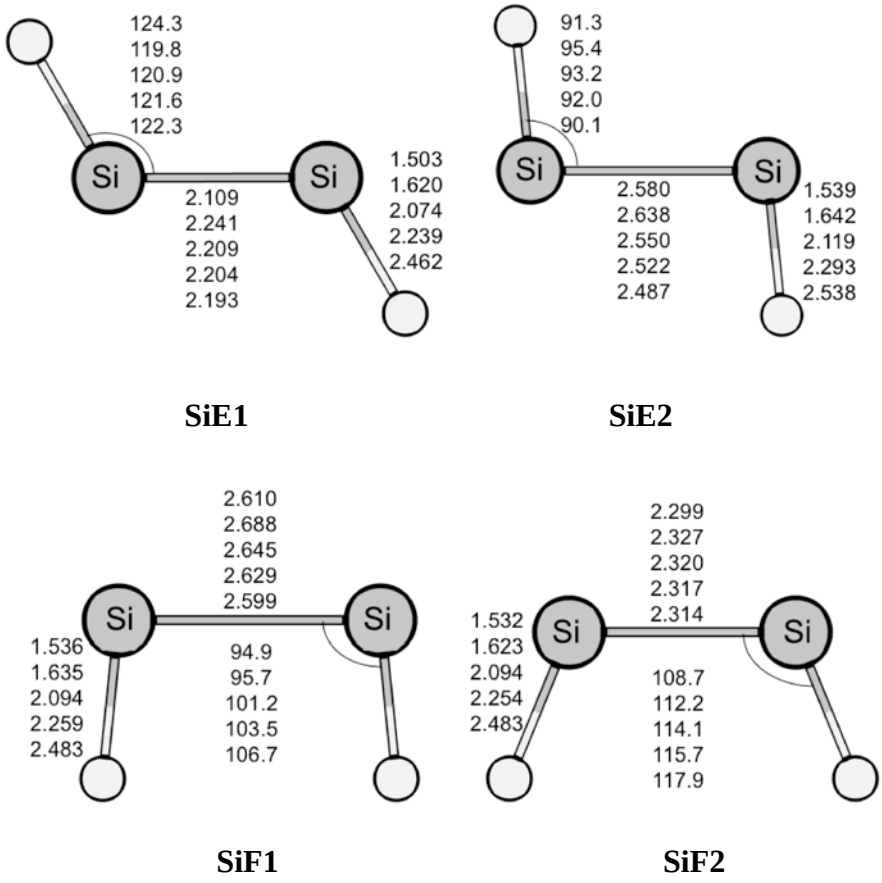

Figure 4.1.1.3. Optimized bent-structures in their singlet state, **SiE1**, **SiE2**, **SiF1** and **SiF2** calculated at BP86/QZ4P level. The bond lengths are given in Å and the angles are given in degree.

The linear structures **SiG** are second order saddle points for all Si_2X_2 compounds (Figure 4.1.1.4). The Si-Si and Si-X distances are the smallest of all Si_2X_2 isomers. The Si-Si distance is in a good correlation with mass of the halogen atoms, but not for Si_2H_2. This point will be discussed later.

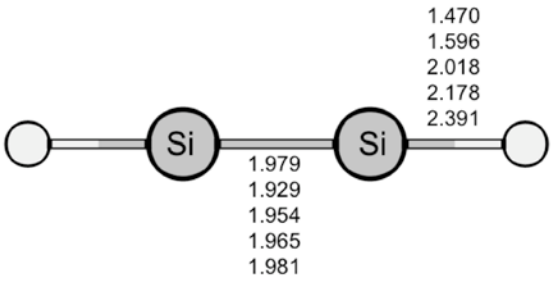

SiG

Figure 4.1.1.4 Optimized linear structures in the singlet state, **SiG**, calculated at BP86/QZ4P level. The bond lengths are given in Å and the angles are in given degree.

Interestingly, the distorted bent structure **SiH** could be only found for Si_2F_2 and the isomer is not a stationary point for Si_2H_2, Si_2Cl_2, Si_2Br_2 and Si_2I_2 (Figure 4.1.1.5). The **SiH** structure is a local minimum with C_2 symmetry. The geometry of **SiH** shows a similarity to **SiE2** and **SiF1**. However, the Si-Si distance is still shorter and the Si-Si-X angle is smaller.

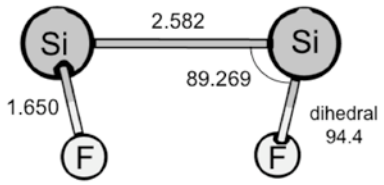

SiH

Figure 4.1.1.5. The optimized distorted bent-structure in the singlet state, **SiH**, calculated at BP86/QZ4P level. The bond lengths are given in Å and the angles are in degree.

A transition state connecting **SiH** and **SiA** exists, where the geometry is quite similar to **SiA** and the relative energy is very small (0.1 kcal/mol at the BP86/QZ4P level).

4.1 Si_2X_2 Molecules

Table 4.1.1.1, Table 4.1.1.2 and Table 4.1.1.3 show the relative energies of the isomers in the singlet state for several methods. Here, the CCSD(T) results are quite reliable due to the fact that the difference between CCSD and CCSD(T) values are relative small. The largest deviation is 4.3 kcal/mol for the cis bent structure **SiF2** of Si_2I_2 except the **SiC** isomers of Si_2F_2, Si_2Cl_2, and Si_2Br_2. The deviations between CCSD and CCSD(T) for these molecules are 9.4, 7.3 and 6.9 kcal/mol, respectively. These large deviations indicate a multi-reference character of the wave functions of these structures. The relative energies between the singlet isomers at BP86/QZ4P level are relatively accurate and the largest difference from CCSD(T)/aug-cc-pVQZ is 9.0 kcal/mol for the structure **SiG** of Si_2F_2 and the mean absolute error form CCSD(T)/aug-cc-pVQZ is 2.3 kcal/mol. The relative energy values of SCS-MP2 and MP4 are very similar and they are close to those of the CCSD(T) calculations. The largest error in MP2, SCS-MP2 and MP4 are 15.7 kcal/mol (**SiE2** isomer of Si_2F_2), 12.6 kcal/mol (**SiC** isomer of Si_2F_2) and 5.1 kcal/mol (**SiC** isomer of Si_2F_2), and the mean absolute errors of these three methods are 2.6, 1.0 and 1.0 kcal/mol, respectively. The SCS-MP2 method gives very accurate results for the relative energies of the molecules in the singlet state.

The relative energies show that the Si_2X_2 molecules are categorized into three groups, Si_2H_2 group, Si_2F_2 group and the group of Si_2Cl_2, Si_2Br_2 and Si_2I_2. The Si_2H_2 isomers present the following order of stability: **SiA** > **SiB** > **SiC** > **SiD** > **SiE1** > **SiG** > **SiE2** > **SiF1** > **SiF2**. Here, the global minimum is the doubly bridged structure, **SiA**. The order of stability shows that Si_2H_2 prefers the bridged structure, followed by the bent-structures. The linear structure is less stable than the trans-bent structure, but more stable than the cis-bent structure. The Si_2F_2 isomers present a different trend to Si_2H_2 and the order of stability is the following: **SiD** > **SiH** > **SiE2** > **SiF1** > **SiE1** > **SiA** > **SiF2** > **SiB** > **SiC** > **SiG**. The most stable isomer is the vinylidene structure, **SiD**. The followings ones are the bent-structures. The order shows that the bridged structures are shifted to higher energies. The last group shows the following order of stability: **SiA** > (**SiD**, **SiE2, SiB**) > **SiE1** > **SiF1** > **SiF2** > **SiC** > **SiG.** This order is between Si_2F_2 and Si_2H_2. The global minimum is **SiA**, but the position of **SiB** in the energetical order is not fixed. The relative energies of Si_2Cl_2, Si_2Br_2 and Si_2I_2 mostly correlate with the halogen atoms and the energy differences become larger as the halogen atoms get heavier.

Table 4.1.1.1 Optimized structures of **SiA-SiD** at BP86/QZ4P level and relative energies calculated with BP86/QZ4P and *ab initio* methods with aug-cc-pVQZ basis set. The bond lengths are given in Å and the angles are given in degree. The relative energies with respect to **SiA** are given in kcal/mol. The values in parentheses are the number of imaginary frequencies.

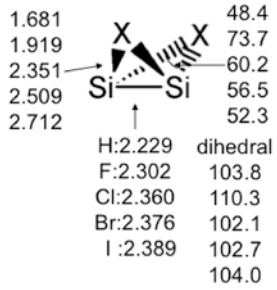

SiA

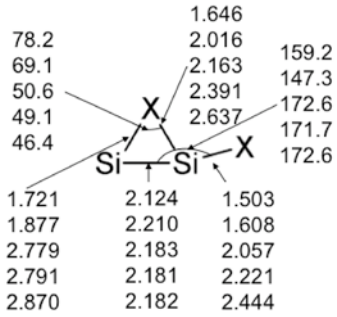

SiB

	H	F	Cl	Br	I	H	F	Cl	Br	I
BP86	0(0)	0(0)	0(0)	0(0)	0(0)	9.9(0)	13.4(1)	18.6(0)	20.4(0)	20.4(0)
HF	0	0	0	0	0	14.0	18.7	17.8	22.7	24.1
MP2	0	0	0	0	0	9.8	12.3	18.2	20.6	21.0
SCS-MP2	0	0	0	0	0	10.0	13.3	17.6	20.3	20.7
MP4	0	0	0	0	0	9.8	12.2	17.2	20.0	20.7
CCSD	0	0	0	0	0	11.5	14.1	17.5	21.0	21.9
CCSD(T)	0	0	0	0	0	10.1	12.3	17.1	20.1	20.8

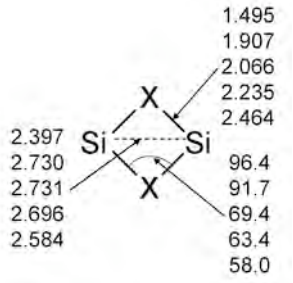

SiC

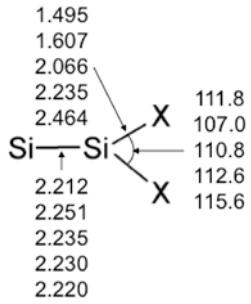

SiD

	H	F	Cl	Br	I	H	F	Cl	Br	I
BP86	11.3(1)	41.9(1)	58.1(1)	58.4(1)	57.9(1)	15.3(0)	-7.3(0)	16.6(0)	21.6(0)	25.9(1)
HF	17.2	58.7	81.6	82.1	62.5	5.4	-23.8	4.8	11.7	16.8
MP2	10.8	45.5	63.8	64.2	62.1	16.0	-13.6	14.6	20.7	26.6
SCS-MP2	11.6	45.5	64.3	64.8	61.3	13.1	-14.5	12.3	18.3	23.8
MP4	10.9	38.0	59.5	60.5	59.3	13.9	-12.3	13.0	19.3	25.0
CCSD	12.8	42.3	66.2	67.5	60.3	11.6	-16.0	10.3	16.7	22.0
CCSD(T)	11.2	32.9	58.9	60.9	58.8	12.5	-14.2	12.0	18.2	23.6

Table 4.1.1.2 Optimized structures of **SiE1-SiF2** at BP86/QZ4P level and relative energies calculated with BP86/QZ4P and *ab initio* methods with aug-cc-pVQZ basis set. The bond lengths are given in Å and the angles are given in degree. The relative energies with respect to **SiA** are given in kcal/mol. The values in parentheses are the number of imaginary frequencies.

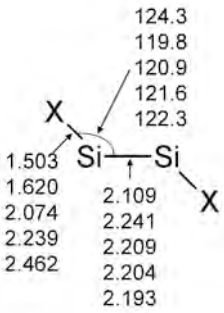

SiE1

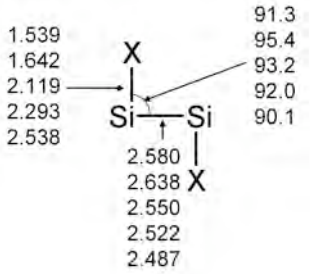

SiE2

	H	F	Cl	Br	I	H	F	Cl	Br	I
BP86	19.9(0)	-0.6(0)	18.2(0)	21.8(0)	24.6(0)	45.6(1)	-1.2(1)	17.9(1)	21.3(1)	24.5(1)
HF	26.9	2.9	25.1	30.0	33.1	28.2	-17.5	4.1	9.2	14.7
MP2	19.3	11.3	18.8	22.9	26.3	47.2	10.3	19.4	24.2	29.8
SCS-MP2	18.7	-1.7	18.4	22.5	25.8	42.0	-5.9	15.6	20.5	25.9
MP4	18.0	-2.2	17.2	21.6	25.2	44.1	-3.4	17.0	21.7	26.8
CCSD	20.8	-0.7	19.8	24.6	28.2	38.7	-8.0	12.5	17.3	22.3
CCSD(T)	17.9	-2.6	17.5	22.2	25.8	41.8	-5.4	15.1	19.7	24.6

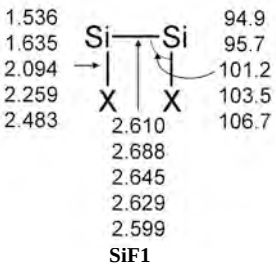

SiF1

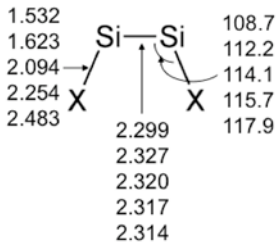

SiF2

	H	F	Cl	Br	I	H	F	Cl	Br	I
BP86	47.7(1)	0.7(1)	21.5(1)	26.0(1)	30.9(1)	57.0(1)	7.5(0)	29.2(1)	33.4(1)	37.6(1)
HF	30.0	-15.3	8.2	14.1	20.3	68.3	15.5	41.6	47.4	53.3
MP2	49.5	-1.2	23.0	28.7	35.8	61.6	8.5	33.2	38.3	44.1
SCS-MP2	44.0	-3.8	19.3	25.0	31.7	59.3	9.0	32.8	38.0	43.6
MP4	46.2	-1.4	20.5	26.1	32.5	55.9	7.2	30.1	35.3	40.6
CCSD	40.7	-5.9	21.8	21.8	27.9	57.3	9.4	33.6	39.4	45.4
CCSD(T)	43.8	-3.3	18.6	24.1	30.2	58.2	6.4	29.9	35.4	41.1

Table 4.1.1.3 Optimized structures of **SiG** and **SiH** at BP86/QZ4P level and relative energies calculated with BP86/QZ4P and *ab initio* methods with aug-cc-pVQZ basis set. The bond lengths are given in Å and the angles are given in degree. The relative energies with respect to **SiA** are given in kcal/mol. The values in parentheses are the number of imaginary frequencies.

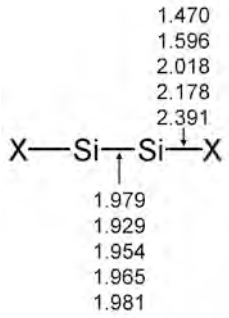

SiG

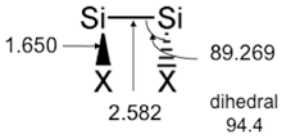

SiH

	H	F	Cl	Br	I	F
BP86	41.4(2)	62.6(2)	66.9(2)	67.6(2)	64.9(2)	-2.0(0)
HF	42.8	55.0	64.6	66.8	64.8	-18.0
MP2	37.5	53.5	61.6	62.6	60.7	-4.1
SCS-MP2	38.1	54.4	61.6	62.5	60.4	-6.7
MP4	38.0	55.5	61.5	62.9	61.2	-4.3
CCSD	40.5	54.8	62.7	64.4	62.6	-8.6
CCSD(T)	38.4	53.6	61.5	63.0	61.3	-6.0

4.1.1.2 Triplet Isomers of Si_2X_2

In the previous chapter, the singlets of Si_2X_2 were investigated. However, energetically low-lying isomers of Si_2X_2 may also exist on the triplet potential energy surface. Scheme 4.1.1.2 shows the investigated triplet isomers. The structures of the stationary points are denoted as doubly bridged structure (**SiA(T)**), singly bridged planar structure (**SiB(T)**), planar doubly bridged structure (**SiC(T)**), vinylidene structure (**SiD(T)**), trans-bent structure (**SiE(T)**), cis-bent structure (**SiF(T)**), linear structure (**SiG(T)**) and distorted singly bridged structure (**SiI(T)**).

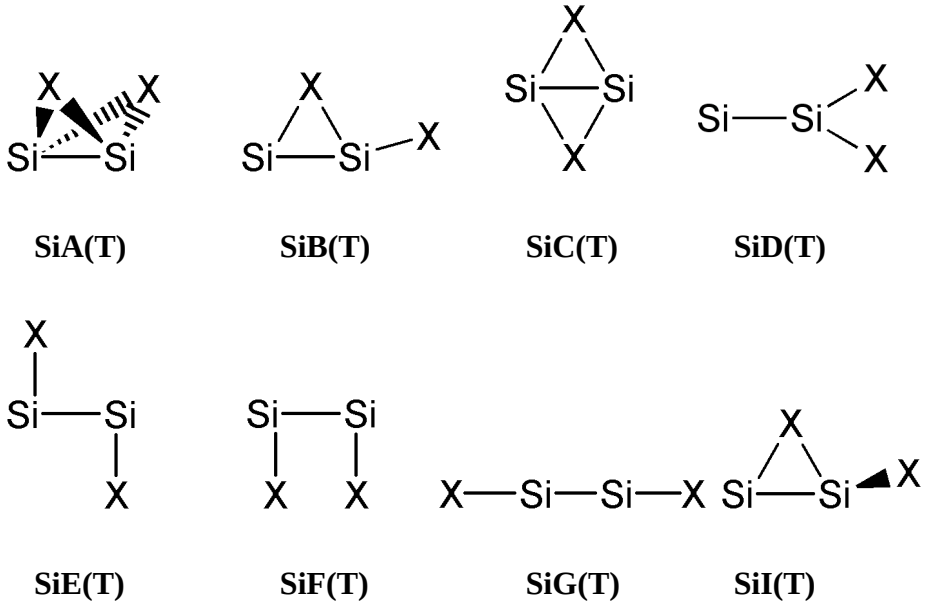

Scheme 4.1.1.2. Investigated triplet isomers of Si_2X_2

The non-planar doubly bridged structures **SiA(T)** have C_{2v} symmetry (Figure 4.1.1.6) and they are local minima except for Si_2F_2. For Si_2F_2, the isomer is a second order saddle point. The Si-Si distance and Si-X-Si angle are in a good correlation with the mass of the X atoms, where the Si-Si distance becomes longer and the Si-X-Si angle becomes smaller with heavier X atom. **SiA(T)** shows a similar trend to **SiA**, but the two Si atoms of Si_2H_2 and Si_2F_2 interact weakly and the Si-Si bonds for Si_2Cl_2, Si_2Br_2 and Si_2I_2 are nearly broken. The Si-X distances are quite similar to those of **SiA**. The Si-X-Si angles are larger than those in **SiA**. This points that the geometric differences stem from the different Si-Si bonding situation.

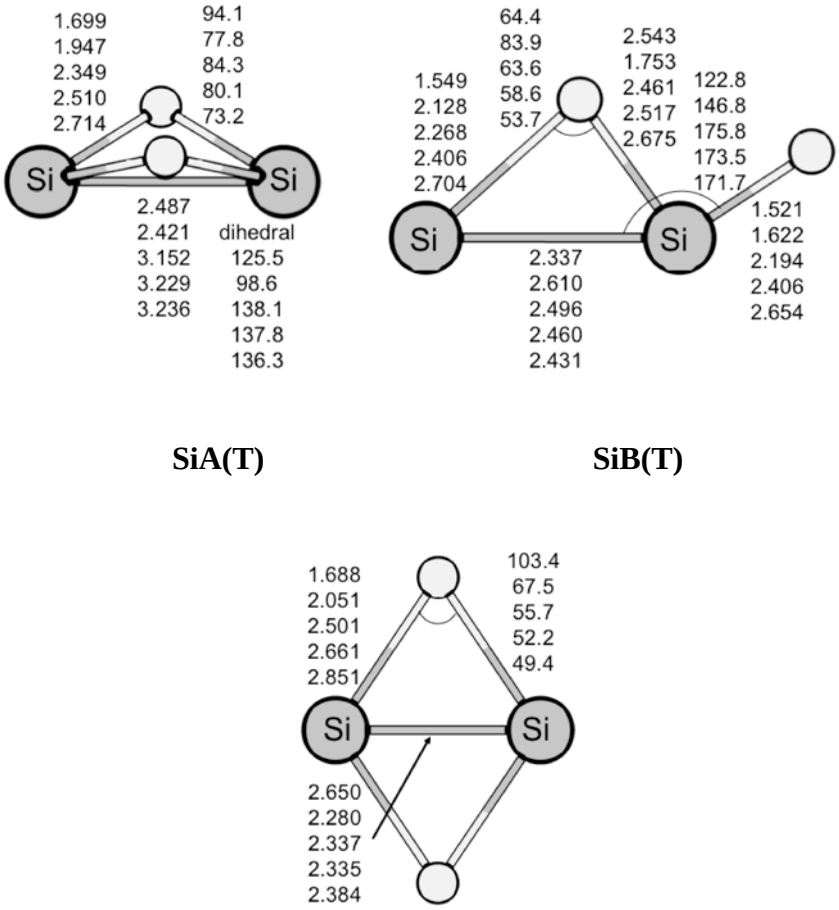

Figure 4.1.1.6. Optimized ring-structures in their triplet state, **SiA(T)**, **SiB(T)** and **SiC(T)** calculated at BP86/QZ4P level of theory. The bond lengths are given in Å and the angles are given in degree.

The singly bridged planar structures **SiB(T)** have C_s symmetry (Figure 4.1.1.6). This structure of Si_2H_2 is predicted to be a minimum. The structure **SiB(T)** has one imaginary frequency for Si_2F_2 and while Si_2Cl_2, Si_2Br_2 and Si_2I_2 present two. The Si-Si bond and Si-X-Si angle becomes smaller with increasing the mass of the halogen atoms. The Si-Si bonds and the Si-X-Si bridging are weaker than that those of **SiB**. The bridging H atom of Si_2H_2 has nearly no interaction with the central Si atom and this structure of **SiB** can be considered as a kind of bent structure.

The planar doubly bridged structures **SiC(T)** have D_{2h} symmetry (Figure 4.1.1.6). The structures of Si_2H_2, Si_2Cl_2, Si_2Br_2 and Si_2I_2 are transition states while the structure of Si_2F_2 is a second-order saddle point. The Si-Si bond and Si-X-Si angle of

Si_2F_2, Si_2Cl_2 and Si_2Br_2 change with the change in the halogen atoms: the Si-Si bond becomes weaker and the Si-X-Si angle gets smaller with the heavier halogen atom. For the Si-X bonds, the Si-X interactions are weaker than those of **SiC**. The geometries show that the Si-Si interactions are stronger and the Si-X-Si bridged structures are weaker than those of **SiC** except for Si_2H_2, where the Si-Si interaction is weaker than that of **SiC**. The Si-H bond is longer and the Si-H-Si angle is larger than those of **SiC**. For Si_2H_2, the bridged structure is weaker in **SiC(T)** than that in **SiC**.

The vinylidene structures **SiD(T)** have C_{2v} symmetry (Figure 4.1.1.7) and these isomers are local minima. For Si_2F_2, the isomer **SiD(T)** is the global minimum. The Si-Si distance shows a clear correlation with the mass of the X atoms. The Si-Si bond length becomes longer with heavier X atoms.

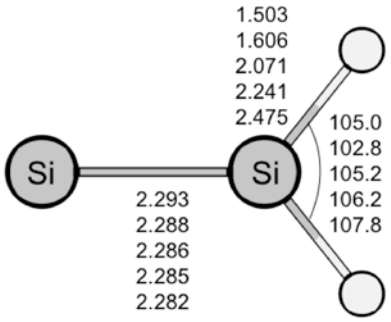

SiD(T)

Figure 4.1.1.7. Optimized vinylidene structures in the triplet state, **SiD(T)** calculated at BP86/QZ4P level of theory. The bond lengths are given in Å and the angles are given in degree.

The trans-bent structures **SiE(T)** have C_{2h} symmetry (Figure 4.1.1.8). These isomers **SiE(T)** are predicted to be minima. **SiE(T)** lies between **SiE1** and **SiE2** in the points of the Si-Si bond lengths and the Si-Si-X angles. The Si-Si distances correlate with the Si-Si-X angles and the Si-Si bond becomes shorter as the angle gets larger. It is the same tendency as in **SiE1** and **SiE2**.

The cis-bent structures **SiF(T)** have C_{2v} symmetry (Figure 4.1.1.8). These isomers, **SiF(T)**, are predicted to be minima except for Si_2H_2. The isomer of Si_2H_2 is predicted to be a saddle point. The isomer of **SiF(T)** lies between **SiF1** and **SiF2** regarding the geometry For Si_2F_2, Si_2Cl_2, Si_2Br_2, Si_2I_2, the Si-Si bond becomes shorter

and the Si-Si-Si angle becomes larger as the X atom becomes heavier. In this correlation, Si_2H_2 is outlier because of the smaller steric effect. The Si-X bonds of **SiE(T)** and **SiF(T)** are similar. From these points, these two isomers differ in the Si-Si bond situation and the steric effect of halogen atoms.

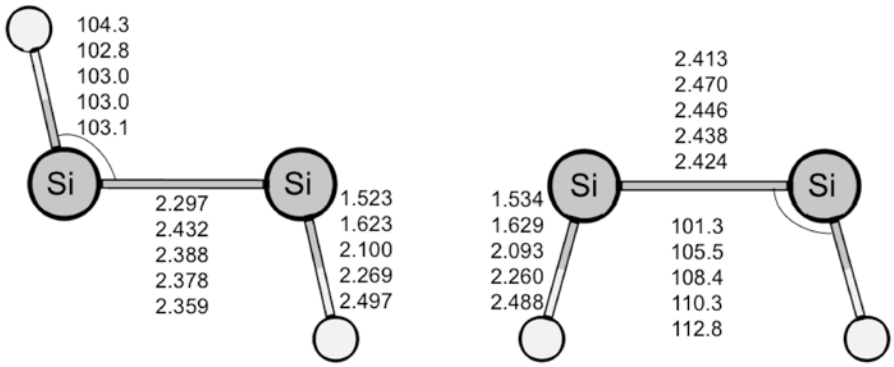

SiE(T) **SiF(T)**

Figure 4.1.1.8. Optimized bent-structures in their triplet state, **SiE(T)** and **SiF(T)**, calculated at BP86/QZ4P level. The bond lengths are given in Å and the angles are given in degree.

The linear structures of **SiG(T)** are in a fourth-order saddle point for Si_2H_2, Si_2Cl_2, Si_2Br_2 and Si_2I_2 (Figure 4.1.1.9). The structure of Si_2F_2 has two imaginary frequencies. The Si-Si bond lengths are quite longer than those of **SiG**. The Si-Si distances become shorter as the halogen atoms get heavier.

SiG(T)

Figure 4.1.1.9. Optimized linear structures in triplet state **SiG(T)** calculated at BP86/QZ4P level. The bond lengths are given in Å and the angles are given in degree.

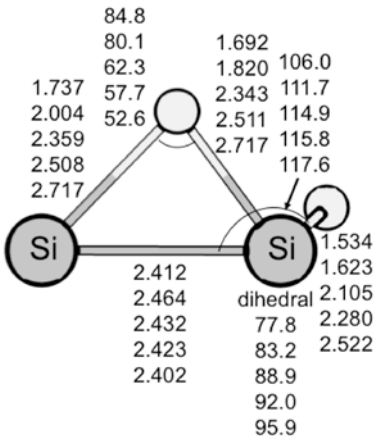

SiI(T)

Figure 4.1.1.10. Optimized distorted singly bridged structure in the triplet state, **SiI(T)**, calculated at BP86/QZ4P. The bond lengths are given in Å and the angles are given in degree.

The distorted singly bridged planar structures **SiI(T)** have C_1 symmetry and these isomers are predicted to be minima (Figure 4.1.1.10). The Si-Si bond length correlates with the mass of the halogen atoms and the bond length becomes smaller as the halogen atom gets heavier. The X atom in the ring is strongly connected to the centered Si atom in Si_2H_2 and Si_2F_2. In Si_2Cl_2, Si_2Br_2 and Si_2I_2, the X atom is bonded to both Si atoms.

Table 4.1.1.4 and Table 4.1.1.5 show the relative energies of the stationary points on the triplet potential energy surface at BP86/QZ4P level. These energies are relatively smaller than those calculated at CCSD(T)/aug-cc-pVQZ//BP86/QZ4P level of theory and the largest difference is 14.9 kcal/mol for the isomer **SiG(T)** of Si_2I_2. The relative energies of the triplets are often underestimated with BP86/QZ4P in the triplets systems and the mean absolute error form CCSD(T)/aug-cc-pVQZ is 6.2 kcal/mol. BP86/QZ4P gives accurate results for minima but the relative energies of the transition states are underestimated. The differences between the CCSD and CCSD(T) values are relatively small and the largest difference is 3.5 kcal/mol for the **SiE(T)** isomer of Si_2Br_2. This indicates that the isomers in the triplet state only have a small multi-reference character and that the CCSD(T) results are reliable and accurate. For the stationary points on the potential energy surface of the triplets, SCS-UMP2/aug-cc-pVQZ gives worse results than UMP2/aug-cc-pVQZ. The largest

deviation for UMP2/aug-cc-pVQZ from CCSD(T)/aug-cc-pVQZ is 5.9 kcal/mol for the **SiB(T)** structure of Si_2Cl_2, where the largest difference for SCS-UMP2 is 8.6 kcal/mol for the **SiG(T)** structure of Si_2I_2. The mean absolute errors from CCSD(T)/aug-cc-pVQZ are 2.9 and 4.3 kcal/mol for UMP2/aug-cc-pVQZ and SCS-UMP2/aug-cc-pVQZ, respectively. For the stationary points on the potential energy surface of the triplets, SCS-UMP2/aug-cc-pVQZ gives worse results than UMP2/aug-cc-pVQZ. This is due to the fact that the parameters of the SCS correction are optimized for the singlets but not for triplets. The UMP4/aug-cc-pVQZ gives the results, which are close to the CCSD(T)/aug-cc-pVQZ results, where the largest deviation is 3.8 kcal/mol for the **SiE(T)** structure of Si_2Br_2 and in the **SiF(T)** structure of Si_2I_2 and the mean absolute error is 2.2 kcal/mol. RMP2 presents similar values to CCSD(T), where the largest deviation is 2.9 kcal/mol for the **SiD(T)** structure of Si_2F_2 and mean absolute error are 1.0 kcal/mol.

The relative energy shows that triplet Si_2X_2 molecules are categorized into three groups, analogues to the singlet isomers: Si_2H_2 group, Si_2F_2 group and the group of Si_2Cl_2, Si_2Br_2 and Si_2I_2. The Si_2H_2 isomers present the following order of stability; **SiD(T)** > **SiE(T)** > **SiI(T)** > **SiB(T)** > **SiF(T)** > **SiA(T)** > **SiC(T)** > **SiG(T)**. These isomers are always higher in energy than the corresponding singlets. Here, the most stable isomer **SiD(T)** is a local minimum. The order of stability shows that Si_2H_2 prefers the vinylidene structure while the linear structure is the most unfavorable. However, between them, the isomers show a clear preference of structure.

The isomers of Si_2F_2 show the following order of stability: **SiD(T)** > **SiE(T)** > **SiF(T)** > **SiI(T)** > **SiG(T)** > **SiB(T)** > **SiA(T)** > **SiC(T)**. The isomer **SiD(T)** is the global minimum of Si_2F_2. **SiD(T)**, **SiE(T)**, **SiF(T)** and **SiG(T)** are lower in energy than the corresponding singlets. Some triplets of Si_2F_2 are more stable than **SiA**. The instability of the structure comes from the weakness of the bridged structure and the destabilization of **SiA**. Si_2F_2 prefers the vinylidene structure followed by bent-structures. The bridged structures are the most unfavorable isomers.

The group of Si_2Cl_2, Si_2Br_2 and Si_2I_2 shows different trends from Si_2H_2 and Si_2F_2. The stability is as follows: **SiE(T)** > **SiD(T)** > **SiF(T)** > **SiI(T)** > **SiA(T)**, **SiB(T)**, **SiC(T)**, **SiG(T)**, where the order of **SiA(T)**, **SiB(T)**, **SiC(T)** and **SiG(T)** depends on halogen atom. The trans-bent bent structure is the most stable isomer of the Si_2Cl_2,

Si_2Br_2 and Si_2I_2 isomers. The isomers of this group prefer the bent structure and the vinylidene structure is slightly higher isomer than **SiE(T)**. The bridged structures are less favorable structures in the triplet state.

Table 4.1.1.4 Optimized structures of **SiA(T)-SiD(T)** at BP86/QZ4P level and the relative energies calculated with BP86/QZ4P and *ab initio* methods with aug-cc-pVQZ basis sets. The bond lengths are given in Å and the angles are given in degree. The relative energies with respect to **SiA** in singlet state and given in kcal/mol. The values in parentheses are the number of imaginary frequencies.

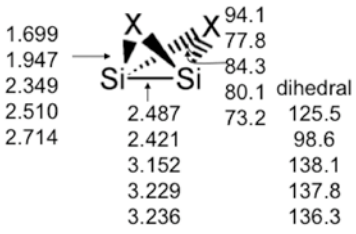

SiA(T)

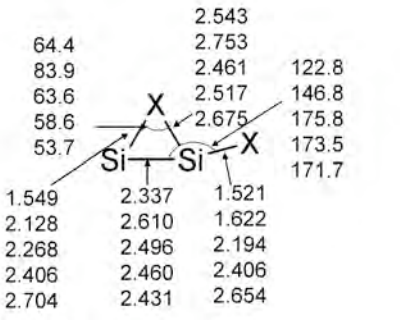

SiB(T)

	H	F	Cl	Br	I	H	F	Cl	Br	I
BP86	40.3(0)	34.9(2)	38.1(0)	39.9(0)	41.2(0)	29.9(0)	12.9(1)	35.8(2)	36.2(2)	36.1(2)
HF	47.0	46.4	25.5	28.8	33.5	13.6	0.7	42.8	42.6	41.4
RMP2	48.3	44.0	41.3	44.6	48.5	36.1	15.3	47.7	46.0	45.1
UMP2	51.9	45.9	44.0	47.3	48.4	36.4	17.2	52.6	50.8	50.4
SCS-UMP2	55.8	51.7	44.0	47.2	51.0	36.8	19.4	54.1	52.6	51.5
UMP4	50.3	45.4	43.5	46.7	49.9	35.7	18.4	50.6	48.9	48.3
CCSD	49.5	47.0	38.9	41.8	45.2	32.0	14.6	47.6	47.2	46.0
CCSD(T)	48.7	44.8	41.0	43.9	46.9	34.1	16.0	46.7	46.2	45.4

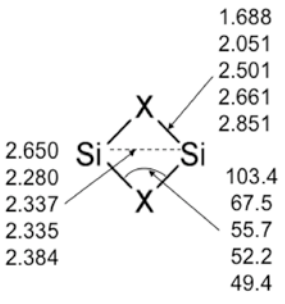

SiC(T)

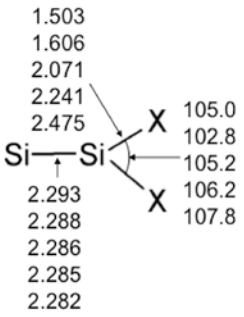

SiD(T)

	H	F	Cl	Br	I	H	F	Cl	Br	I
BP86	40.8(1)	40.3(2)	36.9(1)	34.9(1)	34.1(1)	20.2(0)	-17.1(0)	11.2(0)	17.1(0)	23.2(0)
HF	48.0	60.3	42.0	40.3	40.1	0.9	-39.8	-6.9	1.1	8.3
RMP2	48.4	46.7	49.4	47.8	47.4	23.0	-21.5	12.0	19.5	28.0
UMP2	51.8	52.5	49.9	49.2	48.7	24.9	-19.6	14.1	20.6	30.3
SCS-UMP2	56.2	56.6	52.1	48.4	51.1	24.9	-16.2	15.6	23.4	32.1
UMP4	50.5	51.3	48.1	47.8	47.2	24.3	-16.5	13.8	22.0	30.8
CCSD	50.7	43.2	48.4	46.5	45.7	20.0	-21.1	9.6	17.1	24.3
CCSD(T)	49.8	48.4	47.5	45.6	44.8	22.7	-18.6	12.3	19.7	27.1

Table 4.1.1.5 Optimized structures of **SiE(T)-SiI(T)** at BP86/QZ4P level and the relative energies calculated with BP86/QZ4P and *ab initio* methods with aug-cc-pVQZ basis sets. The bond lengths are given in Å and the angles are given in degree. The relative energies with respect to **SiA** in singlet state and given in kcal/mol. The values in parentheses are the number of imaginary frequencies.

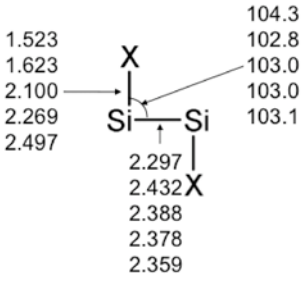

SiE(T)

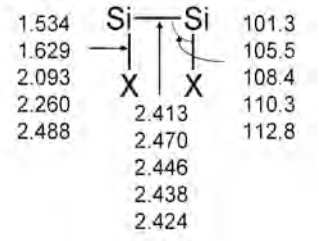

SiF(T)

	H	F	Cl	Br	I	H	F	Cl	Br	I
BP86	22.7(0)	-14.2(0)	7.5(0)	12.0(0)	16.5(0)	34.7(2)	-12.0(0)	10.8(0)	15.7(0)	21.1(0)
HF	13.1	-26.2	-1.1	4.8	10.3	25.1	-23.5	3.0	9.5	16.3
RMP2	26.6	-12.7	11.9	17.3	23.3	42.1	-9.4	16.7	22.6	30.0
UMP2	30.1	-10.1	14.9	20.1	26.9	44.3	-7.7	18.7	24.8	32.5
SCS-MP2	29.8	-17.8	15.5	22.3	28.5	43.8	-5.7	19.3	26.7	33.8
UMP4	28.5	-9.0	13.6	20.7	27.0	41.9	-6.7	17.1	24.5	31.6
CCSD	25.4	-12.5	10.3	20.4	21.2	38.1	-9.6	14.4	20.4	27.0
CCSD(T)	26.5	-11.1	11.6	16.9	22.4	39.3	-8.3	15.5	21.3	27.8

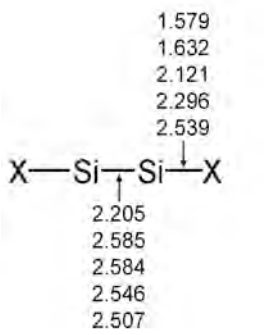

SiG(T)

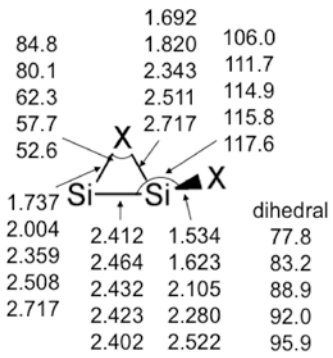

SiI(T)

	H	F	Cl	Br	I	H	F	Cl	Br	I
BP86	68.9(4)	6.7(2)	32.6(4)	36.6(4)	41.6(4)	30.6(0)	2.1(0)	18.6(0)	21.1(0)	23.4(0)
HF	74.9	6.0	36.7	42.7	49.6	21.8	-0.5	9.8	13.5	16.7
RMP2	74.9	13.4	45.4	51.2	58.6	35.7	2.7	22.2	25.9	29.9
UMP2	77.6	13.7	45.8	54.3	62.0	39.0	5.7	25.4	27.0	31.3
SCS-MP2	79.7	18.5	49.0	58.2	65.1	39.3	7.9	26.4	30.5	34.1
UMP4	76.1	14.6	44.0	52.8	59.5	37.8	7.5	24.8	29.1	32.6
CCSD	77.2	15.4	44.8	50.8	57.8	33.9	2.6	21.0	24.5	27.7
CCSD(T)	75.3	14.9	43.9	49.7	56.5	35.2	4.3	22.4	25.8	29.0

4.1.1.3 Summary of Geometries and Relative energies

In chapter 4.1.1, the geometries and relative energies of the isomers of Si_2X_2 (X=H, F, Cl, Br and I) were investigated. The Si_2X_2 molecules are categorized to three groups in the viewpoint of the stability of the isomers: Si_2H_2, Si_2F_2, and the group of Si_2Cl_2, Si_2Br_2 and Si_2I_2.

For Si_2H_2, the investigated isomers present the following order of stability: **SiA** > **SiB** > **SiC** > **SiD** > **SiE1** > **SiD(T)** > **SiE(T)** > ... > **SiG(T)**. The most stable isomer is SiA and the Si-H-Si ring structures stabilize Si_2H_2. For Si_2H_2, the stabilizing effect of the bridged is the most important one.

The isomers of Si_2F_2 show a different behavior from Si_2H_2. The stability of the investigated isomers are as follows; **SiD(T)** > **SiD** > **SiE(T)** > **SiF(T)** > **SiH** > **SiE2** > **SiF1** > **SiE1** > **SiA** > … > **SiG**. The most stable isomer is **SiD(T)**. The order shows that Si_2F_2 prefers vinylidene structure and the bent structures, where the ring structures are unstable in Si_2F_2. This means that the Si-Si bond plays a more important role than the Si-X-Si bridged structure in Si_2F_2.

The stability of Si_2Cl_2, Si_2Br_2 and Si_2I_2 isomers exhibits a relatively similar behavior to Si_2H_2. These isomers show the following order of stability; **SiA** > **SiE(T)** > **SiD** > **SiD(T)** > **SiE1** > ... > **SiG**. In these molecules, the doubly bridged structure **SiA** is the most stable isomer. However, the other bridged structures are higher in energy. The order shows that the X-Si-X bridged structure contributes to the stabilization of these molecules, but the Si-Si bond is still important, too. In general, the relative energies of all isomers increase with respect to **SiA**, as the halogen atom X becomes heavier.

4.1.2 Orbital Interactions and Bond Situations

4.1.2.1. Orbital Analyses

The last section shows that an energetically low-lying isomer exists in the singlet state, except for Si_2F_2, and the difference is mainly due to the bond situation of the Si-Si bond. **SiA**, **SiB**, **SiC**, **SiE1**, **SiE2**, **SiF1**, **SiF2**, and **SiG,** which have a X-Si-Si-X structure can be divided into two SiX fragments and the bonding situation in these molecules can be described as interactions between the two SiX fragments. The orbital interactions between the diatomic species are analyzed with a similar approach to the Trinquier/Malrieu/Carter/Goddard model [81, 82, 83], which is able to explain the E_2H_2 bonding situation in the previous report [87].

4.1.2.1.1 SiX Fragment

Figure 4.1.2.1 shows schematic pictures of the electronic ground state ($X^2\Pi$) and Table 4.1.2.1 shows the first excited state ($a^4\Sigma^-$) of SiX and the calculated excitation energies $a^4\Sigma^- \leftarrow X^2\Pi$ at BP86/QZ4P level and MRCI-SD/aug-cc-pvQZ//BP86/QZ4P level. A (5,5) full-valence CASSCF/aug-cc-pVQZ wave function was used as a reference in the MRCI-SD calculation of SiH and a (11,8) full-valence CASSCF/aug-cc-pVQZ wave function was used as a reference in the MRCI-SD calculations of SiF, SiCl, SiBr and SiI. The excitation energies at BP86/QZ4P level are in relative good agreement with those of MRCI-SD/aug-cc-pVQZ//BP86/QZ4P level and that of the full-CI calculation of SiH (36.4 kcal/mol) from the previous reports [260, 261]. The largest deviation from the MRCI-SD(Q) result and the full-CI calculation are found for SiH with 1.2 and 2.1 kcal/mol, respectively. The MRCI-SD results of SiH and SiF are similar to those of the previous report by Sax et al [262].

As shown in Section 4.1.1, the linear structure is the energetically highest lying stationary point of the investigated structure in the Si_2X_2 system and this situation is quite different from the C_2X_2 system, where the linear structure is the global minimum. Figure 4.1.2.1 shows clearly that the electronic configuration of the SiX moiety must be in the $a^4\Sigma^-$ excited state and not in the $X^2\Pi$ ground state to form the triply bonded linear species XSi≡SiX. Therefore the SiX fragments must at first become excited into the $a^4\Sigma^-$ state in order to bind through one σ and two degenerate

π bonds in XSi≡SiX. The previous study showed that it is energetically much easier to excite CH from the $^2\Pi$ ground state to the $^4\Sigma^-$ excited state to form a triple bond than for the SiH species because the carbon species CH has a lower excitation energy (15.4 kcal/mol) [263] than SiH (38.6 kcal/mol). The possible gain in binding energy after the $^4\Sigma^- \leftarrow {}^2\Pi$ excitation is much larger for C_2H_2 than for Si_2H_2 and the other heavier homologues. Table 4.1.2.1 shows that the excitation energy becomes larger as the halogen atoms get heavier, and the excitation energies of the halogen containing molecules are much larger than that of SiH. This is due to the fact that the halogen atoms are electron-withdrawing groups and the halogen atoms stabilize the $X^2\Pi$ ground state, where the main contribution is the stabilizing of the σ-lone-pair. Figure 4.1.2.1(b) shows that the electron configuration of the $X^2\Pi$ ground state only allows an electron sharing single bond between two SiX moieties. The other possibility to form bonds is the donor-acceptor bond between two moieties in the $X^2\Pi$ ground state.

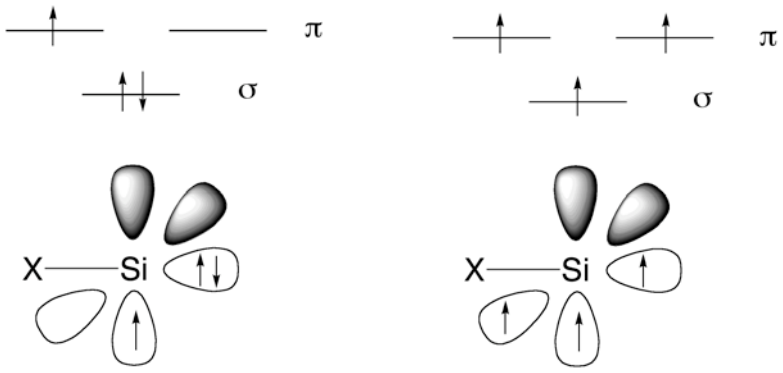

$X^2\Pi$ $a^4\Sigma^-$

(a) ground state (b) excited state

Figure 4.1.2.1 Schematic pictures of the $X^2\Pi$ ground state and the $a^4\Sigma^-$ excited state for the SiX fragments

4.1 Si_2X_2 Molecules

Table 4.1.2.1 Calculated excitation energies from the $X^2\Pi$ ground state to the $a^4\Sigma^-$ excited state at BP86/QZ4P level of theory, MRCI-SD/aug-cc-pVQZ// BP86/QZ4P and MRCI-SD(Q)/aug-cc-pVQZ//BP86/QZ4P levels, where (Q) indicates the inclusion of the Davidson correction. The energies are given in kcal/mol.

	BP86/QZ4P	MRCI-SD/ aug-cc-pVQZ	MRCI-SD(Q)/ aug-cc-pVQZ
SiH	38.56	37.82	39.75
SiF	83.88	79.42	84.36
SiCl	70.86	68.32	72.00
SiBr	66.56	63.66	66.71
SiI	59.33	57.25	59.67

Table 4.1.2.2 Calculated dissociation energies D_e and theoretical bond energies D_e- $2\Delta E_{exc}$ of linear X-Si-Si-X into 2 SiX fragments and excitation energies from $X^2\Pi$ ground state to the $a^4\Sigma^-$ excited state of SiX at BP86/QZ4P level. The energies are given in kcal/mol.

	D_e	ΔE_{exc}	D_e- $2\Delta E_{exc}$
H	121.6	38.6	44.5
F	136.7	83.9	-31.0
Cl	128.5	70.9	-13.2
Br	124.0	66.6	-9.1
I	117.7	59.3	-1.0

Table 4.1.2.2 shows the theoretically predicted bond dissociation energies D_e- $2\Delta E_{exc}$ for breaking the triple bond in linear X-Si≡Si-X yielding 2 SiX ($a^4\Sigma^-$). The linear isomers of Si_2H_2, Si_2F_2, Si_2Cl_2, Si_2Br_2 and Si_2I_2 have similar dissociation energies and the dissociation energies are much weaker than those of acetylene. After correcting the D_e values by the excitation energy of the two SiX fragments from the $X^2\Pi$ ground state to the $a^4\Sigma^-$ state, the calculated values D_e give theoretical bond energies D_e- $2\Delta E_{exc}$. The theoretical bond energy correlates with ΔE_{exc} and the excitation energy dominates the trend of D_e- $2\Delta E_{exc}$. Si_2F_2, Si_2Cl_2 and Si_2Br_2 exhibit higher dissociation energies than Si_2H_2, but the theoretical dissociation energies of Si_2F_2, Si_2Cl_2, Si_2Br_2 and Si_2I_2 are negative because of the high excitation energies. Due to the high excitation energies, the formation of the triple bond is unfavorable for these isomers.

The calculated bond dissociation energy D_e and theoretical dissociation energy D_e- $2\Delta E_{exc}$ show that it is energetically unfavorable for the SiX fragments to form a XSi≡SiX triple bond through the $a^4\Sigma^-$ excited state because the Si-Si single bond, that can be formed from the $X^2\Pi$ ground state, would deliver a much larger binding energy. The typical bond dissociation energies of Si-Si single bonds are about 75-80 kcal/mol [264]. This is much less than the stabilization energy that can be expected from the formation of an electron-sharing XSi-SiX single bond between two SiX fragments in the $X^2\Pi$ ground state. The possibility of additional stabilizations through lone-pair and/or Si-X donor acceptor interactions, which are described below, will be enough to gain the much higher bond energy of the triple bond. It follows that it is energetically more profitable for two SiX species to bind in their $X^2\Pi$ ground state than in the $a^4\Sigma^-$ excited state.

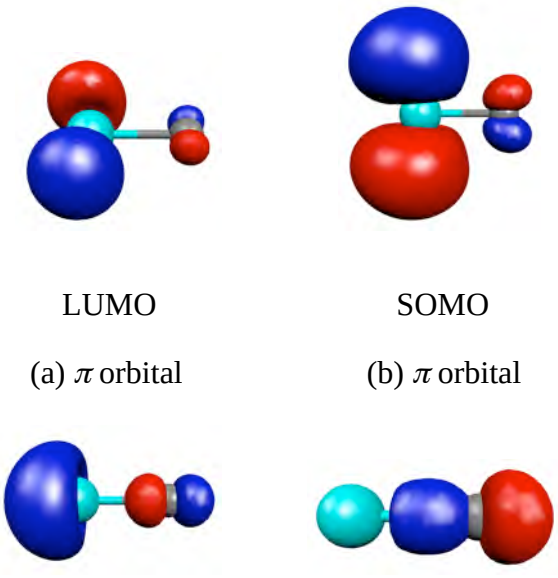

LUMO SOMO

(a) π orbital (b) π orbital

(c) σ-lone-pair orbital (d) σ-Si-X orbital

Figure 4.1.2.2. Important orbitals of the SiX fragment in the $X^2\Pi$ ground to from the Si-Si bond.

Figure 4.1.2.2 shows the selected orbitals of the SiX fragments. Two π orbitals are found as LUMO and SOMO, respectively. Two types of σ orbitals, the lone-pair orbitals and Si-X orbitals are found as occupied orbitals. These orbitals of SiH, SiF, SiCl, SiBr and SiI are quite similar in each other for the region near Si atom. Table

4.1.2.3 and Figure 4.1.2.3 show the orbital energies of the selected orbitals in Figure 4.1.2.2. Figure 4.1.2.3 shows that orbital energies exhibit the clear correlation. SOMO and LUMO become lower in energy as the halogen atom gets heavier. The energies of the lone-pair orbital and the Si-X bond orbital show the opposite trend and they become higher with heavier halogen atoms. The deviation of orbital energies is larger in the lone-pair orbital and the Si-X bond orbital than HOMO and LUMO because the Si-X bond orbital and the lone-pair orbital have σ-symmetry and the effect of X atom is larger in the orbitals with σ-symmetry. The $\Delta E_{\pi\text{-lone-pair}}$ values show the energy difference between LUMO and the lone-pair orbital. $\Delta E_{\pi\text{-lone-pair}}$ shows a clear correlation with the energy of the lone-pair and $\Delta E_{\pi\text{-lone-pair}}$ values are smaller as the energy of lone-pair becomes higher. The $\Delta E_{\pi\text{-Si-X}}$ values show the energy difference between LUMO and the Si-X bond orbital. $\Delta E_{\pi\text{-Si-X}}$ shows a similar correlation to $\Delta E_{\pi\text{-lone-pair}}$ and $\Delta E_{\pi\text{-SiX}}$ values are smaller as the energy of Si-X bond orbital becomes higher. They are due to that the X atom has little effect on the π orbitals.

Table 4.1.2.3. Calculated orbital energies of SiX molecules in their $X^2\Pi$ ground state at BP86/QZ4P level. The energies are given in eV.

	SiH	SiF	SiCl	SiBr	SiI
π orbital (LUMO)	-4.2032	-3.7307	-3.9305	-3.9679	-4.0238
π orbital (SOMO)	-4.0101	-3.5175	-3.7113	-3.7476	-3.8059
lone-pair orbital	-6.8281	-8.8880	-8.1647	-7.8638	-7.4337
Si-X bond orbital	-11.9789	-13.3636	-12.2078	-11.9270	-11.5366
$\Delta E_{\pi\text{-lone-pair}}$	2.6204	5.1573	4.2342	3.8959	3.4099
$\Delta E_{\pi\text{-SiX}}$	7.7757	9.6329	8.2773	7.9591	7.5128

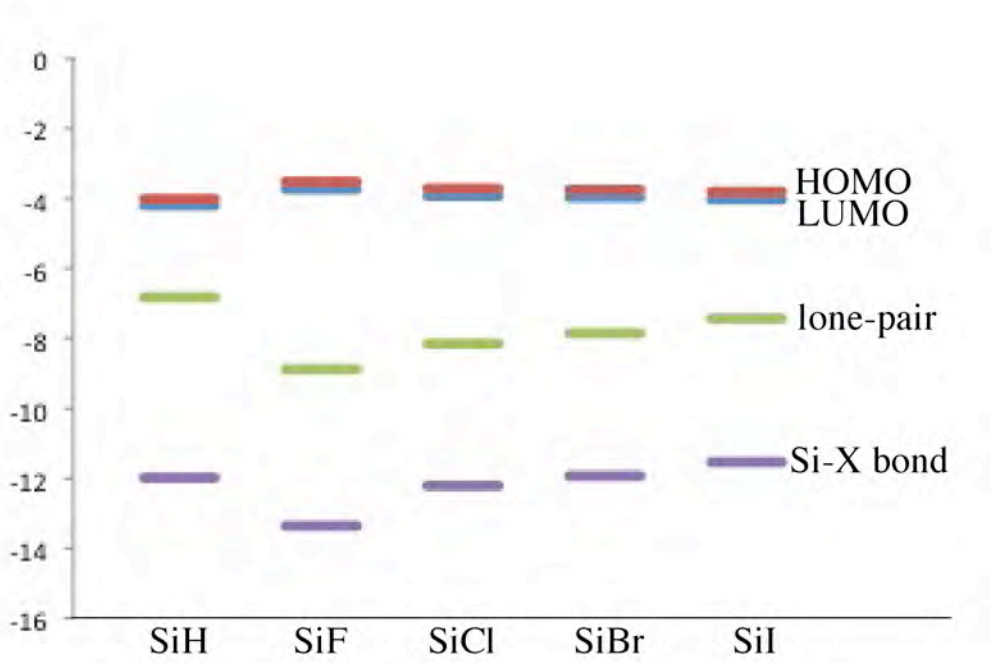

Figure 4.1.2.3. Correlation of the orbital energies of the SiX fragments in Figure 4.1.2.2.

Table 4.1.2.4 Each percentage contribution of selected orbitals corresponds to the indicated atomic orbitals

	SiH(%)	SiF(%)	SiCl(%)	SiBr(%)	SiI(%)
π orbital (LUMO)	Si: p_y 95.92 H: p_y 3.76	Si: p_x 48.03 p_y 44.98	Si: p_z 86.97 Cl: p_z 7.91	Si: p_y 86.77 Br: p_y 9.09	Si: p_y 57.04 p_x 28.48 I: p_y: 7.16
π orbital (SOMO)	Si: p_z 96.74 H: p_z 3.06	Si: p_z 93.39 F: p_z 4.77	Si: p_y 70.42 p_x 18.12 Cl: p_y 6.08	Si: p_z 88.70 Br: p_z 8.74	Si: p_z 86.79 I: p_z 10.11
Lone-pair orbital	Si: s 25.86 p_x 39.53 H: s 35.47	Si: s 65.11 p_y 7.03 p_x 6.58 F: p_y 9.48 p_x 8.88	Si: s 40.66 p_x 17.11 Cl: p_x 27.50 p_y 7.07	Si: s 31.34 p_x 23.78 Br: p_x 40.97	Si: s 18.78 p_x 21.37 p_y 10.67 I: p_x 28.46 p_y 14.21
Si-X orbital	Si: s 61.20 H: s 34.76	Si: s 23.76 F: p_y 34.83 p_x 32.62	Si: s 52.21 Cl: p_x 32.13 p_y 8.27	Si: s 63.35 Br: p_x 31.15	Si: s 73.80 I: p_x 13.73 s 7.34

Table 4.1.2.4 shows the contribution of atomic orbitals for each Kohn-Sham molecular orbital. In this table, LUMO and SOMO show a similar contribution of atomic orbitals and these orbitals are constructed by just *p* orbitals, which show a similar trend for their orbital energies.

For the lone-pair orbital, the contribution of the *s* orbital becomes smaller as the halogen atom gets heavier and the contribution of the *p* orbital of the Si atom shows the opposite trend to the *s* orbital. The contribution of the *p* atomic orbital in the lone-pair is in a correlation with the orbital energy of the lone-pair, and the energy of the lone-pair becomes higher as the contribution of *p* orbital grows.

The Si-X bond orbital is built from the *s* orbitals of Si atom and *s* orbital of hydrogen and *p* orbital of halogen atoms. The contribution of the X atom in the Si-X bond correlates with the energy of the Si-X bond and the orbital energy becomes lower in energy with a larger contribution of the halogen atom X.

4.1.2.1.2 σ-type Isomers, **SiA**, **SiE2** and **SiF1**

As shown before, the linear arrangement of two SiX fragments of the $X^2\Pi$ ground state is unfavorable for the bond formation between the unpaired electrons. The bond formation must rather take place in a sideways fashion. Figure 4.1.2.4 shows some different orientations for two SiX fragments each in the $X^2\Pi$ state which lead to Si-Si σ bonds.

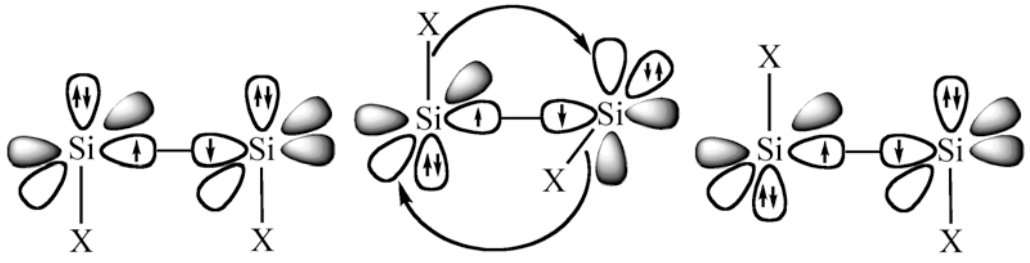

(a) (b) (c)

Figure 4.1.2.4. Qualitative model for σ-type orbital interaction between two SiX molecules in different orientation where the unpaired electrons yield a σ orbital.

Figure 4.1.2.4 (a) shows a syn-planar arrangement of the SiX moieties, which gives the isomer **SiF1**. This arrangement is not favorable because the vacant *p(π)* orbitals remain unoccupied while the Si-X bonds and the electron lone-pairs of the two molecules repel each other. The geometry optimization of Si_2X_2 with a syn-planar arrangement gives a transition state.

The rotation around the σ-bond axis by 90° gives a much more favorable arrangement. In this bond situation, the empty *p*(π) orbitals (LUMOs) of SiX can interact with the Si-X bond and with the electron lone-pair of the other SiX. The donor-acceptor interactions between the Si-X bond and the vacant *p*(π) are more stabilizing than the donation from the electron lone-pairs to the p(π) because of more effective orbital combination. The acceptor orbital is a *p* orbital and the lone-pair orbitals have also *p*-character, as shown in Table 4.1.2.4. These orbitals have both directional properties and the combination leads to a weaker overlap of the orbitals. The Si-X bond has a large *s* character, which leads to less directional properties, and the Si-X donor-acceptor interaction leads to a three-center two-electron bond. This means that the Si-X bonds are better donors than the lone-pairs. The Si-X bonds interact with the empty *p(π)* orbitals of the other SiX moiety. This arrangement gives the isomer **SiA** as shown in Figure 4.1.2.4 (b). This explains why the global energy minimum is the halogen-bridged geometry **SiA**, which is not planar but has a perpendicular arrangement of the two Si_2X planes with a dihedral angle between 103.8° and 110.3°. For Si_2F_2, **SiA** is not the global minimum because the bonding situation is different from the other Si_2X_2 molecules. The discussion about Si_2F_2 is carried out later. The quantitative model indicates that there are three bonding components of the orbital interactions in **SiA**: one σ bond and two Si-X donor-acceptor bonds.

Figure 4.1.2.4 (c) shows the anti-planar arrangement of the SiX fragments, which gives the isomers **SiE2**. The only Si-Si bonding contribution is the σ orbital between two Si atoms. The structure of **SiE2** lacks the two Si-X donor-acceptor interactions of **SiA**, and so that the vacant *p*(π) orbitals remain unoccupied. The geometry optimization of Si_2X_2 with an anti-planar arrangement gives structures that are transition states.

Table 4.1.2.5. Selected orbitals and their energies of σ-type isomers, **SiA**, **SiE2** and **SiF2**. The energy levels are given in eV.

	SiA	**SiE2**	**SiF1**
orbital	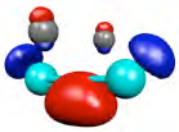	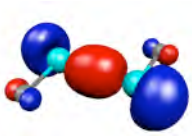	
	σ-type bond	σ-type bond	σ-type bond
H	-5.1759	-4.8863	-5.0400
F	-4.9672	-4.5597	-4.5144
Cl	-5.3488	-4.9332	-4.8045
Br	-5.3610	-5.0079	-4.8469
I	-5.4025	-5.0959	-4.8992
orbital	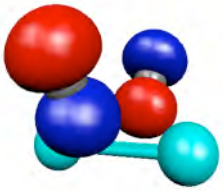	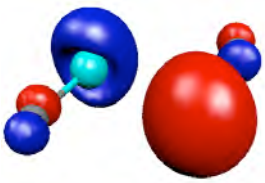	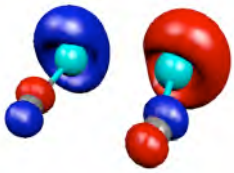
	Si-X donor	lone-pair	lone-pair
H	-9.3955	-6.8245	-5.9110
F	-10.0343	-7.9517	-7.8480
Cl	-9.9588	-7.4683	-7.2761
Br	-9.3912	-7.1324	-6.9804
I	-8.7596	-6.6344	-6.4801
orbital			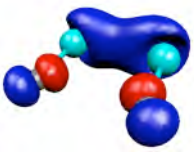
	Si-X donor	lone-pair	lone-pair
H	-15.3092	-6.9136	-7.6617
F	-14.5823	-9.5561	-9.7792
Cl	-13.5908	-8.0775	-8.8216
Br	-13.4258	-7.5025	-8.7684
I	-13.0054	-6.8398	-8.2664

4.1 Si_2X_2 Molecules

In the previous section, the bond situation is discussed with a qualitative model. Table 4.1.2.5 shows the shapes of the selected orbitals and their orbital energies of **SiA**, **SiE2** and **SiF1** concerning the Si-Si bond. The first orbitals of **SiA**, **SiE2** and **SiF1** in Table 4.1.2.5 are σ-type Si-Si bonds. The second one and third one of **SiA** are Si-X donor-acceptor bonds while those of **SiE2** and **SiF1** are lone-pair orbitals. These orbitals show that the qualitative model is sensible in these σ system isomers.

Table 4.1.2.5 indicates that the Si-Si σ bonds constitute the HOMO for **SiA**, **SiE2** and **SiF2** in all Si_2X_2 molecules, which are categorized to a σ type structure in Figure 4.1.2.4. The energies of the HOMOs are presented in Table 4.1.2.3. SiF has the highest HOMO energy of all Si_2X_2 systems and the orbital energy decreases with heavier halogen atoms. In the Si_2F_2, Si_2Cl_2, Si_2Br_2 and Si_2I_2 systems, the energy level of the σ type orbital clearly correlates with the orbital energy of π orbital of the SiX fragments. The Si-Si bond lengths in **SiE2** and **SiF1** are longer than the Si-Si single bond of $X_3Si\text{-}SiX_3$ (Si_2H_6: 2.351Å, Si_2F_6: 2.345Å, Si_2Cl_6: 2.352Å, Si_2Br_6: 2.361Å, Si_2I_6: 2.375Å at BP86/QZ4P), because the σ bonds in **SiE2** and **SiF1** are formed by the two π orbitals of SiX moieties, which are the SOMOs shown in Figure 4.1.2.2 (b) and the σ bond has little *s* character, whereas the normal Si-Si σ bond has sp^3 character. Table 4.1.2.6 shows the orbital energies. The energy of the σ type orbital in Si_2F_2 is the highest in **SiA**, **SiE2** and **SiF1**, wherein the orbital energies become lower when halogen atom X gets heavier.

SiA clearly shows two Si-X donor-acceptor bonds as shown in Table 4.1.2.5. These two orbitals in Table 4.1.2.5 are very similar except for the node on the Si-Si bond. The energetically higher orbital has a node on the Si-Si bond while the lower one does not. From these orbital figures, it can be thought that the energetically higher orbital is the anti-bonding orbital of the lower one (Table 4.1.2.5). The energetically lower orbital has a large coefficient on the Si-Si bond and this orbital contributes to the Si-Si bond. The energetically higher orbital has a large coefficient between the two Si atoms and the X atom and this orbital contributes to the formation of the Si-X-Si ring structure. This can explain the Si-Si bond lengths in **SiA**, which are shorter than that in the Si-Si single bond of **SiE2** and **SiF1**. The energies of the σ-type orbitals correlate with the Si-Si bond distances and the Si-Si bond distance becomes shorter as the energy of the σ-type orbital gets lower. For **SiA**, this correlation is not

found because the Si-X donor-acceptor interactions concern the Si-Si bond, too.

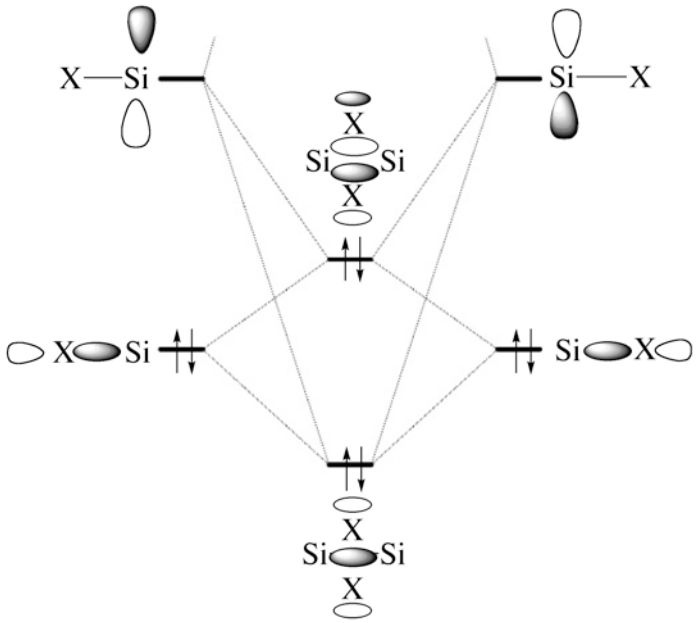

Figure 4.1.2.5 Orbital correlation model for donor-acceptor interaction between the Si-X bond and the vacant *p*(π) orbital in ground state of two Si-X fragments to yield bridged structures.

Figure 4.1.2.5 is the correlation model of the Si-X bond orbital and the vacant π-orbital. In principle, the orbital energy level of the two new formed orbitals depend on the energy level of the original orbitals, i.e. the energy level of the vacant π orbital and the Si-X bond orbital. Table 4.1.2.5 shows that the orbital energies of the two Si-X donor-acceptor bonds become higher as the halogen atom gets heavier. This trend corresponds to the orbital energies of the Si-X bond because the main contribution of the orbital is the Si-X bond.

Figure 4.1.2.6 shows the orbital correlation model of **SiE2** and **SiE1**. In **SiE2** and **SiF1**, the two lone-pair orbitals interact with each other and they form a bonding orbital between the two SiX moieties. However, they form an anti-bonding orbital at the same time. This system can be viewed as a four-electron-two-orbital interaction and the interaction between two lone-pair orbitals is almost canceled. Therefore, they have little contribution to the Si-Si bond formation.

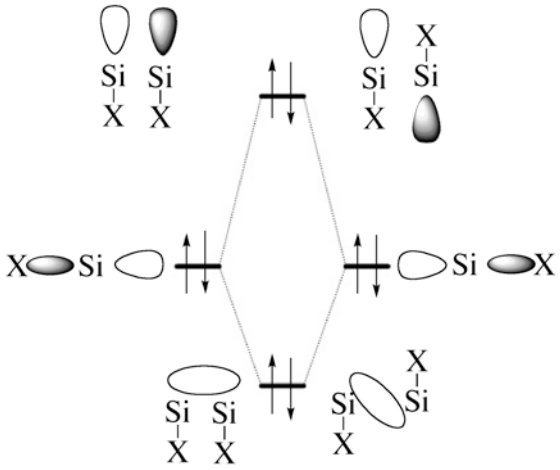

Figure 4.1.2.6. Orbital correlation diagram between two lone-pair orbitals in ground state of the two Si-X fragments in σ-type bent-structures, **SiE2** and **SiF1**.

4.1.2.1.3 π-type Isomers, **SiB**, **SiC**, **SiE1** and **SiF2**

The unpaired electrons in the $X^2\Pi$ ground state of the Si-X may also be paired in an electron-sharing bond between the two SiX fragments, which has a π symmetry with respect to the molecular structure. Figure 4.1.2.7 shows different orientations for two ($X^2\Pi$) SiX molecules which lead to a Si-Si π bond.

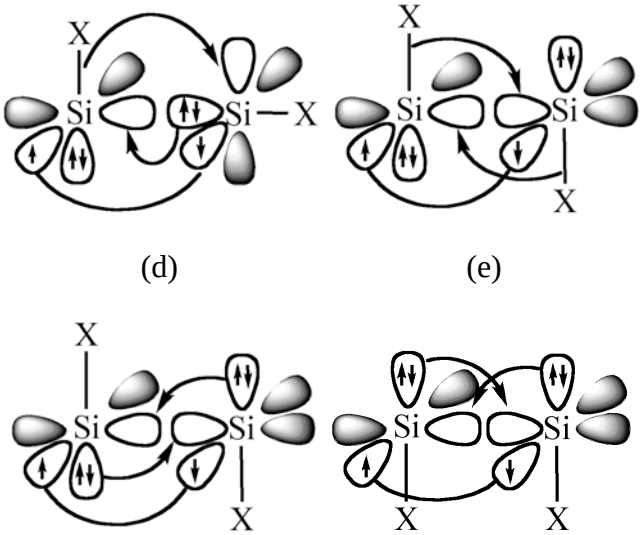

(d) (e)

(f) (g)

Figure 4.1.2.7 Qualitative model for the π-type orbital interactions between two SiX molecules in different orientations where the unpaired electrons yield a π orbital.

The arrangement given in Figure 4.1.2.7 has an electron lone-pair on one SiX moieties pointing in the direction of the empty π orbital of the other SiX species. This orbital interaction now has a σ symmetry with respect to the SiX dimer plane. Besides the electron-sharing π bond and the lone-pair donor-acceptor σ bond, further stabilizing orbital interactions are possible in the structure shown in Figure 4.1.2.7. Another possibility is the donation of the SiX bonding orbital, which is shown in the orbital of **SiA** in Figure 4.1.2.4(b). As noted before, the donation from the SiX bonding orbital is stronger than from the lone-pair orbital. The former interaction becomes stronger when the SiX donor orbital and the empty π orbital of the interacting fragments are tilted toward each other, which leads to the structure **SiB** (Figure 4.1.2.7(d)). The tilting of the empty π orbital of the acceptor SiX moiety (top SiX in Figure 4.1.2.7(d)) means that the terminal atom moves toward the bridging halogen atom. The syn orientation of the terminal atom with respect to the bridging X atom can be explained as a secondary effect of optimizing the SiX donor-acceptor interaction, which is shown in Figure 4.1.2.7(d). The unusual singly bridged geometry of **SiB**, which has a terminal halogen atom with syn-orientation to the bridging atom, can thus be explained as a stereoelectronic effect that comes from the orbital interactions between two SiX fragments in their $X^2\Pi$ ground state.

Figure 4.1.2.7 (e) displays another orientation of two SiX molecules where the unpaired electrons form a π bond, while the SiX bonds are in an anti-periplanar arrangement. The π orbital interaction between the SiX fragments is enhanced by two equal donor-acceptor interactions between the SiX bonding orbitals and the empty π orbitals of the interacting fragments. The latter orbital interactions become stronger, when the hydrogen atom bridge in a doubly bridged planar (D_{2h}) structure. The D_{2h} symmetric stationary point is an energetically low-lying structure on the PES. The inspection of the Hessian matrix reveals, however, that it is a transition state for the degenerate rearrangement of the global energy minimum structure **SiA**. It is the wing-flapping motion of the butterfly geometry. The structure **SiA** has a Si-Si σ bond and two SiX donor-acceptor bonds (Figure 4.1.2.4(b)), while the transition state has a Si-Si π bond and two SiX donor-acceptor bonds (Figure 4.1.2.7(e)).

The electron lone-pair donation is weaker than the SiX bond donation, but it leads to another structure of $(SiX)_2$, which is a minimum on the PES. Figure 4.1.2.7(f)

and Figure 4.1.2.7(g) show that the donation of the lone-pair of SiX to the vacant p_π orbital becomes enhanced tilting the Si-X bond outwardly, which yields the trans and cis form **SiE1** and **SiF2**, respectively. According to the orbital analysis, the structures **SiE1** and **SiF2** have three bonding orbital components, which are one π bond and two lone-pair donor-acceptor bonds. The structures **SiE1** and **SiF2** of Si_2H_2 are energetically higher lying than the planar transition state with two bridging hydrogen atoms, which has one π bond and two Si-X donor-acceptor bonds, whereas those in Si_2F_2, Si_2Cl_2, Si_2Br_2 and Si_2I_2 lie energetically lower than the planar transition state with two bridging halogen atoms.

Table 4.1.2.6 shows the orbital of energies of the important orbitals in **SiB, SiC**, **SiE1** and **SiF2**, which involve the Si-Si bond. Table 4.1.2.6 presents the Si-Si π bonds of **SiB, SiC**, **SiE1** and **SiF2**, which are categorized to a π type structure in Figure 4.1.2.7. In these isomers, the Si-Si π bond is found to be the HOMO. The energy of the π type orbital in Si_2F_2 is the highest in **SiB**, **SiC**, **SiE1** and **SiF2**, where the orbital energies become lower with the heavier halogen atom X. The orbital energy correlates with the energy of the SOMO of the SiX fragment (Table 4.1.2.3). Moreover, these orbital energies correlate with the Si-Si bond length because the π bonding is very sensitive to the bond length. The isomers **SiB**, **SiE1** and **SiF2** are often found as minima because they have a π bond and the rotation needs energy to break the π bond. The isomers **SiC** of Si_2F_2, Si_2Cl_2, Si_2Br_2 and Si_2I_2 are transition states because the energy of the π orbital is relatively higher than that of σ bond in **SiA**. The Si-Si bond distance is quite long and the π bond is unstable and the π bond can rotate easily.

In principle, a π bond is weaker than a σ bond and a "single" π bond should be longer than a σ bond, because a π bond usually has less orbital overlap than σ bond. However, the Si-Si bond lengths in **SiB, SiE1** and **SiF2** are shorter than the Si-Si single bond in **SiE2** and **SiF1** as shown in the chapter 4.1.1.1. This suggests that another interaction, besides the π orbital interaction, could exist between the Si-Si atoms as expected in Figure 4.1.2.7.

Table 4.1.2.6. Selected orbitals and orbital energies of the π-type isomers, **SiB, SiC**, **SiE1** and **SiF2**. The energy levels are given in eV.

	SiB	**SiC**	**SiE1**	**SiF2**
orbital		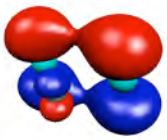	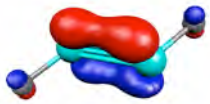	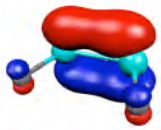
	π-type bond	π-type bond	π-type bond	π-type bond
H	-5.2694	-5.2332	-5.2378	-5.2109
F	-4.7670	-3.8513	-4.9462	-4.8408
Cl	-4.9730	-4.1995	-5.0570	-4.9526
Br	-4.9084	-4.2817	-5.0477	-4.9532
I	-4.8754	-4.3565	-5.0321	-4.9496
orbital	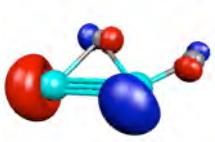		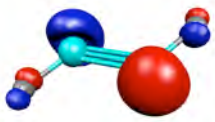	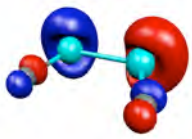
	Lone-pair donor	Si-X donor	lone-pair	lone-pair
H	-6.8651	-10.3875	-6.5184	-5.9421
F	-7.6887	-11.5504	-7.5830	-7.6191
Cl	-7.2156	-9.9922	-7.1486	-7.0826
Br	-6.9939	-9.5008	-6.9526	-6.8525
I	-6.6475	-8.9325	-6.6269	-6.5003
orbital	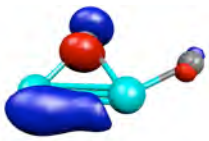		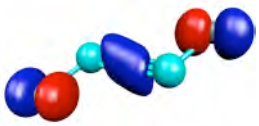	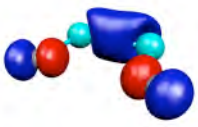
	Si-X donor	Si-X donor	lone-pair	lone-pair
H	-8.2060	-15.6233	-8.6005	-8.3344
F	-9.8627	-14.3002	-10.7711	-10.7573
Cl	-8.9749	-13.1861	-9.9561	-9.8047
Br	-8.2876	-13.1043	-9.3957	-9.2838
I	-7.5500	-12.7691	-8.7168	-8.6595

The second orbital of **SiB** of Table 4.1.2.6 shows that the orbital has the largest coefficient between the two Si atoms and the shape of the orbital is similar to the lone-pair donor-acceptor bond model in Figure 4.1.2.7(d). The energy level of this orbital correlates with the energy of the lone-pair of the Si-X fragment (Table 4.1.2.3), where the orbital energy level becomes lower, when halogen atom X is heavier. To form the donor-acceptor bond, the lone-pair orbital interacts with the vacant π orbital of the Si-X fragment. The formed donor-acceptor orbital mainly has the character of the original lone-pair orbital and the energy level of the formed orbital exhibits the correlation with the lone-pair orbital.

The third orbital of **SiB** in Table 4.1.2.6 shows that the largest coefficient comes from the Si atoms and the main contribution is not a Si-X donor-acceptor bond. However, the orbital has the second largest coefficient in the Si-X-Si region. The energy level of this orbital is moderately higher than that of the Si-X donor-acceptor bond of **SiA**. The energy level of the orbital shows a similar trend with the orbital energy of Si-X bond in the SiX fragment (Table 4.1.2.3), where the orbital energy level becomes lower, when the halogen atom X gets heavier.

The **SiC** isomers have a π bond and two Si-X donor-acceptor bonds. The Si-X donor-acceptor bond orbitals are quite similar to those of **SiA**. The two Si-X donor-acceptor bonds form two new orbitals and the main contributions of these orbitals are the Si-Si bond are the Si-X-Si ring structure, which is the same as the bond correlation in Figure 4.1.2.7. The energy level of the π orbital is higher than that of σ orbital of **SiA**. Due to this, **SiC** is unstable and these structures are transition states.

The two orbitals of **SiE1** and **SiF2** are similar to the two lone-pair orbitals of **SiE2** and **SiF1**, respectively. The energetically higher lying orbital has a node along the Si-Si bond while the lower lying one does not. The energetically lower lying orbital has a large coefficient on the Si-Si bond and this orbital contributes to the Si-Si bond. The energetically higher orbital is similar to the original lone-pair orbital. From these orbital figures, it can be guessed that the energetically higher orbital is the anti-bonding orbital of the lower one. When the energy levels of these orbitals are compared, the lower lying “lone-pair like” orbital energy of **SiE1** is 1.2 to 1.7 eV lower than the energies of the lone-pair orbital in **SiE2**, where the lone-pairs in **SiE2** do not contribute to the Si-Si bond. The orbital energy differences between **SiF1** and

SiF2 are 0.39 to 0.97 eV. The stabilization can be attributed to the contribution of the vacant π orbital, as shown in Figure 4.1.2.7(f) and Figure 4.1.2.7(g). Figure 4.1.2.8 and Figure 4.1.1.9 show the correlation diagram of **SiE1** and **SiF2**. These figures exhibit that the Si-Si bond has a σ type bonding orbital and the **SiE1** and **SiF2** have two bonding orbitals between two Si atoms. This can explain the Si-Si bond lengths in **SiE1** and **SiF2**, which are shorter than those of the Si-Si single bond in **SiE2** and **SiF1**. The Si-Si bond lengths of **SiE1** and **SiF2** correlate with the orbital energies of the lone-pair and the bond length becomes longer as the energy becomes lower, where the Si-Si bond of **SiE2** and **SiF1** has no correlation with the orbital energy of lone-pair. This suggests also that the lone-pair is important for the Si-Si bond of **SiE1** and **SiF2**.

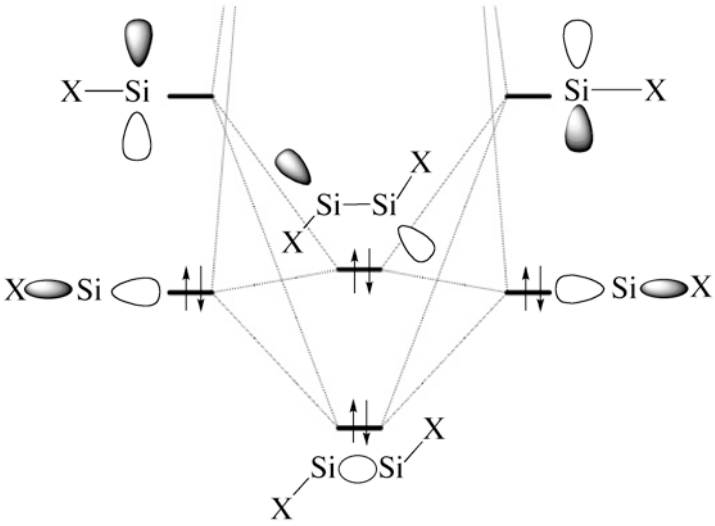

Figure 4.1.2.8 Orbital correlation diagram between two lone-pair orbitals in ground state of the two Si-X fragments in **SiE1**.

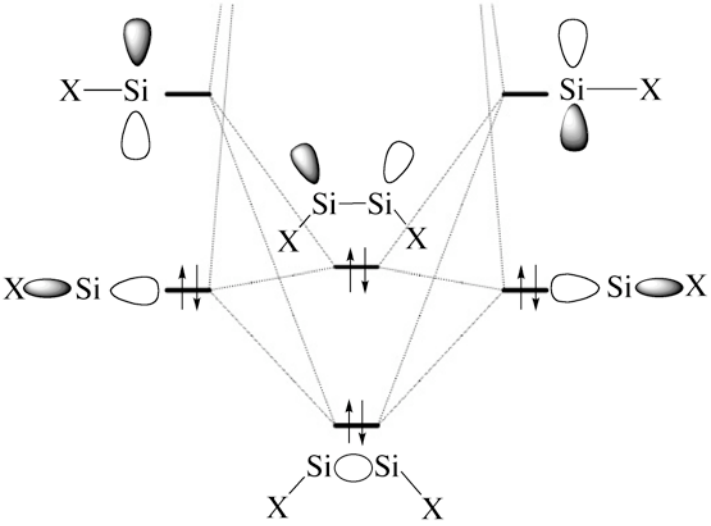

Figure 4.1.2.9 Orbital correlation diagram between two lone-pair orbitals in ground state of the two Si-X fragments in **SiF2**.

4.1.2.1.4 **SiH** Isomer

In the chapter 4.1.1.1, it has been shown that the **SiH** structure of Si_2F_2 is the most stable isomer of the F-Si-Si-F structures. The orbital interaction of **SiH** is here investigated. Figure 4.1.2.10 shows three possibilities of the orbital interaction between the two Si-F fragments in the structural point of view. Figure 4.1.2.10(b) has two Si-X donor-acceptor interactions and one σ-bond, and this model is the quantitative model of **SiA** and exact the same as Figure 4.1.2.4(b). The model (g) has only one σ bond, and the model (h) has a σ bond and two lone-pair donor-acceptor bonds. In the structural points, the isomer **SiH** is similar to **SiE1** and **SiF2**, which have two lone-pair donor-acceptor, as mentioned in the chapter 4.1.1.1.

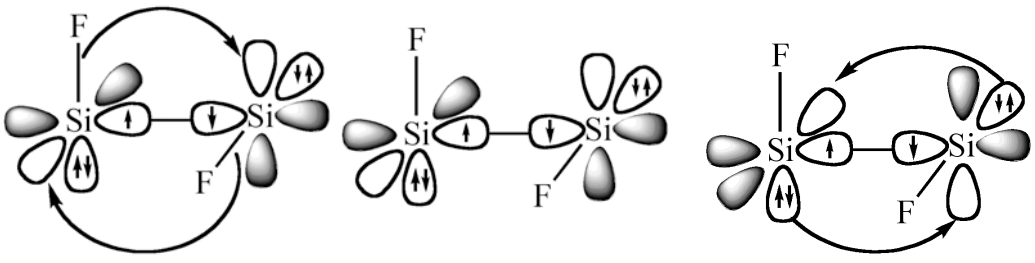

(b) (g) (h)

Figure 4.1.2.10 Qualitative models for orbital interaction between two SiX fragments to yield **SiH** structure.

Table 4.1.2.7. Selected orbitals and orbital energies of the **SiH** isomer of Si_2F_2. The energies are given in eV.

orbital	σ-type	lone-pair	lone-pair
	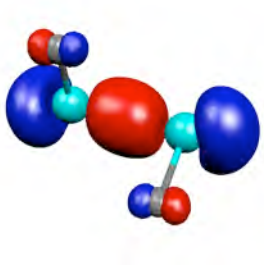	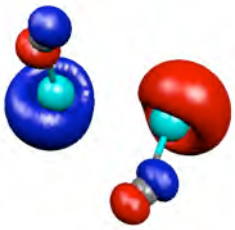	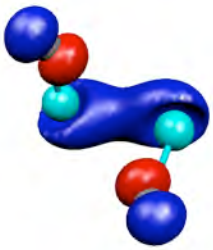
Energy level	-4.5900	-7.9358	-9.5711

Table 4.1.2.7 shows the shapes of the selected orbitals and the orbital energies for **SiH** of Si_2F_2. As shown in Table 4.1.2.7, the isomer **SiH** has a σ orbital and two lone-pair orbitals. The shapes of these orbitals are similar to those of **SiE2** and **SiF1**, where the isomers have just a σ orbital. The orbital energies are also quite similar to those of **SiE2** (Table 4.1.2.5). From the viewpoint of orbitals and orbital energies, the qualitative model (g) is suitable for the **SiH** isomer and **SiH** only has a σ bond and this isomer has no donor-acceptor bond.

The Si-X donor is the best way to form the donor-acceptor bond in the systems for Si_2H_2, Si_2Cl_2, Si_2Br_2, and Si_2I_2, as mentioned before. Table 4.1.2.3 showed that the orbital energy of the SiX fragments and the energy gap between the Si-X bond orbital and the LUMO, $\Delta E_{\pi\text{-SiX}}$. The SiH molecule has the smallest energy difference, $\Delta E_{\pi\text{-SiX}}$. The energy differences for SiCl, SiBr and SiI are larger than that for SiH, but the energy gain from the Si-X donor-acceptor bond is still larger than the energetic loss to form the bridged structure, i.e. form the elongation of the Si-X bond. The difference $\Delta E_{\pi\text{-SiX}}$ for SiF is the largest of all SiX molecules. The Si-F-Si bridged formation needs to elongate the Si-F bond and the energy gain from the bridging cannot compensate the destabilization of the Si-F bond.

Si_2H_2 prefers the bridged structure. This bridging also stabilizes the molecules in

Si_2Cl_2, Si_2Br_2 and Si_2I_2. However, the effect is not as large as that of Si_2H_2. Si_2F_2 disfavors the bridged structure and it prefers a non-bridged Si-Si bond. This trend can be explained by the shape of the orbitals shown in Figure 4.1.2.11. The H atom just has an *s* orbital and the bridging is the favorable structure because the *s* orbital is non-directional. However, halogen atoms of Si_2X_2 have *p* orbitals and these orbitals are directional. It is less favorable to form the bridged structure with a *p* orbital than with an *s* orbital because of the directional character of the halogen *p* orbital. The heavier halogen atoms have the more diffused orbitals and so the bridged structure is favored. From these points, the stability of the isomers depends on the stability of the Si-X-Si ring-structure and the Si-Si bond situation.

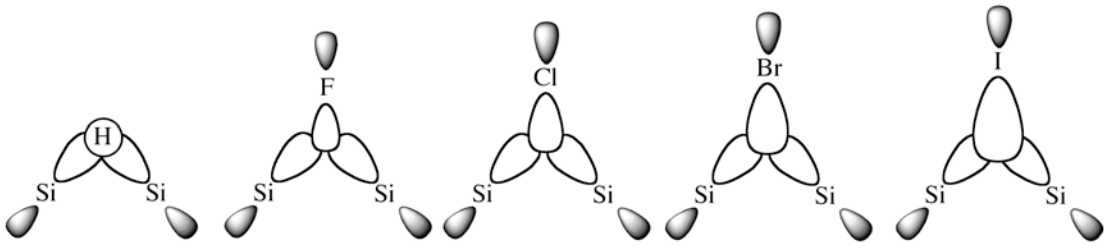

Figure 4.1.2.11. Orbital interaction model for the Si-X-Si bridged structure.

4.1.2.1.5 Vinylidene Isomers, **SiD** and **SiD(T)**

In the previous two chapters, the Si-Si bond between two SiX moieties have been investigated. As shown in the chapter 4.1.1, the vinylidene structure is the most stable structure for Si_2F_2 and the Si-X-Si bridging is not as important as for the other Si_2X_2 molecules to stabilize the isomers of Si_2F_2. Figure 4.1.2.12 shows the qualitative model of **SiD** and **SiG**, which are assumed to have a double and a triple bond, respectively. **SiG** shows the typical triple bond as expected. The orbital energy level of π type bond of **SiD** in Figure 4.1.2.12 is similar to the π bond of **SiG**. The σ type orbital in **SiD** is not equivalent in the Si-Si bond and the shape of the σ type orbital is quite similar to the lone-pair donor-acceptor bond of **SiB**. The bond lengths correlate with the orbital energy of **SiD** and **SiG**, where the bond length becomes shorter as the energy gets lower. The energies of the π type orbital of **SiD** have no correlation with the halogen atoms. However, the π type orbital of Si_2F_2 is the highest in Si_2X_2

molecules. The orbital energies show that the F atom stabilizes the σ-orbital of the vinylidene structure of **SiD** and it destabilizes the π orbital of **SiD**.

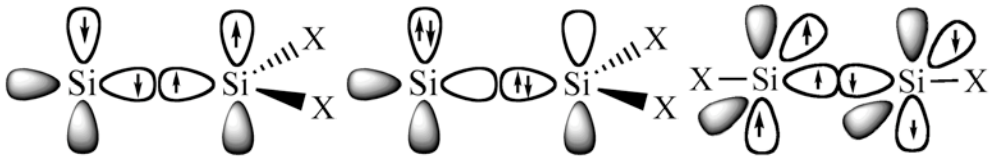

(i) (j) (k)

Figure 4.1.2.12 Qualitative models for the orbital interaction of the vinylidene type isomers and the linear molecule in the different orientation where the electron configurations yield a double bond and a triple bond, respectively. In the model of (i) and (j), the *s* orbital of Si atom is omitted.

Table 4.1.2.8. Orbital energies of **SiD** and **SiG**. The energies are given in eV.

	SiD	**SiG**
Orbital		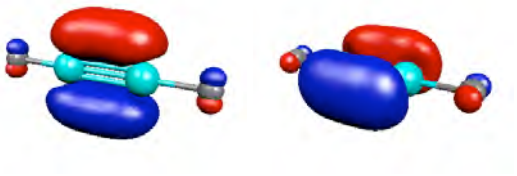
	π-type bond	π-type bond
H	-5.1509	-5.3954
F	-5.0494	-5.4738
Cl	-5.1196	-5.3038
Br	-5.1112	-5.1990
I	-5.0971	-5.0901
orbital	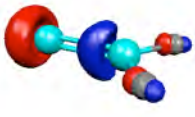	
	σ-type bond	σ-type bond
H	-6.4202	-9.6588
F	-7.4306	-12.1750
Cl	-7.0964	-10.7763
Br	-6.9463	-10.1954
I	-6.6702	-9.4343

The orbital model of the **SiD** structure shows that the orbital interaction is divided into two parts, Si atom and the silylene SiX_2. Table 4.1.2.9 shows the orbitals of the silylene of SiX_2. On one hand, the silylene of SiH_2 prefers the triplet state as its ground state and the σ type orbital and the π orbital are singly occupied. On the other hand, SiF_2, $SiCl_2$, $SiBr_2$ and SiI_2 prefer the singlet state and the σ type orbital is doubly occupied. From the orbital analysis of silylene, the model (i), which shows an electron-sharing type Si-Si double bond, is suitable for Si_2H_2 to form the Si-Si double bond, although the donor-acceptor type Si-Si bonding model (j) is preferable for Si_2F_2, Si_2Cl_2, Si_2Br_2 and Si_2I_2. The energy levels of σ-type bond show a correlation with those of silylene due to that the σ-type bonding bonds are composed from σ-type orbital of the silylene.

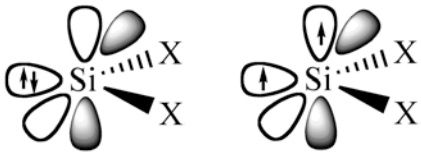

singlet triplet

Figure 4.1.2.13 Orbital model of the silylene SiX_2.

Table 4.1.2.9 Orbital energies of silylene SiX_2, where σ type orbitals are doubly occupied for SiF_2, $SiCl_2$, $SiBr_2$ and SiI_2 while σ type orbital and π type orbital are singly occupied. The energies are given in eV.

	$\pi_{\|\|}$-type bond	$\pi_{\perp}$-type bond	σ-type bond
orbital	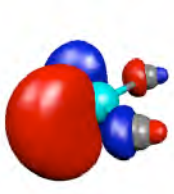	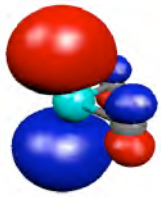	
H	-0.2341	-4.1042	-5.9866
F	-0.7850	-3.1921	-7.3352
Cl	-1.1748	-3.8454	-6.8841
Br	-1.4198	-3.9528	-6.6677
I	-1.7198	-4.1004	-6.3354

Table 4.1.2.10 Orbital energies of **SiD(T)**. The energies are given in eV.

SiD(T)	$\pi_{\|}$-type bond	$\pi_{\perp}$-type bond	σ-type bond
orbital	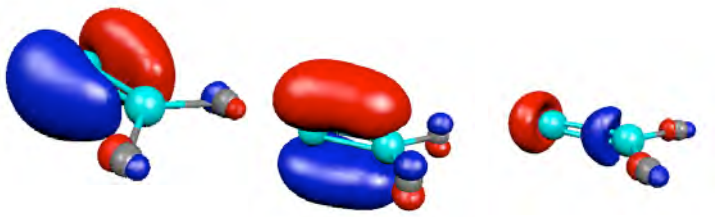		
	(SOMO)	(SOMO)	
H	-4.6941	-5.8744	-6.6302
F	-5.2488	-5.7681	-7.6877
Cl	-5.1498	-5.7700	-7.3207
Br	-5.1192	-5.7401	-7.1485
I	-5.0529	-5.6861	-6.8332

SiD(T)

Figure 4.1.2.14 Orbital model of **SiD(T)**.

Table 4.1.2.10 shows the orbitals of **SiD(T)**. For **SiD(T)**, the σ type orbital is occupied and two types of π orbitals, $\pi_{\|}$-type and $\pi_{\perp}$-type are singly occupied. The energy of the $\pi_{\|}$-type orbitals is higher than those of the $\pi_{\perp}$-type orbitals. The orbital energies of the $\pi_{\|}$-type orbitals and the σ-type orbitals show a clear correlation with the orbitals of the silylene. However, the $\pi_{\perp}$-type does not show a clear correlation. Si_2F_2 has a π-type orbital as its SOMO and the energy level is lower than the one in $SiCl_2$, $SiBr_2$ and SiI_2. It is found that the F atom stabilizes either $\pi_{\|}$-type or σ-type orbitals. The electronic states of **SiD(T)** and silylene SiX_2 indicate that the orbital model of **SiD(T)** of Figure 4.1.2.14 is sensible, which shows the donor-acceptor type Si-Si bonding model. The orbital model of **SiD(T)** suggest that the bond formation of $Si{=}SiH_2$ with the triplet state needs the excitation of SiH_2 from singlet to triplet state and the Si=Si bond formation of **SiD(T)** is less favorable than that of **SiD**, although

Si_2F_2, Si_2Cl_2, Si_2Br_2 and Si_2I_2 prefer the **SiD(T)** structure because the ground state of SiX_2 is triplet and the bond formation needs no excitation of *p* orbital of Si atom.

4.1.2.1.6 Summary of Orbital Analyses

In this chapter, the orbital analyses of the SiX fragment and the Si_2X_2 isomers are shown. The analyses of SiX fragments showed that the formation of the linear structures is unfavorable because of the large excitation energy from the $X^2\Pi$ ground state to the $a^4\Sigma^-$ excited state, although the interactions between two SiX fragments in the $X^2\Pi$ ground state are favorable. The orbital analyses of Si_2X_2 exhibited that qualitative models are sensible as the models of the Si_2X_2 isomers and the XSi-SiX structures are categorized to two groups: σ-type isomers and π-type isomers. The doubly bridged structures, **SiA** are categorized to σ-type isomers and these isomers have three components, one σ-bond and two Si-X donor-acceptor bonds, where the Si-X bond donor-acceptor is a quite favorable bond situation due to the formation of the three-center-two-electron interaction, although **SiE2** and **SiF1** have just a σ-type orbital. The **SiH** isomer is categorized to the σ-type structure because the orbitals and the orbital energies are quite similar to those of **SiE2** and **SiF1**. **SiB**, **SiC**, **SiE1** and **SiF2** are categorized to π-type isomers. The comparison of the orbital energies of **SiE1** and **SiF2** with **SiE2** and **SiF1** indicates the donor-acceptor interaction between the lone-pair orbital and the vacant π orbital. The orbital analyses of silylene SiX_2 showed that SiH_2 prefers the triplet state and the singlets are favorable for the other SiX_2 molecules. Due to that, the singlet isomer **SiD** of Si_2H_2 is more stable than triplet isomer **SiD(T)**, although the other isomers Si_2X_2 prefer triplets.

4.1.2.2 AIM Analyses

In the previous section, the orbitals and their energy levels were investigated. However, the charge distribution between the considered two fragments remains not clear. For that reason and to gain more insight into the bonding situation, we used the AIM method to compare the electron densities in the Si_2X_2 systems. Figure 4.1.2.15 – Figure 4.1.2.22 show the Bader plots of the isomers **SiA** – **SiF2**. In general, the charge accumulation and zero flux surfaces exhibits that Si-F bond have more ionic character and Si_2H_2 and Si_2I_2 molecules have more covalent character.

Figure 4.1.2.15 shows the Bader plot of the isomer **SiA** in the Si_2X plane. The bond paths of each isomer show the Si-X-Si bridged structure. A charge accumulation between the two Si atoms is explained as a Si-Si electron-sharing bond. The charge accumulation at the side of Si atom is interpreted as a lone-pair. This is very similar to the qualitative model of **SiA**. A charge accumulation shows that the Si-X-Si interactions of Si_2F_2, Si_2Cl_2, Si_2Br_2 and Si_2I_2 have more ionic character than that of Si_2H_2 because of less charge accumulation. The zero flux surfaces are not drawn here due to the technical reasons.

In the sections 4.1.1.1 and the section 4.1.2.1, the bonding situations in **SiB** have been discussed. There, the lone-pair donor bond and Si-X donor-acceptor bond could not be found clearly in **SiB**. The bond paths in Figure 4.1.2.16 show that Si_2F_2 has a Si-X-Si ring structure and the other molecules do not have. This is consistent with the discussion from the bond lengths (chapter 4.1.1.1). The charge accumulation between the two Si atoms is interpreted as a Si-Si bond and the zero-flux surface indicates that the Si-Si bond is a polar electron-sharing bond. The charge accumulation on the side of Si atom is explained as a lone-pair orbital.

The bond paths of Figure 4.1.2.17 show that the isomers **SiC** have a Si-X-Si bridged structure. The small charge accumulation is interpreted as a small electron-sharing bond and the ionic interaction plays an important role in Si-X-Si bridged structure. The charge accumulation on the side of Si atom is explained as lone-pair orbitals of the Si atom.

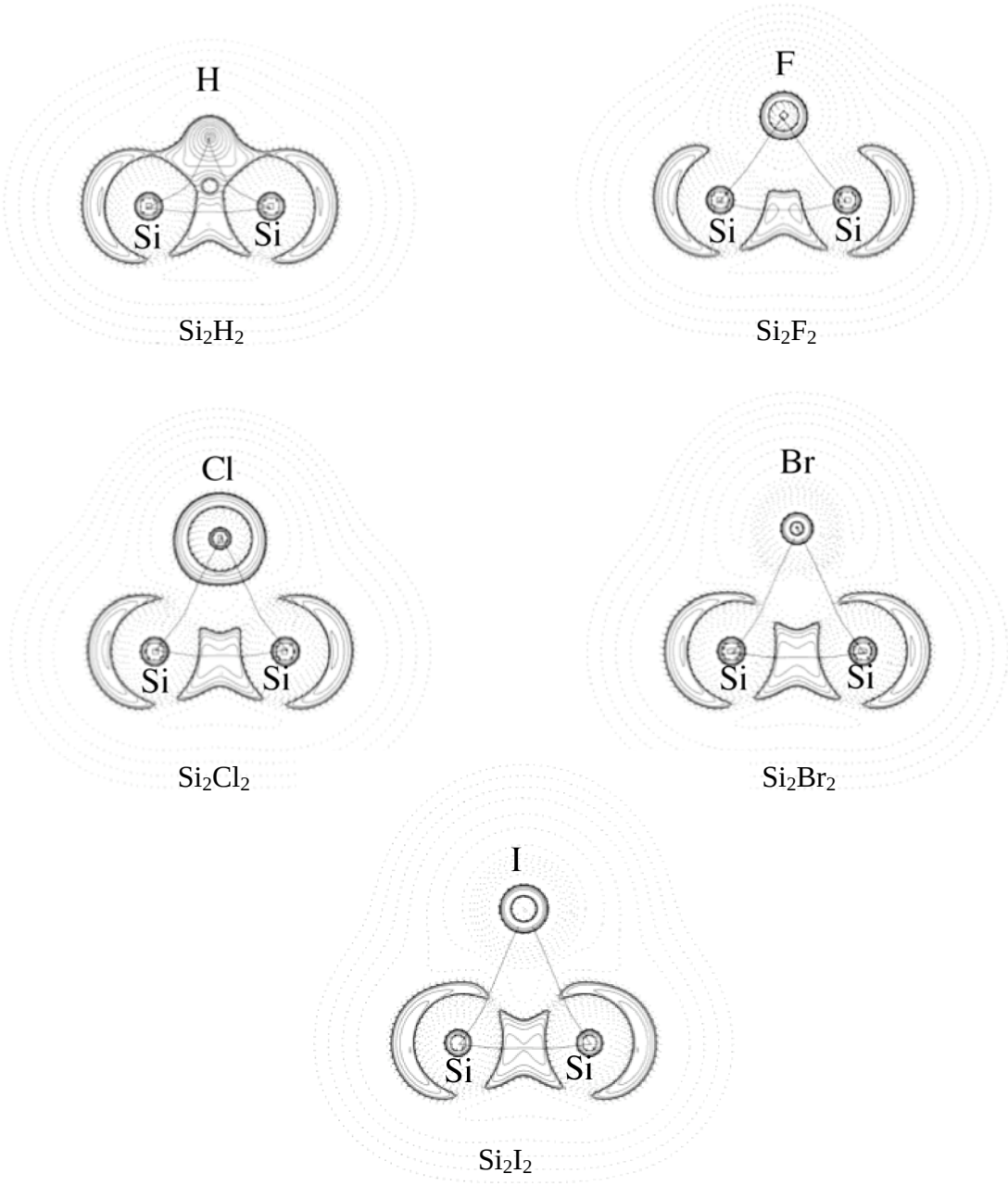

Figure 4.1.2.15 Contour line diagram $\nabla^2\rho(r)$ of isomer **SiA**. Solid lines indicate areas of charge concentration ($\nabla^2\rho(r) < 0$), while dashed lines show areas of charge depletion ($\nabla^2\rho(r) > 0$). Solid lines that connect the atomic nuclei are the bond paths.

4.1 Si_2X_2 Molecules

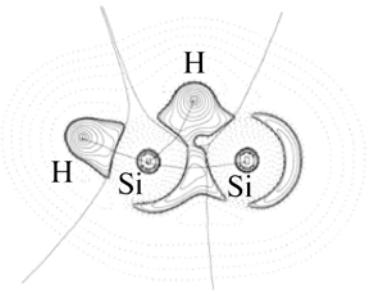

Si_2H_2

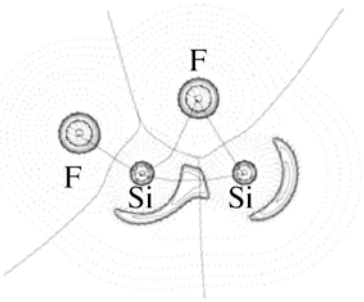

Si_2F_2

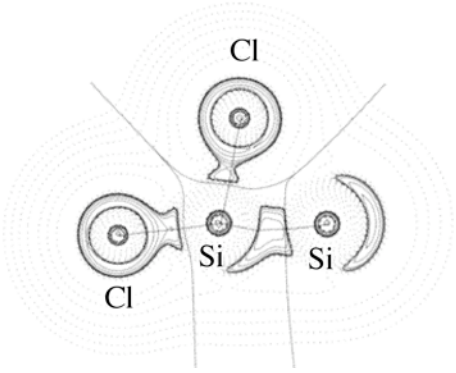

Si_2Cl_2

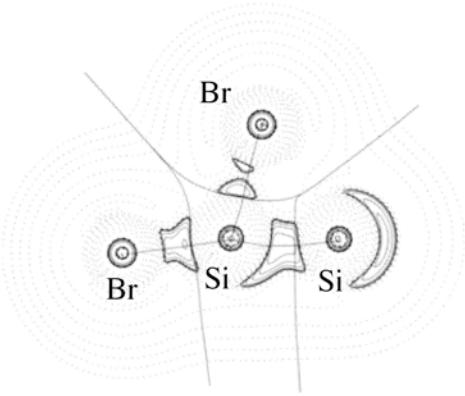

Si_2Br_2

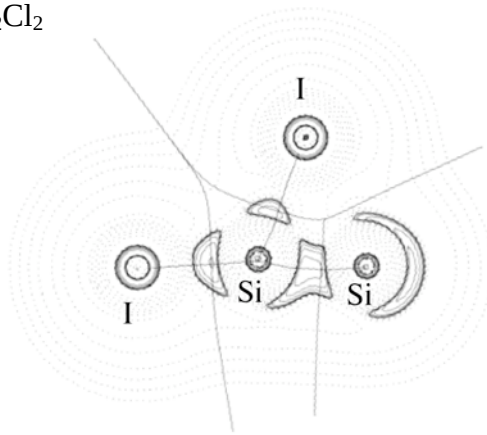

Si_2I_2

Figure 4.1.2.16 Contour line diagram $\nabla^2\rho(r)$ of isomer **SiB**. Solid lines indicate areas of charge concentration ($\nabla^2\rho(r) < 0$), while dashed lines show areas of charge depletion ($\nabla^2\rho(r) > 0$). Solid lines that connect the atomic nuclei are the bond paths, while solid lines that separate the atomic basins give the zero-flux surfaces in the molecular plane.

4.1 Si_2X_2 Molecules

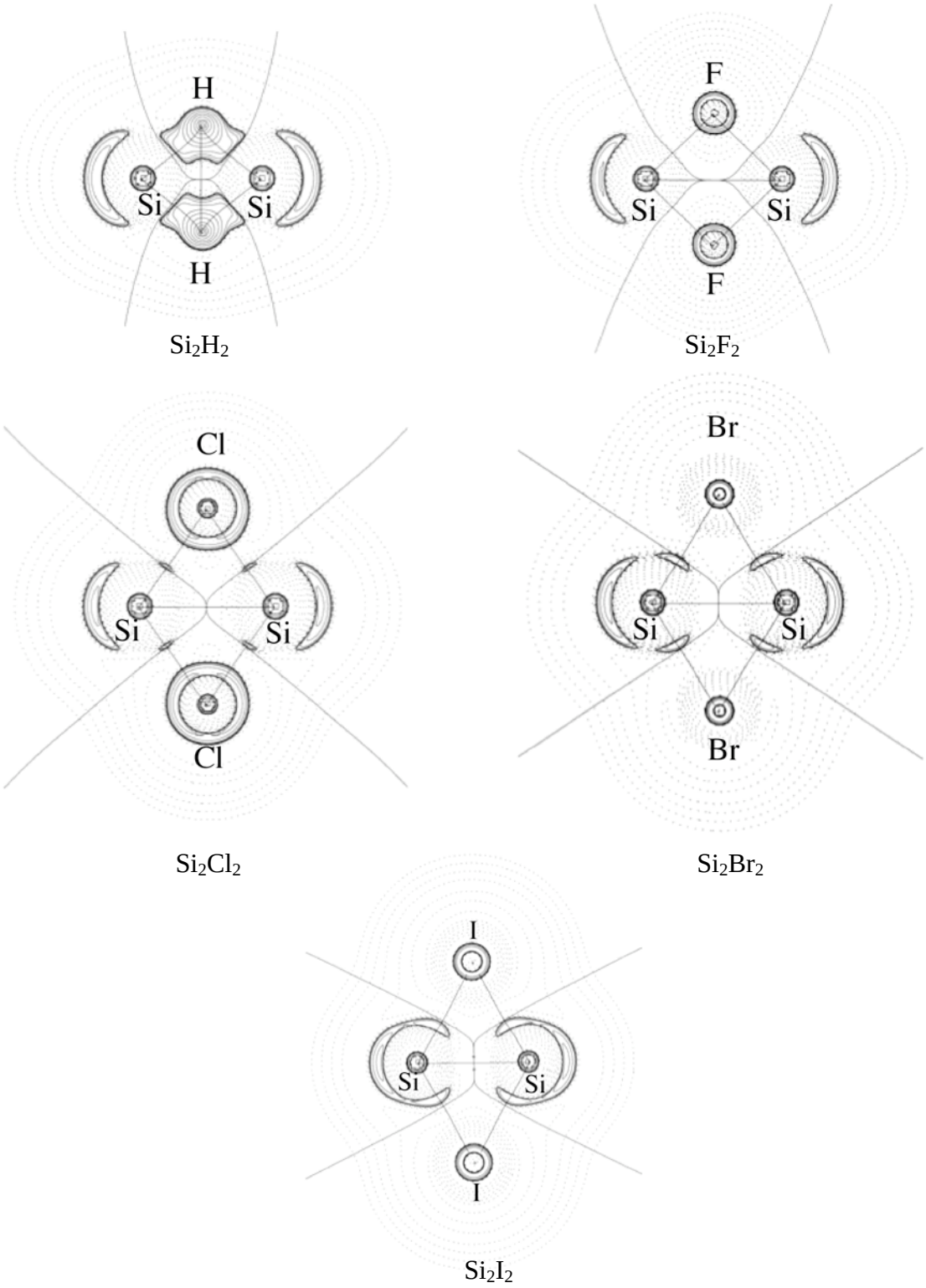

Si_2H_2 Si_2F_2

Si_2Cl_2 Si_2Br_2

Si_2I_2

Figure 4.1.2.17 Contour line diagram $\nabla^2\rho(r)$ of isomer **SiC**. Solid lines indicate areas of charge concentration ($\nabla^2\rho(r) < 0$), while dashed lines show areas of charge depletion ($\nabla^2\rho(r) > 0$). Solid lines that connect the atomic nuclei are the bond paths, while solid lines that separate the atomic basins give the zero-flux surfaces in the molecular plane.

The bond paths of Figure 4.1.2.18 show the Si-Si bond and Si-X bonds for **SiD**. The charge accumulation between the two Si-Si atoms is elucidated as a polar electron-sharing bond or a donor-acceptor bond. The charge accumulation of the side Si atom is interpreted as a lone-pair.

Figure 4.1.2.19 shows the bond paths of the Si-Si bond and the Si-X bonds of **SiE1**. The charge accumulation of the Si-Si bond is interpreted as a Si-Si electron sharing or a lone-pair donor-acceptor bond. The charge accumulation on the Si atom is interpreted as lone-pairs, which is consistent with the orbital analysis.

Figure 4.1.2.20 shows the bond paths of the Si-Si bond and Si-X bonds in **SiE2**. The charge accumulation in the Si-Si region is interpreted as a covalent Si-Si bond and that of each Si atom explained as a lone-pair. This agrees with the orbital analysis (chapter 4.1.2.1.2). The charge accumulation in the Si-Si region of **SiE2** is larger than that of **SiE1** and it indicates the differences of the Si-Si bonding situation.

The charge accumulation of **SiF1** shown in Figure 4.1.2.21 is quite similar to that of **SiE2**. The bond paths of **SiF1** present the Si-Si and Si-X bonds. The charge accumulation between the two Si atoms is interpreted as Si-Si bond and the zero flux surface shows the covalent character of the Si-Si bond. Figure 4.1.2.21 shows bond paths between two Br and I atoms. It is due to the fact that the Si-Si-X angle is nearly 90 degree and Br and I have large radii.

In Figure 4.1.2.22 **SiF2** shows a similar Badar plot to **SiE1**. The Si-Si bond and the Si-X bonds are represented by the bond paths of **SiE1**. A charge accumulation in Figure 4.1.2.22 is elucidated as a Si-Si bond and the other one as lone-pairs on the Si atoms. The situation is similar to that of **SiE1**. However, the charge accumulation is smaller than that in **SiE1**.

The results of AIM analysis showed the charge accumulation of the isomers and their interpretations by means of the bonding interactions. The interpretation of figures of charge accumulation comes to the similar results as the orbitals analyses. The AIM analyses proved the bridged structures of all **SiA** and **SiC** isomers and **SiB** of Si_2F_2. The bent structures suggested that the isomers have a Si-Si bond and two lone-pairs.

4.1 Si_2X_2 Molecules

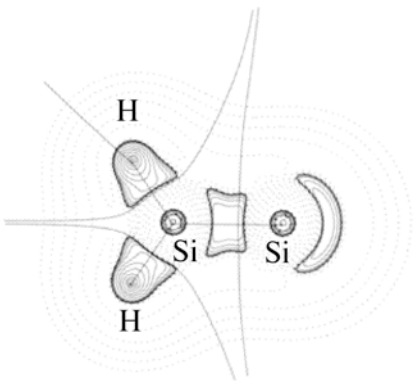

Si_2H_2

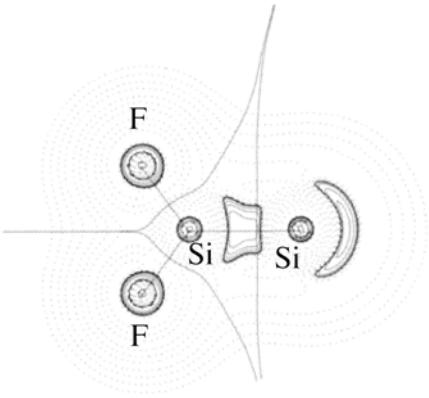

Si_2F_2

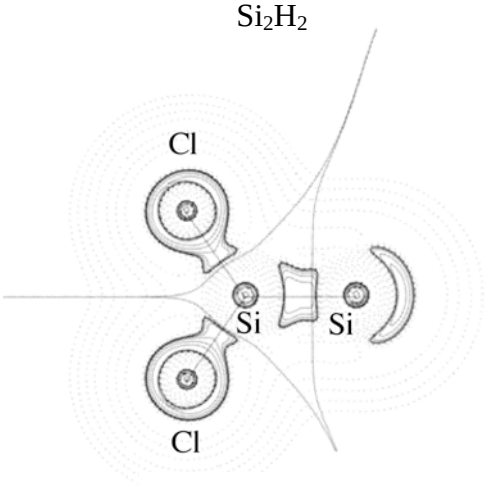

Si_2Cl_2

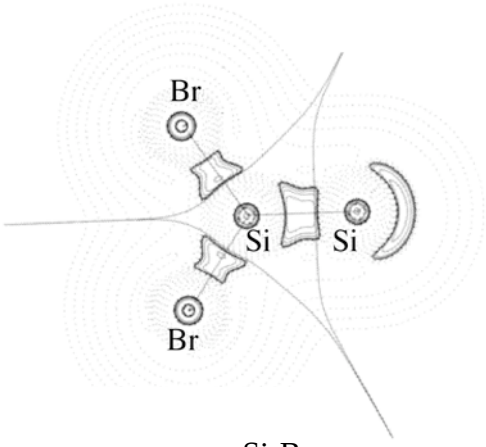

Si_2Br_2

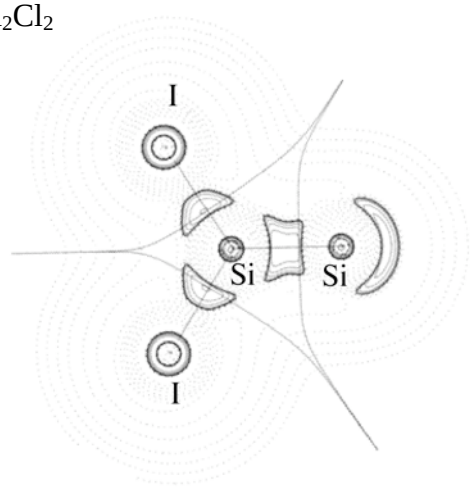

Si_2I_2

Figure 4.1.2.18 Contour line diagram $\nabla^2\rho(r)$ of isomer **SiD**. Solid lines indicate areas of charge concentration ($\nabla^2\rho(r) < 0$), while dashed lines show areas of charge depletion ($\nabla^2\rho(r) > 0$). Solid lines that connect the atomic nuclei are the bond paths, while solid lines that separate the atomic basins give the zero-flux surfaces in the molecular plane.

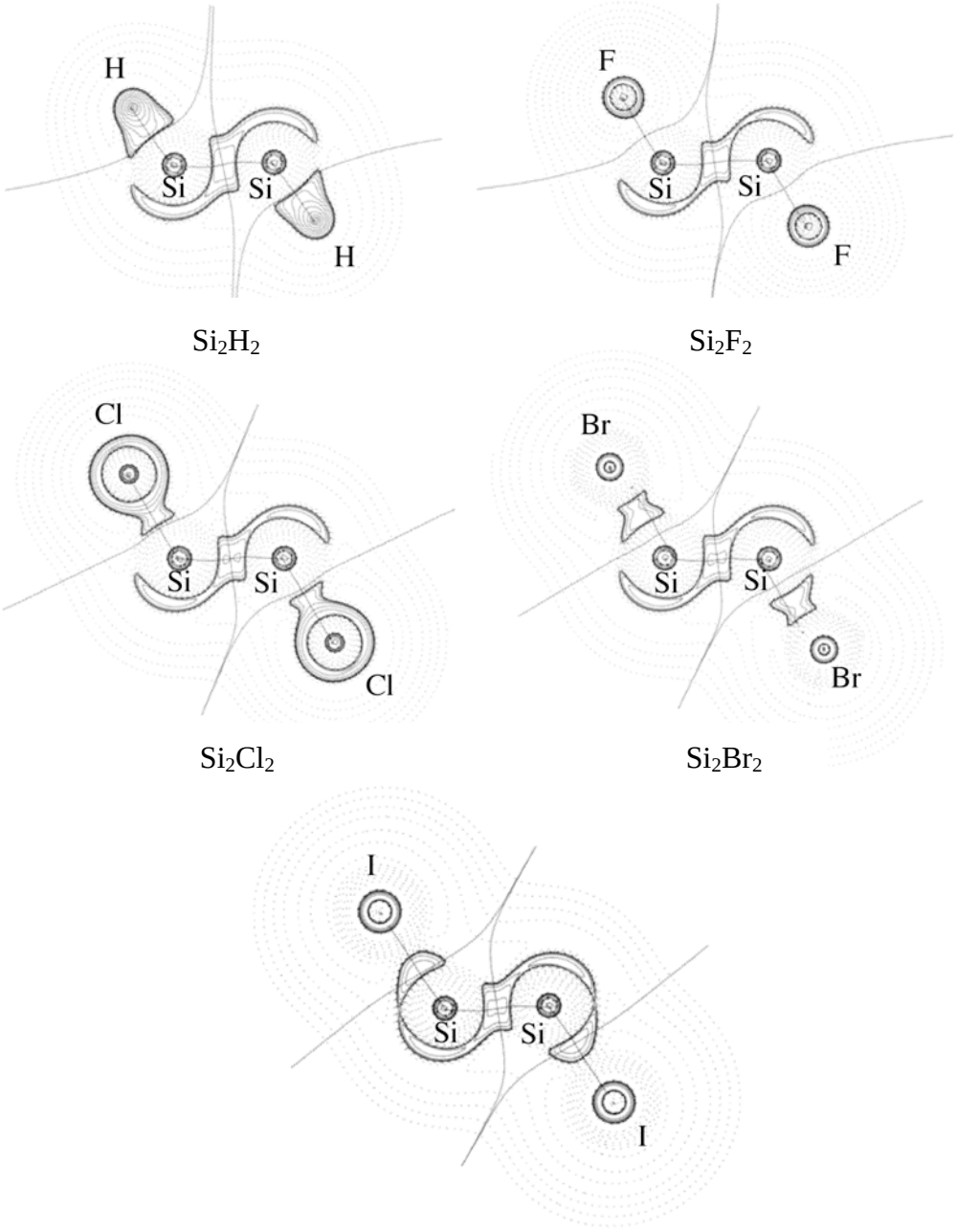

Si_2H_2 Si_2F_2

Si_2Cl_2 Si_2Br_2

Si_2I_2

Figure 4.1.2.19 Contour line diagram $\nabla^2\rho(r)$ of isomer **SiE1**. Solid lines indicate areas of charge concentration ($\nabla^2\rho(r) < 0$), while dashed lines show areas of charge depletion ($\nabla^2\rho(r) > 0$). Solid lines that connect the atomic nuclei are the bond paths, while solid lines that separate the atomic basins give the zero-flux surfaces in the molecular plane.

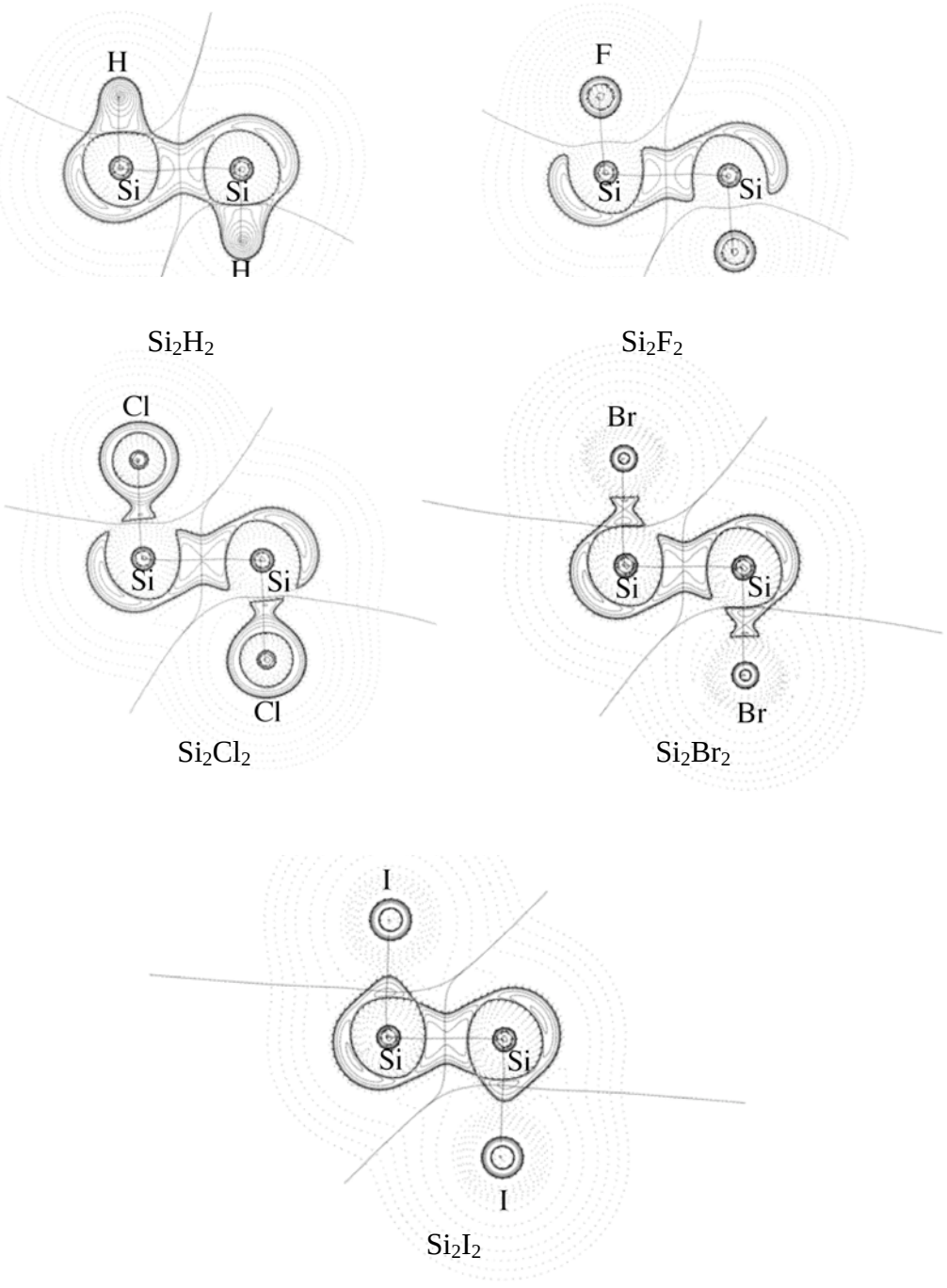

Si_2H_2 Si_2F_2 Si_2Cl_2 Si_2Br_2 Si_2I_2

Figure 4.1.2.20 Contour line diagram $\nabla^2\rho(r)$ of isomer **SiE2**. Solid lines indicate areas of charge concentration ($\nabla^2\rho(r) < 0$), while dashed lines show areas of charge depletion ($\nabla^2\rho(r) > 0$). Solid lines that connect the atomic nuclei are the bond paths, while solid lines that separate the atomic basins give the zero-flux surfaces in the molecular plane.

4.1 Si_2X_2 Molecules

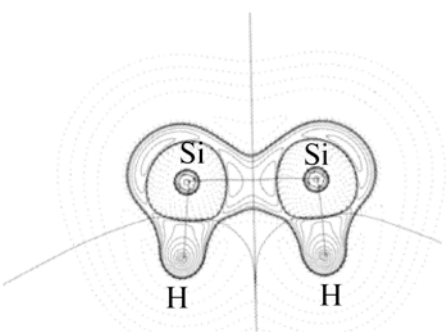

Si_2H_2

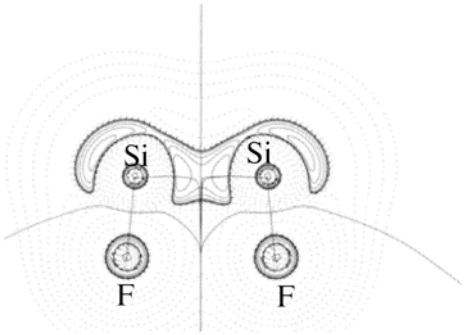

Si_2F_2

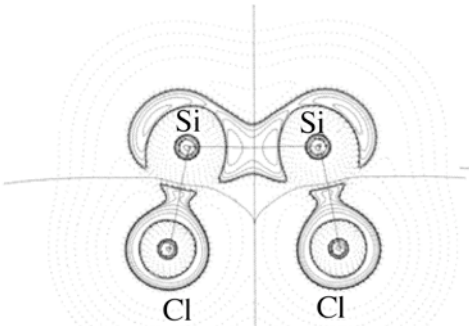

Si_2Cl_2

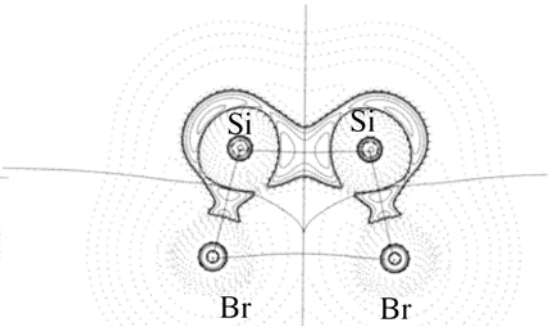

Si_2Br_2

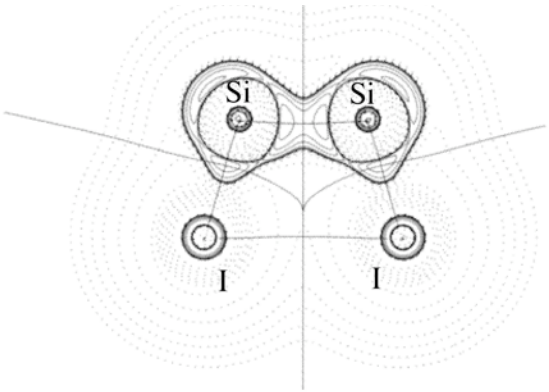

Si_2I_2

Figure 4.1.2.21 Contour line diagram $\nabla^2\rho(r)$ of isomer **SiF1**. Solid lines indicate areas of charge concentration ($\nabla^2\rho(r) < 0$), while dashed lines show areas of charge depletion ($\nabla^2\rho(r) > 0$). Solid lines that connect the atomic nuclei are the bond paths, while solid lines that separate the atomic basins give the zero-flux surfaces in the molecular plane.

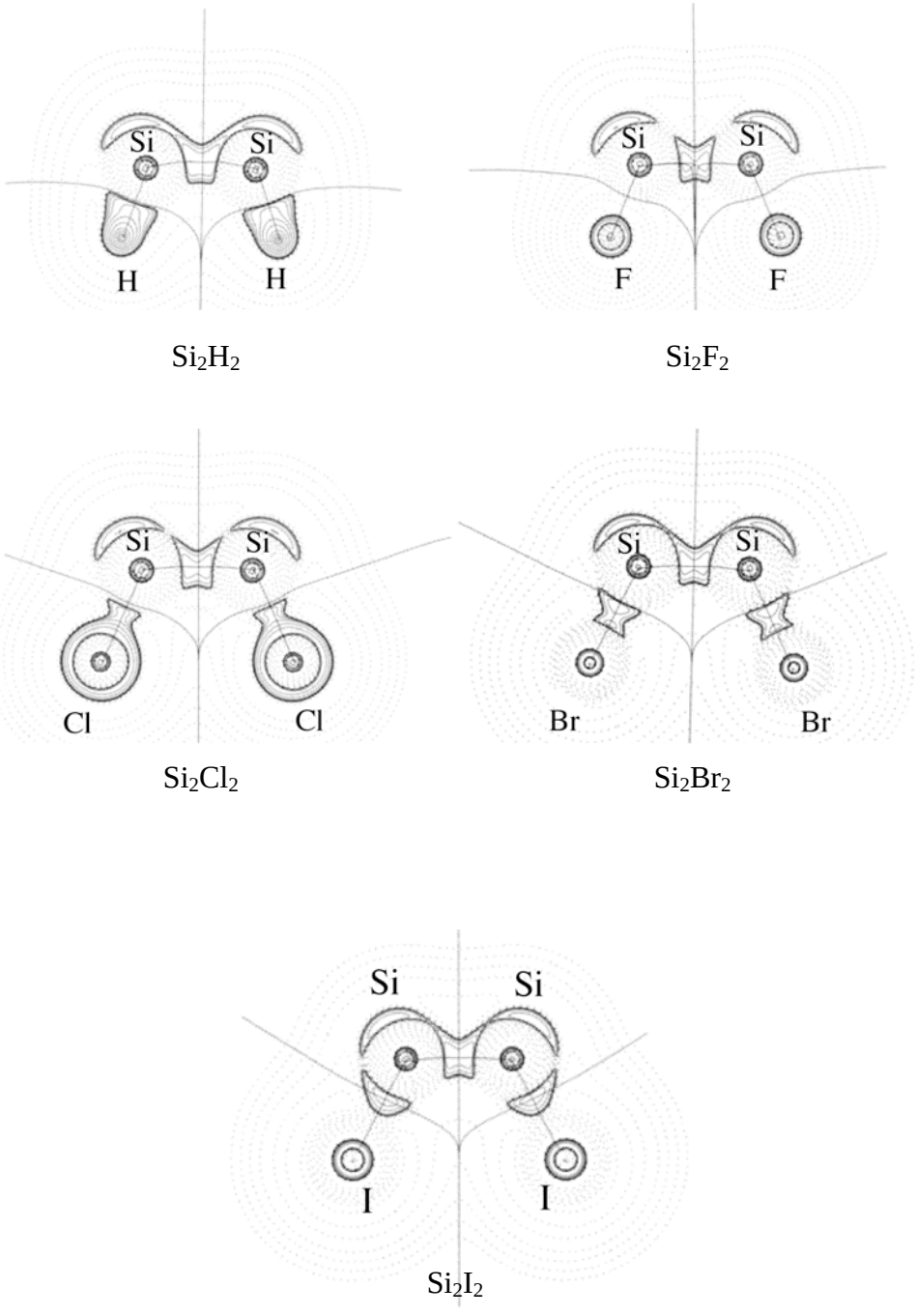

Si_2H_2 Si_2F_2

Si_2Cl_2 Si_2Br_2

Si_2I_2

Figure 4.1.2.22 Contour line diagram $\nabla^2\rho(r)$ of isomer **SiF2**. Solid lines indicate areas of charge concentration ($\nabla^2\rho(r) < 0$), while dashed lines show areas of charge depletion ($\nabla^2\rho(r) > 0$). Solid lines that connect the atomic nuclei are the bond paths, while solid lines that separate the atomic basins give the zero-flux surfaces in the molecular plane.

4.1.2.3. Charge Analyses

The orbital interactions are investigated in the chapter 4.1.2.1 and the orbital interaction with two fragments may explain the geometry of each isomer. Chapter 4.1.2.2 showed the AIM analyses and they presented the bondings and their bonding character. However, the contribution of charge is not clear yet. This chapter shows the charge analyses.

4.1.2.3.1 SiX Fragment

Table 4.1.2.11 shows the computed Hirshfeld charge of the SiX molecules. It is found that the Si atom is always positively charged and that the hydrogen atom and the halogen atom are always negatively charged because the halogen atoms and hydrogen are more electronegative than the Si atom, as expected. The order of charge shift from Si to X is as follows: SiF > SiH > SiCl > SiBr > SiI. The charge analysis of the Si-X molecule shows that the Si-Si donor acceptor interactions are not favorable because of the repulsion of the two dipolar SiX fragments. In the contrast to that, the Si-X donor-acceptor interactions come along with attractive dipole-dipole interactions. This is another reason why the doubly bridged structure is more favorable than the bent structure.

Table 4.1.2.11 Hirshfeld charge of the SiX fragments calculated at BP86/QZ4P level.

	SiH	SiF	SiCl	SiBr	SiI
Si	0.1251	0.1853	0.1152	0.0930	0.0642
X	-0.1251	-0.1853	-0.1152	-0.0930	-0.0642

4.1.2.3.2 Si_2X_2 Isomers

Table 4.1.2.12 shows the Hirshfeld charge of the Si_2X_2 molecules. The Hirshfeld charges show that Si_2F_2 is the most polarized molecule and that Si_2I_2 exhibits a small charge redistribution. This means that the former has more ionic character and the latter has more covalent character, which is in the agreement with the results of AIM. Although the charge distribution has no correlation with the relative energies, it shows the character of each isomer.

Table 4.1.2.12 Calculated Hirshfeld charges at BP86/QZ4P level.

	SiA	**SiB**	**SiC**	**SiE1**	**SiE2**	**SiF1**	**SiF2**	**SiG**	**SiH**
					Si_2H_2				
Si_1	0.0570	0.0746	0.0626	0.0525	0.1216	0.1174	0.1023	0.0029	
Si_2	0.0570	0.0275	0.0626	0.0525	0.1216	0.1174	0.1023	0.0029	
H_1	-0.0570	-0.0587	-0.0626	-0.0525	-0.1216	-0.1174	-0.1023	-0.0029	
H_2	-0.0570	-0.0434	-0.0626	-0.0525	-0.1216	-0.1174	-0.1023	-0.0029	
					Si_2F_2				
Si_1	0.1466	0.2243	0.1438	0.1697	0.1968	0.1889	0.1706	0.1253	0.1944
Si_2	0.1466	0.0978	0.1438	0.1697	0.1968	0.1889	0.1706	0.1253	0.1944
F_1	-0.1466	-0.1604	-0.1438	-0.1697	-0.1968	-0.1889	-0.1706	-0.1253	-0.1944
F_2	-0.1466	-0.1617	-0.1438	-0.1697	-0.1968	-0.1889	-0.1706	-0.1253	-0.1944
					Si_2Cl_2				
Si_1	0.0716	0.1010	0.0900	0.0850	0.1283	0.1187	0.0899	0.0102	
Si_2	0.0716	0.0535	0.0900	0.0850	0.1283	0.1187	0.0899	0.0102	
Cl_1	-0.0716	-0.0813	-0.0900	-0.0850	-0.1283	-0.1187	-0.0899	-0.0102	
Cl_2	-0.0716	-0.0732	-0.0900	-0.0850	-0.1283	-0.1187	-0.0899	-0.0102	
					Si_2Br_2				
Si_1	0.0459	0.0601	0.0660	0.0595	0.1047	0.0963	0.0657	-0.0261	
Si_2	0.0459	0.0352	0.0660	0.0595	0.1047	0.0963	0.0657	-0.0261	
Br_1	-0.0459	-0.0520	-0.0660	-0.0595	-0.1047	-0.0963	-0.0657	0.0261	
Br_2	-0.0459	-0.0433	-0.0660	-0.0595	-0.1047	-0.0963	-0.0657	0.0261	
					Si_2I_2				
Si_1	0.0128	0.0138	0.0260	0.0269	0.0710	0.0660	0.0347	-0.0662	
Si_2	0.0128	0.0167	0.0260	0.0269	0.0710	0.0660	0.0347	-0.0662	
I_1	-0.0128	-0.0203	-0.0260	-0.0269	-0.0710	-0.0660	-0.0347	0.0662	
I_2	-0.0128	-0.0102	-0.0260	-0.0269	-0.0710	-0.0660	-0.0347	0.0662	

SiE2 and **SiF1** show the largest charge separations and they are almost the same as the free SiX fragment. It indicates that they need little change of the charge distribution for the Si-Si bond formation for **SiE2** and **SiF1**. **SiE1** and **SiF2** are also similar bent-structures. However, the charge decreases in these isomers. This indicates that the X atoms have to donate the electron density to the Si atoms to form the Si-Si bond. However, this is an unfavorable situation because the X atoms have large electronegativities.

The ring-structures **SiA** and **SiC** show smaller atomic charges. Although the charge donation form the X atom to the Si atom is considered, the electron donation in the ring-structures is quite favorable because the direction of charge donation is the same as the orbital interaction of orbital analyses. The bridged structure is favorable in the point of intramolecular charge transfer.

4.1.2.3.3 Vinylidene Isomers, **SiD** and **SiD(T)**

Table 4.1.2.13 shows the Hirshfeld charges of the vinylidene structures **SiD** and **SiD(T)**. The charges of **SiD** show that both silicon atoms are positively charged. The charge of Si_1 of Si_2F_2, Si_2Cl_2, Si_2Br_2 and Si_2I_2 becomes less positive as the halogen atom gets heavier, although the charge of Si_2 shows the opposite trend. The table clearly shows the charge transfer from Si_2 to Si_1. This charge transfer becomes larger as the halogen atom gets heavier.

In **SiD(T)**, the Si_2 atoms are always negatively charged. It means the charge donation from Si_1 to Si_2. This is the same direction as the donation of the σ-type orbital, and the donation is favorable. The charges of Si_1 in Si_2F_2, Si_2Cl_2, Si_2Br_2 and Si_2I_2 become smaller as the halogen atom gets heavier.

Table 4.1.2.13 Calculated Hirshfeld charges at BP86/QZ4P level. The Si_1 and Si_2 mean the Si atoms described at the bottom of the table.

Si_2H_2	**SiD**	**SiD(T)**	Si_2F_2	**SiD**	**SiD(T)**
Si_1	0.0485	0.1813	Si_1	0.2901	0.3653
Si_2	0.0721	-0.0332	Si_2	0.0524	-0.0216
H_1	-0.0603	-0.0741	F_1	-0.1713	-0.1718
H_2	-0.0603	-0.0741	F_2	-0.1713	-0.1718
Si_2Cl_2	**SiD**	**SiD(T)**	Si_2Br_2	**SiD**	**SiD(T)**
Si_1	0.1079	0.1934	Si_1	0.0587	0.1465
Si_2	0.0752	-0.0084	Si_2	0.0780	-0.0033
Cl_1	-0.0916	-0.0925	Br_1	-0.0684	-0.0716
Cl_2	-0.0916	-0.0925	Br_2	-0.0684	-0.0716
Si_2I_2	**SiD**	**SiD(T)**			
Si_1	-0.0006	0.0906			
Si_2	0.0782	-0.0007			
I_1	-0.0388	-0.0449			
I_2	-0.0388	-0.0449			

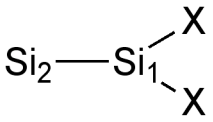

4.1.2.4 Energy Decomposition Analysis

Chapter 4.1.2.1 has shown that the unusual equilibrium geometries **SiA**-**SiG** of Si_2X_2 can be explained in terms of orbital interactions between the SiX fragments in the $X^2\Pi$ ground state. Table 4.1.2.14 and Table 4.1.2.15 give the EDA results for the structures **SiA**, **SiB**, **SiC**, **SiE1**, **SiE2**, **SiF1**, **SiF2** and **SiH** using two SiX molecules in the $X^2\Pi$ ground state as interacting fragments. The $a^4\Sigma$ excited state of SiX is used for the EDA calculations of the structure **SiG**. The $a^4\Sigma \leftarrow X^2\Pi$ excitation energy is then considered as part of the preparation energy of the SiX fragments, which is the reason why the linear species **SiG** have rather large ΔE_{prep} values. The EDA data directly lead to an estimation of the bonding contributions of the σ and π orbital components of the calculated heavier acetylene analogue of the linear form **SiG**.

The EDA results show that **SiA**, **SiB** and **SiC** often show large electrostatic interaction values and large orbital interaction energies. The large electrostatic interaction stems from the large electron charge redistribution of the Si-X molecules (Table 4.1.2.11), which is important in the formation of the Si-X-Si bridged structure. This is consistent with the result of the orbital analyses (chapter 4.1.2.1) and AIM (chapter 4.1.2.2). The large orbital interaction energies show that the Si-X donor-acceptor bond leads to a very effective bonding situation and the Si-X-Si bridging is a desirable structure. These isomers also show relatively large preparation energies and the large preparation energies stem from the formation of the Si-X-Si bridged structure where the Si-X bond is elongated. Si_2F_2 shows quite small orbital interaction energies because of the large energy gap between the Si-F σ bond orbital and the LUMO. Si_2F_2 cannot compensate the increase of the preparation energy by the orbital interactions (Table 4.1.2.3).

The bent structures, **SiE1**, **SiE2**, **SiF1** and **SiF2** often show weaker electrostatic interactions and weaker orbital interactions than the bridged structures **SiA**, **SiB** and **SiC**. The smaller electrostatic interactions of the bent structures are due to the small electrostatic interaction between the two SiX dipoles as explained in chapter 4.1.2.2. The small orbital interactions stem from the less effective orbital interaction than those of the ring structures in the viewpoint of the orbital combinations, as described in the orbital analyses of chapter 4.1.2.1, where **SiE1** and **SiF2** have a π-type bond

and two lone-pair donor acceptor bond, although **SiE2** and **SiF1** have just a σ-type bond. **SiE1** and **SiF2** show smaller electrostatic interactions than **SiE2** and **SiF1** because **SiE1** and **SiF2** have a shorter Si-Si bond and this leads to larger electrostatic repulsions. The orbital interactions for Si_2H_2 and other Si_2X_2 isomers show a different trend in **SiE1** and **SiE2**. The different trends stem from the difference of the energy gap between the lone-pair orbital and the vacant π orbital (Table 4.1.2.3). For **SiE1** and **SiF2**, the orbital interactions of Si_2H_2 and other Si_2X_2 isomers show the same trend, and the orbital interactions of **SiF1** are larger than those of **SiF2** because of ineffective orbital interactions caused by geometrical reasons.

The π isomers, **SiB**, **SiC**, **SiE1** and **SiF2**, have small $\Delta E_{orb}(\pi)$ components and the components indicate that the π orbital interactions are often weak for **SiC** and **SiF2**. Because of the small π orbital interaction, the Si-Si bond of these isomers can easily rotate along the Si-Si axis, and these isomers are found as transition states or higher order saddle points.

Table 4.1.2.14 and Table 4.1.2.15 show that, in general, Si_2H_2 and Si_2F_2 do not follow the correlation of Si_2Cl_2, Si_2Br_2 and Si_2I_2 because of the large polarization of Si-F fragment and the different character of the Si-H bond. The stability of the isomers **SiA, SiB** and **SiC** depends on three important factors: orbital energy, polarizability of the Si-X fragment and the character of the Si-X bond. For Si_2F_2, the electrostatic interaction is very strong, but the orbital interaction is smaller than the expected values from the correlation. For Si_2H_2, the character of the Si-H bond is different from the other SiX bonds because hydrogen has just an *s* orbital, and halogen atoms bind the Si atom with their *p* orbitals. Accounting from that, the Si_2X_2 molecules are categorized into three groups: Si_2H_2, Si_2F_2 and the group of Si_2Cl_2, Si_2Br_2 and Si_2I_2.

Table 4.1.2.14 Energy decomposition analysis of Si_2H_2, Si_2F_2 and Si_2Cl_2 at BP86/QZ4P of the Si-Si bond using two doublet fragments for **SiA**-**SiF2** and **SiH**. Two quartet fragments are used for **SiG** The symmetry in the analysis is C_s except the **SiA** isomer. Energy values are given in kcal/mol.

Term	**SiA**	**SiB**	**SiC**	**SiE1**	**SiE2**	**SiF1**	**SiF2**	**SiG**	**SiH**
					Si_2H_2				
ΔE_{int}	-93.0	-82.3	-77.9	-68.5	-42.4	-40.3	-31.01	-125.78	
ΔE_{Pauli}	276.8	232.3	179.0	164.5	102.0	98.4	84.08	110.76	
ΔE_{elstat}	-136.2	-119.5	-90.6	-84.0	-69.0	-65.2	-24.56	-63.22	
	36.9%	38.0%	35.3%	36.1%	47.8%	47.0%	21.34%	26.73%	
ΔE_{orb}	-233.5	-195.0	-166.4	-149.0	-75.4	-73.5	-90.53	-173.31	
	63.1%	62.0%	64.7%	63.9%	52.2%	53.0%	78.66%	73,27%	
ΔE_{orb}(a')	-233.5	-151.0	-129.4	-107.1	-75.4	-73.48	-57.34	-96.81	
	100.00%	77.5%	77.8%	71.9%	>99.9%	99.98%	63.34%	55.86%	
ΔE_{orb}(a'')		-44.0	-37.0	-41.82	-0.0	-0.02	-33.19	-76.51	
		22.5%	22.2%	28.1%	<0.1%	0.03%	36.66%	44.15%	
ΔE_{prep}	7.0	6.2	3.24	2.5	2.0	2.0	2.0	81.27	
ΔE(=-*De*)	-86.0	-76.1	-74.4	-66.0	-40.4	-38.3	-29.0	-44.51	
					Si_2F_2				
ΔE_{int}	-65.02	-33.05	-20.4	-34.19	-34.81	-32.88	-25.94	-143.19	-35.86
ΔE_{Pauli}	340.53	172.28	205.1	105.01	110.51	100.63	80.19	58.13	79.5
ΔE_{elstat}	-175.85	-75.94	-118.9	-38.03	-74.63	-65.74	-23.17	-18.97	-44.25
	43.36%	36.98%	52.7%	27.32%	51.36%	49.24%	21.84%	9.42%	38.36%
ΔE_{orb}	-229.7	-129.39	-106.6	-101.16	-70.69	-67.76	-82.95	-182.35	-71.1
	56.64%	63.02%	47.3%	72.68%	48.64%	50.76%	78.16%	90.58%	61.64%
ΔE_{orb}(a')	-229.70	-89.80	-103.8	-60.48	-70.25	-67.43	-47.09	-93.28	-71.10
	100.00%	69.40%	97.4%	59.78%	99.38%	99.51%	56.77%	51.16%	100.00%
ΔE_{orb}(a'')		-39.59	-2.8	-40.68	-0.44	-0.33	-35.86	-89.07	
		30.60%	2.6%	40.21%	0.62%	0.49%	43.23%	48.85%	
ΔE_{prep}	33.4	14.1	30.8	2.0	2.1	2.0	2.0	174.23	2.2
ΔE(=-*De*)	-31.6	-19.0	10.3	-32.2	-32.8	-30.1	-23.9	31.04	-33.6
					Si_2Cl_2				
ΔE_{int}	-71.91	-70.57	-18.9	-37.66	-38.18	-34.28	-26.54	-136.69	
ΔE_{Pauli}	341.5	319.34	179.5	119.49	126.54	105.25	86.97	84.64	
ΔE_{elstat}	-172.21	-142.97	-88.50	-46.00	-82.43	-66.82	-27.43	-35.79	
	41.66%	36.67%	44.6%	29.27%	50.04%	47.89%	24.16%	16.17%	
ΔE_{orb}	-241.21	-246.93	-109.9	-111.15	-82.29	-72.71	-86.08	-185.55	
	58.34%	63.33%	55.4%	70.73%	49.96%	52.11%	75.84%	83.83%	
ΔE_{orb}(a')	-241.21	-192.04	-98.6	-70.36	-80.67	-71.85	-51.14	98.52	
	100.00%	77.77%	89.7%	63.30%	98.04%	98.82%	59.41%	53.10%	
ΔE_{orb}(a'')		-54.89	-11.3	-40.79	-1.61	-0.87	-34.94	-87.02	
		22.23%	10.3%	36.70%	1.96%	1.20%	40.59%	46.90%	
ΔE_{prep}	18.2	35.5	23.3	2.1	2.4	2.1	2.1	149.9	
ΔE(=-*De*)	-53.7	-35.1	4.39	-35.5	-35.8	-32.2	-24.5	13.21	

Table 4.1.2.15 Energy decomposition analysis of Si_2Br_2 and Si_2I_2 at BP86/QZ4P of the Si-Si bond using two doublet fragments for **SiA**-**SiF2**. Two quartet fragments are used for **SiG**. The symmetry in the analysis is C_s except the **SiA** isomer. Energy values are given in kcal/mol.

Term	**SiA**	**SiB**	**SiC**	**SiE1**	**SiE2**	**SiF1**	**SiF2**	**SiG**
				Si_2Br_2				
ΔE_{int}	-74.03	-61.46	-20.7	-38.91	-39.82	-34.68	-27.30	-175.04
ΔE_{Pauli}	302.08	282.86	173.3	122.4	135.78	108.42	89.62	88.22
ΔE_{elstat}	-158.52	-125.35	-83.6	-47.5	-87.63	-68.4	-29.27	-38.89
	42.15%	36.41%	43.1%	29.45%	49.90%	47.80%	25.04 %	14.77%
ΔE_{orb}	-217.59	-218.97	-110.5	-113.8	-87.98	-74.7	-87.64	-224.37
	57.85%	63.59%	56.9%	70.55%	50.10%	52.20%	74.96 %	85.23%
ΔE_{orb}(a')	-217.59	-169.60	-95.8	-73.02	-85.46	-73.52	-52.71	-118.58
	100.00%	77.45%	86.7%	64.16%	97.14%	98.42%	60.14%	52.85%
ΔE_{orb}(a")		-49.37	-14.7	-40.79	-2.52	-1.18	-34.93	-105.79
		22.55%	13.3%	35.84%	2.86%	1.58%	39.86%	47.15%
ΔE_{prep}	15.5	23.3	20.6	2.2	2.6	2.2	2.2	184.2
ΔE(=-*De*)	-58.5	-38.1	-0.1	-36.7	-37.2	-32.5	-25.1	9.1
				Si_2I_2				
ΔE_{int}	-76.11	-57.19	-22.5	-41.53	-42.34	-35.28	-28.56	-160.28
ΔE_{Pauli}	298.2	253.8	173.2	128.74	149.49	113.42	94.27	104.3
ΔE_{elstat}	-158.37	-112.79	-82.2	-51.37	-94.87	-70.4	-32.57	-45.72
	42.31%	36.27%	42.0%	30.17%	49.45%	47.34%	26.52%	17.28%
ΔE_{orb}	-215.94	-198.19	-113.5	-118.9	-96.96	-78.3	-90.26	-218.86
	57.69%	63.73%	58.0%	69.83%	50.55%	52.66%	73.48%	82.72%
ΔE_{orb}(a')	-215.94	-152.77	-96.1	-78.19	-92.59	-76.48	-55.59	-117.47
	100.00%	77.08%	84.7%	65.76%	95.49%	97.68%	61.59%	53.67%
ΔE_{orb}(a")		-45.42	-17.4	-40.71	-4.37	-1.82	-34.67	-101.38
		22.92%	15.3%	34.24%	4.51%	2.32%	38.41%	46.32%
ΔE_{prep}	12.3	13.8	16.6	2.2	3.0	2.3	2.3	161.29
ΔE(=-*De*)	-63.8	-43.4	-5.9	-39.3	-39.4	-33.0	-26.3	1.01

4.1 Si_2X_2 Molecules

The order of the dissociation energies of the Si_2H_2 isomers is as follows: **SiA** > **SiB** > **SiC** > **SiD** > **SiE1** > **SiG** > **SiE2** > **SiF1** > **SiF2**. **SiA** has the largest dissociation energy and the order is consistent with the relative energies. The bridged structures **SiA**, **SiB** and **SiC** show large electrostatic interactions ΔE_{elstat} and large orbital interactions ΔE_{orb}. The large ΔE_{elstat} values of the bridged structures are due to the large dipole-dipole interactions between the two Si-H fragments, where the Si-H fragment is a dipole described in chapter 4.1.2.1.1. The large ΔE_{orb} values stem from the three-center-two-electron bonding of the Si-X donor-acceptor interaction. The stability of **SiA** is determined by the favorable bonding situation and the large electrostatic interaction. The stabilities of **SiE1**, **SiE2**, **SiF1** and **SiF2** are decided by the smaller electrostatic interactions and the smaller orbital interactions. In the bent-structures, the hydrogen atoms are away from the Si-Si bond and the electrostatic interaction between Si and H cannot compensate the electrostatic repulsion between two positively charged Si atoms. It leads to small electrostatic interactions. **SiE1** and **SiF2** have two lone-pair donor-acceptor bonds and one π type interaction, although **SiE2** and **SiF1** have just one σ type orbital. **SiE2** and **SiF1** show similar values for ΔE_{orb} and ΔE_{elstat}, because these isomers have the same σ type interaction, as explained in the orbital analysis (chapter 4.1.2.1.2). The difference is just the relative position of the Si-H fragment. Apart from **SiE2** and **SiF2**, **SiF2** presents moderately smaller values for ΔE_{elstat} and ΔE_{orb} than **SiE1**, although **SiF2** is the cis isomer of **SiE1**. The SiH fragments are parallel in **SiF2** and this configuration is unfavorable in the point of electrostatic interactions. For that reason, the ΔE_{elstat} of **SiF2** is smaller than that of **SiE1**. The qualitative models of Figure 4.1.2.9 show the orbital interactions of **SiE1** and **SiF2** between two SiH fragments. The model (f) indicates that two SiH fragments rotate into the same direction to form the lone-pair donor-acceptor interactions. This rotation enhances the lone-pair donor-acceptor interaction in the point of orbital interactions. On the other hand, the model (g) exhibits that two SiH fragments rotate into the different direction with each other and this rotation weakens the lone-pair donor-acceptor interaction. As a result, the ΔE_{orb} value of **SiF2** becomes smaller than that of **SiE1**. The large interaction energy of **SiG** stems from the large orbital energy due to the ideal triple bond. However, **SiG** is an unstable isomer because of the large excitation energy.

Si_2F_2 shows a different trend for the dissociation energies from Si_2H_2 and it

exhibits the following order of dissociation energies: **SiH** > **SiE2** > **SiE1** > **SiA** > **SiF1** > **SiF2** > **SiB** > **SiC** > **SiG**. **SiH** shows the largest dissociation energy of all Si_2F_2 isomers. This order correlates with the stability of the Si_2F_2 isomers in chapter 4.1.1.1. The bridged structures **SiA**, **SiB** and **SiC** show large electrostatic interactions, ΔE_{elstat}, and large orbital interactions, ΔE_{orb}, which are similar to those of Si_2H_2. However, **SiA**, **SiB** and **SiC** show large preparation energies, which stems from the elongation of the Si-F bond which is necessary to form the Si-F-Si bridged structure. As a result, the Si-X-Si bridged structures become unfavorable and the bent-structures become relatively stable. The order of bent structures, **SiE1**, **SiE2**, **SiF1** and **SiF2** is different from Si_2H_2. **SiE1** has a smaller dissociation energy than **SiE2**. The difference comes from the orbital energy gap of the Si-X fragments between the σ-lone-pair orbital and vacant π-orbital, $\Delta E_{\pi\text{-lone-pair}}$. In SiF, $\Delta E_{\pi\text{-lone-pair}}$ is larger than that of SiH, and the lone-pair donor acceptor interaction is weaker than that in Si_2H_2. The dissociation energy of **SiH** is the largest of the Si_2F_2 isomers. The orbital interaction of **SiH** is quite similar to that of **SiE2**, which arises from the same σ-type interaction. The electrostatic interaction of **SiH** is ca. 30 kcal/mol smaller than that of **SiE2**, because the conformation leads to a larger electrostatic repulsion between the F atoms. However, the energetic loss is compensated by the smaller Pauli repulsion. As a result, **SiH** becomes the favorable structure. **SiG** has an ideal triple bond and it shows a large interaction energy and the orbital energy. However, **SiG** is an unfavorable isomer because of the quite large excitation energy, which is similar to Si_2H_2, but **SiG** of Si_2F_2 shows large negative dissociation energy because of the larger excitation energy.

The group of Si_2Cl_2, Si_2Br_2 and Si_2I_2 shows the trend between Si_2H_2 and Si_2F_2, and it shows the order of the dissociation energies as follows: **SiA** > (**SiB**, **SiE2**) > **SiE1** > **SiF1** > **SiF2** > **SiC** > **SiG**. The **SiA** isomers have the largest dissociation energies and this order is consistent with the stability of the isomers of Si_2Cl_2, Si_2Br_2 and Si_2I_2. For the bridged isomers, the dissociation energies show a clear correlation with the preparation energies. The dissociation energy becomes larger as the preparation energy gets smaller. For **SiA** isomers, the electrostatic interactions and the orbital interactions exhibit a clear correlation with the charge of the SiX molecules and the orbital energy of the Si-X bond, respectively. The dissociation energies of **SiC** show a correlation with the orbital interactions. The dissociation energy becomes

larger as the orbital interaction increases. The bridged structures **SiA**, **SiB** and **SiC** show large electrostatic interactions, ΔE_{elstat} and large orbital interactions ΔE_{orb}. However, the preparation energies are large, too. **SiA** is still global minima for these isomers due to the large electrostatic interaction and the orbital interaction, but the other bridged isomers become less stable due to the large preparation energies. The trans bent structures show a similar trend to those of Si_2F_2. The dissociation energy of **SiE1** and **SiF2** has a correlation with the orbital energy, and the dissociation energy becomes larger as the orbital energy becomes larger. The orbital energy term shows that the π-bonding components (a") are quite similar in the **SiE2** and **SiF1** molecules, and the difference comes from the part of the lone-pair donor-acceptor interaction (a'). The difference of the orbital interaction stems from the energy gap between the lone-pair and the vacant π orbital of the Si-X fragments. The orbital energy correlates with the orbital energy gap $\Delta E_{\pi\text{-lone-pair}}$, and the $\Delta E_{orb}(\sigma)$ energy becomes larger as the $\Delta E_{\pi\text{-lone-pair}}$ value gets smaller. The preparation energies are almost constant for **SiE1** and **SiF2**.

The EDA results shows that the Si_2X_2 molecules of **SiA**, **SiB**, **SiC**, **SiE1**, **SiE2**, **SiF1**, **SiF2**, **SiG** and **SiH** are categorized into three groups and the categories are the same group as the relative energies, where the categories are same as those of relative energies.

It was presented in chapter 4.1.1 that **SiA** is the most stable isomer for Si_2H_2, Si_2Cl_2, Si_2Br_2 and Si_2I_2, and **SiD(T)** is the most stable isomer of Si_2F_2. In this chapter, EDA result showed that the **SiA** of Si_2F_2 cannot be the most stable isomer because the energetic loss during the elongation of the Si-F bond is quite large and the energetic gain from the formation of Si-X-Si bridging cannot compensate the energetic loss. Due to that, the bridged structures become unfavorable and the other isomers get more stable.

Table 4.1.2.16, Table 4.1.2.17 and Table 4.1.2.18 give the EDA results for the vinylidene structures, **SiD** and **SiD(T)** using SiX_2 and a Si atom as fragments. For **SiD**, the fragment has two possible orbital interactions as shown in chapter 4.1.2.1. One is the covalent model (m) and the other is the donor-acceptor model (n). The isomers of **SiD(T)** have just a donor-acceptor model (o). For each model, the isomer of Si_2H_2 shows the largest dissociation energy, which stems from the large

electrostatic interaction. For the halogen isomers, the bond strength correlates with the halogen atoms, and the dissociation energies become larger as the halogen atom gets heavier.

The vinylidene isomers of **SiD** are categorized into two groups: Si_2H_2 and the other isomers. Si_2H_2 prefers the covalent Si-Si double bond because the covalent bond model shows a smaller orbital interaction energy and a smaller preparation energy. The group of Si_2F_2, Si_2Cl_2, Si_2Br_2 and Si_2I_2 shows a different trend. The isomers of **SiD** prefer the donor acceptor Si-Si double bond, because the model (o) gives smaller ΔE_{orb} values and smaller ΔE_{prep} values. The different behavior of the preparation energy stems from the ground state of the SiX_2 molecules, where the ground state of Si_2H_2 is a triplet although that of Si_2F_2, Si_2Cl_2, Si_2Br_2 and Si_2I_2 is singlet (chapter 4.1.2.1).

The EDA results of the covalent model (m) show that the dissociation energy correlates with the electrostatic interactions, and the D_e value becomes larger as the ΔE_{elstat} value gets larger. The preparation energy and the orbital interaction energy show a correlation with the mass of the halogen atom, and the ΔE_{prep} value becomes smaller and the ΔE_{orb} value becomes larger as the halogen atom gets heavier. The analysis of the ΔE_{orb} value shows that the σ-interaction correlates with the halogen atom, but π interaction is nearly constant. It indicated that the halogen atom has an effect on the σ-interaction in the model (m). The results of the donor-acceptor model (n) show a correlation between the dissociation energy and the orbital energy, and the D_e value becomes larger as the ΔE_{orb} value gets larger. The electrostatic interactions are nearly constant and they do not show a clear correlation. The analysis of ΔE_{orb} shows that both σ and π interactions become larger as the halogen atom gets heavier for model (n).

The **SiD(T)** isomer shows a clear correlation of the dissociation energy with the electrostatic interaction, and the D_e value becomes larger as the ΔE_{orb} value gets larger. The electrostatic interaction does not show a clear correlation, which is similar to that of **SiD**. The analysis of the orbital interaction presents the correlation of each component with the halogen atom, and both σ– and π– interactions become larger as the halogen atom gets heavier, which is similar to the donor-acceptor model of **SiD**.

The comparison of **SiD** with **SiD(T)** presents that the **SiD** isomer of Si_2H_2 shows much larger dissociation energies than in **SiD(T)**. The dissociation energies for **SiD** of Si_2F_2, Si_2Cl_2, Si_2Br_2 and Si_2I_2 are still larger, but the differences are smaller. Especially, the difference between **SiD** and **SiD(T)** for Si_2F_2 is quite small. The preparation energies are smaller for **SiD(T)** than for **SiD**. The EDA results agree with the orbital analyses of **SiD** and **SiD(T)**.

As a summary, Si_2H_2 prefers the **SiD** structure with the electron-sharing bond due to the smaller orbital interaction and smaller preparation energies. **SiD** of Si_2F_2, Si_2Cl_2, Si_2Br_2 and Si_2I_2 show slightly larger electrostatic interaction and orbital interaction than **SiD(T)**. However, the preparation energies of **SiD(T)** are smaller than those of **SiD**.

Table 4.1.2.16 Energy decomposition analysis of Si_2H_2 and Si_2F_2 at BP86/QZ4P of the Si-Si bond using Si atom and SiX_2 fragment for **SiD** and **SiD(T)**. The symmetry in the analyses is C_{2v}. Energy values are given in kcal/mol.

	Si_2H_2		
	SiD		**SiD(T)**
Term	covalent	donor-acceptor	donor-acceptor
ΔE_{int}	-86.94	-101.37	-49.66
ΔE_{Pauli}	158.57	165.24	136.22
ΔE_{elstat}	-113.48	-100.57	-79.94
	46.22%	37.72%	43.01%
ΔE_{orb}	-132.03	-166.05	-105.94
	53.78%	62.28%	56.99%
$\Delta E_{orb}(\sigma)$	-95.92	-101.82	-83.75
	(72.65%)	(61.32%)	(79.06%)
$\Delta E_{orb}(\delta)$	0.00	0.00	0.00
	(0.00%)	(0.00%)	(0.00%)
$\Delta E_{orb}(\pi_{\|\|})$	-3.25	-3.24	0.09
	(2.46%)	(1.95%)	(0.08%)
$\Delta E_{orb}(\pi_{\perp})$	-32.86	-60.98	-22.28
	(24.89%)	(36.73%)	(21.03%)
ΔE_{prep}	13.76	28.19	4.19
$\Delta E(=-D_e)$	-73.18	-73.18	-45.47
	Si_2F_2		
	SiD		**SiD(T)**
Term	covalent	donor-acceptor	donor-acceptor
ΔE_{int}	-103.49	-58.20	-23.11
ΔE_{Pauli}	115.53	127.09	116.19
ΔE_{elstat}	-90.58	-64.31	-57.9
	41.36%	34.71%	41.56%
ΔE_{orb}	-128.44	-120.98	-81.41
	58.64%	65.29%	58.44%
$\Delta E_{orb}(\sigma)$	-89.78	-74.98	-66.35
	(69.90%)	(61.98%)	(81.51%)
$\Delta E_{orb}(\delta)$	-0.05	-0.01	0.00
	(0.04%)	(0.01%)	(0.00%)
$\Delta E_{orb}(\pi_{\|\|})$	-0.85	-0.84	-1.92
	(0.66%)	(0.69%)	(2.36%)
$\Delta E_{orb}(\pi_{\perp})$	-37.75	-45.15	-13.13
	(29.39%)	(37.32%)	(16.13%)
ΔE_{prep}	74.18	28.89	1.15
$\Delta E(=-D_e)$	-29.31	-29.31	-21.96

Table 4.1.2.17 Energy decomposition analysis of Si_2Cl_2 and Si_2Br_2 at BP86/QZ4P of the Si-Si bond using Si atom and SiX_2 fragment for **SiD** and **SiD(T)**. The symmetry in the analyses is C_{2v}. Energy values are given in kcal/mol.

	Si_2Cl_2		
	SiD	**SiD(T)**	
term	covalent	donor-acceptor	donor-acceptor
ΔE_{int}	-92.89	-68.00	-29.00
ΔE_{Pauli}	141.78	132.29	116.84
ΔE_{elstat}	-98.63	-67.79	-58.5
	42.03%	33.85%	40.11%
ΔE_{orb}	-136.03	-132.5	-87.33
	57.97%	66.15%	59.89%
$\Delta E_{orb}(\sigma)$	-97.27	-79.88	-69.1
	(71.51%)	(60.29%)	(79.12%)
$\Delta E_{orb}(\delta)$	-0.07	-0.02	-0.01
	(0.05%)	(0.02%)	(0.01%)
$\Delta E_{orb}(\pi_{\|\|})$	-2.44	-2.34	-2.39
	(1.79%)	(3.54%)	(2.74%)
$\Delta E_{orb}(\pi_{\perp})$	-36.25	-50.26	-15.83
	(26.65%)	(37.93%)	(18.13%)
ΔE_{prep}	54.89	30.00	1.51
$\Delta E(=-D_e)$	-38.00	-38.00	-27.49
	Si_2Br_2		
	SiD	**SiD(T)**	
term	covalent	donor-acceptor	donor-acceptor
ΔE_{int}	-89.8	-69.45	-29.9
ΔE_{Pauli}	150.83	131.71	115.27
ΔE_{elstat}	-100.36	-66.16	-56.46
	41.71%	0.3289	38.89%
ΔE_{orb}	-140.27	-135.00	-88.71
	58.29%	0.6711	61.11%
$\Delta E_{orb}(\sigma)$	-100.44	-80.31	-69.34
	(71.61%)	(59.49%)	(78.16%)
$\Delta E_{orb}(\delta)$	-0.08	-0.02	-0.01
	(0.06%)	(0.01%)	(0.01%)
$\Delta E_{orb}(\pi_{\|\|})$	-3.53	-3.29	-2.97
	(2.52%)	(2.44%)	(3.35%)
$\Delta E_{orb}(\pi_{\perp})$	-36.21	-51.39	-16.4
	(25.82%)	(0.39%)	(18.49%)
ΔE_{prep}	50.39	30.04	1.44
$\Delta E(=-D_e)$	-39.41	-39.41	-28.46

Table 4.1.2.18 Energy decomposition analysis of Si_2I_2 at BP86/QZ4P of the Si-Si bond using Si atom and SiX_2 fragment for **SiD** and **SiD(T)**. The symmetry in the analyses is C_{2v}. Energy values are given in kcal/mol.

	Si_2I_2		
	SiD		**SiD(T)**
term	covalent	donor-acceptor	donor-acceptor
ΔE_{int}	-85.43	-73.51	-32.4
ΔE_{Pauli}	164.83	133.39	114.89
ΔE_{elstat}	-104.44	-66.29	-55.53
	41.73%	32.04%	37.70%
ΔE_{orb}	-145.82	-140.61	-91.76
	58.27%	67.96%	62.30%
$\Delta E_{orb}(\sigma)$	-104.31	-82.39	-70.71
	(71.53%)	(58.59%)	(77.06%)
$\Delta E_{orb}(\delta)$	-0.09	-0.02	0.00
	(0.06%)	(0.01%)	(0.00%)
$\Delta E_{orb}(\pi_{\|\|})$	-5.32	-5.00	-3.64
	(3.65%)	(3.56%)	(3.97%)
$\Delta E_{orb}(\pi_{\perp})$	-36.09	-53.20	-17.40
	(24.75%)	(37.84%)	(18.96%)
ΔE_{prep}	42.50	30.54	1.45
$\Delta E(=-D_e)$	-42.97	-42.97	-30.95

4.1.3 Summary

In chapter 4.1, the results of the investigated Si_2X_2 isomers are shown. The geometries and the relative energies are discussed in chapter 4.1.1 and the doubly bridged structures, **SiA**, are the global minima for Si_2H_2, Si_2Cl_2, Si_2Br_2 and Si_2I_2, while the vinylidene structure in the triplet state, **SiD(T)**, is the global minimum for Si_2F_2. The order of the stability for the isomers showed that the bridged structures are unfavorable for Si_2F_2 and the isomers are shifted to the energetically unstable direction.

The analyses of the SiX fragments showed that the SiX fragments have very high excitation energies from the $X^2\Pi$ ground state to the $a^4\Sigma^-$ excited state. Due to that, the linear structure is unfavorable and the SiX fragments prefer the bond formation in the $X^2\Pi$ ground state. The orbital analyses showed that the qualitative model of the Si_2X_2 isomers from two SiX fragments gives a good understanding of the bonding situation. **SiA** has three bonding components: one σ-bond and two Si-X bond donor-acceptor bonds, and **SiA** shows most effective bond situation.

AIM analyses showed the bridged structures of **SiA**, **SiB** of Si_2F_2 and **SiC**. The charge accumulation presented the difference of the bonding situations of two types of bent-structures: **SiE1**, **SiF2** and **SiE2**, **SiF1**. **SiE1** and **SiE2** present the different pictures of charge accumulation for **SiE2** and **SiF1**. The different pictures indicate the different bond situations of these isomers as described in the orbital analyses. This agrees with the results of the orbital analyses.

Charge analyses of the SiX fragments presented the large dipole character of the SiX molecules, and the charge becomes larger as the halogen atom gets heavier. The large electrostatically polarized SiX molecules lead to the large dipole-dipole interaction, and the interaction enhances the bridged structures. The analyses of Si_2X_2 presented that the bent structures are unfavorable due to the large intramolecular charge transfer to form the Si-Si bond, although the bridged structure is favorable because the direction of charge transfer is the same as that of the donor-acceptor bond.

The results of the EDA showed that the dissociation energy correlates with the

stability of the Si_2X_2 isomers. The doubly bridged structure **SiA** has the largest dissociation energy for Si_2H_2, Si_2Cl_2, Si_2Br_2 and Si_2I_2. The large dissociation energies stem from the large orbital interaction energies from the Si-X bond donor-acceptor and the electrostatic interaction between two SiX dipoles. In Si_2F_2, the bridged structures are not the favorable structures because the donor-acceptor bond formation needs much larger energy to elongate the SiF bond. Due to that, the bridged structures become unstable and the other isomers become relatively more stable.

4.2 Ge_2X_2 Molecules (X=H, F, Cl, Br and I)

4.2.1 Geometries and Relative Energies

Figures 4.2.1.1 – Figure 4.2.1.9 show the optimized geometries of several isomers of Ge_2X_2 (X=H, F, Cl, Br and I). The singlet isomers **GeA-GeG** and the triplet isomers **GeA(T)-GeG(T)** and **GeI(T)** are optimized at BP86/QZ4P. Table 4.2.1.1, Table 4.2.1.2 and Table 4.2.1.3 show the relative energies of the stationary points on the singlet potential energy surface calculated with BP86/QZ4P. Additionally to this, single point energies for singlets were calculated with HF, MP2, SCS-MP2, MP4, CCSD and CCSD(T). For these calculations, the aug-cc-pVQZ basis set was used. Table 4.2.1.4 and Table 4.2.1.5 show the energies of the stationary points on the triplet potential energy surface calculated with BP86/QZ4P. The single point energies for triplets were calculated with HF, MP2, SCS-MP2, MP4, RCCSD and RCCSD(T) and the aug-cc-pVQZ basis sets was used for these calculation. The energies are relative to the isomer **GeA**, which is the global minimum of Ge_2H_2. The results in Table 4.2.1.1 – Table 4.2.1.5 and figure show that the optimized geometries and relative energies are in agreement with previous theoretical calculations of Ge_2H_2 and Ge_2F_2 at DFT [21, 29, 64, 87] and ab initio levels [15, 26, 27, 28, 29].

4.2.1.1 Singlet Isomers of Ge_2X_2

Scheme 4.2.2.1 shows the types of different isomers of Ge_2X_2 investigated here and they are denoted as follows: non-planer doubly bridged structure (**GeA**), singly bridged planar structure (**GeB**), planar doubly bridged structure (**GeC**), vinylidene structure (**GeD**), trans-bent structure (**GeE**), cis-bent structure (**GeF**) and linear structure (**GeG**). The structural trend of Ge_2X_2 is relatively similar to the trend of Si_2X_2.

The non-planar doubly bridged structures of **GeA** have C_{2v} symmetry and these isomers are the global minima for all Ge_2X_2 isomers, which is similar to the comparable isomers for Si_2H_2, Si_2Cl_2, Si_2Br_2 and Si_2I_2 of **SiA** (Figure 4.2.1.1). The Ge-Ge bond lengths and Ge-X-Ge angles have a correlation and they become longer and larger as the X atom gets heavier. Figure 4.2.1.1 shows the Ge-X bond length of

GeX fragments and the difference of the bond lengths suggests that the Ge-X bond is elongated to form the Ge-X-Ge bridged structure, as the halogen atom X is lighter. Ge_2H_2 is an outlier of the correlation, because of the different character of the Ge-X bond, which is discussed later in chapter 4.2.2.1. The trend of **GeA** is similar to **SiA** in the structural points.

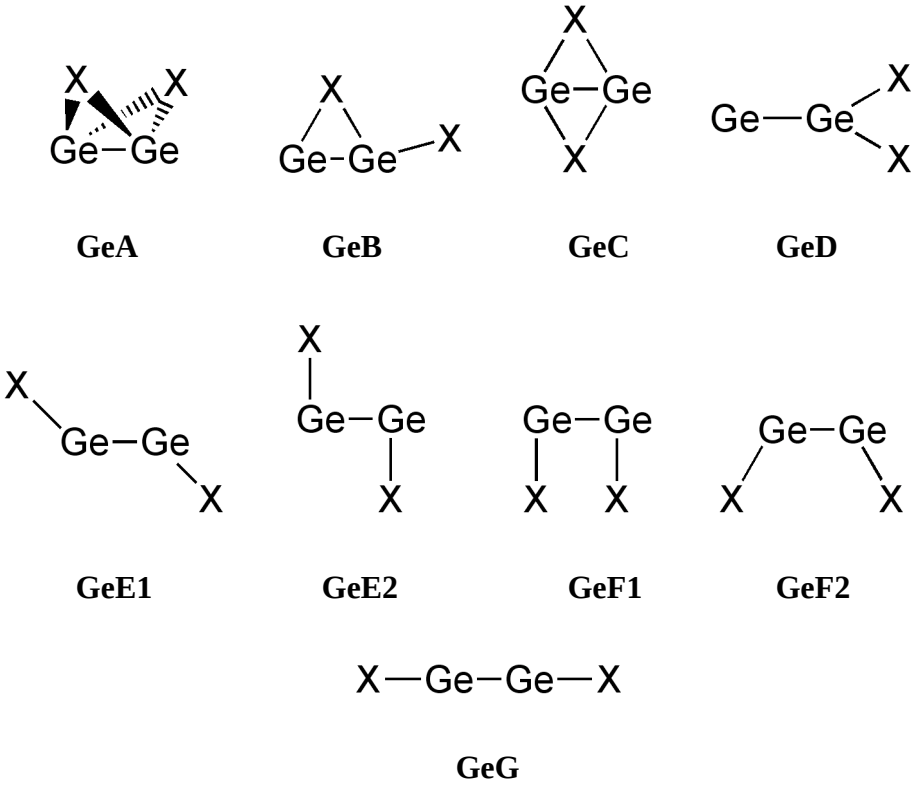

GeA **GeB** **GeC** **GeD**

GeE1 **GeE2** **GeF1** **GeF2**

GeG

Scheme 4.2.1.1. Investigated singlet isomers of Ge_2X_2

The singly bridged planar structures of **GeB** have C_s symmetry, and this isomer is predicted as a minimum for Ge_2H_2 and Ge_2I_2 (Figure 4.1.1.1), which is similar to Si_2H_2 and Si_2I_2. For Ge_2F_2, Ge_2Cl_2 and Ge_2Br_2, the structure **GeB** is a transition state and it has one imaginary frequency, where the isomers of Si_2Cl_2 and Si_2Br_2 are local minima. The Ge-Ge bond lengths and the Ge-X-Ge angles correlate with the large halogen atoms and the Ge-Ge bond becomes longer as the halogen atom gets heavier. However, the Ge-Ge bond lengths of Ge_2Cl_2, Ge_2Br_2 and Ge_2I_2 are nearly constant. The Ge-Ge bond of Ge_2H_2 is the exception of the correlation, and it is due to the different Si-X-Si bridging situation, which is discussed later. The Ge-X bond lengths show that the X atom in the ring interacts with both Ge atoms in all Ge_2X_2 molecules, which is similar to Si_2H_2, Si_2F_2 and Si_2I_2, whereas the Si(side)-Cl and Si(side)-Br

bonds of **SiB** are almost broken.

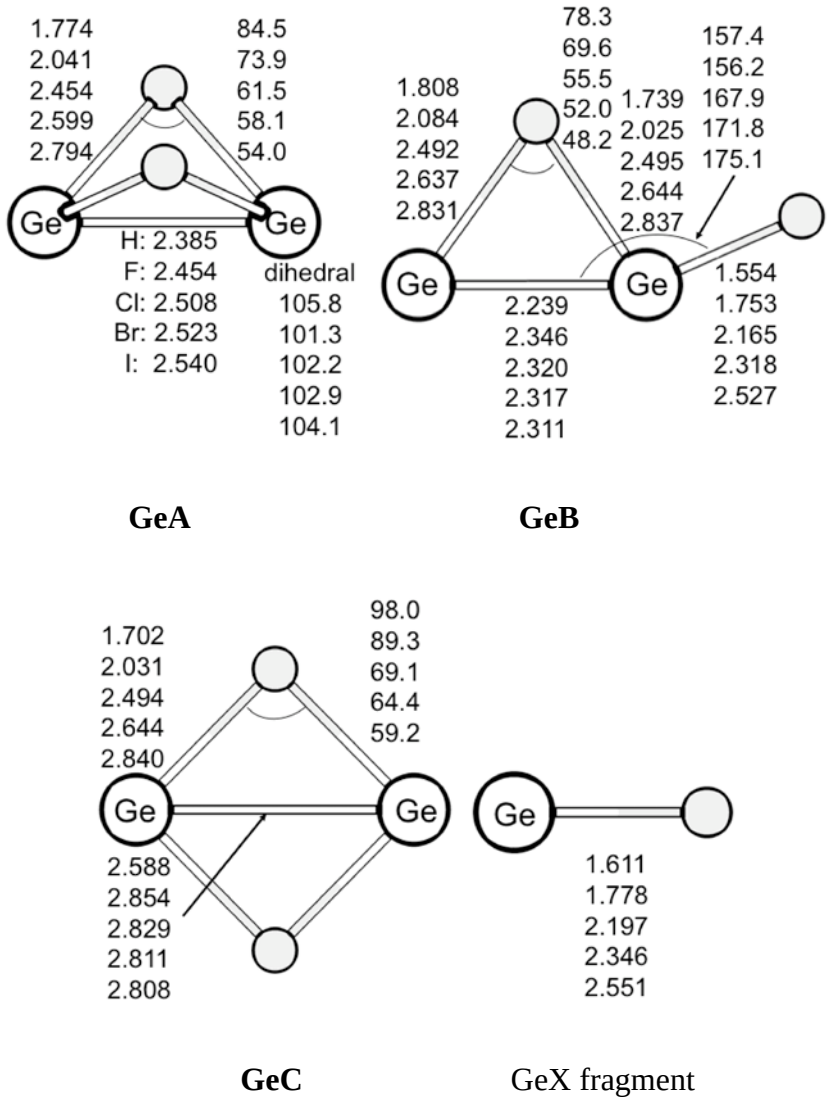

Figure 4.2.1.1. Optimized bridged structures in their singlet state, **GeA**, **GeB** and **GeC**, and Ge-X fragments in their $X^2\Pi$ ground state, calculated with BP86/QZ4P level. The bond lengths are given in Å and the angles are given in degree.

The planar doubly bridged structures **GeC** have D_{2h} symmetry and they are transition states in all cases except for Ge_2I_2 (Figure 4.2.1.1). In Ge_2I_2, the isomer is found as a minimum, where the isomers of **SiB** are found as transition states. A correlation is found between the Ge-Ge bonds and the Ge-X-Ge angles. The bond

lengths and the angles become shorter and smaller with the heavier halogen atoms. The Ge-Ge bond of Ge_2H_2 is not the longest because of the different Ge-X-Ge bridging situation. When the Ge-Ge bond lengths are considered, the two Ge atoms of Ge_2H_2 still interact, and the Ge-Ge interaction is very weak in Ge_2F_2, Ge_2Cl_2, Ge_2Br_2 and Ge_2I_2. The trend of the Ge-Ge bond is similar to that of the Si-Si bond. The Ge-X bonds become weaker than those of the GeX molecules to form the Ge-X-Ge bridged structure. Considering these points, it is found that the Ge-Ge bond lengths depend on the halogen atoms, because the main interaction take place in the Ge-X-Ge bridged structure, which is similar to the Si_2X_2 system.

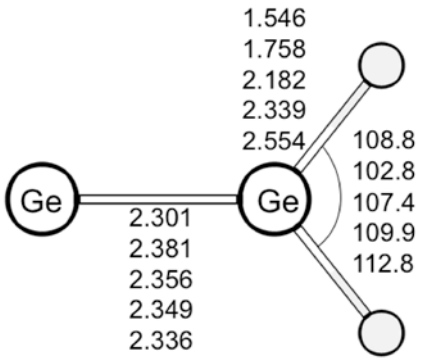

GeD

Figure 4.2.1.2. Optimized structures in the singlet state, **GeD** calculated with BP86/QZ4P level. The bond lengths are given in Å and the angles are given in degree.

The vinylidene structures **GeD** have C_{2v} symmetry and they are local minima for Ge_2H_2, Ge_2F_2 and Ge_2Cl_2 (Figure 4.2.1.2). For Ge_2Br_2 and Ge_2I_2, these isomers are transition states. This is similar to the **SiD** isomers of Si_2X_2 except for Si_2Br_2, where the isomer of Si_2Br_2 is a local minimum. The Ge-Ge bond becomes shorter as the halogen atom gets heavier, but the difference is very small, which is similar to **SiD**.

The trans-bent structure has two types of isomers, **GeE1** and **GeE2**, which both have C_{2h} symmetry (Figure 4.2.1.3). The isomer **GeE1** of Ge_2H_2 is predicted as a minimum and the other trans-bent structures **GeE1** of Ge_2F_2, Ge_2Cl_2, Ge_2Br_2 and Ge_2I_2 are transition state, whereas the isomers of Si_2X_2 are all local minima. All **GeE2** isomers of Ge_2X_2 are transition states, which is similar to **SiE2** of Si_2X_2. The isomers **GeE1** and **GeE2** differ from each other in the Ge-Ge bond distance and the Ge-X-Ge

angle. For **GeE1**, the Ge-Ge distance of correlates with the Ge-Ge-X angle and the Ge-Ge bond becomes shorter as the angle becomes larger. This suggests that the Ge-Ge interaction becomes stronger as the Ge-Ge-X angle becomes larger. **GeE2** shows the opposite trend to **GeE1**. The GeX bonds of both isomers are quite similar. It means that the difference of **GeE1** and **GeE2** stems from the different Ge-Ge bond situation. The Ge_2H_2 structure of **GeE2** does not fit to the trend due to the different character of GeH fragment.

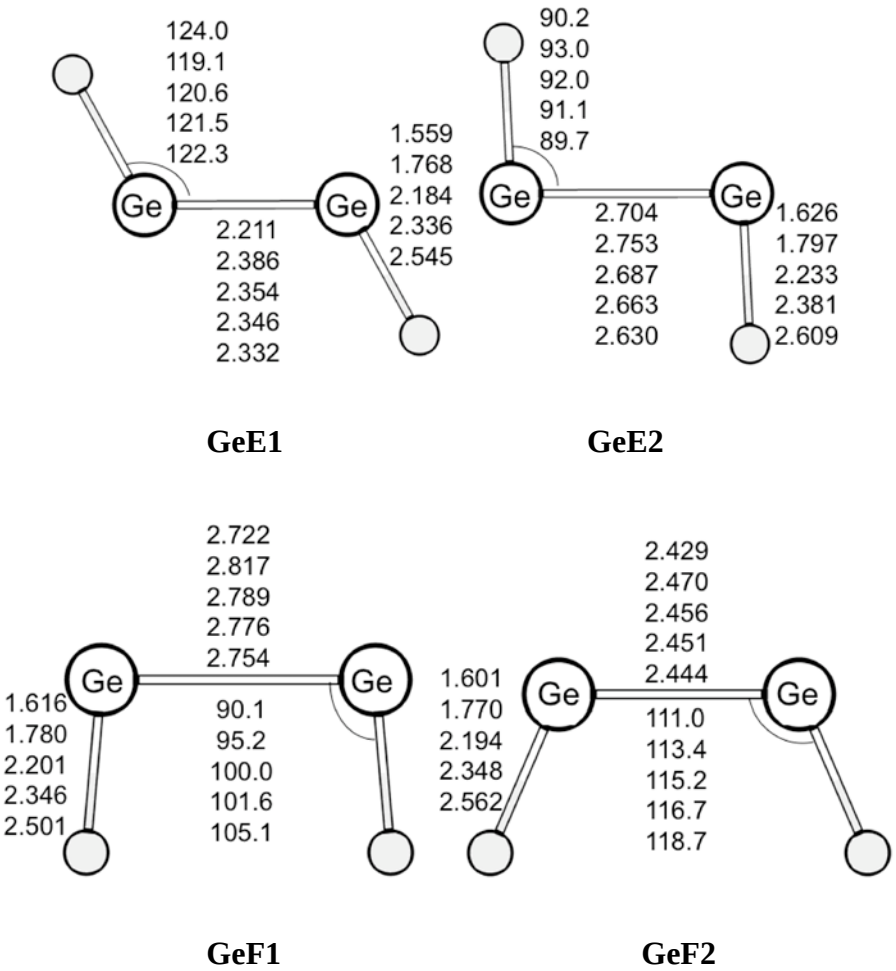

Figure 4.2.1.3. Optimized bent-structures in their singlet state, **GeE1**, **GeE2**, **GeF1** and **GeF2** calculated with BP86/QZ4P level. The bond lengths are given in Å and the angles are given in degree.

The cis-bent structures also have two types of isomers, **GeF1** and **GeF2**, which both have C_{2v} symmetry (Figure 4.2.1.3). The isomers **GeF1** and **GeF2** are both

transition states. This is similar to the isomers of **SiF1** and **SiF2** except the **SiF2** isomer of Si_2F_2, which is a local minimum. The Ge-Ge interaction of **GeF1** and **GeF2** becomes stronger as the halogen atom gets heavier. The Ge-Ge-X angle of **GeF1** and **GeF2** becomes larger as the halogen atom gets heavier, which is similar to **SiF1** and **SiF2**. The isomers **GeF1** have larger Ge-Ge-X angles than **GeE2**, which due to steric effects, whereas the Ge-Ge-X angles in **GeF2** are smaller than those in **GeE1**. **GeF1** and **GeF2** have very similar Ge-X distances. This means that the structural difference stem from the Ge-Ge bond. The trend of the **GeF1** and **GeF2** structure is quite similar to that of **SiF1** and **SiF2**.

The linear structures **GeG** are second order saddle points for Ge_2H_2 and Ge_2Cl_2 and the structures for Ge_2F_2 Ge_2Cl_2 and Ge_2Cl_2, are fourth order saddle points (Figure 4.2.1.4), where all linear isomers of **SiG** are second order saddle points. The Ge-Ge and Ge-X distances are the smallest of all Ge_2X_2 isomers. The Ge-Ge distances become longer as the halogen atom gets heavier, but they are nearly constant in these isomers

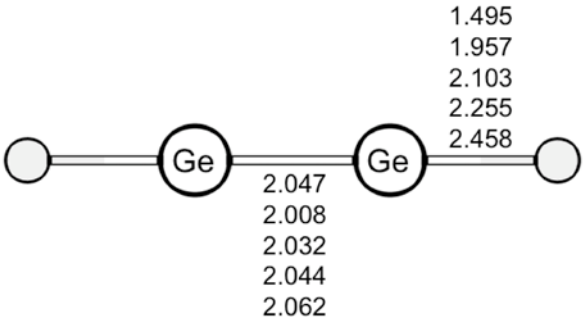

GeG

Figure 4.2.1.4 Optimized linear structures in the ground state, **GeG** calculated with BP86/QZ4P level. The bond lengths are given in Å and the angles are given in degree.

For Ge_2X_2, the distorted bent structure **GeH** is not found. The optimization from the predicted **GeH** structure leads to **GeA** and there are no minima between **GeA** and **GeF1** or **GeE2**. This situation is similar to Si_2H_2, Si_2Cl_2, Si_2Br_2 and Si_2I_2.

Table 4.2.1.1, Table 4.2.1.2 and Table 4.2.1.3 show the relative energies of the singlet state of stationary points on the singlet potential energy surface at BP86/QZ4P level. Here, the CCSD(T) results are quite reliable due to the fact that the difference between CCSD and CCSD(T) values are relative small and the largest deviation is 3.7 kcal/mol in the cis-bent structure **GeF2** of Ge_2H_2 except for the **GeC** isomer of Ge_2F_2 and Ge_2Cl_2, where the deviations between CCSD and CCSD(T) are 7.7 and 9.0 kcal/mol, respectively. These large deviations indicate a multi-reference character of the wave function in these structures. The relative energies between the singlet isomers at BP86/QZ4P level are relatively accurate and the largest difference from CCSD(T)/aug-cc-pVQZ is 17.7 kcal/mol for the structure **GeG** of Ge_2Cl_2 and the mean absolute error form CCSD(T)/aug-cc-pVQZ is 3.9 kcal/mol. The relative energy values of SCS-MP2 and MP4 are very similar and they are close to those of CCSD(T) calculations. The largest error in MP2, SCS-MP2 and MP4 are 19.8, 20.0 and 15.7 kcal/mol for the structure **GeC** of Ge_2Cl_2, where the isomer has multi-reference character, and the mean absolute errors of these three methods are 2.5, 1.5 and 1.4 kcal/mol, respectively. The SCS-MP2 method gives very accurate results for the singlet isomers.

Table 4.2.1.1, Table 4.2.1.2 and Table 4.2.1.3 present that Ge_2H_2 and the other Ge_2X_2 isomers behave different. Therefore, the isomers can be divided into two categories: Ge_2H_2 and the others. The following order presents the stability of Ge_2H_2: **GeA** > **GeC** > **GeB** > **GeD** > **GeE1** > **GeE2** > **GeF1** > **GeG** > **GeF2**. The global minimum is the doubly bridged structure **GeA**. Ge_2H_2 prefers to take the bridged structure, and the vinylidene structure is following one. The linear structures are unstable isomers. This trend and relative energies of Ge_2H_2 are relatively similar to those of Si_2H_2.

The other group shows a different trend as follows: **GeA** > **GeE2** > **GeF1** > **GeD** > **GeE1** > (**GeB)** > **GeF2** > **GeC** > **GeG**. The global minimum is **GeA**. The following one is **GeE2**, where the trans-bent structures are transition states connecting two minima of **GeA**. This bridging also stabilizes the molecules. However, the effect is not as large as that in Ge_2H_2. The stability of **GeB** depends on the halogen atoms. Ge_2I_2 prefers **GeB**, but for Ge_2F_2 and Ge_2Cl_2, the isomer is unstable. The stability of bent-structures is different from that of Ge_2H_2. From these points, the stability of the

isomers depends on the stability of the Ge-X-Ge ring-structure and the Ge-Ge bond situation. The relative energies are slightly larger than those of Si analogues.

Table 4.2.1.1 Optimized structures of **GeA-GeD** at BP86/QZ4P level and relative energies calculated on these geometries with BP86/QZ4P and with some ab initio methods with aug-cc-pVQZ basis set. The bond lengths are given in Å and the angles are in degree. The relative energies are given in kcal/mol with respect to **GeA** and given. The values in parentheses are the number of imaginary frequencies.

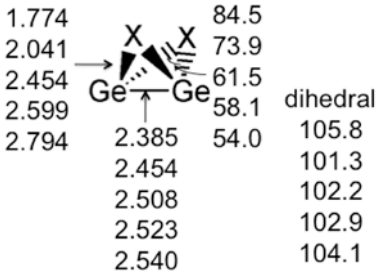

GeA

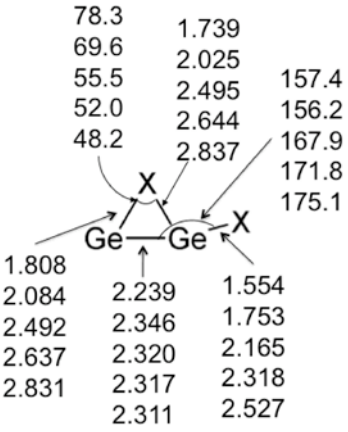

GeB

	H	F	Cl	Br	I	H	F	Cl	Br	I
BP86	0(0)	0(0)	0(0)	0(0)	0(0)	10.9(0)	25.0(1)	28.7(1)	28.7(1)	27.5(0)
HF	0	0	0	0	0	13.8	28.5	32.74	33.0	31.4
MP2	0	0	0	0	0	9.8	23.8	27.8	27.9	26.9
SCS-MP2	0	0	0	0	0	10.1	24.8	27.9	28.0	26.7
MP4	0	0	0	0	0	9.9	24.0	27.0	27.4	26.6
CCSD	0	0	0	0	0	11.2	25.4	28.7	29.2	28.1
CCSD(T)	0	0	0	0	0	10.1	24.0	27.3	27.8	26.8

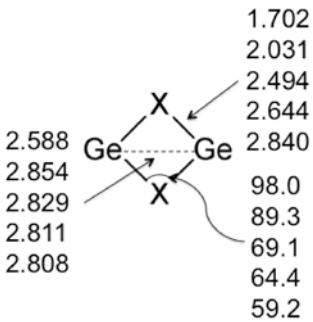

GeC

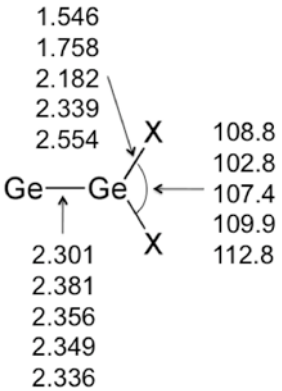

GeD

	H	F	Cl	Br	I	H	F	Cl	Br	I
BP86	8.8(1)	35.7(1)	48.2(1)	49.1(1)	49.1(0)	16.5(0)	21.9(0)	32.0(0)	34.3(1)	36.0(1)
HF	14.9	51.7	70.0	35.2	70.8	5.1	6.9	19.5	23.3	25.8
MP2	8.3	38.7	53.7	41.8	54.2	14.8	15.1	27.4	31.0	34.4
SCS-MP2	9.0	38.6	53.9	40.0	54.7	12.4	14.7	25.4	28.8	31.8
MP4	8.4	31.7	49.6	39.1	51.3	13.1	16.8	25.8	29.5	32.8
CCSD	10.2	35.6	42.9	38.3	57.5	10.7	13.7	23.7	27.4	30.2
CCSD(T)	8.8	27.9	33.9	38.5	51.9	11.9	15.0	25.0	28.6	31.5

Table 4.2.1.2 Optimized structures of **GeE1-GeF2** at BP86/QZ4P level and relative energies calculated with BP86/QZ4P and with some ab initio methods with aug-cc-pVQZ basis set. The bond lengths are given in Å and the angles are in degree. The relative energies are given in kcal/mol with respect to **GeA** and given. The values in parentheses are the number of imaginary frequencies.

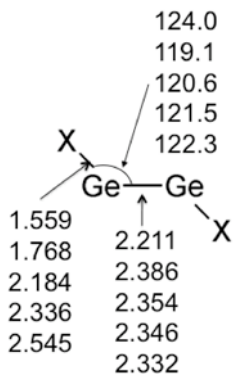

GeE1

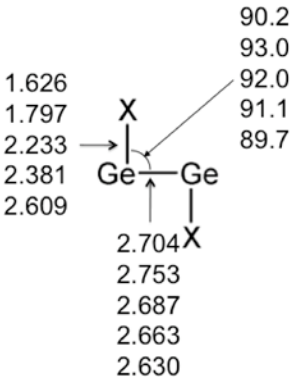

GeE2

	H	F	Cl	Br	I	H	F	Cl	Br	I
BP86	22.3(0)	21.7(1)	28.9(1)	30.4(1)	31.4(1)	37.7(1)	10.6(1)	19.0(1)	21.0(1)	23.0(1)
HF	24.8	24.2	32.8	35.3	36.8	20.6	-2.6	6.5	9.6	13.1
MP2	19.6	22.0	28.9	31.3	33.3	38.6	10.7	20.6	24.0	28.1
SCS-MP2	19.0	22.7	28.4	30.7	32.4	33.7	8.6	17.2	20.5	24.4
MP4	18.5	22.3	27.4	29.9	31.9	35.8	11.2	18.6	21.8	25.5
CCSD	20.0	23.3	28.9	31.6	33.5	30.7	7.2	14.5	17.7	21.2
CCSD(T)	18.1	21.9	27.4	30.0	32.0	33.8	9.6	17.0	20.1	23.4

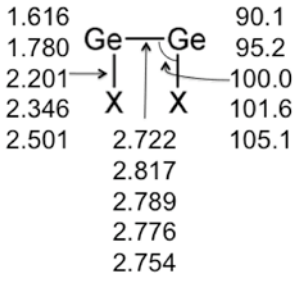

GeF1

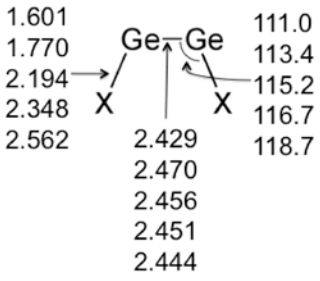

GeF2

	H	F	Cl	Br	I	H	F	Cl	Br	I
BP86	39.6(1)	13.5(1)	23.0(1)	25.8(1)	28.9(1)	54.4(1)	27.6(1)	36.4(1)	38.3(1)	40.3(1)
HF	22.6	0.8	11.2	14.9	19.0	59.9	33.5	44.7	48.0	51.6
MP2	40.6	14.1	24.6	28.4	33.6	57.4	29.6	39.9	43.1	46.8
SCS-MP2	35.7	12.1	21.3	25.0	29.9	55.0	30.2	39.3	42.3	45.9
MP4	37.7	14.4	22.4	30.8	30.8	52.5	28.7	37.1	40.2	43.6
CCSD	32.6	10.7	18.6	22.2	26.5	52.2	30.2	39.1	42.6	46.3
CCSD(T)	35.6	12.9	20.9	24.4	28.7	48.5	27.8	36.5	39.9	43.5

Table 4.2.1.3 Optimized structures of **GeG** at BP86/QZ4P level and relative energies calculated on these geometries with BP86/QZ4P and with some ab initio methods with aug-cc-pVQZ basis set. The bond lengths are given in Å and the angles are given in degree. The relative energies are given in kcal/mol with respect to **GeA** and given. The values in parentheses are the number of imaginary frequencies.

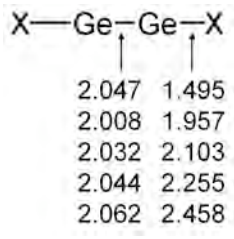

GeG

	H	F	Cl	Br	I
BP86	55.7(2)	124.1(4)	109.5(2)	105.3(4)	96.3(4)
HF	49.6	106.9	96.8	94.4	87.4
MP2	45.0	109.8	92.6	89.5	83.0
SCS-MP2	45.7	111.4	92.6	89.3	82.5
MP4	45.8	112.2	92.1	89.5	83.3
CCSD	47.3	111.4	93.2	90.7	84.3
CCSD(T)	46.0	109.3	91.8	89.4	83.3

4.2.1.2 Triplet Isomers of Ge_2X_2

The singlet isomers of Ge_2X_2 are investigated before in chapter 4.2.1.1. However, energetically low-lying isomers of Ge_2X_2 may exist on the triplet potential energy surface. Scheme 4.2.1.2 shows the triplet structures of the stationary points. They are denoted as follows: doubly bridged structure (**GeA(T)**), singly bridged planar structure (**GeB(T)**), planar doubly bridged structure (**GeC(T)**), vinylidene structure (**GeD(T)**), trans-bent structure (**GeE(T)**), cis-bent structure (**GeF(T)**), linear structure (**GeG(T)**) and distorted singly bridged structure (**GeI(T)**). The trend of the structures of Ge_2X_2 isomers is quite similar to that of Si_2X_2.

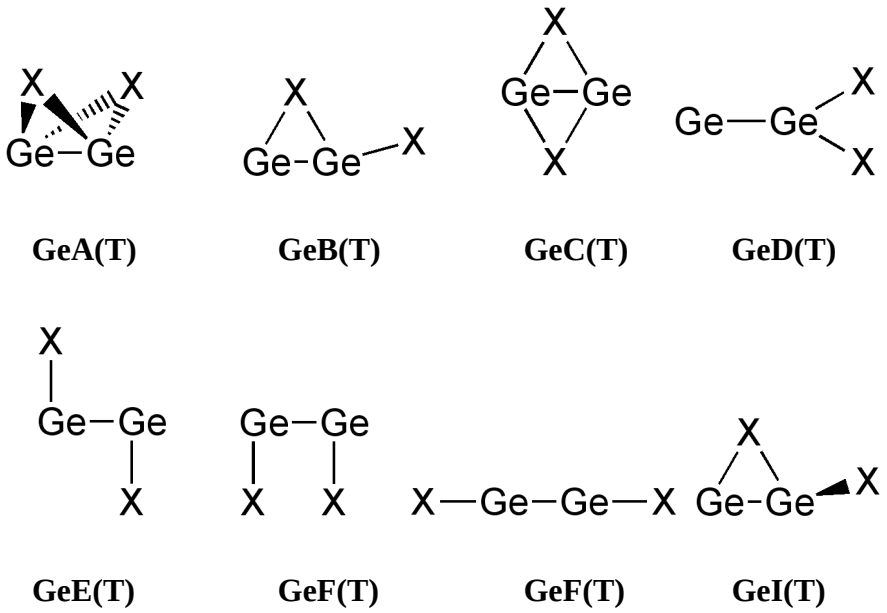

Scheme 4.2.1.2. Investigated triplet isomers of Ge_2X_2

The non-planar doubly bridged structures **GeA(T)** have C_{2v} symmetry and they are local minima for Ge_2H_2, Ge_2Cl_2, Ge_2Br_2 and Ge_2I_2 (Figure 4.2.1.5). For Ge_2F_2, the isomer is a second order saddle point, which is similar to **SiA(T)**. The geometries are quite different from **GeA**. The Ge-Ge bond and Ge-Ge-X angles show a correlation with the X atom and the Ge-Ge bond length are longer with heavier X atoms. However, the correlation of the Ge-Ge-X angle does not exist for Ge_2H_2 because of the different Ge-X bond character. Nevertheless, The two Ge atoms still interact weakly. The trend of the **GeA(T)** structure is quite similar to the trend of **SiA(T)**.

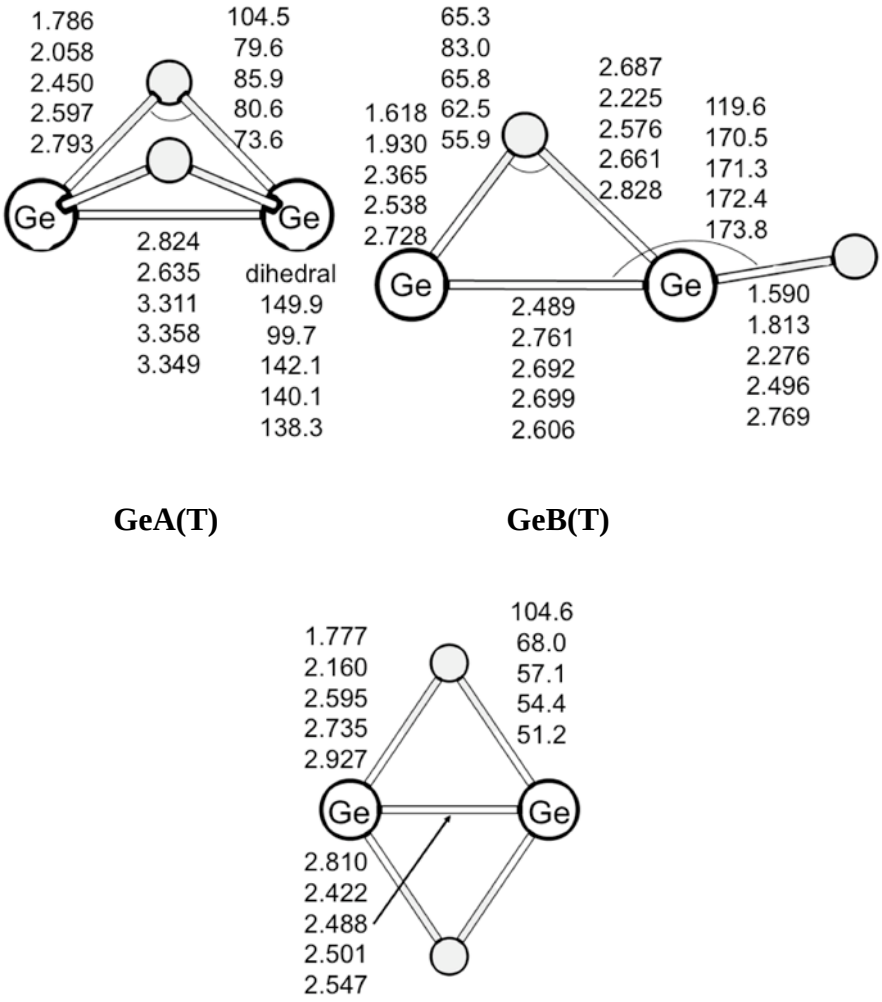

Figure 4.2.1.5. Optimized bridged structures in their triplet state, **GeA(T)**, **GeB(T)** and **GeC(T)** calculated with BP86/QZ4P level. The bond lengths are given in Å and the angles are given in degree.

The singly bridged planar structures **GeB(T)** have C_s symmetry and these isomers are predicted to be a transition states except for Ge_2H_2, where the isomer of Ge_2H_2 is a minimum (Figure 4.2.1.5). The X atoms in the ring are strongly connected to the Ge(side) atom and the ring structure is very weak. Especially, the isomer of Ge_2H_2 has a very small Ge-X-Ge bridging interaction. The Ge-Ge bond and Ge-X-Ge angle show a clear correlation with halogen atoms, and the bond length and the angle become shorter and smaller, respectively, as the halogen atom gets heavier. The Ge_2H_2 does not follow the correlation, because of the different character of the Ge-X-Ge bridged structure.

The planar doubly bridged structures **GeC(T)** have D_{2h} symmetry (Figure 4.2.1.5). The structures of Ge_2F_2, Ge_2Cl_2, Ge_2Br_2 and Ge_2I_2 are transition states. This is similar to **SiC(T)** of Si_2Cl_2, Si_2Br_2 and Si_2I_2. The isomer of Ge_2H_2 is predicted to be a minimum, where the **SiC(T)** of Si_2H_2 is transition state. The Ge-Ge bond and the Ge-X-Ge angle correlate with the halogen atoms and the bond lengths and bond angles become larger and smaller as the halogen atom gets heavier. Ge_2H_2 behaves different form the other halogen isomers. The Ge-Ge interaction of Ge_2H_2 is weaker than the other **GeC** isomers.

The vinylidene structures **GeD(T)** have C_{2v} symmetry and these isomers are predicted to be local minima (Figure 4.2.1.6), which are similar to the isomers of **SiD(T)**, except Si_2X_2. The Ge-Ge interactions are slightly smaller than those in **GeD** and the Ge-Ge distance becomes shorter as the halogen atoms gets heavier in the halogen isomers.

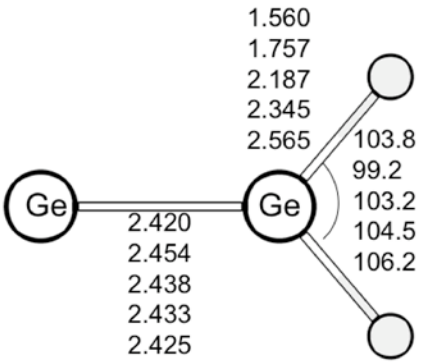

GeD(T)

Figure 4.2.1.6. Optimized vinylidene structures in the triplet state, **GeD(T)** calculated with BP86/QZ4P level. The bond lengths are given in Å and the angles are given in degree.

The trans-bent structures **GeE(T)** are C_{2h} symmetric and these isomers **GeE(T)** are predicted to be minima (Figure 4.2.1.7), which is similar to the Si_2X_2 analogues, **SiE(T)**. The Ge-Ge distance correlates with the Ge-Ge-X angle and the Ge-Ge bond becomes shorter as the Ge-Ge-X angle gets larger.

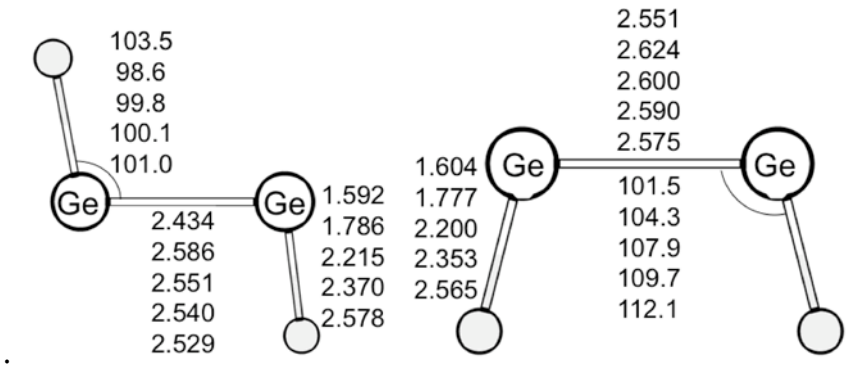

GeE(T) **GeF(T)**

Figure 4.2.1.7. Optimized bent-structures in the triplet state, **GeE(T)** and **GeF(T)** calculated with BP86/QZ4P level. The bond lengths are given in Å and the angles are given in degree.

The cis-bent structures **GeF(T)** have C_{2v} symmetry (Figure 4.2.1.7). These isomers **GeF(T)** are predicted to be minima except for Ge_2H_2. The **GeF(T)** isomer of Ge_2H_2 is a second order saddle point, which is identical to the Si_2X_2 isomers of **SiF(T)**. The Ge-Ge bond and the Ge-Ge-X angle do not show a clear correlation, because of the steric effect of the X atoms. The deviation of the bond lengths is smaller in **GeF(T)** than in **GeE(T)**, whereas the deviation of the Ge-Ge-X angle is larger in **GeF(T)**. From these points, the halogen atoms affect the Ge-Ge distance in **GeE(T)** and the steric effect is important for the Ge-Ge-X angle in **GeF(T)**.

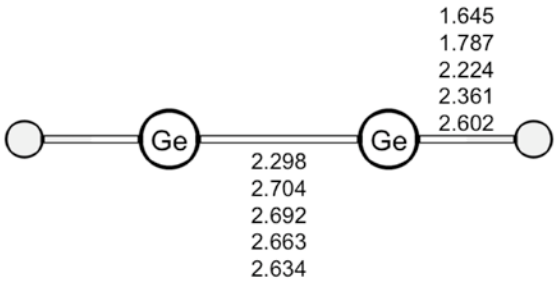

GeG(T)

Figure 4.2.1.8. Optimized linear structure in the triplet state, **GeG(T)** calculated with BP86/QZ4P level. The bond lengths are given in Å and the angles are given in degree.

The linear structures **GeG(T)** are fourth order saddle points for Ge_2H_2 and Ge_2I_2 (Figure 4.2.1.8). The **GeG(T)** structures of Ge_2F_2, Ge_2Cl_2 and Ge_2Br_2 are second order saddle points, where the **SiG(T)** structures of Si_2Cl_2, Si_2Br_2 and Si_2I_2 are fourth order transition states. The Ge-Ge bond lengths are longer in all Ge_2X_2 structures than in **GeG**. The Ge-Ge bond length has a correlation for halogen isomers, and the Ge-Ge distance becomes shorter as the halogen atom gets heavier.

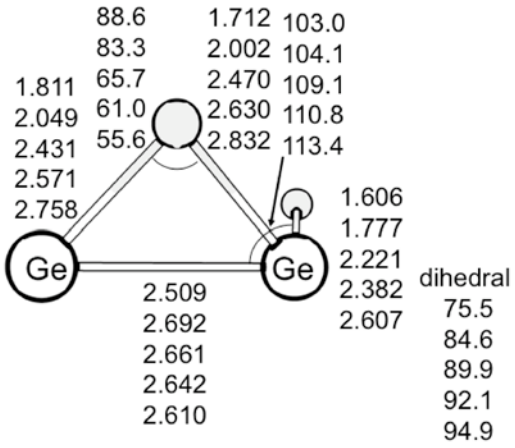

GeI(T)

Figure 4.2.1.9. Optimized distorted singly bridged structures, **GeI(T)** calculated with BP86/QZ4P level. The bond lengths are given in Å and the angles are given in degree.

The distorted singly bridged planar structures **GeI(T)**, have C_1 symmetry and these isomers are predicted to be minima for all Ge_2X_2 (Figure 4.2.1.9), which is similar to the **SiI(T)** of Si_2X_2. The Ge-Ge bond distance becomes slightly shorter if the halogen atom gets heavier. In **GeI(T)**, the Ge-X-Ge ring structure is weak.

Table 4.2.1.4 and Table 4.2.1.5 exhibit that the relative energies of the stationary points on the triplet energy potential surface at triplets at BP86/QZ4P level of theory are relatively smaller than those calculated at CCSD(T)/aug-cc-pVQZ//BP86/QZ4P level of theory and the largest difference is 13.8 kcal/mol for the **GeG(T)** structure of Ge_2I_2. The relative energies of the triplets are often underestimated with BP86/QZ4P in these systems and the mean absolute error from CCSD(T)/aug-cc-pVQZ is 5.8

kcal/mol. BP86/QZ4P gives accurate results for minima, but the transition states are calculated to be lower in energies than those of CCSD(T)/aug-cc-pVQZ. The differences between CCSD and CCSD(T) values are relatively small and the largest difference is 2.7 kcal/mol for the **GeD(T)** isomer of Ge_2H_2. It indicates that the isomers in triplet state have only a small multi-reference character and that the CCSD(T) results are reliable and accurate. For the stationary points on the triplet energy potential surface, SCS-UMP2 methods are slightly more accurate than UMP2. The largest deviation from CCSD(T)/aug-cc-pVQZ for UMP2 is 15.5 kcal/mol for the **GeG(T)** structure of Ge_2F_2, whereas the large difference in SCS-UMP2 is 10.2 kcal/mol for the **GeG(T)** structure of Ge_2Br_2. However, the mean absolute error from CCSD(T)/aug-cc-pVQZ is 6.2 kcal/mol in UMP2 and SCS-UMP2, and the mean absolute error in SCS-UMP2 is nearly same as that in UMP2. This is due to the fact that the parameters of the SCS-correction are optimized for singlets not for triplets [ref]. The UMP4 method gives better results than SCS-UMP2 and UMP2, where the largest deviation is 7.4 kcal/mol for the **GeA(T)** structure in Ge_2H_2 and mean absolute error is 4.5 kcal/mol. RMP2 presents similar values to CCSD(T) and the largest deviation and mean absolute error are 2.4 kcal/mol for the **GeF(T)** structure of Ge_2H_2 and 1.1 kcal/mol, respectively.

In the triplet state, the isomers are categorized into three groups, Ge_2H_2, Ge_2F_2 and the group of Ge_2Cl_2, Ge_2Br_2 and Ge_2I_2. Ge_2H_2 shows the following order of stability: **GeD(T)** > **GeE(T)** > **GeB(T)** > **GeI(T)** > **GeF(T)** > **GeA(T)** > **GeC(T)** > **GeG(T)**. These isomers are always higher in energy than the singlet. For the triplets, the vinylidene structure **GeD(T)** is most stable, which is similar to Si_2H_2. The order of stability shows the bent-structure and singly bridged structure is relatively favorable, but the doubly bridged structures and linear structures are unfavorable structures. The relative energies of Ge_2H_2 are often higher than those of Si_2H_2.

For Ge_2F_2, the order of stability for each isomer is as follows: **GeE(T)** > **GeD(T)** > **GeF(T)** > **GeI(T)** > **GeG(T)** > **GeB(T)** > **GeA(T)** > **GeC(T)**. The order shows that **GeE(T)** is the most stable isomer for triplets and Ge_2F_2 prefers bent-structures. The vinylidene structure is the second stable isomer, where the corresponding isomer of Si_2F_2 is a global minimum. The doubly bridged structures and linear structures are unfavorable structures, which is a similar trend to Ge_2H_2.

4.2 Ge_2X_2 Molecules

The group of Ge_2Cl_2, Ge_2Br_2 and Ge_2I_2 shows the following order of stability as follows: **GeE(T)** > **GeF(T)** > **GeI(T)** > **GeD(T)** > **GeA(T)** > **GeC(T)** > **GeB(T)** > **GeG(T)**. This order is similar to that of Ge_2F_2, but vinylidene structures become unstable. **GeE(T)** is the most stable isomer for triplets, but they are still local minima and the isomers of **GeA** are still more stable. The relative energies of Ge_2F_2, Ge_2Cl_2 Ge_2Br_2 and Ge_2I_2 are often higher than those of corresponding Si_2X_2 isomers.

Table 4.2.1.4 Optimized structures of **GeA(T)-GeD(T)** at BP86/QZ4P level and relative energies calculated on the geometries with BP86/QZ4P and ab initio methods with aug-cc-pVQZ basis set. The bond lengths are given in Å and the angles are given in degree. The relative energies are given in kcal/mol with respect to **GeA** in singlet state. The values in parentheses are the number of imaginary frequencies.

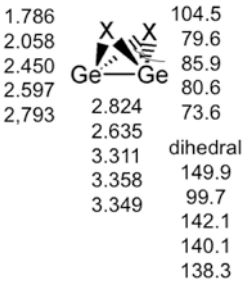

GeA(T)

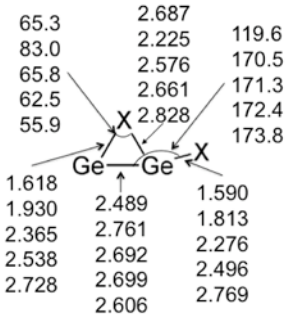

GeB(T)

	H	F	Cl	Br	I	H	F	Cl	Br	I
BP86	34.8(0)	30.8(2)	32.3(0)	34.0(0)	35.1(0)	27.7(0)	26.7(2)	34.2(2)	34.6(2)	35.0(2)
HF	21.0	39.5	16.2	19.4	23.9	11.0	27.8	37.3	38.4	39.7
RMP2	38.3	36.3	32.8	36.2	40.1	31.5	36.2	44.7	45.3	44.7
UMP2	46.5	41.2	39.3	42.2	45.6	35.6	42.5	52.4	52.1	52.2
SCS-UMP2	49.7	46.5	38.2	41.0	44.5	35.2	43.9	52.9	53.2	52.7
UMP4	45.0	40.7	38.8	41.5	44.5	34.1	42.5	50.5	50.2	49.8
CCSD	35.4	39.1	30.7	33.6	36.8	27.4	36.4	43.9	44.7	44.7
CCSD(T)	37.6	37.2	33.1	35.9	38.9	29.5	36.3	43.7	44.4	44.3

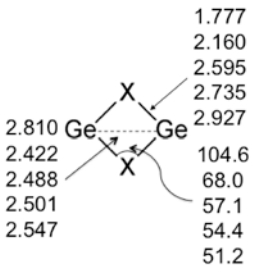

GeC(T)

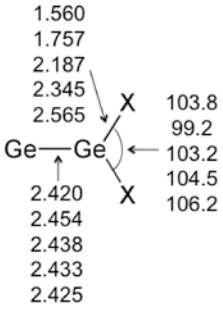

GeD(T)

	H	F	Cl	Br	I	H	F	Cl	Br	I
BP86	33.0(0)	32.3(1)	31.1(1)	30.3(1)	29.6(1)	22.1(0)	12.0(0)	28.8(0)	28.8(0)	32.2(0)
HF	38.2	40.8	35.5	34.5	34.7	-0.1	-10.4	6.1	10.9	15.2
RMP2	39.0	40.1	42.3	41.6	41.8	21.5	6.2	23.7	28.6	34.2
UMP2	45.4	44.9	45.1	45.8	46.0	25.5	7.2	28.0	34.1	39.8
SCS-UMP2	46.9	48.4	46.9	47.3	47.1	25.2	10.3	29.2	34.8	39.7
UMP4	44.1	44.2	43.7	44.1	43.9	24.5	10.1	27.4	33.4	38.4
CCSD	41.1	42.1	41.7	40.6	40.3	18.4	7.1	21.6	26.2	30.8
CCSD(T)	40.5	40.8	41.2	40.1	39.7	21.1	9.2	23.8	28.5	33.3

Table 4.2.1.5 Optimized structures of **GeE(T)-GeI(T)** at BP86/QZ4P level and relative energies calculated on the geometries with BP86/QZ4P and ab initio methods with aug-cc-pVQZ basis set. The bond lengths are given in Å and the angles are given in degree. The relative energies are given in kcal/mol with respect to **GeA** in singlet state. The values in parentheses are the number of imaginary frequencies.

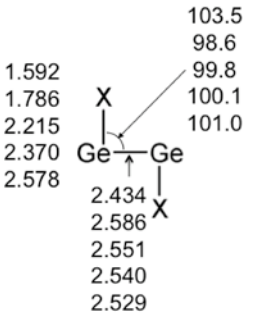

GeE(T)

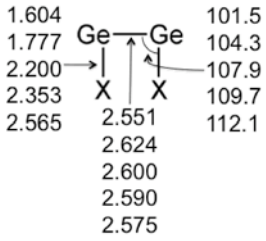

GeF(T)

	H	F	Cl	Br	I	H	F	Cl	Br	I
BP86	21.9(0)	2.8(0)	13.0(0)	15.8(0)	18.9(0)	29.9(2)	4.9(0)	15.6(0)	18.6(0)	22.0(0)
HF	8.7	-8.2	3.3	7.0	10.9	17.4	-5.6	6.6	10.7	15.3
RMP2	23.2	5.4	16.6	20.4	25.0	34.7	8.6	20.3	24.4	29.6
UMP2	28.8	6.9	21.6	27.5	31.7	40.3	9.6	25.0	31.1	35.7
SCS-MP2	28.1	8.9	22.0	27.4	31.2	39.3	11.6	25.5	31.1	35.4
UMP4	26.9	8.0	20.3	26.1	30.0	37.9	10.5	23.5	29.4	33.7
CCSD	21.2	5.9	14.8	18.4	22.3	30.6	9.0	18.2	22.0	26.5
CCSD(T)	22.7	7.4	16.3	19.9	23.8	32.3	10.3	19.5	23.3	27.8

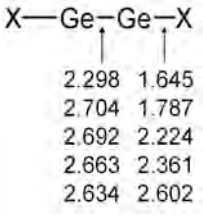

GeG(T)

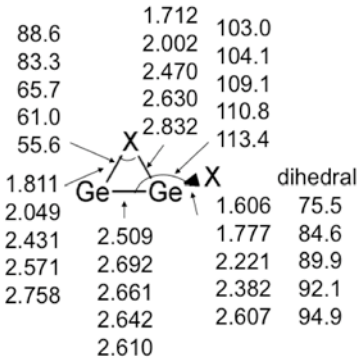

GeI(T)

	H	F	Cl	Br	I	H	F	Cl	Br	I
BP86	69.3(4)	20.4(2)	32.1(2)	34.6(2)	37.9(4)	28.3(0)	10.8(0)	20.8(0)	22.6(0)	23.4(0)
HF	72.6	20.5	34.5	38.3	43.0	15.8	-4.3	8.7	11.7	14.9
RMP2	71.1	28.5	44.3	48.3	53.9	30.9	10.7	22.4	25.2	28.5
UMP2	77.3	45.4	55.0	54.7	60.0	36.3	13.5	27.6	31.3	34.3
SCS-MP2	79.0	34.5	51.4	56.9	61.8	35.7	14.9	27.7	31.2	33.9
UMP4	75.2	30.7	47.3	53.0	57.9	34.7	15.2	26.9	30.4	33.1
CCSD	73.0	30.3	43.2	47.1	52.1	28.4	10.9	20.9	23.6	26.3
CCSD(T)	71.4	29.9	42.9	46.7	51.7	30.1	12.8	22.6	25.2	27.9

4.2.1.3 Summary of Geometry and Relative Energies

The chapter 4.2.1 presented the geometries and relative energies of the isomers of Ge_2H_2, Ge_2F_2, Ge_2Cl_2 Ge_2Br_2 and Ge_2I_2. The order of the stability of the Ge_2H_2 isomers are as follows: **GeA** > **GeC** > **GeB** > **GeD** > ... > **GeG > GeF2**. It clearly shows that Ge_2H_2 prefers to have the bridged structures. For Ge_2H_2, the stabilizing effect of the bridging is the most important, which is similar to Si_2H_2.

Ge_2F_2, Ge_2Cl_2, Ge_2Br_2 and Ge_2I_2 show a different trend to Ge_2H_2, and they shows the order of the stability as follows: **GeA** > **GeE(T)**, **GeE2**, **GeF(T)** >… > **GeG**. The doubly bridged structure **GeA** is the most stable isomer. However, the Ge-X-Ge bridgings do not form as stable isomers as that of Ge_2H_2. These isomers also prefer the trans-bent structures. It suggests that the Ge-X-Ge bridged structure in these molecules contributes to the less stabilization of these molecules than Ge_2H_2, but the Ge-Ge bond is still important, too.

The vinylidene structures **GeD** and **GeD(T)** exhibit higher relative energies and they are local minima or transition state although the **SiD(T)** structure of Si_2F_2 is a global minimum.

4.2.2 Orbital Interactions and Bond Situations

4.2.2.1. Orbital Analyses

The last section showed that there exist several stationary points on the singlet potential energy surface, which differ mainly in the bond situation around the Ge-Ge bond. **GeA**, **GeB**, **GeC**, **GeE1**, **GeE2**, **GeF1**, **GeF2**, and **GeG,** which have a X-Ge-Ge-X structure, can be divided into two GeX fragments and the bonding situation in these molecules can be described as interactions between the two GeX fragments. The orbital interactions between the diatomic species are analyzed with a similar approach to the Trinquier/Malrieu/Carter/Goddard model [81, 82, 83], which was able to explain the E_2H_2 bonding situation well in the previous report [87] and chapter 4.1.

4.2.2.1.1 GeX Fragment

Figure 4.2.2.1 shows schematic pictures of the electronic ground state ($X^2\Pi$) and Table 4.2.2.1 presents the first excited state ($a^4\Sigma^-$) of GeX and the calculated excitation energies $a^4\Sigma^- \leftarrow X^2\Pi$ at BP86/QZ4P level and MRCI-SD/aug-cc-pvQZ//BP86/QZ4P level. A (5,5) full-valence CASSCF/aug-cc-pVQZ wave function was used as a reference in the MRCI-SD calculation of GeH and a (11,8) full-valence CASSCF/aug-cc-pVQZ wave function was used as reference in the MRCI-SD calculation of GeF, GeCl, GeBr and GeI. The excitation energies at BP86/QZ4P are in relatively good agreement with those of MRCI-SD/aug-cc-pVQZ//BP86/QZ4P level and the experimental value of GeH (47.8 kcal/mol) [263]. The largest deviation of BP86/QZ4P from the MRCI-SD(Q) /aug-cc-pVQZ result and the experimental value are found for GeH with 4.35 and 0.66 kcal/mol, respectively. The largest deviation from the MRCI-SD(Q)/aug-cc-pVQZ in GeX fragments is 9.6 kcal/mol for the excitation energy calculation with BP86/QZ4P for GeF. The excitation energy is underestimated in BP86/QZ4P. However, the excitation energies calculated with BP86/QZ4P are still acceptable.

As shown in Section 4.2.1, the linear structure is the energetically highest lying stationary point of the investigated structures in the Ge_2X_2 system. This situation is quite different from the C_2X_2 system, where the linear structure is the global

minimum. Figure 4.2.2.1 shows clearly that the electronic configuration of GeX moiety must be the $a^4\Sigma^-$ excited state and not the $X^2\Pi$ ground state to form the triply bonded linear species XGe≡GeX. The situation is similar to SiX molecules. Therefore the GeX fragments must at first become excited into the $a^4\Sigma^-$ state in order to bind through one σ and two degenerate π bonds in XGe≡GeX. The previous study showed that it is energetically much easier to excite CH from the $X^2\Pi$ ground state to the $a^4\Sigma^-$ excited state because the carbon species CH has a lower excitation energy (15.4 kcal/mol) than GeH (47.1 kcal/mol) to form a triple bond than for the GeH species [263]. The possible gain in binding energy after $a^4\Sigma^- \leftarrow X^2\Pi$ excitation is much larger for C_2H_2 than for Ge_2H_2 and the other heavier homologues. Table 4.2.2.1 shows that the excitation energy becomes larger as the halogen atoms heavier and the excitation energies of halogen molecules are much larger than that of GeH. This is due to that the halogen atoms are electron-withdrawing groups and the halogen atoms stabilize the $X^2\Pi$ ground state, where the main contribution is σ-lone pair. The electron configuration of the $X^2\Pi$ ground state allows only an electron sharing single bond between the two GeX moieties. The other possibility to form bond is the donor-acceptor bond between two moieties in the $X^2\Pi$ ground state. This orbital interaction is similar to the SiX molecules.

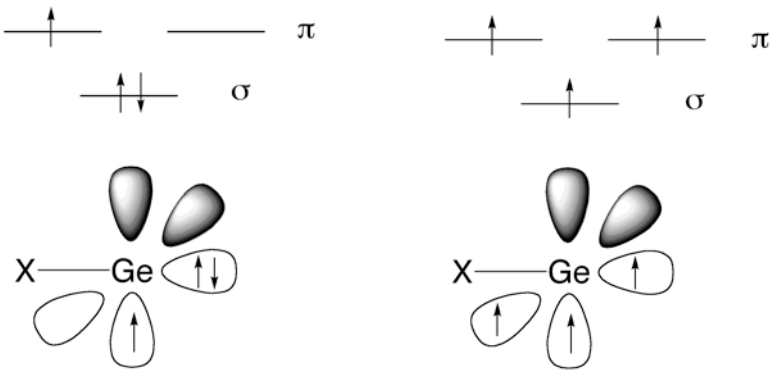

$X^2\Pi$ $a^4\Sigma^-$

ground state excited state

Figure 4.2.2.1 Schematic pictures of the $X^2\Pi$ ground state and the $a^4\Sigma^-$ excited state for the GeX fragment.

Table 4.2.2.1 Calculated excitation energies from $X^2\Pi$ ground state to $a^4\Sigma$ excited state at BP86/QZ4P, MRCI-SD/aug-cc-pVQZ//BP86/QZ4P and MRCI-SD(Q)/aug-cc-pVQZ//BP86/QZ4P levels, where (Q) indicates the inclusion of the Davidson correction. The energies are given in kcal/mol.

	BP86/QZ4P	MRCI-SD/ aug-cc-pVQZ	MRCI-SD(Q)/ aug-cc-pVQZ
GeH	47.12	41.49	42.57
GeF	101.90	85.05	90.42
GeCl	85.06	74.27	76.87
GeBr	78.36	68.96	71.72
GeI	68.29	60.86	63.04

Table 4.2.2.2 Calculated dissociation energies D_e of linear X-Ge≡Ge-X into 2GeX fragments and excitation energies between $X^2\Pi$ ground state and $a^4\Sigma$ excited state at BP86/QZ4P level. The energies are given in kcal/mol

	D_e	ΔE_{exc}	D_e- $2\Delta E_{exc}$
H	113.3	47.1	19.0
F	122.6	101.9	-81.2
Cl	113.9	85.1	-56.3
Br	107.7	78.4	-49.0
I	99.9	68.3	-36.6

Table 4.2.2.2 shows the theoretically predicted bond dissociation energies for breaking the triple bond in linear X-Ge≡Ge-X yielding 2 GeX ($a^4\Sigma^-$) and it indicate that linear Ge_2H_2, Ge_2F_2, Ge_2Cl_2, Ge_2Br_2 and Ge_2I_2 have similar dissociation energies, and they are much weaker than that of acetylene and the linear structure of Si_2X_2. The correction of dissociation energies of Ge_2X_2 by the $a^4\Sigma^- \leftarrow X^2\Pi$ excitation energies gives theoretical bond energies of D_e-$2\Delta E_{exc}$. The excitation energies of two GeX fragments are even higher than the bond dissociation energy of linear XGe≡GeX in Ge_2F_2, Ge_2Cl_2, Ge_2Br_2 and Ge_2I_2. Ge_2F_2 and Ge_2Cl_2 give higher dissociation energies than Ge_2H_2. However, Ge_2F_2 Ge_2Cl_2 Ge_2Br_2 and Ge_2I_2 need much higher excitation energies than Ge_2H_2 and the theoretical dissociation energies of Ge_2F_2, Ge_2Cl_2, Ge_2Br_2 and Ge_2I_2 are negative. The excitation energy, ΔE_{exc} correlates with D_e- $2\Delta E_{exc}$ and this factor dominate the stability of the linear structure. The dissociation energy is smaller and ΔE_{exc} is larger than those of SiX molecules. Due to the high excitation

energies, the formation of the triple bond is unfavorable for these isomers.

The theoretically predicted bond dissociation energy D_e- $2\Delta E_{exc}$ shows that it is energetically unfavorable for the GeX fragments to form an XGe≡GeX triple bond through the $a^4\Sigma^-$ excited states because the Ge-Ge single bond that can be formed from the $X^2\Pi$ ground state, would deliver much a larger binding energy. The typical bond dissociation energies of the Ge-Ge single bonds of Ge_2X_6 are 33.6-60.9 kcal/mol, which are calculated with BP86/QZ4P level. This is much less than the stabilization energy that can be expected from the formation of an electron-sharing XGe-GeX single bond between GeX in the $X^2\Pi$ ground state. The possibility of additional stabilizations through lone-pair and/or Ge-X donor acceptor interactions, which are described below, will be enough to gain the much higher bond energy of the triple bond. It follows that it is energetically more profitable for two GeX species to bind in their $X^2\Pi$ ground state than in the $a^4\Sigma^-$ excited state, which is similar to the SiX molecules.

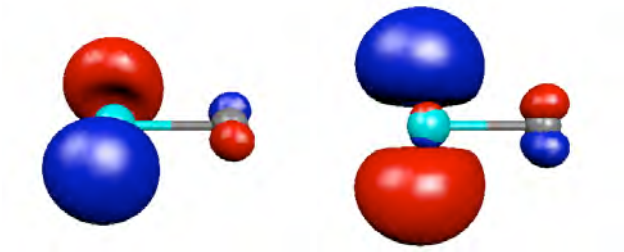

LUMO SOMO

(a) π orbital (b) π orbital

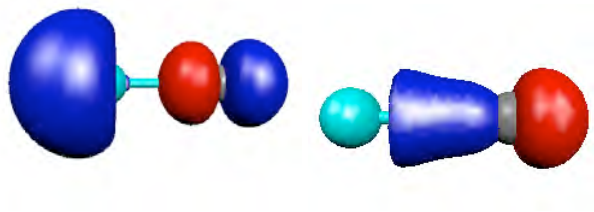

(c) σ-lone-pair orbital (d) σ-Ge-X orbital

Figure 4.2.2.2. Important orbitals of GeX fragment in the $X^2\Pi$ ground state to form the Ge-Ge bond.

Table 4.2.2.3. Calculated orbital energies of the GeX molecules in their $X^2\Pi$ ground state at BP86/QZ4P level. The energies are given in eV.

	GeH	GeF	GeCl	GeBr	GeI
π orbital (LUMO)	-4.1069	-3.8622	-3.9825	-3.9905	-4.0156
π orbital (SOMO)	-3.8844	-3.6323	-3.7429	-3.7492	-3.7764
lone-pair orbital	-6.7893	-9.1749	-8.3278	-7.9588	-7.4830
Ge-X bond orbital	-12.6408	-13.1588	-12.6998	-12.5833	-12.3235
$\Delta E_{\pi\text{-lone-pair}}$	2.6824	5.3127	4.3453	3.8063	3.1545
$\Delta E_{\pi\text{-GeX}}$	8.5339	9.2966	8.7133	8.5928	8.3079

Figure 4.2.2.2 shows the selected orbitals of the GeX fragments. Two π orbitals are found as LUMO and SOMO, respectively. Two types of σ orbitals, the lone-pair orbitals and Ge-X orbitals are found as occupied orbitals. These orbitals of GeH, GeF, GeCl, GeBr and GeI are quite similar in each other for the region near Ge atom. Table 4.2.2.3 shows the orbital energies of the selected orbitals in Figure 4.2.2.2. The orbital energies exhibit the clear correlation for GeF, GeCl, GeBr and GeI molecules (Figure 4.2.2.3). The LUMO and SOMO show a clear correlation and the energy of LUMO becomes higher as the energy of SOMO gets higher, because both orbitals are mainly built from the *p* orbital of Ge atom, (Figure 4.2.2.2 and Table 4.2.2.4). The lone-pair orbitals and Si-X bond shows a clear correlation and the energy of lone-pair orbital gets higher with higher energy of Si-X bond because it contains *s* orbital of Ge atom. The GeF molecule has the highest energy for SOMO and the lowest energies for the lone-pair orbital and the Ge-X bond orbital, which is a similar trend to SiX_2. However, the deviation of orbital energy of Si-X bond is larger than that of lone-pair and Si-X bond depends stronger on X atom than lone-pair. The $\Delta E_{\pi\text{-lone-pair}}$ values show the energy difference between LUMO and the lone-pair orbital. $\Delta E_{\pi\text{-lone-pair}}$ shows a correlation with the orbital energy of lone-pair and $\Delta E_{\pi\text{-lone-pair}}$ becomes larger as the orbital energy of lone-pair gets lower. The $\Delta E_{\pi\text{-GeX}}$ values show the energy

difference between LUMO and Ge-X bond orbital. $\Delta E_{\pi\text{-GeX}}$ shows a correlation with the orbital energy of Ge-X bond and $\Delta E_{\pi\text{-GeX}}$ becomes larger as the orbital energy of Ge-X bond orbital gets lower. Figure 4.2.2.3 shows the clear correlation of $\Delta E_{\pi\text{-lone-pair}}$ with $\Delta E_{\pi\text{-GeX}}$, and $\Delta E_{\pi\text{-lone-pair}}$ becomes smaller as the $\Delta E_{\pi\text{-GeX}}$ gets smaller. The $\Delta E_{\pi\text{-lone-pair}}$ and $\Delta E_{\pi\text{-GeX}}$ values depend on the energies of lone-pair and Ge-X bond because the energy of LUMO is nearly constant.

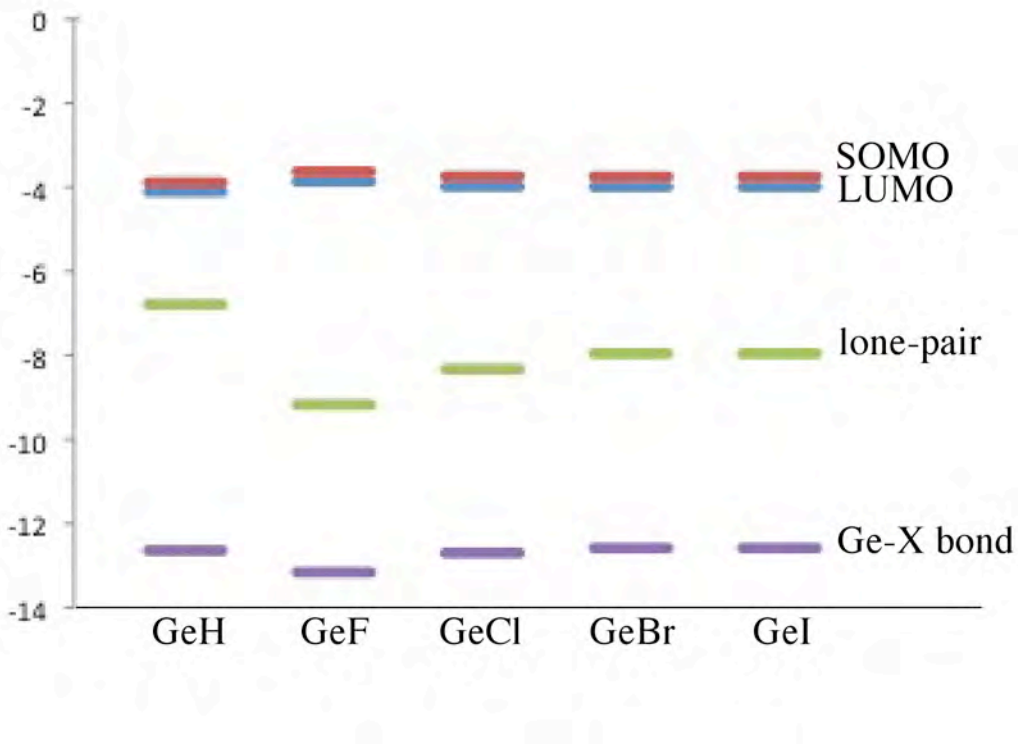

Figure 4.2.2.3 The correlation for GeX orbitals in Figure 4.2.2.2

Table 4.2.2.4 shows the contribution of atomic orbitals for each Kohn-Sham molecular orbital. In this table, LUMO and SOMO show the similar contribution of atomic orbital and these orbitals are constructed by just *p* orbitals, which show a similar trend for their orbital energies, which is similar to the orbitals of the SiX molecules.

For the lone-pair orbital, the trend of the contributions is similar to that of SiX. The contribution of *s* orbital becomes smaller as the halogen atom gets heavier and the contribution of *p* orbital of Ge atom shows the opposite trend to *s* orbital. The

contribution of the *p* atomic orbital in the lone-pair has a correlation with the orbital energy of the lone-pair, and the energy of the lone-pair becomes higher in energy as the contribution of *p* orbital larger.

The Ge-X bond orbital is built from the *s* orbitals of Ge atom and the *s* orbital of hydrogen or the *p* orbitals of halogen atoms. The contribution of X atom in Si-X bond correlates with the energy of Ge-X bond and the orbital energy becomes lower in energy with the larger contribution of the orbital of X atom.

The comparison with the SiX molecules shows that the contribution of atomic orbitals of X atom becomes larger in lone-pair orbitals and smaller in Ge-X orbital. It suggests that Ge-X bond orbitals show the stronger character of the atomic orbital of Ge atom and the lone-pair gets stronger influence of X atoms. It agrees with the trend of orbital energy

Table 4.2.2.4 Each percentage contribution of selected orbitals corresponds to the indicated atomic orbitals

	GeH(%)	GeF(%)	GeCl(%)	GeBr(%)	GeI(%)
π orbital (LUMO)	Ge: p_x 55.14 p_y 41.73	Ge: p_x 47.47 p_y 46.28 F: p_y 2.69 p_x 2.63	Ge: p_y 69.58 p_x 18.81 Cl: p_y 6.01	Ge: p_x 63.96 p_y 23.62 Br: p_x 6.30	Ge: p_x 62.32 p_y 23.69 I: p_y: 7.37
π orbital (SOMO)	Ge: p_z 97.32 H: p_z 2.61	Ge: p_z 94.27 F: p_z 4.97	Ge: p_z 89.48 Cl: p_z 7.09	Ge: p_z 88.70 Br: p_z 7.95	Ge: p_z 87.10 I: p_z 9.24
Lone-pair orbital	Ge: *s* 15.93 p_x 24.38 p_y 18.46 H: *s* 41.01	Ge: *s* 39.06 p_x 6.88 p_x 6.71 F : p_x 22.46 p_y 21.90	Ge: *s* 21.99 p_x 16.80 Cl: p_x 41.34 P_y 11.18	Si: *s* 17.08 p_y 17.07 Br: p_y 40.76 p_x 15.05	Ge: s 11.77 p_y 19.97 p_x 7.59 I: p_y 41.18 p_x 15.65
Ge-X orbital	Ge: *s* 75.48 H: *s* 21.45	Ge: *s* 53.76 F: p_x 20.73 p_y 20.21	Ge: *s* 71.34 Cl: p_x 18.20 *s* 6.00	Si: *s* 78.01 Br: p_y 13.06 p_x 4.82	Ge: *s* 80.72 I: p_x 9.18 *s* 7.20

4.2.2.1.2 σ-type Isomers, **GeA**, **GeE2** and **GeF1**

As shown before, the linear arrangement of two GeX fragments of the $X^2\Pi$ state is unfavorable for the bond formation between the unpaired electrons and the bond formation must rather take place in a sideways fashion. Figure 4.1.2.4 shows some different orientations for two GeX fragments in the $X^2\Pi$ state which leads to a Ge-Ge σ bond.

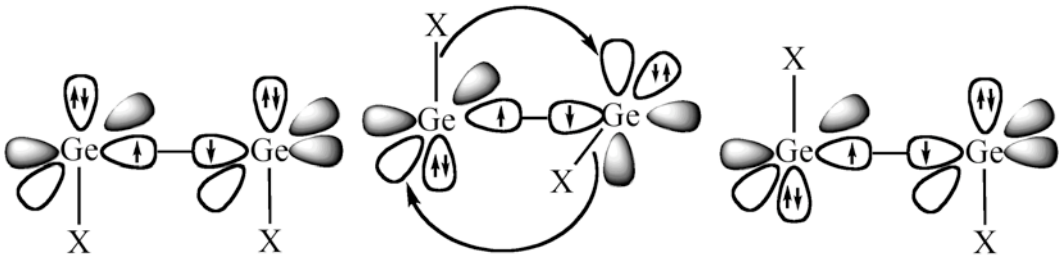

(a) (b) (c)

Figure 4.2.2.4. Qualitative model for the σ-type orbital interaction between two GeX molecules in different orientation where the unpaired electrons yield a σ orbital.

Figure 4.2.2.4 (a) shows a syn-planar arrangement of the GeX moieties, which gives the cis-bent isomer **GeF1**. This arrangement is not favorable because the vacant *p*(π) orbitals remain unoccupied while the Ge-X bonds and the electron lone-pairs of the two molecules repel each other. The geometry optimization of Ge_2X_2 with a syn-planar arrangement gives a structure which is a transition state.

The rotation around the σ-bond axis by 90° gives a much more favorable arrangement. In this bond situation, the empty *p(π)* orbitals of GeX can interact with the Ge-X bond and with the electron lone-pair of the other GeX fragment. The donor-acceptor interactions between the Ge-X bond and the vacant *p(π)* is more stabilizing than the donation from the electron lone-pairs to the *p(π)* because of more effective orbital combination. The acceptor bond is the *p* orbital and the lone-pair orbitals have also *p*-character, as shown in Table 4.2.2.4. These orbitals have both directional properties and the combination leads to a lower overlap of the orbitals. The Ge-X bond has large *s* character, which has less directional properties, and the Ge-X donor-acceptor leads to a three-center two-electron bond. This indicates that the Ge-X bonds are better donors than the lone-pairs. The Ge-X bonds interact with the empty *p(π)*

orbitals of the other GeX moiety. This arrangement gives the isomer **GeA** as shown in Figure 4.2.2.4 (b). This is similar to Si_2X_2 molecules. This explains why the global energy minimum is the doubly bridged butterfly structure **GeA** that is not planar but has a perpendicular arrangement of the two Ge_2X planes which have a dihedral angle between 101.3° and 105.8°. From the quantitative model, it is found that there are three bonding components of the orbital interactions in **GeA**: one σ bond and two Ge-X donor-acceptor bonds.

Figure 4.2.2.4 (c) shows the anti-planar arrangement of the GeX fragments, which gives the trans-bent isomer **GeE2**. The only Ge-Ge bonding contribution is the σ orbital between the two Ge atoms. The structure **GeE2** lacks the two Ge-X donor-acceptor interactions of **GeA**, and the vacant $p(\pi)$ orbitals remain unoccupied. This is similar to **GeF1**. The geometry optimization of Ge_2X_2 with an anti-planar arrangement gives structure which is a transition state.

In the previous session, the bond situation has been discussed with a qualitative model. Table 4.2.2.5 shows the shapes of the selected orbitals and their orbital energies of **GeA**, **GeE2** and **GeF1** concerning the Ge-Ge bonds. The first orbitals of **GeA**, **GeE2** and **GeF1** in Table 4.2.2.5 seem σ-type Ge-Ge bonds. The second one and third one of **GeA** seem Ge-X donor-acceptor bonds and those of **GeE2** and **GeF1** seem lone-pair orbitals. These orbitals show that the qualitative model is sensible in these σ system isomers.

Table 4.2.2.5 presents the Ge-Ge σ bonds and the orbitals are found as the HOMO in **GeA**, **GeE2** and **GeF1** of all Ge_2X_2 molecules, which are categorized as σ type structure in Figure 4.2.2.4. The energies of the HOMOs are presented in Table 4.2.2.3 and for GeF it has the highest HOMO energy of Ge_2X_2 system and the orbital energy decreases with heavier halogen atoms. They are similar to **SiA**, **SiE2** and **SiF1**. In the Ge_2X_2 system (X=F, Cl, Br and I), the energy level of σ type orbital clearly correlates with orbital energy of the SOMO of the GeX fragment. The Ge-Ge bond lengths in **GeE2** and **GeF1** are longer than the Ge-Ge single bond of X_3Ge-GeX_3 (Ge_2H_6: 2.424Å, Ge_2F_6: 2.457Å, Ge_2Cl_6: 2.481Å, Ge_2Br_6: 2.489Å, Ge_2I_6: 2.581Å at BP86/QZ4P level) because the σ bond in **GeE2** and **GeF1** is formed by the π orbitals of two GeX moieties, which are the SOMOs shown in Figure 4.2.2.2(b),

Table 4.2.2.5. Selected orbitals and orbital shapes and energies of σ-type isomers, **GeA**, **GeE2** and **GeF2**, which have a σ orbital. The energy levels are given in eV.

	GeA	**GeE2**	**GeF1**
orbital		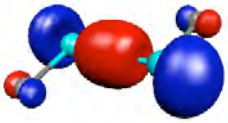	
	σ-type bond	σ-type bond	σ-type bond
H	-4.9343	-4.8376	-4.9036
F	-4.8014	-4.7061	-4.6294
Cl	-5.1566	-4.9601	-4.8032
Br	-5.1649	-4.9875	-4.7673
I	-5.2081	-5.0324	-4.8327
orbital	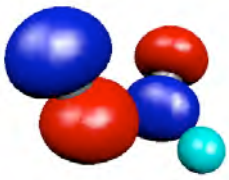	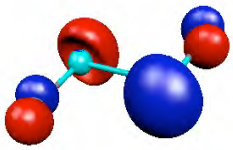	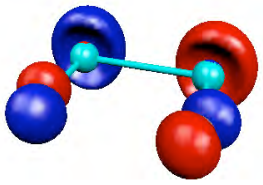
	Ge-X donor	lone-pair	lone-pair
H	-7.2164	-6.4754	-5.9603
F	-10.4398	-8.5813	-8.4571
Cl	-9.3580	-7.7011	-7.8200
Br	-8.9018	-7.2248	-7.3994
I	-8.3763	-6.6771	-6.9910
orbital	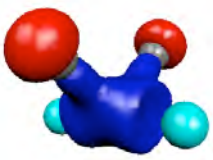	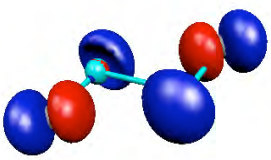	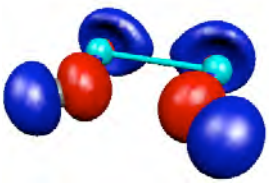
	Ge-X donor	lone-pair	lone-pair
H	-15.2314	-6.9388	-7.2985
F	-14.2042	-9.1699	-9.4276
Cl	-13.8073	-7.9352	-8.7999
Br	-13.7558	-7.4323	-8.3639
I	-13.4201	-6.8606	-7.9635

and the σ bond has little *s* character, whereas the normal Ge-Ge σ bond has sp^3 character. The energy level of the σ type orbital in Ge_2F_2 is the highest in **GeA**, **GeE2** and **GeF1**, where the orbital energies become lower when the halogen atom X gets heavier.

GeA clearly has two Ge-X donor-accepter bonds as shown in Table 4.2.2.5. These two orbitals in Table 4.2.2.5 are very similar except the node on the Ge-Ge bond. The energetically higher orbital has a node on the Ge-Ge bond and the lower one does not. From these orbital figures, it can be determined that the energetically higher orbital is the anti-bonding orbital of lower (Figure 4.2.2.5). The energetically lower orbital has large coefficients on both Ge atoms and this orbital contributes to the Ge-Ge bond. The energetically higher orbital has large coefficients on two Ge atoms and the X atom and this orbital contributes to the formation of the Ge-X-Si ring structure. This can explain the Ge-Ge bond lengths in **GeA**, which are shorter than the Ge-Ge single bond of **GeE2** and **GeF1**. These results are very similar to Si_2X_2 system.

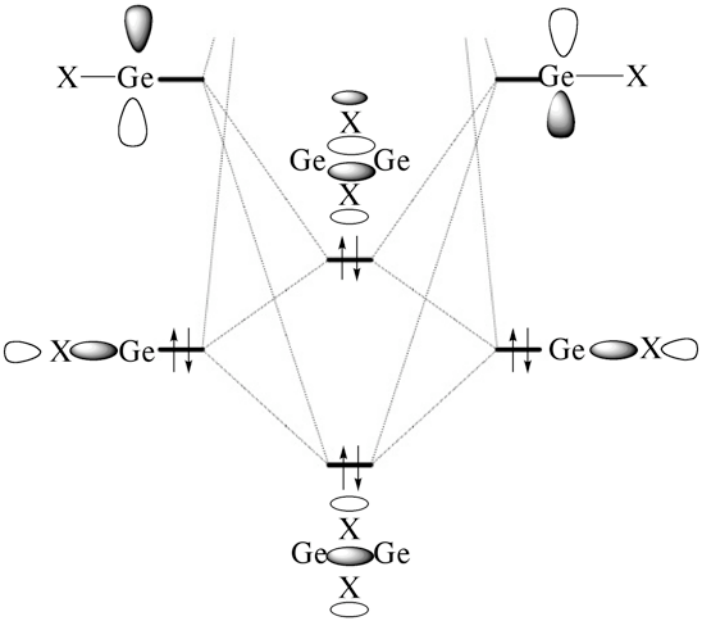

Figure 4.2.2.5. Orbital correlation model for the donor-acceptor interaction between the Ge-X bond and the vacant $p(\pi)$ orbital in the $X^2\Pi$ ground state of two Ge-X fragments to produce bridged structures.

Figure 4.2.2.5 shows that the two Ge-X donor-acceptor bonds interact and form new two orbitals, which is similar to Figure 4.1.2.5. In principle, the orbital energy level of the two new formed orbitals depends on the energy level of original orbitals, i.e. the energy level of the vacant π orbital and the Ge-X bond orbital. Table 4.2.2.5 shows that the orbital energies of two Ge-X donor-acceptor bonds become higher as the halogen atom gets heavier and it is similar trend to orbital energies of the Ge-X bond because the main contribution of the orbital is the Ge-X bond.

In **GeE2** and **GeF1**, the two lone-pair orbitals interact with each other and they form a bonding orbital between the two GeX moieties. However, they form an occupied anti-bonding orbital at the same time (Figure 4.2.2.6). This system is the four-electron two-orbital interaction and the interaction between two lone-pair orbitals almost cancels; for the bond formation, therefore, this interaction has only a little contribution to the Ge-Ge bond. This is similar to **SiE2** and **SiF1**.

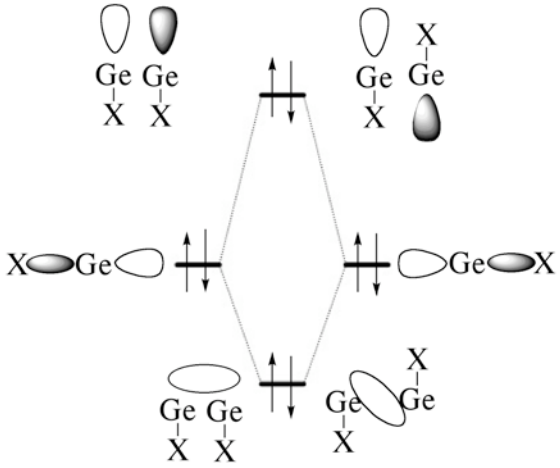

Figure 4.2.2.6 Orbital correlation diagram between two lone-pair orbitals of two Ge-X fragments in the $X^2\Pi$ ground state in σ-type bent-structures, **GeE2** and **GeF1**.

4.2.2.1.3 π-type Isomers, **GeB**, **GeC**, **GeE1** and **GeE2**

The unpaired electrons in the $X^2\Pi$ ground state of Ge-X fragments may also be paired in an electron-sharing Ge-Ge bond between the two Ge-X fragments, which has a π symmetry with respect to the molecular structure. Figure 4.2.2.7 shows different orientations for two ($X^2\Pi$) GeX molecules which lead to a Ge-Ge π bond, which is similar to Figure 4.1.2.7.

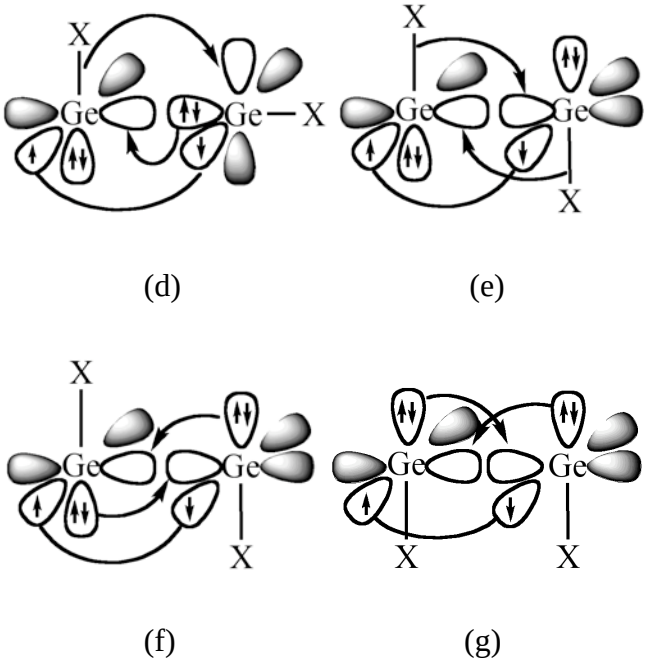

Figure 4.2.2.7 Qualitative model for the π-type orbital interaction between two GeX molecules in different orientations where the unpaired electrons yield a π orbital.

The arrangement that is given in Figure 4.2.2.7(d) has an electron lone-pair on one GeX moiety pointing in the direction of the empty π orbital of the other GeX species. This orbital interaction has σ symmetry with respect to the $(GeX)_2$ dimer plane. Besides the electron-sharing π bond and the lone-pair donor-acceptor σ bond, further stabilizing orbital interactions are possible in the structure shown in Figure 4.2.2.7(d). Another possibility is the donation of the GeX bonding orbital, which is shown in the orbital of **GeA** in Figure 4.2.2.4(b). As noted before, the donation from the GeX bonding orbital is stronger than that from the lone-pair orbital. The former interaction becomes stronger when the GeX donor orbital and the empty π orbital of the interacting fragments are tilted toward each other, which leads to the structure **GeB** (Figure 4.2.2.7(d)). The tilting of the empty π orbital of the acceptor GeX moiety (top GeX in Figure 4.2.2.7(d)) means that the terminal atom moves toward the bridging halogen atom. The syn orientation of the terminal atom with respect to the bridging X atom can be explained as a secondary effect of optimizing the GeX donor-acceptor interaction, which is shown in Figure 4.2.2.7(d) and which is similar to Si_2X_2. The unusual singly bridged geometry of **GeB**, which has a terminal halogen atom with syn-orientation to the bridging atom, can thus be explained as a

Table 4.2.2.6. Selected orbitals and orbital energies of π-type isomers, **GeB, GeC**, **GeE1** and **GeF**. The energy levels are given in eV.

	GeB	**GeC**	**GeE1**	**GeF2**
orbital	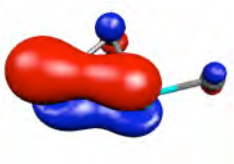	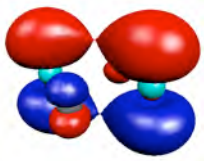		
	π-type bond	π-type bond	π-type bond	π-type bond
H	-5.0268	-4.8519	-5.0525	-4.9935
F	-4.7764	-3.8078	-4.9903	-4.8968
Cl	-4.8786	-4.1531	-5.0240	-4.9155
Br	-4.8397	-4.1881	-4.9829	-4.8796
I	-4.8138	-4.2419	-4.9454	-4.8446
orbital			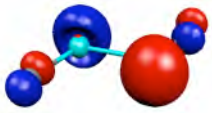	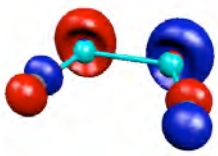
	lone-pair donor	Ge-X donor	lone-pair	lone-pair
H	-7.0698	-9.4833	-6.6924	-6.0952
F	-8.3883	-10.4655	-8.4816	-8.4520
Cl	-7.6260	-9.4689	-7.7557	-7.6682
Br	-7.2230	-9.0705	-7.3957	-7.3098
I	-6.7214	-8.5865	-6.9066	-6.8370
orbital	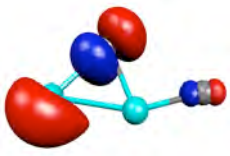		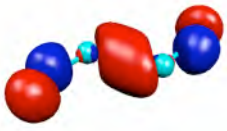	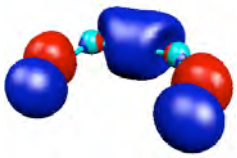
	Ge-X donor	Ge-X donor	lone-pair	lone-pair
H	-8.1934	-15.3959	-8.3697	-8.0444
F	-9.7893	-13.7414	-10.7823	-10.6163
Cl	-8.5847	-13.5164	-9.6118	-9.4763
Br	-8.0374	-13.5266	-9.1153	-9.0159
I	-7.4315	-13.2565	-8.5108	-8.4494

stereoelectronic effect that comes from the orbital interactions between two GeX fragments in their $X^2\Pi$ ground states. Figure 4.2.2.7 (e) displays another orientation of two GeX molecules where the unpaired electrons form a π bond, while the GeX bonds are in an anti-planar arrangement. The π orbital interaction between the GeX fragments is enhanced by two equal donor-acceptor interactions between the GeX bonding orbitals and the empty π orbitals of the interacting fragments. The latter orbital interactions become stronger when the halogen atoms bridge in a doubly bridged planar (D_{2h}) structure. Geometry optimizations of $(GeX)_2$ show that the D_{2h} symmetric stationary points is an energetically low-lying structure on the potential energy surface. The inspection of the Hessian matrix reveals, however, that it is a transition state for the degenerate rearrangement of the global energy minimum structure **GeA**. It is the wing-flapping motion of the butterfly geometry. The structure **GeA** has a Ge-Ge σ bond and two GeX donor-acceptor bonds (Figure 4.2.2.4(b)), while the transition state has a Ge-Ge π bond and two GeX donor-acceptor bonds (Figure 4.2.2.7(e)).

The donation of the electron lone-pair is less stabilizing than the GeX donation, and it leads to another structure of $(GeX)_2$. Figure 4.2.2.7(f) and Figure 4.2.2.7(g) show that the donation of lone-pair of the GeX fragment to the vacant p_π orbital becomes enhanced tilting the Ge-X bond outwardly, which yields the trans and cis form **GeE1** and **GeF2**, respectively. According to the orbital analysis, the structures **GeE1** and **GeF2** have three bonding orbital components, which are one π bond and two lone-pair donor-acceptor bonds. The structures **GeE1** and **GeF2** of Ge_2H_2 are energetically higher lying than the planar transition state with two bridging hydrogen atoms, **GeC**, which has one π bond and two Ge-X donor-acceptor bonds, whereas those for Ge_2F_2, Ge_2Cl_2, Ge_2Br_2 and Ge_2I_2 are energetically lower lying than the planar transition state with two bridging halogen atoms.

Table 4.2.2.6 shows the orbital energies of important orbitals in **GeB**, **GeC**, **GeE1** and **GeF2**, which concern the Ge-Ge bond. Table 4.2.2.6 presents the Ge-Ge π bond of **GeB, GeC**, **GeE1** and **GeF1**, which are categorized to a π type structure in Figure 4.2.2.7. In these isomers, the Ge-Ge π bond is found as the HOMO. The energy of the π type orbital in Ge_2F_2 is the highest in **GeB**, **GeC**, **GeE1** and **GeF2**, where the orbital energies become lower when the halogen atom X becomes heavier.

This correlates with the energy level of SOMO of the GeX fragment. However the π orbital energy is higher in energy than those of Si_2X_2 molecules. Here, the **GeE1** structures in Ge_2F_2, Ge_2Cl_2, Ge_2Br_2 and Ge_2I_2 are transition states, where the same trans-bent structures of **SiE1** of Si_2X_2 are minima. The difference comes from the character of π orbital of GeX molecules. The π orbital of GeX molecules is larger than that of SiX. However, the Ge-Ge distance in Ge_2F_2, Ge_2Cl_2, Ge_2Br_2 and Ge_2I_2 is also longer and the overlap between two Ge atoms is still small. These energetically higher π bonds are not strong enough to stabilize the planar structure and the rotation does not need a large energy to break the Ge-Ge π bond. In account of that, the isomers **GeE1** are transition states. The isomers **GeC** of Ge_2F_2, Ge_2Cl_2, Ge_2Br_2 and Ge_2I_2 are transition states because the energy of the π orbital is relative high. The isomers of **GeF2** show relative energetically high π bond, and due to that, they are transition state. The π bond is weak and the rotate is easy.

In principle, a π bond is weaker than a σ bond and a "single" π bond should be longer than a σ bond, because a π bond usually has less orbital overlap than a σ bond. However, the Ge-Ge bond lengths in **GeB, GeE1** and **GeF2** are shorter than the Ge-Ge single bond in **GeE2** and **GeF1** as shown in the chapter 4.2.1.1. This suggests that other interactions except the π orbital interaction could exist between Ge-Ge atoms as expected in Figure 4.2.2.7. These interactions are the donor-acceptor bond from the Ge-X bond and lone pair, respectively, to vacant π orbital, which is similar to the Si_2X_2 isomers.

The second orbital of **GeB** of Table 4.2.2.6 shows that a huge amount of electron density from these orbital is located between the two Ge atoms and the shape of the orbital is similar to the lone-pair donor-acceptor bond model in Figure 4.2.2.7(d). The orbital figure is quite similar to that of **SiB**. The energy levels of this orbital correlate with the energies of lone-pairs of the Ge-X fragments (Table 4.2.2.6), where the orbital energy level becomes lower when halogen atom X gets heavier. The trend is similar to that of **SiB**. To form the donor-acceptor bond, the lone-pair orbital interacts with the vacant π orbital of the GeX fragment. The formed donor-acceptor orbital mainly has the character of original lone-pair orbital and the energy level of the formed orbital exhibits the correlation with the lone-pair orbital.

The third orbital of **GeB** in Table 4.2.2.6 shows that a huge amount of electron density from these orbital is located between Ge atoms and the main contribution is not Ge-X bond donor-acceptor bond. However, the orbital has a large amount of electron density in the Ge-X-Ge region. The energy level of this orbital is moderately higher than that of Ge-X donor-acceptor bond in **GeA**. The energy level of the orbital shows a similar trend with the orbital energy of Ge-X bond in the GeX fragment (Table 4.2.2.6), where the orbital energy level becomes lower when halogen atom X gets heavier, which is similar trend of **SiB**.

The structures **GeC** have a π bond and two Ge-X bond donor-acceptor bonds (Table 4.2.2.6). The Ge-X donor-acceptor bond orbitals are quite similar to those of **GeA**. The two Ge-X donor-acceptor bonds form two new orbitals and the main contributions are the regions of Ge-Ge bond and Ge-X-Ge ring structure, respectively, which are same as the bond correlation in Figure 4.2.2.7(e). The energy level of π orbital is higher than that of σ orbital of **GeA**. Due to this, **GeC** is unstable and it is a transition state.

These two orbitals of **GeE1** and **GeF1** are similar to the two lone-pair orbitals in **GeE2** and **GeF1**, respectively (Table 4.2.2.6). When the energy levels of these orbitals are compared, the lower “lone-pair like” orbital energies of **GeE1** are 1.43 to 1.67 eV lower than the energies of lone-pair orbital in **GeE2**, where the lone-pairs in **GeE2** do not contribute to the Ge-Ge single bond. The orbital energy differences between **GeF1** and **GeF2** are 0.49 to 1.18 eV. The stabilization comes from the contribution of vacant π orbital of the fragment, where the stabilization is similar to that of **SiE1** and **SiF2.** The energetically higher lying orbital has a node along the Ge-Ge bond and the lower one does not. From these orbital figures, it can be thought that the energetically higher orbital is the anti-bonding orbital of lower one and the two equivalent lone-pair donor-acceptor orbitals produce two orbitals (Figure 4.2.2.8 and Figure 4.2.2.9). The energetically lower lying orbital has a large coefficient on the Ge-Ge bond and this orbital contributes to the Ge-Ge bond. The energetically higher lying orbital is similar to the original lone-pair orbital. This can explain the Ge-Ge bond lengths in **GeE1** and **GeF2**, which are shorter than Ge-Ge single bond of **GeE2** and **GeF1**.

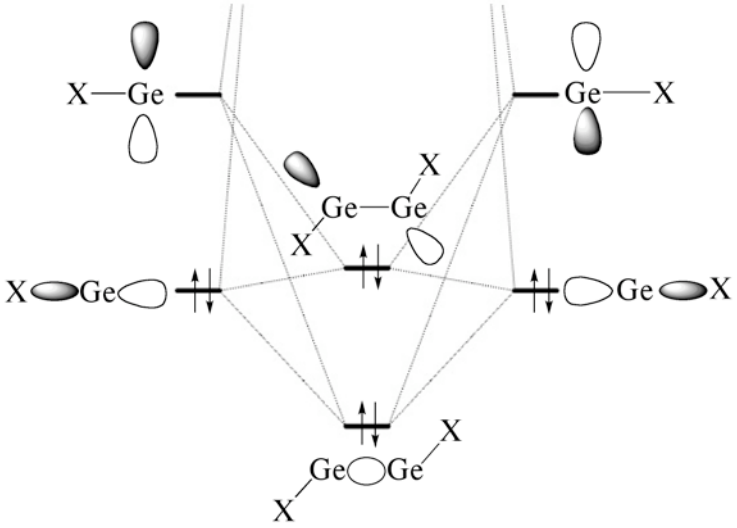

Figure 4.2.2.8. Orbital correlation diagram between two lone-pair orbitals and vacant *p*(π) orbitals of two Ge-X fragments in their ground state in **GeE1**.

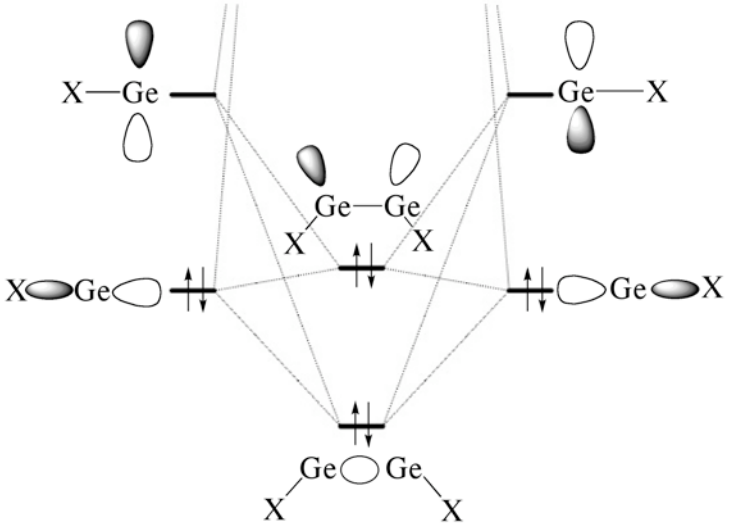

Figure 4.2.2.9. Orbital correlation diagram between two lone-pair orbitals and the vacant *p*(π) orbitals of two Ge-X fragments in their ground state in **GeF2**.

4.2.2.1.4 Summary of Orbital Analyses

In this chapter, the orbital analyses of the Ge_2X_2 molecules and their fragments GeX are investigated. The analyses of GeX fragments showed the high excitation energy from the $X^2\Pi$ ground state to the $a^4\Sigma^-$ excited state, where the energies are larger than those of the SiX molecules. Due to that, the linear structures shows negative dissociation energies and the structures are unfavorable. Instead of that, GeX molecules prefer the interactions between two GeX fragments in their ground state. The orbital analyses of fragments showed that the orbital energy exhibits a correlation with the X atom.

The orbital analyses of Ge_2X_2 molecules show that qualitative models between two GeX fragments are sensible as the orbital interaction models of the Ge_2X_2 isomers. The isomers with the XGe-GeX structure are categorized to two groups: σ-type isomers and π-type isomers. The doubly bridged structure **GeA** is categorized to the σ-type structure and the structure shows three components of the bondings: one σ-orbital and two Ge-X donor-acceptor interactions, although the other σ-type isomers, **GeE2** and **GeF1** have just σ-orbital, where the Ge-X donor-acceptor bond is a reasonable bonding situation between Ge-X molecules for the reason that the bonding leads the three-center-two-electron-bond.

The orbital analyses of π-type isomers, **GeB**, **GeC**, **GeE1** and **GeF2** show the energetically high π orbital. Due to that, their π bonds are not stable and they are transition states. The orbital energies of the lone-pair type orbitals for **GeE1** and **GeE2** are different from those for **GeF2** and **GeF1**. Especially, the lower lone-pair like orbitals of **GeE1** and **GeF2** are more stable than those of **GeE2** and **GeF1**. The difference of orbital energies suggests the interaction of the lone-pair orbitals with the vacant *p*-orbital.

4.2.2.2 AIM Analyses

In the previous section, the orbitals and their energies were investigated and they showed the interactions between two GeX fragments are reasonable. However, the charge distributions between two fragments are not clear. It is interesting to compare the electron densities in Ge_2X_2 systems with each other. Figure 4.2.2.10 – Figure 4.2.2.17 show the Bader plots of Ge_2X_2 isomers. In general, the zero flux surfaces exhibits that Ge_2F_2 molecules have more ionic character and Ge_2I_2 molecules have more covalent character of Ge-X bond.

Figure 4.2.2.10 shows the Bader plot of the isomers **GeA** in the Ge_2X plane. The bond paths indicate that all **GeA** isomers have Ge-X-Ge bridged structures, which is consistent with the results of the geometry and orbital analyses. For Ge_2F_2, Ge_2Cl_2, Ge_2Br_2 and Ge_2I_2 molecules, a charge accumulation is found between two Ge atoms. However, the accumulated region is quite smaller compared to that of Si_2X_2 molecules. This suggests that Ge_2X_2 has smaller orbital interaction contributions and the ionic interaction is more important for the Ge-X-Ge bridging.

In the chapter 4.2.1.1 and 4.2.2.1, the bond situations in **GeB** in Figure 4.2.2.11 have been discussed. However, the lone-pair donor-acceptor bonds and Ge-X donor-acceptor bonds were not clear in **GeB** in the orbital analysis and the viewpoint of the geometry. The AIM results show that all **GeB** isomers have a Ge-X-Ge ring structure, which agrees with the orbital interaction model of **GeB**. The bond situation is different from **SiB** isomers, where the **SiB** isomers do not have a ring-structure except Si_2F_2. The small charge accumulation for all **GeB** isomers and the bond paths indicates the importance of the electrostatic interaction in the ring structures.

Figure 4.2.2.12 shows the **GeC** isomers have Ge-X-Ge bridged structure. The AIM results show that Ge_2H_2, Ge_2Cl_2, Ge_2Br_2 and Ge_2I_2 molecules have a Ge-Ge bond, whereas Ge_2F_2 shows no Ge-Ge bonding but F-F interaction. The result of Ge-Ge bond path agrees with the discussions of their geometries. The charge accumulation is not found in all Ge_2X_2 molecules, which is similar to **SiC**. It indicated that the ionic interaction plays an important role in Ge-X-Ge bridged structure.

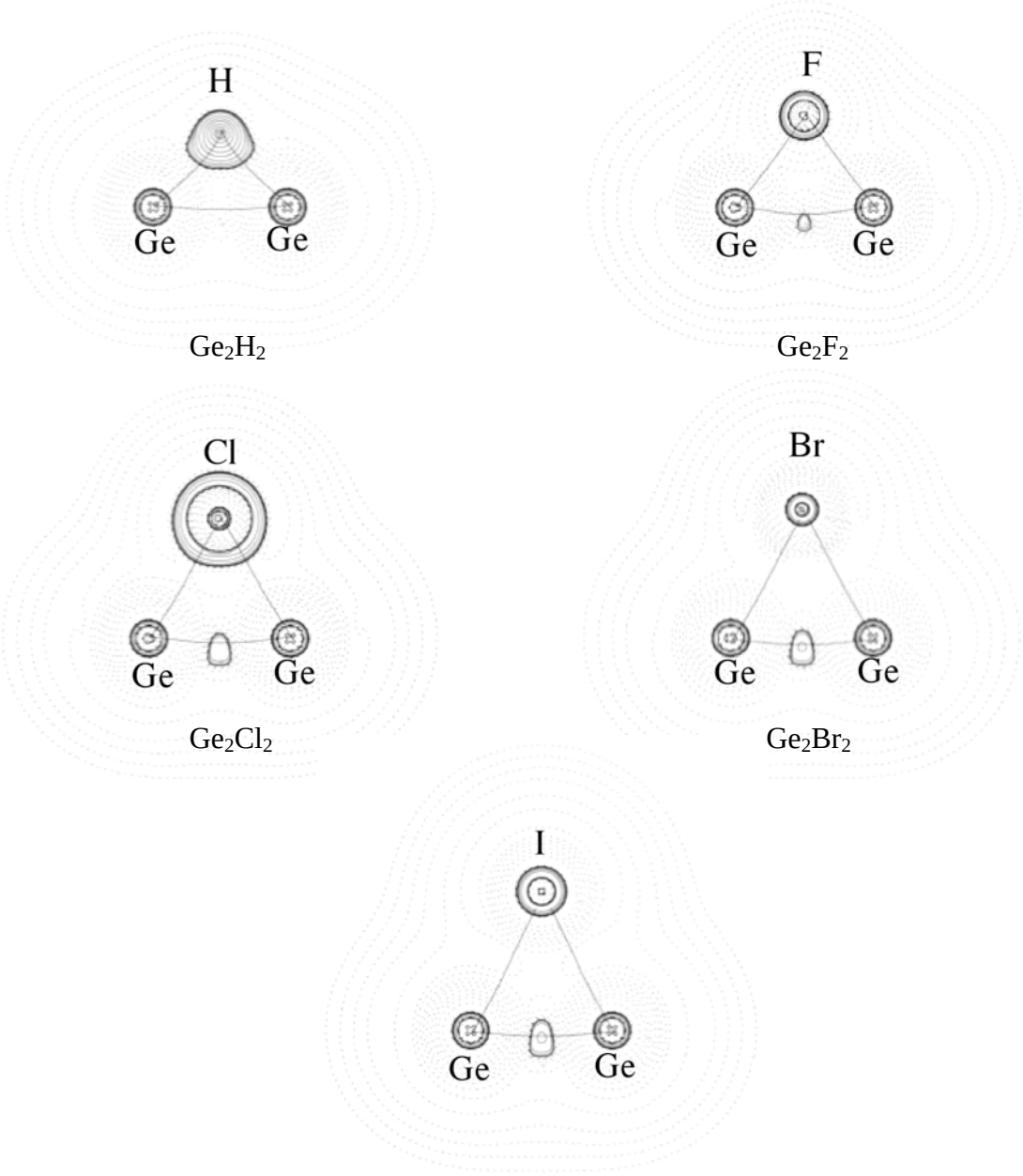

Ge_2H_2 Ge_2F_2

Ge_2Cl_2 Ge_2Br_2

Ge_2I_2

Figure 4.2.2.10 Contour line diagram $\nabla^2\rho(r)$ of isomer **GeA** in the plane of two Ge atoms and one of the X atoms. Solid lines indicate areas of charge concentration ($\nabla^2\rho(r) < 0$), while dashed lines show areas of charge depletion ($\nabla^2\rho(r) > 0$). Solid lines that connect atomic nuclei are bond paths.

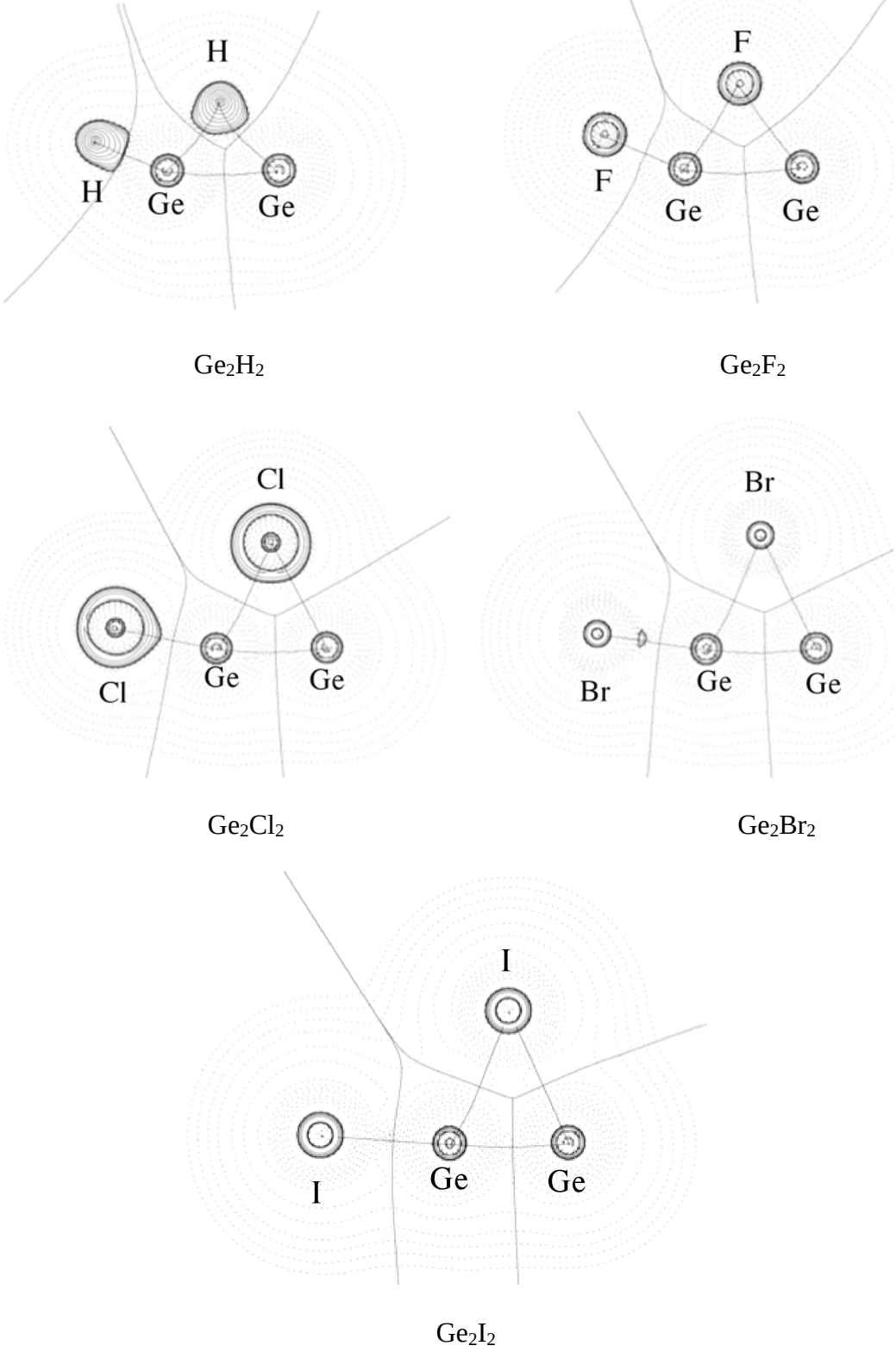

Ge_2H_2 Ge_2F_2

Ge_2Cl_2 Ge_2Br_2

Ge_2I_2

Figure 4.2.2.11 Contour line diagram $\nabla^2\rho(r)$ of isomer **GeB**. Solid lines indicate areas of charge concentration ($\nabla^2\rho(r) < 0$), while dashed lines show areas of charge depletion ($\nabla^2\rho(r) > 0$). Solid lines that connect atomic nuclei are bond paths.

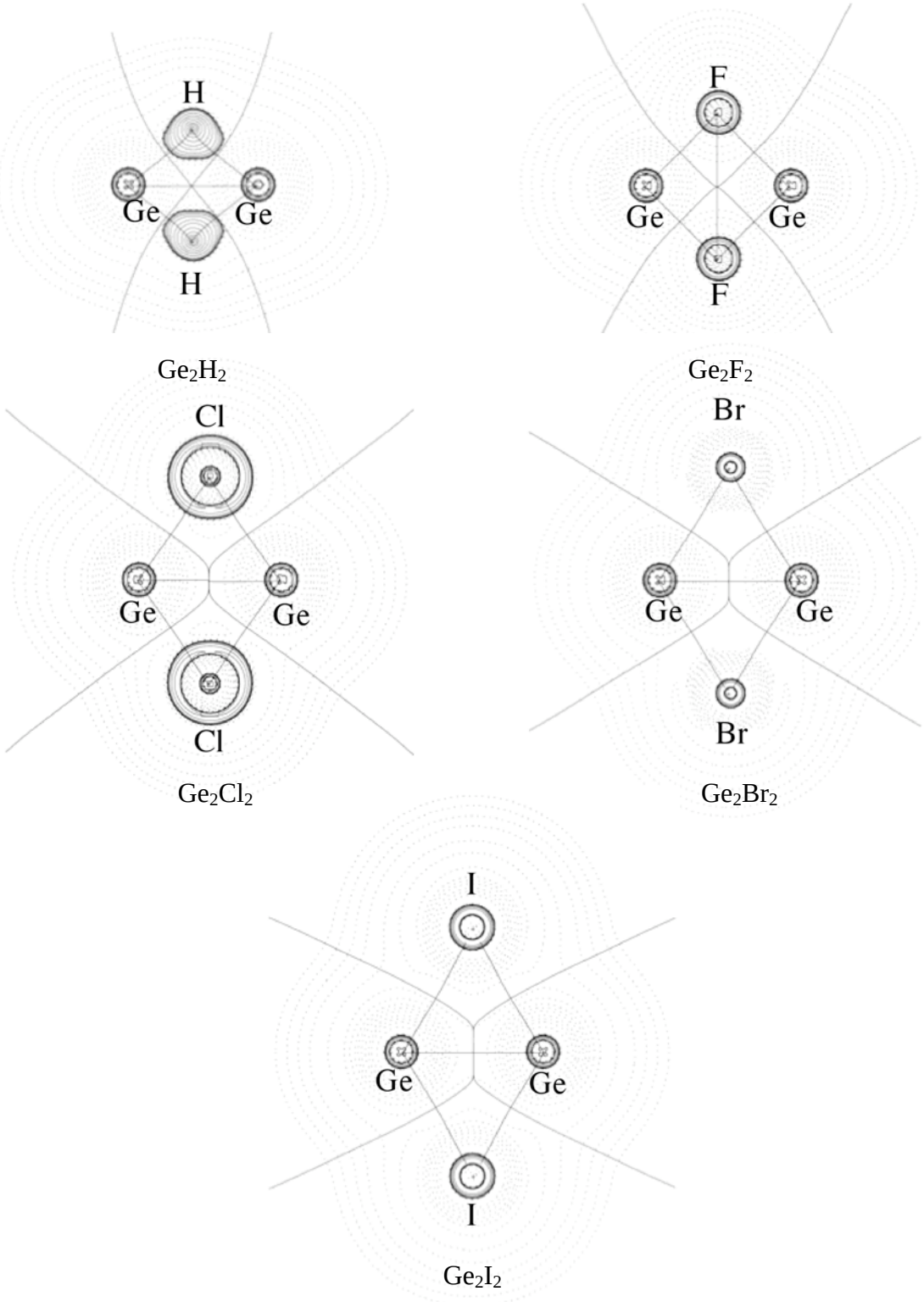

Ge_2H_2 Ge_2F_2

Ge_2Cl_2 Ge_2Br_2

Ge_2I_2

Figure 4.2.2.12 Contour line diagram $\nabla^2\rho(r)$ of isomer **GeC**. Solid lines indicate areas of charge concentration ($\nabla^2\rho(r) < 0$), while dashed lines show areas of charge depletion ($\nabla^2\rho(r) > 0$). Solid lines that connect the atomic nuclei are the bond paths.

Figure 4.2.2.13 shows bond paths and the Laplacian of the densities for the vinyl isomers **GeD**. The figure indicates the Ge-Ge bond and the Ge-X bond. A charge accumulation indicates the covalent character of the Ge-Ge bonds. However, the covalent character of Ge-Ge bond is smaller than that of Si-Si bond of **SiD** because charge accumulation is smaller than that of **SiD**.

The contour line diagrams in Figure 4.2.2.14 show that the Ge-Ge bonds and Ge-X bonds of **GeE1** isomers. No charge accumulation is found in the region of Ge-Ge bond, although **SiE1** showed large charge accumulations and they are interpreted as a Si-Si bond. In Chapter 4.2.2.1, the orbital figures of **GeE1** showed two lone-pair donor-acceptor bonds. However, the lone-pair donor-acceptor orbital showed smaller contribution for the Ge-Ge bond than those of **SiE1**. Due to that, **GeE1** shows no charge accumulation.

Bond paths of Figure 4.2.2.15 show that **GeE2** has the Ge-Ge bonds and Ge-X bonds. The charge accumulation among the Ge-Ge bond region shows that the Ge-Ge bond has electron-sharing covalent bond character. **GeE2** showed different pictures of charge accumulation from **GeE1.** It clearly shows the difference of bond situation between **GeE1** and **GeE2**, where the qualitative models of Figures 4.2.2.4 and Figure 4.2.2.7 indicates that **GeE2** has a Ge-Ge σ bond and **GeE1** has a π bond and two donor-acceptor bonds. It is consistent with the orbital analyses in the previous chapter 4.2.2.1.

The AIM results of **GeF1** in Figure 4.2.2.16 show Ge-Ge bonds and Ge-X bonds. The figures of **GeF1** are similar to **SiF1**, but the charge accumulation is quite smaller. The Ge-Ge bonding situation is quite similar to that of **GeE2**, and the Ge-Ge bond has still a covalent character. Bond paths between two halogen atoms indicate the X-X interaction in Ge_2Cl_2, Ge_2Br_2 and Ge_2I_2. It is due to that the Ge-Ge-X angle is nearly 90° and Br and I have large radius.

Figure 4.2.2.17 shows the Ge-Ge bonding and Ge-X bonding of **GeF2**. No charge accumulation in the region of the Ge-Ge bond indicates the less covalent character of the Ge-Ge bond, where the Si-Si bond of **SiF2** showed a covalent character. The situation is similar to that of **GeE1**.

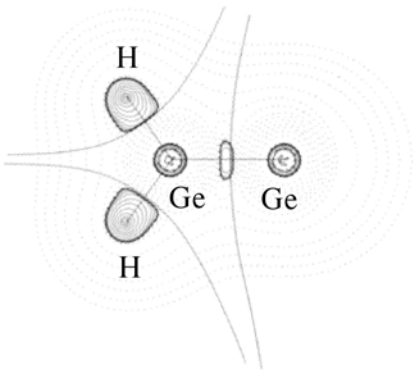

Ge_2H_2

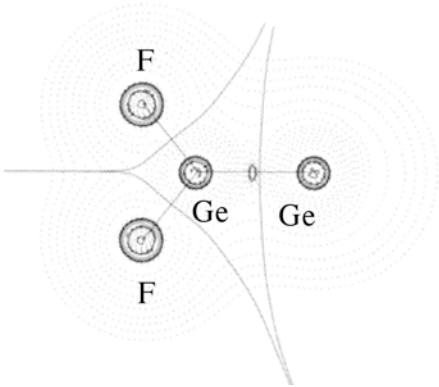

Ge_2F_2

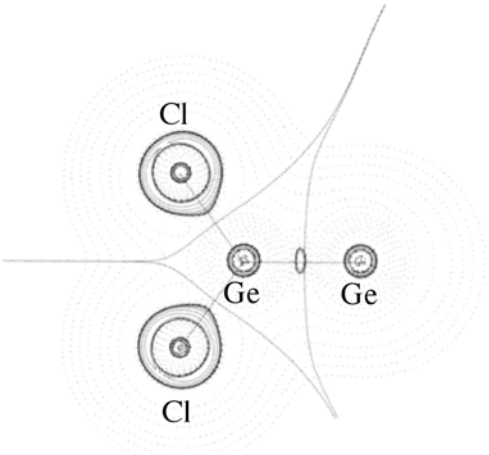

Ge_2Cl_2

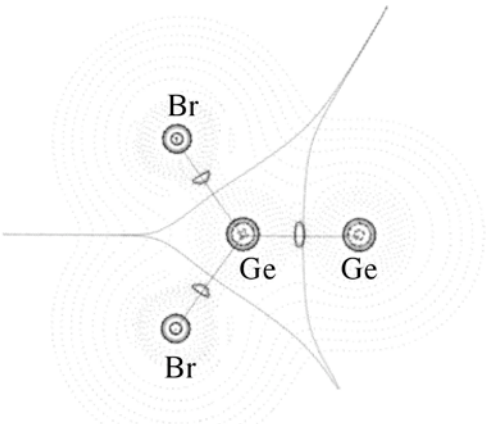

Ge_2Br_2

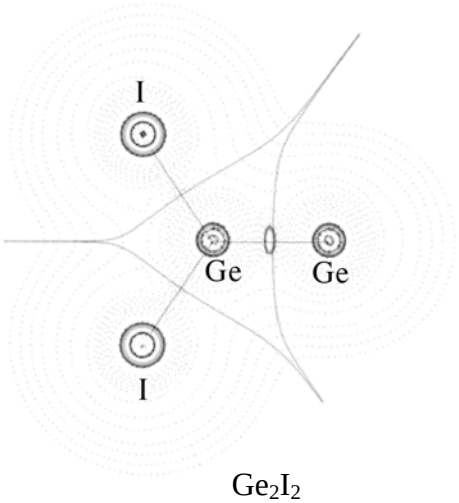

Ge_2I_2

Figure 4.2.2.13 Contour line diagram $\nabla^2\rho(r)$ of isomer **GeD**. Solid lines indicate areas of charge concentration ($\nabla^2\rho(r) < 0$), while dashed lines show areas of charge depletion ($\nabla^2\rho(r) > 0$). Solid lines that connect the atomic nuclei are the bond paths.

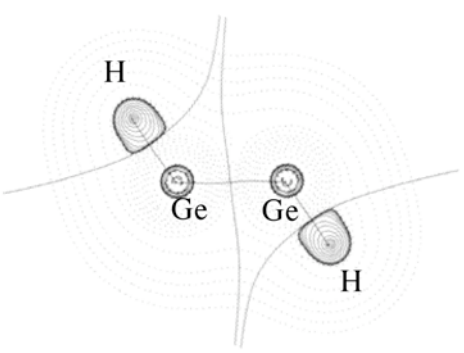

Ge_2H_2

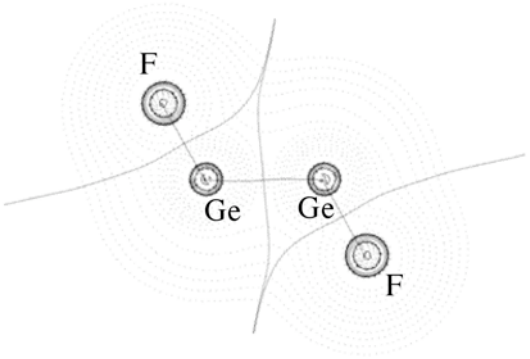

Ge_2F_2

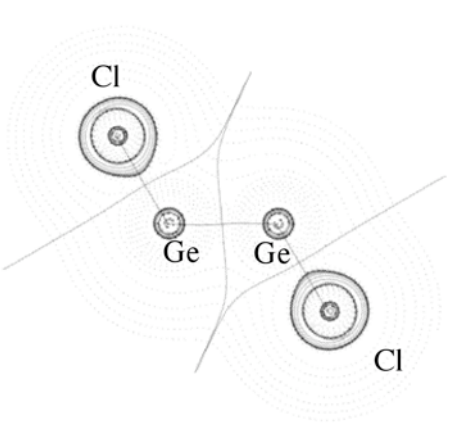

Ge_2H_2

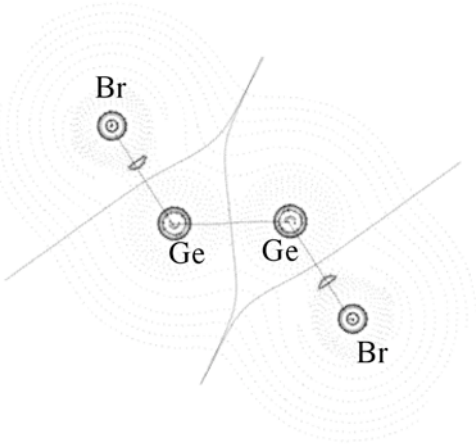

Ge_2F_2

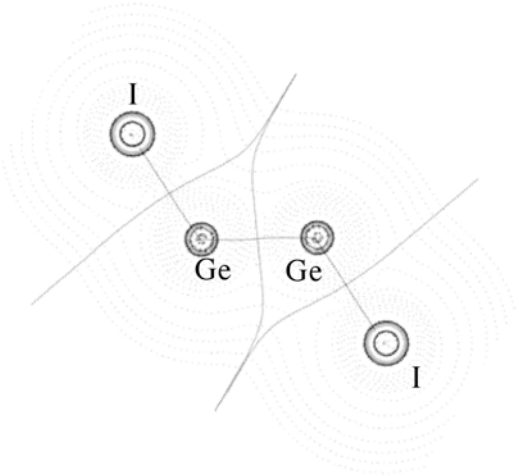

Ge_2H_2

Figure 4.2.2.14 Contour line diagram $\nabla^2\rho(r)$ of isomer **GeE1**. Solid lines indicate areas of charge concentration ($\nabla^2\rho(r) < 0$), while dashed lines show areas of charge depletion ($\nabla^2\rho(r) > 0$). Solid lines that connect the atomic nuclei are the bond paths.

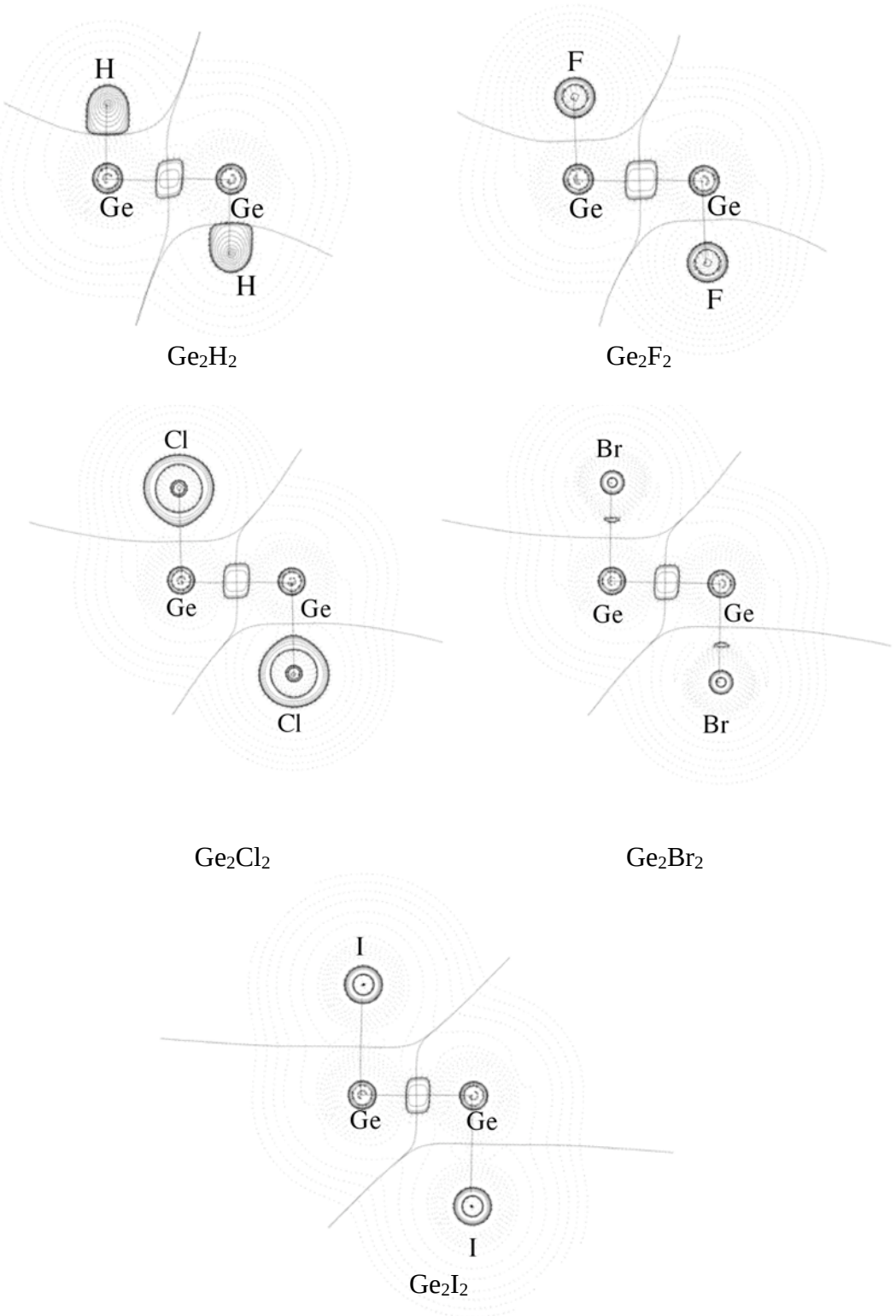

Ge_2H_2 Ge_2F_2

Ge_2Cl_2 Ge_2Br_2

Ge_2I_2

Figure 4.2.2.15 Contour line diagram $\nabla^2\rho(r)$ of isomer **GeE2**. Solid lines indicate areas of charge concentration ($\nabla^2\rho(r) < 0$), while dashed lines show areas of charge depletion ($\nabla^2\rho(r) > 0$). Solid lines that connect the atomic nuclei are the bond paths.

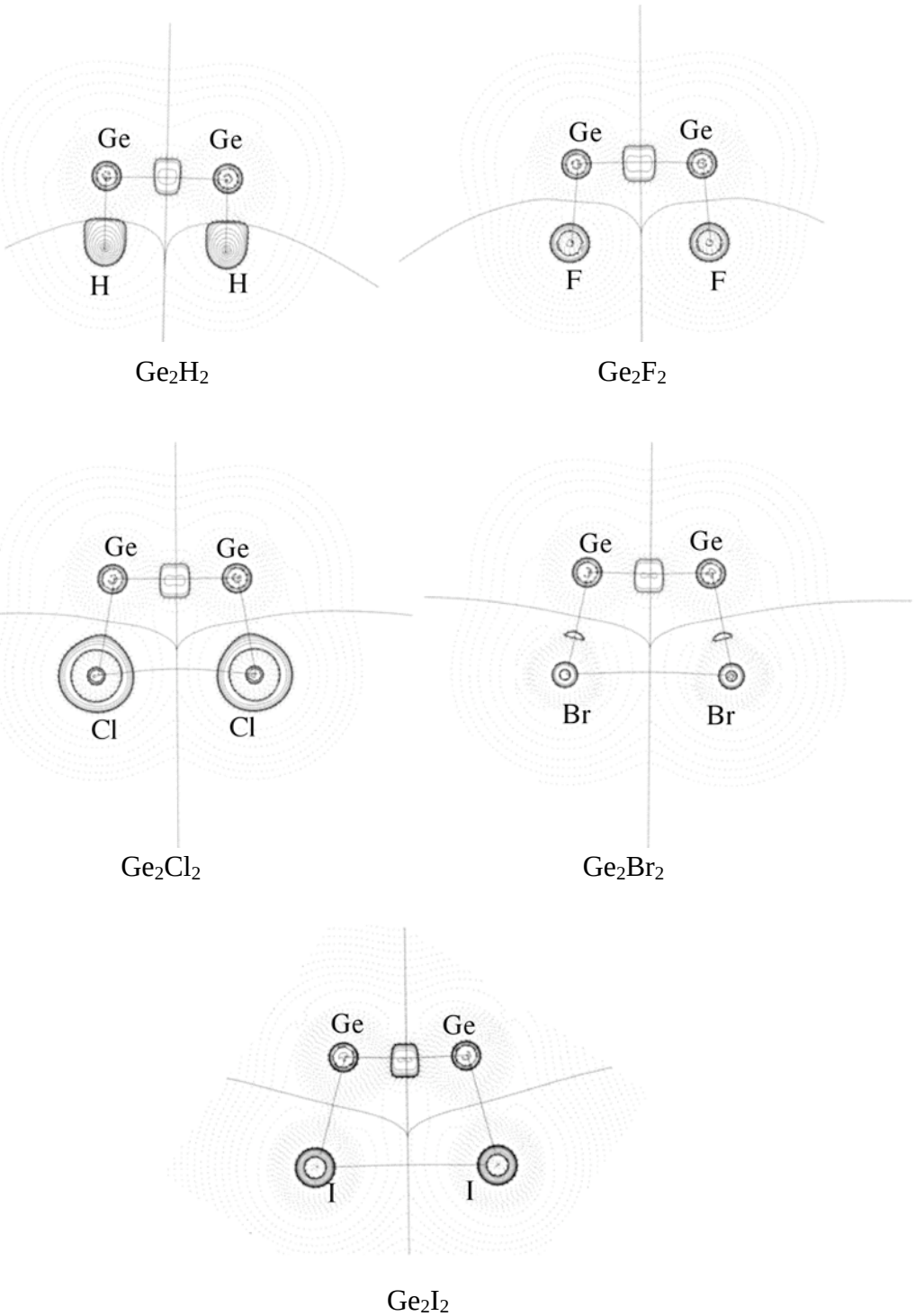

Ge_2H_2 Ge_2F_2

Ge_2Cl_2 Ge_2Br_2

Ge_2I_2

Figure 4.2.2.16 Contour line diagram $\nabla^2\rho(r)$ of isomer **GeF1**. Solid lines indicate areas of charge concentration ($\nabla^2\rho(r) < 0$), while dashed lines show areas of charge depletion ($\nabla^2\rho(r) > 0$). Solid lines that connect the atomic nuclei are the bond paths

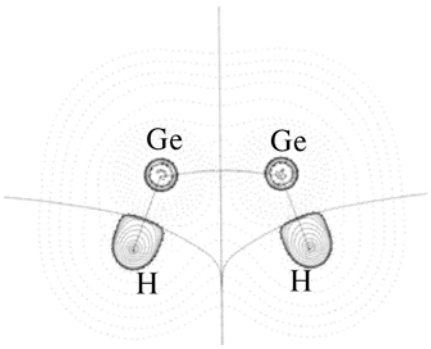

Ge_2H_2

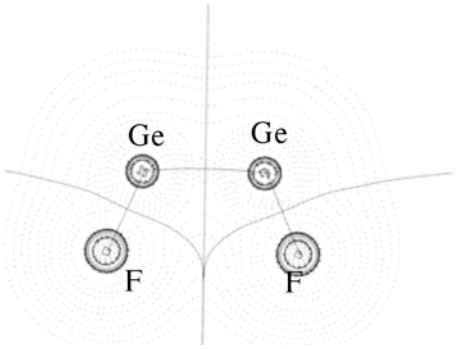

Ge_2F_2

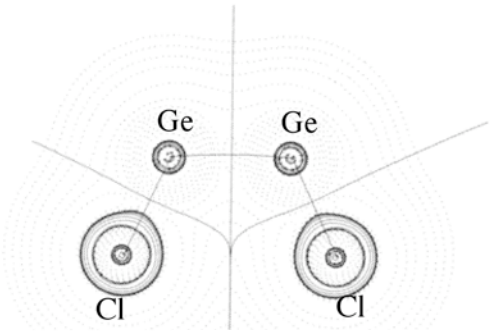

Ge_2H_2

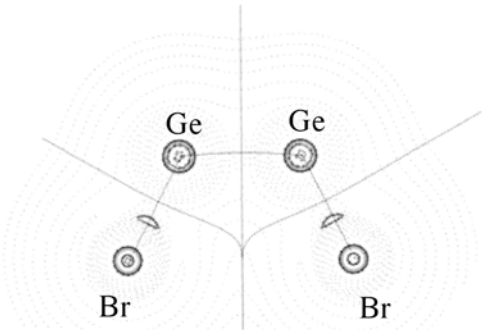

Ge_2F_2

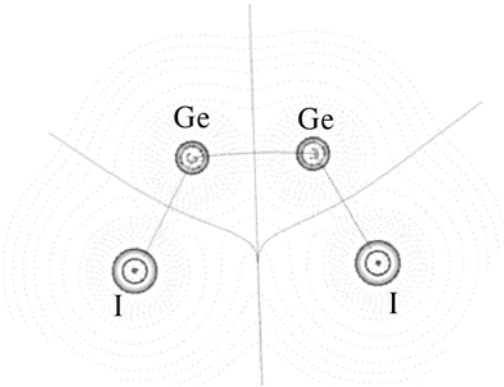

Ge_2I_2

Figure 4.2.2.17 Contour line diagram $\nabla^2\rho(r)$ of isomer **GeF2**. Solid lines indicate areas of charge concentration ($\nabla^2\rho(r) < 0$), while dashed lines show areas of charge depletion ($\nabla^2\rho(r) > 0$). Solid lines that connect the atomic nuclei are the bond paths

As a summary of AIM analyses, the AIM results showed that **GeA**, **GeB** and **GeC** have ring-structures and these isomers show small charge accumulation, which is consistent with the results, that electrostatic interaction is important for the bridged structures. The charge accumulation of bent structures indicated the difference of the electro-sharing σ-bond of **GeE2** and **GeF1**, and the lone-pair donor-acceptor bond of **GeE1** and **GeF2**. The charge accumulation is quite smaller than that of Si_2X_2 isomers.

4.2.2.3. Charge Analyses

In chapter 4.2.2.1, the orbital interactions of the two fragments are shown, and the orbital interaction could explain the geometry of each isomer well. AIM analyses were carried out and described in chapter 4.2.2.2 and the AIM results presented the Ge-Ge and Ge-X bonding and the Ge-Ge bonding character. However, the contribution of charge is not clear. This chapter shows the charge analyses of the GeX fragments and the Ge_2X_2 isomers.

4.2.2.3.1 GeX fragment

Table 4.2.2.7 shows the computed Hirshfeld charges of the GeX molecules. The table presents that Ge atom is always positively charged and hydrogen atom and the halogen atom are always negatively charged because the halogen atoms are more electronegative than the Ge atom. The order of polarizability is as follows: GeF > GeCl > GeBr > GeH > GeI. The charge analysis of the GeX molecule shows that the lone-pair donor-acceptor is not favorable because of the large electric repulsion from two positive Ge atoms, but the GeX donor-acceptor leads to an effective Ge-X···Ge-X dipole-dipole interaction. This is another reason why the doubly bridged structure is more favorable than the bent-structure. The comparison of the absolute charge values with those of SiX molecules indicates that the GeX molecules are more polarized than the SiX molecules. It suggests that the bridged structures of Ge_2X_2 become more stable and the bent-structures are less stable because the larger polarization leads to the larger dipole-dipole interaction for bridged structures and the larger electrostatic reposition for bent-structures.

Table 4.2.2.7 Hirshfeld charge of the GeX fragment calculated at BP86/QZ4P level.

	GeH	GeF	GeCl	GeBr	GeI
Ge	0.1345	0.2416	0.1675	0.1401	0.1061
X	-0.1345	-0.2416	-0.1675	-0.1401	-0.1061

4.2.2.3.2 Ge_2X_2 molecules

Table 4.2.2.8 shows Hirshfeld charge of Ge_2X_2 isomers. The charge distribution does not show a clear correlation with relative energies of the Ge_2X_2 isomers. However the charge distribution presents the character of the molecules. Hirshfeld charges show that Ge_2F_2 is relatively large polarized and Ge_2I_2 exhibits small charge distribution. In general in Ge_2F_2, Ge atoms have relatively large positive charge. It means that the former has more ionic character and the latter has more covalent character. It agrees with the results of AIM.

The bent-structures of Ge_2X_2 show a different trend to each other, and they are categorized to two groups, where the categories are same as those of orbital analyses. **GeE2** and **GeF1** show the largest positive charge of all Ge_2X_2 isomers and the charge values are similar to those of the GeX molecules. It suggests that the Ge-Ge bond formation of **GeE2** and **GeF1** from two GeX fragments need no intramolecular charge transfer. On the other hand, **GeE1** and **GeF2** have less positive charge than **GeE2** and **GeF1**. It indicates the intramolecular charge transfer from the halogen atoms to the Ge atoms. However, the charge transfer is unfavorable because the halogen atoms are more electronegative than the Ge atom.

The ring structures, **GeA**, **GeB** and **GeC** show smaller charge distribution than the GeX fragments and these isomers also need intramolecular charge transfer. However, these charge transfers are favorable because the direction of charge transfer is the same as the orbital donation. According to the charge transfer, the bridged structures are favorable.

Table 4.2.2.8 Calculated charge distribution given by Hirshfeld charge at BP86/QZ4P level

	GeA	**GeB**	**GeC**	**GeE1**	**GeE2**	**GeF1**	**GeF2**	**GeG**
				Ge_2H_2				
Ge_1	0.0719	0.0482	0.0762	0.0534	0.1346	0.1270	0.1117	-0.0250
Ge_2	0.0719	0.0644	0.0762	0.0534	0.1346	0.1270	0.1117	-0.0250
H_1	-0.0719	-0.0697	-0.0762	-0.0534	-0.1346	-0.1270	-0.1117	0.0250
H_2	-0.0719	-0.0429	-0.0762	-0.0534	-0.1346	-0.1270	-0.1117	0.0250
				Ge_2F_2				
Ge_1	0.2067	0.2602	0.2096	0.2213	0.2576	0.2412	0.2220	0.1320
Ge_2	0.2067	0.1616	0.2096	0.2213	0.2576	0.2412	0.2220	0.1320
F_1	-0.2067	-0.2130	-0.2096	-0.2213	-0.2576	-0.2412	-0.2220	-0.1320
F_2	-0.2067	-0.2088	-0.2096	-0.2213	-0.2576	-0.2412	-0.2220	-0.1320
				Ge_2Cl_2				
Ge_1	0.1265	0.1349	0.1443	0.1325	0.1870	0.1674	-0.1351	0.0110
Ge_2	0.1265	0.1180	0.1443	0.1325	0.1870	0.1674	-0.1351	0.0110
Cl_1	-0.1265	-0.1431	-0.1443	-0.1325	-0.1870	-0.1674	-0.1351	-0.0110
Cl_2	-0.1265	-0.1098	-0.1443	-0.1325	-0.1870	-0.1674	-0.1351	-0.0110
				Ge_2Br_2				
Ge_1	0.0956	0.0936	0.1137	0.1015	0.1584	0.1405	0.1048	-0.0320
Ge_2	0.0956	0.0977	0.1137	0.1015	0.1584	0.1405	0.1048	-0.0320
Br_1	-0.0956	-0.1129	-0.1137	-0.1015	-0.1584	0.1405	-0.1048	0.0320
Br_2	-0.0956	-0.0784	-0.1137	-0.1015	-0.1584	0.1405	-0.1048	0.0320
				Ge_2I_2				
Ge_1	0.0585	0.0425	0.0718	0.0632	0.1206	0.1064	0.0678	-0.0664
Ge_2	0.0585	0.0731	0.0718	0.0632	0.1206	0.1064	0.0678	-0.0664
I_1	-0.0585	-0.0754	-0.0718	-0.0632	-0.1206	-0.1064	-0.0678	0.0664
I_2	-0.0585	-0.0402	-0.0718	-0.0632	-0.1206	-0.1064	-0.0678	0.0646

4.2.2.4 Energy Decomposition Analysis

It was shown in chapter 4.2.2.1 that the unusual equilibrium geometries of **GeA**-**GeG** of Ge_2X_2 can be nicely explained in terms of orbital interactions between the **GeX** fragments in the $X^2\Pi$ ground state. Table 4.2.2.9 and Table 4.2.2.10 give the EDA results for the structures **GeA**, **GeB**, **GeC**, **GeE1**, **GeE2**, **GeF1** and **GeF2** using two GeX molecules in the $X^2\Pi$ ground state as interacting fragments, and for **GeG** using two GeX molecules in the $a^4\Sigma^-$ excited state as interacting fragments. The $a^4\Sigma \leftarrow X^2\Pi$ excitation energy is then considered as preparation energy of the GeX fragment, which is the reason that the linear species **GeG** have rather large ΔE_{prep} values. In general, the isomers of Ge_2X_2 show smaller energies than those of Si_2X_2. It suggests that the interactions between two GeX fragments are weaker than those between two SiX fragments .The ratio of ΔE_{elstat} and ΔE_{orb} shows that the interactions between the GeX fragments are more electrostatic and less orbital interaction character than those between the SiX fragments.

GeA, **GeB** and **GeC** show the relatively large orbital energies and large electrostatic interaction values, where the trend is similar to that in Si_2X_2 system. The large electrostatic interaction energy indicates that the electrostatic interaction is important for the formation of the Ge-X-Ge bridged structure. This is consistent with the result of AIM analysis. The large orbital interaction energies suggest that the Ge-X bond donor-acceptor interaction leads to a very effective bond situation and that the Ge-X-Ge bridging is a desirable structure. These isomers show relatively large preparation energies due to the elongation of the Ge-X bonds to form the Ge-X-Ge bridged structures. The preparation energies of Ge_2X_2 are smaller than those in the Si_2X_2 system. Therefore, the formation of the Ge-X-Ge bridging can compensate the energetic loss to elongate the Ge-X bonds. Due to that, **GeA** shows the largest dissociation energies, D_e, of all Ge_2X_2 isomers, apart from **SiA** of the Si_2X_2 molecules.

The bent-structures, **GeE1**, **GeE2**, **GeF1** and **GeF2** often show smaller electrostatic interaction energies and smaller orbital interaction energies than the bridged structures, **GeA**, **GeB** and **GeC**. The smaller electrostatic interaction is due to the electrostatic repulsion between two positively charged Ge atoms in the GeX

fragments, as explained in the part of the charge analyses (chapter 4.2.2.3). **GeE2** and **GeF1** show smaller interaction energies because they have just a σ-type bond. The small orbital interactions of **GeE1** and **GeF2** stem from the unfavorable donor-acceptor interaction between the lone-pair orbital and the vacant π orbital, as described in the orbital analysis of the chapter 4.2.2.1. As a result, the smaller ΔE_{elstat} and ΔE_{orb} values lead to smaller dissociation energies. **GeE1** and **GeF2** often show smaller electrostatic interaction than **GeE2** and **GeF1** because **GeE1** and **GeF2** have shorter Ge-Ge bond lengths and they lead to larger electrostatic repulsions. For Ge_2H_2, the electrostatic interaction of **GeE1** is larger than that of **GeE2** because GeH fragment is less polarized than the other GeX fragments. **GeE2** and **GeF1** show the similar dissociation energies and these dissociation energies show little dependence from the halogen atom due to the independence of the SOMO orbital.

The orbital interaction term of $\Delta E_{orb}(\pi)$ shows that the π type orbital interactions of **GeB**, **GeC**, **GeE1** and **GeF2** are smaller than those of **SiB**, **SiC**, **SiE1** and **SiE2**. Due to the small π orbital interaction, these isomers can easily rotate along the Ge-Ge axis, and these isomers are found as transition states or higher order saddle points.

Ge_2X_2 isomers are categorized into two groups as the dissociation energies are concerned: Ge_2H_2 and the other Ge_2X_2 isomers. These categories are similar to those of the relative energies. For Ge_2H_2, the order of dissociation energies for the Ge_2H_2 isomers is as follows: **GeA** > **GeB** > **GeC** > **GeE1** > **GeE2** > **GeF1** > **GeF2** > **GeG**. This order agrees with the stability of the Ge_2H_2 isomers. **GeA** has the largest dissociation energy. The bridged structures, **GeA**, **GeB** and **GeC** show large electrostatic interactions, ΔE_{elstat}, and large orbital interactions ΔE_{orb}, which are similar to **SiA**, **SiB** and **SiC** of Si_2H_2. The large ΔE_{elstat} values of the bridged structures stem from the large dipole-dipole interactions between two Ge-H fragments, where the GeH fragment is a dipole, described in chapter 4.1.2.1.1. These ΔE_{elstat} values are larger than those of **SiA**, **SiB** and **SiC** because the GeH fragment is more polarized than the SiH fragment. The large ΔE_{orb} values arise from the three-center-two-electron bond of the Si-X bond donor-acceptor interactions. The bent structures are always higher in energy than the bridged structures. The order of stability for **GeE1**, **GeE2**, **GeF1** and **GeF2** is determined by the small electrostatic

interaction and the different orbital interaction situation. In the bent-structure, the electrostatic interaction between Ge and H cannot compensate the electrostatic repulsion between two Ge atoms because the hydrogen atoms are away from Ge-Ge bond. The charge of the Ge atom of the GeH molecule is larger than that of the Si atom of the SiH molecule. It leads to less electrostatic interactions between two GeH fragments as expected in chapter 4.2.2.1. As shown in the orbital analyses, **GeE1** and **GeF2** have two lone-pair donor-acceptor bonds and one π type interaction, where **GeE2** and **GeF1** have just one σ type orbital. The orbital interaction of **GeE1** for Ge_2H_2 is larger than that of **GeE2** because of the different bonding situation. **GeE2** and **GeF1** show similar ΔE_{elstat} and ΔE_{elstat} values because these isomers have the same σ type interactions, as explained in chapter 4.2.2.1.2. **GeF2** is the cis-trans isomer of **GeE1**. However, **GeF2** presents moderately smaller ΔE_{elstat} and ΔE_{orb} than **GeE1**. The qualitative orbital models of Figure 4.2.2.7 showed the orbital interactions of the π-type isomers between two GeH fragments. The model (f) indicated that two GeH fragments rotate to the same direction with each other to form lone-pair donor-acceptor interactions and this rotation increases the lone-pair donor-acceptor interaction in the point of orbital interaction. On the other hand, the model (g) exhibits that two GeH fragments rotate to the different directions, but this lone-pair donor-acceptor interaction is still ineffective. As a result, the ΔE_{orb} of **GeF2** becomes smaller than that of **GeF1**. **GeG** shows the ideal triple bond and the large interaction energy of **GeG** stems from the large orbital energy. However, **GeG** is an unstable isomer because of the large excitation energy.

The group of Ge_2F_2, Ge_2Cl_2, Ge_2Br_2 and Ge_2I_2 shows the similar trend compared to the group of Si_2Cl_2, Si_2Br_2 and Si_2I_2 The dissociation energy of Ge_2F_2, Ge_2Cl_2, Ge_2Br_2 and Ge_2I_2 shows the following order: **GeA** > **GeE2** > **GeF1** > **GeE1** > (**GeB**) > **GeF2** > **GeC** > **GeG**. The order of **GeB** depends on the halogen atoms. For **GeA**, the dissociation energies show a clear correlation with the electrostatic interaction and orbital interaction, and they show the same trend. The electrostatic interactions and the orbital interactions exhibit clear correlations with the charge of the GeX fragments and the orbital energy of the Ge-X bonds, respectively. The dissociation energies also show a correlation with the preparation energy, and the dissociation energy becomes larger as the preparation energy gets smaller. **GeA** shows always the largest

dissociation energy due to that largest electrostatic interaction and the largest orbital interaction can compensate the energetic loss of the elongation of the Ge-X bonds. However, **GeB** and **GeC** show smaller electrostatic interactions and smaller orbital interaction and they cannot compensate the energetic loss of the Ge-X-Ge bridge formation. For this reason, **GeB** and **GeC** show small dissociation energies and the **GeB** and **GeC** isomers are energetically unfavorable structures. The electrostatic interactions of **GeE2** and **GeF1** are always larger than those of **GeE1** and **GeF2** in the isomers of this group. The small electrostatic interaction stems from the electrostatic repulsion and the electrostatic interaction correlates with the Ge-Ge bond lengths of these isomers. The orbital interactions of **GeE1** and **GeE2** in this group show a different trend from Ge_2H_2. For Ge_2F_2, Ge_2Cl_2, Ge_2Br_2 and Ge_2I_2, the orbital interactions of **GeE1** are smaller than those of **GeE2**, although the interactions for Ge_2H_2 show an opposite tend. The difference stems from the lone-pair donor-acceptor interaction, i.e. the energy gap of the lone-pair orbital and the vacant π orbital, $\Delta E_{\pi\text{-lone-pair}}$, because the orbital energies of π bond, $\Delta E_{orb}(\pi)$, are similar for all **GeE1** isomers. For the GeX molecules, $\Delta E_{\pi\text{-lone-pair}}$ values strongly depend on the halogen atoms and the $\Delta E_{\pi\text{-lone-pair}}$ values of the GeH fragment are smaller than those of the other GeX fragments, whereas $\Delta E_{\pi\text{-lone-pair}}$ values of the SiX molecules are smaller than those of GeX molecules. As a result, the **GeE1** structures become less favorable than **GeE2**. The isomers of **GeG** show larger interaction energy than that of Ge_2H_2, but **GeG** are unstable isomers because of the large excitation energy.

The EDA results shows that the Ge_2X_2 molecules of **GeA**, **GeB**, **GeC**, **GeE1**, **GeE2**, **GeF1**, **GeF2**, and **GeG** can be categorized into two groups and they are of the same group as the relative energies. **GeA** always shows large dissociation energy apart from Si_2X_2 molecules due to the large electrostatic interaction and the large orbital interaction from the large dipole-dipole interaction and the favorable orbital interaction.

Table 4.2.2.9 Energy decomposition analysis of Ge_2H_2, Ge_2F_2 and Ge_2Cl_2 at BP86/QZ4P of the Ge-Ge bond using two doublet fragments for **GeA-GeF2**. Two quartet fragments are used for **GeG**. The symmetry in the analysis is C_s except for the **GeA** isomer. Energy values are given in kcal/mol.

Term	**GeA**	**GeB**	**GeC**	**GeE1**	**GeE2**	**GeF1**	**GeF2**	**GeG**
				Ge_2H_2				
ΔE_{int}	-82.0	-69.7	-69.27	-54.61	-38.54	-36.59	-21.72	-118.58
ΔE_{Pauli}	286.32	217.83	171.87	146.30	95.63	93.05	66.35	135.97
ΔE_{elstat}	-144.52	-127.8	-100.83	-82.50	-69.93	-66.78	-21.66	-85.54
	39.24%	44.45%	41.81%	41.06%	52.12%	51.51%	24.59%	33.60%
ΔE_{orb}	-223.81	-159.73	-140.32	-118.41	-64.25	-62.86	-66.41	-169.02
	60.76%	55.55%	58.19%	58.94%	47.88%	48.49%	75.41%	66.40%
ΔE_{orb}(a')	-223.81	-121.93	-111.16	-81.74	-64.15	-62.77	-38.56	-96.39
	100.00%	76.34%	79.22%	69.03%	99.85%	99.85%	58.06%	57.03%
ΔE_{orb}(a'')		-37.80	-29.16	-36.67	-0.10	-0.10	-27.85	-72.72
		23.66%	20.78%	30.97%	0.16%	0.16%	41.94%	43.02%
ΔE_{prep}	7.25	5.88	3.36	2.17	1.46	1.40	1.41	99.56
ΔE(=-*De*)	-74.75	-63.82	-65.90	-52.44	-37.08	-35.19	-20.30	-19.02
				Ge_2F_2				
ΔE_{int}	-66.52	-33.58	-29.52	-22.69	-33.87	-30.85	-16.78	-129.84
ΔE_{Pauli}	274.72	166.57	157.39	73.02	99.52	88.07	54.93	85.41
ΔE_{elstat}	-152.72	-83.42	-102.29	-24.63	-72.18	-61.6	-13.33	-33.09
	44.75%	41.68%	54.72%	25.73%	54.11%	51.80%	18.59%	15.37%
ΔE_{orb}	-188.53	-116.73	-84.63	-71.09	-61.21	-57.32	-58.38	-182.16
	55.25%	58.32%	45.28%	74.27%	45.89%	48.20%	81.41%	84.63%
ΔE_{orb}(a')	-188.53	-80.30	-82.07	-38.14	-60.71	-56.94	-29.34	-98.9
	100.00%	68.79%	96.98%	53.65%	99.18%	99.34%	50.25%	54.33%
ΔE_{orb}(a'')		-36.43	-2.56	-32.95	-0.50	-0.38	-29.04	-83.36
		31.21%	3.03%	46.35%	0.82%	0.66%	49.74%	45.76%
ΔE_{prep}	23.56	15.66	22.22	1.41	1.53	1.37	1.37	211.01
ΔE(=-*De*)	-42.96	-17.92	-7.30	-21.28	-32.34	-29.48	-15.41	81.17
				Ge_2Cl_2				
ΔE_{int}	-68.56	-34.80	-24.2	-25.9	-36.13	-31.7	-18.36	-156.5
ΔE_{Pauli}	285.12	170.47	147.4	85.90	111.38	90.15	62.11	103.12
ΔE_{elstat}	-154.08	-80.20	-80.34	-32.83	-78.69	-61.9	-18.31	-49.25
	43.56%	39.07%	46.82%	29.37%	53.35%	50.80%	22.76%	18.97%
ΔE_{orb}	-199.61	-125.08	-91.26	-78.97	-68.82	-59.95	-62.16	-210.37
	56.44%	60.93%	53.18%	70.63%	46.65%	49.20%	77.24%	81.03%
ΔE_{orb}(a')	-199.61	-88.68	-81.83	-45.47	-67.50	-59.19	-33.28	-113.81
	100.00%	70.90%	89.67%	57.58%	98.08%	98.73%	53.54%	54.10%
ΔE_{orb}(a'')		-36.40	-11.3	-33.49	-1.33	-0.76	-28.87	-96.68
		29.10%	10.3%	36.70%	1.96%	1.27%	46.45%	45.96%
ΔE_{prep}	15.34	10.31	19.16	1.54	1.87	1.50	1.50	212.76
ΔE(=-*De*)	-53.22	-24.49	-5.04	-24.36	-34.26	-30.20	-16.86	56.26

Table 4.2.2.10 Energy decomposition analysis of Ge_2Br_2 and Ge_2I_2 at BP86/QZ4P of the Ge-Ge bond using two doublet fragments for **GeA**-**GeF2**. Two quartet fragments are used for **GeG**. The symmetry in the analysis is C_s except for the **GeA** isomer. Energy values are given in kcal/mol.

Term	**GeA**	**GeB**	**GeC**	**GeE1**	**GeE2**	**GeF1**	**GeF2**	**GeG**
				Ge_2Br_2				
ΔE_{int}	-69.63	-36.66	-24.27	-27.39	-37.29	-32.04	-19.5	-146.09
ΔE_{Pauli}	284.64	173.14	145.59	90.05	118.9	120.39	65.45	109.6
ΔE_{elstat}	-157.02	-81.86	-77.42	-35.7	-83.38	-63.7	-20.89	-51.24
	44.32%	39.02%	45.58%	30.40%	53.38%	41.78%	24.59%	20.04%
ΔE_{orb}	-197.25	-127.95	-92.44	-81.74	-72.81	-88.74	-64.07	-204.45
	55.68%	60.98%	54.42%	69.60%	46.62%	58.22%	75.41%	79.96%
$\Delta E_{orb}(a')$	-197.25	-91.69	-81.19	-48.13	-70.86	-87.76	-35.11	-110.8
	100.00%	71.66%	87.83%	58.88%	97.33%	98.89%	54.80%	54.23%
$\Delta E_{orb}(a'')$		-36.26	-11.25	-33.61	-1.94	-0.98	-28.95	-93.69
		28.34%	12.17%	41.12%	2.66%	1.10%	45.19%	45.83%
ΔE_{prep}	13.39	9.13	17.10	1.58	2.05	1.55	1.56	195.1
$\Delta E(=-De)$	-56.24	-27.53	-7.17	-25.81	-35.24	-30.49	-17.94	49.01
				Ge_2I_2				
ΔE_{int}	-70.73	-39.86	-24.85	-29.91	-39.06	-32.51	-21.11	-133.25
ΔE_{Pauli}	286.33	180.3	146.92	97.64	129.82	95.55	70.81	119.61
ΔE_{elstat}	-160.01	-86.63	-76.55	-40.97	-89.76	-64.88	-24.98	-56.44
	44.81%	39.35%	44.57%	32.12%	53.15%	50.66%	27.18%	22.32%
ΔE_{orb}	-197.05	-133.53	-95.21	-86.58	-79.11	-63.18	-66.94	-196.42
	55.19%	60.65%	55.43%	67.88%	46.85%	49.34%	72.82%	77.68%
$\Delta E_{orb}(a')$	-197.05	-97.36	-81.97	-52.80	-75.92	-61.76	-38.04	-106.78
	100.00%	72.91%	86.09%	60.98%	95.97%	97.75%	56.83%	54.36%
$\Delta E_{orb}(a'')$		-36.17	-13.24	-33.78	-3.19	-1.42	-28.90	-89.73
		27.09%	13.91%	39.01%	4.03%	2.25%	43.18%	45.68%
ΔE_{prep}	11.06	7.72	14.31	1.68	2.37	1.71	1.70	169.89
$\Delta E(=-De)$	-59.67	-32.14	-10.54	-28.23	-36.69	-30.80	-19.40	36.64

4.2.3. Summary

Chapter 4.2 showed the investigated Ge_2X_2 isomers. The geometries and the relative energies are shown in chapter 4.2.1, and the doubly bridged structure, **GeA**, is a global minimum for all Ge_2X_2 molecules, while Si_2X_2 in chapter 4.1 showed a different global minimum for Si_2F_2.

The investigation of the GeX fragments showed that the linear triple bond formation of X-Ge≡Ge-X is quite unfavorable due to the negative dissociation energies, which stem from the large excitation energies from the ground state to the excited state. The Ge-Ge triple bond formation is less favorable than the Si-Si triple bond. Therefore, the interaction of the GeX fragments occurs in the $X^2\Pi$ ground state.

The orbital analyses showed that the qualitative model of the Ge_2X_2 isomers from two GeX fragments gives explanations of the bonding situation of the Ge_2X_2 isomers, and it is found that the orbital models are sensible in Ge_2X_2 system. The XGe-GeX isomers are categorized into two groups: σ-type isomer and π-type isomer. **GeA** are categorized into the σ-type isomer, and moreover, **GeA** has also two GeX donor-acceptor interactions, where the Ge-X bond donor-acceptor interaction is quite favorable because it leads to the three-center-two-electron bond. The two types of bent-structures show similar orbital pictures, but those orbital energies are different. The difference stems from the interaction between the lone-pair orbitals and vacant *p*-orbital.

The investigation of bond paths proved the Ge-Ge and Ge-X bonding, and **GeA**, **GeB** and **GeC** have bridged structures. Ge_2X_2 showed smaller charge accumulations, although those of Si_2X_2 are larger. It indicates the smaller orbital interaction of the Ge_2X_2 molecules than of Si_2X_2. **GeE1** and **GeF2** present different pictures of the charge accumulation in **GeE2** and **GeF1**. It suggests the different Ge-Ge bond situation of **GeE1**, **GeF2** and **GeE2**, **GeF2**, which agrees with the orbital analyses.

Charge analyses showed that GeX fragments are large dipoles and it indicates that the bent-structures are unfavorable, although the bridged structures become more favorable, due to that the bridged structures lead to the favorable geometries for the dipole-dipole electrostatic interaction. Furthermore, the GeX molecules are more

charged than the SiX molecules, and it leads to larger dipole-dipole interaction for the ring structures.

The results of EDA showed that the dissociation energy correlates with the stability of the isomers. The doubly bridged structure **GeA** has the largest dissociation energy. The large dissociation energy stems from the large orbital interaction energy from the Ge-X bond donor-acceptor and electrostatic interaction between two GeX dipoles. The bent structures show smaller dissociation energies due to the less favorable geometries for the dipole-dipole interaction and less effective orbital interactions.

4.3 Sn_2X_2 Molecules (X=H, F, Cl, Br and I)

4.3.1 Geometries and Relative Energies

Figure 4.3.1.1 – Figure 4.3.1.9 show the optimized geometries of several isomers of Sn_2X_2 (X=H, F, Cl, Br and I). The isomers in the singlet state **SnA**-**SnG** and the isomers in the triplet state **SnA(T)**-**SnI(T)** are optimized at the BP86/QZ4P level. Table 4.3.1.1, Table 4.3.1.2 and Table 4.3.1.3 show the relative energies of the stationary points on the singlet energy surface calculated with BP86/QZ4P. In addition to this, single point energies for the singlets are calculated with HF, MP2, SCS-MP2, MP4, CCSD and CCSD(T). For these calculations the aug-cc-pVQZ basis sets are used. Table 4.3.1.4 and Table 4.3.1.5 show the energies on the triplet potential energy surface calculated with BP86/QZ4P. Additionally, the single point energies for the triplets are calculated with HF, MP2, SCS-MP2, MP4, RCCSD and RCCSD(T). For these calculations, the aug-cc-pVQZ basis sets are used. All energies are given relative to the energy of the isomer **SnA**, which is the global minimum of Sn_2H_2. The results in the tables and figures show that the optimized geometries and relative energies are in agreement with previous theoretical calculations of Sn_2H_2 with DFT [21, 64, 87].

4.3.1.1 Singlet Isomers of Sn_2X_2

Scheme 4.3.1.1 shows the investigated species are named as follows: non-planar, doubly bridged structure (**SnA**), singly bridged planar structure (**SnB**), planar doubly bridged structure (**SnC**), vinylidene structure (**SnD**), trans-bent structure (**SnE**), cis-bent structure (**SnF**), and linear structure (**SnG**).

The non-planar doubly bridged structures of **SnA** have C_{2v} symmetry and these isomers are the global minima for all Sn_2X_2 species (Figure 4.3.1.1), which is similar to Ge_2X_2. The Sn-Sn bond lengths have a correlation with the Sn-X-Sn angle and the Sn-Sn distance becomes longer as the angle gets smaller. The comparison of the Sn-X bond with the Sn-X fragment suggests that the Sn-X bond length is elongated to form the Sn-X-Sn bridged structure. The trend of **SnA** is similar to the Si_2X_2 and Ge_2X_2 system.

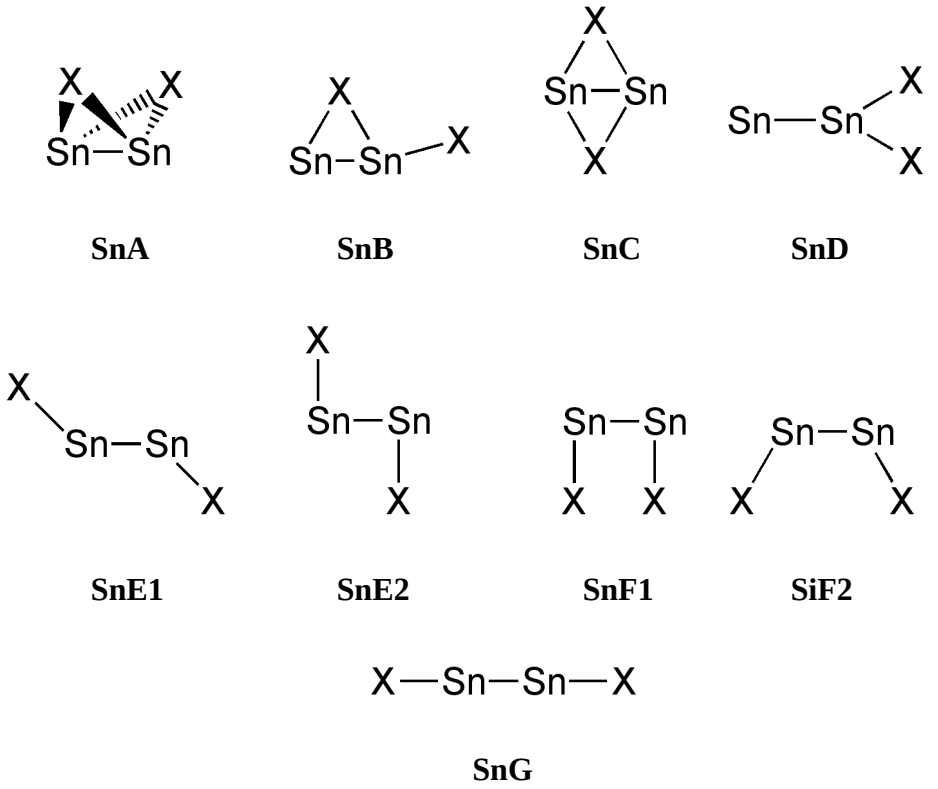

Scheme 4.3.1.1. Investigated singlet isomers of Sn_2X_2

The singly bridged planar structures of **SnB** have C_s symmetry and these isomers are predicted as transition states for all Sn_2X_2 isomers (Figure 4.3.1.1), which is similar to **SiB** of Si_2F_2 and **GeB** of Ge_2F_2, Ge_2Cl_2 and Ge_2Br_2, whereas the those isomers of Si_2H_2, Si_2Cl_2 and Si_2Br_2, Si_2I_2, Ge_2H_2 and Ge_2I_2 are local minima. The Sn-Sn bond length has no correlation with the halogen atom, and the Sn-Sn bond lengths in Sn_2Cl_2, Sn_2Br_2 and Sn_2I_2 are almost constant. The Sn-X-Sn angles show a correlation with the X atom and the angle becomes smaller as the X atom gets heavier. In account of the bond lengths, the X atoms in the ring interact with both Sn atoms and the Sn-X-Sn ring depends on the Sn-X-Sn structure.

The planar doubly bridged structures **SnC** have D_{2h} symmetry and they are transition states in all cases (Figure 4.3.1.1), which are similar to corresponding structure of Si_2X_2 and Ge_2X_2, **SiC** and **GeC**, except Ge_2I_2. The Sn-Sn interactions of **SnC** are smaller than those of **SnA** because of the longer Sn-Sn bond. However, a clear correlation between the bond lengths and the halogen atoms could not be found. When the Sn-Sn bond lengths are considered, the two Sn atoms of Sn_2H_2 still interact with each other, but the Sn-Sn distances in Sn_2F_2, Sn_2Cl_2, Sn_2Br_2 and Sn_2I_2 are quite

long and the two Sn atoms interact very weakly. In the **SnC** structures, the Sn-Sn bond does not show a clear correlation. The Sn-X-Sn angles are smaller, as the X atom becomes heavier. The Sn-X bond is elongated to form the bridged structure.

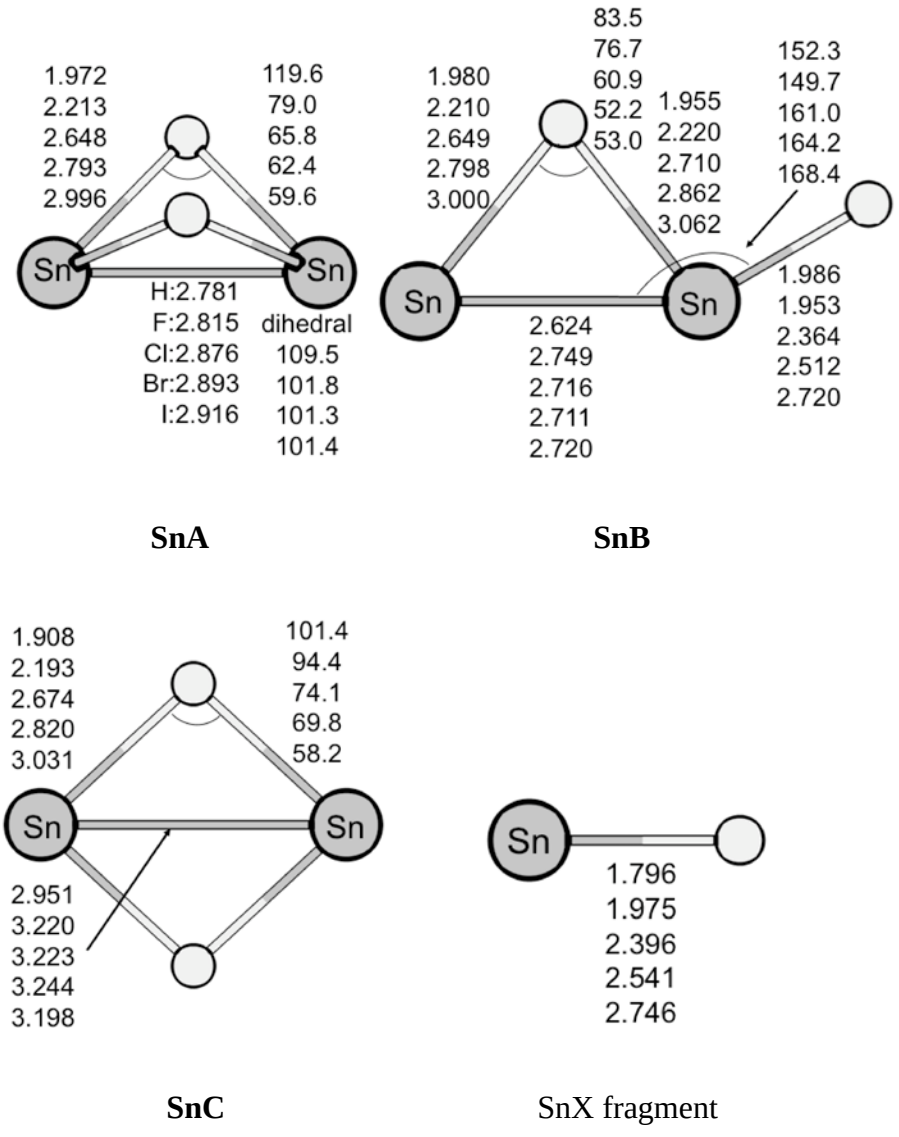

Figure 4.3.1.1. Optimized bridged structures in their singlet state, **SnA**, **SnB**, **SnC** and SnX fragments of the $X^2\Pi$ ground state calculated at BP86/QZ4P level. The bond lengths are given in Å and the angles are given in degree.

The vinylidene structures **SnD** have C_{2v} symmetry and they are minima for Sn_2F_2 and Sn_2Cl_2. For Sn_2H_2, Sn_2Br_2 and Sn_2I_2, these isomers are transition states (Figure 4.3.1.2). This is similar to the **GeD** isomers of Ge_2X_2 except Ge_2H_2, where the isomer of Ge_2H_2 is a local minimum. The Sn-Sn bond lengths do not show a clear correlation.

Therefore, the halogen atoms have nearly no influence on the Sn-Sn bond length in the vinylidene structure of Sn_2X_2. The trend of the **SnD** structure is quite similar to that of **SiD** and **GeD**.

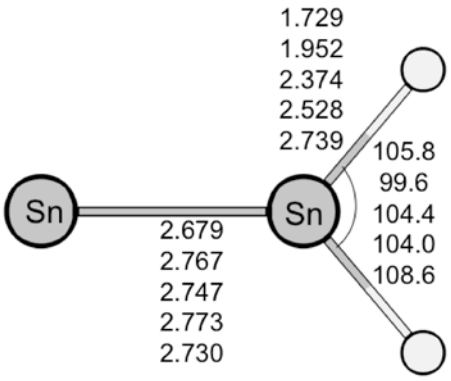

SnD

Figure 4.3.1.2. Optimized vinylidene structures in their singlets state, **SnD**, at BP86/QZ4P level. The bond lengths are given in Å and the angles are given in degree

The trans-bent structure has two types of isomers, **SnE1** and **SnE2**, which both have C_{2h} symmetry (Figure 4.3.1.3). The **SnE1** isomers for Sn_2H_2, Sn_2F_2 and Sn_2Cl_2 are second order saddle points and those of Sn_2Br_2 and Sn_2I_2 are transition states, whereas the isomers **SiE1** of Si_2X_2 and **GeE1** of Ge_2H_2 are all local minima, and **GeE1** of Ge_2F_2, Ge_2Cl_2, Ge_2Br_2, Ge_2I_2 are transition states. The isomers of **SnE2** for Sn_2H_2, Sn_2F_2 and Sn_2Br_2, Sn_2I_2 are transition state and that for Sn_2Cl_2 is a second order saddle point, with a very small second imaginary mode (-6.5 cm^{-1}). The isomers, **SnE1** and **SnE2**, differ from each other in the Sn-Sn bond lengths and the Sn-Sn-X angles. The Sn-Sn bond lengths of **SnE1** correlate with the Sn-Sn-X angle and the Sn-Sn bond becomes shorter as the Sn-Sn-X angle gets smaller. The Sn-Sn bond and the Sn-Sn-X angle of **SnE2** correlate with the halogen atoms and the bond length becomes smaller as the angle gets smaller. The **SnE2** isomer of Sn_2H_2 does not follow the correlation. Due to these points, it can be considered that the difference in the structures stems form the difference of the Sn-Sn bond situation.

The cis-bent structures also have two types of isomers, **SnF1** and **SnF2**, which have both C_{2v} symmetry (Figure 4.3.1.3). The isomers **SnF1** and **SnF2** are transition states. This is similar to the isomers of **SiF1**, **SiF2**, **GeF1** and **GeF2** except the **SiF2**

isomer of Si_2F_2, which is a local minimum. The Sn-Sn bond interactions of **SnF1** and **SnF2** become stronger and the Sn-Sn-X bonds become larger as the halogen atom becomes heavier, which is similar to **SnE2** and the corresponding Si_2X_2 and Ge_2X_2 isomers, **SiF1**, **SiF2**, **GeF1** and **GeF2**. The **SnF1** and **SnF2** isomers of Sn_2H_2 are outlier of the correlation because the larger Sn-Sn-X angles of the halogen compounds of **SnF1** and **SnF2** are mainly caused by steric effects, but the Sn-Sn bond interactions are still important for these isomers.

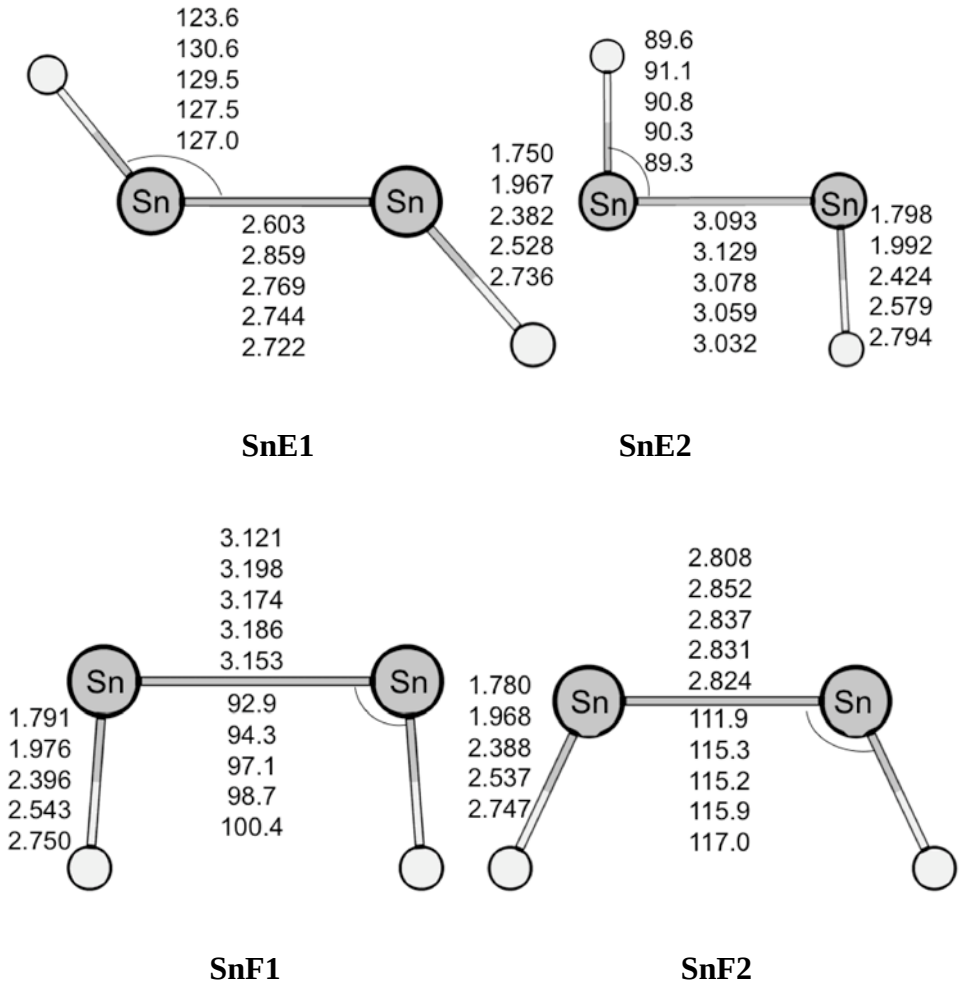

Figure 4.3.1.3. Optimized bent structures in their singlet state, **SnE1** and **SnE2**, **SnF1** and **SnF2** at BP86/QZ4P level. The bond lengths are given in Å and the angles are given in degree.

The linear structure **SnG** for Sn_2H_2 is a second order saddle point and those for Sn_2F_2, Sn_2Cl_2 Sn_2Br_2 and Sn_2I_2 are predicted to be fourth order saddle points (Figure 4.3.1.4). The Sn-Sn distances are nearly same for all **SnG**, which is similar to **SiG** and **GeG**. The halogen atoms have an influence on the bond length in the linear structures and the Sn-Sn bond lengths become larger as the halogen atom gets heavier.

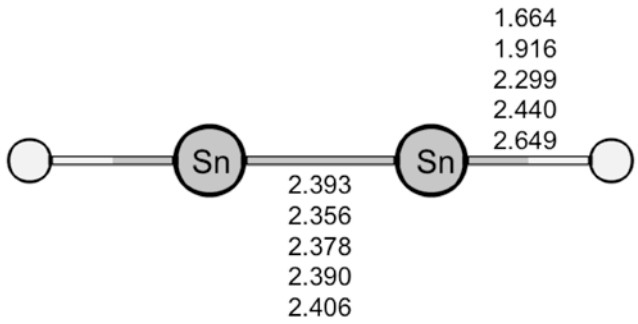

SnG

Figure 4.3.1.4 Optimized linear structures in the singlet state, **SnG** at BP86/QZ4P level. The bond lengths are given in Å and the angles are in given degree.

For Sn_2X_2, the distorted bent structure **SnH** is not found. The optimization from **SnH** structure leads to **SnA** and there are no minima between **SnA** and **SnF1** or **SnE2**, which is similar to Ge_2X_2.

Table 4.3.1.1, Table 4.3.1.2 and Table 4.3.1.3 show the relative energies of the isomers in the singlet state for several methods. Here, the CCSD(T) results are quite reliable due to the fact that the difference between the CCSD and CCSD(T) values are relative small (~5 kcal/mol) except for the isomer **SnC** of Sn_2F_2 and Sn_2Cl_2. The deviations between CCSD and CCSD(T) for these isomers are 7.2 and 6.0 kcal/mol, respectively. These large deviations suggest a multi-reference character of the wave functions for these structures. The relative energies between the singlet isomers at BP86/QZ4P level are relatively accurate and the largest difference from CCSD(T)/aug-cc-pVQZ is 19.7 kcal/mol for the structure **SnG** of Si_2F_2, and which is energetically very high. The mean absolute error form CCSD(T)/aug-cc-pVQZ is 3.4 kcal/mol. For the minima, the energy differences are not so large and they are ca. 5

kcal/mol and the error becomes larger for the transition states and higher order saddle points. The relative energy values of SCS-MP2 and MP4 are very similar and they are close to those of the CCSD(T) calculations. The largest error in MP2, SCS-MP2 and MP4 are 10.5 kcal/mol (**SnC** isomer of Sn_2F_2), 10.2 kcal/mol (**SnC** isomer of Sn_2F_2) and 6.4 kcal/mol (**SnG** isomer of Sn_2F_2), respectively. The mean absolute error of these three methods are 2.6, 1.7 and 1.1 kcal/mol, respectively. The SCS-MP2 method gives very accurate results for the relative energies of the molecules in the singlet state.

The relative energies in Table 4.3.1.1 and Table 4.3.1.2 show that the Sn_2X_2 molecules are categorized into two groups regarding their stability: Sn_2H_2 and the others. The following order is the stability for Sn_2H_2: **SnA** > **SnC** > **GeB** > **SnD** > **SnE1** > **SnE2** > **SnF1** > **SnF2** > **SnG**. This trend and the relative energies of Sn_2H_2 are relatively similar to those of Si_2H_2 and Ge_2H_2. The global minimum is the doubly bridged structure **SnA**. Sn_2H_2 prefers to have bridged structures, and the vinylidene structure is relatively stable. The linear structures are unstable isomers.

The other group shows a different trend as follows: **SnA** > **SnE2** > **SnF1** > **SnD** > (**SnE1**, **SnB, SnF2**, **SnC**) > **SnG**. The doubly bridged isomers **SnA** are the global minima for Sn_2F_2, Sn_2Cl_2, Sn_2Br_2 and Sn_2I_2. The following one is **SnE2**, where the trans-bent structures are transition states or higher order saddle points connecting the two minima of **SnA**. The order of stability shows that the Sn-X-Sn bridging also stabilizes the Sn_2X_2 molecules. However, the stabilizing effect is not as large as that in Ge_2H_2, because of the instability of **SnB** and **SnC**. The bent-structures are the following ones. The stabilization of the bent-structures is different from that of Sn_2H_2. Consequently, the stability of the isomers depends on the stability of the Ge-X-Ge ring-structure and the Ge-Ge bond situation. The vinylidene structures **SnD** are not stable like the corresponding isomers of Si_2X_2 and Ge_2X_2. The relative energies are slightly larger than those of Si_2X_2 and Ge_2X_2.

Table 4.3.1.1 Optimized structures of the **SnA-SnD** isomers calculated at BP86/QZ4P level and relative energies calculated with BP86/QZ4P and ab initio methods with aug-cc-pVQZ basis sets. The bond lengths are given in Å and the angles are given in degree. The relative energies with respect to **SnA** are given in kcal/mol. The values in parentheses are the number of imaginary frequencies.

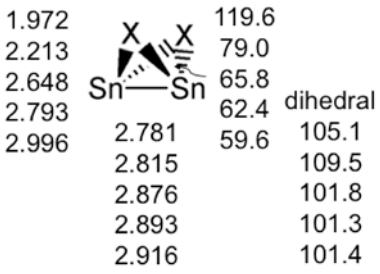

SnA

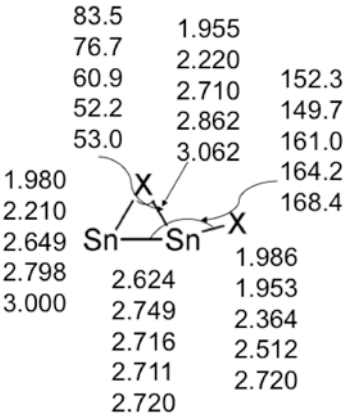

SnB

	H	F	Cl	Br	I	H	F	Cl	Br	I
BP86	0(0)	0(0)	0(0)	0(0)	0(0)	13.5(1)	27.4(1)	29.7(1)	29.8(1)	29.2(1)
HF	0	0	0	0	0	17.3	33.4	35.7	36.0	35.2
MP2	0	0	0	0	0	13.6	26.6	31.3	31.4	30.8
SCS-MP2	0	0	0	0	0	13.8	27.2	31.4	31.4	30.7
MP4	0	0	0	0	0	13.3	25.5	30.2	30.4	30.0
CCSD	0	0	0	0	0	14.4	27.4	31.7	32.1	31.6
CCSD(T)	0	0	0	0	0	13.4	25.7	30.3	30.6	30.2

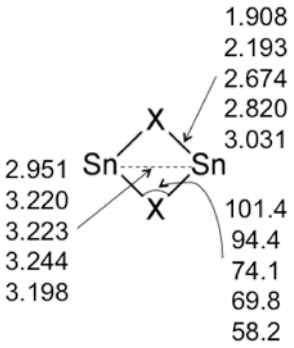

SnC

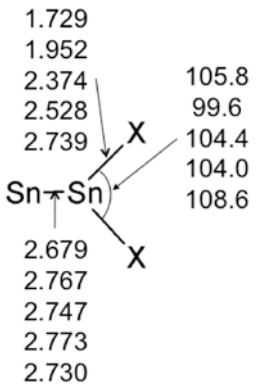

SnD

	H	F	Cl	Br	I	H	F	Cl	Br	I
BP86	5.4(1)	25.6(1)	38.2(1)	39.8(1)	40.3(1)	19.3(1)	31.1(0)	34.9(0)	36.3(1)	37.5(1)
HF	10.4	37.6	56.0	57.8	53.3	10.8	25.3	28.3	30.3	31.8
MP2	4.9	26.5	41.7	43.4	52.3	18.7	24.3	34.3	36.5	38.6
SCS-MP2	5.5	26.2	41.8	43.5	51.9	16.8	24.0	32.9	34.8	36.6
MP4	5.0	20.0	37.5	39.6	50.8	17.2	24.2	32.8	34.8	36.9
CCSD	6.5	23.2	41.8	44.2	51.1	15.1	23.7	31.5	33.5	35.2
CCSD(T)	5.2	16.0	35.8	38.4	50.3	16.0	23.8	32.2	34.1	30.6

Table 4.3.1.2 Optimized structures of the **SnE1-SnF2** isomers calculated at BP86/QZ4P level and relative energies calculated with BP86/QZ4P and ab initio methods with aug-cc-pVQZ basis sets. The bond lengths are given in Å and the angles are given in degree. The relative energies are respect to **SnA** and they are given kcal/mol. The values in parentheses are the number of imaginary frequencies.

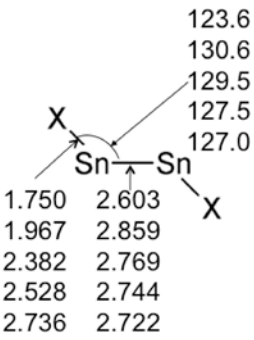

SnE1

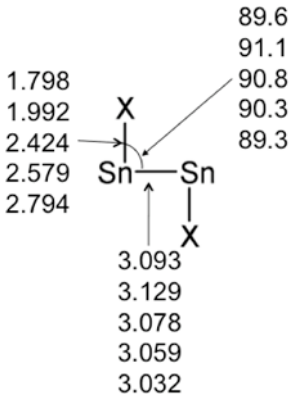

SnE2

	H	F	Cl	Br	I	H	F	Cl	Br	I
BP86	25.3(2)	31.5(2)	32.9(2)	33.2(1)	33.8(1)	29.3(1)	15.8(1)	18.4(2)	19.7(1)	21.2(1)
HF	28.2	38.4	38.2	39.0	39.6	14.0	8.1	8.3	9.7	11.5
MP2	25.5	28.2	37.1	37.8	39.0	29.5	12.2	20.5	22.4	25.1
SCS-MP2	24.7	28.1	36.3	37.0	37.9	25.5	10.0	17.6	19.4	21.9
MP4	24.0	26.0	34.0	36.1	37.2	27.5	10.9	19.0	20.8	23.2
CCSD	20.6	28.4	36.3	37.0	38.0	23.0	9.0	15.6	17.2	19.3
CCSD(T)	23.2	26.6	35.1	35.9	36.9	28.5	10.4	17.8	19.5	21.6

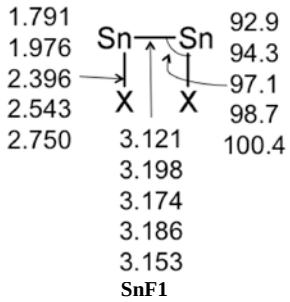

SnF1

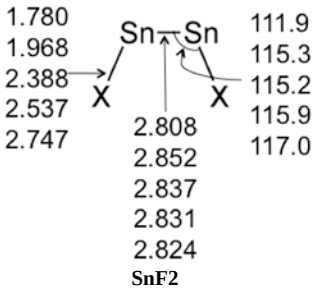

SnF2

	H	F	Cl	Br	I	H	F	Cl	Br	I
BP86	30.7(1)	19.1(1)	22.3(1)	23.7(1)	25.8(1)	46.8(1)	34.9(1)	37.4(1)	38.2(1)	39.3(1)
HF	15.3	12.3	13.3	15.0	17.2	50.4	43.3	44.7	46.1	48.0
MP2	31.1	15.3	24.7	26.7	29.9	50.3	32.0	42.6	44.2	46.5
SCS-MP2	27.0	13.1	21.9	23.8	26.7	48.2	31.8	41.8	43.3	45.4
MP4	29.0	13.7	23.1	24.9	27.7	46.5	29.3	40.1	41.6	43.7
CCSD	24.4	12.1	20.0	21.7	24.1	45.5	31.4	41.0	42.6	44.8
CCSD(T)	27.3	13.4	21.9	23.6	26.1	42.9	28.8	39.0	40.6	42.8

Table 4.3.1.3 Optimized structures of the **SnG** isomers calculated at BP86/QZ4P level and relative energies calculated with BP86/QZ4P and ab initio methods with aug-cc-pVQZ basis set. The bond lengths are given in Å and the angles are given in degree. The relative energies are respect to **SnA** and they are given kcal/mol. The values in parentheses are the number of imaginary frequencies.

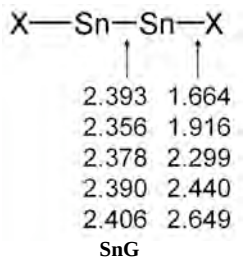

SnG

	H	F	Cl	Br	I
BP86	64.6(2)	138.8(4)	122.9(4)	116.5(4)	107.5(4)
HF	64.9	140.49	122.72	118.05	109.56
MP2	58.2	127.23	115.23	109.96	101.91
SCS-MP2	59.2	128.42	115.37	109.94	101.65
MP4	58.5	125.57	113.38	108.49	100.81
CCSD	60.5	127.93	115.77	111.06	103.32
CCSD(T)	58.8	119.15	111.97	107.73	100.74

4.3.1.2 Triplet Isomers of Sn_2X_2

In the section 4.3.1.1, the singlet isomers are investigated and maybe the triplet potential energy surface has energetically lower isomers. Scheme 4.3.1.2 shows the investigated structures of the triplets and the stationary points are denoted as non-planar doubly bridged butterfly structure (**SnA(T)**), singly bridged planar structure (**SnB(T)**), planar doubly bridged structure (**SnC(T)**), vinylidene structure (**SnD(T)**), trans-bent structure (**SnE(T)**), cis-bent structure (**SnF(T)**), linear structure (**SnG(T)**) and distorted singly bridged structure (**SnI(T)**).

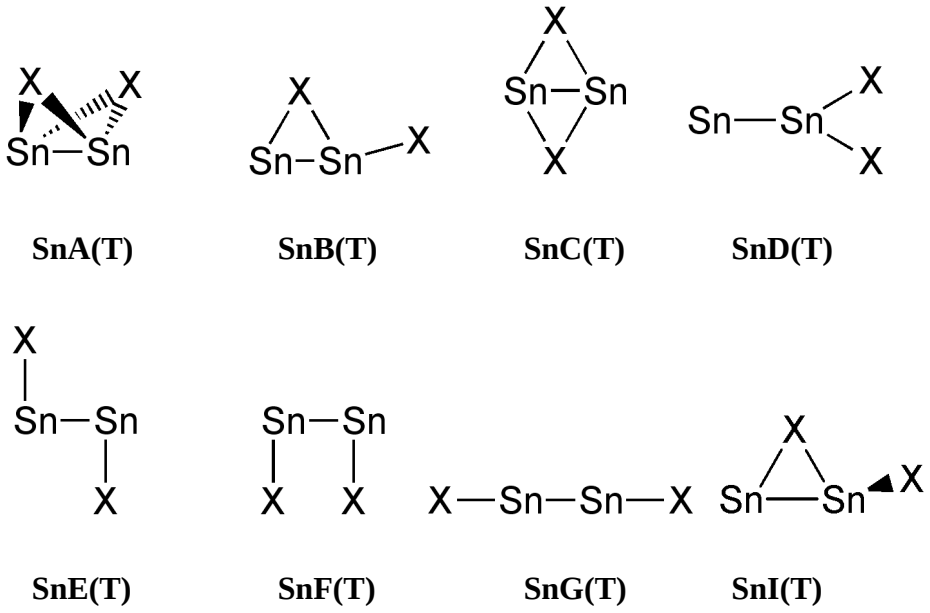

Scheme 4.3.1.2. Investigated triplet isomers of Sn_2X_2

The non-planar doubly bridged structures **SnA(T)** have C_{2v} symmetry and they are predicted to be local minima for Sn_2Cl_2, Sn_2Br_2 and Sn_2I_2. For Sn_2H_2 and Sn_2F_2, the structures are second order saddle points (Figure 4.3.1.5). The Sn-Sn bond correlates with the X atom and the Sn-Sn interaction becomes weaker as the X atom gets heavier. However, the geometries are quite different from **SnA**. Although the two Sn atoms for Sn_2H_2 and Sn_2F_2 interact weakly, the Sn-Sn bonds are nearly broken for Sn_2Cl_2, Sn_2Br_2 and Sn_2I_2. The Sn-X distances are slightly shorter than the bond lengths of **SnA**. The Sn-X-Sn angles show a correlation with the halogen atoms for Sn_2F_2, Sn_2Cl_2, Sn_2Br_2 and Sn_2I_2 and the angle becomes smaller as the halogen atom gets heavier. The Sn-X-Sn angle of Sn_2H_2 does not show a clear correlation with X

atom and the differences are mainly due to the different Sn-Sn bonding situation.

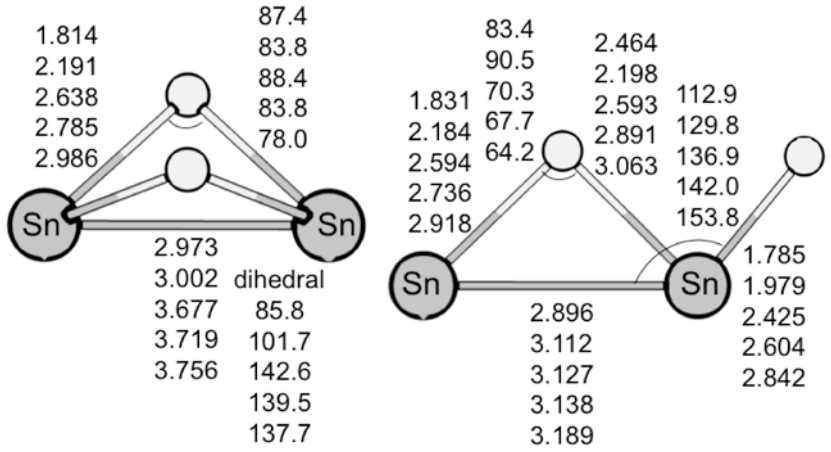

SnA(T) **SnB(T)**

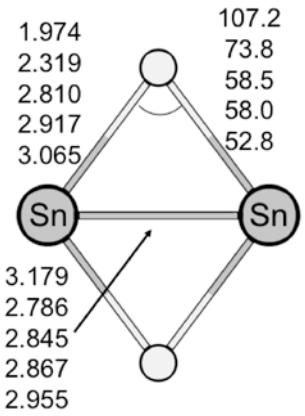

SnC(T)

Figure 4.3.1.5. Optimized bridged structures in their triplet state, **SnA(T)**, **SnB(T)** and **SnC(T)** calculated at BP86/QZ4P level. The bond lengths are given in Å and the angles are given in degree.

The singly bridged planar structures **SnB(T)** have C_s symmetry and these isomers are predicted to be the transition states for Sn_2H_2, Sn_2F_2 and Sn_2I_2, and second order saddle points for Sn_2Cl_2, Sn_2Br_2 (Figure 4.3.1.5). The Sn-Sn bond has a correlation with the X atom and the bond length gets longer as the X atom becomes heavier. The Sn-X bond lengths of the ring show that the isomers of Sn_2Cl_2, Sn_2Br_2 and Sn_2I_2 have Sn-X-Sn ring structures, but that of Sn_2H_2 does not. The Sn-X-Sn angle correlates

with the halogen atoms and the angle becomes smaller as the halogen atom gets heavier. The angle of Sn_2H_2 does not correlate with the X atoms and this trend is similar to the ring-structure.

The planar doubly bridged structures **SnC(T)** have D_{2h} symmetry (Figure 4.3.1.5). The **SnC(T)** structures of Sn_2F_2, Sn_2Cl_2, Sn_2Br_2 and Sn_2I_2 are transition states. The structure of Sn_2H_2 is predicted to be a minimum. This is similar to **GeC(T)**. Sn_2H_2 and the halogen isomers behave different with respect to the comparison of **SnC** and **SnC(T)**. On the one hand, in Sn_2H_2, the Sn-Sn interaction is weaker than that of **SnC**. On the other hand, for Sn_2F_2, Sn_2Cl_2, Sn_2Br_2 and Sn_2I_2 the Sn-Sn interaction is stronger. The isomers of Sn_2F_2, Sn_2Cl_2 and Sn_2Br_2 show a correlation between the Sn-Sn bond length and the Sn-X-Sn angle, and the Sn-Sn bond becomes weaker as the angle gets smaller.

The vinylidene structures **SnD(T)** have C_{2v} symmetry and these isomers are predicted to be local minima (Figure 4.3.1.6), which is similar to the isomers of **GeD(T)**. The bond lengths show that the Sn-Sn interactions are weaker than those of **SnD**. The Sn-Sn bond correlates with the X atom, but the isomer of Sn_2H_2 is an exception. The Sn-Sn interaction becomes slightly stronger as the halogen atom X gets heavier.

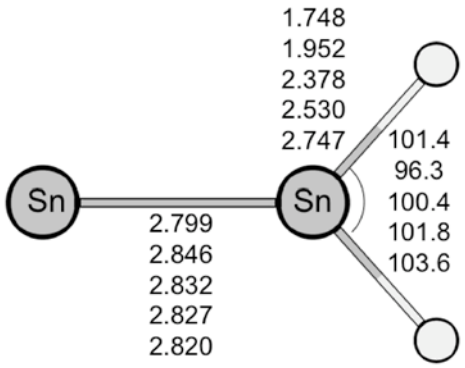

SnD(T)

Figure 4.3.1.6. Optimized vinylidene structures in their triplet state, **SnD(T)** calculated at BP86/QZ4P level. The bond lengths are given in Å and the angles are given in degree.

The trans-bent structures **SnE(T)** have C_{2h} symmetry (Figure 4.3.1.7). These isomers **SnE(T)** are predicted to be minima for all Sn_2X_2 molecules, which is similar to the Si_2X_2 and Ge_2X_2 analogues. The Sn-Sn distance gets shorter as the halogen atom becomes heavier. The angle becomes slightly larger as the halogen atom gets heavier.

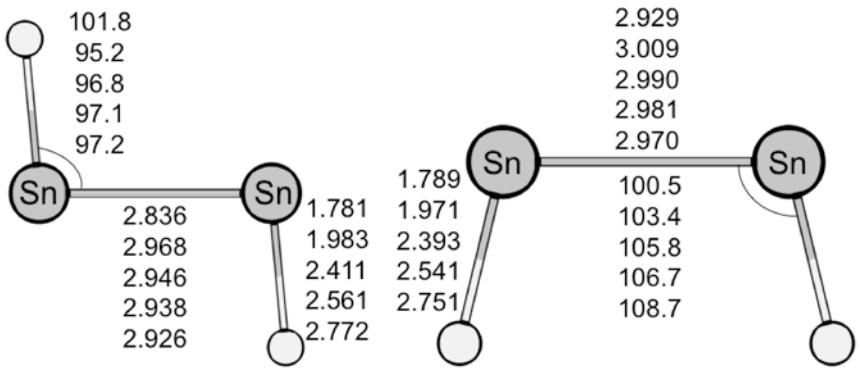

SnE(T) **SnF(T)**

Figure 4.3.1.7. Optimized bent structures in their triplet state, **SnE(T)** and **SnF(T)** calculated at BP86/QZ4P level. The bond lengths are given in Å and the angles are given in degree.

The cis-bent structures **SnF(T)** have C_{2v} symmetry (Figure 4.3.1.7). These isomers, **SnF(T)**, are predicted to be local minima except for Sn_2H_2. The isomer **SnF(T)** of Sn_2H_2 is a second order saddle point. This is similar to **SiF(T)** and **GeF(T)**. The Sn-Sn bond lengths correlate with the Sn-Sn-X angle, and the Sn-Sn interaction becomes smaller as the angle gets larger. **SnF(T)** shows a different correlation and the Sn-Sn-X angle correlates with the X atoms, where the angle becomes larger as the X atom gets heavier, which comes from the steric effect. The Sn-Sn bond lengths of Sn_2F_2, Sn_2Cl_2, Sn_2Br_2 and Sn_2I_2 show a correlation with the halogen atoms, and the Sn-Sn interaction becomes larger as the halogen atom gets heavier. The deviation in the bond lengths in **SnF(T)** is smaller than that in **SnE(T)**, whereas the deviation in the Sn-Sn-X angle is larger in **SnF(T)** than in **SnE(T)**. From these points, the halogen atoms affect on the Sn-Sn distance in **SnE(T)**, while they affect sterically in **SnF(T)**.

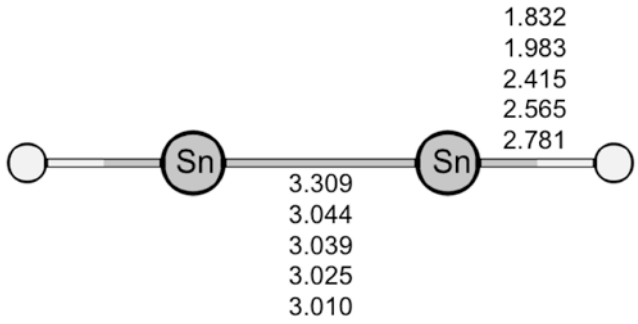

SnG(T)

Figure 4.3.1.8. Optimized linear structures in the triplet state, **SnG(T)** calculated at BP86/QZ4P level. The bond lengths are given in Å and the angles are given in degree.

The linear structures **SnG(T)** are a fourth order saddle point for Sn_2H_2 and the structures of Sn_2F_2, Sn_2Cl_2, Sn_2Br_2, Sn_2I_2 are second order saddle points (Figure 4.3.1.8). As shown in Figure 4.3.1.8, the Sn-Sn distances become shorter as the halogen atoms get heavier.

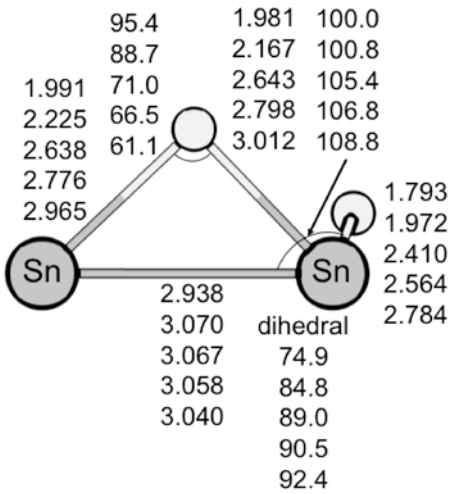

Figure 4.3.1.9. Optimized distorted singly bridged structures in their triplet state, **SnI(T)** calculated at BP86/QZ4P level. The bond lengths are given in Å and the angles are given in degree.

The distorted singly bridged planar structures **SnI(T)** have C_1 symmetry and these isomers are predicted to be minima for all Sn_2X_2 molecules (Figure 4.3.1.9), which is similar to **SiI(T)**, and **GeI(T)**. The bond lengths show that the isomers have a

Sn-X-Sn ring structure. The Sn-Sn bond length becomes slightly shorter as the halogen atom becomes heavier.

Table 4.3.1.4 and Table 4.3.1.5 show the relative energies relative to the structure **SnA** of the stationary points on the triplet potential energy surface at BP86/QZ4P level. These energies are smaller than those calculated at CCSD(T)/aug-cc-pVQZ//BP86/QZ4P level of theory and the largest difference is 11.5 kcal/mol for the isomer **SnG(T**) of Sn_2F_2. The relative energies of the triplets are often underestimated with BP86/QZ4P in these systems and the mean absolute error form CCSD(T)/aug-cc-pVQZ is 3.3 kcal/mol. BP86/QZ4P gives accurate results for minima but the transition states are calculated as to be stable. The differences between the CCSD and CCSD(T) values are relatively small and the largest difference is 3.6 kcal/mol for the **SnG(T)** isomer of Sn_2Cl_2. This indicates that the isomers in the triplet state wave functions only have small multi-reference character and that the CCSD(T) results are reliable and very accurate. For the stationary points on the triplet potential energy surface, SCS-UMP2 methods gives worse results than UMP2/aug-cc-pVQZ. The largest deviation from CCSD(T)/aug-cc-pVQZ for UMP2 is 13.5 kcal/mol for the **SnG(T)** structure of Sn_2H_2, where the largest difference for SCS-UMP2 is 14.1 kcal/mol for the **SnG(T)** structure of Sn_2H_2. The mean absolute errors from CCSD(T)/aug-cc-pVQZ are 5.8 and 6.3 kcal/mol in UMP2 and SCS-UMP2, respectively. This is due to the fact that the parameters of the SCS-MP2 correction are mainly optimized for singlets and not for triplets. The UMP4 method gives results very close to the CCSD(T), where the largest deviation is 10.5 kcal/mol for the **SnE(T)** structure of Sn_2F_2 and mean absolute error is 5.2 kcal/mol. RMP2 presents similar values to CCSD(T) and the largest deviation is 4.5 kcal/mol of the **SnG(T)** structure of Sn_2H_2 and the mean absolute error is 0.5 kcal/mol, respectively.

Table 4.3.1.4 and Table 4.3.1.5 show that the isomers in the triplet state are categorized to three groups, Sn_2H_2, Sn_2F_2 and the group of Sn_2Cl_2, Sn_2Br_2 and Sn_2I_2. Sn_2H_2 shows the following order of stability: **SnE(T)** > **SnD(T)** > **SnI(T)** > **SnF(T)** > **SnB(T)** > **SnC(T)** > **SnA(T)** > **SnG(T)**. These isomers are higher are always higher in energy than the singlets. For the triplets, the trans-bent structure **SnE(T)** is the most stable, which is different trend to Si_2H_2 and Ge_2H_2. The order of stability shows that the bent-structure and the vinylidene structure are relatively favorable, but the doubly

bridged structures and linear structures are unfavorable structures. The relative energies of Sn_2H_2 are often similar to Ge_2H_2.

For Sn_2F_2, the order of stability for each isomer is as follows: **SnE(T)** > **SnI(T)** > **SnF(T)** > **SnD(T)** > **SnB(T)** > **SnG(T)** > **SnA(T)** > **SnC(T)**. The order shows that **SnE(T)** is the most stable isomer for the triplets and Sn_2F_2 prefers bent structures. The vinylidene structure is a relative stable isomer, but the corresponding isomers of Si_2F_2 and Ge_2F_2 are more stable. The doubly bridged structures and linear structures are unfavorable structures, which is a similar trend to Sn_2H_2.

The group of Sn_2Cl_2, Sn_2Br_2 and Sn_2I_2 shows the following order of stability: **SnE(T)** > **SnI(T)** > **SnF(T)** > **SnA(T)** > **SnC(T)** > **SnD(T)** > **SnB(T)** > **SnG(T)**. This order is similar to that of Ge_2F_2. The isomers of this group prefer the bent-structure, but they are still local minima. The vinylidene structures and the linear structures are unfavorable. The relative energies of Ge_2F_2, Ge_2Cl_2 Ge_2Br_2 and Ge_2I_2 are often higher in energy than those of the corresponding Si_2X_2 isomers.

Table 4.3.1.4 Optimized structures of the **SnA(T)-SnD(T)** isomers calculated at BP86/QZ4P level and relative energies. The bond lengths are given in Å and the angles are in degree. The relative energies are respect to **SnA** in singlet state and given in kcal/mol. The values in parentheses are the number of imaginary frequencies.

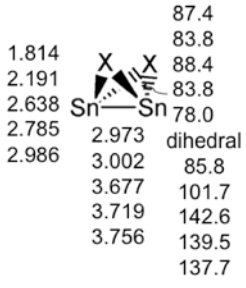

SnA(T)

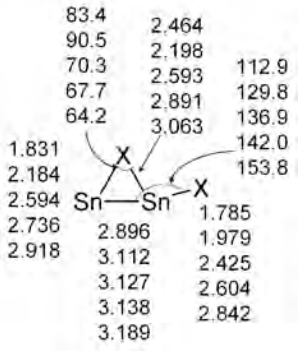

SnB(T)

	H	F	Cl	Br	I	H	F	Cl	Br	I
BP86	32.6(2)	21.5(2)	24.7(0)	27.5(0)	28.0(0)	23.7(1)	18.4(1)	26.2(2)	27.6(2)	30.0(1)
HF	26.0	27.4	7.3	10.4	14.1	16.3	11.3	23.2	24.9	28.1
RMP2	39.0	26.7	22.5	25.9	29.7	27.5	19.2	33.0	35.2	39.4
UMP2	39.5	30.6	31.2	34.1	37.5	34.1	26.4	44.1	44.4	48.1
SCS-UMP2	39.6	35.5	29.9	32.7	36.0	34.6	28.1	41.7	44.6	47.9
UMP4	38.0	30.4	30.9	33.6	36.7	32.6	27.8	40.0	43.2	46.6
CCSD	35.6	28.6	21.4	24.2	27.3	25.9	19.4	31.9	33.8	37.2
CCSD(T)	36.8	27.3	23.7	26.5	29.5	27.1	20.3	32.3	34.3	37.7

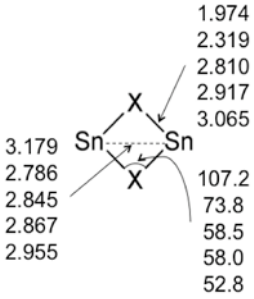

SnC(T)

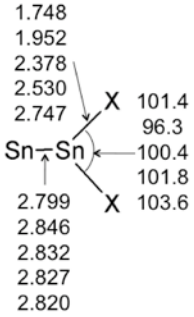

SnD(T)

	H	F	Cl	Br	I	H	F	Cl	Br	I
BP86	24.4(0)	26.9(1)	25.7(1)	25.0(1)	24.9(1)	20.8(0)	20.8(0)	27.0(0)	28.9(0)	31.4(0)
HF	28.1	32.5	6.7	26.9	27.4	2.2	6.7	12.2	14.9	17.8
RMP2	29.0	34.6	22.9	33.7	34.4	20.9	16.4	27.9	30.8	34.8
UMP2	35.7	37.8	32.2	39.0	40.2	27.1	22.3	34.2	39.7	43.4
SCS-UMP2	39.3	41.1	30.6	40.4	41.3	27.0	24.9	35.2	40.1	43.2
UMP4	35.1	38.0	31.9	38.2	39.0	25.9	19.4	33.7	38.9	42.1
CCSD	31.1	36.9	21.5	33.1	33.4	18.6	17.5	26.5	29.2	32.3
CCSD(T)	30.7	33.3	24.0	33.0	33.2	21.0	18.7	28.4	31.0	34.4

Table 4.3.1.5 Optimized structures of **SnE(T)-SnI(T)** at BP86/QZ4P level. The bond lengths are given in Å and the angles are in degree. The relative energies are respect to **SnA** in singlet state and given kcal/mol. The values in parentheses are the number of imaginary frequencies.

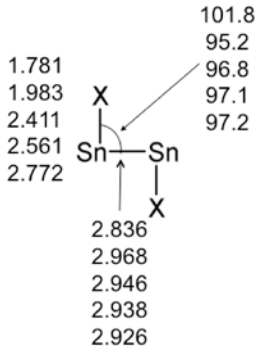

SnE(T)

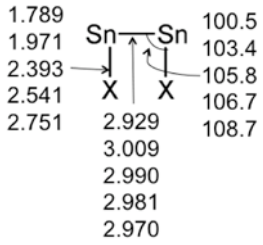

SnF(T)

	H	F	Cl	Br	I	H	F	Cl	Br	I
BP86	19.1(0)	10.2(0)	14.1(0)	15.8(0)	18.1(0)	23.7(2)	12.7(0)	16.7(0)	18.3(0)	20.7(0)
HF	7.2	4.3	6.3	8.2	7.2	11.8	7.2	9.3	11.3	13.9
RMP2	21.2	7.9	18.9	21.2	24.5	27.9	10.3	22.4	24.5	27.9
UMP2	28.3	18.6	25.6	30.7	33.5	35.0	21.7	28.9	34.0	36.9
SCS-MP2	28.1	20.4	26.0	30.6	32.9	34.2	23.5	29.3	33.9	36.4
UMP4	26.7	19.5	24.7	29.6	32.1	33.1	22.4	27.9	32.7	35.2
CCSD	19.0	8.3	17.5	19.4	22.0	24.4	10.6	20.7	22.5	25.2
CCSD(T)	20.7	8.9	18.9	20.9	23.6	26.3	11.9	22.1	23.9	26.6

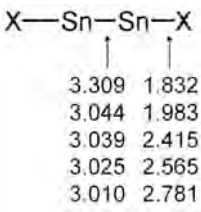

SnG(T)

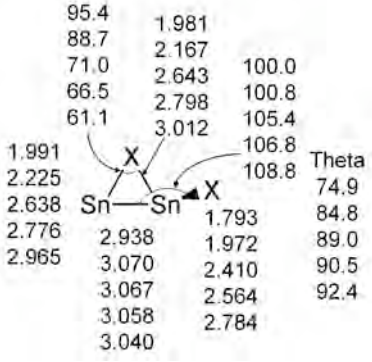

SnI(T)

	H	F	Cl	Br	I	H	F	Cl	Br	I
BP86	51.6(4)	26.0(2)	30.5(2)	31.9(2)	34.2(2)	22.3(0)	11.4(0)	17.6(0)	19.1(0)	21.0(0)
HF	50.0	28.6	31.5	33.3	36.2	8.6	-1.2	5.6	7.7	10.3
RMP2	63.5	25.9	40.8	43.3	47.4	24.5	8.5	19.0	21.2	24.2
UMP2	72.5	36.0	46.3	44.3	55.4	27.3	11.2	21.9	28.8	31.5
SCS-MP2	73.1	40.0	48.6	46.2	56.7	26.7	12.4	21.9	28.5	30.8
UMP4	69.1	37.0	45.7	43.6	59.5	26.1	13.0	21.5	28.2	30.5
CCSD	59.0	27.3	40.1	42.3	45.6	21.8	8.6	17.9	19.8	22.1
CCSD(T)	59.0	26.5	40.0	42.3	45.7	23.9	10.2	19.7	21.6	24.0

4.3.1.3 Summary of Geometry and Relative Energies

The chapter 4.3.1 presented the geometries and relative energies of the isomers of Sn_2H_2, Sn_2F_2, Sn_2Cl_2 Sn_2Br_2 and Sn_2I_2. Table 4.3.1.1 – Table 4.3.1.5 show that the isomers are categorized to three groups, Sn_2H_2, Sn_2F_2 and the group of Sn_2Cl_2, Sn_2Br_2 and Sn_2I_2. The isomers **SnA**, **SnB** and **SnC** have ring-structure in the geometric viewpoint.

Sn_2H_2 shows the following order of stability: **SnA** > **SnC** > **SnB** > **SnD** > **SnE(T)** > **SnD(T)** > ... > **SnG(T)**. The order shows that Sn_2H_2 prefers to have bridged structures.

The isomers of Sn_2F_2 show a different behavior from Sn_2H_2. The stability of the investigated isomers are as follows: **SnA** > **SnE(T)** > **SnI(T)** > **SnE2** > **SnF(T)** > **SnF1** > … > **SiG**. Sn_2F_2 also prefers to have the doubly bridged structure, but the other ring structures are unstable for Sn_2F_2.

The stability of Sn_2Cl_2, Sn_2Br_2 and Sn_2I_2 isomers exhibit a relatively similar behavior to Sn_2F_2. These isomers show the following order of stability: **SnA** > **SnE2** > **SnD** > **SnE(T)** > **SnI(T)** > **SnF1** > **SnF(T)** > … > **SnG**. These isomers prefer still prefer the doubly bridged structure **SnA**, but the other bridged structures are less stable. Instead of those, the bent structures become the second stable isomer.

The Sn_2X_2 molecules exhibit global minima in the doubly bridged butterfly structures, **SnA** and the linear structures are the most unstable isomers. This is similar to the Ge_2X_2 isomers.

4.3.2 Orbital Interactions and Bond Situations

4.3.2.1. Orbital Analyses

The section 4.3.1 shows that energetically low-lying isomers exist on the singlet energy potential surface and the difference in these isomers is mainly due to the bond situation around the Sn-Sn bond. **SnA**, **SnB**, **SnC**, **SnE1**, **SnE2**, **SnF1**, **SnF2** and **SnG,** which have a X-Sn-Sn-X structure, can be divided to two SnX fragments and the bonding situation in these molecules can be described as interactions between two SnX fragments. The orbital interactions between the diatomic species are analyzed with a similar approach to the Trinquier/Malrieu/Carter /Goddard model [81, 82, 83], which is able to explain the E_2H_2 bonding situation [87].

4.3.2.1.1 SnX Fragments

Figure 4.3.2.1 shows schematic pictures of the electronic ground state ($X^2\Pi$) and the first excited state ($a^4\Sigma^-$) of SnX and Table 4.3.2.1 presents the calculated $a^4\Sigma^- \leftarrow X^2\Pi$ excitation energies at BP86/QZ4P and MRCI-SD/aug-cc-pVQZ//BP86/ QZ4P. A (5,5) full-valence CASSCF/aug-cc-pVQZ wave function was used as a reference in the MRCI-SD calculation of SnH and a (11,8) full-valence CASSCF/aug-cc-pVQZ wave function was used as a reference in the MRCI-SD calculation of SnF, SnCl, SnBr and SnI. The excitation energies at BP86/QZ4P are in relative good agreement with those at MRCI-SD(Q)/aug-cc-pVQZ//BP86/QZ4P level. The largest deviation from the MRCI-SD(Q) result is 7.3 kcal/mol for SnF. The excitation energies are overestimated with BP86/QZ4P level.

As is shown in section 4.3.1.1, the linear structure is an energetically high lying stationary point on the potential energy surface of the Sn_2X_2 system and this situation is quite different from the C_2X_2 system, where the linear structure is a global minimum, which is similar to Si_2X_2 and Ge_2X_2 systems. In order to form the triply bonded linear species XE≡EX, the EX moiety must be excited to the $a^4\Sigma^-$ excited state. The previous study showed that it is energetically much easier to excite CH from the $X^2\Pi$ ground state to the $a^4\Sigma^-$ excited state (15.4 kcal/mol) than SnH (45.9 kcal/mol) [263]. The possible gain in binding energy after the $a^4\Sigma^- \leftarrow X^2\Pi$ excitation is

much larger for C_2H_2 than for Sn_2H_2. The situation is similar for all EX with E=Si, Ge and Sn. The electron configuration of the $X^2\Pi$ ground state only allows an electron sharing single bond between two SnX moieties. Another possibility to form bonds is the formation of donor-acceptor bond between two moieties in the $X^2\Pi$ ground state. The situation is similar to SiX and GeX.

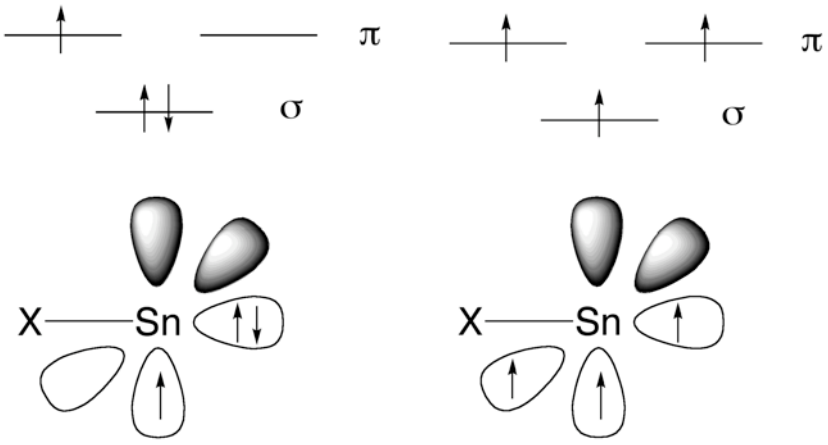

$X^2\Pi$ $a^4\Sigma^-$

ground state excited state

Figure 4.3.2.1 Schematic pictures of the $X^2\Pi$ ground state and the $a^4\Sigma^-$excited state for the GeX fragment.

Table 4.3.2.1 Calculated excitation energies from $^2\Pi$ ground state to $^4\Sigma$ excited state at BP86/QZ4P, MRCI-SD/aug-cc-pVQZ//BP86/QZ4P and MRCI-SD(Q)/aug-cc-pVQZ//BP86/QZ4P levels, where (Q) indicates the inclusion of the Davidson correction. The energies are given in kcal/mol.

	BP86/QZ4P	MRCI-SD/ aug-cc-pVQZ	MRCI-SD(Q)/ aug-cc-pVQZ
SnH	45.85	41.51	42.39
SnF	92.97	82.27	85.70
SnCl	80.35	72.24	74.52
SnBr	74.77	66.08	67.63
SnI	66.66	60.71	62.50

Table 4.3.2.2 Calculated dissociation energies D_e of linear X-Sn-Sn-X into 2 SnX fragments and excitation energies from the $^2\Pi$ ground state to the $^4\Sigma$ excited state of SnX at BP86/QZ4P level. The energies are given in kcal/mol

	D_e	ΔE_{exc}	D_e- $2\Delta E_{exc}$
H	89.4	45.9	-2.3
F	93.0	93.0	-92.9
Cl	88.9	80.4	-71.8
Br	87.5	74.8	-62.0
I	80.9	66.7	-52.5

Table 4.3.2.2 shows the theoretically predicted bond dissociation energies for breaking the triple bond in linear X-Sn≡Sn-X yielding two SnX ($a^4\Sigma^-$), D_e- $2\Delta E_{exc}$. Linear Sn_2H_2, Sn_2F_2, Sn_2Cl_2, Sn_2Br_2 and Sn_2I_2 have similar dissociation energies D_e and they are much weaker than that of acetylene and the linear structures of Si_2X_2 and Ge_2X_2. After correcting for the excitation energy of the two SnX fragments from the $X^2\Pi$ ground state to the $a^4\Sigma^-$ state, the calculated values give theoretical bond energies D_e- $2\Delta E_{exc}$. The excitation energies of the two SnX fragments are even higher than the bond dissociation energies of the linear X-Sn≡Sn-X of Sn_2F_2, Sn_2Cl_2, Sn_2Br_2 and Sn_2I_2. Sn_2F_2 has a slightly higher dissociation energy than Sn_2H_2. However, the excitation energies for SnF, SnCl, SnBr and SnI are much higher than for Sn_2H_2 and the theoretical dissociation energies of Sn_2F_2, Sn_2Cl_2, Sn_2Br_2 and Sn_2I_2 are negative. The excitation energy, ΔE_{exc} correlates with D_e- $2\Delta E_{exc}$ and the excitation energy dominates the stability of the linear structure. The ΔE_{exc} values are similar to those of GeX, but the dissociation energy is smaller than those of the SiX and GeX molecules. Due to the high excitation energies, the formation of the Sn-Sn triple bond is unfavorable for the Sn_2X_2 isomers.

The calculated bond dissociation energy D_e shows that it is energetically impossible for the SnX fragments to form an XSn≡SnX triple bond through the $a^4\Sigma^-$ excited state because the Sn-Sn single bond that can be formed from the $X^2\Pi$ ground state, would deliver a much larger binding energy. The typical bond dissociation energies of Sn-Sn single bonds in Sn_2X_6 are 28.3 - 57.1 kcal/mol, which are calculated at BP86/QZ4P level. This is much less than the stabilization energy that

can be expected from the formation of an electron-sharing XSn-SnX single bond between two SnX fragments in the $X^2\Pi$ ground state. The possibility of additional stabilizations through lone-pair and/or Sn-X donor acceptor interactions, which are described below, will be enough to gain the much higher bond energy of the triple bond. It follows that it is energetically more profitable for two SnX species to bind in their $X^2\Pi$ ground state than in the $a^4\Sigma^-$ excited state.

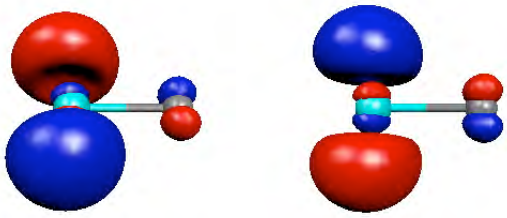

LUMO SOMO

(a) π orbital (b) π orbital

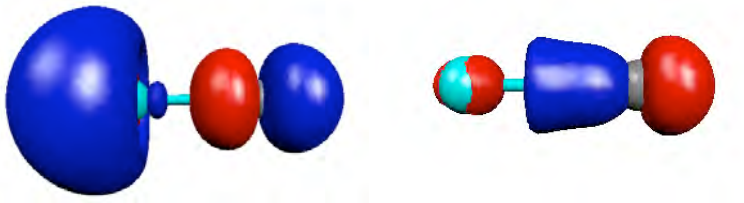

(c) σ lone-pair orbital (d) σ Sn-X orbital

Figure 4.3.2.2. Important orbitals of the SnX fragment in the $X^2\Pi$ ground state to form the Sn-Sn bond.

Figure 4.3.2.2 shows the selected orbitals of the SnX fragment. The orbitals are similar to SiX and GeX. Two π orbitals are found as LUMO and SOMO. The lone-pair orbitals and Sn-X orbitals are found as occupied orbitals with σ symmetry. These orbitals of SnH, SnF, SnCl, SnBr and SnI are quite similar in each other in the region near Sn atom. Table 4.3.2.3 shows the orbital energies of the selected orbitals in Figure 4.3.2.2. The orbital energies of SOMO and LUMO are nearly constant. The lone-pair orbital and the Sn-X bond orbital show a similar correlation and the orbital

energy becomes higher as the halogen atoms get heavier. This trend is similar to those of the SiX and GeX molecules. However, the deviation of eigenvalue of the lone-pair orbital is larger than the deviation of the eigenvalue of Sn-X bond orbital and it suggests that the X atom has larger effect on lone-pair orbital than on the Sn-X bond orbital.

Table 4.3.2.3 Calculated orbital energies of the SnX molecules on their $X^2\Pi$ ground state at BP86/QZ4P level. The energies are given in eV.

	SnH	SnF	SnCl	SnBr	SnI
π orbital (LUMO)	-3.9429	-3.8348	-3.9439	-3.9447	-3.9561
π orbital (SOMO)	-3.7202	-3.6068	-3.7104	-3.7098	-3.7227
lone-pair orbital	-6.4001	-8.4799	-7.8923	-7.5883	-7.1877
Sn-X bond orbital	-11.3856	-11.7939	-11.5918	-11.5052	-11.3167
$\Delta E_{\pi\text{-lone-pair}}$	2.4572	4.6451	3.9484	3.6436	3.2316
$\Delta E_{\pi\text{-SnX}}$	7.4427	7.9591	7.6479	7.5585	7.3606

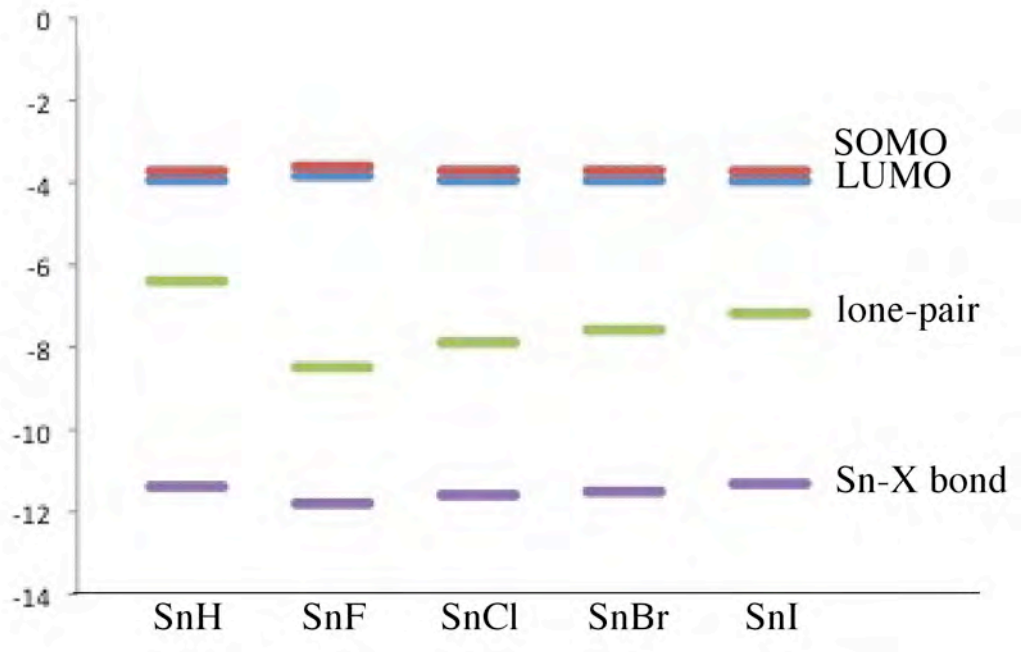

Figure 4.3.2.3. The orbital energies of LUMO, SOMO, lone-pair orbital and Sn-X orbital in Figure 4.3.2.2.

The $\Delta E_{\pi\text{-lone-pair}}$ values show the energy differences between the LUMO and the lone-pair orbital, where these orbitals are important for the lone-pair donor acceptor interaction, and the $\Delta E_{\pi\text{-Sn-X}}$ values show the energy difference between the LUMO and the Sn-X bond orbital, which concern for the Sn-X donor-acceptor interaction. Table 4.3.2.3 shows that the $\Delta E_{\pi\text{-lone-pair}}$ and $\Delta E_{\pi\text{-Sn-X}}$ have correlations with the mass of the halogen atoms and $\Delta E_{\pi\text{-lone-pair}}$ and $\Delta E_{\pi\text{-Sn-X}}$ become smaller as the halogen atom gets heavier. Compared to the SiX and GeX molecules, the $\Delta E_{\pi\text{-lone-pair}}$ and $\Delta E_{\pi\text{-Sn-X}}$ are smaller than those of SiX and GeX, and it suggests that the orbital interaction is more favorable.

Table 4.3.2.4 Each percentage contribution of selected orbitals corresponds to the indicated atomic orbitals of SnX fragment

	SnH(%)	SnF(%)	SnCl(%)	SnBr(%)	SnI(%)
π orbital (LUMO)	Sn: p_x 58.38 p_y 39.18	Sn: p_y 94.86 F: p_y 2.69	Sn: p_y 82.78 p_x 8.80 Cl: p_y 5.70	Sn: p_y 69.43 p_x 21.05 Br: p_y 5.55	Sn: p_y 70.81 p_x 17.73 I: p_y: 6.80
π orbital (SOMO)	Sn: p_z 97.91 H: p_z 2.06	Sn: p_z 95.41 F: p_z 4.05	Sn: p_z 92.99 Cl: p_z 5.87	Sn: p_z 92.07 Br: p_z 6.70	Sn: p_z 89.86 I: p_z 7.72
Lone-pair orbital	Sn: s 16.65 p_y 22.22 p_x 14.91 H: s 47.89	Sn: s 36.51 p_x 11.54 F : p_x 50.07	Sn: s 23.33 p_x 15.38 Cl: p_x 52.22 p_y 5.55	Sn: s 18.04 p_x 15.04 Br: p_x 46.03 p_y 13.96	Sn: s 13.29 p_y 18.07 p_x 4.52 I: p_y 49.66 p_x 12.43
Sn-X orbital	Sn: s 75.78 H: s 21.83	Sn: s 58.46 F: p_x 37.24	Sn: s 71.08 Cl: p_x 21.59 s 3.34	Sn: s 77.65 Br: p_y 14.53 p_x 4.40	Sn: s 80.22 I: p_x 11.56 s 3.81

Table 4.3.2.4 shows the contributions of the atomic orbitals for selected Kohn-Sham molecular orbitals. In this table, LUMO and SOMO show a similar contribution of atomic orbital and these orbitals are constructed by just *p* orbitals, which is the same for the SiX and GeX molecules. In the lone-pair orbital, the contribution of the

Sn atom and X atom is nearly the same. The contributions of the *s* orbitals are 11% - 16%, and this is quite smaller than for SiX and GeX, where *s* orbital contributes smaller as the halogen atom gets heavier. The contributions of the *p* orbitals of Sn atom are 11% - 36% and the *p* orbital shows the opposite trend to the *s* orbital. The comparison with SiX and GeX shows that the contribution of the X atom becomes larger as the atom of carbon family gets heavier, and the lone-pair contains more X atom character. The lone-pair of SnF has the largest *s* character and the contribution of *s* orbital becomes larger as the halogen atom gets heavier. The Sn-X bond orbital is built from the *s* orbitals of Sn atom and *s* orbital of Hydrogen and *p* orbital for halogen atoms. The Sn-X orbital is mainly consisted from the atomic orbital of Sn atom. The Sn-F bond orbital shows smallest *s* contribution and the contribution of *s* orbital becomes larger as the halogen atom gets heavier. The percentage of Sn-X bond shows that the contribution of X atom becomes smaller as the atom of carbon family gets heavier, and the Sn-X bond contains more *s* character of the Sn atom.

4.3.2.1.2 σ-type Isomers, **SnA**, **SnE2** and **SnF1**

As shown before, the linear arrangement of two SnX fragments of the $X^2\Pi$ state is unfavorable for the bond formation between the unpaired electrons. The bond formation must rather take place in a sideways fashion. Figure 4.3.2.4 shows some different orientations for two SnX fragments, each in the $X^2\Pi$ state, which lead to a Sn-Sn σ bond,

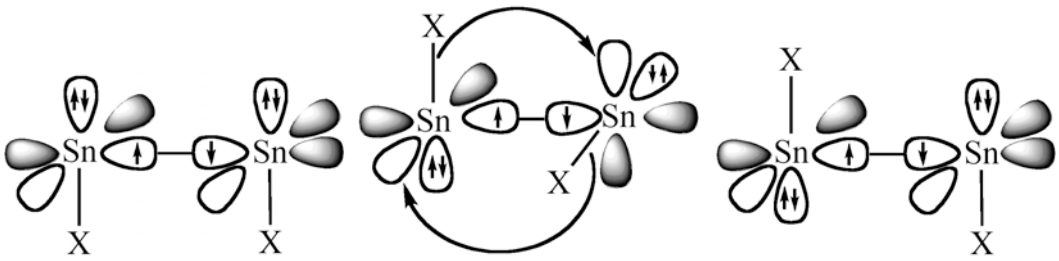

(a) (b) (c)

Figure 4.3.2.4. Qualitative model for σ-type orbital interaction between two SnX molecules in different orientation where the unpaired electrons yield a σ orbital.

Figure 4.3.2.4 (a) shows a syn-planar arrangement of the SnX moieties, which gives the isomer **SnF1**. This arrangement is not favorable because the vacant *p(π)*

orbitals remain unoccupied while the Sn-X bonds and the electron lone-pairs of the two fragments repel each other. The geometry optimization of Sn_2X_2 with a syn-planar arrangement gives a structure which is a transition state.

The rotation around the σ-bond axis by 90° gives a much more favorable arrangement. In this bond situation, the empty *p*(π) orbitals of SnX can interact with the Sn-X bond and with the electron lone-pair of the other SnX fragment. The donor-acceptor interactions between the Sn-X bond and the vacant *p*(π) is more stabilizing than the donation from the electron lone-pairs to the *p*(π) because of the more effective orbital combination. The acceptor bond is a *p* orbital and the lone-pair orbitals have also *p*-character, as shown in Table 4.3.2.4. These orbitals have both directional properties and the combination leads to a lower overlap of the two orbitals. The Sn-X bond has a large *s* character, which has less directional properties, and the Sn-X donor-acceptor leads to a three-center-two-electron bond. The three-center two-electron bond is favorable in the point of the overlap of the orbitals. This means that the Sn-X bonds are better donors than the lone-pairs. The Sn-X bonds interact with the empty p(π) orbitals of the other SnX moiety. This arrangement gives the isomer **SnA** as shown in Figure 4.3.2.4 (b), which is similar to Si_2X_2 and Ge_2X_2. This explains why the global energy minimum is the halogen-bridged geometry **SnA** that is not planar but has a nearly perpendicular arrangement of the two Sn_2X planes which have a dihedral angle between 101.3° and 109.5°. From the quantitative model, it is found that there are three bonding components of the orbital interactions in **SnA**: one σ electron sharing bond and two Sn-X donor-acceptor bonds.

Figure 4.3.2.4 (c) shows the anti-planar arrangement of the two SnX fragments, which gives the isomers **SnE2**. The only Sn-Sn bonding contribution is the σ orbital between two Sn atoms. The structure of **SnE2** lacks the two Sn-X donor-acceptor interactions of **SnA**, and so that the vacant *p(π)* orbitals remain unoccupied. The geometry optimization of Sn_2X_2 with an anti-planar arrangement gives structures that are transition states.

Table 4.3.2.5. Selected orbitals and orbital shapes and energies of σ-isomers **SnA**, **SnE2** and **SnF2**. The energy levels are given in eV.

	SnA	**SnE2**	**SnF1**
orbital		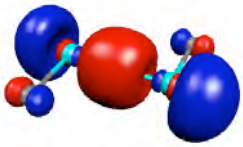	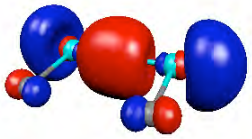
	σ-type bond	σ-type bond	σ-type bond
H	-4.5358	-4.5884	-4.6007
F	-4.3862	-4.5749	-4.5184
Cl	-4.7478	-4.7727	-4.6546
Br	-4.7797	-4.7827	-4.6530
I	-4.8269	-4.8057	-4.6608
Orbital		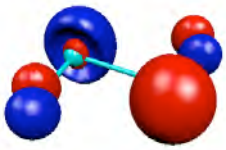	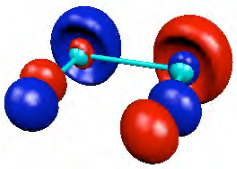
	Sn-X donor	lone-pair	lone-pair
H	-8.0032	-6.1673	-5.8146
F	-9.6493	-8.0620	-7.9560
Cl	-8.7540	-8.0108	-7.4973
Br	-8.3679	-7.7497	-7.1980
I	-7.8995	-7.4508	-6.8117
Orbital		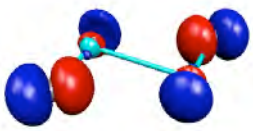	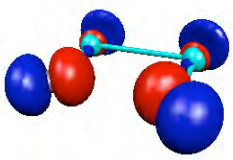
	Sn-X donor	lone-pair	lone-pair
H	-13.4103	-6.4710	-6.7595
F	-12.6494	-8.4748	-8.6225
Cl	-12.4472	-8.1710	-8.1930
Br	-12.4054	-7.7843	-7.8834
I	-12.1699	-7.3104	-7.5019

4.3 Sn_2X_2 Molecules

In the previous section, the bond situation has been discussed with a qualitative model. Table 4.3.2.5 shows the selected orbitals and their orbital energies of **SnA**, **SnE2** and **SnF1** concerning the Sn-Sn bonds. The first orbitals of **SnA**, **SnE2** and **SnF1** in Table 4.3.2.5 seem σ-type Sn-Sn bonds. The second one and third one of **SnA** seem to be Sn-X donor-acceptor bonds and those of **SnE2** and **SnF1** seem to be lone-pair orbitals. These orbitals show that the qualitative model is sensible in these σ system isomers.

The Sn-Sn σ bonds and the orbitals are found as the HOMO in **SnA**, **SnE2** and **SnF1** of all Sn_2X_2 molecules. The orbitals are also found as the HOMOs in Si_2X_2, Ge_2X_2 and Sn_2X_2 molecules. The energies of the HOMOs are presented in Table 4.3.2.5 and for SnF it has the highest HOMO energy of Sn_2X_2 system and the orbital energy mostly decreases with heavier halogen atoms. In the Sn_2F_2, Sn_2Cl_2, Sn_2Br_2 and Sn_2I_2 system, the energy level of the σ type orbital clearly correlates with the orbital energy of the π orbital, which is the SOMO of the SnX fragment. The Sn-Sn bond lengths in **SnE2** and **SnF1** are longer than the Sn-Sn single bond of $X_3Sn\text{-}SnX_3$ (Sn_2H_6: 2.795Å, Sn_2F_6: 2.836Å, Sn_2Cl_6: 2.866Å, Sn_2Br_6: 2.881Å, Sn_2I_6: 2.897Å at BP86/QZ4P), because the σ bonds in **SnE2** and **SnF1** are formed by the two π orbitals of SnX moieties which are the SOMOs shown in Figure 4.3.2.2(b) and the σ bond has little *s* character, whereas the normal Sn-Sn σ bond has sp^3 character. Table 4.3.2.5 shows the orbital energies of these structures. The energy level of the σ type orbital in Sn_2F_2 is the highest in **SnA**, **SnE2** and **SnF1**, where the orbital energies become lower when halogen atom X gets heavier.

SnA clearly has two Sn-X donor-acceptor bonds as shown in Table 4.3.2.5. These two orbitals in Table 4.3.2.5 are very similar except the node on the Sn-Sn bond. The energetically higher orbital has a node on the Sn-Sn bond and the lower one does not. From these orbital figures, it can be thought that the energetically higher lying orbital is the anti-bonding orbital of lower lying one (Figure 4.3.2.5). The energetically lower lying orbital has large coefficients on the Sn-Sn bond and this orbital contributes to the Sn-Sn bond, whereas the energetically higher orbital has large coefficients between two Sn atoms and the X atom and this orbital contributes to the formation of the Sn-X-Sn ring structure. This can explain the Sn-Sn bond lengths

in **SnA**, which are shorter than those of the Sn-Sn single bond of Sn_2X_6. This bonding situation is qualitatively the same as for the corresponding structures of **SiA** and **GeA**. This similarity results in the fact that the doubly bridged non-planar structures **SiA**, **GeA** and **SnA** are the global minimum in all cases except for Si_2F_2.

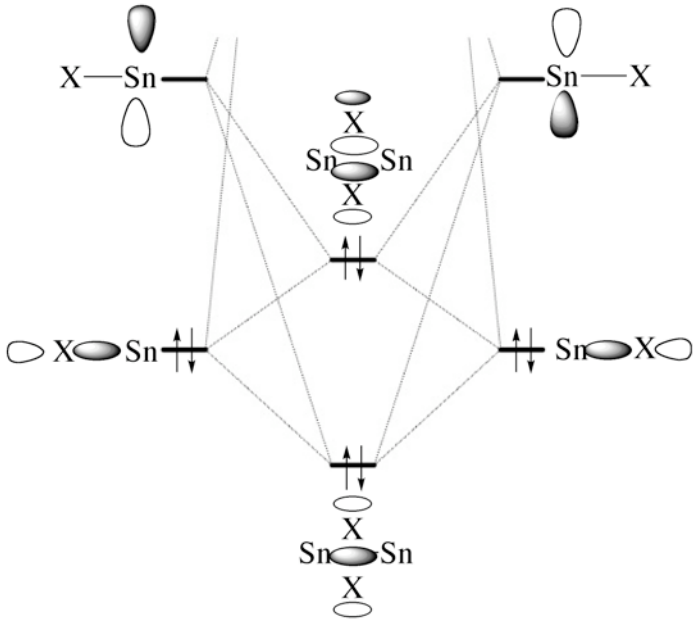

Figure 4.3.2.5 Orbital correlation model for donor-acceptor interaction between the Sn-X bond and the vacant $p(\pi)$ orbital in ground state of two Sn-X fragments to yield bridged structures.

Figure 4.3.2.5 shows that the two Sn-X donor-acceptor bonds interact with each other and form two new orbitals. In principle, the orbital energy level of the new formed orbitals depend on the energy level of the orbitals of the fragment i.e. the energy level of the vacant π orbital and the Sn-X σ bond orbital. Table 4.3.2.5 shows that the orbital energies of two Sn-X donor-acceptor bonds become higher as the halogen atom gets heavier and it is similar trend to the orbital energies of the Sn-X bond because the main contribution of these orbitals is the Sn-X bond.

In **SnE2** and **SnF1**, the two lone-pair orbitals interact with each other and they form a bonding orbital between the two SnX moieties. However, they form an occupied anti-bonding orbital at the same time (Figure 4.3.2.6). This system is the four-electron-two-orbital interaction and the interaction between two lone-pair orbitals almost cancels; for the bond formation, therefore, they have nearly no

contribution to the Sn-Sn bond, which is similar to **SiE2**, **SiF1**, **GeE2** and **GeF1**.

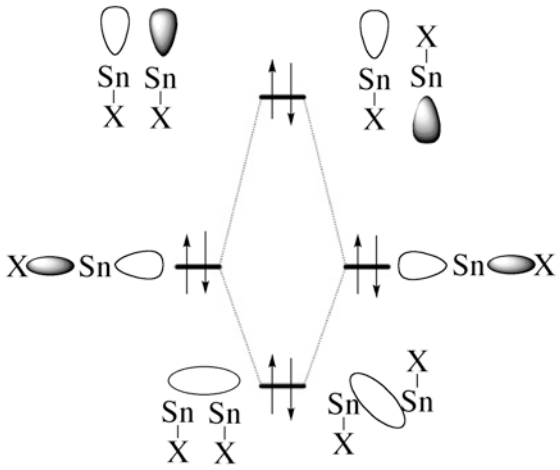

Figure 4.3.2.6 Orbital correlation diagram between two lone-pair orbitals of the two Si-X fragments in ground state in σ-type bent structures, **SnE2** and **SnF1**.

4.3.2.1.3 π-type Isomers, **SnB**, **SnC**, **SnE1** and **SnF2**

The unpaired electrons in the $X^2\Pi$ ground state of the Sn-X may also be paired in an electron-sharing Sn-Sn bond between the two SnX fragments, which has π symmetry with respect to the molecular structure. Figure 4.3.2.7 shows different orientations for two ($X^2\Pi$) SnX molecules which lead to such a Sn-Sn π bond.

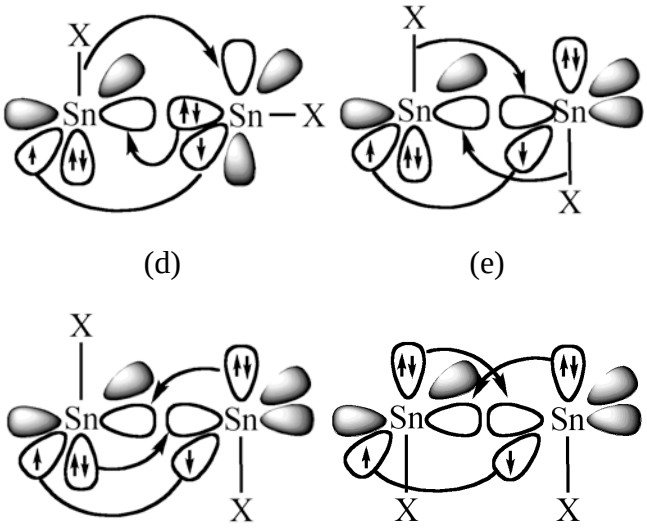

Figure 4.3.2.7 Qualitative model for the π-type orbital interaction between two SnX molecules in different orientations where the unpaired electrons yield a π orbital.

The arrangement that is given in Figure 4.3.2.7(d) has an electron lone-pair of one SnX moieties pointing in the direction of the empty π orbital of the other SnX species. This orbital interaction now has σ symmetry with respect to the SnX dimer plane. Besides the electron-sharing π bond and the lone-pair donor-acceptor σ bond, further stabilizing orbital interactions are possible, which are shown in Figure 4.3.2.7(d). Another possibility is the donation of the SnX σ bonding orbital, which is shown in the orbital of **SnA** in Figure 4.3.2.4(b). As noted before, the donation from the SnX bonding orbital is stronger than from the lone-pair orbital. The former interaction becomes stronger when the SnX donor orbital and the empty π orbital of the interacting fragments are tilted toward each other, which leads to the structure **SnB** (Figure 4.3.2.7(d)). The tilting of the empty π orbital to the acceptor SnX moiety (top SnX in Figure 4.3.2.7(d)) means that the terminal atom moves toward the bridging X atom. The unusual singly bridged geometry of **SnB**, which has a terminal X atom with syn-orientation to the bridging atom, can thus be explained as a stereoelectronic effect that comes from the orbital interactions between two SnX fragments in their $X^2\Pi$ ground states.

Figure 4.3.2.7(e) displays another orientation of two SnX molecules where the unpaired electrons form a π bond, while the SnX bonds are in an anti-planar arrangement. The π orbital interaction between the SnX fragments is enhanced by two equal donor-acceptor interactions between the SnX bonding orbitals and the empty π orbitals of the interacting fragments. The latter orbital interactions become stronger, when the X atom bridge in a doubly bridged planar (D_{2h}) structure. Geometry optimizations of $(SnX)_2$ show that the D_{2h} symmetric stationary point is an energetically low-lying structure on the potential energy surface. The inspection of the Hessian matrix reveals, however, that it is a transition state for the degenerate rearrangement of the global energy minimum structure **SnA**. It is the wing-flapping motion of the butterfly geometry. The structure **SnA** has a Sn-Sn σ bond and two SnX donor-acceptor bonds (Figure 4.3.2.4(b)), while the transition state has a Sn-Sn π bond and two SnX donor-acceptor bonds (Figure 4.3.2.7(e)).

Table 4.3.2.6. Selected orbitals and orbital energies of the π isomers, **SnB, SnC**, **SnE1** and **SnF2**. The energy levels are given in eV.

	SnB	**SnC**	**SnE1**	**SnF2**
orbital	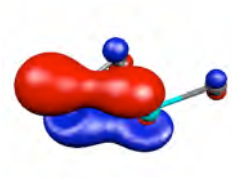	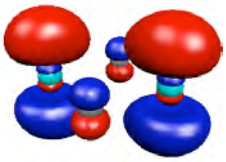	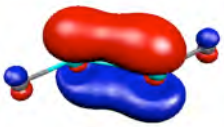	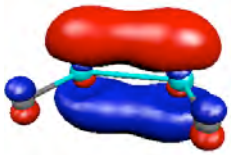
	π-type bond	π-type bond	π-type bond	π-type bond
H	-4.6183	-4.4269	-4.6773	-4.6368
F	-4.4638	-3.6269	-4.7320	-4.7012
Cl	-4.6036	-3.9234	-4.8231	-4.7274
Br	-4.5797	-3.9549	-4.8074	-4.6845
I	-4.5614	-4.0351	-4.7449	-4.6395
orbital	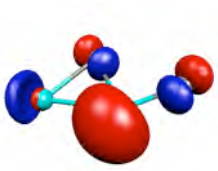	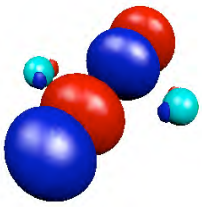	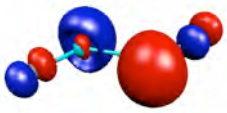	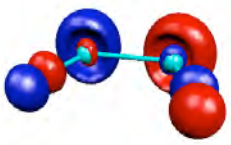
	lone-pair donor	Sn-X donor	lone-pair	lone-pair
H	-6.6407	-8.5481	-6.3478	-5.9225
F	-7.9807	-9.7528	-8.0334	-8.0481
Cl	-7.4336	-8.9032	-7.4801	-7.4830
Br	-7.0816	-8.5136	-7.2108	-7.1707
I	-6.6164	-8.1224	-6.7884	-6.7446
orbital		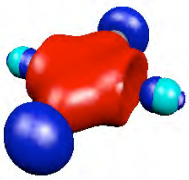	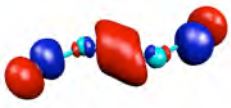	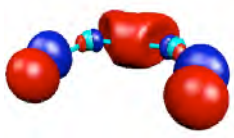
	Sn-X donor	Sn-X donor	lone-pair	lone-pair
H	-7.6233	-13.5530	-7.7239	-7.4239
F	-9.2204	-12.3443	-9.8244	-9.6378
Cl	-8.2950	-12.2157	-9.0910	-8.8562
Br	-7.6933	-12.1725	-8.6593	-8.4814
I	-7.4624	-12.0555	-8.1584	-8.0025

The electron lone-pair donation is weaker than the SnX σ-bond donation, but it leads to another structure of $(SnX)_2$ which is a saddle point on the potential energy surface.

Figure 4.3.2.7(f) and 4.3.2.7(g) show that the donation of the lone-pair of one SnX fragment to the vacant p_π orbital of the other SnX fragment becomes enhanced tilting the Sn-X bond outwardly, which yields the trans and cis form **SnE1** and **SnF2**, respectively. According to the orbital analysis, the structures **SnE1** and **SnF2** have three bonding orbital components, which are one π bond and two lone-pair donor-acceptor bonds. The structure **SnE1** and **SnF2** of Sn_2H_2 is energetically higher lying than the planar transition state with two bridging hydrogen atoms, **SnC**, which has one π bond and two Sn-X donor-acceptor bonds, whereas **SnE1** for Sn_2F_2, Sn_2Cl_2, Sn_2Br_2 and Sn_2I_2 lie energetically lower than **SnC**.

Table 4.3.2.6 shows the orbital energies of important orbitals in **SnB, SnC**, **SnE1** and **SnF2**, which concern the Sn-Sn bond. The Sn-Sn π bonds of **SnB, SnC**, **SnE1** and **SnF1**, which are categorized to a π type structure in Figure 4.3.2.7, are found as the HOMO. The energy of the π type orbital in Sn_2F_2 is the highest in **SnB**, **SnC**, **SnE1** and **SnF2**, where the orbital energies become lower, when the halogen atom X gets heavier. This correlates with the orbital energy of the SOMO of the SnX fragment and also the energies of π orbitals correlate with the Sn-Sn bond lengths. The π type isomers **SnB**, **SnC**, **SnE1** and **SnF2** are found as transition states because the energies of their π orbitals are relatively higher than that of σ bond of **SnA**, where the corresponding isomers of Si_2X_2, Ge_2X_2 are often found as minima because the rotation of their Si-Si bond and Ge-Ge bond needs more energy to break the π bond. The π bond is weak and the π bond can rotate easily in Sn_2F_2, Sn_2Cl_2, Sn_2Br_2 and Sn_2I_2 molecules. In principle, a π bond is weaker than a σ bond and a "single" π bond must be longer than a σ bond, because a π bond usually has less orbital overlap than a σ bond. However the Sn-Sn bond lengths in **SnB, SnE1** and **SnF2** are shorter than the Sn-Sn single bonds of **SnE2** and **SnF1** as shown in the chapter 4.3.1.1. This suggests that another interaction, in addition to the π orbital interaction, could exist between the Sn-Sn atoms as expected in Figure 4.3.2.7. These interactions are the donor-acceptor bond form the lone-pair to the vacant π orbital.

The second figure of **SnB** of Table 4.3.2.6 shows that the orbital has the large amount of electron density between the two Sn atoms and the shape of the orbital is similar to the lone-pair donor-acceptor bond model in Figure 4.3.2.7(d). The energy level of this orbital correlates with the energies of the lone-pairs of the Sn-X fragments (Table 4.3.2.3), where the orbital energy level becomes lower, when the halogen atom X gets heavier. To form the donor-acceptor bond, the lone-pair orbital interacts with the vacant π orbital of the Sn-X fragment and the formed donor-acceptor orbital has mainly the character of the original lone-pair orbital and the energy level of the formed orbital exhibits the correlation with the lone-pair orbital. These orbitals are similar to those of **SiB** and **GeB**.

The third orbital of **SnB** in Table 4.3.2.6 shows that the largest coefficient comes from two Sn atoms and the main contribution is not a Sn-X donor-acceptor bond. However, the orbital contributes to the Sn-X-Sn bonding. The energy level of this orbital is moderately higher than that of Sn-X donor-acceptor bond in **SnA**. The energy level of the orbital shows a similar trend with the orbital energy of the Sn-X bond in the SnX fragment (Table 4.3.2.3), where the orbital energy level becomes lower when the halogen atom X is heavier. The orbitals of **SiB** and **GeB** show similar orbitals to **SnB**.

The **SnC** structures have a π bond and two Sn-X donor-acceptor bonds. The Sn-X donor-acceptor bond orbitals are quite similar to those of **SnA**. The two Sn-X donor-acceptor bonds mainly contribute to the Sn-Sn bond and the Sn-X-Sn ring structure, which is same as the bond correlation in Figure 4.3.2.7(e). The energy level of the π orbital is higher than that of the σ orbital of **SnA** and the π orbitals of **SnB**, **SnE1** and **SnF2**.

The two orbitals shown in Table 4.3.2.6 of **SnE1** and **SnF2** are similar to the two lone-pair orbitals of **SnE2** and **SnF1**. When the energy levels of these orbitals are compared, the lower “lone-pair like” orbital energy of **SnE1** is 0.8480 – 1.3496 eV lower than the energy of the lone-pair orbital of **SnE2**, where the lone-pairs in **SnE2** do not contribute to the Sn-Sn bond. The orbital energy differences between **SnF1** and **SnF2** are 0.5006 – 0.6644 eV. The stabilization comes from the contribution of the vacant π orbital. The energetically higher lying orbital has a node along the Sn-Sn

bond and the lower lying one does not. From these orbital figures, it can be thought that the energetically higher orbital is the anti-bonding orbital of the lower one (Figure 4.3.2.8 and 4.3.2.9). The energetically lower lying orbital contributes to the Sn-Sn bond. The energetically higher orbital looks similar to the localized lone-pair orbital. This can explain the Sn-Sn bond lengths in **SnE1** and **SnF2**, which are shorter than the Sn-Sn single bonds of **SnE2** and **SnF1**. The Sn-X bond lengths in **SnE1** and **SnF2** are shorter than those of **SnE2** and **SnF1**, as the lone-pair orbital also contributes to the Sn-X bond and the orbital interaction between the lone-pair orbitals and the vacant orbitals stabilize the Sn-X bond.

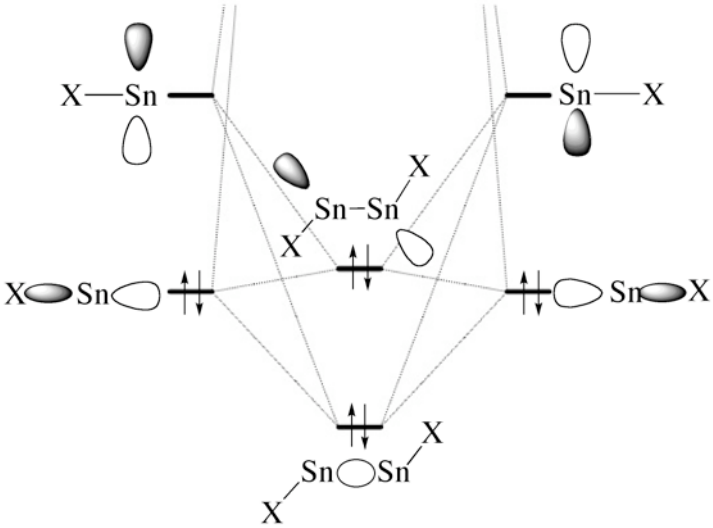

Figure 4.3.2.8 Orbital correlation diagram between two lone-pair orbitals in $X^2\Pi$ ground state of the two Sn-X fragments in **SnE1** to yield donor-acceptor bonds.

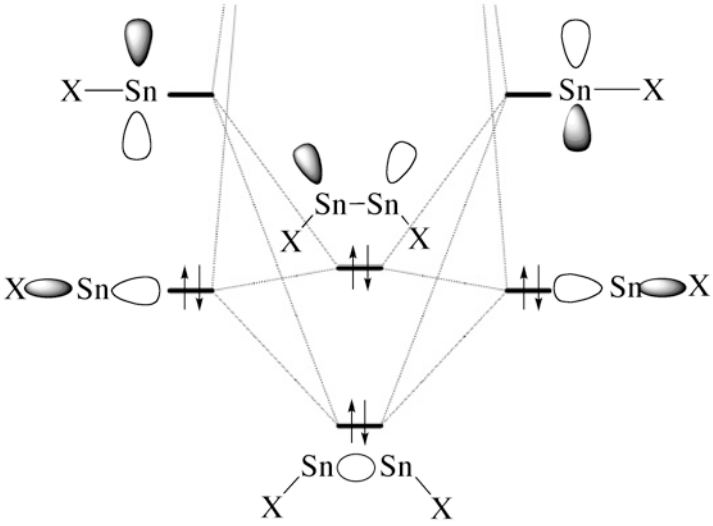

Figure 4.3.2.9 Orbital correlation diagram between two lone-pair orbitals in $X^2\Pi$ ground state of the two Sn-X fragments in **SnF2** to yield donor-acceptor bonds.

4.3.2.1.4 Summary of Orbital Analyses

In this chapter, the orbital analyses of the SnX fragments and Sn_2X_2 molecules have been shown. The orbital analyses of the SnX fragment show that the SnX molecules need very high excitation energies from $X^2\Pi$ state to $a^4\Sigma$ state. Due to that, the bond dissociation energies of the linear XSn≡SnX structure become negative and the triple bond formation is quite unfavorable. Alternatively, X-Sn-Sn-X bond formation happens through the SnX fragments in the $X_2\Pi$ ground state.

The orbital analyses of Sn_2X_2 presented that the interaction models between two SnX fragments are quite sensible for the Sn_2X_2 molecules, and the structural difference stems from the orbital interaction between two SnX fragments. The orbital models presented that the X-Sn-Sn-X isomers are categorized to two groups: σ-type isomers and π-isomers. The doubly bridged structures **SnA** are categorized to the σ-type isomer, and **SnA** has three bonding components: one σ-type bond and two Sn-X bond donor-acceptor bonds. Here, the Sn-X donor-acceptor interaction leads a favorable bridging situation, three-center-two-center bond, although the lone-pair donor-acceptor interaction is less favorable due to the less orbital interaction. Due to that, the Sn-X-Sn bridging is the favorable bonding situation.

SnB, **SnC**, **SnE1** and **SnF2** are categorized to π-isomers and these isomers are transition states, due to the energetically high π-orbital, which is similar to π isomers of Ge_2X_2. The lone-pair-type orbital of **SnE1** and **SnF2** show lower energies than **SnE2** and **SnF1**. It suggests that the lone-pair orbitals of **SnE1** and **SnF2** interact with the vacant π orbitals.

4.3.2.2 AIM Analyses

In the chapter 4.3.1, the bond situation is discussed for the several geometries of Sn_2X_2, and the orbitals and their energies were investigated in the previous chapter. However, there are still some questions unanswered about the bonding situation. An additional possibility of bonding analysis is the topological analysis of the electron density. Figure 4.3.2.10 – Figure 4.1.2.17 show the Bader plots. In general, Laplacians $\nabla^2\rho$ exhibit that Sn_2F_2 molecules have a more ionic character and Sn_2I_2 molecules have a more covalent character, considering the charge accumulation.

Figure 4.3.2.10 shows the Bader plot of the isomer **SnA** in the Sn_2X plane. The results show that **SnA** has an Sn-X-Sn ring structure, as expected at the geometry part. A charge accumulation is not found and it suggests that the Sn-X and Sn-Sn interaction has a large ionic character, although the charge accumulation is found for Si_2X_2 and Ge_2X_2.

In the chapter 4.3.1 and 4.3.2.1, the lone-pair donor bond and the Sn-X donor-acceptor bond could not be found clearly in **SnB** from the point of geometries and orbitals. The AIM results show that **SnB** has a Sn-X-Sn ring structure, which is consistent with the results of the geometry analyses (Figure 4.3.2.11). Although the charge accumulation is found for Si_2X_2 and Ge_2X_2, no charge accumulation is found for Sn_2X_2, The lack of the charge accumulation indicates the less covalent character of the Sn-Sn bond and the Sn-X bond.

The AIM results show that all **SnC** isomers have Sn-X-Sn ring structures, and Sn_2H_2, Sn_2Br_2 and Sn_2I_2 molecules have Sn-Sn bonds, although Sn_2F_2 and Sn_2Cl_2 show no bond path between the Sn atoms (Figure 4.3.2.12). This agrees with the discussion of the differences of the geometry. The X atoms in **SnC** have a bond path to each Sn atom. Considering that no charge accumulation in the region between Sn and X is found in all Sn_2X_2 molecules, the ionic interaction plays an important role in Sn-X-Sn bridging, even though the charge accumulation is found for Si_2X_2 and Ge_2X_2.

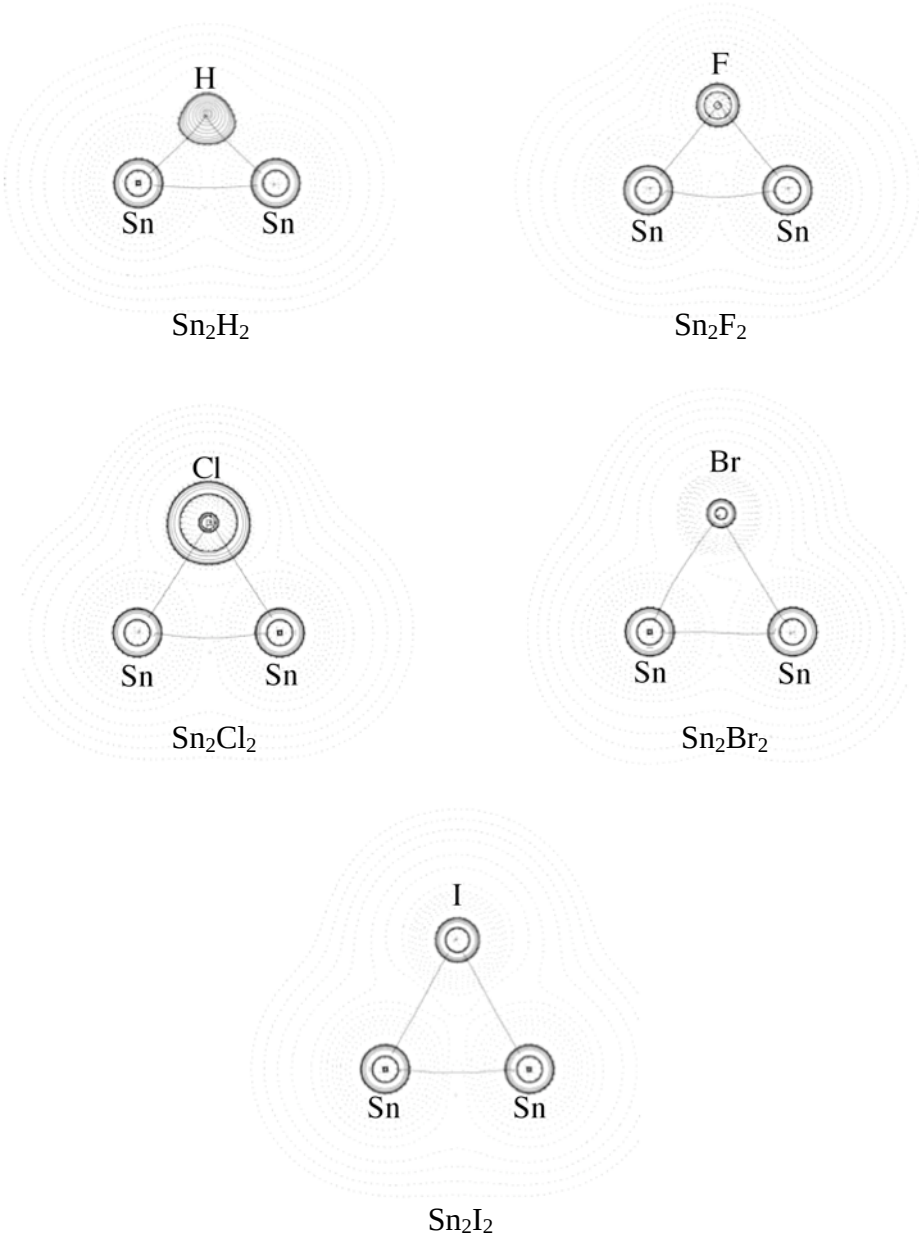

Sn_2H_2 Sn_2F_2

Sn_2Cl_2 Sn_2Br_2

Sn_2I_2

Figure 4.3.2.10 Contour line diagram $\nabla^2\rho(r)$ of isomer **SnA**. Solid lines indicate areas of charge concentration ($\nabla^2\rho(r) < 0$), while dashed lines show areas of charge depletion ($\nabla^2\rho(r) > 0$). Solid lines that connect the atomic nuclei are the bond paths.

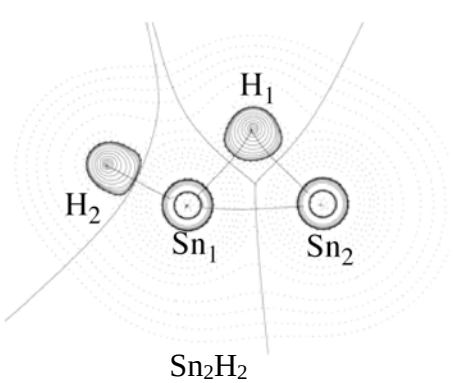

Sn_2H_2

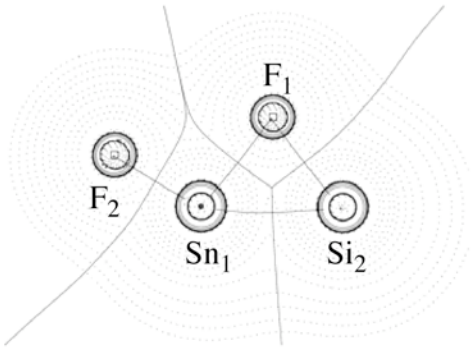

Sn_2F_2

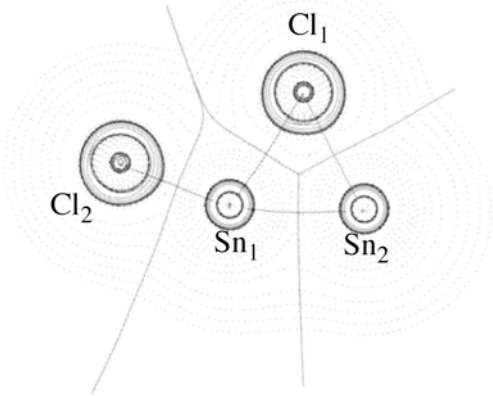

Sn_2Cl_2

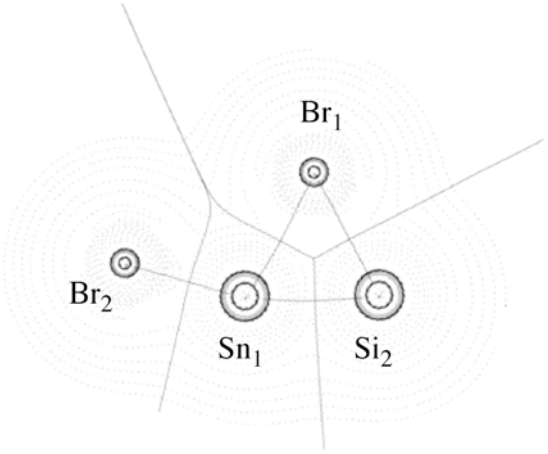

Sn_2Br_2

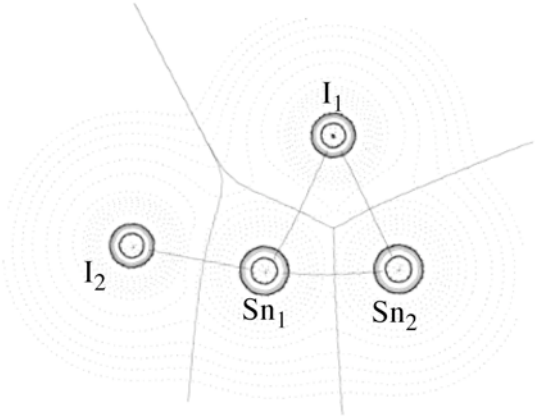

Sn_2I_2

Figure 4.3.2.11 Contour line diagram $\nabla^2\rho(r)$ of isomer **SnB**. Solid lines indicate areas of charge concentration ($\nabla^2\rho(r) < 0$), while dashed lines show areas of charge depletion ($\nabla^2\rho(r) > 0$). Solid lines that connect the atomic nuclei are the bond paths.

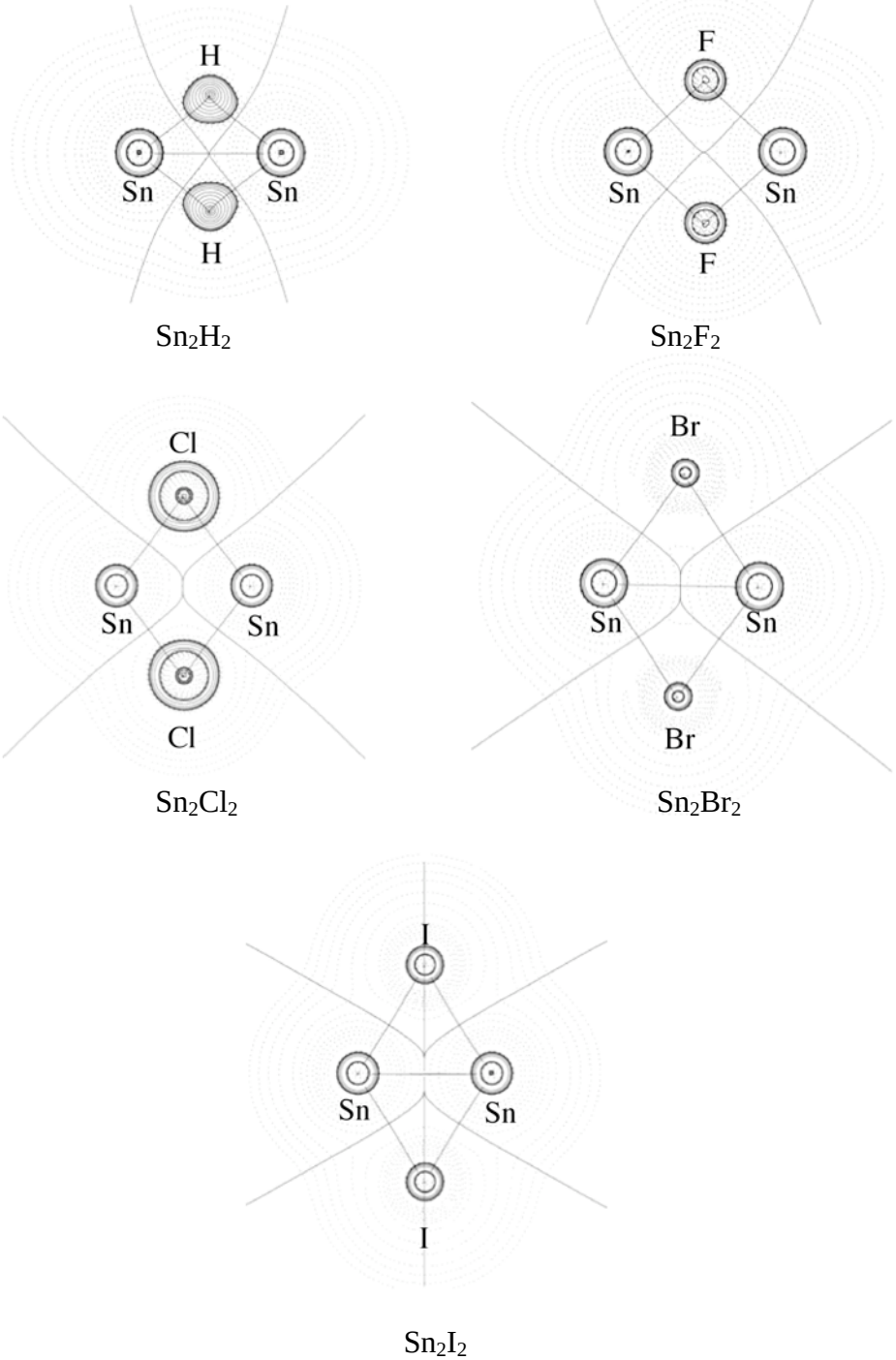

Sn_2H_2 Sn_2F_2

Sn_2Cl_2 Sn_2Br_2

Sn_2I_2

Figure 4.3.2.12 Contour line diagram $\nabla^2\rho(r)$ of isomer **SnC**. Solid lines indicate areas of charge concentration ($\nabla^2\rho(r) < 0$), while dashed lines show areas of charge depletion ($\nabla^2\rho(r) > 0$). Solid lines that connect the atomic nuclei are the bond paths.

Figure 4.3.2.13 shows the isomers of **SnD** have Sn-Sn and Sn-X bonds. No charge accumulation is found between the two Sn atoms, although charge accumulation is found in Si_2X_2 and Ge_2X_2 systems. The less charge accumulation indicates that Sn-Sn bond has a more ionic character than Si-Si bonds of **SiD** and Ge-Ge bonds of **GeD**.

The AIM results of **SnE1** are shown in Figure 4.3.2.14 and it presents the Sn-Sn bonds and Sn-X bonds. The contour line diagrams show that no charge accumulation is found in the region of the Sn-Sn bond, although the charge accumulation is found for Si_2X_2 and Ge_2X_2. It suggests that the **SnE1** isomers have smaller orbital interaction between Sn atoms than the isomers of **SiE1** and **GeE1**. The isomers of **SnE2** have Sn-Sn and Sn-X bonds as shown in Figure 4.3.2.15. A slight charge accumulation is found among the Sn-Sn bond region, although no charge accumulation is found in **SnE1**. The difference of **SnE1** and **SnE2** suggests the different orbital situation and it agrees with the results of the orbital analyses, which indicated the Sn-Sn σ bond for **SnE2** and the lone-pair donor-acceptor bond for **SnE1**.

Figure 4.3.2.16 shows that the isomers of **SnF1** have Sn-Sn and Sn-X bonds. For Sn_2Cl_2, Sn_2Br_2 and Sn_2I_2, two halogen atoms have the X-X bond because the Sn-Sn-X angle is nearly 90° and Cl, Br and I have a large radius, which is similar to the situation in Si_2X_2 and Ge_2X_2. The figures of the charge accumulation are quite similar to those of **SnE2** and it suggests that the **SnF1** isomers have a similar bond situation to **SnE2**. The bond path proved that the **SnF2** isomers have Sn-Sn bonds and Sn-X bonds as shown in Figure 4.3.2.17. A charge accumulation is not found in the region of the Sn-Sn bond. The figures show that the bonding situations are similar to those of **SnE1**.

In this chapter, the AIM analyses of Sn_2X_2 isomers are shown. The analyses of the Sn_2X_2 molecules show smaller charge accumulations than the Si_2X_2 isomers and Ge_2X_2 isomers, and it indicates the smaller orbital interacting between the two Sn atoms. The AIM results proved that **SnA**, **SnB** and **SnC** have Sn-X-Sn bridged structures. The bent-structures **SnE1** and **SnF2** showed the different charge accumulation figures from **SnE2** and **SnF1**, and it suggests the different Sn-Sn

bonding situation as discussed before (chapter 4.3.2.1).

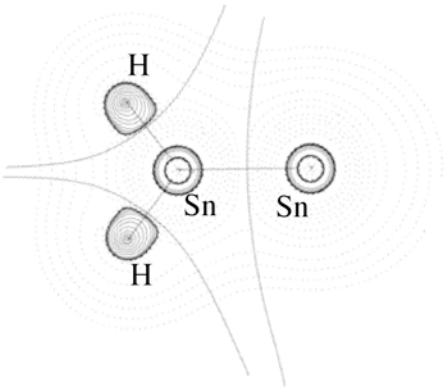

Sn_2H_2

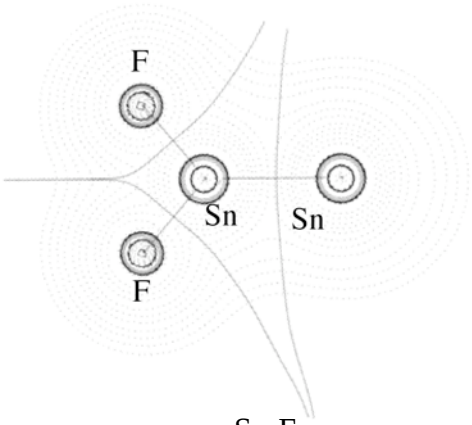

Sn_2F_2

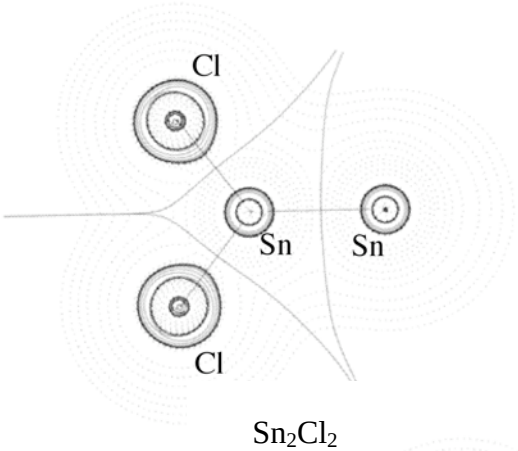

Sn_2Cl_2

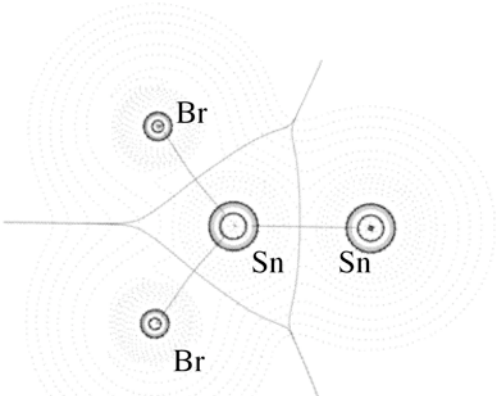

Sn_2Br_2

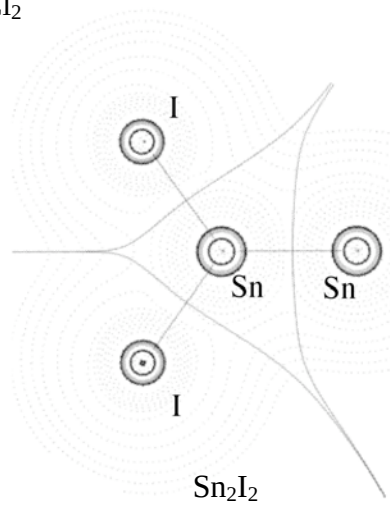

Sn_2I_2

Figure 4.3.2.13 Contour line diagram $\nabla^2\rho(r)$ of isomer **SnD**. Solid lines indicate areas of charge concentration ($\nabla^2\rho(r) < 0$), while dashed lines show areas of charge depletion ($\nabla^2\rho(r) > 0$). Solid lines that connect the atomic nuclei are the bond paths, while solid lines that separate the atomic basis give the zero-flux surface in the molecular plane.

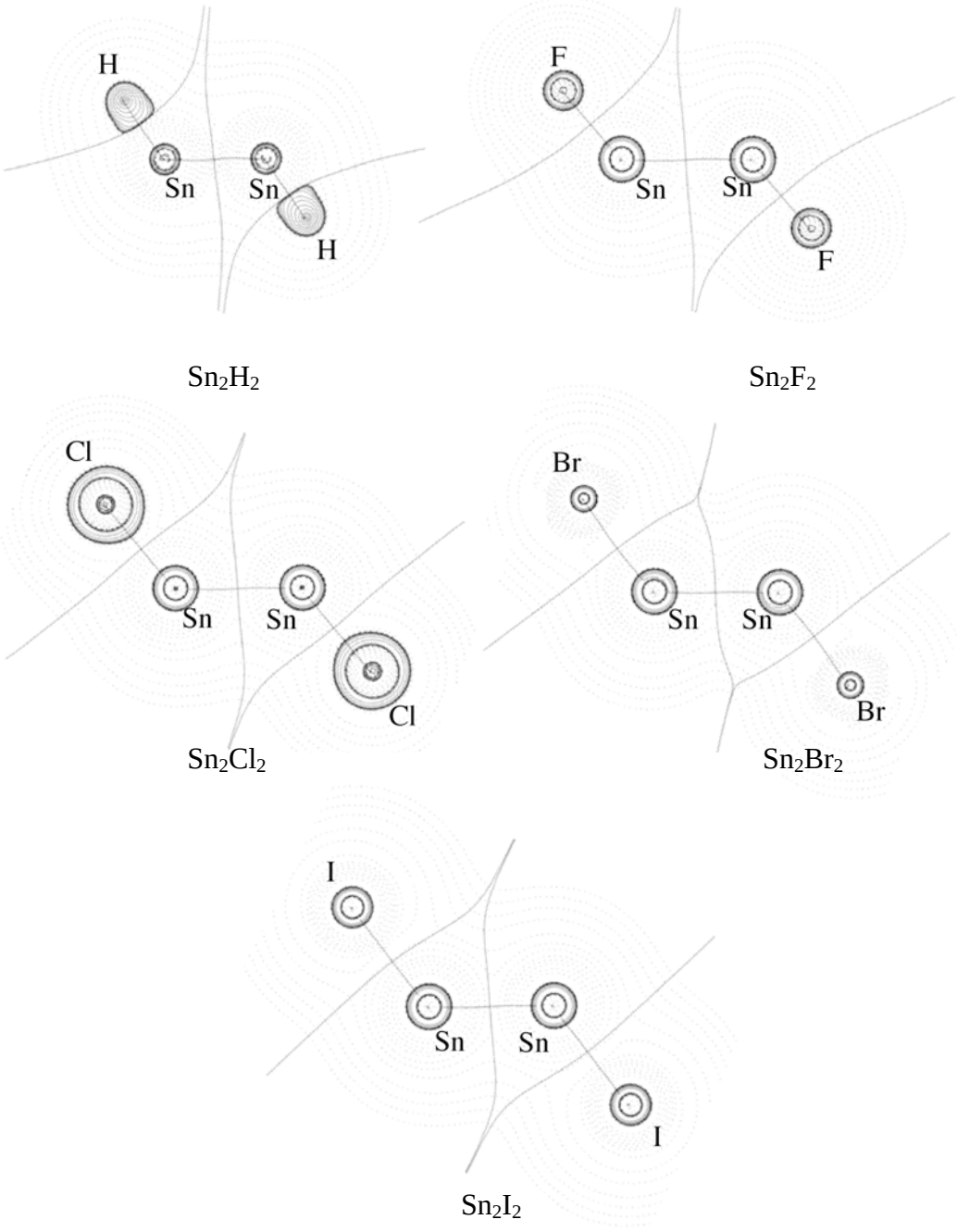

Sn_2H_2 Sn_2F_2

Sn_2Cl_2 Sn_2Br_2

Sn_2I_2

Figure 4.3.2.14 Contour line diagram $\nabla^2\rho(r)$ of isomer **SnE1**. Solid lines indicate areas of charge concentration ($\nabla^2\rho(r) < 0$), while dashed lines show areas of charge depletion ($\nabla^2\rho(r) > 0$). Solid lines that connect the atomic nuclei are the bond paths, while solid lines that separate the atomic basis give the zero-flux surface in the molecular plane.

4.3 Sn_2X_2 Molecules

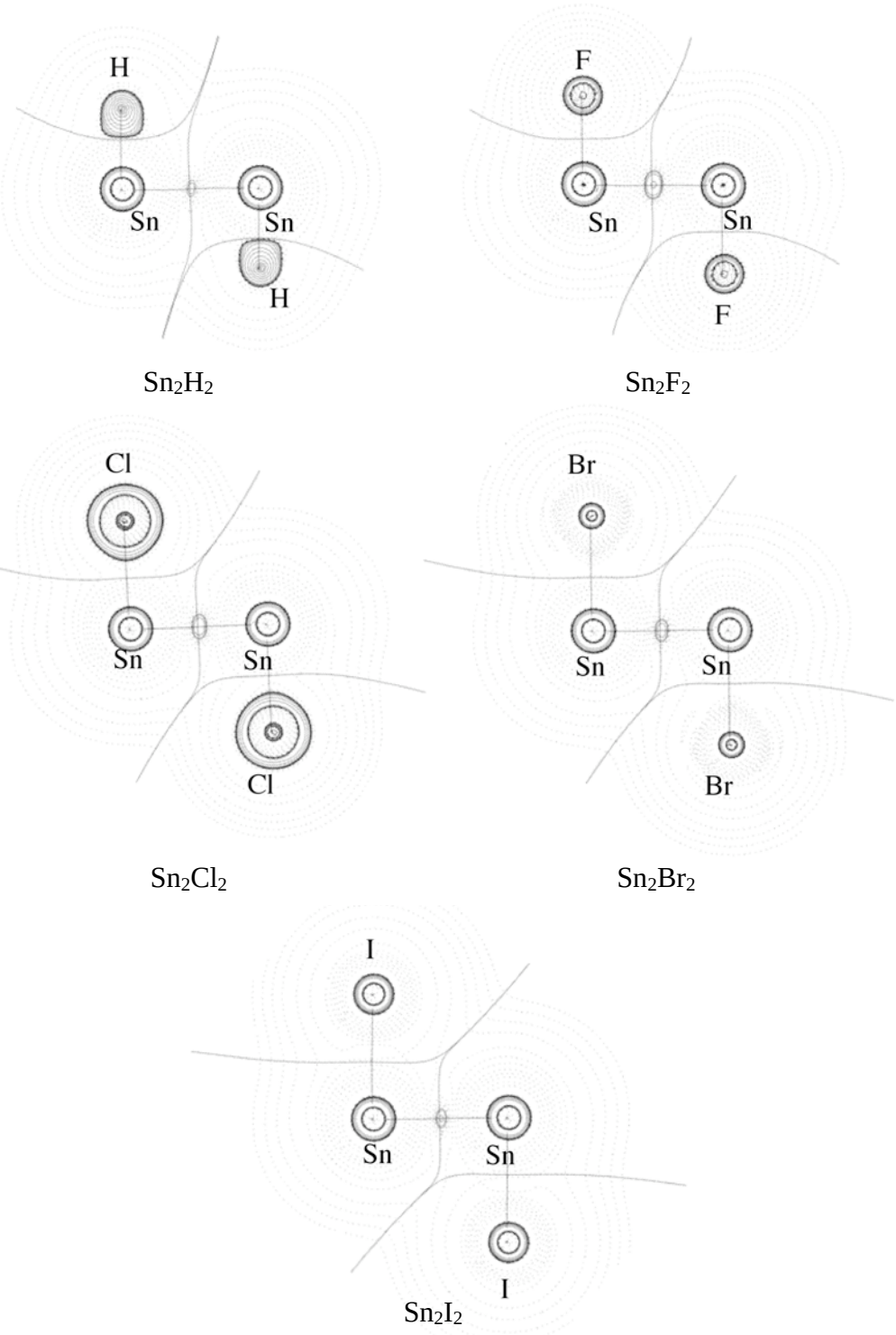

Sn_2H_2 Sn_2F_2

Sn_2Cl_2 Sn_2Br_2

Sn_2I_2

Figure 4.3.2.15 Contour line diagram $\nabla^2\rho(r)$ of isomer **SnE2**. Solid lines indicate areas of charge concentration ($\nabla^2\rho(r) < 0$), while dashed lines show areas of charge depletion ($\nabla^2\rho(r) > 0$). Solid lines that connect the atomic nuclei are the bond paths, while solid lines that separate the atomic basis give the zero-flux surface in the molecular plane.

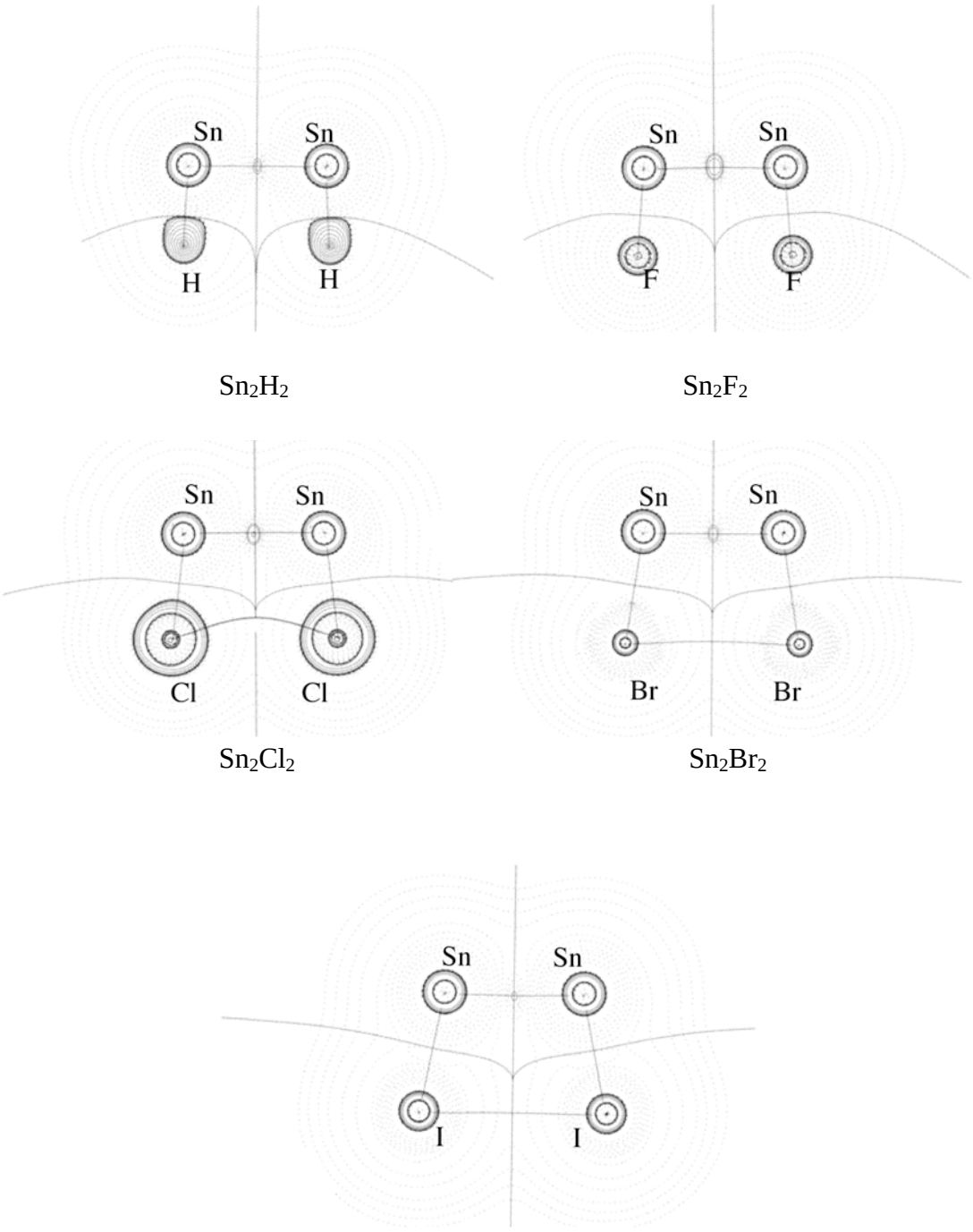

Sn_2H_2 Sn_2F_2

Sn_2Cl_2 Sn_2Br_2

Sn_2I_2

Figure 4.3.2.16 Contour line diagram $\nabla^2\rho(r)$ of isomer **SnF1**. Solid lines indicate areas of charge concentration ($\nabla^2\rho(r) < 0$), while dashed lines show areas of charge depletion ($\nabla^2\rho(r) > 0$). Solid lines that connect the atomic nuclei are the bond paths, while solid lines that separate the atomic basis give the zero-flux surface in the molecular plane.

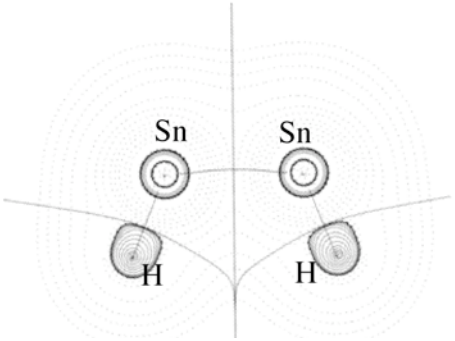

Sn_2H_2

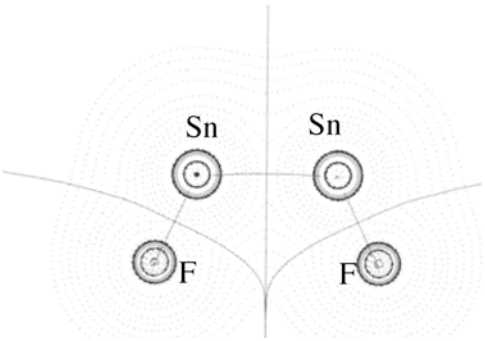

Sn_2F_2

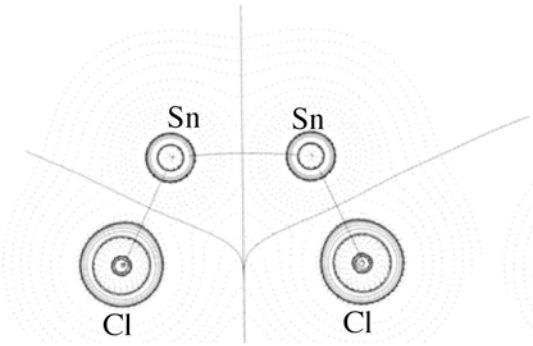

Sn_2H_2

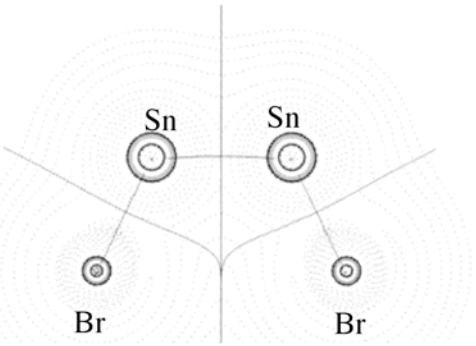

Sn_2F_2

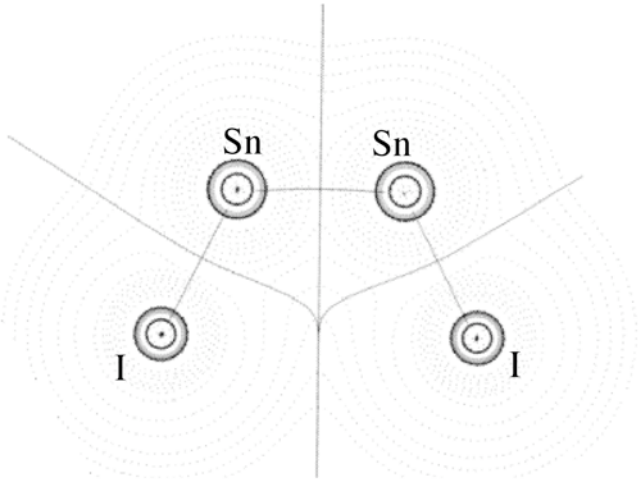

Sn_2I_2

Figure 4.3.2.17 Contour line diagram $\nabla^2\rho(r)$ of isomer **SnF2**. Solid lines indicate areas of charge concentration ($\nabla^2\rho(r) < 0$), while dashed lines show areas of charge depletion ($\nabla^2\rho(r) > 0$). Solid lines that connect the atomic nuclei are the bond paths, while solid lines that separate the atomic basis give the zero-flux surface in the molecular plane.

4.3.2.3. Charge Analyses

In chapter 4.3.2.1, the orbital analyses were presented, and they showed that the orbital interactions of the two SnX fragments could give a good explanation for their geometries. Chapter 4.3.2.2 illustrated the AIM analyses presenting the Sn-Sn bond and the Sn-X bonds. The charge accumulation indicated the bond character of the Sn-Sn bonds. However, the contribution of charge is not clear. In this chapter, the charge analyses of the SnX fragments and the Sn_2X_2 isomers are discussed.

4.3.2.3.1 SnX Fragment

Table 4.3.2.7 shows the Hirshfeld charges of the SnX molecules and it shows that the Sn atom is always positively charged and the hydrogen atom and the halogen atoms are always negative charged, because hydrogen atom and halogen atoms are more electronegative than the Sn atom, as expected. The order of the polarizability is as follows: SnF > SnCl > SnBr > SnI > SnH. The large positive charge of Sn atom in the SnX molecules indicates that the lone-pair donor-acceptor is not favorable because the geometries lead to a large electric repulsion from two positive Sn atoms. Although the Sn-X bond donor-acceptor also leads to small Sn-Sn bond lengths, the donor-acceptor interaction leads to an effective Sn-X···Sn-X electrostatic interaction due to the fact that the Sn-X molecules are dipoles. This is another reason why the doubly bridged structure **SnA** is a favorable structure compared to the bent structures. The SnX molecules are more polarized than SiX and GeX molecules because absolute charge values are larger than those of SiX and GeX. The larger polarization leads the larger dipole-dipole interaction for the bridged structures and the larger electrostatic repulsion for the bent-structures.

Table 4.3.2.7 Hirshfeld charges of the SnX fragment calculated at BP86/QZ4P level.

	SnH	SnF	SnCl	SnBr	SnI
Sn	0.1613	0.3030	0.2295	0.1991	0.1628
X	-0.1613	-0.3030	-0.2295	-0.1991	-0.1628

4.3.2.3.2 Sn_2X_2 Molecules

Table 4.3.2.8 shows the Hirshfeld charges of the Sn_2X_2 molecules. Although the charges do not show any clear correlations with the relative energies, the charge distribution shows the character of each Sn_2X_2 isomer. The Hirshfeld charges show that Sn_2F_2 is relatively strong polarized and Sn_2I_2 exhibits a small charge distribution due to the smaller charge distribution in the SnI fragments. It means that the former has a more ionic character and the latter has a more covalent character. It agrees with the results of the AIM analyses.

The bent structures, **SnE2** and **SnF1,** have the largest positive charges for the Sn atoms of the isomers and the absolute values are quite similar to those of the SnX fragment. The similar charge values indicate that the Sn-Sn bond formation of **SnE2** and **SnF1** needs quite small intermolecular charge transfers in the Sn-X fragments. The other bent structures **SnE1** and **SnF2** show smaller charge values, which indicates an intramolecular charge transfer from the halogen atoms to the Sn atoms. However, the charge transfer is quite unfavorable. This is a reason that **SnE1** and **SnF2** are less favorable structures than **SnA**.

The ring structures **SnA**, **SnB** and **SnC** show smaller charges than the free SnX fragments. It indicates the intramolecular charge transfer to form the Sn-Sn bond. Although that is similar to **SnE1** and **SnF2**, the intramolecular charge transfer in **SnA**, **SnB** and **SnC** is favorable because the donation of electrons is the same as the donation in terms of the orbital interactions. The bridged structures are favorable as the intramolecular charge transfer is concerned.

Table 4.3.2.8 Calculated Hirshfeld charges at BP86/QZ4P level

	SnA	**SnB**	**SnC**	**SnE1**	**SnE2**	**SnF1**	**SnF2**	**SnG**
				Sn_2H_2				
Sn_1	0.1078	0.0855	0.1097	0.0915	0.1612	0.1538	0.1402	0.0002
Sn_2	0.1078	0.0984	0.1097	0.0915	0.1612	0.1538	0.1402	0.0002
H_1	-0.1078	-0.1041	-0.1097	-0.0915	-0.1612	-0.1538	-0.1402	-0.0002
H_2	-0.1078	-0.0798	-0.1097	-0.0915	-0.1612	-0.1538	-0.1402	-0.0002
				Sn_2F_2				
Sn_1	0.2549	0.3260	0.2535	0.2853	0.3171	0.2989	0.2851	0.1812
Sn_2	0.2549	0.2028	0.2535	0.2853	0.3171	0.2989	0.2851	0.1812
F_1	-0.2549	-0.2543	-0.2535	-0.2853	-0.3171	-0.2989	-0.2851	-0.1812
F_2	-0.2549	-0.2745	-0.2535	-0.2853	-0.3171	-0.2989	-0.2851	-0.1812
				Sn_2Cl_2				
Sn_1	0.1784	0.2020	0.1899	0.1955	0.2490	0.2234	0.1961	0.0564
Sn_2	0.1784	0.1627	0.1899	0.1955	0.2490	0.2234	0.1961	0.0564
Cl_1	-0.1784	-0.1877	-0.1899	-0.1955	-0.2490	-0.2234	-0.1961	-0.0564
Cl_2	-0.1784	-0.1770	-0.1899	-0.1955	-0.2490	-0.2234	-0.1961	-0.0564
				Sn_2Br_2				
Sn_1	0.1460	0.1575	0.1621	0.1638	0.2189	0.1938	0.1619	0.0111
Sn_2	0.1460	0.1418	0.1621	0.1638	0.2189	0.1938	0.1619	0.0111
Br_1	-0.1460	-0.1574	-0.1621	-0.1638	-0.2189	-0.1938	-0.1619	-0.0111
Br_2	-0.1460	-0.1419	-0.1621	-0.1638	-0.2189	-0.1938	-0.1619	-0.0111
				Sn_2I_2				
Sn_1	0.1077	0.1036	0.1206	0.1191	0.1816	0.1579	0.1206	-0.0383
Sn_2	0.1077	0.1163	0.1206	0.1191	0.1816	0.1579	0.1206	-0.0383
I_1	-0.1077	-0.1204	-0.1206	-0.1191	-0.1816	-0.1579	-0.1206	0.0383
I_2	-0.1077	-0.0994	-0.1206	-0.1191	-0.1816	-0.1579	-0.1206	0.0383

4.3.2.4 Energy Decomposition Analyses

The section 4.3.2.1 has shown that the unusual equilibrium geometries of **SnA**-**SnG** of Sn_2X_2 can be nicely explained in terms of orbital interactions between the SnX fragments in the $X^2\Pi$ ground state. Tables 4.3.2.9 and Table 4.3.2.10 give the EDA results for the structures **SnA**, **SnB**, **SnC**, **SnE1**, **SnE2**, **SnF1** and **SnF2** using two SnX molecules in the $X^2\Pi$ ground state as interacting fragments and the $a^4\Sigma$ excited state of SnX is used for the EDA calculations of the structure **SnG**. The $a^4\Sigma^- \leftarrow X^2\Pi$ excitation energy is the major part of the preparation energy of the SnX fragments, which is the reason that the linear species **SnG** have rather large ΔE_{prep} values. In general, the contributions of ΔE_{orb} in Sn_2F_2, Sn_2Cl_2, Sn_2Br_2 and Sn_2I_2 are smaller than that in Sn_2H_2 and the contribution becomes smaller when the halogen atom gets heavier. In general, the Sn_2X_2 isomers show smaller interactions than the Si_2X_2 and Ge_2X_2 isomers and it indicates the weaker interaction between two SnX fragments than between two SiX and GeX fragments, respectively. The ratio of ΔE_{elstat} and ΔE_{orb} shows that the interactions between the SnX fragments have more electrostatic character and less orbital interaction character than those between the SiX and GeX fragments.

The EDA results present that **SnA**, **SnB** and **SnC** generally show large interaction energies arising from large electrostatic interactions and large orbital interactions. This is a similar situation to Si_2X_2 and Ge_2X_2 system. The large electrostatic interaction arises from the large charge distribution of the SnX fragments, which means that the electrostatic interaction is important for the Sn-X-Sn bridging formation. This agrees with the results of the AIM analyses and the charge analyses. The large orbital interaction stems from the effective Sn-X bond donor-acceptor interaction, which is the three-center-two-electron interaction, as explained in chapter 4.3.2.1. The large orbital interaction indicates that the Sn-X-Sn bridging is a favorable structure in the point of orbital interactions. Although the preparation energies in these isomers are larger than those of bent isomers due to the elongation of the Sn-X bonds, they can overcompensate the energetic loss with the large electrostatic interaction and the large orbital interaction. The compensation is easier than in the Si_2X_2 and Ge_2X_2 system, because the preparation energies ΔE_{prep} are quite

smaller.

The bent structures, **SnE1**, **SnE2**, **SnF1** and **SnF2** often show weaker electrostatic interactions and weaker orbital interactions than the bridged structures. The smaller electrostatic interactions stem form the unfavorable geometries, which produce the large electrostatic repulsions between the two positively charged Sn atoms. This agrees with the charge analyses in chapter 4.3.2.3. The small orbital interactions of **SnE1** and **SnF2** come form the less favorable lone-pair donor-acceptor interactions than the Sn-X bond donor-acceptor interaction, as explained at chapter 4.3.2.1. **SnE2** and **SnF1** also present smaller orbital interaction terms than those of the ring structures and these interactions are similar in each other, due to that both isomers have just a σ-type bonding situation. **SnE1** of Sn_2H_2 shows larger electrostatic interactions and larger orbital interactions than those of the other Sn_2X_2 isomers. The smaller orbital interaction energies of Sn_2F_2, Sn_2Cl_2, Sn_2Br_2 and Sn_2I_2 arise from the larger energy gaps of $\Delta E_{\pi\text{-lone-pair}}$ of their fragments (Table 4.3.2.3). The smaller electrostatic interaction stems from the more positive charge of the Sn atom.

The π isomers of **SnB, SnC**, **SnE1** and **SnF2** show smaller π interactions than those of the Si_2X_2 and Ge_2X_2 isomers. Due to that, the rotation around the Sn-Sn axis is easier in these isomers, and these isomers are found as transition states or higher order saddle points. This indicated that the small π interactions affect on the geometrical stability of the π structures.

The isomers of Sn_2X_2 are categorized to two groups: Sn_2H_2 and the other isomers. These categories are similar to those of Ge_2X_2. The dissociation energies of Sn_2H_2 show the order as follows: **SnA** > **SnB** > **SnC** > **SnE1** > **SnE2** > **SnF1** > **SnF2** > **SnG**. The bridged structures **SnA**, **SnB** and **SnC** show larger electrostatic interactions and larger orbital interactions. The large electrostatic interactions stem from the large dipole-dipole electrostatic interaction between the SnH fragments, and the large orbital interactions arise from the favorable Sn-X bond donor-acceptor interactions, which leads the three-center-two-electrons interaction. The bent structures show smaller electrostatic interactions and smaller orbital interactions than bridged structures due to the less favorable geometries for the dipole-dipole electrostatic interactions and due to the less favorable orbital interactions than the

bridged structures, respectively

The other isomers, Sn_2F_2, Sn_2Cl_2, Sn_2Br_2 and Sn_2I_2, show a different trend to Sn_2H_2 and the order is as follows: **SnA** > **SnE1** > **SnF1** > (**SnB**) > **SnC** > **SnE1** > **SnF2** > **SnG**. The position of **SnB** depends on the halogen atom X. Although the bridged structures shows large orbital interactions in Sn_2F_2, Sn_2Cl_2, Sn_2Br_2 and Sn_2I_2, the orbital interactions of these isomers are smaller than those of Sn_2H_2 due to the larger energy gaps between the Sn-X bond orbitals and the vacant π-orbitals, $\Delta E_{\pi\text{-Sn-X}}$ (Table 4.3.2.3). The electrostatic interactions of **SnA** for Sn_2F_2, Sn_2Cl_2, Sn_2Br_2 and Sn_2I_2 are stronger than those of Sn_2H_2, although **SnB** and **SnC** show smaller interactions. The trans-bent structures show a different trend to those of Sn_2H_2. The dissociation energies of **SnE1** are quite smaller than those of **SnE2**, and the smaller dissociation energies stem from the ΔE_{elstat} values and the ΔE_{orb} values. The smaller ΔE_{elstat} values arise from the larger electrostatic repulsions of the two Sn atoms in the Sn-X fragments with shorter Sn-Sn distances. The smaller ΔE_{orb} values stem from the smaller lone-pair donor-acceptor interactions, ΔE_{orb}(a") caused by the larger orbital energy gaps between the lone-pair orbital and the LUMO ($\Delta E_{\pi\text{-lone-pair}}$) (Table 4.3.2.3), where the π-interactions for all **SnE1** isomers are quite similar. The preparation energies for **SnA**, **SnB** and **SnC** are larger than those for **SnE1**, **SnE2**, **SnF1** and **SnF2**. As a result, the Sn-X-Sn bridging becomes relatively unstable and the bent-structures become more stable. However, the **SnA** isomers are still global minima due to the large orbital interaction and electrostatic interaction.

The bond situation of **SnA** is the most favorable because the **SnA** isomers give the largest interaction energies and dissociation energies in the interactions between two SnX fragments in their ground state. The bridged structures need large preparation energies and the preparation energies strongly depend on the halogen atom. The second largest dissociation energies are shown by the isomer **SnB** in Sn_2H_2 and the isomers **SnE2** in Sn_2F_2, Sn_2Cl_2, Sn_2Br_2 and Sn_2I_2. This indicates that Sn_2H_2 prefers the Sn-X-Sn bridged structure and the σ-type isomers are favorable for Sn_2F_2, Sn_2Cl_2, Sn_2Br_2 and Sn_2I_2.

Table 4.3.2.9 Energy decomposition analysis of Sn_2H_2, Sn_2F_2 and Sn_2Cl_2 on BP86/QZ4P level of the Sn-Sn bond using two doublet fragments for **SnA**-**SnF2**. Two quartet fragments are used for **SnG**. The symmetry in the analysis is C_s except for the **SnA** isomer. Energy values are given in kcal/mol.

term	**SnA**	**SnB**	**SnC**	**SnE1**	**SnE2**	**SnF1**	**SnF2**	**SnG**
				Sn_2H_2				
ΔE_{int}	-69.16	-53.53	-60.52	-38.68	-34.16	-32.76	-16.73	-94.85
ΔE_{Pauli}	243.38	170.92	153.18	108.98	80.13	76.8	52.66	115.79
ΔE_{elstat}	-133.24	-109.46	-102.99	-65.14	-63.29	-59.88	-19.7	-78.33
	42.63%	48.77%	48.19%	44.11%	55.38%	54.65%	28.39%	37.19%
ΔE_{orb}	-179.29	-114.98	-110.71	-82.52	-51.00	-49.68	-49.69	-132.31
	57.37%	51.23%	51.81%	55.89%	44.62%	45.35%	71.61%	62.81%
ΔE_{orb}(a')	-179.29	-86.59	-88.87	-55.12	-50.87	-49.56	-28.31	-77.25
	100.00%	75.31%)	80.28%	66.79%	99.74%	99.76%	56.98%	58.38%
ΔE_{orb}(a'')		-28.40	-21.84	-27.40	-0.13	-0.12	-21.38	-55.21
		24.70%	19.73%	33.20%	0.25%	0.24%	43.03%	41.73%
ΔE_{prep}	6.85	4.76	3.64	1.66	1.16	1.16	1.19	97.12
$\Delta E(=-D_e)$	-62.30	-48.77	-56.87	-37.02	-33.00	-31.60	-15.4	-2.27
				Sn_2F_2				
ΔE_{int}	-63.24	-27.67	-35.44	-15.61	-31.37	-27.91	-12.19	-135.94
ΔE_{Pauli}	225.51	120.01	134.12	46.48	82.58	72.85	41.03	71.38
ΔE_{elstat}	-138.79	-67.72	-101.47	-17.38	-64.34	-54.45	-9.92	-32.43
	48.07%	45.85%	59.84%	27.99%	56.47%	54.04%	18.64 %	15.64%
ΔE_{orb}	-149.95	-79.96	-68.1	-44.71	-49.61	-46.31	-43.29	-174.89
	51.93%	54.15%	40.16%	72.01%	43.53%	45.96%	81.36 %	84.36%
ΔE_{orb}(a')	-149.95	-53.53	-66.01	-21.95	-49.24	-46.01	-20.80	-96.34
	100.00%	66.94%	96.93%	49.10%	99.26%	99.36%	48.04%	55.09%
ΔE_{orb}(a'')		-26.43	-2.09	-22.75	-0.37	-0.29	-22.50	-78.83
		33.05%	3.07%	50.89%	0.75%	0.63%	51.97%	45.07%
ΔE_{prep}	17.31	9.15	15.10	1.14	1.23	1.12	1.15	228.84
$\Delta E(=-D_e)$	-45.93	-18.52	-20.33	-14.46	-30.13	-26.78	-11.04	92.9
				Sn_2Cl_2				
ΔE_{int}	-62.34	-26.95	-26.20	-17.93	-32.56	-28.48	-13.36	-95.43
ΔE_{Pauli}	233.08	123.48	124.49	63.21	89.58	74.31	45.14	88.94
ΔE_{elstat}	-136.55	-63.48	-77.92	-26.74	-68.07	-54.59	-12.65	-43.59
	46.22%	42.20%	51.71%	32.96%	55.73 %	53.10%	21.62%	23.64%
ΔE_{orb}	-158.87	-86.95	-72.76	-54.39	-54.06	-48.20	-45.85	-140.78
	53.78%	57.80%	48.29%	67.04%	44.27 %	46.90%	78.38%	76.36%
ΔE_{orb}(a')	-158.87	-60.09	-66.77	-29.30	-53.28	-47.67	-23.40	-79.5
	100.00%	69.11%	91.77%	53.87%	98.55%	98.89%	51.03%	56.52%
ΔE_{orb}(a'')		-26.85	-5.99	-25.09	-0.79	-0.54	-22.45	-61.43
		30.88%	8.23%	46.13%	1.46%	1.12%	48.96%	43.64%
ΔE_{prep}	12.79	7.13	14.83	1.25	1.45	1.21	1.23	167.74
$\Delta E(=-D_e)$	-53.7	-19.82	-11.36	-16.67	-31.10	-27.26	-12.12	72.31

Table 4.3.2.10 Energy decomposition analysis of Sn_2Br_2 and Sn_2I_2 on BP86/QZ4P level of the Sn-Sn bond using two doublet fragments for **SnA**-**SnF2**. Two quartet fragments are used for **SnG**. The symmetry in the analysis is C_s except for the **SnA** isomer. Energy values are given in kcal/mol.

term	**SnA**	**SnB**	**SnC**	**SnE1**	**SnE2**	**SnF1**	**SnF2**	**SnG**
				Sn_2Br_2				
ΔE_{int}	-62.68	-28.04	-26.79	-19.26	-33.12	-28.77	-14.25	-91.71
ΔE_{Pauli}	236.06	126.72	123.66	67.56	94.15	75.69	47.4	92.57
ΔE_{elstat}	-140.36	-65.21	-75.90	-28.92	-70.97	-55.47	-14.47	-45.35
	46.99%	42.14%	50.45%	33.31%	55.76%	53.11%	23.47%	24.61%
ΔE_{orb}	-158.37	-89.55	-74.55	-57.9	-56.31	-48.98	-47.19	-138.93
	53.01%	57.86%	49.55%	66.69%	44.24%	46.89%	76.53%	75.39%
ΔE_{orb}(a')	-158.37	-62.75	-68.04	-32.18	-55.21	-48.31	-24.70	-78.22
	100.00%	70.07%	91.26%	55.58%	98.05%	98.62%	52.35%	56.30%
ΔE_{orb}(a")		-26.80	-6.51	-25.72	-1.10	-0.67	-22.48	-60.90
		29.93%	8.73%	44.42%	1.95%	1.37%	47.64%	43.84%
ΔE_{prep}	11.44	6.59	15.32	1.26	1.55	1.26	1.26	156.99
$\Delta E(=-D_e)$	-51.23	-21.44	-11.46	-17.99	-31.56	-27.50	-12.98	65.28
				Sn_2I_2				
ΔE_{int}	-63.23	-30.13	-24.88	-21.07	-34.11	-29.07	-15.51	-86.42
ΔE_{Pauli}	238.83	133.04	124.24	73.61	100.68	77.27	51.00	99.15
ΔE_{elstat}	-142.54	-69.04	-72.42	-33.37	-74.87	-56.31	-17.49	-49.39
	47.19%	42.31%	48.56%	35.24%	55.55%	52.95%	26.29%	26.62%
ΔE_{orb}	-159.53	-94.13	-76.7	-61.31	-59.92	-50.03	-49.03	-136.18
	52.81%	57.69%	51.44%	64.76%	44.45%	47.05%	73.71%	73.38%
ΔE_{orb}(a')	-159.53	-67.28	-67.53	-35.47	-58.19	-49.12	-26.66	-76.25
	100.00%	71.48%	88.04	57.85%	97.11%	98.18%	54.38%	55.99%
ΔE_{orb}(a")		-26.85	-9.17	-25.85	-1.73	-0.91	-22.37	-60.08
		28.52%	11.96%	42.16%	2.89%	1.82%	45.63%	44.12%
ΔE_{prep}	9.71	5.83	12.10	1.34	1.74	1.33	1.33	140.37
$\Delta E(=-D_e)$	-53.51	-24.29	-12.77	-19.72	-32.36	-27.73	-14.17	53.95

4.3.3 Summary

The chapter 4.3 showed the relative energies, orbital analyses, AIM analyses, charge analyses and EDA results of Sn_2X_2 isomers. The chapter 4.3.1 presented that the doubly bridged structures **SnA** are the global minima for all Sn_2X_2 isomers, which is similar to the Ge_2X_2 molecules. The geometries presented the correlation for the Sn-Sn bond lengths and the angles with the halogen atoms.

The investigation of the Sn-X molecules showed that the very large excitation energies of the SnX molecules. The large excitation energies suggested that the linear Sn-Sn triple bond formation is quite unfavorable because the high excitation energies lead to negative Sn-Sn bond dissociation energies, where the excitation energies are larger than those of SiX and GeX molecules. Alternatively, two SnX molecules interact with each other in the $X^2\Pi$ ground state, and they form the Sn-Sn bond in a sideway fashion. The orbital analyses of Sn_2X_2 showed that these isomers can be categorized into the σ-type isomers and π-type isomers. The isomers of **SnA**, **SnE2** and **SnF1** are categorized as σ-type isomers and the orbital analyses presented a σ-type Sn-Sn bond orbital. In addition to the σ-type Sn-Sn interaction, **SnA** shows two Sn-X donor-acceptor orbitals, where the Sn-X bond donor-acceptor interaction is favorable from the reason that this donor-acceptor interaction leads to the three-center-two-electron interaction. **SnB**, **SnC**, **SnE1** and **SnF2** are categorized as π-type isomers. These isomers are all found as transition states, because the orbital energies of the π-type orbitals are high and the orbital interactions are weak. The lone-pair type orbitals of **SnE1** and **SnF2** are energetically more stable than those of **SnE2** and **SnF1**. The different orbital energies indicated the donor-acceptor interaction in **SnE1** and **SnF2** between the lone-pair orbital and the vacant π-orbital.

The AIM analyses showed that **SnA**, **SnB** and **SnC** have ring structures and the charge accumulation of the bent structures suggested that the Sn-Sn bond situations of **SnE1** and **SnF2** are different from those of **SnE2** and **SnF1**. For the Sn_2X_2 molecules, the electrostatic interactions are quite important because the charge accumulation of the Sn_2X_2 molecules is quite smaller than that of the Si_2X_2 and Ge_2X_2 molecules.

The charge analyses of the Sn-X fragments show that the SnX molecules are

more polarized than SiX and GeX molecules. This points out that the bent structures are less favorable than the bridged structures because the bent structures lead to the larger electrostatic repulsion, although the bridged structures lead to larger dipole-dipole interactions, which is similar to the orbital analyses.

The EDA results presented that the dissociation energies show a good correlation with the stability of the Sn_2X_2 isomers. The doubly bridged structures **SnA** show the largest dissociation energies, due to the large orbital interactions and large electrostatic interactions, which stems from the large orbital interaction from the efficient three-center-two-electron bond and from the large electrostatic interaction between the large dipoles, respectively. The bent structures are less favorable due to the less effective electrostatic interaction and less favorable orbital interaction.

4.4 Pb_2X_2 Molecules (X=H, F, Cl, Br and I)

4.4.1 Geometries and Relative Energies

Figure 4.4.1.1 – Figure 4.4.1.9 show the optimized geometries of several isomers of Pb_2X_2 (X=H, F, Cl, Br and I). The isomers in the singlet state **PbA-PbG** and the isomers in the triplet state **PbA(T)-PbG(T)** and **PbI(T)** are optimized with BP86/QZ4P level. Table 4.4.1.1, Table 4.4.1.2 and Table 4.4.1.3 show the relative energies of the stationary points on the singlet potential energy surface calculated with BP86/QZ4P. In addition to this, single point energies for the singlets were calculated with HF, MP2, SCS-MP2, MP4, CCSD and CCSD(T). For these calculations, the aug-cc-pVQZ basis sets were used. Table 4.4.1.4 and Table 4.4.1.5 show the energies of the stationary points on the triplet potential energy surface of BP86/QZ4P. The single point energies for triplets were calculated with HF, MP2, SCS-MP2, MP4, RCCSD and RCCSD(T). For these calculations, the aug-cc-pVQZ basis sets were used, too. The energies are given relative to the isomer **PbA**, which is the global minimum of Pb_2H_2. The results in the tables and figures show that the optimized geometries and relative energies of Pb_2H_2 are in agreement with previous theoretical calculations with DFT [21, 32, 64, 87] and ab initio levels [31].

4.4.1.1 Singlet Isomers of Pb_2X_2

Scheme 4.4.1.1 shows some singlets isomers of Pb_2X_2 investigated here. The investigated isomers are denoted as follows, as non-planar, doubly bridged structure (**PbA**), as singly bridged planar structure (**PbB**), as planar doubly bridged structure (**PbC**), as vinylidene structure (**PbD**), as trans-bent structure (**PbE**), as cis-bent structure (**PbF**) and as linear structure (**PbG**).

The non-planar doubly bridged structures of **PbA** have C_{2v} symmetry and these isomers are predicted to be the global minima for all Pb_2X_2 molecules (Figure 4.4.1.1), which is similar to Si_2X_2 except Si_2F_2, Ge_2X_2 and Sn_2X_2. The Pb-Pb bond length and the Pb-X-Pb angle show a good correlation with the mass of the X atom and the distance becomes longer and the angle becomes smaller as the X atom becomes heavier. The Pb-X bonds are 8-11% longer than those of the PbX molecules

due to the Pb-X-Pb bridging. This suggests that the Pb-X bond is elongated to form the Pb-X-Pb bridging structure. This trend of **PbA** is similar to the doubly bridged non-planar structures of Si_2X_2, Ge_2X_2 and Sn_2X_2.

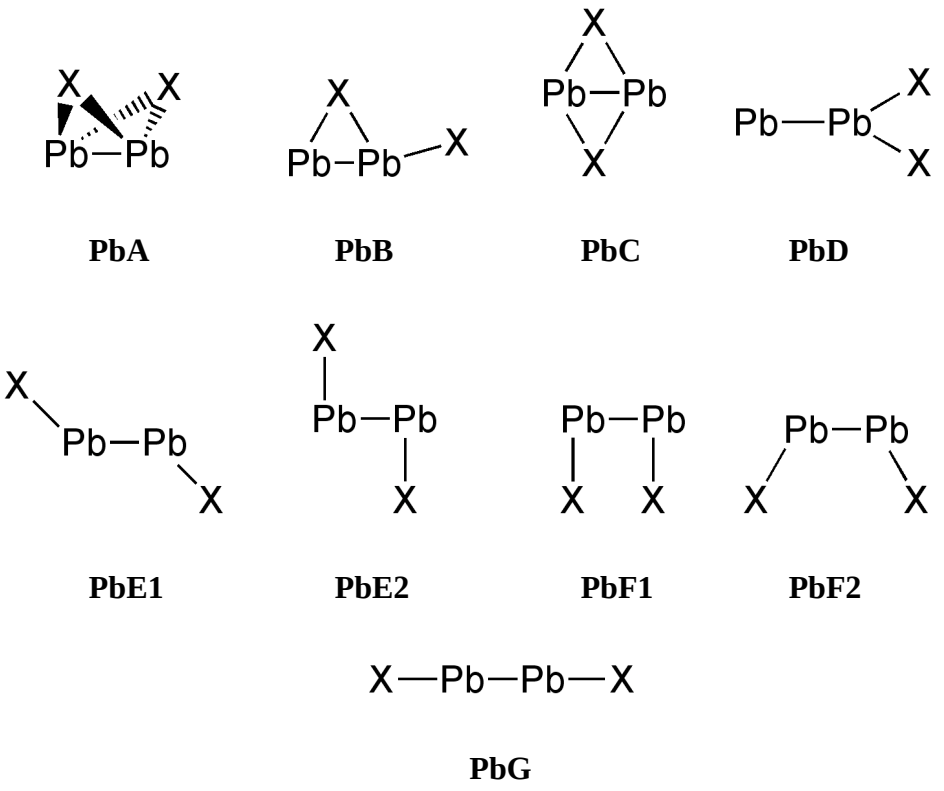

Scheme 4.4.1.1. Investigated singlet isomers of Pb_2X_2.

The singly bridged planar structures of **PbB** have C_s symmetry and these isomers are predicted to be transition states for Pb_2F_2, Pb_2Br_2 and Pb_2I_2 and these isomers are predicted as second order saddle points for Pb_2H_2 and Pb_2Cl_2 (Figure 4.4.1.1). However, the second imaginary frequency of Pb_2Cl_2 is very small (6.6 *i* cm^{-1}). The Pb-Pb bond length and Pb-X-Pb angle show a correlation with the halogen atom for Pb_2F_2, Pb_2Cl_2, Pb_2Br_2 and Pb_2I_2, and the bond length and the angle become smaller when the halogen atom X gets heavier, which is similar to the trend of **GeB**. Pb_2H_2 shows different trend, which stems from the different Pb-X bond character expressed later in chapter 4.4.2.1. In account of the Pb-Pb and Pb-X bond lengths, halogen X in the ring interacts with both Pb atoms.

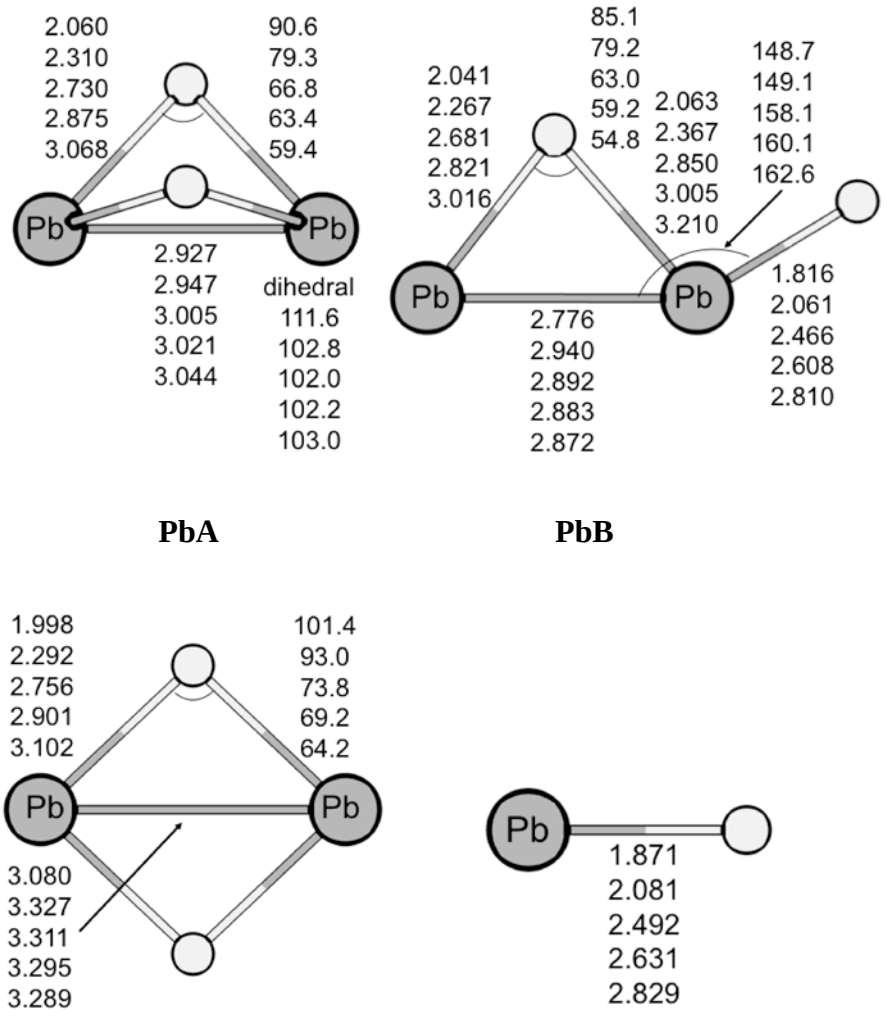

Figure 4.4.1.1. Optimized bridged structures in their singlet state, **PbA**, **PbB**, **PbC** and the PbX fragments in the $X^2\Pi$ ground state calculated at BP86/QZ4P level. The bond lengths are given in Å and the angles are given in degree.

The planar doubly bridged structures **PbC** have D_{2h} symmetry and they are transition states for every case (Figure 4.4.1.1), which is similar to **SnC** of Sn_2X_2. The Pb-Pb bond lengths are longer than those of **PbA**, which also have a doubly bridged structure. The bond lengths of Pb_2X_2 show that two Pb atoms of Pb_2H_2 still interact with each other, but two Pb atoms of Pb_2F_2, Pb_2Cl_2, Pb_2Br_2 and Pb_2I_2 interact only very weakly with each other. From this point, it is found that the Pb-Pb bond lengths depend on the halogen atoms and the main interaction in these isomers of Pb_2F_2, Pb_2Cl_2, Pb_2Br_2, and Pb_2I_2 is the Pb-X-Pb bridging. The Pb-Pb bond length and

the Pb-X-Pb angle of Pb_2F_2, Pb_2Cl_2, Pb_2Br_2 and Pb_2I_2 show a clear correlation with the halogen atom and the Pb-Pb distance becomes shorter and the Pb-X-Pb angle is larger when the halogen atom X gets heavier. This trend is similar to **SiC**, **GeC**, and **SnC**. Pb_2H_2 does not obey the correlation because of the different character of Pb-X bond and the Pb-X-Pb bridging.

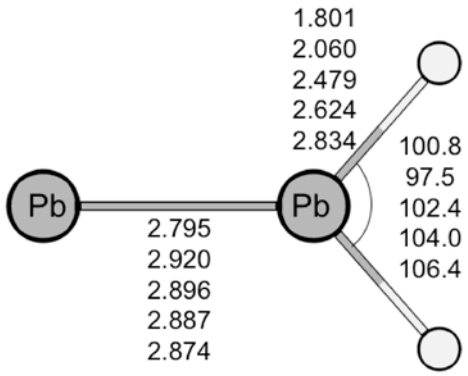

PbD

Figure 4.4.1.2. Optimized vinylidene structures in their singlet state, **PbD** calculated at BP86/QZ4P level. The bond lengths are given in Å and the angles are given in degree.

The vinylidene structures **PbD** have C_{2v} symmetry and they are second order saddle points with two imaginary frequencies for all Pb_2X_2 molecules (Figure 4.4.1.2), where the corresponding isomers of Si_2X_2, Ge_2X_2 and Sn_2X_2, **SiD, GeD** and **SnD**, respectively, are local minima or transition states. The Pb-Pb bond lengths show a clear correlation with the halogen atoms and the Pb-Pb bond length becomes shorter as the halogen atom gets heavier. The Pb-Pb distance is an outlier of the correlation and the Pb-Pb bond is much shorter. The trend of the Pb-Pb bonds is similar to **SiD**, **GeD** and **SnD**.

The trans-bent structure has two types of isomers, **PbE1** and **PbE2**, which both have C_{2h} symmetry (Figure 4.4.1.3). The isomers **PbE1** are predicted as second order saddle points, which is similar to **SnE1** of Sn_2H_2, Sn_2F_2 and Sn_2Cl_2, where the isomers **SiE1** and **GeE1** of Ge_2H_2 are all local minima, and the isomers **SnE1** of Sn_2Br_2 and Sn_2I_2 are transition states. The isomers **PbE2** are predicted as transition states for Pb_2H_2 and Pb_2F_2, and second order saddle points for Pb_2Cl_2, Pb_2Br_2 and

Pb_2I_2, where the isomers **SiE2**, **GeE2** and **SnE2** are transition states. The isomers, **PbE1** and **PbE2** differ from each other in the Pb-Pb bond lengths and the Pb-Pb-X angles. The Pb-Pb bond lengths of **PbE1** and **PbE2** have a correlation with the halogen atom and the Pb-Pb interaction becomes stronger as the halogen atom X gets heavier. The Pb-Pb-X angles in **PbE1** are nearly constant (ca. 125º) and the Pb-Pb-X angle of **PbE2** isomers becomes smaller as the halogen atom becomes heavier. The isomers of Pb_2H_2 are exceptions and this point is discussed later. The Pb-X distances are very similar. Accounting this, the different structures of **PbE1** and **PbE2** stem from a different Pb-Pb bond situation.

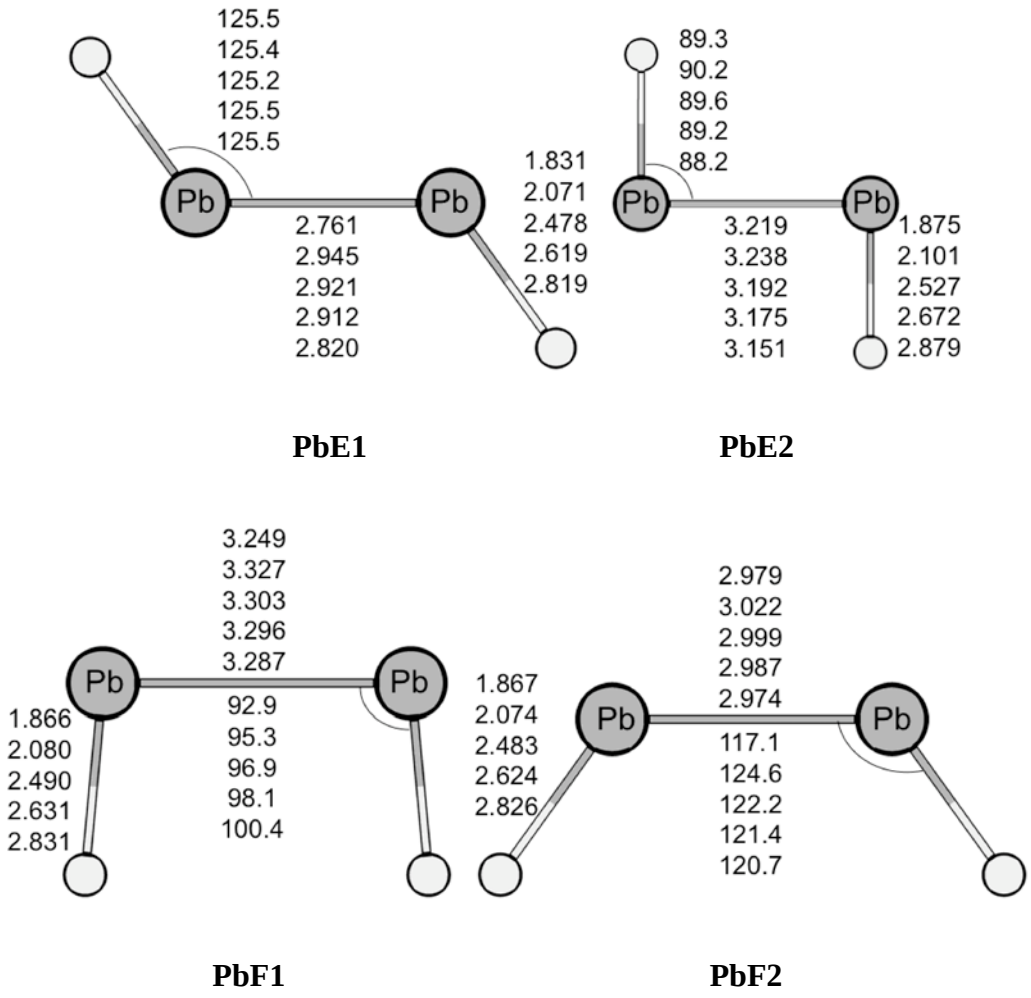

Figure 4.4.1.3. Optimized bent-structures in their singlet state, **PbE1**, **PbE2**, **PbF1** and **PbF2** calculated at BP86/QZ4P level. The bond lengths are given in Å and the angles are given in degree.

The cis-bent structures also have two types of isomers, **PbF1** and **PbF2**, which have both C_{2v} symmetry (Figure 4.4.1.3). The isomers **PbF1** are transition states, which is the same for **SiF1**, **GeF1** and **SnF1**. The isomers **PbF2** are second order saddle points, and this isomer of Pb_2I_2 is predicted as a transition state, where **SiF2** except Si_2F_2, **GeF2** and **SnF2** are transition states. The Pb-Pb bond lengths and the Pb-Pb-X angle show a correlation with the halogen atom for **PbF1** and the Pb-Pb interaction becomes stronger and the Pb-Pb-X angle becomes larger as the halogen atom gets heavier, which is the same as for **PbE2**. The **PbF1** structures have larger Pb-Pb-X angles than the **PbE2** structure, which is due to steric effects. The Pb-Pb bond lengths and Pb-Pb-X angles of **PbF2** also show a correlation with the halogen atom, and the Pb-Pb bond interaction becomes larger and the Pb-Pb-X angles of **PbF2** becomes smaller with the heavier halogen atom, where the angle exhibits the different trend from **SiF2**, **GeF2**, and **SnF2**. The isomers of **PbF1** and **PbF2** have very similar Pb-X distances. It means that the structural differences arise form the Pb-Pb bonding situation.

The linear structures **PbG** are second order saddle points for Pb_2H_2 and Pb_2F_2, Pb_2Cl_2, Pb_2Br_2 and Pb_2I_2, where the corresponding isomers of Si_2X_2, Ge_2X_2 and Sn_2X_2 are second order or fourth order saddle points. The Pb-Pb and Pb-X distances are the smallest of all Pb_2X_2 molecules. The Pb-Pb distances becomes slightly longer as the halogen atom gets heavier, which is a similar trend to the ones of **SiG**, **GeG** and **SnG**.

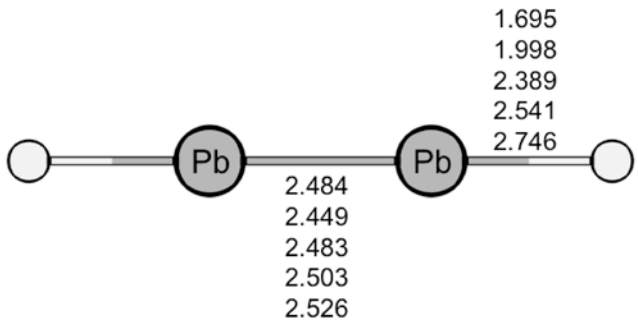

PbG

Figure 4.4.1.4. Optimized linear structures in the singlet state, **PbG**, calculated at BP86/QZ4P level. The bond lengths are given in Å and the angles are given in degree.

4.4 Pb_2X_2 Molecules

In Pb_2X_2, the distorted bent structure **PbH** is not found. The optimization from the **PbH** structure leads to **PbA** and there are no minima between **PbA** and **PbF1** or **PbE2**. This is similar to the situation of Ge_2X_2 and Sn_2X_2 and the distorted bent structure is found only for Si_2F_2.

Table 4.4.1.1, Table 4.4.1.2 and Table 4.4.1.3 show the relative energies of the stationary points on the singlet potential energy surface for several methods. Here, the CCSD(T) results are quite reliable due to the fact that the difference between CCSD and CCSD(T) values are relative small. The largest deviation is 6.3 kcal/mol in the planar doubly bridged structure **PbC** structure of Pb_2F_2 except for the **PbG** isomer of Pb_2Cl_2, Pb_2Br_2 and Pb_2I_2. The deviations between CCSD and CCSD(T) for the **PbG** structures of Pb_2Cl_2, Pb_2Br_2 and Pb_2I_2 are 23.6, 15.3 and 7.4 kcal/mol, respectively. These large deviations indicate a multi-reference character of the wave functions of these structures. The relative energies of the singlet isomers at BP86/QZ4P level are relatively accurate and the largest difference from CCSD(T)/aug-cc-pVQZ is 17.0 kcal/mol for the structure **PbG** of Pb_2F_2 and the mean absolute error form CCSD(T)/aug-cc-pVQZ is 2.9 kcal/mol. The relative energy values of SCS-MP2 and MP4 are very similar and they are close to those of the CCSD(T) calculations. The largest error in MP2, SCS-MP2 and MP4 are 19.6, 22.7 and 20.1 kcal/mol of the **PbG** isomer of Pb_2Cl_2, and the mean absolute error of these three methods are 3.6, 2.8 and 1.7 kcal/mol, respectively. The SCS-MP2 method gives very accurate results for the relative energies of the molecules in the singlet state.

The Pb_2X_2 isomers can be categorized into three groups, Pb_2H_2, Pb_2F_2 and the other isomers. These categories are similar to those of Si_2X_2. The Pb_2H_2 isomers present the following order of stability: **PbA** > **PbC** > **PbB** > **PbE2** > **PbD** > **PbF1** > **PbE1** > **PbF2** > **PbG**. The order shows that Pb_2H_2 prefers the bridged structures. **PbE2** and **PbF1** are more stable than **PbE2** and **PbF2** and this is different trend to Si_2H_2, Ge_2H_2 and Sn_2H_2.

The Pb_2F_2 isomers present the following order of stability: **PbA** > **PbC** > **PbE2** > **PbF1** > **PbB** > **PbE1** > **PbF2** > **PbD** > **PbG**. The bridged structure, **PbA**, is the most stable isomer and the bridged structures are relatively stable. The order shows that vinylidene structure **PbD** shifted to the unstable direction.

4.4 Pb_2X_2 Molecules

The group of Pb_2Cl_2, Pb_2Br_2 and Pb_2I_2 shows another trend for the stability of the isomers and the order is as follows: **PbA** > **PbE2** > **PbF1** > (**PbC**, **PbB**, **PbE1**) > **PbF2** > **PbD** > **PbG**. The doubly bridged structures **PbA** are still the global minima. However, the other bridged structures become unstable and the bent-structures are shifted to the direction of lower energy. The vinylidene structures and the linear structures are unfavorable isomers. The relative energies of Pb_2Cl_2, Pb_2Br_2 and Pb_2I_2 show a correlation with the halogen atoms and the relative energies become larger as the halogen atom gets heavier.

Table 4.4.1.1 Optimized structures of the **PbA**-**PbD** isomers calculated at BP86/QZ4P level and relative energies calculated with BP86/QZ4P and ab initio methods with aug-cc-pVQZ basis sets. The bond lengths are given in Å and the angles are given in degree. The relative energies are respect to **PbA** and given in kcal/mol. The values in parentheses are the number of imaginary frequencies.

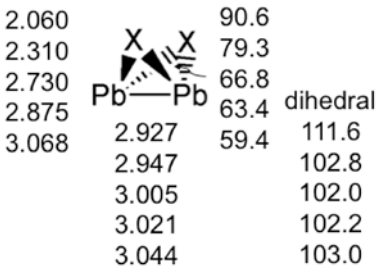

PbA

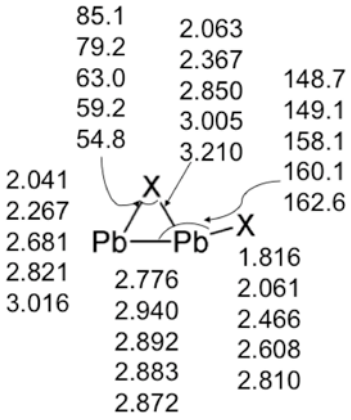

PbB

	H	F	Cl	Br	I	H	F	Cl	Br	I
BP86	0(0)	0(0)	0(0)	0(0)	0(0)	17.0(2)	31.8(1)	34.0(2)	33.9(1)	33.4(1)
HF	0	0	0	0	0	19.7	36.5	39.1	39.3	38.9
MP2	0	0	0	0	0	18.2	31.4	35.8	37.2	36.9
SCS-MP2	0	0	0	0	0	18.1	31.3	35.3	36.8	36.4
MP4	0	0	0	0	0	17.3	29.9	33.6	35.5	35.4
CCSD	0	0	0	0	0	17.5	30.8	34.3	36.2	36.2
CCSD(T)	0	0	0	0	0	16.8	29.5	33.1	35.0	35.0

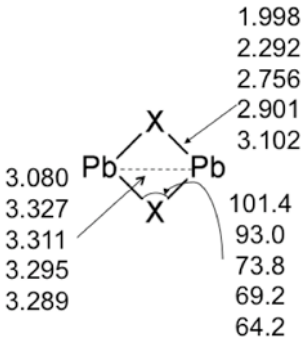

PbC

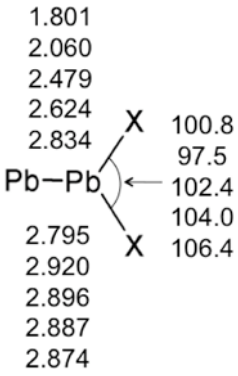

PbD

	H	F	Cl	Br	I	H	F	Cl	Br	I
BP86	4.4(1)	22.4(1)	32.7(1)	34.2(1)	35.4(1)	27.1(2)	43.7(2)	45.3(2)	45.6(2)	46.0(2)
HF	8.7	32.5	47.0	48.6	45.8	20.0	40.2	41.0	41.8	42.6
MP2	3.8	22.8	33.4	36.4	45.4	27.5	40.3	45.8	48.6	50.1
SCS-MP2	4.4	22.1	33.0	36.2	45.0	26.0	40.0	44.0	46.9	48.1
MP4	3.9	16.5	28.6	32.6	44.2	25.9	39.6	43.3	46.7	48.1
CCSD	5.2	19.1	31.8	35.9	44.2	23.8	39.1	41.9	45.1	46.2
CCSD(T)	4.0	12.8	26.5	31.1	43.7	24.5	39.1	42.2	45.5	46.7

Table 4.4.1.2 Optimized structures of the **PbE1**-**PbF2** isomers calculated at BP86/QZ4P level and relative energies calculated with BP86/QZ4P and ab initio methods with aug-cc-pVQZ basis sets. The bond lengths are given in Å and the angles are given in degree. The relative energies are respect to **PbA** and given in kcal/mol. The values in parentheses are the number of imaginary frequencies.

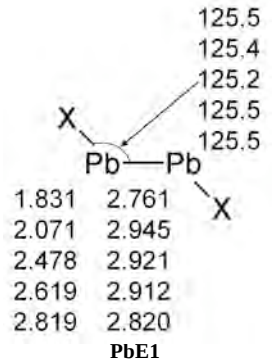

PbE1

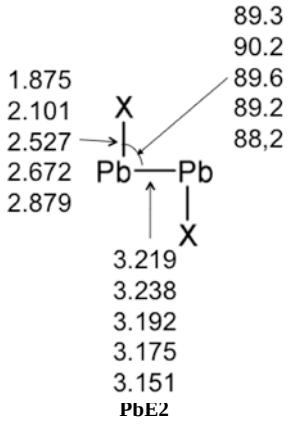

PbE2

	H	F	Cl	Br	I	H	F	Cl	Br	I
BP86	31.0(2)	38.2(2)	38.4(2)	38.4(2)	38.5(2)	26.5(1)	18.8(1)	19.2(2)	20.0(2)	20.7(2)
HF	31.4	44.6	42.4	42.5	42.7	11.9	13.7	11.0	11.3	12.0
MP2	33.4	38.9	43.1	44.8	45.7	26.4	18.1	20.2	22.6	24.6
SCS-MP2	32.2	38.5	41.9	43.5	44.2	22.8	17.2	17.4	19.9	21.6
MP4	31.2	36.5	40.5	42.6	43.3	24.7	18.5	18.3	21.2	23.0
CCSD	30.5	38.2	40.6	42.4	43.0	20.6	17.1	15.6	17.8	19.6
CCSD (T)	30.1	36.8	39.9	41.8	42.5	23.3	18.3	17.3	20.1	21.6

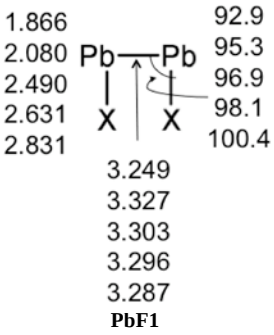

PbF1

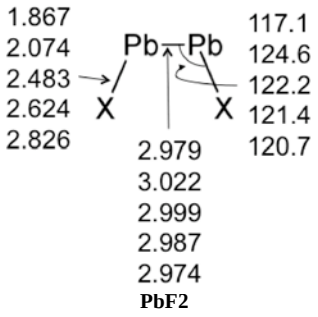

PbF2

	H	F	Cl	Br	I	H	F	Cl	Br	I
BP86	27.9(1)	23.2(1)	24.2(1)	24.9(1)	26.0(1)	47.7(2)	41.4(2)	42.0(2)	42.2(2)	42.5(1)
HF	13.3	19.7	17.7	18.3	19.3	46.3	48.0	53.7	47.2	48.1
MP2	28.1	23.5	26.5	28.5	30.4	51.2	42.6	51.5	49.3	51.0
SCS-MP2	24.4	22.3	23.7	25.9	27.6	48.8	41.8	49.4	47.9	49.3
MP4	26.2	23.1	24.3	26.8	28.5	47.6	39.4	46.1	46.5	47.9
CCSD	22.1	22.1	22.0	24.3	25.6	45.1	40.6	46.1	42.1	47.5
CCSD (T)	24.8	23.1	23.4	25.8	27.2	43.9	38.7	42.0	44.9	46.3

Table 4.4.1.3 Optimized structures of the **PbG** isomer calculated at BP86/QZ4P level and relative energies calculated with BP86/QZ4P and ab initio methods with aug-cc-pVQZ basis sets. The bond lengths are given in Å and the angles are in degree. The relative energies are respect to **PbA** and given in kcal/mol. The values in parentheses are the number of imaginary frequencies.

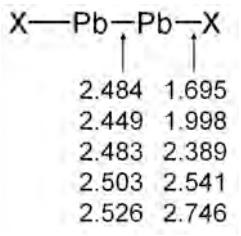

PbG

	H	F	Cl	Br	I
BP86	92.5(2)	198.1(2)	170.1(2)	160.6(2)	145.5(2)
HF	95.1	213.6	183.9	174.2	159.0
MP2	85.2	190.5	179.8	163.2	143.3
SCS-MP2	87.1	191.8	182.9	165.0	143.8
MP4	86.1	184.2	180.3	162.6	141.3
CCSD	88.8	182.7	183.8	167,3	146.9
CCSD (T)	86.6	181.1	160.2	152.1	139.5

4.4.1.2 Triplet Isomers of Pb_2X_2

Although the singlets of Pb_2X_2 are investigated in the last chapter, energetically low-lying isomers of Pb_2X_2 may exist on the triplet potential energy surface. Scheme 4.4.1.2 shows the investigated triplet isomers. The structures of the stationary points are named as doubly bridged structure (**PbA(T)**), singly bridged planar structure (**PbB(T)**), planar doubly bridged structure (**PbC(T)**), vinylidene structure (**PbD(T)**), trans-bent structure (**PbE(T)**), cis-bent structure (**PbF(T)**), linear structure (**PbG(T)**) and distorted singly bridged structure (**PbI(T)**).

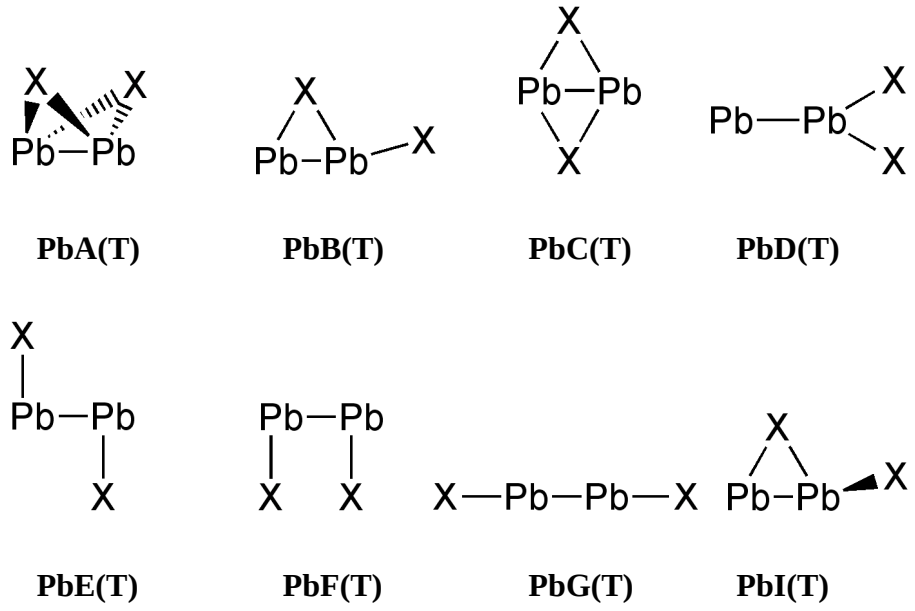

Scheme 4.4.1.2. Investigated triplet isomers of Pb_2X_2

The non-planar doubly bridged structures **PbA(T)** have C_{2v} symmetry (Figure 4.4.1.5). This isomer of Pb_2H_2 is a second order saddle point and those of Pb_2F_2 and Pb_2Cl_2 are transition states. The isomers of Pb_2Br_2 and Pb_2I_2 are predicted to be local minima, which is similar to **SiA(T)**, **GeA(T)** and **SnA(T)**. The geometries are quite different from **PbA**. For Pb_2H_2 and Pb_2F_2, the two Pb atoms still interact weakly, although the Pb-Pb bonds for Pb_2Cl_2, Pb_2Br_2 and Pb_2I_2 are nearly broken. The Pb-X distances are quite similar to those of **PbA** for Pb_2F_2**,** Pb_2Cl_2, Pb_2Br_2 and Pb_2I_2. The Pb-X-Pb angles show the similar trend as the corresponding angles in **SnA(T)**. The larger angles come from the larger Pb-Pb distance, which suggests that the geometric differences are due to the Pb-Pb bonding situation. The relative energies of the triplets

are higher than those of **PbA** for all Pb_2X_2.

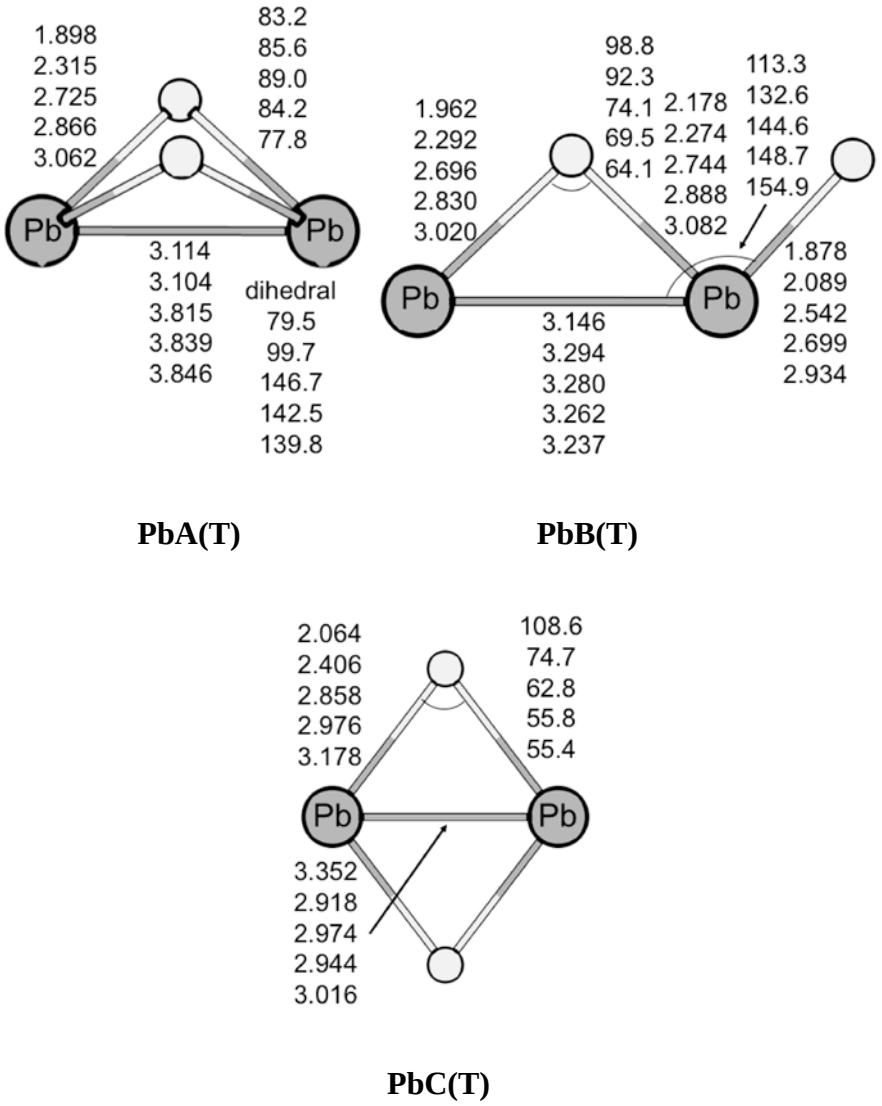

Figure 4.4.1.5. Optimized ring-structures in their triplet state, **PbA(T)**, **PbB(T)** and **PbC(T)** calculated at BP86/QZ4P level. The bond lengths are given in Å and the angles are given in degree.

The singly bridged planar structures **PbB(T)** have C_s symmetry (Figure 4.4.1.5). The isomers are predicted to be transition states. The Pb-Pb bond length bond and the Pb-X-Pb angle show a correlation with the halogen atom and the Pb-Pb interaction becomes stronger and the angle becomes smaller as the halogen atom gets heavier. For the **PbB(T)** structures, the Pb-Pb interaction is stronger than those of the **PbB** structures. For Pb_2F_2, Pb_2Cl_2, Pb_2Br_2 and Pb_2I_2, the **PbB(T)** isomer has a Pb-X-Pb

bridged structure, but the bridged structure is weak in Pb_2H_2.

The planar doubly bridged structures **PbC(T)** have D_{2h} symmetry (Figure 4.4.1.5). The **PbC(T)** structures are transition states. Pb_2H_2 and the halogen isomers behave different with respect to the comparison of **PbC** and **PbC(T)**. For Pb_2H_2, the Pb-Pb interaction is weaker than that of **PbC**. For the halogen isomers, the Pb-Pb interactions are stronger than those of **PbC** and the Pb-X-Pb bridgings become weaker. The Pb-Pb bond lengths and the Pb-X-Pb angle show a correlation with the halogen atom and the Pb-Pb interaction becomes stronger as the angle becomes smaller.

The vinylidene structures **PbD(T)** have C_{2v} symmetry and these isomers are second order saddle points (Figure 4.4.1.6). The bond length shows that the Pb-Pb bond is weaker than in **PbD**. The Pb-Pb distance correlates with halogen atom and the Pb-Pb interaction becomes stronger as the halogen atom gets heavier.

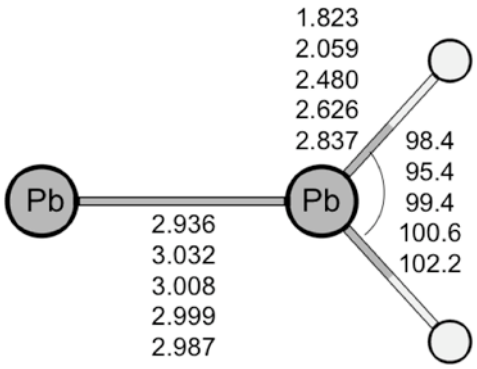

PbD(T)

Figure 4.4.1.6. Optimized structures of vinylidene structures in the triplet state, **PbD(T)** calculated at BP86/QZ4P level. The bond lengths are given in Å and the angles are given in degree.

The trans-bent structures **PbE(T)** have C_{2h} symmetry (Figure 4.4.1.7). These isomers **PbE(T)** of Pb_2H_2 and Pb_2F_2 are predicted to be a second order saddle point and a transition state, respectively, where the structures of **SiE(T)**, **GeE(T)** and **SnE(T)** are local minima. The structures of Pb_2Cl_2, Pb_2Br_2 and Pb_2I_2 are predicted to be minima, which is the same as for **SiE(T)**, **GeE(T)** and **SnE(T)**. The Pb-Pb bonds

and the Pb-Pb-X angles show a correlation with halogen atoms for the halogen isomers and the Pb-Pb distance becomes shorter and the angle becomes smaller as the halogen atom gets heavier. The Pb-Pb bonds of **PbE(T)** show a similar trend to those of **SiE(T)**, **GeE(T)** and **SnE(T)**.

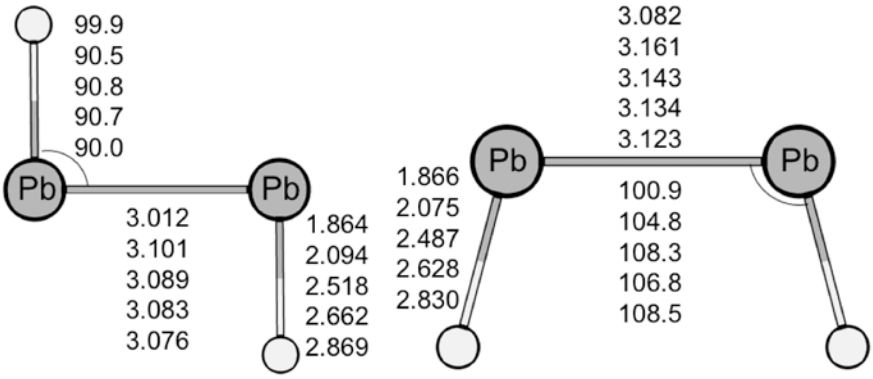

PbE(T) **PbF(T)**

Figure 4.4.1.7. Optimized structures of the bent-structures in their triplet state, **PbE(T)** and **PbF(T)** isomer calculated at BP86/QZ4P level. The bond lengths are given in Å and the angles are given in degree.

The cis-bent structures **PbF(T)** have C_{2v} symmetry (Figure 4.4.1.7). **PbF(T)** is predicted to be a minimum for Pb_2F_2. The **PbF(T)** isomers of Pb_2H_2 and Pb_2Cl_2 are a third order saddle point and a second order saddle point, respectively. The isomers of Pb_2Br_2 and Pb_2I_2 are transition states. This is different from the isomers of Si_2X_2, Ge_2X_2 and Sn_2X_2, although **SiF(T)** of Si_2H_2, **GeF(T)** of Ge_2H_2 and **SnF(T)** of Sn_2H_2 are found as second order saddle points and the other molecules are local minima. The Pb-Pb interactions are stronger than those of **PbE(T)**. The Pb-Pb bond lengths show a correlation with the halogen atoms and the Pb-Pb interaction becomes stronger as the halogen atom gets heavier. The Pb-Pb-X angles correlate with the X atoms and the angle becomes larger as the X atom larger. It suggests that the steric effect plays an important role for **PbF(T)**. The deviation in the bond lengths of **PbF(T)** is smaller that that of **PbE(T)**, whereas the deviation in the Pb-Pb-X angles is larger in **PbF(T)**. The Pb-X distances are similar to those of **PbE(T)**. From these points, the halogen atoms affect on the Pb-Pb distance in **PbE(T)**, while they affect on the Pb-Pb-X angle, namely sterically, in **PbF(T)**.

The linear structures **PbG(T)** of Pb_2H_2 and Pb_2Cl_2 are fourth order saddle points (Figure 4.4.1.8). The **PbG(T)** structures of Pb_2F_2, Pb_2Br_2 and Pb_2I_2 are second order saddle points. The bond lengths show that the Pb-Pb bonds have smaller interactions than those of the **PbG** structure and The Pb-Pb distances become shorter as the halogen atoms get heavier.

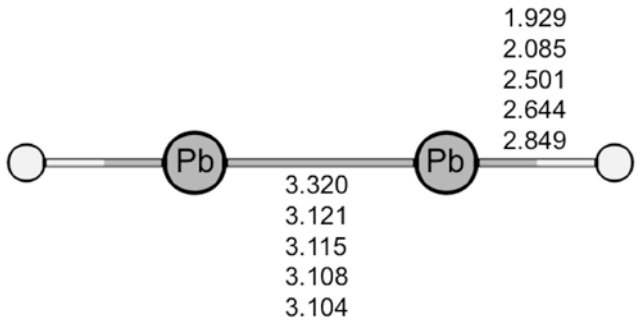

PbG(T)

Figure 4.4.1.8. Optimized linear structures in the triplet state, **PbG(T)**, calculated at BP86/QZ4P level. The bond lengths are given in Å and the angles are given in degree.

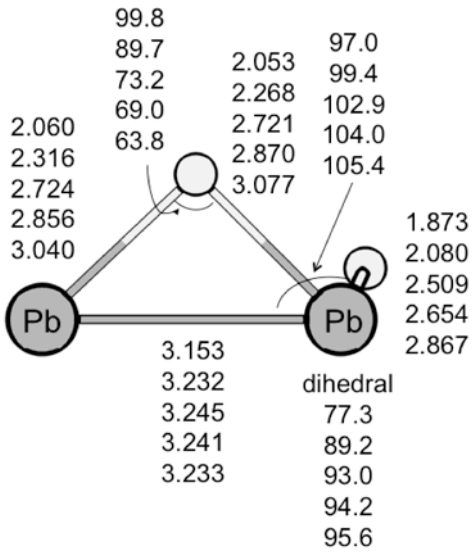

PbI(T)

Figure 4.4.1.9. Optimized geometries of singly bridged structures in the triplet state, **PbI(T)** calculated at BP86/QZ4P level. The bond lengths are given in Å and the angles are given in degree.

4.4 Pb_2X_2 Molecules

The distorted singly bridged planar structures, **PbI(T),** have C_1 symmetry and these isomers are predicted as minima for all Pb_2X_2 (Figure 4.4.1.9), which is similar to **SiI(T)**, **GeI(T)** and **SnI(T)**. The Pb-Pb bond lengths do not show a clear correlation. The Pb-X bonds show that **PbI(T)** has a Pb-X-Pb bridged structure. The trend of **PbI(T)** is often similar to that of **SiI(T)**, **GeI(T)** and **SnI(T)**.

Table 4.4.1.4 and Table 4.4.1.5 show the relative energies of the stationary points on the triplet potential energy surface at BP86/QZ4P level of theory. These energies are relatively smaller than those calculated at CCSD(T)/aug-cc-pVQZ// BP86/QZ4P level of theory and the largest difference is 10.4 kcal/mol for the isomer **PbG(T)** of Pb_2I_2. The relative energies of the triplets are often underestimated with BP86/QZ4P and the mean absolute error form CCSD(T)/aug-cc-pVQZ is 3.8 kcal/mol. BP86/QZ4P gives accurate results for minima but the transition states and the higher order saddle points are calculated as to be stable. The differences between the CCSD and CCSD(T) values are relatively small and the largest difference is 2.7 kcal/mol for the **PbC(T)** isomer of Pb_2H_2. This indicates that the wave function of the isomers in the triplet state only has a very small multi-reference character and that the CCSD(T) results are reliable and very accurate. For the stationary points on the potential energy surface of the triplets, SCS-UMP2/aug-cc-pVQZ gives worse results than UMP2/aug-cc-pVQZ. The largest deviation from CCSD(T)/aug-cc-pVQZ is 14.2 kcal/mol for the **PbG(T)** structure of Pb_2H_2, where the large difference for SCS-UMP2 is 14.7 kcal/mol for the **PbC(T)** structure of Pb_2H_2. The mean absolute errors from CCSD(T)/aug-cc-pVQZ are 8.4 and 8.6 kcal/mol for UMP2/aug-cc-pVQZ and SCS-UMP2/aug-cc-pvQZ, respectively. This is the due to the fact that the parameters of the SCS correction are optimized for singlets and not for triplets. The UMP4/aug-cc-pVQZ gives better the results, compared to the CCSD(T)/aug-cc-pVQZ values than UMP2/aug-cc-pVQZ and SCS-UMP2/aug-cc-pVQZ, where the largest deviation is 11.4 kcal/mol for the **PbC(T)** structure of Pb_2Cl_2 and the mean absolute error is 7.9 kcal/mol. RMP2/aug-cc-pvQZ presents similar values to CCSD(T)/aug-cc-pVQZ and the largest deviation is 4.2 kcal/mol of the **PbG(T)** structure of Pb_2F_2 and the mean absolute error is 1.2 kcal/mol, respectively.

Table 4.4.1.3 and Table 4.3.4.5 show that the isomers in the triplet state are categorized to three groups, Pb_2H_2, Pb_2F_2 and the group of the other Pb_2X_2 isomers.

4.4 Pb_2X_2 Molecules

The Pb_2X_2 molecules show completely different trend compared to Si_2H_2, Ge_2H_2 and Sn_2H_2. Pb_2H_2 shows the following order of stability: **PbC(T)** > **PbI(T)** > **PbE(T)** > **PbF(T)** > **PbB(T)** > **PbD(T)** > **PbA(T)** > **PbG(T)**. These isomers are higher are always higher in energy than the corresponding singlets. For the triplets, the doubly bridged structure **PbC(T)** is most stable, which is a completely different trend to Si_2H_2, Ge_2H_2 and Sn_2H_2. The order of stability shows that Pb_2H_2 does not show a clear preference of the structures. The doubly bridged structures and the linear structures are unfavorable. The relative energies of Pb_2H_2 are often smaller than those of Ge_2H_2.and Sn_2H_2.

For Pb_2F_2, the order of stability of the isomers is as follows: **PbI(T)** > **PbB(T)** > **PbE(T)** > **PbF(T)** > **PbA(T)** > **PbD(T)** > **PbC(T)** > **PbG(T)**. The order shows that **PbI(T)** is the most stable isomer of the triplets and Sn_2F_2 prefers the singly bridged structure. The bent-structures are relatively preferable, which is different to Si_2X_2, Ge_2X_2 and Sn_2X_2. The doubly bridged structures and the linear structures are unfavorable, which is a similar trend to Pb_2H_2.

The group of Pb_2Cl_2, Pb_2Br_2 and Pb_2I_2 shows the order of stability as follows: **PbI(T)** > (**PbE(T)**, **PbC(T)**, **PbA(T))** > **PbF(T)** > **PbB(T)** > **PbD(T)** > **PbG(T)**. The singly bridged structures **PbI(T)** are the most stable local minima for the triplet state. The vinylidene structures and the linear structures are unfavorable structures for the isomers in this group.

Table 4.4.1.4 Optimized structures of **PbA(T)**-**PbD(T)** calculated at BP86/QZ4P level. The bond lengths are given in Å and the angles are in degree. The relative energies are respect to **PbA** in the singlet state and given in kcal/mol. The values in parentheses are the number of imaginary frequencies.

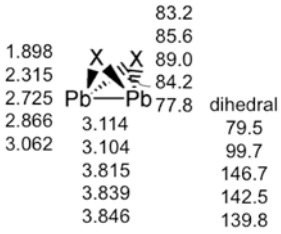

PbA(T)

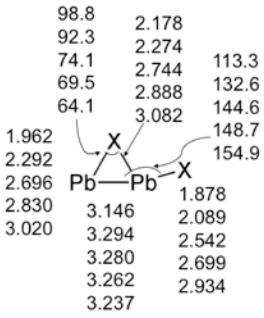

PbB(T)

	H	F	Cl	Br	I	H	F	Cl	Br	I
BP86	30.0(2)	19.7(1)	21.5(1)	23.2(0)	24.7(0)	22.1(1)	19.9(1)	25.5(1)	26.5(1)	27.9(1)
HF	21.1	23.4	1.5	4.4	8.0	13.5	11.1	18.8	20.6	23.2
RMP2	36.2	23.6	20.7	21.4	24.7	27.0	16.9	32.5	33.4	36.2
UMP2	41.4	27.0	27.5	30.4	33.9	33.0	27.9	39.2	42.7	45.2
SCS-UMP2	40.8	31.6	25.4	28.2	31.6	33.4	28.8	39.0	42.1	44.3
UMP4	39.9	27.3	32.0	29.9	33.1	31.8	29.4	38.8	42.0	44.1
CCSD	31.9	25.9	20.8	20.0	22.3	24.4	16.9	31.6	31.7	33.8
CCSD(T)	33.6	25.1	23.4	22.4	24.7	25.9	18.2	32.8	32.8	34.9

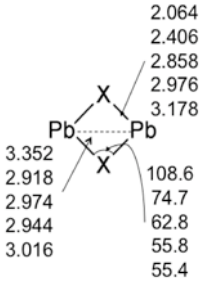

PbC(T)

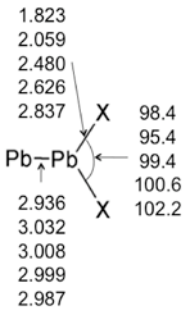

PbD(T)

	H	F	Cl	Br	I	H	F	Cl	Br	I
BP86	20.7(1)	21.8(1)	21.3(1)	21.2(1)	21.2(1)	26.6(2)	32.0(2)	42.2(2)	36.5(2)	38.1(2)
HF	2.0	24.4	21.1	20.4	21.1	8.7	18.0	20.8	22.3	24.4
RMP2	19.8	26.9	22.7	27.0	28.8	27.7	25.9	35.2	39.6	43.0
UMP2	32.0	31.2	32.3	33.9	39.6	33.9	35.1	45.3	50.0	52.9
SCS-UMP2	35.2	34.2	33.8	34.9	37.9	33.8	36.5	45.2	49.3	51.9
UMP4	31.7	31.8	32.0	33.4	38.5	32.7	37.3	45.0	49.3	51.8
CCSD	17.8	29.0	20.6	25.7	27.6	24.7	26.1	32.3	37.1	39.9
CCSD(T)	20.5	28.9	20.6	26.0	27.9	27.1	27.7	34.1	39.0	42.0

Table 4.4.1.5 Optimized structures of **PbE(T)-PbI(T)** calculated at BP86/QZ4P level. The bond lengths are given in Å and the angles are in degree. The relative energies are respect to **PbA** in the singlet state and given in kcal/mol. The values in parentheses are the number of imaginary frequencies.

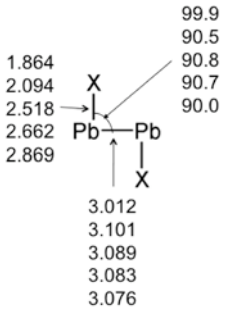

PbE(T)

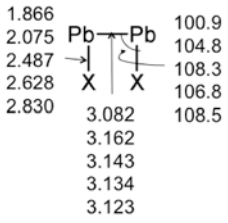

PbF(T)

	H	F	Cl	Br	I	H	F	Cl	Br	I
BP86	20.8(2)	15.2(1)	16.8(0)	17.8(0)	19.3(0)	23.2(3)	18.5(0)	20.3(2)	21.1(1)	22.6(1)
HF	7.2	10.3	9.4	10.3	11.8	9.5	14.5	13.7	14.4	9.5
RMP2	23.4	17.4	20.5	23.7	26.4	26.8	20.5	25.6	28.2	30.6
UMP2	34.5	24.6	29.7	34.1	36.1	34.6	29.0	34.8	39.1	41.3
SCS-MP2	33.4	26.4	30.0	33.9	35.5	33.4	30.9	35.1	38.9	40.6
UMP4	29.3	25.6	28.9	33.1	34.9	32.9	29.7	33.6	37.7	35.2
CCSD	20.1	18.9	18.1	21.4	23.5	22.9	20.6	23.2	25.9	27.6
CCSD(T)	22.4	19.9	19.5	23.0	25.2	25.3	21.5	24.5	27.4	29.2

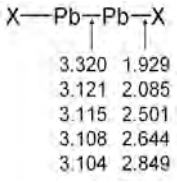

PbG(T)

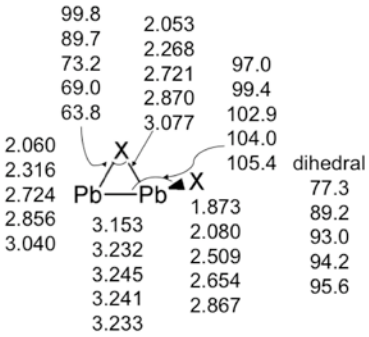

PbI(T)

	H	F	Cl	Br	I	H	F	Cl	Br	I
BP86	44.6(4)	29.1(2)	30.9(4)	31.7(2)	33.1(2)	20.5(0)	13.2(0)	17.6(0)	18.8(0)	20.4(0)
HF	39.4	30.5	30.0	30.8	32.4	4.38	0.4	4.6	6.0	4.4
RMP2	54.3	41.0	38.6	42.3	45.5	21.9	6.6	18.6	20.8	23.5
UMP2	64.6	40.4	48.0	52.7	55.9	28.6	17.7	25.9	29.1	31.7
SCS-MP2	64.7	43.8	49.7	53.8	56.4	27.4	18.4	25.3	28.3	30.4
UMP4	61.6	41.2	47.1	51.8	54.3	27.5	19.4	25.7	28.7	30.9
CCSD	49.5	37.0	36.3	40.3	42.9	19.0	6.7	17.4	19.2	21.2
CCSD(T)	50.4	36.8	36.6	40.8	43.5	21.5	8.4	19.3	21.2	23.2

4.4.1.3 Summary of Geometry and Relative Energies

Chapter 4.4.1.1 and 4.4.1.2 showed the investigated isomers of Pb_2X_2. The geometries of **PbA**, **PbB** and **PbC** show that these isomers have Pb-X-Pb bridged structures, although the Pb-Pb interactions of **PbC** for Pb_2F_2, Pb_2Cl_2, Pb_2Br_2 and Pb_2I_2 are weak.

The relative energies of Pb_2H_2 and Pb_2F_2 behave different from those of the other Pb_2X_2 isomers and the Pb_2X_2 molecules are categorized to three groups. The order of stability of Pb_2H_2 is as follows: **PbA** > **PbC** > **PbB** > **PbC(T)** > **PbI(T)** > **PbE(T)** > ... > **PbG**. This order is similar to that of Sn_2H_2. The order clearly indicates that Pb_2H_2 prefers the bridged structures. This suggests that the Pb-H-Pb bridging can stabilize the Pb_2H_2 molecule most effectively.

Pb_2F_2 shows a different order of the stability and it is as follows: **PbA** > **PbI(T)** > **PbC** > **PbB(T)** > **PbE2** > **PbE(T)** > ... > **PbG**. Pb_2F_2 also prefers bridged structures. However the stabilization effect of the bridging is not so large as for the isomers of Pb_2H_2. The following ones are bent structures.

Pb_2Cl_2, Pb_2Br_2 and Pb_2I_2 show a different order and the order is as follows: **PbA** > **PbE2** > **PbI(T)** > **PbE(T)** > (**PbF1**, **PbC(T)**) > ... > **PbG**. Pb_2Cl_2, Pb_2Br_2 and Pb_2I_2 show that the bridged structures make the molecule stable, which is similar to Pb_2F_2. The bent-structures are also relatively stable.

4.4.2 Orbital Interactions and Bond Situations

4.4.2.1. Orbital Analyses

The last section showed that several energetically low-lying stationary points on the singlet potential energy surface, which differ mainly in the bond situation of the Pb-Pb bond. **PbA**, **PbB**, **PbC**, **PbE1**, **PbE2**, **PbF1**, **PbF2** and **PbG,** which have a X-Pb-Pb-X structure, can be divided into two PbX fragments and the bonding situation in these molecules can be described as interactions between the two PbX fragments. The orbital interactions between the diatomic species are analyzed with the similar approach to the Trinquier/Malrieu/Carter/Goddard model [81, 82, 83], which is able to explain the E_2H_2 bonding situation [87]. This approach was also used for the lighter homologues in the chapter 4.1.2, 4.2.2 and 4.3.2.

4.4.2.1.1. Pb-X Fragments

Figure 4.4.2.1 shows schematic pictures of the electronic ground state ($X^2\Pi$) and the first excited state ($a^4\Sigma^-$) of PbX and Table 4.4.2.1 presents the calculated excitation energies $a^4\Sigma^- \leftarrow X^2\Pi$ at BP86/QZ4P level and MRCI-SD/aug-cc-pvQZ//BP86/QZ4P level. A (5,5) full-valence CASSCF/aug-cc-pVQZ wave functions were used as reference in the MRCI-SD calculation of PbH and (11,8) full-valence CASSCF/aug-cc-pVQZ wave functions were used as a reference in the MRCI-SD calculation of PbF, PbCl, PbBr and PbI. The excitation energies at BP86/QZ4P are in relatively good agreement with those of MRCI-SD/aug-cc-pVQZ//BP86/QZ4P. The largest deviation of BP86/QZ4P from the MRCI-SD(Q) result is found for PbF with 9.2 kcal/mol. The excitation energy is underestimated at BP86/QZ4P for all PbX molecules.

As shown in Section 4.4.1, the linear structure is the energetically highest lying stationary point of the investigated structures in the Pb_2X_2 system and this situation is quite different from the C_2X_2 system, where the linear structure is the global minimum. The previous study showed that it is energetically much easier to excite CH from the $X^2\Pi$ ground state to the $a^4\Sigma^-$ excited state. The carbon species CH has the much lower excitation energy (15.4 kcal/mol) than PbH (52.0 kcal/mol) [263].

Therefore, PbH needs much more energy to reach the $a^4\Sigma^-$ excited state to form a triple bond than for the CH species. The possible gain in binding energy after $a^4\Sigma^- \leftarrow X^2\Pi$ excitation is much larger for C_2H_2 than that for Pb_2H_2. These two facts explain the differences in the potential energy surfaces between C_2X_2 and their higher homologues E_2X_2 (X=Si-Pb, X=H and F-I). Table 4.4.2.1 shows that the excitation energy becomes smaller as the halogen atom gets heavier and the excitation energies of the halogen molecules are much larger than those of SiX, GeX and SnX. Figure 4.4.2.1 clearly shows that the electronic configuration of PbX moiety must be the $a^4\Sigma^-$ excited state and not the $X^2\Pi$ ground state to form the triply bonded linear species XPb≡PbX. Therefore, the PbX fragments must at first become excited into the $a^4\Sigma^-$ state in order to bind through one σ and two degenerate π bonds in XPb≡PbX. The electron configuration of the $X^2\Pi$ ground state only allows an electron sharing single bond between two PbX moieties in a non-linear arrangement. The other possibility to form a bond is a donor-acceptor bond between two moieties in the $X^2\Pi$ ground state. The situation is qualitatively the same as for SiX, GeX and SnX.

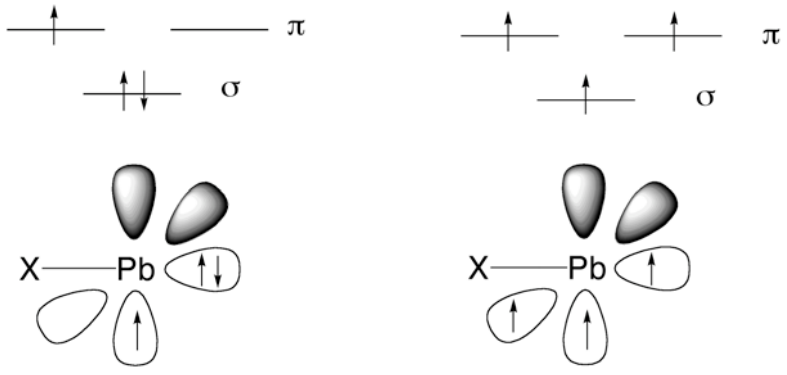

$X^2\Pi$ $a^4\Sigma^-$

ground state excited state

Figure 4.4.2.1 Schematic pictures of the $X^2\Pi$ ground state and the $a^4\Sigma^-$ excited state for the PbX fragment.

Table 4.4.2.1 Calculated excitation energies from the $X^2\Pi$ ground state to the $a^4\Sigma$ excited state at BP86/QZ4P, MRCI-SD/aug-cc-pvQZ//BP86/QZ4P and MRCI-SD(Q)/aug-cc-pvQZ//BP86/QZ4P levels, where (Q) indicates the inclusion of the Davidson correction. The energies are given in kcal/mol.

	BP86/QZ4P	MRCI-SD/ aug-cc-pVQZ	MRCI-SD(Q)/ aug-cc-pVQZ
PbH	52.01	50.22	50.66
PbF	109.41	110.17	113.53
PbCl	90.28	92.53	93.97
PbBr	77.60	82.03	83.68
PbI	65.76	74.62	74.97

Table 4.4.2.2 Calculated dissociation energies D_e of the linear X-Pb≡Pb-X into 2 PbX molecules and the excitation energies from the $X^2\Pi$ ground state to the $a^4\Sigma^-$ excited state of the PbX molecules at BP86/QZ4P level. The energies are given in kcal/mol.

	D_e	ΔE_{exc}	D_e- $2\Delta E_{exc}$
H	69.0	52.0	-35.0
F	69.0	109.4	-149.8
Cl	59.5	90.3	-121.1
Br	45.4	77.6	-109.9
I	38.4	65.8	-93.1

Table 4.4.2.2 shows the theoretically predicted bond dissociation energies for breaking the triple bond in the linear X-Pb≡Pb-X yielding 2 PbX ($a^4\Sigma^-$). Linear Pb_2H_2 and Pb_2F_2 have quite the same dissociation energy of 69.0 kcal/mol and the dissociation energies become smaller as the halogen atom gets heavier. The dissociation energies are much weaker than that of acetylene and the linear structures of Si_2X_2, Ge_2X_2 and Sn_2X_2. After correcting for the excitation energy of the two PbX fragments from the $X^2\Pi$ ground state to the $a^4\Sigma^-$ excited state, the calculated values give theoretical bond energies D_e- $2\Delta E_{exc}$. These theoretical bond energies are more negative than those of SiX, GeX, SnX (Table 4.1.2.2, Table 4.2.2.2 and Table 4.3.2.2). The excitation energies of the two PbX fragments are even higher than the

bond dissociation energy of the linear XPb≡PbX structure of Pb_2H_2, Pb_2F_2, Pb_2Cl_2, Pb_2Br_2 and Pb_2I_2 and the theoretical dissociation energies are negative. From these points, it is found that the interaction is unfavorable because of the large excitation energies, which is similar to SiX, GeX and SnX.

The calculated bond dissociation energy D_e shows that it is energetically unfavorable for the PbX fragments to form an XPb≡PbX triple bond through the $a^4\Sigma^-$ excited states because the Pb-Pb single bond that can be formed from the $X^2\Pi$ ground state would deliver a much larger binding energy. The bond dissociation energies of the Pb-Pb single bonds in Pb_2X_6 are 8.8 - 46.5 kcal/mol, which are calculated at BP86/QZ4P level. This is much less than the stabilization energy that can be expected from the formation of an electron-sharing XPb-PbX single bond between two PbX fragments in the $X^2\Pi$ ground state. The possibility of additional stabilizations through lone-pair and/or Pb-X donor acceptor interactions, which are described below, will be enough to match the much higher bond energy of the triple bond. It follows that it is energetically more profitable for two PbX species to bind in their $X^2\Pi$ ground state than in the $a^4\Sigma^-$ excited state.

Figure 4.4.2.2 shows the selected orbitals of the PbX fragment. Two π orbitals are found as LUMO and SOMO, respectively. Two types of σ orbitals, the lone-pair orbitals and Pb-X orbitals are found as occupied orbitals. However, These orbitals have a different character compared to the ones of the SiX, GeX and SnX fragments. Figure 4.4.2.4(c) shows the Pb-X bond orbital and the orbital figure presents that the Pb-X bond orbital has both lone-pair character and Pb-X bond character. Figure 4.4.2.4(d) shows that the lone-pair orbital is quite similar to the *s* orbital of Pb atom. These orbitals of PbH, PbF, PbCl, PbBr and PbI are quite similar in each other for the region near the Pb atom.

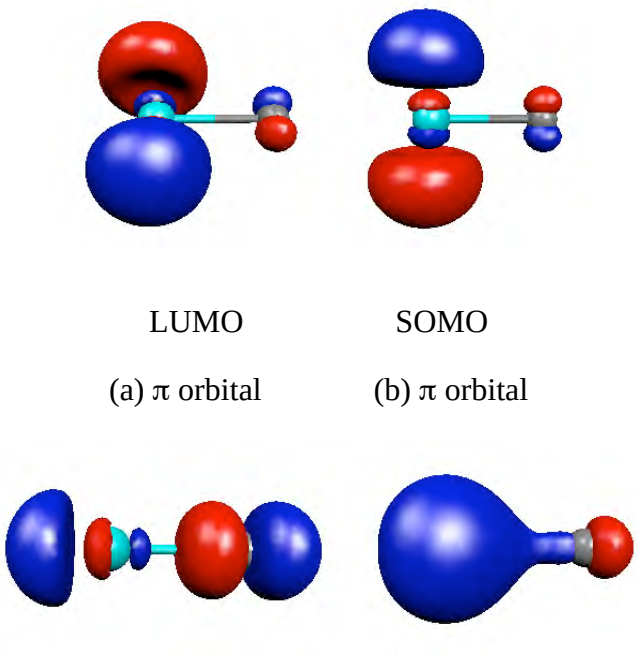

LUMO SOMO

(a) π orbital (b) π orbital

(c) σ-Pb-X bond orbital (d) σ-lone-pair orbital

Figure 4.4.2.2. Important orbitals of the PbX fragment in the $X^2\Pi$ ground state to form the Pb-Pb bond.

Table 4.4.2.3 Calculated orbital energies of the PbX fragment at BP86/QZ4P level. The energies are given in eV.

	PbH	PbF	PbCl	PbBr	PbI
π orbital (LUMO)	-3.7482	-3.7172	-3.8359	-3.8355	-3.8468
π orbital (SOMO)	-3.5471	-3.5184	-3.6251	-3.6214	-3.6308
Pb-X bond orbital	-6.2842	-8.3559	-7.8091	-7.5023	-6.6383
lone-pair orbital (*s*-orbital)	-12.5908	-12.7959	-12.8068	-12.7951	-12.6685
$\Delta E_{\pi\text{-PbX}}$	2.536	4.6387	3.9732	3.6668	2.7915
$\Delta E_{\pi\text{-lone-pair}}$	8.8426	9.0787	8.9709	8.9596	8.8217

Table 4.4.2.3 shows the orbital energies of the selected orbitals in Figure 4.4.2.2. The orbital energies of the PbX molecules differ from those of SiX, GeX and SnX in their order. The energies of HOMOs and the LUMOs are nearly constant similar to the corresponding orbitals of SiX, GeX and SnX. The energies of the Pb-X bond orbitals are higher than those of the lone-pair orbitals, although those of SiX, GeX and SnX are lower. The orbital energies of the Pb-X bond exhibit a clear correlation for PbF, PbCl, PbBr and PbI molecules. The orbital energies of the Pb-X bond orbitals become higher as the halogen atoms get heavier. The trend of the orbital energies is due to the fact that the halogen atoms are electron-withdrawing groups and the halogen atoms stabilize the $X^2\Pi$ ground state of the Pb-X molecules. The energies of the lone-pair orbital are nearly constant and it indicates that the halogen atom has nearly no effect on the lone-pair orbital because the main contribution is *s* orbital of Pb atom (Figure 4.4.2.2) The $\Delta E_{\pi\text{-lone-pair}}$ values show the energy difference between the LUMO and the lone-pair orbital. The $\Delta E_{\pi\text{-lone-pair}}$ values show no clear correlation because of the small contribution of the atomic orbital of X atom. The $\Delta E_{\pi\text{-Pb-X}}$ values show the energy difference between the LUMO and the Pb-X bond orbital, which concern for the Pb-X bond donor-acceptor interaction. The $\Delta E_{\pi\text{-Pb-X}}$ values show a clear correlation with halogen atom and the orbital energy becomes higher as the halogen atom gets heavier.

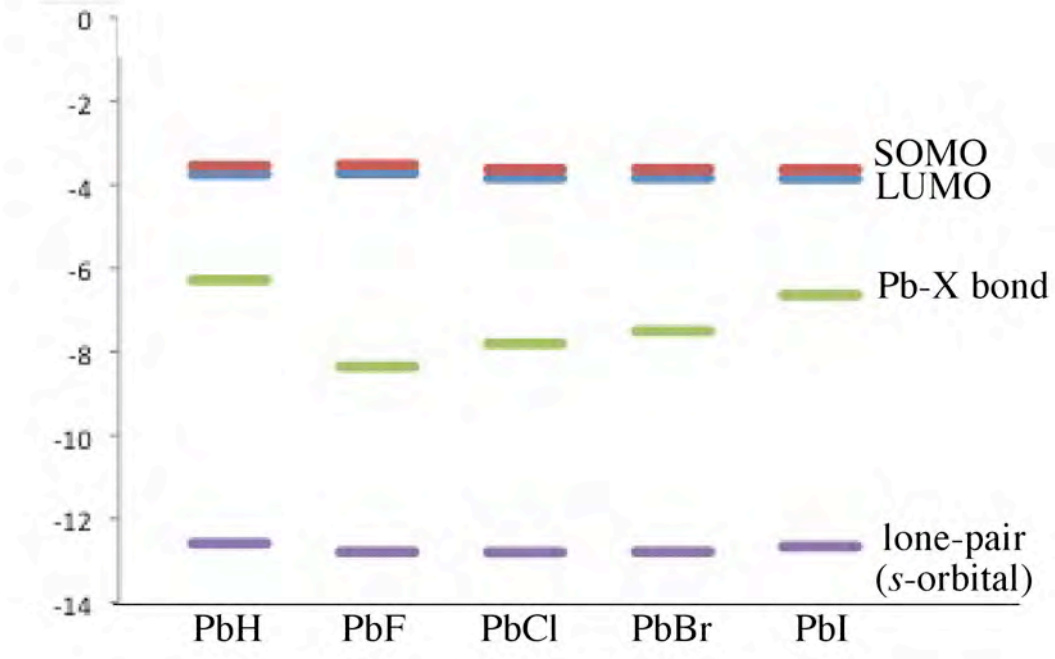

Figure 4.4.2.3 the orbital energies presented in Figure 4.4.2.2

Table 4.4.2.4 shows the contribution of atomic orbitals for each Kohn-Sham molecular orbital of the PbX molecules. It presents that LUMO and SOMO are constructed by just *p* orbitals, which is similar to the SiX, GeX and SnX molecules. The Pb-X bond orbital shows the large contribution from the X atom and the orbital has a large character of the atomic orbital of the X atom. The contributions of *s* orbital from the Pb atom are very small (5% - 13%), where the *s* orbital contributes less as the halogen atom gets heavier. The contributions of the *p* orbital of Pb atom are 10% - 36% and the *p* orbital shows the opposite trend to the *s* orbital. These are quite smaller than the contributions for SiX, GeX and SnX. The lone-pair orbital is composed mainly of the *s* orbital of the Pb atom, which is different to SiX, GeX and PbX. It clearly suggests that the lone-pair orbital is almost a *s* atomic orbital of the Pb atom and the *s* orbital of the Pb atoms does not concern to the Pb-X bond orbital. This is due to that the *s* orbital and the *p* orbital of the Pb atom have a large energy difference and these orbital do not mix. The lone-pair orbital is named as *s*-orbital.

Table 4.4.2.4 Each percentage contribution of selected orbitals corresponds to the indicated atomic orbitals

	PbH(%)	PbF(%)	PbCl(%)	PbBr(%)	PbI(%)
π orbital (LUMO)	Pb: p_y 97.74	Pb: p_y 67.90 p_x 27.07	Pb: p_y 74.17 p_x 17.40 Cl: p_y 4.69	Pb: p_x 58.26 p_y 32.24 Br: p_x 4.27	Pb: p_y 77.54 p_x 11.75 I: p_y: 6.88
π orbital (SOMO)	Pb: p_z 98.25	Pb: p_z 95.57 F: p_z 3.87	Pb: p_z 92.99 Cl: p_z 5.36	Pb: p_z 92.06 Br: p_z 6.12	Pb: p_z 90.66 I: p_z 7.18
Pb-X orbital	Pb: p_x 36.39 H: *s* 56.91	Pb: *s* 13.84 p_x 7.57 p_y 3.02 F : p_x 52.06 p_y 20.75	Pb: *s* 9.31 p_x 13.22 Cl: p_x 58.95 p_y 13.83	Pb: *s* 7.16 p_y 12.58 p_x 6.96 Br: p_y 45.67 p_x 25.27	Pb: *s* 5.14 p_x 20.33 p_y 3.08 I: p_y 59.73 p_x 9.05
lone-pair orbital	Pb: *s* 84.96 H: *s* 12.98	Pb: *s* 82.31 F: p_x 10.44 p_y 4.16	Pb: *s* 85.45 Cl: *s* 3.53 p_x 8.03	Pb: *s* 88.94 Br: *s* 2.97 p_y 5.14	Pb: *s* 88.16 I: *s* 5.32 p_x 5.26

4.4.2.1.2 σ-type Isomers, **PbA**, **PbE2** and **PbF1**

As shown before, the linear arrangement of two PbX fragments of the $X^2\Pi$ state is unfavorable for the bond formation between the unpaired electrons and the bond formation must rather take place in a sideways fashion. Figure 4.4.2.4 shows some different orientations for two PbX fragments each in the $X^2\Pi$ state which lead to a Pb-Pb σ bond.

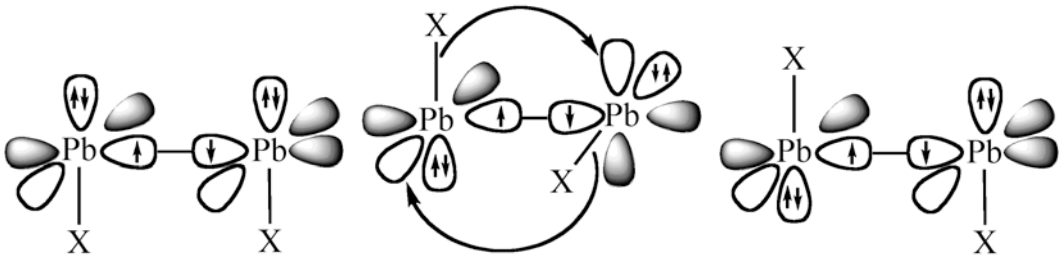

(a) (b) (c)

Figure 4.4.2.4. Qualitative model for the σ-type orbital interaction between two PbX molecules in the different orientation where the unpaired electrons yield a σ orbital.

Figure 4.4.2.4 (a) shows a syn-planar arrangement of the PbX moieties, which gives the isomer **PbF1**. This arrangement is not favorable because the vacant $p(\pi)$ orbitals remain unoccupied while the Pb-X bonds and the electron lone-pairs of the two molecules repel each other. The geometry optimization of Pb_2X_2 with a syn-planar arrangement gives a structure, which is a transition state.

The rotation around the σ-bond axis by 90° gives a much more favorable arrangement. In this bond situation, the empty $p(\pi)$ orbitals of the PbX molecule can interact with the Pb-X bond and with the electron lone-pair of the other PbX fragment. Apart from Si_2X_2, Ge_2X_2 and Sn_2X_2, the PbX donor-acceptor interaction has three possibilities; the Pb-X bond donor-acceptor (b), the σ orbital donor (b') and the lone-pair type donor of the Pb-X bond (b'') (Figure 4.4.2.5).

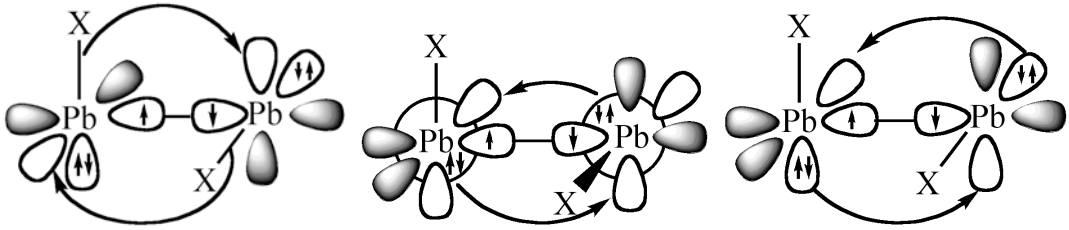

(b) (b') (b'')

Figure 4.4.2.5. Three possibilities of the donor-acceptor interactions. The Pb-X donor-acceptor interaction (b), the *s*-orbital donor-acceptor (b') and the lone-pair type donor of Pb-X bond (b'').

The interaction (b') is not favorable because the lone-pair orbital is mainly composed of the *s* atomic orbital of the Pb atom, as shown in Table 4.4.2.4, and this donor-acceptor interaction has only a small overlap of the orbitals. In addition to that, the orbital energies of the lone-pairs are quite lower in energy and the orbital interactions lead small stabilization energies. The Pb-X bonds are mainly composed of the atomic orbital of the X atom. On the one hand, the lone-pair type donor-accepter (b'') leads to a normal donor-acceptor bond for the reason that the X atom does not concern to the interaction. On the other hand, the Pb-X bond donor-acceptor interaction (b) leads to the three-center-two-electron bond, and the interaction is the most effective orbital combination, as explained in 4.1.2.1, 4.2.2.1, and 4.3.2.1. The Pb-X bonds interact with the empty $p(\pi)$ orbitals of the other PbX moiety. The donor-acceptor interactions between the Pb-X bond and the vacant $p(\pi)$ orbital have the largest stabilizing effect of three possibilities. This arrangement gives the isomer **PbA** as shown in Figure 4.4.2.5 (b). This explains why the global energy minimum is the halogen-bridged geometry **PbA**. The geometry of **PbA** is not planar but it has a nearly perpendicular arrangement of the two Pb_2X planes which have a dihedral angle between 103.8° and 110.3°. From the quantitative model, it is found that there are three bonding components of the orbital interactions in **PbA**: one σ bond and two Pb-X donor-acceptor bonds.

Figure 4.4.2.4 (c) shows the anti-planar arrangement of the PbX fragments, which gives the isomer **PbE2**. The only Pb-Pb bonding contribution is the σ orbital between the two Pb atoms. The structure of **PbE2** lacks the two Pb-X donor-acceptor

interactions of **PbA** and so the vacant $p(\pi)$ orbitals remain unoccupied. The geometry optimization of Pb_2X_2 with an anti-planar arrangement gives structures that are transition states.

In the previous section, the bond situation is discussed with a qualitative model. Table 4.4.2.5 shows the selected orbitals concerning the Pb-Pb bond and their orbital energies of **PbA**, **PbE2** and **PbF1**. The first orbitals of **PbA**, **PbE2** and **PbF1** in Table 4.4.2.5 seem to be σ-type Pb-Pb bonds. The second one and third one of **PbA** seem the Pb-X donor-acceptor bonds and those of **PbE2** and **PbF1** have lone-pair character. These orbitals show that the qualitative model is sensible in these σ system isomers.

Table 4.4.2.5 presents the Pb-Pb σ bonding orbitals, which are found as the HOMO in **PbA**, **PbE2** and **PbF1** for all Pb_2X_2 molecules, which are categorized to a σ type structure in Figure 4.4.2.4. The energies of the HOMOs are presented in Table 4.4.2.5 and for PbF it has the highest HOMO energy of Pb_2X_2 system and the orbital energy mostly decreases with heavier halogen atoms. For the Pb_2F_2, Pb_2Cl_2, Pb_2Br_2 and Pb_2I_2 system, the energy level of the σ type orbital clearly correlates with the orbital energy of π orbital, which is the SOMO, of the PbX fragment. The Pb-Pb bond lengths in **PbE2** and **PbF1** are longer than the Pb-Pb single bond in $X_3Pb\text{-}PbX_3$ (Pb_2H_6: 2.906Å, Pb_2F_6: 3.014Å, Pb_2Cl_6: 3.072Å, Pb_2Br_6: 3.101Å, Pb_2I_6: 3.125Å at BP86/QZ4P level), because the σ bonds in **PbE2** and **PbF1** are formed by the two π orbitals of the PbX moieties, which are the SOMOs shown in Figure 4.4.2.2(b), and the σ bond has little *s* character, whereas the normal Pb-Pb σ bond has sp^3 character. The energy of the σ type orbital in Pb_2F_2 is the highest in **PbA**, **PbE2** and **PbF1**, where the orbital energies become lower when the halogen atom X gets heavier.

Table 4.4.2.5. Orbital shapes and energies of σ-type isomers **PbA**, **PbE2** and **PbF2**. The energy levels are given in eV.

	PbA	**PbE2**	**PbF1**
orbital		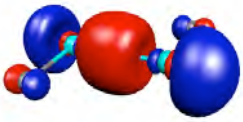	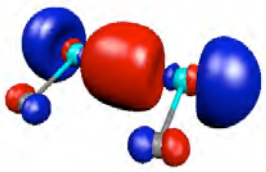
	σ-type bond	σ-type bond	σ-type bond
H	-4.2103	-4.4041	-4.3776
F	-4.1281	-4.4413	-4.3887
Cl	-4.4910	-4.6524	-4.5299
Br	-4.5340	-4.6569	-4.5261
I	-4.5860	-4.6746	-4.5372
orbital		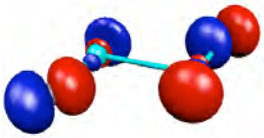	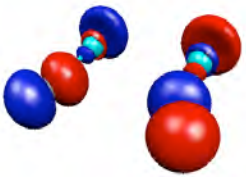
	Pb-X donor	Lone-pair	Lone-pair
H	-7.3967	-5.9037	-5.7595
F	-8.8867	-8.2462	-8.0288
Cl	-8.2557	-7.8024	-7.4889
Br	-7.9408	-7.4700	-7.1832
I	-7.5445	-7.0546	-6.8006
orbital	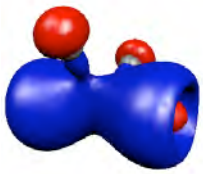		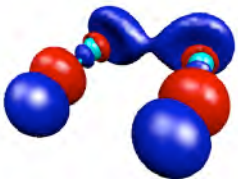
	Pb-X donor	Lone-pair	Lone-pair
H	-13.8448	-6.3517	-6.4365
F	-13.2019	-8.3559	-8.3335
Cl	-13.2757	-7.8739	-7.8483
Br	-13.3134	-7.6267	-7.5695
I	-13.1348	-7.3232	-7.2260

PbA clearly shows two Pb-X donor-accepter bonds. These two orbitals shown in Table 4.4.2.5 are very similar except the node on the Pb-Pb axis. The energetically higher orbital has a node and the lower one does not. From these orbital figures, it can be thought that the energetically higher orbital is the anti-bonding orbital of lower one (Figure 4.4.2.6). The energetically lower lying orbital has no node between the two Pb atoms and this orbital contributes to the Pb-Pb bonding. The energetically higher orbital mainly contributes to the formation of the Pb-X-Pb ring structure. This can explain the short Pb-Pb bond lengths in **PbA**.

Figure 4.4.2.6 shows that the two Pb-X donor-acceptor bonds interact with each other and the orbital interaction forms two new orbitals. In principle, the orbital energy level of the new two formed orbitals depend on the energy level of the original orbitals, i.e., the energy level of the vacant π orbital and the Pb-X σ bond orbital. Table 4.4.2.3 shows that the orbital energies of the two Pb-X donor-acceptor bonds become higher as the halogen atom gets heavier and it is same for the orbital energies of the Pb-X bond.

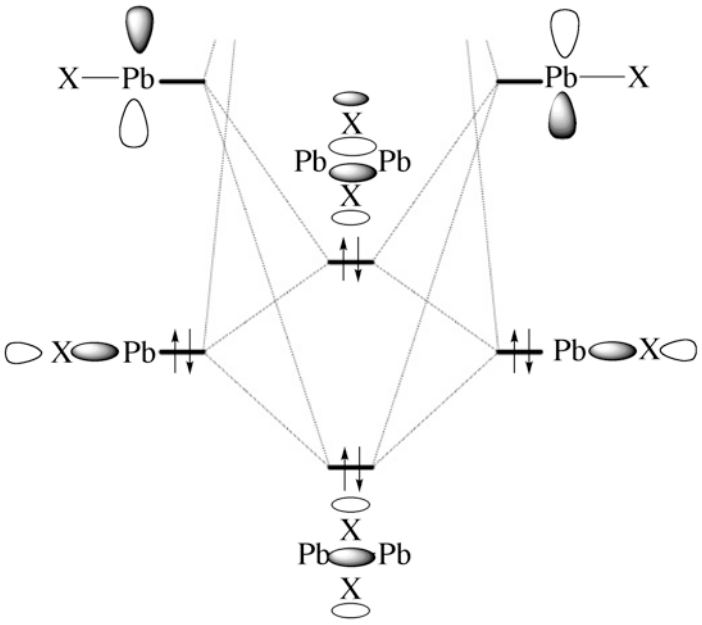

Figure 4.4.2.6 Orbital correlation model for donor-acceptor interaction between the Pb-X bond orbital and the vacant *p(π)* orbital in the $X^2\Pi$ ground state of two Pb-X fragments to yield bridged structures.

In **PbE2** and **PbF1**, the two Pb-X bond orbitals, which have also a lone-pair character, interact with each other and they form a bonding orbital between the two PbX moieties. However, they form an anti-bonding orbital at the same time (Figure 4.4.2.7). This system is the four-electron two-orbital interaction and the interaction between the two lone-pair orbitals almost cancels; for the bond formation, therefore, they have nearly no contribution to the Pb-Pb bond.

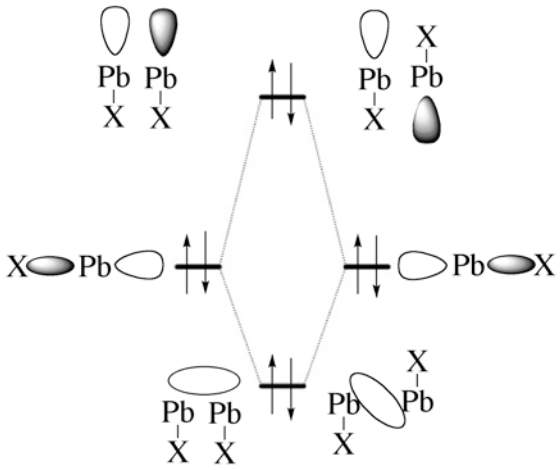

Figure 4.4.2.7 Orbital correlation diagram between two Pb-X orbitals in their $X^2\Pi$ ground state of the two Pb-X fragments in the σ-type bent-structures **PbE2** and **PbF1**.

4.4.2.1.3 π-type Isomers, **PbB**, **PbC**, **PbE1** and **PbE2**

The unpaired electrons in the $X^2\Pi$ ground state of the Pb-X may also be paired in an electron-sharing bond between the two PbX fragments, which has π symmetry with respect to the molecular structure. Figure 4.4.2.8 shows different orientations for two ($X^2\Pi$) PbX molecules, which lead to a Pb-Pb π bond.

The arrangement given in Figure 4.4.2.8 has an electron lone-pair on one of the PbX moieties pointing in the direction of the empty π orbital of the other PbX species. This orbital interaction now has a σ symmetry with respect to the PbX dimer plane. Besides the electron-sharing π bond and the "lone-pair type" donor-acceptor σ bond, further stabilizing orbital interactions are possible in the structures shown in Figure 4.4.2.3. Another possibility is the donation of the Pb-X bonding orbital, which is shown in the orbital of **PbA** in Figure 4.4.2.4(b). As noted before, the donation from

the PbX bonding orbital is stronger than the lone-pair orbital and the lone-pair type donor of the PbX bond. The former interaction becomes stronger when the PbX donor orbital and the empty π orbital of the interacting fragments are tilted toward each other, which leads to structure **PbB** (Figure 4.4.2.8(d)). The tilting of the empty π orbital of the acceptor PbX moiety (top PbX in Figure 4.2.2.8(d)) means that the terminal atom moves toward the bridging halogen atom. The *syn* orientation of the terminal atom with respect to the bridging X atom can be explained as a secondary effect of optimizing the PbX donor-acceptor interaction between their PbX in the $X^2\Pi$ ground state, which is shown in Figure 4.4.2.8(d).

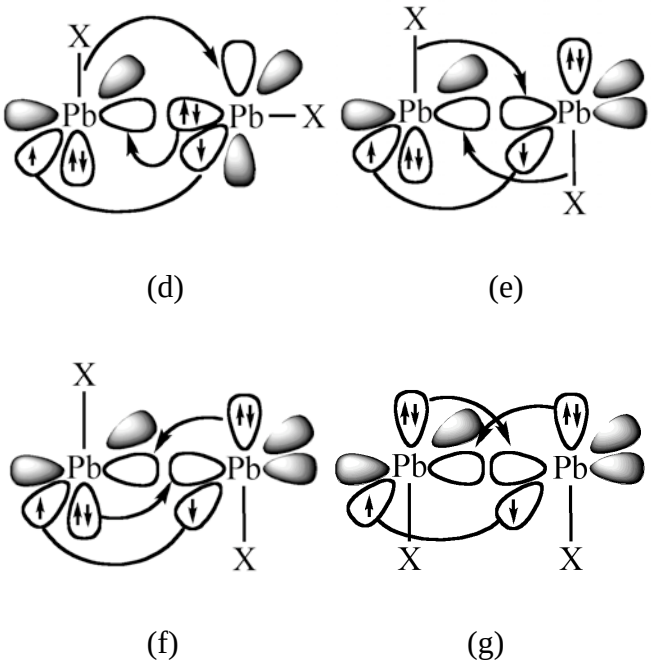

Figure 4.4.2.8 Qualitative model for the π-type orbital interactions between two PbX molecules in different orientations where the unpaired electrons yield a π orbital.

Figure 4.4.2.8(e) displays another orientation of two PbX molecules where the unpaired electrons form a π bond while the PbX bonds are in an anti-periplanar arrangement. The π orbital interaction between the PbX fragments is enhanced by two equal donor-acceptor interactions between the Pb-X bonding orbitals and the empty π orbitals of the interacting fragments. The latter orbital interactions become stronger, when the halogen atoms bridge in a doubly bridged planar (D_{2h}) structure. The geometry optimizations of $(PbX)_2$ show that the D_{2h} symmetric stationary point is an energetically low-lying structure on the potential energy surface. The inspection of

the Hessian matrix reveals, however, that it is a transition state for the degenerate rearrangement of the global energy minimum structure **PbA**. It is the wing-flapping motion of the butterfly geometry. The structure **PbA** has a Pb-Pb σ bond and two PbX donor-acceptor bonds (Figure 4.4.2.4(b)), while the transition state has a Pb-Pb π bond and two PbX donor-acceptor bonds (Figure 4.4.2.8(e)).

The “lone-pair type” donation is weaker than the PbX donation as explained in the chapter 4.4.2.1, but it leads to another structure of $(PbX)_2$ which is a minimum on the potential energy surface. Figure 4.4.2.8(f) and 4.4.2.8(g) show that the "lone-pair type” donor of the PbX bond to the vacant p_π orbital becomes enhanced by tilting the Pb-X bond out, which yields the trans- and cis-form **PbE1** and **PbF2**, respectively. According to the orbital analysis, the structures **PbE1** and **PbF2** have three bonding orbital components, which are one π electron-sharing bond and two “lone-pair type” donor-acceptor bonds. The structure **PbC** of Pb_2H_2 is energetically higher lying than the planar transition state with two bridging halogen atoms, which has one π bond and two Pb-X donor-acceptor bonds, whereas those of Pb_2F_2, Pb_2Cl_2, Pb_2Br_2 and Pb_2I_2 are energetically lower lying than the planar transition state with two bridging halogen atoms.

Table 4.4.2.6 shows the orbital energies of important orbitals in **PbB, PbC**, **PbE1** and **PbF2**, which concern the Pb-Pb bond. Table 4.4.2.6 presents the Pb-Pb π bonds of **PbB, PbC**, **PbE1** and **PbF2**, which are categorized as a π type structure in Figure 4.4.2.8. In these isomers, the Pb-Pb π bond is found as the HOMO. The eigen value of the π type orbital of Pb_2F_2 is the highest in **PbB**, **PbC**, **PbE1** and **PbF2**, where the orbital energies become lower, when the halogen atom X gets heavier. This correlates with the energy level of the SOMO of the PbX fragment. The isomers **PbB**, **PbC**, **PbE1** and **PbF2** of Pb_2H_2, Pb_2F_2, Pb_2Cl_2, Pb_2Br_2 and Pb_2I_2 are found as transition states or higher order saddle points because the energies of the π orbitals are relatively higher than those of the σ orbital of **PbA**, which is similar to the analogues of Sn_2X_2, where the π type isomers of Si_2X_2 and Ge_2X_2 are often found as minima because they have π bond and the rotation needs energy to break the π bond. For **PbB**, **PbC**, **PbE1** and **PbF2** structures, the π bond is unstable and π bond can rotate easily. In principle, a π bond is weaker than a σ bond and a “single” π bond should be longer than a σ

bond, because a π bond usually has less orbital overlap than a σ bond. However, the Pb-Pb bond lengths in **PbB**, **PbE1** and **PbF2** are shorter than the Pb-Pb single bond of **PbE2** and **PbF1** as shown in Section 4.4.1.1. This suggests that another interaction, except a π orbital interaction, could exist between the Pb-Pb atoms as expected in Figure 4.4.2.8.

The second orbital of **PbB** shown in Table 4.4.2.6 shows that the shape of the orbital is similar to the lone-pair donor-acceptor bond model in Figure 4.4.2.8(d). The energy level of this orbital correlates with the energy of the lone-pair of the Pb-X fragment (Table 4.4.2.3), where the orbital energy level becomes lower when the halogen atom X becomes heavier. To form the donor-acceptor bond, the lone-pair orbital interacts with the vacant π orbital of the Pb-X fragment. The formed donor-acceptor orbital has mainly the character of the original lone-pair orbital and the energy level of the formed orbital exhibits the correlation with the lone-pair orbital.

The third orbital of **PbB** in Table 4.4.2.6 shows that the main contribution is not a Pb-X donor-acceptor bond but a Pb-X bond. The energy level of this orbital is moderately higher than that of Pb-X donor-acceptor bond of **PbA**. The energies of these orbitals have the same trend as the orbital energy of the Pb-X bond in the PbX fragment (Table 4.4.2.3), where the orbital energy level becomes lower, when the halogen atom X gets heavier. However, it is very difficult to determine that this orbital concerns the donor-acceptor bond.

PbC has a π bond and two Pb-X donor-acceptor bonds. The Pb-X donor-acceptor bond orbitals are quite similar to that of **PbA**. The two Pb-X donor-acceptor bonds form two new orbitals and the main contributions are in the region of the Pb-Pb bond and the Pb-X-Pb ring, which is quite similar to the bond correlation in Figure 4.4.2.6. The energy level of the π orbital is higher than that of the σ orbital of **PbA**.

Table 4.4.2.6. Selected orbitals and their orbital energies of π type isomers, **PbB, PbC**, **PbE1** and **PbF**. The energy levels are given in eV.

	PbB	**PbC**	**PbE1**	**PbF2**
orbital		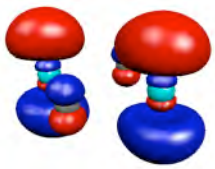		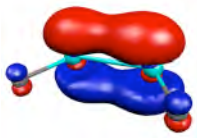
	π-type bond	π-type bond	π-type bond	π-type bond
H	-4.3226	-4.0742	-4.4154	-4.3867
F	-4.2638	-3.4538	-4.6182	-4.5800
Cl	-4.4352	-3.7771	-4.6722	-4.6228
Br	-4.4195	-3.8250	-4.6293	-4.5734
I	-4.4048	-3.8879	-4.5840	-4.5172
orbital	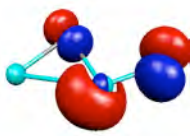		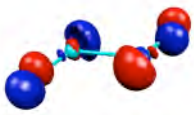	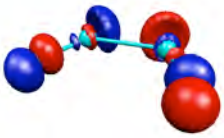
	lone-pair	Pb-X donor	lone-pair	lone-pair
H	-6.6258	-7.8444	-6.4559	-5.9729
F	-8.1675	-9.0207	-8.4251	-8.2997
Cl	-7.9096	-8.4513	-8.0640	-7.8256
Br	-7.5444	-8.1672	-7.7291	-7.4606
I	-7.0778	-7.8022	-7.3256	-7.0169
orbital			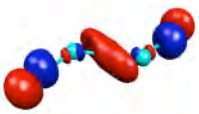	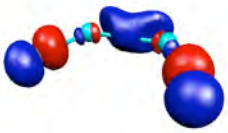
	Pb-X	Pb-X donor	lone-pair	lone-pair
H	-7.4799	-13.9107	-7.3861	-7.1190
F	-9.0535	-12.8873	-9.2904	-9.2142
Cl	-8.1193	-13.1586	-8.6610	-8.5990
Br	-7.7616	-13.2441	-8.3129	-8.2512
I	-7.3600	-13.1245	-7.8589	-7.8001

These two orbitals of **PbE1** and **PbF2** are similar to the two "lone-pair type" orbitals of **PbE2** and **PbF1**, respectively. When the energy levels of these orbitals are compared, the lower lying "lone-pair like" orbital energies of **PbE1** are 0.5357 – 1.0344 eV lower than the energies of the "lone-pair type" orbital of **PbE2**, where the lone-pairs in **PbE2** do not contribute to the Pb-Pb bonding. The orbital energy differences between **PbF1** and **PbF2** are 0.5741- 0.7535 eV. The differences are smaller compared to those in Si_2X_2, Ge_2X_2 and Sn_2X_2. The energetically higher orbital has a node along the Pb-Pb bond and the lower one does not. From these orbital figures, it can be thought that the energetically higher orbital is the anti-bonding orbital of the lower one and the two equivalent "lone-pair type" donor-acceptor orbitals produce two orbitals. The energetically lower lying orbital contributes to the Pb-Pb bond. The energetically higher lying orbital is similar to original lone-pair orbital. This can explain the Pb-Pb bond lengths in **PbE1** and **PbF2**, which are shorter than that in the Pb-Pb single bond of **PbE2** and **PbF1**.

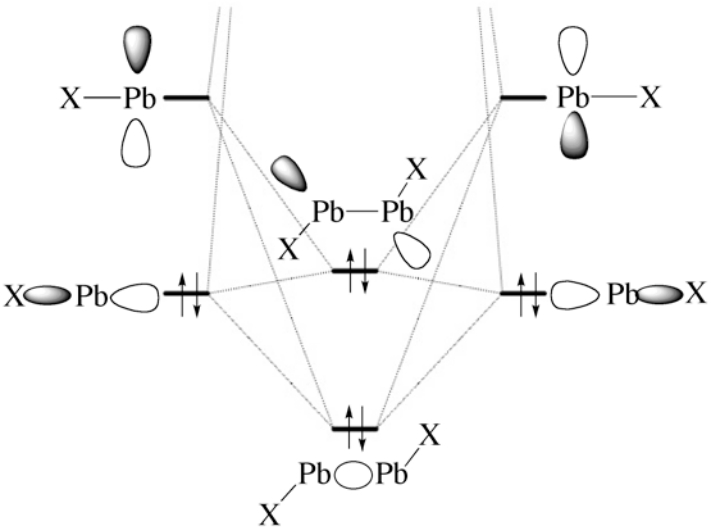

Figure 4.4.2.9 Orbital correlation diagram between two Pb-X orbitals in the $X^2\Pi$ ground state of the two Pb-X fragments in **PbE1**.

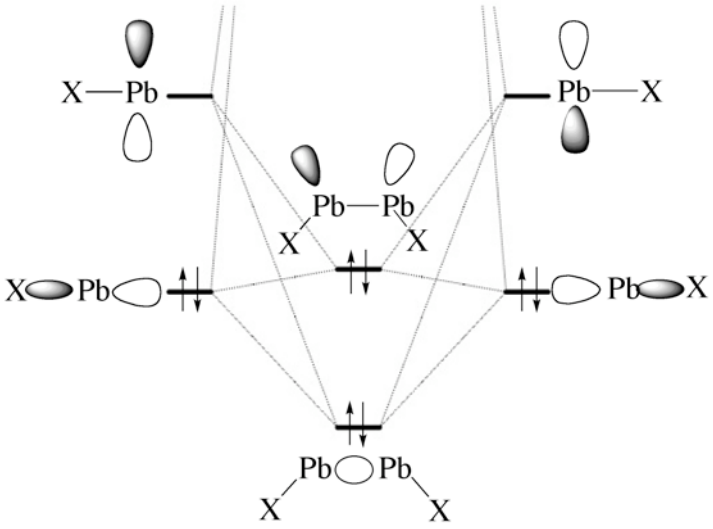

Figure 4.4.2.10 Orbital correlation diagram between two Pb-X orbitals in ground state of the two Pb-X fragments in **PbF2**.

4.4.2.1.4 Summary of Orbital Analyses

In the chapter 4.4.2.1, the orbital analyses of the PbX molecules and the isomers of Pb_2X_2 are presented. The investigation of the PbX molecules shows that the very high excitation energies of PbX molecules from the $X^2\Pi$ ground state to the $a^4\Sigma^-$ excited state lead very large negative bond dissociation energies and it suggests that the linear XPb≡PbX structures are quite unfavorable. The orbital analysis of the PbX molecules shows that the lone-pair orbitals of the PbX molecules are mainly composed from the *s* atomic orbital of the Pb atom, and alternatively, the Pb-X bond orbital has the ”lone-pair character”, where the lone-pair orbitals of the SiX, GeX and SnX molecules are composed of the atomic orbitals of both elements.

The orbital analyses of Pb_2X_2 present that the orbital interaction models of two PbX fragments are quite sensible. The Pb_2X_2 isomers are categorized to σ-type isomers and π-type isomers, where the σ-type isomers are more favorable than the π-type isomers, as explained at the chapter 4.4.1. **PbA** has one σ-type bond and two Pb-X bond donor-acceptor bonds, although the other σ-type isomers have just σ-type orbitals. The Pb-X bond donor-acceptor leads to a strong three-center-two-electron bond, and due to that, **PbA** is the most stable isomer.

The π-type orbitals of **PbB**, **PbC**, **PbE1** and **PbF2** are high in energy. The π

bonds are not stable and the Pb-Pb bond can rotate easily and the isomers become transition states. The orbital energies of “lone-pair like orbital” of **PbE1** and **PbF2** are different from **PbE2** and **PbF1**, although the orbital figures are similar to each other. The stabilization energies stem from the interaction with the vacant π orbital.

4.4.2.2 AIM Analyses

In the chapter 4.4.2.1, the orbitals and their energy levels were investigated. There, some interactions do not become clear in the orbital analysis. In this chapter, the bonding situation will be analyzed by the quantum theory of atoms in molecules. Figure 4.4.2.11 – Figure 4.4.2.18 show the Bader plots of the investigated isomers. The comparison to Si_2X_2, Ge_2X_2 and Sn_2X_2, the charge accumulation correlates with the atom of group 14 and the accumulated region becomes smaller as the atom of the 14 group gets heavier.

Figure 4.4.2.11 shows the Bader plot of the isomer **PbA** in the Pb_2X plane and it shows that **PbA** isomer has a Pb-X-Pb bridged structure. The isomers of **PbA** show no charge accumulation between the two Pb atoms, which explains that the Pb-Pb bonds have a small covalent character.

In session 4.4.1.1 and 4.4.2.1, the Pb-X-Pb ring structures of **PbB** have been discussed with bond length and orbitals. However, the lone-pair donor bond and the Pb-X donor-acceptor bond could not be clearly proved with the orbital analysis. The AIM results in Figure 4.4.2.12 prove that **PbB** has a Pb-X-Pb ring structure, which is consistent with the discussions of the geometry. The figure is quite similar to that of **SnB** apart form **SiB** and **GeB**.

The AIM results of Figure 4.4.2.13 show that the isomers of **PbC** have Pb-X-Pb bridged structures and the figure presents that Pb_2Br_2 and Pb_2I_2 have a Pb-Pb bond, which is different from the geometric viewpoint. No charge accumulation in the Pb-X-Pb ring is found for all Pb_2X_2 molecules. The ionic interaction plays an important role in the Pb-X-Pb bridged structure.

4.4 Pb_2X_2 Molecules

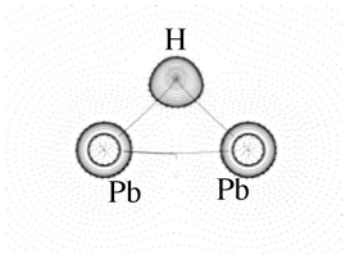

Pb_2H_2

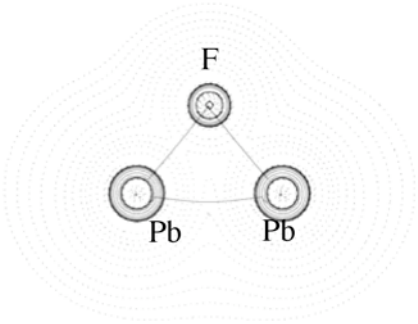

Pb_2F_2

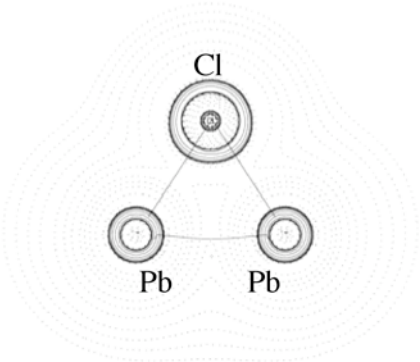

Pb_2Cl_2

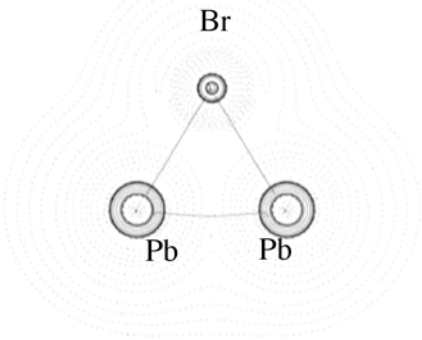

Pb_2Br_2

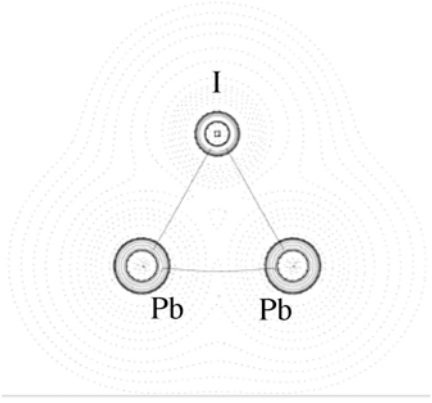

Pb_2I_2

Figure 4.4.2.11 Contour line diagram $\nabla^2\rho(r)$ of isomer **PbA**. Solid lines indicate areas of charge concentration ($\nabla^2\rho(r) < 0$), while dashed lines show areas of charge depletion ($\nabla^2\rho(r) > 0$). Solid lines that connect the atomic nuclei are the bond paths.

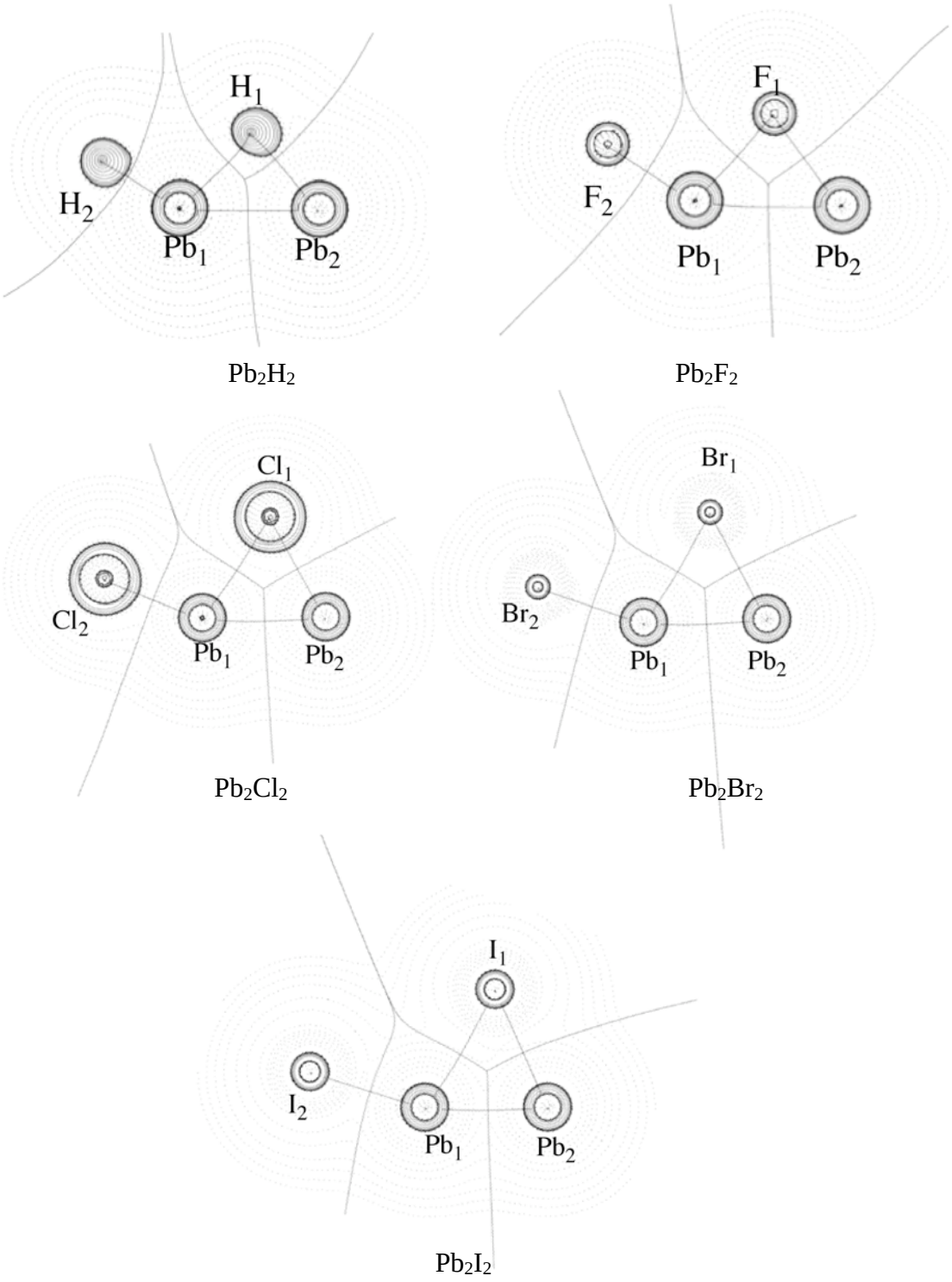

Pb_2H_2 Pb_2F_2

Pb_2Cl_2 Pb_2Br_2

Pb_2I_2

Figure 4.4.2.12 Contour line diagram $\nabla^2\rho(r)$ of isomer **PbB**. Solid lines indicate areas of charge concentration ($\nabla^2\rho(r) < 0$), while dashed lines show areas of charge depletion ($\nabla^2\rho(r) > 0$). Solid lines that connect the atomic nuclei are the bond paths, while solid lines that separate the atomic basis give the zero-flux surface in the molecular plane.

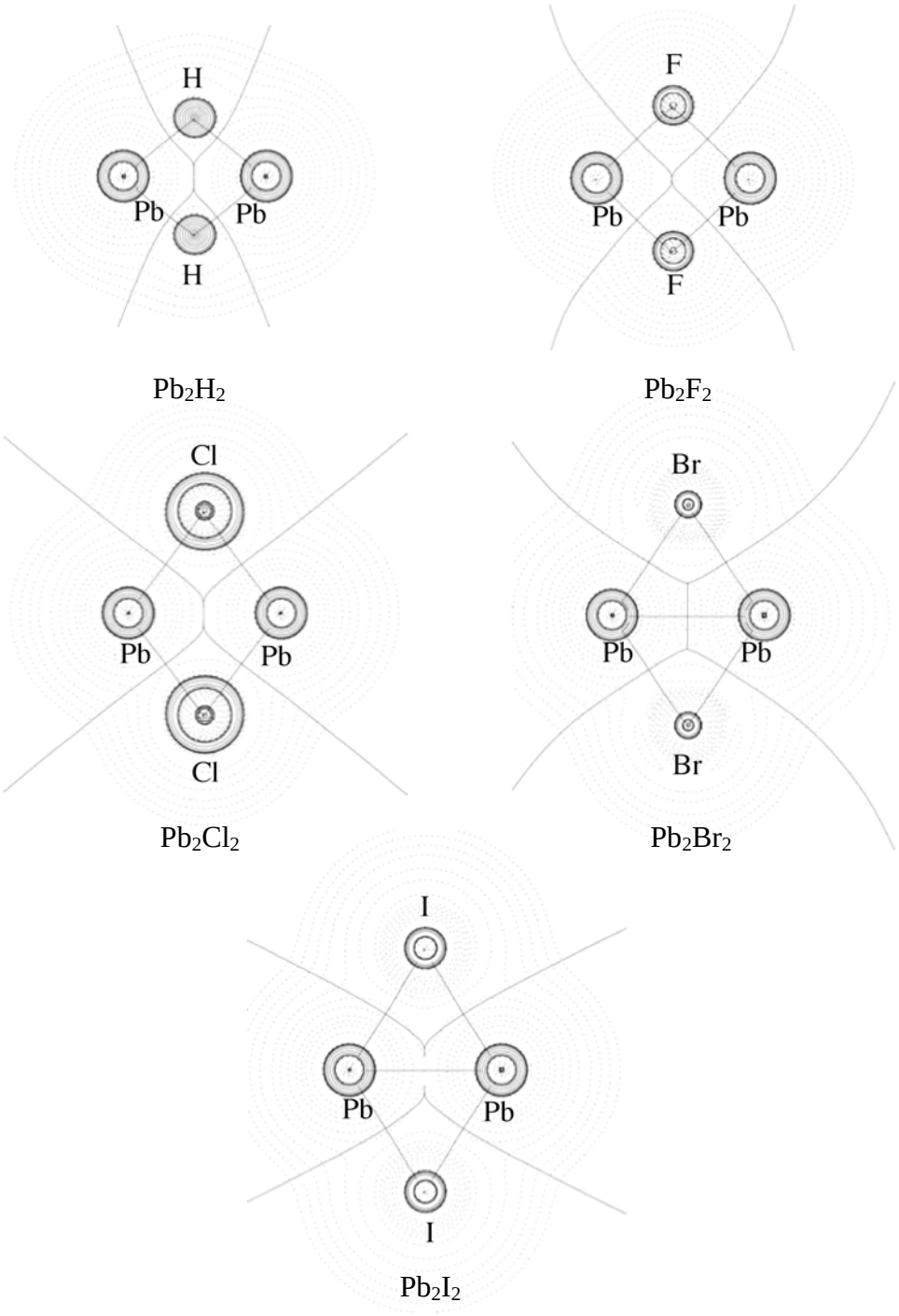

Pb_2H_2 Pb_2F_2 Pb_2Cl_2 Pb_2Br_2 Pb_2I_2

Figure 4.4.2.13 Contour line diagram $\nabla^2\rho(r)$ of isomer **PbC**. Solid lines indicate areas of charge concentration ($\nabla^2\rho(r) < 0$), while dashed lines show areas of charge depletion ($\nabla^2\rho(r) > 0$). Solid lines that connect the atomic nuclei are the bond paths, while solid lines that separate the atomic basis give the zero-flux surface in the molecular plane.

Figure 4.4.2.14 shows the Laplacian, $\nabla^2\rho(r)$, bond paths and zero flux path surfaces of the isomer **PbD** in the molecular plane. This figure shows that **PbD** has a Pb-Pb bond and two Pb-X bonds. A charge accumulation between the two Pb-Pb atoms is not found.

The AIM results of Figure 4.4.2.15 show that **PbE1** has a Pb-Pb bond and a Pb-X bond. The orbital analyses show that the **PbE1** isomer has two lone-pair donor-acceptor bonds, However, **PbE1** shows no charge accumulation in the region of the Pb-Pb bonds. The two lone-pair donor-acceptor interaction is less effective than that in **SiE1** and **GeE1**. Figure 4.4.2.16 shows that **PbE2** has a Pb-Pb bond and two Pb-X bonds. The charge accumulation is not found among the Pb-Pb bond region.

The contour line diagram of $\nabla^2\rho(r)$ for **PbF1** is shown in Figure 4.4.2.17 and it shows a Pb-Pb bond and two Pb-X bonds. For Pb_2Cl_2, Pb_2Br_2 and Pb_2I_2, X-X bonds are found due to that the Pb-Pb-X angle is nearly 90° and Cl, Br and I atoms have larger radii than H and F atom, and H and F atoms repel each other less than the other halogen atoms, which is similar to **SiE1**, **GeE1** and **SnE1**. A charge accumulation is not found among the Pb-Pb bond region similar to **PbE2**. Figure 4.4.2.18 shows that **PbF2** isomer has a Pb-Pb bond and two Pb-X bonds. In the region of the Pb-Pb bond, no charge accumulation is found between two Pb atoms. The situation is similar to that of **PbE1**.

The AIM analyses show the bond paths and it agrees with the discussion of the geometry. **PbA**, **PbB** and **PbC** have ring-structures, as expected in the chapter 4.4.1. However, the charge accumulation between the two E atoms is much smaller than those for Si_2X_2-Sn_2X_2, which indicates that the large electrostatic interactions are important for these isomers.

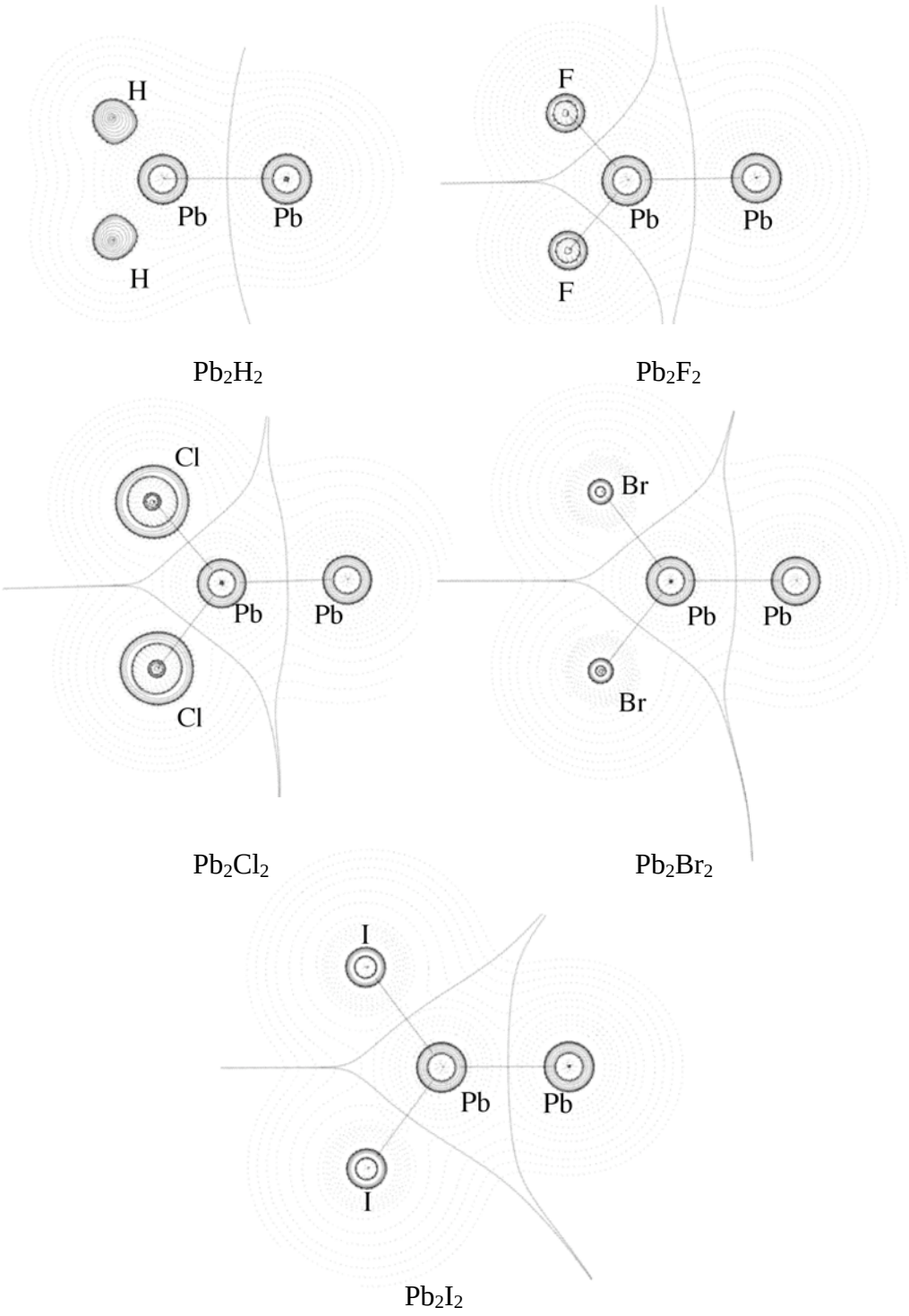

Pb_2H_2 Pb_2F_2 Pb_2Cl_2 Pb_2Br_2 Pb_2I_2

Figure 4.4.2.14 Contour line diagram $\nabla^2\rho(r)$ of isomer **PbD**. Solid lines indicate areas of charge concentration ($\nabla^2\rho(r) < 0$), while dashed lines show areas of charge depletion ($\nabla^2\rho(r) > 0$). Solid lines that connect the atomic nuclei are the bond paths, while solid lines that separate the atomic basis give the zero-flux surface in the molecular plane.

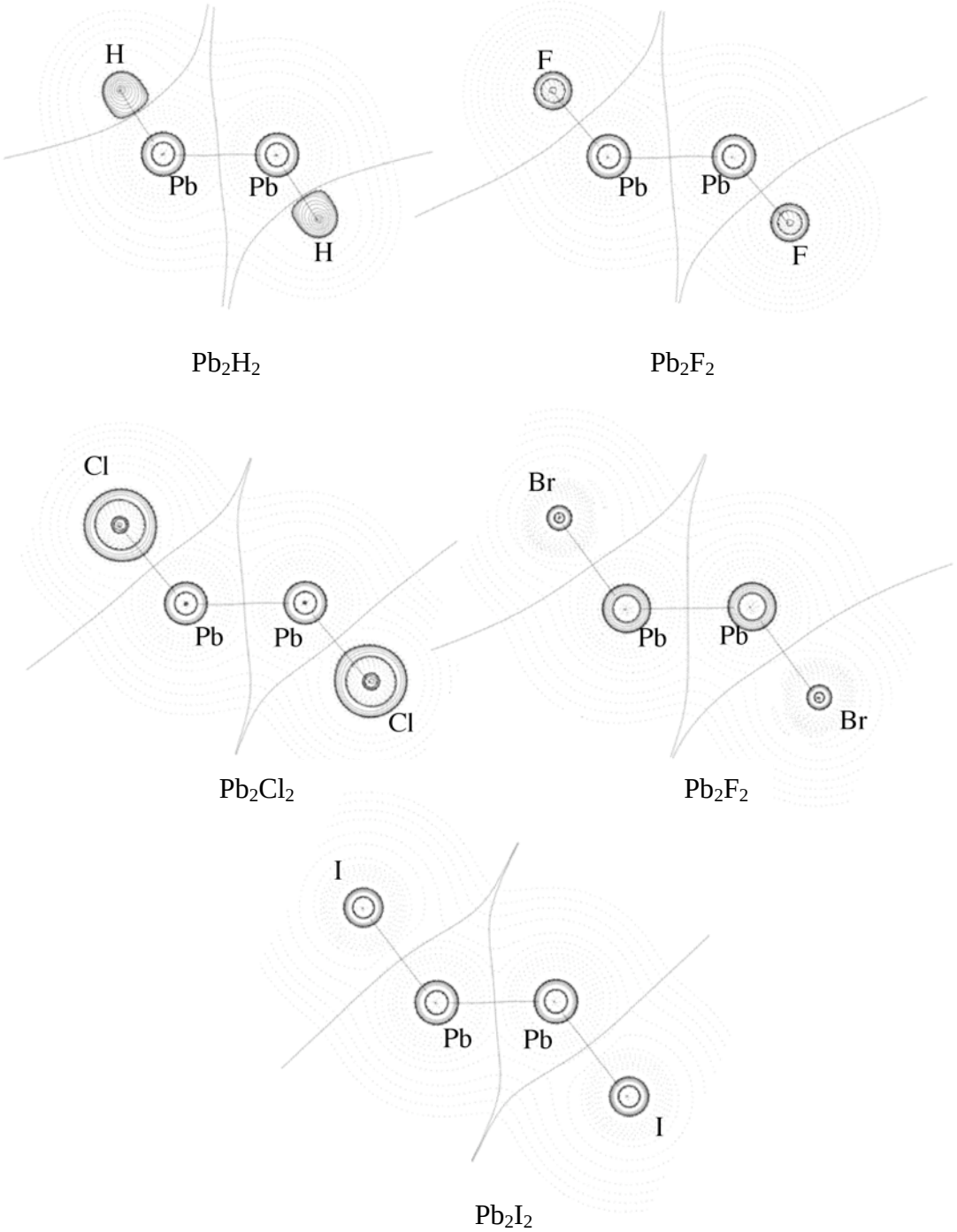

Pb_2H_2 Pb_2F_2

Pb_2Cl_2 Pb_2F_2

Pb_2I_2

Figure 4.4.2.15 Contour line diagram $\nabla^2\rho(r)$ of isomer **PbE1**. Solid lines indicate areas of charge concentration ($\nabla^2\rho(r) < 0$), while dashed lines show areas of charge depletion ($\nabla^2\rho(r) > 0$). Solid lines that connect the atomic nuclei are the bond paths, while solid lines that separate the atomic basis give the zero-flux surface in the molecular plane.

4.4 Pb_2X_2 Molecules

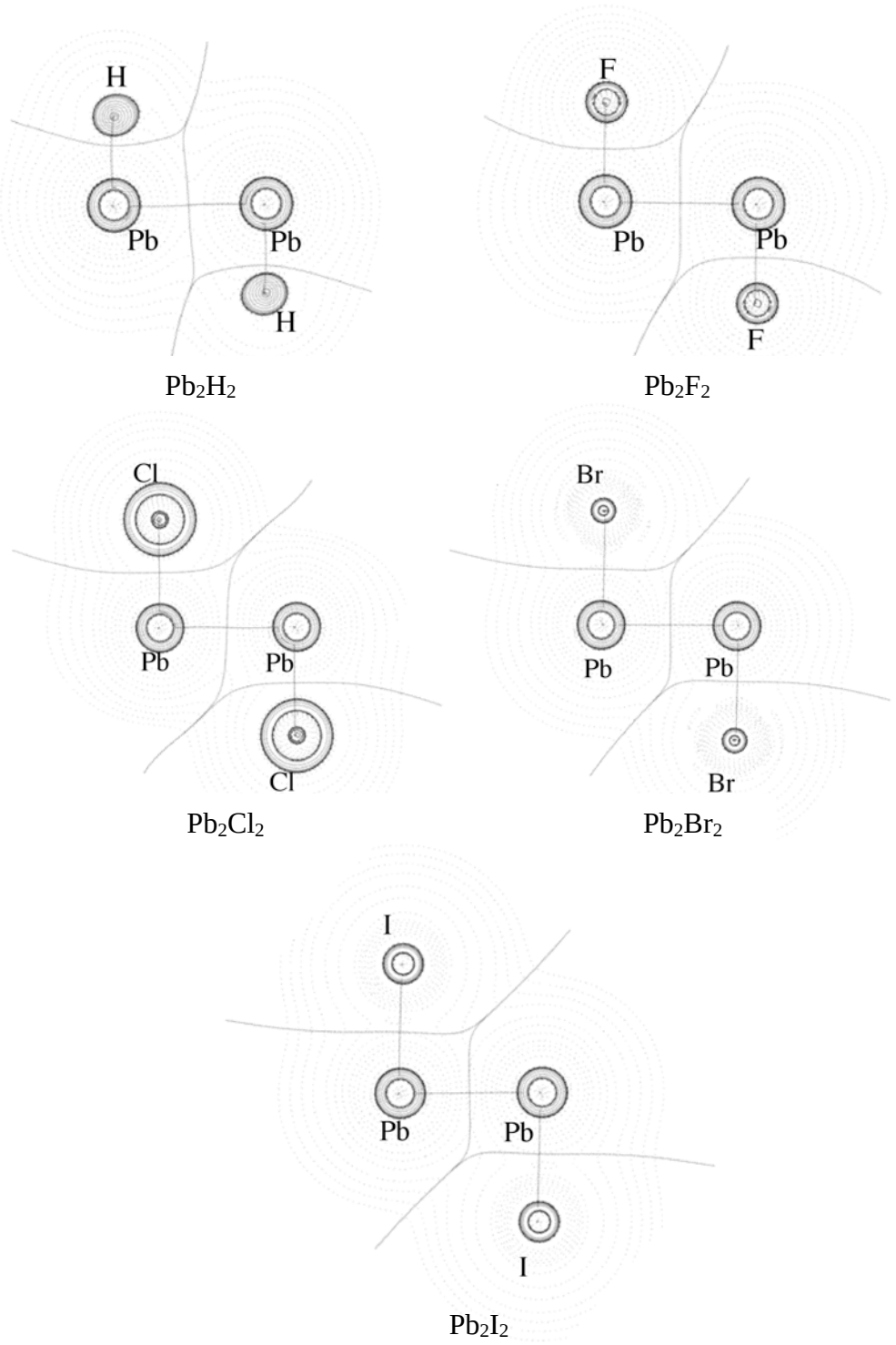

Pb_2H_2 Pb_2F_2

Pb_2Cl_2 Pb_2Br_2

Pb_2I_2

Figure 4.4.2.16 Contour line diagram $\nabla^2\rho(r)$ of isomer **PbE2**. Solid lines indicate areas of charge concentration ($\nabla^2\rho(r) < 0$), while dashed lines show areas of charge depletion ($\nabla^2\rho(r) > 0$). Solid lines that connect the atomic nuclei are the bond paths, while solid lines that separate the atomic basis give the zero-flux surface in the molecular plane.

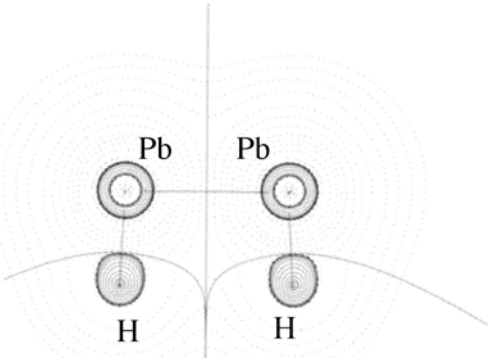

Pb_2H_2

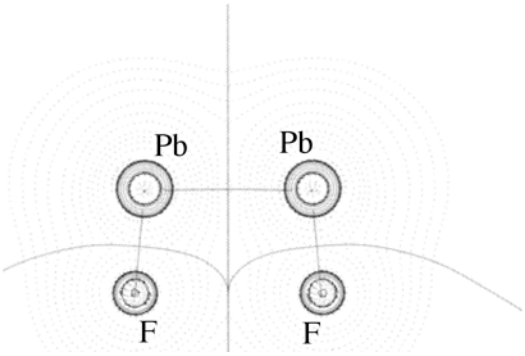

Pb_2F_2

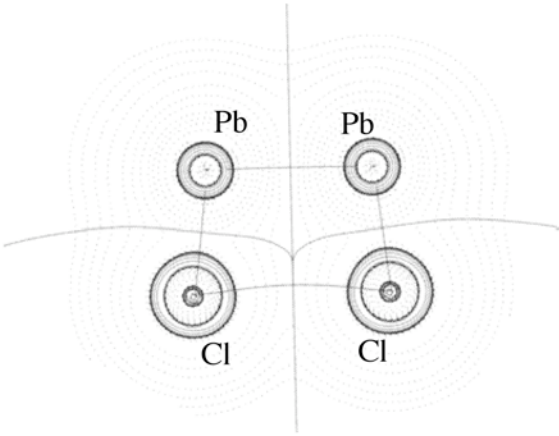

Pb_2Cl_2

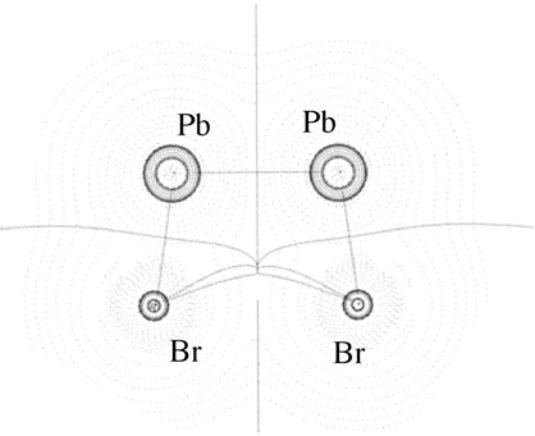

Pb_2Br_2

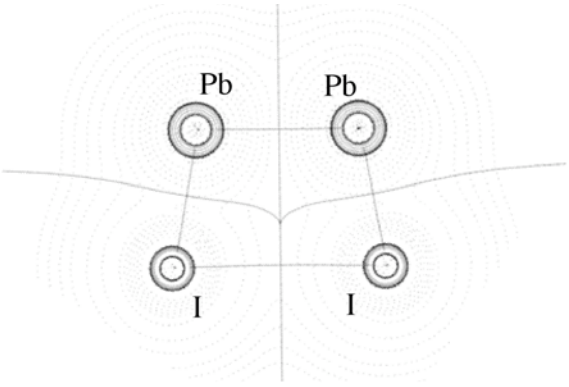

Pb_2I_2

Figure 4.4.2.17 Contour line diagram $\nabla^2\rho(r)$ of isomer **PbF1**. Solid lines indicate areas of charge concentration ($\nabla^2\rho(r) < 0$), while dashed lines show areas of charge depletion ($\nabla^2\rho(r) > 0$). Solid lines that connect the atomic nuclei are the bond paths, while solid lines that separate the atomic basis give the zero-flux surface in the molecular plane.

4.4 Pb_2X_2 Molecules

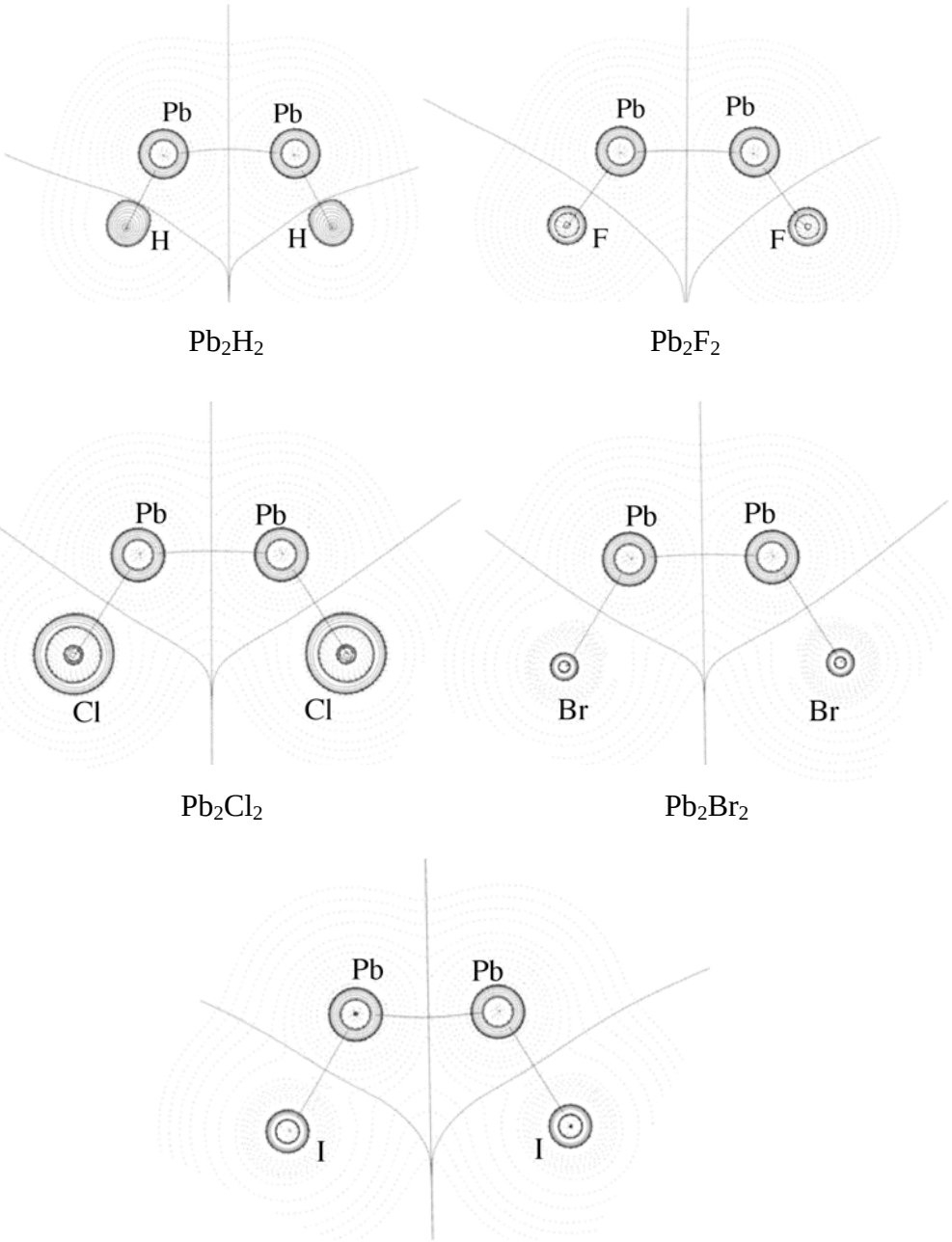

Pb_2H_2 Pb_2F_2

Pb_2Cl_2 Pb_2Br_2

Pb_2I_2

Figure 4.4.2.18 Contour line diagram $\nabla^2\rho(r)$ of isomer **PbF2**. Solid lines indicate areas of charge concentration ($\nabla^2\rho(r) < 0$), while dashed lines show areas of charge depletion ($\nabla^2\rho(r) > 0$). Solid lines that connect the atomic nuclei are the bond paths, while solid lines that separate the atomic basis give the zero-flux surface in the molecular plane.

4.4.2.3. Charge Analyses

As shown in chapter 4.4.2.1, the orbital interactions were investigated and it showed that the orbital interaction with two fragments could explain the geometries of each isomer. The AIM analyses of chapter 4.4.2.2 presented the bond situation and the bonding character. However, the contribution of charge is not clear. This chapter discusses the charge analyses.

4.4.2.3.1. PbX Fragments

Table 4.4.2.7 shows the computed Hirshfeld charges of the PbX molecules. It is found that the Pb atom is always positively charged and the hydrogen atom and the halogen atoms are always negatively charged because the H atom and the halogen atoms are more electronegative than the Pb atom. The charges of the PbX molecules are much larger than that of the PbH molecule. The order of polarization is PbF > PbCl > PbBr > PbI > PbH. The charge analysis of the PbX molecules shows that the Pb-X bond donor-acceptor leads to an effective Pb-X···Pb-X dipole-dipole interaction and the donor-acceptor interaction is quite favorable, although the “lone-pair type” donor-acceptor interaction is less favorable because of the large electric repulsion of two positive charged Pb atoms. This is another reason why the doubly bridged structure **PbA** is more favorable than the bent-structures. The absolute charges of the PbX molecules are larger than those of SiX, GeX and SnX and that indicates that the PbX molecules are more polarized than the SiX, GeX and SnX molecules. This suggests that the bridged structures become more favorable and more stable than the bent-structures because the larger polarization leads to larger dipole-dipole interactions for the bridged structures and larger electrostatic repulsion for the bent-structures

Table 4.4.2.7 Hirshfeld charges of the PbX fragments

	PbH	PbF	PbCl	PbBr	PbI
Pb	0.1786	0.3411	0.2742	0.2426	0.2054
X	-0.1786	-0.3411	-0.2742	-0.2426	-0.2054

4.4.2.3.2 Pb_2X_2 isomers

Table 4.4.2.8 shows the Hirshfeld charge of the Pb_2X_2 isomers. The Hirshfeld charge shows that Pb_2F_2 is the most polarized and Pb_2I_2 exhibits only small partial charges. It means that the former has more ionic character and the latter has more covalent character. This agrees with the results of the AIM. The charges show no correlation with the relative energies, but the charges indicate the character of the bonding situation.

PbE2 and **PbF1** show the largest positive charges of the Pb atom in all isomers and they are similar to the charge of free PbX molecules. It indicates a small intramolecular charge transfer from the X atoms to the Pb atom. On the other hand, **PbE1** and **PbF2** are less positively charged than the PbX molecules, and the Pb-Pb bond formation needs an intramolecular charge transfer from the halogen atoms to the Pb atoms. However, the donation is unfavorable as the electronegativity is concerned, and the Pb-Pb bond formation of **PbE1** and **PbF2** is not favorable.

PbA, **PbB** and **PbC** show smaller charge values of Pb atom than the free Pb-X molecules. It indicated a charge transfer form the Pb atom to the X atom. Apart from the bent-structures, the charge donation is favorable because the direction of the charge donation is the same as that of the orbital donation.

The Pb-Pb bond length correlates with the charge and the Pb-Pb bond becomes longer as the charge gets larger. This suggests that the electrostatic interaction plays an important role for the Pb_2X_2 isomers.

Table 4.4.2.8 Calculated Hirshfeld charges at BP86/QZ4P level.

	PbA	**PbB**	**PbC**	**PbE1**	**PbE2**	**PbF1**	**PbF2**	**PbG**
					Pb_2H_2			
Pb_1	0.1288	0.0878	0.1289	0.1116	0.1816	0.1707	0.1599	-0.0346
Pb_2	0.1288	0.1316	0.1289	0.1116	0.1816	0.1707	0.1599	-0.0346
H_1	-0.1288	-0.1239	-0.1289	-0.1116	-0.1816	-0.1707	-0.1599	0.0346
H_2	-0.1288	-0.0954	-0.1289	-0.1116	-0.1816	-0.1707	-0.1599	0.0346
					Pb_2F_2			
Pb_1	0.2974	0.3648	0.2977	0.3204	0.3585	0.3355	0.3235	0.1417
Pb_2	0.2974	0.2412	0.2977	0.3204	0.3585	0.3355	0.3235	0.1417
F_1	-0.2974	-0.2925	-0.2977	-0.3204	-0.3585	-0.3355	-0.3235	-0.1417
F_2	-0.2974	-0.3135	-0.2977	-0.3204	-0.3585	-0.3355	-0.3235	-0.1417
					Pb_2Cl_2			
Pb_1	0.2241	0.2422	0.2352	0.2390	0.2982	0.2653	0.2404	0.0133
Pb_2	0.2241	0.2070	0.2352	0.2390	0.2982	0.2653	0.2404	0.0133
Cl_1	-0.2241	-0.2261	-0.2352	-0.2390	-0.2982	-0.2653	-0.2404	-0.0133
Cl_2	-0.2241	-0.2232	-0.2352	-0.2390	-0.2982	-0.2653	-0.2404	-0.0133
					Pb_2Br_2			
Pb_1	0.1899	0.1641	0.2030	0.2033	0.2672	0.2344	0.2031	-0.0332
Pb_2	0.1899	0.1555	0.2030	0.2033	0.2672	0.2344	0.2031	-0.0332
Br_1	-0.1899	-0.1632	-0.2030	-0.2033	-0.2672	-0.2344	-0.2031	0.0332
Br_2	-0.1899	-0.1564	-0.2030	-0.2033	-0.2672	-0.2344	-0.2031	0.0332
					Pb_2I_2			
Pb_1	0.1505	0.1406	0.1634	0.1604	0.2295	0.1980	0.1584	-0.0809
Pb_2	0.1505	0.1579	0.1634	0.1604	0.2295	0.1980	0.1584	-0.0809
I_1	-0.1505	-0.1557	-0.1634	-0.1604	-0.2295	-0.1980	-0.1584	0.0809
I_2	-0.1505	-0.1428	-0.1634	-0.1604	-0.2295	-0.1980	-0.1584	0.0809

4.4.2.4 Energy Decomposition Analyses

In the chapter 4.4.2.1, it was shown that the unusual equilibrium geometries **PbA**-**PbG** of Pb_2X_2 could be nicely explained in terms of orbital interactions between the PbX fragments in the $X^2\Pi$ ground state. Table 4.4.2.9 and Table 4.4.2.10 give the EDA results for the structures **PbA**, **PbB**, **PbC**, **PbE1**, **PbE2**, **PbF1**, and **PbF2** using two PbX molecules in the $X^2\Pi$ ground state as interacting fragments and the $a^4\Sigma^-$ excited state of the PbX molecules is used for the EDA calculations of the structure **PbG**. The $a^4\Sigma^- \leftarrow X^2\Pi$ excitation energy is then considered as the most important part of the preparation energy of the Pb fragment, which is the reason that the linear species **PbG** have rather large ΔE_{prep} values. In general, the Pb_2X_2 isomers show smaller interactions compared to Si_2X_2, Ge_2X_2 and Sn_2X_2. It suggests that the interactions between the two PbX fragments are weaker than those between the SiX, GeX and SnX fragments, respectively. The ratio of ΔE_{elstat} and ΔE_{orb} shows that the interactions between the PbX fragments have the most electrostatic character and the least orbital interaction character of all interactions between two EX fragments.

The EDA results present that **PbA**, **PbB** and **PbC** show slightly large preparation energies, large electrostatic interactions and large orbital interactions. The large preparation energies stem from the elongation of the Pb-X bonds to form the Pb-X-Pb bridged structure. Although this situation is similar to that in the Si_2X_2, Ge_2X_2 and Sn_2X_2 systems, the preparation energies of **PbA**, **PbB** and **PbC** are smaller than those of Si_2X_2, Ge_2X_2 and Sn_2X_2. The large electrostatic interaction energy indicates that the electrostatic interaction plays an important role in the formation of the Pb-X-Pb bridged structure in **PbA**, **PbB** and **PbC**, where the large electrostatic interactions arise from the large dipole-dipole interactions between the Pb-X molecules. The importance of electrostatic interaction is similar to Si_2X_2, Ge_2X_2 and Pb_2X_2. The large orbital interaction stems from the Pb-X bond donor-acceptor interaction, which leads to an effective three-center-two-electron interaction.

The bent structures, **PbE1**, **PbE2**, **PbF1** and **PbF2** often show smaller electrostatic interactions and orbital interactions than the bridged structures, **PbA**, **PbB** and **PbC**. The smaller electrostatic interactions come from larger electrostatic repulsions between the positively charged Pb atoms, where the Pb atoms are more

positively charged than Si, Ge and Sn atoms in the corresponding isomers. **PbE1** and **PbF2** show smaller electrostatic interactions than **PbE2** and **PbF1** because **PbE1** and **PbF2** have shorter Pb-Pb bonds, which lead to larger electrostatic repulsions. The smaller orbital interactions of the bent structures stem from the less effective orbital interactions, where **PbE1** and **PbF2** have a π-type bond and two "lone-pair type" donor acceptor interactions, although **PbE2** and **PbF1** have just a σ-type bond, as described in the orbital analyses of chapter 4.4.2.1. The orbital interactions for Pb_2H_2 and the other Pb_2X_2 isomers show a different trend in **PbE1** and **PbE2**, where the orbital interaction of **PbE1** for Pb_2H_2 is larger than that of **PbE2**, whereas for the other Pb_2X_2 isomers the trend is different. The different trend stems from the donor-acceptor interaction part of the orbital interactions, $\Delta E_{orb}(a')$, because the π interactions $\Delta E_{orb}(a'')$ are quite similar in the **PbE1** isomers. It means that the different trend stems from the energy gaps between the Pb-X bond orbital and the vacant π orbital, $\Delta E_{\pi\text{-Pb-X}}$, (Table 4.4.2.3) where the Pb-X bond orbitals of the PbX molecules have a lone-pair orbital character as explained in chapter 4.4.2.1. The $\Delta E_{\pi\text{-Pb-X}}$ values of PbF, PbCl, PbBr and PbI are larger than that of PbH, and it leads smaller orbital interactions in **PbE1**. For **PbE1** and **PbF2**, the orbital interactions in Pb_2H_2 and other Pb_2X_2 isomers show the same trend and the orbital interactions of **PbF1** are larger than those of **PbF2** because of ineffective orbital interaction due to geometrical reasons.

The π isomers, **PbB**, **PbC**, **PbE1** and **PbF2** show smaller π interactions, $\Delta E_{orb}(a'')$ than those for the corresponding isomers of Si_2X_2, Ge_2X_2 and Sn_2X_2. Due to that, the π interaction is very weak, and the π isomers of Pb_2X_2 are found as transition states or higher order saddle points.

The EDA results show that the Pb_2X_2 isomers can be categorized into three groups: Pb_2H_2, Pb_2F_2 and the group of the other Pb_2X_2 isomers. These categories are similar to those of the relative energies. The different groups mainly stem form the following three factors: different orbital energies of the Pb-X bond orbital, the polarity of the Pb-X fragment and the character of the Pb-X bond. For Pb_2H_2, the Pb-H bond has a different character from the other Pb-X bonds because the hydrogen atom has just an *s* orbital and the halogen atoms use a *p* orbital. For Pb_2F_2, the PbF

fragments are more polarized than the other PbX molecules.

The order of dissociation energies for Pb_2H_2 is as follows: **PbA** > **PbC** > **PbB** > **PbG** > **PbE2** > **PbF1** > **PbE1** > **PbF2**. This order is the same as the one of the relative energies as discussed before (chapter 4.4.1). The dissociation energies have a correlation with the electrostatic interactions, and the D_e value becomes larger as the ΔE_{elstat} value gets larger. **PbA**, **PbB** and **PbC** show large electrostatic interactions and large orbital interactions. The large ΔE_{elstat} values arise from the electrostatic interactions between the two dipoles of the PbH molecules. The large ΔE_{orb} value stems from the formation of the three-center-two-electron interaction between the Pb-H bond orbital and the vacant π orbital, as described in chapter 4.4.2.1. The relative energies of the bent structures are smaller than those of the ring structures, where this is similar trend to those of the corresponding isomers of Si_2H_2, Ge_2H_2 and Sn_2H_2. However, **PbE1**, **PbE2**, **PbF1** and **PbF2** show a different trend to the isomers of Si_2H_2, Ge_2H_2 and Sn_2H_2, where the order of the bent structure of Si_2H_2, Ge_2H_2 and Sn_2H_2 is as follows: **E1** > **E2** > **F1** > **F2**. This different trend comes form the very small electrostatic interactions of **PbE1** and **PbF2** because of the strong electrostatic repulsion between the strongly positively charged Pb atoms. **PbE2** and **PbF1** show similar ΔE_{int} and ΔE_{orb} because of the similar bond situation, a σ-type Pb-Pb single bond, as explained in chapter 4.4.2.1. Although **PbF2** is the cis-isomer of **PbE1**, the **PbF2** isomer shows smaller ΔE_{elstat} and ΔE_{orb} values. The smaller ΔE_{elstat} value of **PbF2** arises from the larger electrostatic repulsion due to the parallel configuration of the PbH fragments. The smaller ΔE_{orb} value stems from the less effective “lone-pair type” donor-acceptor interaction. The qualitative model in Figure 4.4.2.8 shows the orbital interactions of **PbE1** and **PbF2** between two PbH fragments. On the one hand, the model (f) indicates that two PbH fragments rotate in the same direction with respect to each other to form the lone-pair donor-acceptor interactions, where this rotation increases the lone-pair donor-acceptor interaction in the point of the orbital interaction. On the other hand, the model (g) exhibits that two PbH fragments rotate in the different directions with respect to each other and this rotation does not increase the lone-pair donor-acceptor interaction due to the configuration of the orbitals. As a result, the ΔE_{orb} value of **PbF2** becomes smaller than that of **PbF1**. **PbG** is relative favorable isomer because of the large orbital interaction and the large electrostatic

interaction arising from the ideal Pb-Pb triple bond, but **PbG** is still an unstable isomer due to the large excitation energy.

Pb_2F_2 shows a different trend of the dissociation energies compared to Pb_2H_2. The order of the dissociation energies is as follows: **PbA** > **PbE2** > **PbC** > **PbF1** > **PbB** > **PbE1** > **PbF2** > **PbG**. This is similar to the order of the stabilities of Pb_2F_2 isomers at BP86/QZ4P level in chapter 4.4.1.1. **PbA** is the most favorable structure in Pb_2F_2 and the following ones are the bent structures of **PbE2** and **PbF1**. The dissociation energies do not show a clear correlation with ΔE_{elstat} or ΔE_{orb}. The doubly bridged structures, **PbA** and **PbC** show large electrostatic interactions and large orbital interactions. The large electrostatic interaction agrees with the charge analysis (chapter 4.4.3) and it is due to the interaction between two large polarized dipoles. The large orbital interaction stems from the favorable donor-acceptor bond as explained at chapter 4.2.1. However, **PbC** is a less stable isomer because the bridged structures show large preparation energies. The order of the bent structures is the same as that of Pb_2H_2. **PbE1** has a smaller dissociation energy than **PbE2** and it comes from the smaller ΔE_{elstat} and ΔE_{orb} values. The smaller ΔE_{elstat} value of **PbE1** arises from the large electrostatic repulsion between two large polarized Pb-F fragments. The smaller ΔE_{orb} stems from the smaller donor-acceptor interaction because the π-interactions of the **PbE1** and **PbF2** isomers are almost the same in each isomers. The smaller donor-acceptor interaction is caused by the larger orbital energy gap between the Pb-F bond orbital and the LUMO of the PbF fragments, $\Delta E_{\pi\text{-PbX}}$, where the Pb-F orbital has a lone-pair orbital character (chapter 4.3.2.1). In the PbF molecule, $\Delta E_{\pi\text{-Pb-X}}$ is larger than that in PbH, and the “lone-pair donor type” acceptor interaction is not so strong as that in Pb_2H_2. **PbB**, **PbE1** and **PbF2** shows smaller electrostatic interactions because of the large polarized PbF molecule.

The group of the other Pb_2X_2 shows a different order of dissociation energies and the order is as follows: **PbA** > **PbE2** > **PbF1** > (**PbB**, **PbC**) > **PbE1** > **PbF2** > **PbG**. The trend of the dissociation energies is similar to that of the relative energies. The isomers of this group prefer the doubly bridged structures **PbA** and the bent structures follow. The dissociation energy does not show a clear correlation with the electrostatic interaction or the orbital interaction, which indicates that both electrostatic interaction and orbital interaction are important for these isomers. The

doubly bridged structures **PbA** and **PbC** lead to a favorable electrostatic interaction because of the strongly polarized PbX fragment and the favorable geometry for the dipole-dipole interaction. **PbA**, **PbB** and **PbC** show larger orbital interactions because of the favorable donor-acceptor bonding situation, the three-center-two-electron bond. However, the dissociation energies of **PbB** and **PbC** are relatively small because of the large preparation energies. **PbE1** and **PbF2** are less favorable than **PbE2** and **PbF1** due to the large electrostatic repulsions and the less effective “lone-pair type” Pb-X bond donor-acceptor interactions.

EDA results presented that the relative energies of Pb_2X_2 isomers correlate with the Pb-Pb bond dissociation energies. The bridged structures **PbA** have the most favorable bond situation of all Pb_2X_2 isomers because the conformation leads the large dipole-dipole electrostatic interactions and the favorable three-center-two-electrons orbital interactions. The bridged structures of Pb_2H_2 show relative large dissociation energies, but the interaction energies of the other isomers are smaller due to the smaller orbital interactions. Due to that, the bent structures become more favorable than **PbB** and **PbC**.

Table 4.4.2.9 Energy decomposition analysis of Pb_2H_2, Pb_2F_2 and Pb_2Cl_2 at BP86/QZ4P level of the Pb-Pb bond using two doublet fragments for **SnA-SnF2**. Two quartet fragments are used for **PbG**. The symmetry in the analysis is C_s except for the **PbA** isomer. All energies are given in kcal/mol.

term	**PbA**	**PbB**	**PbC**	**PbE1**	**PbE2**	**PbF1**	**PbF2**	**PbG**
				Pb_2H_2				
ΔE_{int}	-64.27	-44.16	-56.94	-27.76	-31.96	-30.51	-10.77	-81.13
ΔE_{Pauli}	229.4	138.07	149.21	77.39	74.81	71.11	36.00	117.41
ΔE_{elstat}	-134.86	-94.11	-109.28	-45.70	-61.80	-58.10	-12.38	-73.41
	45.92%	51.64 %	53.01 %	43.46 %	57.89 %	57.18 %	26.48 %	36.98%
ΔE_{orb}	-158.82	-88.11	-96.87	-59.46	-44.96	-43.52	-34.38	-125.13
	54.08%	48.36 %	46.99 %	56.54 %	42.11 %	42.82 %	73.52 %	63.02%
ΔE_{orb}(a')	-158.82	-63.87	-78.70	-36.24	-44.82	-43.38	-16.70	-73.04
	54.08%	72.49%	81.25%	60.95	99.69%	99.69%	48.58%	55.07%
ΔE_{orb}(a'')		-24.25	-18.17	-23.22	-0.14	-0.13	-17.68	-59.70
		27.52%	18.76%	39.05%	0.31%	0.30%	51.43%	45.01%
ΔE_{prep}	6.81	3.72	3.87	1.29	0.98	0.97	0.99	116.17
$\Delta E(=-D_e)$	-57.46	-40.44	-53.07	-26.47	-30.98	-29.54	-9.78	-35.04
				Pb_2F_2				
ΔE_{int}	-62.73	-22.29	-38.69	-11.11	-30.59	-26.07	-7.91	-80.20
ΔE_{Pauli}	194.63	82.49	112.64	32.37	77.57	66.28	25.55	79.16
ΔE_{elstat}	-125.31	-48.28	-93.07	-7.75	-63.02	-51.28	-3.20	-26.72
	48.69 %	46.08 %	61.50 %	17.83 %	58.27 %	55.52 %	9.55%	16.77%
ΔE_{orb}	-132.05	-56.50	-58.26	-35.72	45.14	-41.08	-30.26	-132.63
	51.31 %	53.92 %	38.50 %	82.17 %	41.73 %	44.48 %	90.45%	83.23%
ΔE_{orb}(a')	-132.05	-34.96	-55.88	-14.96	-44.76	-40.78	-11.57	-73.04
	100.00%	61.88%	95.92%	41.88%	99.17%	99.28%	38.24%	55.07%
ΔE_{orb}(a'')		-21.53	-2.38	-20.76	-0.38	-0.30	-18.69	-59.70
		38.11%	4.09%	58.12%	0.84%	0.73%	61.77%	45.01%
ΔE_{prep}	14.40	5.76	12.73	0.99	1.08	0.92	0.97	229.99
$\Delta E(=-D_e)$	-48.33	-16.53	-25.96	-10.12	-29.51	-25.15	-6.94	149.79
				Pb_2Cl_2				
ΔE_{int}	-60.87	-20.19	-29.64	-11.80	-31.87	-26.63	-8.82	-90.89
ΔE_{Pauli}	204.35	83.30	107.33	38.82	84.02	67.63	29.05	83.72
ΔE_{elstat}	-126.00	-42.93	-73.98	-14.60	-67.23	-51.66	-4.86	-34.42
	47.51 %	41.48 %	54.01 %	28.85%	58.01%	54.81%	12.83%	19.71%
ΔE_{orb}	-139.22	-60.57	-63.00	-36.02	-48.66	-42.59	-33.01	-140.18
	52.49%	58.52 %	45.99 %	71.15%	41.99%	45.19%	87.17%	80.29%
ΔE_{orb}(a')	-139.22	-38.56	-57.18	-16.00	-47.93	-42.08	-13.98	-74.50
	100.00%	63.67%	90.77%	44.42%	98.50%	98.80%	42.35%	53.15%
ΔE_{orb}(a'')		-22.00	-5.82	-20.01	-0.73	-0.52	-19.03	-65.72
		36.32%	9.24%	55.55%	1.50%	1.22%	57.65%	46.88%
ΔE_{prep}	11.06	4.35	12.50	0.37	1.31	1.02	1.05	212.00
$\Delta E(=-D_e)$	-49.81	-15.84	-17.14	-11.43	-30.56	-25.61	-7.77	121.11

Table 4.1.2.10. Energy decomposition analysis of Pb_2Br_2 and Pb_2I_2 on BP86/QZ4P level of the Pb-Pb bond using two doublet fragments. The symmetry in the analysis is C_s except for the **PbA** isomer. All energies are given in kcal/mol.

Term	**PbA**	**PbB**	**PbC**	**PbE1**	**PbE2**	**PbF1**	**PbF2**	**PbG**
				Pb_2Br_2				
ΔE_{int}	-60.76	-20.9	-28.26	-13.51	-32.3	-26.99	-9.72	-83.55
ΔE_{Pauli}	209.48	86.33	108.21	40.13	88.21	68.91	31.07	82.96
ΔE_{elstat}	-130.80	-44.57	-71.72	-13.02	-70.1	-52.72	-6.48	-34.59
	48.40 %	41.56 %	52.55%	24.27%	58.17%	54.98%	15.88%	20.77%
ΔE_{orb}	-139.44	-62.66	-64.76	-40.62	-50.41	-43.17	-34.31	-131.91
	51.60 %	58.44 %	47.45%	75.73%	41.83%	45.02%	84.12%	79.23%
ΔE_{orb}(a')	-139.44	-40.66	-57.87	-19.34	-49.43	-42.53	-15.18	-68.88
	100.00%	64.89%	89.36%	47.62%	98.06%	98.51%	44.24%	52.22%
ΔE_{orb}(a")		-22.01	-6.89	-21.28	-0.98	-0.64	-19.13	-63.06
		35.12%	10.64%	52.39%	1.94%	1.48%	55.75%	47.80%
ΔE_{prep}	9.98	4.02	11.72	1.11	1.41	1.07	1.10	193.40
$\Delta E(=-D_e)$	-50.78	-16.88	-16.54	-12.40	-30.89	-25.92	-8.62	109.85
				Pb_2I_2				
ΔE_{int}	-60.86	-22.46	-27.29	-14.93	-33.09	-27.34	-10.94	-75.56
ΔE_{Pauli}	215.14	91.65	110.12	44.22	94.22	70.07	34.06	84.22
ΔE_{elstat}	-134.94	-47.92	-70.14	-16.21	-73.99	-53.53	-8.74	-36.73
	48.89%	42.00 %	51.04%	27.40%	58.12%	54.95%	19.41 %	22.9%
ΔE_{orb}	-141.06	-66.18	-67.27	-42.95	-53.32	-43.89	-36.27	-123.05
	51.11%	58.00 %	48.96%	72.60%	41.88%	45.05%	80.59 %	77.0%
ΔE_{orb}(a')	-141.06	-44.08	-58.94	-21.59	-51.86	-43.07	-17.08	-63.03
	100.00%	66.61%	87.62%	50.27%	97.26%	98.14%	47.09%	51.2%
ΔE_{orb}(a")		-22.10	-8.33	-21.35	-1.46	-0.82	-19.19	-60.04
		33.39%	12.38%	49.71%	2.74%)	1.87%	52.91%	48.7%
ΔE_{prep}	8.63	3.63	10.45	1.16	1.58	1.13	1.16	168.70
$\Delta E(=-D_e)$	-52.23	-18.83	-16.84	-13.77	-31.51	-26.21	-9.78	93.14

4.4.3 Summary

Chapter 4.4 presented the stability, orbital analyses and EDA results of the Pb_2X_2 molecules. The global minima for these isomers are the doubly bridged structures, **PbA**. The Pb-Pb bond length and the angles show a correlation with the halogen atoms.

The analyses of the PbX molecules presented that the formation of the linear X-Pb≡Pb-X with the Pb≡Pb triple bond is quite unfavorable due to the negative dissociation energies arising from the large $a^4\Sigma \leftarrow X^2\Pi$ excitation energies, where the dissociation energies of the X-Pb≡Pb-X triple bond are more negative than those of the Sn≡Sn triple bonds. As a result, the PbX molecules in the $X^2\Pi$ ground state prefer the bond formation in a sideway fashion. The orbital analyses of the PbX molecules clearly showed that the lone-pair orbitals of the PbX molecules are mainly composed of the *s* atomic orbital of Pb, and the X atoms have an effect on only the Pb-X bond orbital, although the orbital energies of the lone-pair orbital and the E-X bond orbitals depend on both E and X elements for SiX, GeX, and SnX. However, the Pb-X bond orbitals have a character of lone-pair orbital, although the corresponding orbitals of SiX, GeX and SnX molecules do not have.

The orbital analyses of Pb_2X_2 presented that the orbital interaction models of two PbX fragments are quite sensible. The Pb_2X_2 isomers are categorized to σ-type isomers and π-type isomers. **PbA** has one σ-type bond and two Pb-X bond donor-acceptor bonds and these donor-acceptor bonds form the effective bonding situation by a three-center-two-electron interaction. Due to that, **PbA** is the most stable isomer. The π-type Pb-Pb bonds of **PbB**, **PbC**, **PbE1** and **PbF2** can rotate easily and the isomers are transition states for the reason that the π-type orbital are high in energy. The orbital energies of the “lone-pair like” orbitals of **PbE1** and **PbF2** are more lower in energy than those of **PbE2** and **PbF1**, and the stabilization energies stem from the interaction with the vacant π orbital.

AIM analyses presented no charge accumulation for the Pb_2X_2 molecules between the Pb atoms. This suggests that the electrostatic interaction is important for the Pb-Pb bond formation. The charge accumulation becomes smaller as the element

of group 14 gets heavier. The bond paths proved that **PbA**, **PbB** and **PbC** have ring structures.

The charge analyses of the PbX fragments showed that the PbX molecules are electrostatically strongly polarized. The large partial charges of the PbX molecules suggest that the bridged structure produces a favorable dipole-dipole interaction, although the geometry of the bent-structures leads to an electrostatic repulsion.

The EDA results presented that the dissociation energies correlate with the stability of the isomers. The doubly bridged structures **PbA** have the most favorable bond situation due to the large orbital interaction arising form the efficient three-center-two-electron bonds and due to the large electrostatic interaction stemming from the large dipole-dipole interactions. The bent structures are less favorable because of the less effective donor-acceptor interactions and the smaller electrostatic interactions.

4.4 Pb_2X_2 Molecules

The nature of the chemical bond
is the problem at the heart of all chemistry.

Bryce L. Crawford Jr. 1953

5. Conclusion

In this study, the isomers of E_2X_2 (E=Si-Pb, X=H, F, Cl, Br and I) were investigated. In most structures, the E-E bond length and the E-X-E angle correlate with the halogen atoms. The relative energies showed that the non-planar doubly bridged structures **A** are global minima for all investigated E_2X_2 molecules except for Si_2F_2, although the global minimum for Si_2F_2 is the vinylidene structure in the triplet state **D(T)**. The linear isomers **G** are always found as energetically higher lying transition states. The relative energies of the E_2H_2 isomers showed a trend that prefers bridged structures, **A**, **B** and **C**, followed by the vinylidene structures. For the Si_2F_2 isomers, the bridged structures **A**, **B** and **C** are less favorable than the bent structures and the isomers are shifted to the energetically unstable direction. As a result, the isomer **SiA** is a local minimum and the vinlylidene structure **SiD(T)** becomes a global minimum. For the other E_2X_2 isomers (X=F, Cl, Br, I), non-planar doubly bridged structures **A** are still found as global minima apart from Si_2F_2. However, the other bridged structures **B** and **C** are less stable than the bent structure **E2**.

The investigation of the EX fragments presented that the molecules need very high excitation energies from the $X^2\Pi$ ground state to the $a^4\Sigma^-$ first excited state. Due to the large excitation energies, the bond dissociation energies of the linear XEEX structures are very small, or negative, and it is found that the E-E triple bond formation is quite unfavorable. Instead of the triple bond formation, the EX molecules interact with each other in a side-ways fashion in their $X^2\Pi$ ground states. The orbital analyses showed that the EX fragments in their $X^2\Pi$ ground state have a half-occupied π-type orbital and two types of occupied orbitals: a σ-type lone-pair orbital and a σ-type E-X bond orbital. The other π-type orbital is found as an unoccupied orbital, and this vacant orbital could work as an acceptor in a donor-acceptor interaction. The character of the σ-type orbitals depends on the E atom, and especially, the orbitals of the PbX molecules present a different character from the other EX molecules. For the SiX, GeX, and SnX molecules, the orbital energies of the

lone-pair orbital and the E-X bond orbitals depend on both E and X elements, although the X atom have an effect on only the Pb-X bond orbital, because the lone-pair orbitals of the PbX molecules are mainly composed of the *s* atomic orbital of Pb. Due to that, the lone-pair orbitals of the PbX molecules does not interact with the vacant π-orbital, although the lone-pair orbital of SiX, GeX and SnX interact with the LUMO and they form lone-pair donor-acceptor bonding. Instead of that, for the PbX molecules, the Pb-X bond orbitals have a character of the lone-pair orbital and the PbX bond orbital can interact with the vacant π orbital. However, the interaction is not as favorable as the Pb-X bond donor-acceptor interaction.

The orbital analyses of E_2X_2 presented that the isomers are categorized to two groups: σ-type isomers and π-type isomers. The σ-type isomers **A**, **E2**, **F1** have a σ-type orbital, and the non-planar doubly bridged structures **A** have also two E-X bond donor-acceptor bonds that lead effective bonding interactions: a three-center-two-electron bond. As a consequence, the structures **A** have three bonding components and the structures **A** have a very effective bonding situation. The π-type isomers, **B**, **C**, **E1** and **F2** have a π-type orbital. The energies of π-type orbitals are higher in energy and the π-type isomers are often found as transition states.

The AIM analyses exhibited the presence of the bondings and their character. The bridged structures **A**, **B** and **C** have E-X-E ring structures. The charge accumulation of the bent structures indicated the different E-E bond character of **E1**, **F2** and **E2**, **F1**. In general, the charge accumulation becomes smaller as the E atom gets heavier.

The charge analyses presented that the EX molecules are dipoles, and the EX molecules behave larger dipoles as the halogen atom gets heavier. The bridged structures lead to effective electrostatic interactions between two EX fragments. On the other hand, the bent structures are unfavorable because these configurations lead to large electrostatic repulsions.

The Energy Decomposion Analyses presented that the stability of the E_2X_2 molecules correlate with the bond dissociation energies. The non-planar doubly bridged structures **A** show the largest dissociation energies. The large dissociation energies of **A** stem from the large dipole-dipole electrostatic interactions and the effective three-center-two-electron orbital interaction. The preparation energies of the

bridged structures are larger than those of the bent structures due to the elongation of E-X bond to form the E-X-E bridged structure. The ring structures of Si_2X_2 show large preparation energies and those of Si_2F_2 are especially quite large. Due to that, the doubly bridged structures cannot compensate the energetic loss of the E-X bond elongation to form bridged structures. As a result, the dissociation energies of **SiA** for Si_2F_2 become smaller and the isomer cannot be the global minimum. The bent structures show often weaker electrostatic interactions and orbital interactions than the bridged structures. The smaller electrostatic interaction values stem from the large electrostatic repulsions between the positively charged E atoms. The smaller orbital interaction values arise from the less effective orbital interactions: the lone-pair donor-acceptor for Si_2X_2, Ge_2X_2 and Sn_2X_2, and the lone-pair type donor-acceptor of Pb-X bond orbitals for Pb_2X_2. The linear structures **G** are always quite unfavorable structures due to the large preparation energies which arise mainly from the $X^2\Pi \leftarrow a^4\Sigma^-$ excitation, although the structures show large orbital interaction energies by forming the ideal E-E triple bond.

No science has ever made more rapid progress
in a shorter time than chemistry.

Martin Heinrich Kloproth, 1791

6. References

[1] Weidenbruch, M. *Angew. Chem., Int. Ed.* **2003**, *42*, 2222.

[2] Weidenbruch, M. *J. Organomet. Chem*. **2002**, *646*, 39.

[3] Power, P. P. *Chem. Rev*. **1999**, *99*, 3463.

[4] Lawrence, S. C.; Wasserman, Z. R.; Moskowitz, J. W. *Int. J. Quantum. Chem.* **1982**, *21*, 565.

[5] Lischka, H.; Köhler, H. *J. Am. Chem. Soc*. **1983**, *105*, 6646.

[6] Binkley, J. S. *J. Am. Chem. Soc.* **1984**, *106*, 603.

[7] Kalcher, J.; Sax, A.; Olbrich, G. *Int. J. Quantum Chem*. **1984,** *25*, 543.

[8] Köhler, H.-J.; Lischka, H. *Chem. Phys. Lett*. **1984**, *112*, 33.

[9] Clabo, D. A.; Schaefer, H. F. *J. Chem. Phys*. **1986**, *84*, 1664.

[10] Luke, B. T.; Pople, J. A.; Krogh-Jespersen, M.-B.; Apeloig, Y.; Karni, M.; Chandrasekhar, J.; Schleyer, P. v. R. *J. Am. Chem. Soc.* **1986**, *108*, 270.

[11] Koseki, S.; Gordon, M. S. *J. Phys. Chem*. **1988**, *92*, 364.

[12] Koseki, S.; Gordon, M. S. *J. Phys. Chem*. **1989**, *93*, 118.

[13] Sax, A. F.; Kalcher, J. *J. Mol. Struct.: THEOCHEM* **1990**, *208*, 123.

[14] Colegrove, B. T.; Schaefer, H. F. *J. Phys. Chem.* **1990**, *94*, 5593.

[15] Grev, R. S. *Adv. Organomet. Chem*. **1991**, *33*, 125.

[16] Grev, R. S.; Schaefer, H. F. *J. Chem. Phys*. **1992**, *97*, 7990.

[17] Hühn, M. M.; Amos, R. D.; Kobayashi, R.; Handy, N. C. *J. Chem. Phys.* **1993**, *98*, 7107.

[18] Jursic, B. S. *J. Mol. Struct.: THEOCHEM* **1999**, *491*, 1.

[19] Jursic, B. S. *J. Mol. Struct.: THEOCHEM* **2000**, *497*, 65.

[20] Krüger, T.; Sax, A. F. *J. Comput. Chem.* **2001**, *22*, 151.

[21] Nagase, S.; Kobayashi, K.; Takagi, N. *J. Organomet. Chem*. **2000**, *611*, 264.

[22] Takahashi, M.; Kawazoe, Y. *Organometallics* **2000**, *611*, 264.

[23] Damrauer, R. Noble, A. L. *Organometallics* **2008**, *27*, 1707.

[24] Dolgonos, G. *Chem. Phys. Lett.* **2008**, *454*, 190.

[25] Dolgonos, G. *Chem. Phys. Lett.* **2008**, *457*, 453.

[26] Yamaguchi, Y.; Deleeuw, B. J.; Richards, C. A.; Schaefer, H. F.; Frenking, G. *J. Am. Chem. Soc.* **1994**, *116*, 11922.

[27] Grev, R. S.; De Leeuw, B. J.; Schaefer, H. F. *Chem. Phys. Lett*. **1990**, *165*, 257.

[28] Palagyi, Z.; Schaefer, H. F.; Kapuy, E. *J. Am. Chem. Soc.* **1993**, *115*, 6901.

[29] Boone, A. J.; Magers, D. H.; Leszczynski, J. *Int. J. Quantum Chem.* **1998**, *70*, 925.

[30] Li, Q.-S.; Lu, R.-H.; Xie, Y.; Schaefer, H. F. *J. Comput. Chem*. **2002**, *23*, 1642.

[31] Han, Y.-K.; Bae, C.; Lee, Y. S.; Lee, S. Y. *J. Comput. Chem.* **1998**, *19*, 1526.

[32] Chen, Y.; Hartmann, M.; Diedenhofen, M.; Frenking, G. *Angew. Chem., Int. Ed*. **2001**, *40*, 2052.

[33] Bogey, M.; Bolvin, H.; Demuyneck, C.; Destombes, J.-L. *Phys. Rev. Lett.* **1991**, *66*, 413.

[34] Bogey, M.; Bolvin, H.; Cordonnier, M.; Demuynck, C.; Destombes, J. L.; Császár, A. G. *J. Chem. Phys.* **1994**, *100*, 8614.

[35] Cordonnier, M.; Bogey, M.; Demuynck, C.; Destombes, J.-L. *J. Chem. Phys.* **1992**, *97*, 7984.

[36] Demuynck, C. *J. Mol. Spectrosc.* **1994**, 168, 215.

[37] Andrews, L.; Wang, X. *J. Phys. Chem. A* **2002**, *106*, 7696.

[38] Nakajima, Y.; Tonokura, K.; Sugimoto, K.; Koshi, M. *Int. J. Chem. Kinet.* **2001**, 33, 136.

[39] Wang, X.; Andrews, L.; Kushto, G. *J. Phys. Chem. A* **2002**, *106*, 5809.

[40] Wang, X.; Andrews, L.; Chertihin, G. V.; Souer, P. F. *J. Phys. Chem. A* **2002**, *106*, 6302.

[41] Wang, X.; Andrews, L. *J. Am. Chem. Soc*. **2003**, *125*, 6581.

[42] Thies, B. S.; Grev, R. S.; Schaefer, H. F. *Chem. Phys. Lett*. **1987**, *140*, 355.

[43] Colegrove, B. T.; Schaefer, H. F. *J. Am. Chem. Soc*. **1991**, *113*, 1557.

[44] Jacobsen. H. *Chem. Eur. J.* **2010**, *16*, 976.

[45] Pu, L.; Twamley, B.; Power, P. P. *J. Am. Chem. Soc.* **2000**, *122*, 3524.

[46] Jung, Y.; Brynda, M.; Power, P. P.; Head-Gordon, M. *J. Am. Chem. Soc.* **2006**, *128*, 7185.

[47] Phillips, A. D.; Wright, R. J.; Olmstead, M. M.; Power, P. P. *J. Am. Chem. Soc.* **2002**, *124*, 5930.

[48] Stender, M.; Phillips, A. D.; Wright, R. J.; Power, P. P. *Angew. Chem., Int. Ed.* **2002**, *41*, 1785.

[49] Pietschnig, R.; West, R.; Powell, D. P.; *Organometallics* **2000,** *19*, 2724-2729

[50] Wiberg, N.; Niedermeyer, Fischer, G.; Nöth, H.; Suter, M. *Eur. J. Inorg. Chem*. **2002**, 1066.

[51] Wiberg, N.; Vasisht, S. K.; Fischer, G.; Mayer, P. *Z. Allg. Anorg. Chem.* **2004**, *630*, 1823.

[52] Takagi, N.; Nagase, S. *Eur. J. Inorg. Chem*. **2002**, 2775.

[53] Karni, M.; Apeloig, Y.; Takagi, N.; Nagase, S. *Organometallics* **2005**, *24*, 6319.

[54] Sekiguchi, A.; Kinjo, R.; Ichinohe, M. *Science* **2004**, *305*, 1755.

[55] Kravchenko, V.; Kinjo, R.; Sekiguchi, A.; Ichinohe, M.; West, R.; Balazs, Y. S.; Schmidt, A.; Karni, M.; Apeloig, Y. *J. Am. Chem. Soc.* **2006**, *128*, 14472.

[56] Kobayashi, K.; Nagase, S. *Organometallics* **1997**, *16*, 2489.

[57] Power, P.P. *Chem. Commun.* **2003**, 2091.

[58] Rivard, E.; Power, P. P. *Inorg. Chem*. **2007**, *46*, 10047.

[59] Allen, T. L.; Fink, W. H.; Power, P. P. *J. Chem. Soc. Dalton Trans.* **2000**, 407.

[60] Kobayashi, K.; Takagi, N.; Nagase, S. *Organometallics* **2001**, *20*, 234.

[61] Takagi, N.; Nagase, S. *Organometallics* **2001**, *20*, 5498.

[62] Danovich, D.; Ogliaro, F.; Karni, M.; Apeloig, Y.; Cooper, D. L.; Shaik, S. *Angew. Chem., Int. Ed.* **2001**, *40*, 4023.

[63] Grunenberg, J. *Angew. Chem., Int. Ed.* **2001**, 40, *113*, 4027.

[64] Bridgtman, A. J.; Ireland, L.R. *Polyhedron* **2001**, *20*, 2841.

[65] Himmel, H.-J.; Schnöckel, H. *Chem. Eur. J*. **2003**, *9*, 748.

[66] Sugiyama, Y.; Sasamori, T.; Hosoi, Y.; Furukawa, Y.; Takagi, N.; Nagase, S.; Tokitoh, N. *J. Am. Chem. Soc*. **2006**, *128*, 1023.

[67] Fischer, R. C.; Fettinger, J. C.; Brynda, M. A.; Power, P. P. *J. Am. Chem. Soc*. **2006**, 128, 11366.

[68] Sekiguchi, A.; Ichinohe, M.; Kinjo, R. *Bull. Chem. Soc. Jpn.* **2006**, *79*, 825.

[69] Scemama, A.; Caffarel, M.; Savin, A. *J. Comp. Chem.* **2007**, *28*, 442.

[70] Takagi, N.; Nagase, S. *Organometallics* **2007**, *26*, 3627

[71] Takagi, N.; Nagase, S. J. *Organomet. Chem.* **2007**, *692*, 217.

[72] Sekiguchi, A. *Pure Appl. Chem.* **2008**, *80*, 447.

[73] Takahashi, M.; Sakamoto, K. *J. Phys. Chem. A* **2004**, *108*, 5710.

[74] Takahashi, M.; Kawazoe, Y. *Organometallics* **2008**, *27*, 4829.

[75] Li, G.; Li, Q.; Xu, W.; Xie, Y.; Schaefer III, H. F.; *Mol. Phys.* **2001**, *99*, 1053.

[76] Li, Q.; Li, G.; Xu, W.; Xie, Y.; Schaefer III, H. F.; *ChemPhysChem* **2002**, *3*, 179.

[77] Malcolm, N. O. J.; Gillespie, R. J.; Popelier, P. L. A. *J. Chem. Soc., Dalton Trans*. **2002**, 3333.

[78] Pignedoli, C. A.; Curioni, A.; Andreoni, W. *ChemPhysChem* **2005**, *6*, 1795.

[79] Chesnut, D. B. *Chem. Phys.* **2006**, 327, 327.

[80] Firme, C. L.; Antunes, O. A. C.; Esteves, P. M. *Chem. Phys. Lett.* **2009**, *468*, 129.

[81] Trinquier, G.; Malrieu, J.-P. *J. Am. Chem. Soc*. **1987**, *109*, 5303.

[82] Malrieu, J.-P.; Trinquier, G. *J. Am. Chem. Soc*. **1989**, *111*, 5916.

[83] Carter, E. A.; Goddard, W. A. *J. Phys. Chem.* **1986**, *90*, 998.

[84] Jacobsen, H.; Ziegler, T., *J. Am. Chem. Soc*. **1994**, *116*, 3667.

[85] Driess, M.; Grützmacher, H. *Angew. Chem., Int. Ed.* **1996**, *35*, 828.

[86] Kapp, J.; Remko, M.; Schleyer, P. v. R. *Inorg. Chem.***1997**, *36*, 4241.

[87] Lein, M.; Krapp, A.; Frenking, G. *J. Am Chem. Soc.* **2005**. *127*, 6290.

[88] Diefenbach, A.; Bickelhaupt, F. M.; Frenking, G. *J. Am. Chem. Soc*. **2000**, *122*, 6449.

[89] Uddin, J.; Frenking, G. *J. Am. Chem. Soc.* **2001**, *123*, 1683.

[90] Lein, M.; Frunzke, J.; Timoshkin, A.; Frenking, G. *Chem. Eur. J.* **2001**, *7*, 4155.

[91] Frenking, G.; Wichmann, K.; Fröhlich, N.; Grobe, J.; Golla, W.; Le Van, D.; Krebs, B.; Läge, M. *Organometallics* **2002**, *21*, 2921.

[92] Frunzke, J.; Lein, M.; Frenking, G. *Organometallics* **2002**, *21*, 3351.

[93] Cases, M.; Frenking, G.; Duran, M.; Solà, M. *Organometallics* **2002**, *21*, 4182.

[94] Rayón, V. M.; Frenking, G. *Chem. Eur. J.* **2002**, *8*, 4693.

[95] Nemcsok, D. S.; Kovács, A.; Rayón, V. M.; Frenking, G. *Organometallics* **2002**, *21*, 5803.

[96] Dörr, M.; Frenking, G. *Z. Allg. Anorg. Chem.* **2002**, *628*, 843.

[97] Loschen, C.; Voigt, K.; Frunzke, J.; Diefenbach, A.; Diedenhofen, M.; Frenking, G. *Z. Allg. Anorg. Chem.* **2002**, *628*, 1294.

[98] Pandey, K. K.; Lein, M.; Frenking, G. *J. Am. Chem. Soc.* **2003**, *125*, 1660.

[99] Lein, M.; Frunzke, J.; Frenking, G. *Angew. Chem., Int. Ed.* **2003**, *42*, 1303.

[100] Lein, M.; Frunzke, J.; Frenking, G. *Inorg. Chem.* **2003**, *42*, 2504.

[101] Massera, C.; Frenking, G. *Organometallics* **2003**, *22*, 2758.

[102] Rayón, V. M.; Frenking, G. *Organometallics* **2003**, *22*, 3304.

[103] Esterhuysen, C.; Frenking, G. *Chem. Eur. J.* **2003**, *9*, 3518.

[104] Dietz, O.; Rayón, V. M.; Frenking, G. *Inorg. Chem.* **2003**, *42*, 4977.

[105] Lein, M.; Szabó, A.; Kovács, A.; Frenking, G. *Faraday Discuss.* **2003**, *124*, 365.

[106] Esterhuysen, C.; Frenking, G. *Chem. Eur. J.* **2003**, *9*, 3518.

[107] Bessac, F.; Frenking, G. *Inorg. Chem.* **2003**, *42*, 7990.

[108] Loschen, C.; Frenking, G. *Inorg. Chem.* **2004**, *43*, 778.

[109] Nechaev, M. S.; Rayón, V. M.; Frenking, G. *J. Phys. Chem. A* **2004**, *108*, 3134.

[110] Pandey, K. K.; Lein, M.; Frenking, G. *Organometallics* **2004**, *23*, 2944.

[111] Petz, W.; Kutschera, C.; Heitbaum, M.; Frenking, G.; Tonner, R.; Neumüller, B. *Inorg. Chem.* **2005**, *44*, 1263.

[112] Frenking, G.; Solà, M.; Vyboishchikov, S. F. *J. Organomet. Chem.* **2005**, *690* 6178.

[113] Poleshchuk, O. K.; Shevchenko, E. L.; Branchadell, V.; Lein, M.; Frenking, G. *Int. J. Quantum Chem.* **2005**, *101*, 869.

[114] Bessac, F.; Frenking, G. *Inorg. Chem.* **2006**, *45*, 6956.

[115] Calhorda, M. J.; Krapp, A.; Frenking, G. *J. Phys. Chem. A* **2007**, *111*, 2859.

[116] Krapp, A.; Pandey, K. K.; Frenking, G. *J. Am. Chem. Soc.* **2007**, *129*, 7596.

[117] Tonner, R.; Frenking, G. *Angew. Chem., Int. Ed.* **2007**, *46*, 8695.

[118] Tonner, R.; Heydenrych, G.; Frenking, G. *Chem. Asian J.* **2007**, *2*, 1555.

[119] Tonner, R.; Frenking, G.; Neumüller, B.; Dehnicke, K. *Z. Allg. Anorg. Chem.* **2007**, *633*, 1183.

[120] Fernández, I.; Uggerud, E.; Frenking, G. *Chem. Eur. J.* **2007**, *13*, 8620.

[121] Fernández, I.; Cerpa, E.; Merino, G.; Frenking, G. *Organometallics* **2008**, *27*, 1106.

[122] Caramori, G. F.; Frenking, G. *Organometallics* **2007**, *26*, 5815.

[123] Tonner, R.; Frenking, G. *Chem. Eur. J.* **2008**, *14*, 3260.

[124] Tonner, R.; Frenking, G. *Chem. Eur. J.* **2008**, *14*, 3273.

[125] Hahn, F. E.; Zabula, A. V.; Pape, T.; Hepp, A.; Tonner, R.; Haunschild, R.; Frenking, G. *Chem. Eur. J.* **2008**, *14*, 10716

[126] Krapp, A.; Frenking, G. *J. Am. Chem. Soc.* **2008**, *130*, 16646.

[127] Caramori, G. F.; Frenking, G. *Theor. Chem. Acc.* **2008**, *120*, 351.

[128] Mück, L. A.; Timoshkin, A. Y.; Hopffgarten, M. v.; Frenking, G. *J. Am. Chem. Soc.* **2009**, *131*, 3942.

[129] Fernández, I.; Frenking, G.; Uggerud, E. *Chem. Eur. J.* **2009**, *15*, 2166.

[130] Heydenrych, G.; Hopffgarten, M, v.; Stander, E.; Schuster, O.; Raubenheimer, H. G.; Frenking, G. *Eur. J. Inorg. Chem.* **2009**, 1892.

[131] Prabusankar, G.; Gemel, C.; Parameswaran, P.; Flener, C.; Frenking, G.; Fischer, R. A. *Angew. Chem., Int. Ed.* **2009**, *48*, 5526.

[132] Erhardt, S.; Frenking, G. *J. Organomet. Chem.* **2009**, *694*, 1091.

[133] Esterhuysen, C.; Frenking, G. *Theor. Chem. Acc.* **2004**, *111*, 381.

[134] Kovács, A.; Esterhuysen, C.; Frenking, G. *Chem. Eur. J.* **2005**, 11, 1813.

[135] Cappel, D.; Tüllmann, S.; Krapp, A.; Frenking, G. *Angew. Chem., Int. Ed.* **2005**, *44*, 3617.

[136] Szabó, A.; Kovács, A.; Frenking, G. *Z. Anorg. Allg. Chem.* **2005**, *631*, 1803.

[137] Fernández, I.; Frenking, G. *Chem. Commun.* **2006**, 5030.

[138] Fernández, I.; Frenking, G. *Chem. Eur. J.* **2007**, *13*, 5873.

[139] Fernández, I.; Frenking, G. *J. Phys. Chem. A* **2007**, *111*, 8028.

[140] Fernández, I.; Frenking, G. *J. Org. Chem.* **2007**, *72*, 7367.

[141] Gayatri, G.; Soujanya, Y.; Fernández, I.; Frenking, G.; Sastry, G. N. *J. Phys. Chem. A* **2008**, *112*, 12919.

[142] Planck, M. *Ann. Phys.* **1901**, *4*, 553.

[143] Einstein, A, *Ann. Phys.* **1905**, *17*, 132.

[144] de Broglie, L. *Ann, de Physique* **1925**, *3*, 22.

[145] Szabo, A.; Ostlund, N. S. *Modern Quantum Chemistry: Introduction to Advanced Electonic Structure Theory 1st. Ed.* McGraw-Hill, New York, 1989.

[146] Jensen, F. *Introduction to Computational Chemistry* Wiley, Chichester, England, 1999.

[147] Cramer, C. J. *Essentials of Computational Chemistry. Theories and Models.* Wiley, Chichester, England, 2002.

[148] Atkins, P.; Friedman, R. *Molecular Quantum Mechanics* Oxford University Press, USA, 2005.

[149] Parr, R. G.; Yang, W. *Density-Functional Theory of Atoms and Molecules* Oxford University Press, USA, 1994.

[150] Fiolhais, C.; Nogueira, F.; Marques, Miguel A.L. (Eds.) *A Primer in Density Functional Theory (Lecture Notes in Physics)* Springer-Verlag, Berlin, Germany, 2003.

[151] Schrödinger, E. *Ann. Phys.* **1926**, *79*, 361.

[152] Born, M.; Oppenheimer, R. *Ann. Phys.* **1927**, *84*, 457.

[153] MacDonald, J. K. L. *Phys. Rev.* **1933**, *43*, 830.

[154] MacDonald, J. K. L. *Phys. Rev.* **1934**, *46*, 828.

[155] Pauli, W. *Z. Physik* **1925**, *31*, 765.

[156] Slater, J. C. *Phys. Rev.* **1929**, *34*, 1293.

[157] Slater, J. C. *Phys. Rev.* **1951**, *81*, 385.

[158] Hartree, D. R. *Proc. Camb. Phil. Soc.* **1928**, *24*, 89.

[159] Hartree, D. R. *Proc. Camb. Phil. Soc.* **1928**, *24*, 111.

[160] Fock, V.; *Z. Phys.* **1930**, *61*, 126.

[161] Roothaan, C. C. J. *Rev. Mod. Phys.* **1951**, *23*, 69.

[162] Hall, G. G. *Proc. R. Soc. London Ser. A,* **1951**, *205*, 541.

[163] Löwdin, P.-O. *Rev. Modern. Phys.* **1955**, *27*, 1509.

[164] Møller, C.; Plesset, M. S. *Phys. Rev.* **1934**, *46*, 618.

[165] Grimme, S. *J. Chem. Phys.* **2003**, *118*, 9095.

[166] Coester, F. *Nucl. Phys.* **1958**, *7*, 421.

[167] Coester, F.; Kummel, H. *Nucl. Phys.* **1960**, *17*, 477.

[168] Čížek, J. *J. Chem. Phys.* **1960**, *45*, 4256.

[169] Čížek, J. *Adv. Chem. Phys.* **1969**, *14*, 35.

[170] Bartlett, J. *Ann. Rev. Phys. Chem.* **1981**, *32*, 359.

[171] Brillouin, L. *Actualities Sci. Ind.* **1934**, *71*, 159.

[172] Raghavachari, K.; Trucks, G. W.; Pople, J. A.; Head-Gordon, M. *Chem. Phys. Lett.* **1989**, *157*, 479.

[173] Das G.; Wahl, A.C. *J. Chem. Phys.* **1972**, *56*, 1769.

[174] Schmidt, M. W.; Gordon, M. S. *Annu. Rev. Phys. Chem.* **1998**, *49*, 233.

[175] Lie, G.C.; Hinze, J. *J. Chem. Phys.* **1973**, *59*, 1872

[176] Buenker, R. J.; Peyerimhoff, S. D. *Theor. Chim. Acta* **1974**, *35*, 33

[177] Hohenberg, P.; Kohn, W. *Phys. Rev. B* **1964**, *136*, 864.

[178] Levy, M. *Proc. Natl. Acad. Sci.* U.S.A. **1979**, *76*, 6062.

[179] Kohn, W.; Sham, L. J. *Phys. Rev. A*, **1965**, *140*, 1133.

[180] Gritsenko, O. V.; Baerends, E. J. *Theor. Chim. Acta* **1997**, *96*, 44.

[181] Baerends, E. J. *Theor. Chem. Acc.* **2000**, *103*, 265.

[182] Stowasser, R.; Hoffmann, R. *J. Am. Chem. Soc.* **1999**, *121*, 3414.

[183] Kohn, W.; Becke, A. D.; Parr, R. G. *J. Phys. Chem.* **1996**, *100*, 12974.

[184] Bloch, F. *Z. Physik* **1929**, *57*, 545.

[185] Dirac, P. A. M. *Proc. Camb. Phil. Soc.* **1930**, *26*, 376.

[186] Vosko, S. J.; Wilk, L.; Nusair. M. *Can. J. Phys*, **1980**, *58*, 1200.

[187] Ceperley, D. M.; Alder, B. J. *Phys. Rev. Lett.* **1980**, *45*, 566.

[188] Becke, A. D. *Phys. Rev. A* **1988**, *38*, 3098.

[189] Perdew, J. P. *Phys. Rev. B* **1986**, *33*, 8822.

[190] Perdew, J. P. *Phys. Rev. B* **1986**, *34*, 7406.

[191] Slater, J. C. *Phys. Rev.* **1930**, *36*, 57.

[192] Dunning, Jr. T. H. *J. Chem. Phys.* **1989**, *90*, 1007.

[193] Kendall, R.A.; Dunning, Jr. T. H.; Harrison, R. J. *J. Chem. Phys.* **1992**, *96*, 6796.

[194] Woon, D. E.; Dunning, Jr. T. H. *J. Chem. Phys.* **1993**, *98*, 1358.

[195] Woon, D. E.; Dunning, Jr. T. H. *J. Chem. Phys.* **1994**, *100*, 2975.

[196] Dunning, Jr. T. H. *J. Chem. Phys.* **1989**, *90*, 1007.

[197] Woon, D. E.; Dunning, Jr. T. H. *J. Chem. Phys.* **1995**, *103*, 4573.

[198] Wilson, A. K.; Mourik, T. v.; Dunning, Jr. T. H.; *J. Mol. Struct.: THEOCHEM* **1996**, *388*, 339.

[199] Peterson, K. A.; Dunning, Jr. T. H. *J. Chem. Phys.* **1995**, *102*, 2032.

[200] Wilson, A. K.; Woon, D. E.; Peterson, K. A.; Dunning, Jr. T. H. *J. Chem. Phys.* **1999**, *110*, 7667.

[201] Mourik T. v.; Dunning, Jr. T. H. *Int. J. Quantum Chem.* **2000**, *76*, 205.

[202] Wilson, A. K.; Woon, D. E.; Peterson, K. A.; Dunning, Jr. T. H. *J. Chem. Phys.* **1999**, *110*, 7667

[203] Dunning, T. H.; Peterson, K. A. Wilson, A. K. *J. Chem. Phys.* **1999**, *114*, 9244.

[204] Peterson, K. A. *J. Chem. Phys.* **2003**, *119*, 11099.

[205] Peterson, K. A.; Figgen, D.; Goll, E.; Stoll, H.; Dolg, M. *J. Chem. Phys.* **2003**, *119*, 11113.

[206] Peterson, K. A.; Shepler, B. C.; Figgen, D.; Stoll, H. *J. Phys. Chem. A* **2006**, *110*, 13877.

[207] Hellmann, H. *J. Chem. Phys.* **1935**, *3*, 61.

[208] Einstein, A. *Ann. Phys.* **1905**, *17*, 891.

[209] Dirac, P. A. M. *Roy. Soc. Proc. A* **1928**, *117*, 610.

[210] Snijders, J. G.; Baerends, E. J. *Mol. Phys.* **1978**, *36*, 1789.

[211] Snijders, J. G.; Baerends, E. J.; Ros, P. *Mol. Phys.* **1979**, *38*, 1909.

[212] Lenthe, E. v.; Baerends, E. J.; Snijders, J. G. *J. Chem. Phys.* **1993**, *99*, 4597.

[213] Lenthe, E. v.; Baerends, E. J.; Snijders, J. G. *J. Chem. Phys.* **1994**, *101*, 9783.

[214] Lenthe, E. v.; Snijders, J. G.; Baerends, E. J. *J. Chem. Phys.* **1996**, *105*, 6505.

[215] Lenthe, E. v.; Leeuwen, R. v.; Baerends, E. J.; Snijders, J. G. *Int. J. Quantum Chem.* **1996**, *57*, 281.

[216] Lenthe, E. v.; Wormer, P. E. S.; Avoird, A. v. d. *J. Chem. Phys.* **1997**, *107*, 2488.

[217] Lenthe, E. v.; Ehlers, A.; Baerends, E. J. *J. Chem. Phys.* **1999**, *110*, 8943.

[218] Eyring, H. *J. Chem. Phys.* **1935**, *3*, 107.

[219] Morokuma, K. *J. Chem. Phys.* **1971**, *55*, 1236.

[220] Kitaura, K.; Morokuma, K. *Int. J. Quantum Chem.* **1976**, *10*, 325.

[221] Morokuma, K. *Acc. Chem. Res.* **1977**, *10*, 294.

[222] Morokuma, K. *J. Am. Chem. Soc.* **1977**, *99*, 1316.

[223] Morokuma, K.; Umeyama, H. *Chem. Phys. Lett.* **1977**, *49*, 333.

[224] Ziegler, T.; Rauk, A. *Theor. Chim. Acta* **1977**, *46*, 1.

[225] Ziegler, T.; Rauk, A. *Inorg. Chem.* **1979**, *18*, 1558.

[226] Ziegler, T.; Rauk, A. *Inorg. Chem.* **1979**, *18*, 1755.

[227] Ziegler, T.; Tschinke, V.; Ursenbach, C. *J. Am. Chem. Soc.* **1987**, *109*, 4825.

[228] Hirshfeid, F. L. *Theor. Chim. Acta* **1977**, *44*, 129.

[229] Reed, A. E.; Curtiss, L. A.; Weinhold, F. *Chem. Rev.* **1988**, *88*, 899.

[230] Foster, J. P.; Weinhold, F. *J. Am. Chem. Soc.* **1980**, *102*, 7211.

[231] Löwdin, P.-O. *Adv. Phys.* **1956**, *5*, 1.

[232] Reed, A. E.; Weinhold, F. J. *J. Chem. Phys.* **1983**, *78*, 4066.

[233] Reed, A. E.; Weinstock, R. B.; Weinhold, F. *J. Chem. Phys.* **1985**, *83*, 735.

[234] Bader, R. F. W. *Atoms in Molecules: A Quantum Theory*, University of Oxford Press, Oxford, 1990.

[235] Snijders, J. G.; Baerends, E. J.; Vernooijs, P. *At. Nucl. Data Tables* **1982**, *26*, 483.

[236] ADF 2007.01, SCM, Theoretical Chemistry, Vrije Universiteit, Amsterdam, The Netherlands, http://www.scm.com.

[237] Velde, G. t.; Bickelhaupt, F. M.; Baerends, E. J.; Fonseca Guerra, C.; Gisbergen, S. J. A. v.; Snijders, J. G.; Ziegler, T. *J. Comput. Chem.* **2001**, *22*, 931.

[238] Fonseca Guerra, C.; Snijders, J. G.; Velde, G. t.; Baerends, E. J. *Theor. Chem. Acc.* **1998**, *99*, 391.

[239] Hampel, C.; Peterson, K.; Werner, H.-J. *Chem. Phys. Lett.* **1992**, *190*, 1.

[240] Deegan, M. J. O.; Knowles, P. J. *Chem. Phys. Lett.* **1994**, *227*, 321.

[241] Amos, R. D.; Andrews, J. S.; Handy, N. C.; Knowles, P. J.; *Chem. Phys. Lett.* **1991**, *185*, 256.

[242] Krishnan, R.; Pople, J. A. *Int. J. Quantum Chem.* **1978**, *14*, 91.

[243] Krishnan, R.; Pople, J. A, *J. Chem. Phys*. **1980**, *72*, 4244.

[244] Knowles, P. J.; Hampel C.; Werner, H.-J. *J. Chem. Phys.* **1993**, *99*, 5219.

[245] Knowles, P. J.; Hampel C.; Werner, H.-J. *J. Chem. Phys.* **2000**, *112*, 3106.

[246] Werner, H.-J.; Knowles, P. J. *J. Chem. Phys.* **1985**, *82*, 5053.

[247] Knowles, P. J.; Werner, H.-J. *Chem. Phys. Lett.* **1985**, *115*, 259.

[248] Werner, H.-J.; Meyer, W. *J. Chem. Phys.* **1980**, *73*, 2342.

[249] Werner, H.-J.; Meyer, W. *J. Chem. Phys.* **1981**, *74*, 5794.

[250] Werner, H.-J. *Adv. Chem. Phys.* **1987**, *69*, 1.

[251] Werner, H.-J.; Knowles, P. J. *J. Chem. Phys.* **1998**, *89*, 5803.

[252] Knowles, P. J.; Werner, H.-J. *Chem. Phys. Lett.* **1988**, *145*, 514.

[253] Werner, H.-J.; Reinsch, E. A. *J. Chem. Phys.* **1982**, *76*, 3144.

[254] Langhoff, S. R.; Davidson, E. R. *Int. J. Quantum Chem.* **1974**, 8, 61.

[255] MOLPRO, version 2006.1, a package of ab initio programs, Werner, H.-J.; Knowles, P. J.; Lindh, R.; Manby, F. R.; Schütz, M.; Celani, P.; Korona, T.; Rauhut, G.; Amos, R. D.; Bernhardsson, A.; Berning, A.; Cooper, D. L.; Deegan, M. J. O.; Dobbyn, A. J.; Eckert, F.; Hampel C.; Hetzer, G.; Lloyd, A.W.; McNicholas, S. J.; Meyer, W.; Mura, M. E.; Nicklass, A.; Palmieri, P.; Pitzer, R.; Schumann, U.; Stoll, H.; Stone, A. J.; Tarroni R.; Thorsteinsson, T.; see http://www.molpro.net .

[256] Frisch, M. J.; Trucks, G. W.; Schlegel, H. B.; Scuseria, G. E.; Robb, M. A.; Cheeseman, J. R; Montgomery, J. A., Jr.; Vreven T.; Kudin, K. N.; Burant, J. C.; Millam, J. M.; Iyengar, S. S.; Tomasi, J.; Barone, V.; Mennucci, B.; Cossi, M.; Scalmani, G.; Rega, N.; Petersson, G. A.; Nakatsuji, H.; Hada, M.; Ehara, M.; K. Toyota, M.; Fukuda, R.; Hasegawa, J.; Ishida, M.; Nakajima, T.; Honda, Y.; Kitao, O.; Nakai, H.; Klene, M.; Li, X.; Knox, J. E.; Hratchian, H. P.; Cross, J. B.; Bakken, V.; Adamo, C.; Jaramillo, J.; Gomperts, R.; Stratmann, R. E.; Yazyev, O.; Austin, A. J.; Cammi, R.; Pomelli, C.; Ochterski, J. W.; Ayala, P. Y.; Morokuma, K.; Voth, G. A.; Salvador, P.; Dannenberg, J. J.; Zakrzewski, V. G.; Dapprich, S.; Daniels, A. D.; Strain, M. C.; Farkas, O.; Malick, D. K.; Rabuck, A. D.; Raghavachari, K.; Foresman, J. B.; Ortiz, J. V.; Cui, Q.; Baboul, A. G.; Clifford, S.; Cioslowski, J.; Stefanov, B. B.; Liu, G.; Liashenko, A.; Piskorz, P.; Komaromi, I.; Martin, R. L.; Fox, D. J.; Keith, T.; Al-Laham, M. A.; Peng, C. Y.; Nanayakkara, A.; Challacombe, M.; Gill, P. M. W.; Johnson, B.; Chen, W.; Wong, M. W.; Gonzalez, C.; Pople, J. A. Gaussian 03, revision D.01; Gaussian, Inc.: Wallingford, CT, 2004.

[257] Chemcraft, Zhurko, G. A. see, http://www.chemcraftprog.com

[258] Molekel, Flükiger, P.; Lüthi, H. P.; Sortmann, S.; Weber, J. Molekel 4.3, Swiss Center for Scientific Computing, Manno (Schweiz) 2000 - 2002.

[259] AIMPAC Program Package, R. F. W. Bader research group, McMaster University, Hamilton, Canada.

[260] Lewerenz, M.; Bruna, P. J.; Peyerimhoff, S. D.; Buenker, R. J. *Mol. Phys.* **1983**, 49, 1.

[261] Lewerenz, M.; Bruna, P. J.; Peyerimhoff, S. D.; Buenker, R. J. *J. Phys. B* **1983**, *16*, 4511.

[262] Kalcher, J.; Sax, A.; Olbrich, G. *J. Mol. Struct.: THEOCHEM* **1994,** *313*, 41.

[263] Huber, K. P., Herzberg, G. *Molecular Spectra and Molecular Structure IV. Constants of Diatomic Molecules*; Van Nostrand-Reinhold: New York, 1979.

[264] *Handbook of Chemistry and Physics, 79th ed.*; CRC Press: Boca Raton, 1998.

You can know the name of a bird in all the languages of the world,
but when you're finished,
you'll know absolutely nothing whatever about the bird...
So let's look at the bird and see what it's doing
— that's what counts.
I learned very early the difference
between knowing the name of something
and knowing something.

Richard Feynman

7. Abbreviations

AIM	Atoms In Molecules
Aug-cc-pVQZ	Augmented correlation-consistent quadruple zeta basis sets
BP86	Becke88-exchange function with VWN5 and Perdew86-correlation function
CASSCF	Complete Active Space Self-Consistent Field
CC	Coupled Cluster
CCSD	Coupled Cluster Singles and Doubles
CCSD(T)	Coupled Cluster Singles, Doubles and estimated Triples
CI	Configuration Interaction
DFT	Density Functional Theory
D_e	Dissociation Energy
ECP	Effective Core Potential
EDA	Energy Decomposition Analysis
GGA	General Gradient Approximation
GTO	Gaussian Type Orbital
HF	Hartree-Fock
HOMO	Highest Occupied Molecular Orbital
KS	Kohn-Sham
LCAO-MO	Linear Combination of Atomic Orbitals
LDA	Local density approximation
LSDA	Local spin density approximation
LUMO	Lowest Unoccupied Molecular Orbital
MO	Molecular Orbital
MP2	Møller-Plesset perturbation theory including second order correction
MP4	Møller-Plesset perturbation theory including fourth order correction

MRCI-SD	Multi-Reference Configuration Interaction
MRCI-SD(Q)	Multi-Reference Configuration Interaction with Davidson correction
QZ4P	Quadruple Zeta basis set with four Polarization functions
RCCSD	Restricted Coupled Cluster Singles and Doubles
RCCSD(T)	Restricted Coupled Cluster Singles, Doubles and estimated Triples
RHF	Restricted Hartree-Fork
SCS	Spin Component Scale
SCF	Self-Consistent Field
SOMO	Singly Occupied Molecular Orbital
STO	Slater Type Orbital
UHF	Unrestricted Hartree-Fork
UMP2	Unrestricted Møller-Plesset perturbation theory including second order correction
UMP4	Unrestricted Møller-Plesset perturbation theory including fourth order correction
ZORA	Zero-Order Regular Approximation

Quidvis Recte Factum Quamvis Humile Praeclarum

8. Geometries and Energies of the calculated Molecules

This section gives the geometries and the energies of all molecules in this study. The Cartesian coordinates are given in Å and the bond energies are given in a.u.

Si_2H_2

SiA (-0.50783148 a.u.)

Si	-1.114389	0.000000	-0.007135
Si	1.114389	0.000000	-0.007135
H	0.000000	-0.990483	-0.783138
H	0.000000	0.990483	-0.783138

SiB (-0.49212577 a.u.)

Si	0.153790	0.025856	0.000000
Si	2.278134	0.001584	0.000000
H	1.171734	1.319270	0.000000
H	-1.244880	0.575709	0.000000

SiC (-0.48989296 a.u.)

Si	-1.198463	0.000000	0.000000
Si	1.198463	0.000000	0.000000
H	0.000000	1.071142	0.000000
H	0.000000	-1.071142	0.000000

SiD (-0.48339812 a.u.)

Si	0.000000	0.000000	0.017207
Si	0.000000	0.000000	2.228865
H	1.237727	0.000000	-0.821247
H	-1.237727	0.000000	-0.821247

SiE1 (-0.47605174 a.u.)

Si	0.007380	1.054232	0.000000
Si	-0.007380	-1.054232	0.000000
H	1.254202	1.893256	0.000000
H	-1.254202	-1.893256	0.000000

SiE2 (-0.43516647 a.u.)

Si	-1.289847	0.021170	0.000000
Si	1.289847	-0.021170	0.000000
H	-1.298823	1.560055	0.000000
H	1.298823	-1.560055	0.000000

SiF1 (-0.43516647 a.u.)

Si	-1.289847	0.021170	0.000000
Si	1.289847	-0.021170	0.000000
H	-1.298823	1.560055	0.000000
H	1.298823	-1.560055	0.000000

SiF2 -0.41701290 a.u.

Si -1.149263 0.000000 -0.002053

Si 1.149263 0.000000 -0.002053

H -1.639501 0.000000 -1.453013

H 1.639501 0.000000 -1.453013

SiG (-0.44178386 a.u.)

Si 0.000000 0.000000 -0.989682

Si 0.000000 0.000000 0.989682

H 0.000000 0.000000 -2.459605

H 0.000000 0.000000 2.459605

SiA(T) -0.44366463 a.u.

Si -1.243722 0.000000 -0.015683

Si 1.243722 0.000000 -0.015683

H 0.000000 -1.029520 -0.545843

H 0.000000 1.029520 -0.545843

SiB(T) -0.46016640 a.u.

Si -0.017870 -0.041336 0.000000

Si 2.318326 0.020169 0.000000

H 1.980423 1.531593 0.000000

H -0.873132 1.216273 0.000000

SiC(T) -0.44283052 a.u.

Si	0.000000	0.000000	-1.325148
Si	0.000000	0.000000	1.325148
H	1.045858	0.000000	0.000000
H	-1.045858	0.000000	0.000000

SiD(T) -0.47558012 a.u.

Si	0.000000	0.000000	-0.019728
Si	0.000000	0.000000	2.273759
H	1.194944	0.000000	-0.931706
H	-1.194944	0.000000	-0.931706

SiE(T) -0.47170097 a.u.

Si	-0.020196	1.148346	0.000000
Si	0.020196	-1.148346	0.000000
H	1.448649	1.551365	0.000000
H	-1.448649	-1.551365	0.000000

SiF(T) -0.45250328 a.u.

Si	-1.206308	0.000000	0.003290
Si	1.206308	0.000000	0.003290
H	-1.507582	0.000000	-1.501325
H	1.507582	0.000000	-1.501325

SiG(T) -0.39795969 a.u.

Si	0.000000	0.000000	-1.102339
Si	0.000000	0.000000	1.102339
H	0.000000	0.000000	-2.675239
H	0.000000	0.000000	2.675239

SiI(T) -0.45914465 a.u.

Si	0.000249	0.025425	0.026616
Si	2.312200	0.002733	-0.010131
H	1.130837	1.250230	-0.265904
H	-0.447120	0.022417	-1.440298

Si_2F_2

SiA -0.62677298 a.u.

Si	-1.150819	0.000000	-0.003203
Si	1.150819	0.000000	-0.003203
F	0.000000	-1.187555	-0.976484
F	0.000000	1.187555	-0.976484

SiB -0.60667698 a.u.

Si	-0.054977	-0.024459	0.000000
Si	2.151534	0.094248	0.000000
F	1.084317	1.638688	0.000000
F	-1.454227	0.767977	0.000000

SiC -0.56002874 a.u.

Si	1.364831	0.000000	0.000000
Si	-1.364831	0.000000	0.000000
F	0.000000	0.000000	1.325360
F	0.000000	0.000000	-1.325360

SiD -0.63847545 a.u.

Si	0.000000	0.000000	-0.003831
Si	0.000000	0.000000	2.247241
F	1.291062	0.000000	-0.960560
F	-1.291062	0.000000	-0.960560

SiE1 -0.62777802 a.u.

Si	-0.001314	1.120589	0.000000
Si	0.001314	-1.120589	0.000000
F	1.402875	1.927640	0.000000
F	-1.402875	-1.927640	0.000000

SiE2 -0.62864910 a.u.

Si	-1.309102	0.160962	0.000000
Si	1.309102	-0.160962	0.000000
F	-1.261755	1.802226	0.000000
F	1.261755	-1.802226	0.000000

SiF1 -0.62572075 a.u.

Si	-1.343974	0.000000	0.030580
Si	1.343974	0.000000	0.030580
F	-1.507352	0.000000	-1.596093
F	1.507352	0.000000	-1.596093

SiF2 -0.61468042 a.u.

Si	0.000000	1.163401	0.000973
Si	0.000000	-1.163401	0.000973
F	0.000000	1.775922	1.504424
F	0.000000	-1.775922	1.504424

SiG -0.52698543 a.u.

Si	0.000000	0.000000	-0.964292
Si	0.000000	0.000000	0.964292
F	0.000000	0.000000	-2.560732
F	0.000000	0.000000	2.560732

SiA(T) -0.57122456 a.u.

Si	-1.226928	0.000000	-0.377990
Si	1.226928	0.000000	-0.377990
F	0.000000	1.148491	0.588682
F	0.000000	-1.148491	0.588682

SiB(T) -0.60621246 a.u.

Si	-0.002762	-0.000530	0.000000
Si	2.607496	0.000808	0.000000
F	1.580595	1.421902	0.000000
F	3.965787	0.887706	0.000000

SiC(T) -0.56249922 a.u.

Si	-1.136926	0.000000	0.000000
Si	1.136926	0.000000	0.000000
F	0.000000	0.000000	1.708583
F	0.000000	0.000000	-1.708583

SiD(T) -0.65397209 a.u.

Si	0.000000	0.000000	0.003139
Si	0.000000	0.000000	2.291508
F	1.255163	0.000000	-0.998285
F	-1.255163	0.000000	-0.998285

SiE(T) -0.64934083 a.u.

Si	-1.210631	-0.112410	0.000000
Si	1.210631	0.112410	0.000000
F	1.422643	1.730783	0.000000
F	-1.422643	-1.730783	0.000000

SiF(T) -0.64592809 a.u.

Si	-1.235109	0.000000	0.028350
Si	1.235109	0.000000	0.028350
F	-1.670529	0.000000	-1.541748
F	1.670529	0.000000	-1.541748

SiG(T) -0.61614724 a.u.

Si	0.000000	0.000000	-1.292524
Si	0.000000	0.000000	1.292524
F	0.000000	0.000000	-2.924194
F	0.000000	0.000000	2.924194

SiI(T) -0.62347561 a.u.

Si	-0.142224	0.127528	0.402954
Si	2.219357	0.099076	-0.298851
F	0.925811	1.572872	0.114110
F	-1.140465	0.341296	-0.858857

Si_2Cl_2

SiA -0.50273669 a.u.

Si	-1.179987	0.000000	-0.003860
Si	1.179987	0.000000	-0.003860
Cl	0.000000	-1.581103	-1.282856
Cl	0.000000	1.581103	-1.282856

SiB -0.47308885 a.u.

Si	0.190807	0.236729	0.000000
Si	2.305860	-0.303228	0.000000
Cl	1.098890	2.199996	0.000000
Cl	-1.851433	0.482894	0.000000

SiC -0.41018680 a.u.

Si	0.000000	0.000000	-1.365605
Si	0.000000	0.000000	1.365605
Cl	1.973066	0.000000	0.000000
Cl	-1.973066	0.000000	0.000000

SiD -0.47629001 a.u.

Si	0.000000	0.000000	-0.004743
Si	0.000000	0.000000	2.230173
Cl	1.700905	0.000000	-1.177549
Cl	-1.700905	0.000000	-1.177549

SiE1 -0.47379374 a.u.

Si	-0.000140	1.104507	0.000000
Si	0.000140	-1.104507	0.000000
Cl	1.778355	2.170681	0.000000
Cl	-1.778355	-2.170681	0.000000

SiE2 -0.47418493 a.u.

Si	0.144070	-0.023858	0.000000
Si	-0.144119	-2.557253	0.000000
Cl	2.259433	-0.144571	0.000000
Cl	-2.259469	-2.436207	0.000000

SiF1 -0.46847310 a.u.

Si	-1.322709	0.000000	0.294894
Si	1.322709	0.000000	0.294894
Cl	-1.727592	0.000000	-1.759251
Cl	1.727592	0.000000	-1.759251

SiF2 -0.45615651 a.u.

Si	-1.159930	0.000000	0.211741
Si	1.159930	0.000000	0.211741
Cl	-2.011855	0.000000	-1.692724
Cl	2.011855	0.000000	-1.692724

SiG -0.39613843 a.u.

Si	0.000000	0.000000	-0.977232
Si	0.000000	0.000000	0.977232
Cl	0.000000	0.000000	-2.995579
Cl	0.000000	0.000000	2.995579

SiA(T) -0.44194568 a.u.

Si	-1.576144	0.000000	0.142913
Si	1.576144	0.000000	0.142913
Cl	0.000000	1.631114	0.755227
Cl	0.000000	-1.631114	0.755227

SiB(T) -0.44565259 a.u.

Si	-0.035371	0.082149	0.000000
Si	2.458410	-0.027081	0.000000
Cl	1.481840	2.019618	0.000000
Cl	-2.214659	0.339105	0.000000

SiC(T) -0.44395462 a.u.

Si	-1.168415	0.000000	0.000000
Si	1.168415	0.000000	0.000000
Cl	0.000000	-2.210873	0.000000
Cl	0.000000	2.210873	0.000000

SiD(T) -0.48496259 a.u.

Si	0.000000	0.000000	0.153022
Si	0.000000	0.000000	2.438537
Cl	1.645192	0.000000	-1.104338
Cl	-1.645192	0.000000	-1.104338

SiE(T) -0.49078751 a.u.

Si	-1.102488	-0.458997	0.000000
Si	1.102488	0.458997	0.000000
Cl	-2.325421	1.248242	0.000000
Cl	2.325421	-1.248242	0.000000

SiF(T) -0.48551242 a.u.

Si	0.000000	1.223201	-0.147702
Si	0.000000	-1.223201	-0.147702
Cl	0.000000	1.884903	1.838169
Cl	0.000000	-1.884903	1.838169

SiG(T) -0.45077314 a.u.

Si	0.000000	0.000000	-1.291957
Si	0.000000	0.000000	1.291957
Cl	0.000000	0.000000	-3.412704
Cl	0.000000	0.000000	3.412704

SiI(T) -0.47314984 a.u.

Si	0.172226	-0.038691	0.636036
Si	2.360246	-0.351426	-0.379647
Cl	1.498060	1.801815	0.050202
Cl	-1.421591	0.135497	-0.727487

Si_2Br_2

SiA -0.46486709 a.u.

Si	-1.188040	0.000000	-0.002012
Si	1.188040	0.000000	-0.002012
Br	0.000000	-1.725471	-1.382082
Br	0.000000	1.725471	-1.382082

SiB -0.43242386 a.u.

Si	0.015039	0.000369	0.000000
Si	-0.018573	2.180918	0.000000
Br	2.303449	0.631984	0.000000
Br	-0.272182	-2.201686	0.000000

SiC -0.37174028 a.u.

Si	0.000000	0.000000	0.400889
Si	0.000000	0.000000	-2.294459
Br	0.000000	2.182099	-0.946796
Br	0.000000	-2.182099	-0.946796

SiD -0.43043454 a.u.

Si	0.000000	0.000000	0.004229
Si	0.000000	0.000000	-2.225448
Br	0.000000	1.858617	1.245498
Br	0.000000	-1.858617	1.245498

SiE1 -0.43015655 a.u.

Si	-0.642940	0.894802	0.000000
Si	0.642940	-0.894802	0.000000
Br	2.876563	-0.733239	0.000000
Br	-2.876563	0.733239	0.000000

SiE2 -0.43090080 a.u.

Si	0.089905	1.257856	0.000000
Si	-0.089905	-1.257856	0.000000
Br	2.381090	1.174305	0.000000
Br	-2.381090	-1.174305	0.000000

SiF1 -0.42344479 a.u.

Si	0.000000	1.314521	-0.172007
Si	0.000000	-1.314521	-0.172007
Br	0.000000	1.841152	2.025135
Br	0.000000	-1.841152	2.025135

SiF2 -0.41169637 a.u.

Si	0.000000	1.158691	-0.000136
Si	0.000000	-1.158691	-0.000136
Br	0.000000	2.137169	2.031411
Br	0.000000	-2.137169	2.031411

SiG -0.35706145 a.u.

Si	0.000000	0.000000	-0.982389
Si	0.000000	0.000000	0.982389
Br	0.000000	0.000000	-3.160601
Br	0.000000	0.000000	3.160601

SiA(T) -0.40129308 a.u.

Si	-1.614664	0.000000	0.148479
Si	1.614664	0.000000	0.148479
Br	0.000000	1.792548	0.840976
Br	0.000000	-1.792548	0.840976

SiB(T) -0.40719855 a.u.

Si	-0.016407	0.218964	0.000000
Si	2.429383	-0.051164	0.000000
Br	1.451520	2.263959	0.000000
Br	-2.362938	0.750762	0.000000

SiC(T) -0.40932288 a.u.

Si	0.000000	-1.178623	0.000000
Si	0.000000	1.178623	0.000000
Br	-2.374848	0.000000	0.000000
Br	2.374848	0.000000	0.000000

SiD(T) -0.43763158 a.u.

Si	0.000000	0.000000	0.273511
Si	0.000000	0.000000	2.558057
Br	1.792205	0.000000	-1.072309
Br	-1.792205	0.000000	-1.072309

SiE(T) -0.44579534 a.u.

Si	-0.232688	-1.165773	0.000000
Si	0.232688	1.165773	0.000000
Br	1.835894	-2.098560	0.000000
Br	-1.835894	2.098560	0.000000

SiF(T) -0.43990190 a.u.

Si	0.000000	1.218795	-0.295300
Si	0.000000	-1.218795	-0.295300
Br	0.000000	2.003280	1.824685
Br	0.000000	-2.003280	1.824685

SiG(T) -0.40656533 a.u.

Si	0.000000	0.000000	-1.273008
Si	0.000000	0.000000	1.273008
Br	0.000000	0.000000	-3.569413
Br	0.000000	0.000000	3.569413

SiI(T) -0.43125934 a.u.

Si	0.118879	-0.253416	0.449086
Si	2.469324	-0.584238	-0.035814
Br	1.570249	1.755392	0.044633
Br	-1.278855	-0.284996	-1.352211

Si_2I_2

SiA -0.42726791 a.u.

Si	-1.194438	0.000000	0.095501
Si	1.194438	0.000000	0.095501
I	0.000000	-1.917894	-1.403849
I	0.000000	1.917894	-1.403849

SiB -0.39469725 a.u.

Si	-0.061251	0.038340	0.000000
Si	-0.024872	2.219803	0.000000
I	2.465155	0.792332	0.000000
I	-0.416153	-2.379892	0.000000

SiC -0.33492086 a.u.

Si	0.000000	1.341487	0.000000
Si	0.000000	-1.341487	0.000000
I	2.421142	0.000000	0.000000
I	-2.421142	0.000000	0.000000

SiD -0.38605190 a.u.

Si	0.000000	0.000000	0.365291
Si	0.000000	0.000000	-1.854792
I	0.000000	2.084877	1.678523
I	0.000000	-2.084877	1.678523

SiE1 -0.38809909 a.u.

Si	-0.056914	-1.095219	0.000000
Si	0.056914	1.095219	0.000000
I	1.953839	-2.515949	0.000000
I	-1.953839	2.515949	0.000000

SiE2 -0.38824373 a.u.

Si	0.003896	1.243559	0.000000
Si	-0.003896	-1.243559	0.000000
I	2.531813	1.239807	0.000000
I	-2.531813	-1.239807	0.000000

SiF1 -0.37809240 a.u.

Si	0.000000	1.299413	-0.032853
Si	0.000000	-1.299413	-0.032853
I	0.000000	2.012406	2.345401
I	0.000000	-2.012406	2.345401

SiF2 -0.36737480 a.u.

Si 0.000000 1.157238 0.117051

Si 0.000000 -1.157238 0.117051

I 0.000000 2.320324 2.312354

I 0.000000 -2.320324 2.312354

SiG -0.32391228 a.u.

Si 0.000000 0.000000 -0.990442

Si 0.000000 0.000000 0.990442

I 0.000000 0.000000 -3.381815

I 0.000000 0.000000 3.381815

SiA(T) -0.36162517 a.u.

Si -1.617892 0.000000 0.074182

Si 1.617892 0.000000 0.074182

I 0.000000 2.022530 0.884494

I 0.000000 -2.022530 0.884494

SiB(T) -0.36969521 a.u.

Si 0.000094 -0.000248 0.000000

Si 2.430674 -0.000122 0.000000

I 1.184850 2.397994 0.000000

I -2.625832 0.384135 0.000000

SiC(T) -0.37299481 a.u.

Si 0.000000 -1.192053 0.000000

Si 0.000000 1.192053 0.000000

I -2.589679 0.000000 0.000000

I 2.589679 0.000000 0.000000

SiD(T) -0.39022476 a.u.

Si 0.000000 0.000000 0.398175

Si 0.000000 0.000000 2.680118

I 1.998733 0.000000 -1.060983

I -1.998733 0.000000 -1.060983

SiE(T) -0.40094995 a.u.

Si -0.271449 -1.147886 0.000000

Si 0.271449 1.147886 0.000000

I 1.966642 -2.254966 0.000000

I -1.966642 2.254966 0.000000

SiF(T) -0.40094995 a.u.

Si -0.271449 -1.147886 0.000000

Si 0.271449 1.147886 0.000000

I 1.966642 -2.254966 0.000000

I -1.966642 2.254966 0.000000

SiG(T) -0.36101783 a.u.

Si 0.000000 0.000000 -1.253383

Si 0.000000 0.000000 1.253383

I 0.000000 0.000000 -3.792687

I 0.000000 0.000000 3.792687

SiI(T) -0.39001632 a.u.

Si 0.056801 -0.268431 0.505714

Si 2.342281 -0.589932 -0.161479

I 1.529410 1.974182 0.074610

I -1.706956 -0.341889 -1.295739

Ge_2H_2

GeA -0.46747505 a.u.

Ge -1.192458 0.000000 -0.003181

Ge 1.192458 0.000000 -0.003181

H 0.000000 -1.042451 -0.802984

H 0.000000 1.042451 -0.802984

GeB -0.45006201 a.u.

Ge 0.131513 0.002327 0.000000

Ge 2.370357 0.002037 0.000000

H 1.198135 1.375648 0.000000

H -1.303100 0.599348 0.000000

GeC -0.45338361 a.u.

Ge	0.000000	0.000000	-0.108710
Ge	0.000000	0.000000	2.458807
H	1.116874	0.000000	1.175053
H	-1.116874	0.000000	1.175053

GeD -0.44119510 a.u.

Ge	0.000000	0.000000	-0.007544
Ge	0.000000	0.000000	-2.308652
H	0.000000	1.254455	0.891327
H	0.000000	-1.254455	0.891327

GeE1 -0.43192505 a.u.

Ge	-1.105558	0.001926	0.000000
Ge	1.105558	-0.001926	0.000000
H	-1.976689	1.296014	0.000000
H	1.976689	-1.296014	0.000000

GeE2 -0.40745111 a.u.

Ge	-1.352165	0.004129	0.000000
Ge	1.352165	-0.004129	0.000000
H	-1.351789	1.630742	0.000000
H	1.351789	-1.630742	0.000000

GeF1 -0.40442621 a.u.

Ge	0.000000	1.361708	0.000003
Ge	0.000000	-1.361708	0.000003
H	0.000000	1.364541	1.616930
H	0.000000	-1.364541	1.616930

GeF2 -0.38071450 a.u.

Ge	0.000000	1.214915	0.004055
Ge	0.000000	-1.214915	0.004055
H	0.000000	1.787755	1.499473
H	0.000000	-1.787755	1.499473

GeG -0.37866963 a.u.

Ge	0.000000	0.000000	1.023646
Ge	0.000000	0.000000	-1.023646
H	0.000000	0.000000	2.518170
H	0.000000	0.000000	-2.518170

GeA(T) -0.41207683 a.u.

Ge	-1.412413	-0.002346	0.010580
Ge	1.412413	0.002346	0.010580
H	-0.001720	1.056574	0.295162
H	0.001720	-1.056574	0.295162

GeB(T) -0.42336116 a.u.

Ge	-0.003365	-0.027044	0.000000
Ge	2.485764	0.018250	0.000000
H	2.136037	1.598411	0.000000
H	-0.812895	1.341666	0.000000

GeC(T) -0.41484631 a.u.

Ge	0.000000	0.000000	-0.230085
Ge	0.000000	0.000000	2.580183
H	1.087128	0.000000	1.175039
H	-1.087128	0.000000	1.175039

GeD(T) -0.42336116 a.u.

Ge	-0.003365	-0.027044	0.000000
Ge	2.485764	0.018250	0.000000
H	2.136037	1.598411	0.000000
H	-0.812895	1.341666	0.000000

GeE(T) -0.43255502 a.u.

Ge	-1.217435	0.009340	0.000000
Ge	1.217435	-0.009340	0.000000
H	-1.577759	1.560314	0.000000
H	1.577759	-1.560314	0.000000

GeF(T) -0.41981446 a.u.

Ge	0.000000	1.275385	0.000393
Ge	0.000000	-1.275385	0.000393
H	0.000000	1.595267	1.572607
H	0.000000	-1.595267	1.572607

GeG(T) -0.35706011 a.u.

Ge	0.000000	0.000000	1.149973
Ge	0.000000	0.000000	-1.149973
H	0.000000	0.000000	2.794833
H	0.000000	0.000000	-2.794833

GeI(T) -0.42239808 a.u.

Ge	-0.004527	-0.000736	0.003351
Ge	2.505139	0.003008	-0.003428
H	1.227954	1.275362	-0.170770
H	-0.368992	0.184568	-1.549904

Ge_2F_2

GeA -0.58477155 a.u.

Ge	-1.226949	0.000000	-0.000430
Ge	1.226949	0.000000	-0.000430
F	0.000000	-1.260876	-1.034658
F	0.000000	1.260876	-1.034658

GeB -0.54486052 a.u.

Ge	0.058038	-0.010987	0.000000
Ge	2.403931	-0.008797	0.000000
F	1.177634	1.676501	0.000000
F	-1.546158	0.695563	0.000000

GeC -0.52793379 a.u.

Ge	-1.426886	0.000000	0.000000
Ge	1.426886	0.000000	0.000000
F	0.000000	1.445003	0.000000
F	0.000000	-1.445003	0.000000

GeD -0.54985690 a.u.

Ge	0.000000	0.000000	0.022607
Ge	0.000000	0.000000	-2.358919
F	0.000000	1.372710	1.120240
F	0.000000	-1.372710	1.120240

GeE1 -0.55021250 a.u.

Ge	-1.185076	0.138442	0.000000
Ge	1.185076	-0.138442	0.000000
F	-1.858878	1.773067	0.000000
F	1.858878	-1.773067	0.000000

GeE2 -0.56784035 a.u.

Ge -1.376093 0.045963 0.000000

Ge 1.376093 -0.045963 0.000000

F -1.410197 1.842802 0.000000

F 1.410197 -1.842802 0.000000

GeF1 -0.56328310 a.u.

Ge -1.408502 0.000000 -0.000759

Ge 1.408502 0.000000 -0.000759

F -1.564388 0.000000 -1.775738

F 1.564388 0.000000 -1.775738

GeF2 -0.54085868 a.u.

Ge -1.235153 0.000000 -0.030992

Ge 1.235153 0.000000 -0.030992

F -1.937832 0.000000 -1.658107

F 1.937832 0.000000 -1.658107

GeG -0.38695737 a.u.

Ge 0.000000 0.000000 -1.003911

Ge 0.000000 0.000000 1.003911

F 0.000000 0.000000 -2.724499

F 0.000000 0.000000 2.724499

GeA(T) -0.53563915 a.u.

Ge -1.317478 0.000000 0.354498

Ge 1.317478 0.000000 0.354498

F 0.000000 1.208302 -0.664926

F 0.000000 -1.208302 -0.664926

GeB(T) -0.54229934 a.u.

Ge -0.070089 -0.012597 0.000000

Ge 2.689570 0.081989 0.000000

F 1.478681 1.584918 0.000000

F -1.867277 0.224251 0.000000

GeC(T) -0.53325871 a.u.

Ge -1.210811 0.000000 0.000000

Ge 1.210811 0.000000 0.000000

F 0.000000 1.790710 0.000000

F 0.000000 -1.790710 0.000000

GeD(T) -0.56565138 a.u.

Ge 0.000000 0.000000 -0.043753

Ge 0.000000 0.000000 2.410606

F 1.336943 0.000000 -1.184498

F -1.336943 0.000000 -1.184498

GeE(T) -0.58035767 a.u.

Ge -1.292806 0.000000 0.000000

Ge 1.292806 0.000000 0.000000

F -1.559440 1.766146 0.000000

F 1.559440 -1.766146 0.000000

GeF(T) -0.57696021 a.u.

Ge -1.311846 0.000000 0.045351

Ge 1.311846 0.000000 0.045351

F -1.751611 0.000000 -1.676457

F 1.751611 0.000000 -1.676457

GeG(T) -0.55226117 a.u.

Ge 0.000000 0.000000 -1.351851

Ge 0.000000 0.000000 1.351851

F 0.000000 0.000000 -3.139015

F 0.000000 0.000000 3.139015

GeI(T) -0.56754560 a.u.

Ge -0.143873 0.048422 0.361125

Ge 2.488860 0.005355 -0.199073

F 1.172488 1.539976 0.135648

F -0.920741 0.276845 -1.221069

Ge_2Cl_2

GeA -0.47436879 a.u.

Ge	-1.253946	0.000000	-0.001907
Ge	1.253946	0.000000	-0.001907
Cl	0.000000	-1.642439	-1.326170
Cl	0.000000	1.642439	-1.326170

GeB -0.42858800 a.u.

Ge	0.048529	0.146680	0.000000
Ge	2.343187	-0.196202	0.000000
Cl	1.525086	2.157271	0.000000
Cl	-1.977549	0.908812	0.000000

GeC -0.39758657 a.u.

Ge	0.000000	-1.414520	0.000000
Ge	0.000000	1.414520	0.000000
Cl	2.054596	0.000000	0.000000
Cl	-2.054596	0.000000	0.000000

GeD -0.42336449 a.u.

Ge	0.000000	0.000000	0.002124
Ge	0.000000	0.000000	2.358253
Cl	1.764051	0.000000	-1.281365
Cl	-1.764051	0.000000	-1.281365

GeE1 -0.42837819 a.u.

Ge -1.171480 -0.113636 0.000000

Ge 1.171480 0.113636 0.000000

Cl -2.460906 1.648804 0.000000

Cl 2.460906 -1.648804 0.000000

GeE2 -0.44416535 a.u.

Ge 0.060663 -1.342070 0.000000

Ge -0.060663 1.342070 0.000000

Cl 2.293244 -1.317973 0.000000

Cl -2.293244 1.317973 0.000000

GeF1 -0.43768551 a.u.

Ge -1.394684 0.000000 0.041905

Ge 1.394684 0.000000 0.041905

Cl -1.776157 0.000000 -2.125424

Cl 1.776157 0.000000 -2.125424

GeF2 -0.41643240 a.u.

Ge -1.228117 0.000000 -0.016658

Ge 1.228117 0.000000 -0.016658

Cl -2.162850 0.000000 -2.001626

Cl 2.162850 0.000000 -2.001626

GeG -0.29990199 a.u.

Ge	0.000000	0.000000	-1.016213
Ge	0.000000	0.000000	1.016213
Cl	0.000000	0.000000	-3.119543
Cl	0.000000	0.000000	3.119543

GeA(T) -0.42284249 a.u.

Ge	-1.654791	0.028747	0.179481
Ge	1.654791	-0.028747	0.179481
Cl	0.029664	1.708391	0.766396
Cl	-0.029664	-1.708391	0.766396

GeB(T) -0.41986896 a.u.

Ge	0.005973	-0.001703	0.000000
Ge	2.697557	-0.000337	0.000000
Cl	1.544607	2.064927	0.000000
Cl	-2.243874	0.341343	0.000000

GeC(T) -0.42483144 a.u.

Ge	-1.240433	0.000000	0.000000
Ge	1.240433	0.000000	0.000000
Cl	0.000000	-2.279034	0.000000
Cl	0.000000	2.279034	0.000000

GeD(T) -0.43348223 a.u.

Ge	0.000000	0.000000	0.063430
Ge	0.000000	0.000000	2.501639
Cl	1.713465	0.000000	-1.296238
Cl	-1.713465	0.000000	-1.296238

GeE(T) -0.45359279 a.u.

Ge	-0.275780	-0.152699	0.000000
Ge	0.275746	2.338262	0.000000
Cl	1.773262	-0.993419	0.000000
Cl	-1.773189	3.179216	0.000000

GeF(T) -0.44947694 a.u.

Ge	-1.299795	0.000000	0.190341
Ge	1.299795	0.000000	0.190341
Cl	-1.977663	0.000000	-1.902365
Cl	1.977663	0.000000	-1.902365

GeG(T) -0.42319181 a.u.

Ge	0.000000	0.000000	-1.344940
Ge	0.000000	0.000000	1.344940
Cl	0.000000	0.000000	-3.569080
Cl	0.000000	0.000000	3.569080

GeI(T) -0.44129974 a.u.

Ge	-0.113501	-0.058903	0.108784
Ge	2.536068	0.124021	-0.068237
Cl	1.114144	2.091018	0.066042
Cl	-0.980524	-0.066565	-1.936004

Ge_2Br_2

GeA -0.44041059 a.u.

Ge	-1.261481	0.000000	-0.003017
Ge	1.261481	0.000000	-0.003017
Br	0.000000	-1.776553	-1.419811
Br	0.000000	1.776553	-1.419811

GeB -0.39464677 a.u.

Ge	-0.096211	-0.090733	0.000000
Ge	-0.286124	-2.399669	0.000000
Br	2.173041	-1.447138	0.000000
Br	0.437388	2.164953	0.000000

GeC -0.36220049 a.u.

Ge	-1.405628	0.000000	0.000000
Ge	1.405628	0.000000	0.000000
Br	0.000000	-2.239726	0.000000
Br	0.000000	2.239726	0.000000

GeD -0.38575407 a.u.

Ge	0.000000	0.000000	0.000725
Ge	0.000000	0.000000	2.349657
Br	1.914030	0.000000	-1.343059
Br	-1.914030	0.000000	-1.343059

GeE1 -0.39190797 a.u.

Ge	-1.173070	0.003708	0.000000
Ge	1.173070	-0.003708	0.000000
Br	-2.386284	2.000310	0.000000
Br	2.386284	-2.000310	0.000000

GeE2 -0.40693583 a.u.

Ge	0.013907	1.331400	0.000000
Ge	-0.013907	-1.331400	0.000000
Br	2.404331	1.354087	0.000000
Br	-2.404331	-1.354087	0.000000

GeF1 -0.39937251 a.u.

Ge	-1.388584	0.000000	0.109058
Ge	1.388584	0.000000	0.109058
Br	-1.881292	0.000000	-2.190995
Br	1.881292	0.000000	-2.190995

GeF2 -0.37937266 a.u.

Ge	-1.225410	0.000000	0.004517
Ge	1.225410	0.000000	0.004517
Br	-2.281466	0.000000	-2.093074
Br	2.281466	0.000000	-2.093074

GeG -0.27267638 a.u.

Ge	0.000000	0.000000	-1.022063
Ge	0.000000	0.000000	1.022063
Br	0.000000	0.000000	-3.277449
Br	0.000000	0.000000	3.277449

GeA(T) -0.38630625 a.u.

Ge	-1.676782	-0.085637	0.343152
Ge	1.676782	0.085637	0.343152
Br	-0.095003	1.859989	1.018890
Br	0.095003	-1.859989	1.018890

GeB(T) -0.38528227 a.u.

Ge	-0.053915	0.012793	0.000000
Ge	-0.207356	-2.681385	0.000000
Br	2.078504	-1.578991	0.000000
Br	0.418527	2.463713	0.000000

GeC(T) -0.39254448 a.u.

Ge	-1.250546	0.000000	0.000000
Ge	1.250546	0.000000	0.000000
Br	0.000000	-2.431933	0.000000
Br	0.000000	2.431933	0.000000

GeD(T) -0.39454208 a.u.

Ge	0.000000	0.000000	0.197848
Ge	0.000000	0.000000	2.631226
Br	1.853992	0.000000	-1.238443
Br	-1.853992	0.000000	-1.238443

GeE(T) -0.41519560 a.u.

Ge	-0.959182	-0.833006	0.000000
Ge	0.959182	0.833006	0.000000
Br	0.254971	-2.867774	0.000000
Br	-0.254971	2.867774	0.000000

GeF(T) -0.41082652 a.u.

Ge	-1.294870	0.000000	0.369304
Ge	1.294870	0.000000	0.369304
Br	-2.087719	0.000000	-1.845919
Br	2.087719	0.000000	-1.845919

GeG(T) -0.38526056 a.u.

Ge	0.000000	0.000000	-1.331615
Ge	0.000000	0.000000	1.331615
Br	0.000000	0.000000	-3.713045
Br	0.000000	0.000000	3.713045

GeI(T) -0.40442511 a.u.

Ge	-0.106827	0.012223	0.723125
Ge	2.308746	0.070907	-0.345626
Br	1.064618	2.279009	0.086331
Br	-1.774074	-0.194770	-0.965188

Ge_2I_2

GeA -0.40545600 a.u.

Ge	-1.270181	0.000000	0.067626
Ge	1.270181	0.000000	0.067626
I	0.000000	-1.962386	-1.462029
I	0.000000	1.962386	-1.462029

GeB -0.36158632 a.u.

Ge	-0.156198	-0.136774	0.000000
Ge	-0.464787	-2.427148	0.000000
I	2.252976	-1.635138	0.000000
I	0.360935	2.336451	0.000000

GeC -0.32716045 a.u.

Ge -1.403786 0.000000 0.000000

Ge 1.403786 0.000000 0.000000

I 0.000000 -2.468767 0.000000

I 0.000000 2.468767 0.000000

GeD -0.34812037 a.u.

Ge 0.000000 0.000000 -0.071636

Ge 0.000000 0.000000 2.264571

I 2.127270 0.000000 -1.485913

I -2.127270 0.000000 -1.485913

GeE1 -0.35535513 a.u.

Ge -1.165951 0.013193 0.000000

Ge 1.165951 -0.013193 0.000000

I -2.501823 2.179959 0.000000

I 2.501823 -2.179959 0.000000

GeE2 -0.36883032 a.u.

Ge -0.057041 1.314845 0.000000

Ge 0.057041 -1.314845 0.000000

I 2.549592 1.415821 0.000000

I -2.549592 -1.415821 0.000000

GeF1 -0.35944958 a.u.

Ge -1.377145 0.000000 0.232189

Ge 1.377145 0.000000 0.232189

I -2.046044 0.000000 -2.239738

I 2.046044 0.000000 -2.239738

GeF2 -0.34128893 a.u.

Ge -1.222021 0.000000 0.090566

Ge 1.222021 0.000000 0.090566

I -2.451979 0.000000 -2.157243

I 2.451979 0.000000 -2.157243

GeG -0.25197089 a.u.

Ge 0.000000 0.000000 -1.031020

Ge 0.000000 0.000000 1.031020

I 0.000000 0.000000 -3.488568

I 0.000000 0.000000 3.488568

GeA(T) -0.34954826 a.u.

Ge -1.671284 -0.101628 0.344102

Ge 1.671284 0.101628 0.344102

I -0.126739 2.084672 1.139876

I 0.126739 -2.084672 1.139876

GeB(T) -0.34975028 a.u.

Ge -0.150109 -0.126673 0.000000

Ge -0.356706 -2.724401 0.000000

I 2.181976 -1.725481 0.000000

I 0.365431 2.594058 0.000000

GeC(T) -0.35827450 a.u.

Ge -1.263748 0.000000 0.000000

Ge 1.263748 0.000000 0.000000

I 0.000000 -2.640497 0.000000

I 0.000000 2.640497 0.000000

GeD(T) -0.35417095 a.u.

Ge 0.000000 0.000000 0.263994

Ge 0.000000 0.000000 2.689258

I 2.051859 0.000000 -1.274603

I -2.051859 0.000000 -1.274603

GeE(T) -0.37537232 a.u.

Ge -1.003196 -0.764368 0.000000

Ge 1.003196 0.764368 0.000000

I 0.156886 -3.071301 0.000000

I -0.156886 3.071301 0.000000

GeF(T) -0.37032534 a.u.

Ge -1.287565 0.000000 0.554307

Ge 1.287565 0.000000 0.554307

I -2.250451 0.000000 -1.822881

I 2.250451 0.000000 -1.822881

GeG(T) -0.34512580 a.u.

Ge 0.000000 0.000000 -1.317074

Ge 0.000000 0.000000 1.317074

I 0.000000 0.000000 -3.918874

I 0.000000 0.000000 3.918874

GeI(T) -0.36652194 a.u.

Ge -0.016801 0.035661 0.820863

Ge 2.340418 -0.001852 -0.299577

I 1.184033 2.478888 0.037624

I -1.970073 -0.336476 -0.866532

Sn_2H_2

SnA -0.42118975 a.u.

Sn 0.000000 1.390358 -0.162273

Sn 0.000000 -1.390358 -0.162273

H 1.142558 0.000000 0.645266

H -1.142558 0.000000 0.645266

SnB -0.39961310 a.u.

Sn	0.070244	-0.052868	0.000000
Sn	2.693268	0.020098	0.000000
H	1.318124	1.452298	0.000000
H	-1.492767	0.712043	0.000000

SnC -0.41252839 a.u.

Sn	0.000000	0.000000	-1.475687
Sn	0.000000	0.000000	1.475687
H	1.208897	0.000000	0.000000
H	-1.208897	0.000000	0.000000

SnD -0.39049192 a.u.

Sn	0.000000	0.000000	-0.119903
Sn	0.000000	0.000000	-2.799836
H	0.000000	1.377635	0.925693
H	0.000000	-1.377635	0.925693

SnE1 -0.38090085 a.u.

Sn	-1.301385	-0.010464	0.000000
Sn	1.301385	0.010464	0.000000
H	-2.280586	1.440372	0.000000
H	2.280586	-1.440372	0.000000

SnE2 -0.37449586 a.u.

Sn	0.011966	1.546385	0.000000
Sn	-0.011966	-1.546385	0.000000
H	1.808775	1.521937	0.000000
H	-1.808775	-1.521937	0.000000

SnF1 -0.37226023 a.u.

Sn	0.000000	1.560612	-0.010603
Sn	0.000000	-1.560612	-0.010603
H	0.000000	1.649804	1.778111
H	0.000000	-1.649804	1.778111

SnF2 -0.34667069 a.u.

Sn	0.000000	1.403868	-0.009505
Sn	0.000000	-1.403868	-0.009505
H	0.000000	2.071507	1.647513
H	0.000000	-2.071507	1.647513

SnG -0.31828683 a.u.

Sn	0.000000	0.000000	-1.196396
Sn	0.000000	0.000000	1.196396
H	0.000000	0.000000	-2.860563
H	0.000000	0.000000	2.860563

SnA(T) -0.36927681 a.u.

Sn	-1.486999	0.000001	-0.000006
Sn	1.486999	-0.000001	-0.000006
H	-0.446966	1.011095	1.088620
H	0.446966	-1.011095	1.088620

SnB(T) -0.38344273 a.u.

Sn	-0.070101	-0.072645	0.000000
Sn	2.824024	0.032108	0.000000
H	1.790318	1.542893	0.000000
H	-0.824184	1.545549	0.000000

SnC(T) -0.38237836 a.u.

Sn	0.000000	0.000000	-1.589706
Sn	0.000000	0.000000	1.589706
H	1.170802	0.000000	0.000000
H	-1.170802	0.000000	0.000000

SnD(T) -0.38801654 a.u.

Sn	0.000000	0.000000	-0.061578
Sn	0.000000	0.000000	-2.860178
H	0.000000	1.352556	1.045634
H	0.000000	-1.352556	1.045634

SnE(T) -0.39069260 a.u.

Sn	-1.417925	-0.019613	0.000000
Sn	1.417925	0.019613	0.000000
H	-1.806839	1.718658	0.000000
H	1.806839	-1.718658	0.000000

SnF(T) -0.38334685 a.u.

Sn	0.000000	1.464641	-0.010358
Sn	0.000000	-1.464641	-0.010358
H	0.000000	1.791427	1.748983
H	0.000000	-1.791427	1.748983

SnG(T) -0.33891851 a.u.

Sn	0.000000	0.000000	-1.654709
Sn	0.000000	0.000000	1.654709
H	0.000000	0.000000	-3.488913
H	0.000000	0.000000	3.488913

SnI(T) -0.38563860 a.u.

Sn	-0.098006	-0.001698	0.003891
Sn	2.839842	0.002805	-0.002294
H	1.361556	1.325653	-0.175597
H	-0.414337	0.227902	-1.746437

Sn_2F_2

SnA -0.55820581 a.u.

Sn	0.000000	1.407532	-0.164527
Sn	0.000000	-1.407532	-0.164527
F	1.325253	0.000000	0.913392
F	-1.325253	0.000000	0.913392

SnB -0.51452031 a.u.

Sn	0.008284	-0.057572	0.000000
Sn	2.756822	0.021172	0.000000
F	1.340612	1.718150	0.000000
F	-1.704924	0.878052	0.000000

SnC -0.51741636 a.u.

Sn	-1.609915	0.000000	0.000000
Sn	1.609915	0.000000	0.000000
F	0.000000	1.489603	0.000000
F	0.000000	-1.489603	0.000000

SnD -0.50860733 a.u.

Sn	0.000000	0.000000	-0.055889
Sn	0.000000	0.000000	-2.822934
F	0.000000	1.489777	1.205581
F	0.000000	-1.489777	1.205581

SnE1 -0.50806384 a.u.

Sn	-1.429413	-0.008087	0.000000
Sn	1.429413	0.008087	0.000000
F	-2.717678	1.478809	0.000000
F	2.717678	-1.478809	0.000000

SnE2 -0.53303934 a.u.

Sn	0.011112	1.564582	0.000000
Sn	-0.011112	-1.564582	0.000000
F	2.002803	1.588966	0.000000
F	-2.002803	-1.588966	0.000000

SnF1 -0.52769827 a.u.

Sn	0.000000	1.599154	-0.300693
Sn	0.000000	-1.599154	-0.300693
F	0.000000	1.748644	1.669204
F	0.000000	-1.748644	1.669204

SnF2 -0.50262066 a.u.

Sn	0.000000	1.426051	-0.274753
Sn	0.000000	-1.426051	-0.274753
F	0.000000	2.266005	1.505493
F	0.000000	-2.266005	1.505493

SnG -0.33696911 a.u.

Sn	0.000000	0.000000	-1.177933
Sn	0.000000	0.000000	1.177933
F	0.000000	0.000000	-3.090240
F	0.000000	0.000000	3.090240

SnA(T) -0.52386559 a.u.

Sn	-1.500790	0.015921	0.004383
Sn	1.500790	-0.015921	0.004383
F	0.053190	1.264714	1.035322
F	-0.053190	-1.264714	1.035322

SnB(T) -0.52888525 a.u.

Sn	0.024064	-0.038438	0.000000
Sn	3.134752	0.071854	0.000000
F	1.534245	1.559010	0.000000
F	-1.298331	1.434747	0.000000

SnC(T) -0.51530708 a.u.

Sn	-1.392848	0.000000	0.000000
Sn	1.392848	0.000000	0.000000
F	0.000000	1.855015	0.000000
F	0.000000	-1.855015	0.000000

SnD(T) -0.52502456 a.u.

Sn 0.000000 0.000000 0.049815

Sn 0.000000 0.000000 2.896107

F 1.454691 0.000000 -1.251601

F -1.454691 0.000000 -1.251601

SnE(T) -0.54192700 a.u.

Sn -1.482889 -0.062194 0.000000

Sn 1.482889 0.062194 0.000000

F -1.746228 1.902834 0.000000

F 1.746228 -1.902834 0.000000

SnF(T) -0.53803014 a.u.

Sn -1.504533 0.000000 0.057053

Sn 1.504533 0.000000 0.057053

F -1.963519 0.000000 -1.860071

F 1.963519 0.000000 -1.860071

SnG(T) -0.51670633 a.u.

Sn 0.000000 0.000000 -1.521784

Sn 0.000000 0.000000 1.521784

F 0.000000 0.000000 -3.504709

F 0.000000 0.000000 3.504709

SnI(T) -0.53997100 a.u.

Sn	-0.024040	0.015070	-0.035120
Sn	3.046087	0.015808	0.006373
F	1.470708	1.583337	-0.099846
F	-0.367023	0.084889	-1.975717

Sn_2Cl_2

SnA -0.44701448 a.u.

Sn	-1.437977	0.000000	-0.002018
Sn	1.437977	0.000000	-0.002018
Cl	0.000000	-1.716627	-1.415624
Cl	0.000000	1.716627	-1.415624

SnB -0.39963578 a.u.

Sn	-0.136872	-0.089499	0.000000
Sn	2.578852	-0.045588	0.000000
Cl	1.244052	2.241984	0.000000
Cl	-2.384700	0.643325	0.000000

SnC -0.38617643 a.u.

Sn	1.611727	0.000000	0.000000
Sn	-1.611727	0.000000	0.000000
Cl	0.000000	2.133371	0.000000
Cl	0.000000	-2.133371	0.000000

SnD -0.39134015 a.u.

Sn	0.000000	0.000000	0.051332
Sn	0.000000	0.000000	-2.695355
Cl	0.000000	1.875900	1.506877
Cl	0.000000	-1.875900	1.506877

SnE1 -0.39462434 a.u.

Sn	-1.383399	0.000051	0.000000
Sn	1.383399	-0.000051	0.000000
Cl	-2.898631	1.838050	0.000000
Cl	2.898631	-1.838050	0.000000

SnE2 -0.41762124 a.u.

Sn	1.539071	-0.020132	0.000000
Sn	-1.539071	0.020132	0.000000
Cl	1.541943	-2.447096	0.000000
Cl	-1.541943	2.447096	0.00000

SnF1 -0.41150703 a.u.

Sn	-1.587200	0.000000	-0.002410
Sn	1.587200	0.000000	-0.002410
Cl	-1.881954	0.000000	-2.379986
Cl	1.881954	0.000000	-2.379986

SnF2 -0.38737605 a.u.

Sn	-1.418352	0.000000	-0.051202
Sn	1.418352	0.000000	-0.051202
Cl	-2.433552	0.000000	-2.212690
Cl	2.433552	0.000000	-2.212690

SnG -0.25271435 a.u.

Sn	0.000000	0.000000	-1.189339
Sn	0.000000	0.000000	1.189339
Cl	0.000000	0.000000	-3.488197
Cl	0.000000	0.000000	3.488197

SnA(T) -0.40766004 a.u.

Sn	-1.833913	-0.126950	0.108679
Sn	1.833913	0.126950	0.108679
Cl	-0.123631	1.787202	0.715302
Cl	0.123631	-1.787202	0.715302

SnB(T) -0.40528996 a.u.

Sn	0.185380	0.011924	0.000000
Sn	3.312662	0.015530	0.000000
Cl	1.947814	2.221351	0.000000
Cl	-1.587488	1.667001	0.000000

SnC(T) -0.40604802 a.u.

Sn	-1.422198	0.000000	0.000000
Sn	1.422198	0.000000	0.000000
Cl	0.000000	2.390908	0.000000
Cl	0.000000	-2.390908	0.000000

SnD(T) -0.40395190 a.u.

Sn	0.000000	0.000000	0.134501
Sn	0.000000	0.000000	2.966167
Cl	1.826886	0.000000	-1.388489
Cl	-1.826886	0.000000	-1.388489

SnE(T) -0.42451705 a.u.

Sn	-1.456240	-0.221120	0.000000
Sn	1.456240	0.221120	0.000000
Cl	-2.096122	2.103830	0.000000
Cl	2.096122	-2.103830	0.000000

SnF(T) -0.42046163 a.u.

Sn	-1.494752	0.000000	0.181068
Sn	1.494752	0.000000	0.181068
Cl	-2.148340	0.000000	-2.120851
Cl	2.148340	0.000000	-2.120851

SnG(T) -0.39847048 a.u.

Sn	0.000000	0.000000	-1.519539
Sn	0.000000	0.000000	1.519539
Cl	0.000000	0.000000	-3.934222
Cl	0.000000	0.000000	3.934222

SnI(T) -0.41894219 a.u.

Sn	-0.133641	-0.061976	0.507192
Sn	2.831927	-0.045406	-0.276447
Cl	1.379553	2.090247	0.259354
Cl	-1.344298	0.132591	-1.567819

Sn_2Br_2

SnA -0.41340079 a.u.

Sn	-1.446560	0.000000	-0.623147
Sn	1.446560	0.000000	-0.623147
Br	0.000000	1.848925	0.890229
Br	0.000000	-1.848925	0.890229

SnB -0.36593231 a.u.

Sn	0.090220	0.008769	0.000000
Sn	2.801348	0.026320	0.000000
Br	1.496608	2.500924	0.000000
Br	-2.331576	0.676211	0.000000

SnC -0.35010514 a.u.

Sn	1.602159	0.000000	0.000000
Sn	-1.602159	0.000000	0.000000
Br	0.000000	-2.327907	0.000000
Br	0.000000	2.327907	0.000000

SnD -0.35552525 a.u.

Sn	0.000000	0.000000	-0.064464
Sn	0.000000	0.000000	-2.837833
Br	0.000000	1.993170	1.490054
Br	0.000000	-1.993170	1.490054

SnE1 -0.36043697 a.u.

Sn	-1.369888	-0.034582	0.000000
Sn	1.369888	0.034582	0.000000
Br	-2.966967	1.943152	0.000000
Br	2.966967	-1.943152	0.000000

SnE2 -0.38204863 a.u.

Sn	-0.983382	1.171169	0.000000
Sn	0.983382	-1.171169	0.000000
Br	0.982367	2.840448	0.000000
Br	-0.982367	-2.840448	0.000000

SnF1 -0.37558941 a.u.

Sn	0.000000	1.583142	-1.034945
Sn	0.000000	-1.583142	-1.034945
Br	0.000000	1.969044	1.478264
Br	0.000000	-1.969044	1.478264

SnF2 -0.35244643 a.u.

Sn	0.000000	1.415490	-0.943163
Sn	0.000000	-1.415490	-0.943163
Br	0.000000	2.523169	1.338817
Br	0.000000	-2.523169	1.338817

SnG -0.22772544 a.u.

Sn	0.000000	0.000000	-1.194929
Sn	0.000000	0.000000	1.194929
Br	0.000000	0.000000	-3.641307
Br	0.000000	0.000000	3.641307

SnA(T) -0.37124568 a.u.

Sn	-1.847968	-0.205331	0.010392
Sn	1.847968	0.205331	0.010392
Br	-0.214923	1.933406	0.728410
Br	0.214923	-1.933406	0.728410

SnB(T) -0.36934535 a.u.

Sn	0.115896	0.111984	0.000000
Sn	3.248718	-0.075028	0.000000
Br	1.960297	2.338244	0.000000
Br	-1.837238	1.834180	0.000000

SnC(T) -0.37350720 a.u.

Sn	0.000000	-1.433471	0.000000
Sn	0.000000	1.433471	0.000000
Br	-2.549749	0.000000	0.000000
Br	2.549749	0.000000	0.000000

SnD(T) -0.36739040 a.u.

Sn	0.000000	0.000000	0.257739
Sn	0.000000	0.000000	3.084624
Br	1.962801	0.000000	-1.339281
Br	-1.962801	0.000000	-1.339281

SnE(T) -0.38819147 a.u.

Sn	-1.438119	-0.298507	0.000000
Sn	1.438119	0.298507	0.000000
Br	-2.265596	2.125063	0.000000
Br	2.265596	-2.125063	0.000000

SnF(T) -0.38418914 a.u.

Sn	-1.490638	0.000000	0.370393
Sn	1.490638	0.000000	0.370393
Br	-2.222841	0.000000	-2.062746
Br	2.222841	0.000000	-2.062746

SnG(T) -0.36260841 a.u.

Sn	0.000000	0.000000	-1.512400
Sn	0.000000	0.000000	1.512400
Br	0.000000	0.000000	-4.077735
Br	0.000000	0.000000	4.077735

SnI(T) -0.38295495 a.u.

Sn	-0.123794	-0.034809	0.723307
Sn	2.710570	-0.195114	-0.414657
Br	1.439518	2.210810	0.136689
Br	-1.725462	0.020539	-1.278194

Sn_2I_2

SnA -0.37841984 a.u.

Sn	-1.457889	0.000000	-0.686900
Sn	1.457889	0.000000	-0.686900
I	0.000000	2.036131	0.950350
I	0.000000	-2.036131	0.950350

SnB -0.33185562 a.u.

Sn 0.085303 0.015443 0.000000

Sn 2.788009 -0.058289 0.000000

I 1.580206 2.688174 0.000000

I -2.563316 0.632645 0.000000

SnC -0.31349645 a.u.

Sn 1.599216 0.000000 0.000000

Sn -1.599216 0.000000 0.000000

I 0.000000 2.574603 0.000000

I 0.000000 -2.574603 0.000000

SnD -0.31858601 a.u.

Sn 0.000000 0.000000 -0.038949

Sn 0.000000 0.000000 -2.769527

I 0.000000 2.224611 1.560259

I 0.000000 -2.224611 1.560259

SnE1 -0.32457051 a.u.

Sn -1.361278 -0.000731 0.000000

Sn 1.361278 0.000731 0.000000

I -3.009987 2.183942 0.000000

I 3.009987 -2.183942 0.000000

SnE2 -0.34471047 a.u.

Sn -1.023091 1.118666 0.000000

Sn 1.023091 -1.118666 0.000000

I 1.062270 2.978085 0.000000

I -1.062270 -2.978085 0.000000

SnF1 -0.33732830 a.u.

Sn 0.000000 1.576697 -1.128040

Sn 0.000000 -1.576697 -1.128040

I 0.000000 2.118961 1.567669

I 0.000000 -2.118961 1.567669

SnF2 -0.31571952 a.u.

Sn 0.000000 1.412151 -1.000681

Sn 0.000000 -1.412151 -1.000681

I 0.000000 2.658630 1.447337

I 0.000000 -2.658630 1.447337

SnG -0.20715747 a.u.

Sn 0.000000 0.000000 -1.202978

Sn 0.000000 0.000000 1.202978

I 0.000000 0.000000 -3.851593

I 0.000000 0.000000 3.851593

SnA(T) -0.33379503 a.u.

Sn -1.857830 -0.275787 -0.048391

Sn 1.857830 0.275787 -0.048391

I -0.317901 2.141687 0.789919

I 0.317901 -2.141687 0.789919

SnB(T) -0.33066418 a.u.

Sn 0.027061 0.060147 0.000000

Sn 3.207255 -0.039675 0.000000

I 1.832546 2.534409 0.000000

I -2.483277 1.392392 0.000000

SnC(T) -0.33871201 a.u.

Sn 0.000000 -1.447089 0.000000

Sn 0.000000 1.447089 0.000000

I -2.770320 0.000000 0.000000

I 2.770320 0.000000 0.000000

SnD(T) -0.32839556 a.u.

Sn 0.000000 0.000000 0.384488

Sn 0.000000 0.000000 3.204137

I 2.157483 0.000000 -1.316147

I -2.157483 0.000000 -1.316147

SnE(T) -0.34962011 a.u.

Sn -1.417901 -0.358597 0.000000

Sn 1.417901 0.358597 0.000000

I -2.445241 2.216089 0.000000

I 2.445241 -2.216089 0.000000

SnF(T) -0.34544716 a.u.

Sn -1.485176 0.000000 0.568353

Sn 1.485176 0.000000 0.568353

I -2.367179 0.000000 -2.036993

I 2.367179 0.000000 -2.036993

SnG(T) -0.32393748 a.u.

Sn 0.000000 0.000000 -1.504887

Sn 0.000000 0.000000 1.504887

I 0.000000 0.000000 -4.285818

I 0.000000 0.000000 4.285818

SnI(T) -0.34499377 a.u.

Sn -0.051456 -0.063806 0.847675

Sn 2.691931 -0.341765 -0.433551

I 1.575509 2.355168 0.089856

I -1.987576 -0.089953 -1.153697

Pb_2H_2

PbA -0.39995866 a.u.

Pb	0.000000	1.463511	-0.108406
Pb	0.000000	-1.463511	-0.108406
H	1.198938	0.000000	0.705719
H	-1.198938	0.000000	0.705719

PbB -0.37283660 a.u.

Pb	0.223011	0.004170	0.000000
Pb	2.999305	-0.000810	0.000000
H	1.630284	1.513135	0.000000
H	-1.327123	0.950867	0.000000

PbC -0.39296967 a.u.

Pb	0.000000	0.000000	-1.544960
Pb	0.000000	0.000000	1.544960
H	0.000000	1.266252	0.000000
H	0.000000	-1.266252	0.000000

PbD -0.35683151 a.u.

Pb	0.000000	0.000000	-0.089857
Pb	0.000000	0.000000	-2.884956
H	0.000000	1.388430	1.057632
H	0.000000	-1.388430	1.057632

PbE1 -0.35058242 a.u.

Pb	-1.380734	0.001763	0.000000
Pb	1.380734	-0.001763	0.000000
H	-2.443370	1.493545	0.000000
H	2.443370	-1.493545	0.000000

PbE2 -0.35777093 a.u.

Pb	1.609733	-0.013322	0.000000
Pb	-1.609733	0.013322	0.000000
H	1.569848	-1.888121	0.000000
H	-1.569848	1.888121	0.000000

PbF1 -0.35547203 a.u.

Pb	0.000000	1.624684	0.002419
Pb	0.000000	-1.624684	0.002419
H	0.000000	1.718798	1.865694
H	0.000000	-1.718798	1.865694

PbF2 -0.32397566 a.u.

Pb	0.000000	1.489869	0.003391
Pb	0.000000	-1.489869	0.003391
H	0.000000	2.341205	1.665054
H	0.000000	-2.341205	1.665054

PbG -0.25255039 a.u.

Pb	0.000000	0.000000	-1.242564
Pb	0.000000	0.000000	1.242564
H	0.000000	0.000000	-2.937499
H	0.000000	0.000000	2.937499

PbA(T) -0.35216659 a.u.

Pb	-1.556841	0.000000	-0.000002
Pb	1.556841	0.000000	-0.000002
H	-0.595689	1.046671	1.258721
H	0.595689	-1.046671	1.258721

PbB(T) -0.36475037 a.u.

Pb	-0.063967	-0.008637	0.000000
Pb	3.082390	0.006175	0.000000
H	1.645324	1.341713	0.000000
H	-0.815770	1.712352	0.000000

PbC(T) -0.36691315 a.u.

Pb	0.000000	0.000000	-1.675954
Pb	0.000000	0.000000	1.675954
H	0.000000	1.204329	0.000000
H	0.000000	-1.204329	0.000000

PbD(T) -0.35755880 a.u.

Pb	0.000000	0.000000	-0.001634
Pb	0.000000	0.000000	-2.938085
H	0.000000	1.378930	1.192363
H	0.000000	-1.378930	1.192363

PbE(T) -0.36685780 a.u.

Pb	-1.505982	-0.000073	0.000000
Pb	1.505982	0.000073	0.000000
H	-1.825679	1.835938	0.000000
H	1.825679	-1.835938	0.000000

PbF(T) -0.36300813 a.u.

Pb	0.000000	1.541137	-0.000929
Pb	0.000000	-1.541137	-0.000929
H	0.000000	1.892389	1.831363
H	0.000000	-1.892389	1.831363

PbG(T) -0.32884287 a.u.

Pb	0.000000	0.000000	-1.664810
Pb	0.000000	0.000000	1.664810
H	0.000000	0.000000	-3.574287
H	0.000000	0.000000	3.574287

PbI(T) -0.36736109 a.u.

Pb	-0.128542	-0.000283	0.007019
Pb	3.024309	0.001749	-0.004159
H	1.443641	1.317474	-0.129333
H	-0.363692	0.224722	-1.837770

Pb_2F_2

PbA -0.53934716 a.u.

Pb	0.000000	1.473649	-0.109788
Pb	0.000000	-1.473649	-0.109788
F	1.389877	0.000000	1.000205
F	-1.389877	0.000000	1.000205

PbB -0.48867632 a.u.

Pb	0.146585	0.046227	0.000000
Pb	3.085307	-0.025539	0.000000
F	1.720280	1.785063	0.000000
F	-1.596132	1.145938	0.000000

PbC -0.50370043 a.u.

Pb	0.000000	0.000000	-1.663481
Pb	0.000000	0.000000	1.663481
F	0.000000	1.577398	0.000000
F	0.000000	-1.577398	0.000000

PbD -0.46976550 a.u.

Pb	0.000000	0.000000	0.249045
Pb	0.000000	0.000000	-2.670778
F	0.000000	1.549280	1.607056
F	0.000000	-1.549280	1.607056

PbE1 -0.47845736 a.u.

Pb	-1.472744	0.004320	0.000000
Pb	1.472744	-0.004320	0.000000
F	-2.668275	1.694326	0.000000
F	2.668275	-1.694326	0.000000

PbE2 -0.50935127 a.u.

Pb	1.619010	-0.012575	0.000000
Pb	-1.619010	0.012575	0.000000
F	1.608688	-2.113572	0.000000
F	-1.608688	2.113572	0.000000

PbF1 -0.50240655 a.u.

Pb	0.000000	1.663201	-0.204796
Pb	0.000000	-1.663201	-0.204796
F	0.000000	1.855225	1.865933
F	0.000000	-1.855225	1.865933

PbF2 -0.47341111 a.u.

Pb 0.000000 1.513176 -0.172419

Pb 0.000000 -1.513176 -0.172419

F 0.000000 2.723858 1.511500

F 0.000000 -2.723858 1.511500

PbG -0.22362569 a.u.

Pb 0.000000 0.000000 -1.224402

Pb 0.000000 0.000000 1.224402

F 0.000000 0.000000 -3.222137

F 0.000000 0.000000 3.222137

PbA(T) -0.50798428 a.u

Pb -1.571587 0.000000 -0.105985

Pb 1.571587 0.000000 -0.105985

F 0.000000 1.315342 0.959799

F 0.000000 -1.315342 0.959799

PbB(T) -0.50766675 a.u.

Pb 0.005122 -0.035158 0.000000

Pb 3.295584 0.065998 0.000000

F 1.589606 1.596823 0.000000

F -1.456453 1.457706 0.000000

PbC(T) -0.50465671 a.u.

Pb -1.459013 0.000000 0.000000

Pb 1.459013 0.000000 0.000000

F 0.000000 1.912856 0.000000

F 0.000000 -1.912856 0.000000

PbD(T) -0.48840812 a.u.

Pb 0.000000 0.000000 0.046407

Pb 0.000000 0.000000 3.078228

F 1.521041 0.000000 -1.341620

F -1.521041 0.000000 -1.341620

PbE(T) -0.51509514 a.u.

Pb -1.553717 -0.036452 0.000000

Pb 1.553717 0.036452 0.000000

F -1.622211 2.056404 0.000000

F 1.622211 -2.056404 0.000000

PbF(T) -0.50992714 a.u.

Pb -1.580804 0.000000 0.042408

Pb 1.580804 0.000000 0.042408

F -2.109790 0.000000 -1.964243

F 2.109790 0.000000 -1.964243

PbG(T) -0.49292983 a.u.

Pb	0.000000	0.000000	-1.560527
Pb	0.000000	0.000000	1.560527
F	0.000000	0.000000	-3.645190
F	0.000000	0.000000	3.645190

PbI(T) -0.51833513 a.u.

Pb	-0.078209	0.007180	0.049346
Pb	3.152691	0.009721	-0.037783
F	1.501380	1.633450	-0.013957
F	-0.473629	0.012487	-1.993033

Pb_2Cl_2

PbA -0.43571558 a.u.

Pb	1.502533	0.000000	-0.247064
Pb	-1.502533	0.000000	-0.247064
Cl	0.000000	-1.777179	1.191995
Cl	0.000000	1.777179	1.191995

PbB -0.38159471 a.u.

Pb	0.083248	0.081818	0.000000
Pb	2.968947	-0.115088	0.000000
Cl	1.847604	2.320591	0.000000
Cl	-2.134097	1.162749	0.000000

PbC -0.38366462 a.u.

Pb	0.000000	0.000000	1.655582
Pb	0.000000	0.000000	-1.655582
Cl	0.000000	2.203325	0.000000
Cl	0.000000	-2.203325	0.000000

PbD -0.36354328 a.u.

Pb	0.000000	0.000000	-0.117574
Pb	0.000000	0.000000	-3.013429
Cl	0.000000	1.932269	1.435494
Cl	0.000000	-1.932269	1.435494

PbE1 -0.37455920 a.u.

Pb	-1.460901	-0.003123	0.000000
Pb	1.460901	0.003123	0.000000
Cl	-2.889629	2.021808	0.000000
Cl	2.889629	-2.021808	0.000000

PbE2 -0.40504509 a.u.

Pb	-1.596125	-0.018702	0.000000
Pb	1.596125	0.018702	0.000000
Cl	-1.610536	2.508641	0.000000
Cl	1.610536	-2.508641	0.000000

PbF1 -0.39716164 a.u.

Pb	-1.651460	0.000000	0.000159
Pb	1.651460	0.000000	0.000159
Cl	-1.949489	0.000000	-2.472408
Cl	1.949489	0.000000	-2.472408

PbF2 -0.36873150 a.u.

Pb	-1.500997	0.000000	-0.056260
Pb	1.500997	0.000000	-0.056260
Cl	-2.856885	0.000000	-2.136856
Cl	2.856885	0.000000	-2.136856

PbG -0.16334925 a.u.

Pb	0.000000	0.000000	-1.241530
Pb	0.000000	0.000000	1.241530
Cl	0.000000	0.000000	-3.630159
Cl	0.000000	0.000000	3.630159

PbA(T) -0.40143780 a.u.

Pb	-1.908106	-0.006197	0.016786
Pb	1.908106	0.006197	0.016786
Cl	-0.006056	1.864593	0.571863
Cl	0.006056	-1.864593	0.571863

PbB(T) -0.39513217 a.u.

Pb	-0.044078	-0.071278	0.000000
Pb	3.232550	0.039644	0.000000
Cl	1.561580	2.154814	0.000000
Cl	-2.165304	1.329073	0.000000

PbC(T) -0.40179090 a.u.

Pb	0.000000	0.000000	-1.486763
Pb	0.000000	0.000000	1.486763
Cl	2.440824	0.000000	0.000000
Cl	-2.440824	0.000000	0.000000

PbD(T) -0.37896546 a.u.

Pb	0.000000	0.000000	0.112135
Pb	0.000000	0.000000	3.120085
Cl	1.891324	0.000000	-1.492027
Cl	-1.891324	0.000000	-1.492027

PbE(T) -0.40896843 a.u.

Pb	-1.544086	-0.048894	0.000000
Pb	1.544086	0.048894	0.000000
Cl	-1.658125	2.466541	0.000000
Cl	1.658125	-2.466541	0.000000

PbF(T) -0.40344015 a.u.

Pb	-1.571316	0.000000	0.127698
Pb	1.571316	0.000000	0.127698
Cl	-2.268486	0.000000	-2.259480
Cl	2.268486	0.000000	-2.259480

PbG(T) -0.38643213 a.u.

Pb	0.000000	0.000000	-1.557605
Pb	0.000000	0.000000	1.557605
Cl	0.000000	0.000000	-4.058818
Cl	0.000000	0.000000	4.058818

PbI(T) -0.40760773 a.u.

Pb	-0.028397	0.000685	0.092516
Pb	3.214269	0.006997	-0.047151
Cl	1.585196	2.189654	-0.018539
Cl	-0.693089	-0.177172	-2.319784

Pb_2Br_2

PbA -0.40358956 a.u.

Pb	-1.510447	0.000000	0.000436
Pb	1.510447	0.000000	0.000436
Br	0.000000	-1.902941	-1.536012
Br	0.000000	1.902941	-1.536012

PbB -0.34957207 a.u.

Pb	0.097229	0.017942	0.000000
Pb	2.976444	-0.129687	0.000000
Br	1.850621	2.456864	0.000000
Br	-2.305411	1.033216	0.000000

PbC -0.34903152 a.u.

Pb	-1.647735	0.000000	0.000000
Pb	1.647735	0.000000	0.000000
Br	0.000000	2.388236	0.000000
Br	0.000000	-2.388236	0.000000

PbD -0.33093811 a.u.

Pb	0.000000	0.000000	-0.279565
Pb	0.000000	0.000000	-3.167274
Br	0.000000	2.068495	1.336584
Br	0.000000	-2.068495	1.336584

PbE1 -0.34242528 a.u.

Pb	-1.456022	-0.029194	0.000000
Pb	1.456022	0.029194	0.000000
Br	-3.019102	2.072102	0.000000
Br	3.019102	-2.072102	0.000000

PbE2 -0.37189970 a.u.

Pb	-1.587605	0.014645	0.000000
Pb	1.587605	-0.014645	0.000000
Br	-1.526602	2.686162	0.000000
Br	1.526602	-2.686162	0.000000

PbF1 -0.36397783 a.u.

Pb	-1.648049	0.000000	0.000147
Pb	1.648049	0.000000	0.000147
Br	-2.017699	0.000000	-2.604575
Br	2.017699	0.000000	-2.604575

PbF2 -0.33640630 a.u.

Pb	-1.494857	0.000000	-0.105341
Pb	1.494857	0.000000	-0.105341
Br	-2.892703	0.000000	-2.326578
Br	2.892703	0.000000	-2.326578

PbG -0.14761726 a.u.

Pb	0.000000	0.000000	-1.251563
Pb	0.000000	0.000000	1.251563
Br	0.000000	0.000000	-3.792451
Br	0.000000	0.000000	3.792451

PbA(T) -0.36664505 a.u.

Pb	-1.903070	-0.260492	0.326016
Pb	1.903070	0.260492	0.326016
Br	-0.273289	1.996748	1.007173
Br	0.273289	-1.996748	1.007173

PbB(T) -0.36135877 a.u.

Pb	0.038453	0.080553	0.000000
Pb	3.301336	-0.063785	0.000000
Br	1.825744	2.351007	0.000000
Br	-2.197828	1.590219	0.000000

PbC(T) -0.37007548 a.u.

Pb	-1.496705	0.000000	0.000000
Pb	1.496705	0.000000	0.000000
Br	0.000000	2.596508	0.000000
Br	0.000000	-2.596508	0.000000

PbD(T) -0.34538168 a.u.

Pb	0.000000	0.000000	0.215415
Pb	0.000000	0.000000	3.214111
Br	2.020829	0.000000	-1.461537
Br	-2.020829	0.000000	-1.461537

PbE(T) -0.37524663 a.u.

Pb	-0.467956	-1.468918	0.000000
Pb	0.467956	1.468918	0.000000
Br	2.058148	-2.309352	0.000000
Br	-2.058148	2.309352	0.000000

PbF(T) -0.36990950 a.u.

Pb	-1.567091	0.000000	0.278700
Pb	1.567091	0.000000	0.278700
Br	-2.335877	0.000000	-2.234469
Br	2.335877	0.000000	-2.234469

PbG(T) -0.35315316 a.u.

Pb	0.000000	0.000000	-1.553995
Pb	0.000000	0.000000	1.553995
Br	0.000000	0.000000	-4.197849
Br	0.000000	0.000000	4.197849

PbI(T) -0.37362904 a.u.

Pb	0.068114	0.106587	-0.052827
Pb	3.306175	-0.043182	-0.033391
Br	1.805415	2.371716	0.240400
Br	-0.552074	0.256639	-2.629547

Pb_2I_2

PbA -0.36976385 a.u.

Pb	-1.522179	0.000000	0.046845
Pb	1.522179	0.000000	0.046845
I	0.000000	-2.084293	-1.611635
I	0.000000	2.084293	-1.611635

PbB -0.31653918 a.u.

Pb	0.133540	-0.014332	0.000000
Pb	2.998664	-0.210175	0.000000
I	1.962340	2.622121	0.000000
I	-2.485674	1.003794	0.000000

PbC -0.31336119 a.u.

Pb	0.000000	0.000000	0.258566
Pb	0.000000	0.000000	-3.030613
I	0.000000	2.628296	-1.386029
I	0.000000	-2.628296	-1.386029

PbD -0.29642501 a.u.

Pb	0.000000	0.000000	-0.085635
Pb	0.000000	0.000000	-2.960198
I	0.000000	2.267172	1.614730
I	0.000000	-2.267172	1.614730

PbE1 -0.30846553 a.u.

Pb -1.449656 0.002054 0.000000

Pb 1.449656 -0.002054 0.000000

I -3.086440 2.297944 0.000000

I 3.086440 -2.297944 0.000000

PbE2 -0.33673441 a.u.

Pb -1.573047 -0.088672 0.000000

Pb 1.573047 0.088672 0.000000

I -1.647804 2.789453 0.000000

I 1.647804 -2.789453 0.000000

PbF1 -0.32829131 a.u.

Pb -1.642786 0.000000 0.068108

Pb 1.642786 0.000000 0.068108

I -2.154046 0.000000 -2.715805

I 2.154046 0.000000 -2.715805

PbF2 -0.30211719 a.u.

Pb -1.488172 0.000000 0.003726

Pb 1.488172 0.000000 0.003726

I -2.958439 0.000000 -2.410295

I 2.958439 0.000000 -2.410295

PbG -0.13810360 a.u.

Pb 0.000000 0.000000 -1.263069

Pb 0.000000 0.000000 1.263069

I 0.000000 0.000000 -4.010358

I 0.000000 0.000000 4.010358

PbA(T) -0.33046591 a.u.

Pb -1.881841 -0.395742 0.396664

Pb 1.881841 0.395742 0.396664

I -0.460450 2.189581 1.216265

I 0.460450 -2.189581 1.216265

PbB(T) -0.32527459 a.u.

Pb 0.086903 0.113219 0.000000

Pb 3.321262 -0.182646 0.000000

I 1.999055 2.532097 0.000000

I -2.455036 1.567097 0.000000

PbC(T) -0.33604053 a.u.

Pb 0.000000 -1.509517 0.000000

Pb 0.000000 1.509517 0.000000

I -2.814433 0.000000 0.000000

I 2.814433 0.000000 0.000000

PbD(T) -0.30910381 a.u.

Pb	0.000000	0.000000	0.257555
Pb	0.000000	0.000000	3.244294
I	2.209962	0.000000	-1.520675
I	-2.209962	0.000000	-1.520675

PbE(T) -0.33907550 a.u.

Pb	-0.389819	-1.487349	0.000000
Pb	0.389819	1.487349	0.000000
I	2.382918	-2.224913	0.000000
I	-2.382918	2.224913	0.000000

PbF(T) -0.33376301 a.u.

Pb	-1.561412	0.000000	0.343006
Pb	1.561412	0.000000	0.343006
I	-2.459623	0.000000	-2.340738
I	2.459623	0.000000	-2.340738

PbG(T) -0.31702538 a.u.

Pb	0.000000	0.000000	-1.552132
Pb	0.000000	0.000000	1.552132
I	0.000000	0.000000	-4.401153
I	0.000000	0.000000	4.401153

PbI(T) -0.33725521 a.u.

Pb	0.094966	0.098265	-0.034310
Pb	3.320304	-0.101501	-0.041210
I	1.902159	2.565804	0.304852
I	-0.653439	0.234949	-2.797447